

Optimisation of plate girders

Roland Abspoel

Optimisation of plate girders

Proefschrift

Ter verkrijging van de graad van doctor
aan de Technische Universiteit Delft,
op gezag van de Rector Magnificus prof. ir. K.C.A.M. Luyben,
voorzitter van het College voor Promoties,
in het openbaar te verdedigen op
donderdag 3 december 2015 om 10.00 uur

door

Roland ABSPOEL

Civil ingenieur
geboren te Leiden

Dit proefschrift is goedgekeurd door de promotor:

Prof. ir. F.S.K. Bijlaard

Samenstelling promotiecommissie:

Rector Magnificus	Voorzitter
Prof. ir. F.S.K. Bijlaard	Technische Universiteit Delft, promotor
Prof. ir. J.W.B. Stark	Technische Universiteit Delft

Onafhankelijke leden:

Prof. dr. ir. M.A.N. Hendriks	Norwegian University of Science and Technology (NTNU) Trondheim Norway, Technische Universiteit Delft
Dr. M.H. Kolstein	Technische Universiteit Delft
Prof. Dr. –Ing habil. H. Pasternak	Brandenburgische Technische Universität (BTU) Cottbus, Germany
Prof. ir. H.H. Snijder	Technische Universiteit Eindhoven
Prof. dr. ir. M. Veljkovic	Technische Universiteit Delft
Prof. dr. ir. J. Wardenier	Technische Universiteit Delft, National University of Sin- gapore, reservelid



ISBN: 978-94-6259-949-9

Printed by: Ipskamp Drukkers. B.V.

Cover design: Roland Abspoel

Cover photo: Copyright © 2015 Roland Abspoel

Keywords: plate girders, web slenderness, flange induced buckling, effective width method

Copyright © 2015 Roland Abspoel. All rights reserved. No part of this publication may be reproduced, stored in a retrieval system or transmitted in any form or by any means, electronic, mechanical, photocopying, recording or otherwise, without the prior permission in writing from the proprietor.

ACKNOWLEDGEMENTS

In 1992/1993, Prof. Jan Stark moved from the Eindhoven University of Technology to the Delft University of Technology and became supervisor of my MSc-thesis about plate girders. I was surprised that a lot of research was done to improve the theory of tension field action, a method to determine the shear resistance of plate girders, while there was not much interest for bending. To improve the bending moment resistance, the maximum web slenderness is an important factor and in a Draft Eurocode the requirements for this maximum web slenderness were implemented, based on only one test result from the 1960's, which completely confused me.

My interest in the maximum bending moment resistance did not stop after graduation, but because this graduation work was realised in addition to my job at an engineering office, I did not have the time and energy to start a PhD research next to my work and I was really delighted that Prof. Jaap Wardenier gave me the opportunity to work at Delft University of Technology and gave me also some time to continue this research on plate girders under pure bending. I loved my work at the university, teaching enthusiastic young people about steel structures, very much, so that it consumed all my office time and more than that, leaving no time for my promotion project. Later on, I spent a lot of free time on the improvement of civil structures to harvest safe drinking water, at 30 primary schools with about 24000 pupils in one of the poorest areas of Kenya. Knowing that around 5% of the young children will die due to water related diseases, I can not say I wasted my time, but the progress on my PhD-research was very limited during these four years. Apart from this, I had the possibility to send two groups of civil engineering students to Kenya to do research on water facilities, knowing that they would be "infected" for life; they will be the volunteers of the future.

A long time there was not interest to reduce the material use, because labour costs were by far determining the costs of a steel structure. Nowadays more people show interest in the reduction of material use. Reducing the cost of structures, but maybe more important, the influence of life cycle analysis, the effect of structures on the environment, expressed in the carbon footprint, is a hot issue and fit very well with the aim to determine the optimal plate girder, the plate girder with the smallest cross-sectional area to restrain the bending moment as the effect of the load.

First, I would like to apologize to my initial promotor, Prof. Jan Stark, that I did not finish my PhD under his supervision, but I am glad he is one of the members of the committee. Secondly, I would like to thank my promotor, Prof. Frans Bijlaard, for his dedicated guidance and for the possibility to do laboratory tests on a macro scale, but also for giving me the possibility to finish this research. I would like to thank Dr. Henk Kolstein and Prof. Max Hendriks for their guidance and help during the last part of the research. Furthermore, I would like to acknowledge the valu-

able discussions and input from the committee members Prof. Jaap Wardenier, Prof. Hartmut Pasternak and Prof. Bert Snijder. Prof. Milan Veljkovic's position as a member of the PhD-committee changed in the course of time, because at the moment of the PhD-defense he will be the chairman of the department of Steel and Composite Structures at Delft University of Technology and I wish to thank him for the valuable discussions and input. Especially, I am curious about our future cooperation to continue research on the bending moment resistance of plate girders with a very slender web in high strength steels.

I extend my special gratitude to the technicians in the laboratory, Kees van Beek , Albert Bosman and John Hermesen. Without their help, it would, as an unexperienced researcher, never have been possible for me to set up all the frames and instrumentation for these experiments.

Special gratitude goes also to my closest colleagues for having listened for so many years to me talking about the progress or better, the lack of progress in this PhD-research, during the coffee breaks: Wolfgang Gard, Nol Gresnigt, Jan-Willem van de Kuilen, Geert Ravenshorst and Peter de Vries of the Steel and Timber group.

Finally, I would like to thank my parents and brother and parents, brothers and sisters in law, and my friends for their everlasting support. I am sure my dad and my father in law would be very proud of me.

I express my deepest gratitude to my beloved wife, Yvonne, supporting me all the time with all my activities, to my both daughters, Quirina and Rowena, who have missed me the most during their lifetime, and for their husband Marc and boy friend Daan respectively, who, by the way, did not miss me at all.

Sophie, my granddaughter, does not care about this thesis, she gives me her unconditional love and will be happy with the remaining time after finishing this PhD research.

SUMMARY

Optimisation of plate girders

Although plates of nominal steel grades up to 1100 MPa have been available on the market for many years, the optimisation of plate girders under pure bending is, focusing on material use, still uncommon in civil engineering. Lack of design rules, manufacturing experience and conservatism, but especially the lack of economical interest limit the current structural application of plate girders with very slender webs. The introduction of the effective width method in the previous Dutch code NEN6771 [62] in 1990 did not change this lack of interest for plate girders with very slender webs, notwithstanding the interest of this method in the application of cold formed sections and profiled sheeting for roofs, floors and walls.

This lack of interest took a turn because of the great demand for steel by booming economies in e.g. China and India, but also in Brazil, in addition to the increasing interest in sustainability of building activities in the first world countries.

The main goal of this research work is the determination of the maximum bending moment resistance of a double symmetric plate girder for a certain amount of steel. The terms “maximum” and “resistance” seem to be a pleonasm, but the addition “for a certain amount of steel” justifies the use of both terms together. With a certain amount of steel, many different combinations of web and flange dimensions can be used to create a plate girder, each combination with a bending moment resistance. However, there is only one combination of flange and web dimensions that gives the maximum bending moment resistance.

The emphasis is put on the optimal distribution of the amount of steel over the web and the flanges to achieve the maximum bending moment resistance. The research comprises a literature study, an experimental study, an analysis of the experimental results, numerical simulations of the experiments, a parametric research and a design strategy.

The application of the optimised plate girders is focused on roofs and floors in building structures. It is assumed that the compressive flange is fully restrained against lateral torsional buckling, which means that the flange is laterally supported by a roof or floor system. Ideally, most of the material will be put into the flanges and as little as possible in the web to realise the maximum bending moment resistance. The height of the plate girders has to be as large as possible, which means that the web should be as slender as possible.

In most steel structures built up from standard hot-rolled sections up to class 3 cross-sections, the stiffness is governing for the dimensions of the section and not the strength. Beside stiffness, in-

stability can be decisive for the dimensions of the section. This instability can be flange buckling in the direction of the web and plate buckling of the web. In the literature review attention is paid on both types of instabilities. Vertical buckling of the compressive flange into the web determines the maximal web slenderness according to one laboratory test by Basler et al. at the Lehigh University in America in the end of the 1950's and begin of the 1960's.

The bending moment resistance of a plate girder with a very slender web, defined as a class 4 cross-section, is based on the effective width method according to EN-1993-1-5 [30]. The method is developed as alternative to the more conservative linear plate buckling theory, in which the maximum compressive stress is limited to the design value of the buckling stress, to avoid plate buckling. In the effective width method it is accepted that the web buckles. Iterative calculations are necessary to determine the effective bending moment resistance, because of the shift of the neutral axis by neglecting of the non-effective part of the web under compression.

In the literature review also attention is paid to methods, developed by different researchers, to determine the effective bending moment resistance without iterative calculations. None of these methods lead to the maximum bending moment resistance for a certain amount of steel.

The Basler test girder that failed by vertical buckling of the compressive flange into the web is simulated with a FEM-model. Different residual stress distributions were used in the FEM-model and the FEM-results are compared with the test results of the experiment of Basler.

Because of the very limited number of laboratory tests related to vertical buckling of the web into the web, 10 additional model scale laboratory tests were conducted with different ratios of area and different web slenderness in the Stevin 2 Laboratory of the Delft University of Technology. These laboratory tests are used to verify the requirement of the maximum web slenderness and to determine the bending moment resistances of such plate girders with very slender webs. The bending moment resistances are compared with theoretical bending moment resistances.

In addition to this comparison, the test girders are also simulated with a FEM-model. The residual stress distributions according two previous national codes are used and the one that fitted best in the FEM-model for the Basler test girder, is used in the FEM-model to simulate the Delft experiments.

A parametric study was conducted by using the FEM-model, to determine the maximum bending moment resistance for a certain amount of steel for steel grades S235 and S460. By using different approaches, the dimensions of the web and flanges are varied, while the cross-sectional area is kept constant. The author developed a model to calculate the bending moment resistance, based on a simplified effective width method, without the need of iterative calculations. This

method takes into account the truss beam-like behaviour of the double symmetric plate girder with a very slender web and so only the flanges and a small part of the web contribute to the bending moment resistance. This means that, apart from an effective width of the compressive web, there is also an effective width in the tensile part of the web. The model is based on the results of the Delft experiments and on the results of the parametric research using FEM. Additional parametric research is conducted, based on this simplified effective width method, to develop a design procedure to determine the minimal cross-sectional area and the optimal dimensions of the web and flanges of a plate girder to restrain a certain bending moment as an effect of the factored loading.

It is concluded that the maximum web slenderness can be increased relative to the requirement in international standards based on the Basler research. Because of this increase, the stiffness would no longer be the governing criterion, depending of the static scheme, and so it is of interest to do additional research on plate girders of higher steel grades than the steel grades S235 and S355 used in the Delft experiments. Nevertheless, for an optimised plate girder under pure bending, using steel grades up to S355, a reduction of the material use of 50% is possible.

SAMENVATTING

Ondanks dat platen met nominale vloeispanningen tot 1100 MPa al vele jaren beschikbaar zijn op de markt, is het optimaliseren van plaatliggers belast op zuivere buiging, gericht op het materiaalgebruik, nog steeds ongebruikelijk in de civiele techniek. Het ontbreken van ontwerpregels, ervaring bij de fabricage en conservatisme, maar speciaal het ontbreken van economische interesse beperkt de huidige constructieve toepassing van plaatliggers met een bijzonder slank lijf. De introductie van de effectieve breedtemethode in de vorige Nederlandse norm NEN6771 [62] uit 1990 veranderde deze desinteresse voor plaatliggers met een bijzonder slank lijf niet, ondanks de interesse in de toepassing van koudgevormde profielen en geprofileerde platen voor vloeren, daken en wanden.

Het gemis aan interesse veranderde door de grote vraag naar staal door de opkomende economie in bijvoorbeeld China en India, maar ook in Brazilië, naast de groeiende interesse in duurzaamheid in de Westerse wereld.

Het hoofddoel van dit onderzoek is de bepaling van de maximale momentcapaciteit van dubbel symmetrische plaatliggers voor een bepaalde hoeveelheid staal. De termen “maximale” en “capaciteit” lijken een pleonasme te zijn, maar de toevoeging “voor een bepaalde hoeveelheid staal” rechtvaardigt het gebruik van beide termen. Met een bepaalde hoeveelheid staal kunnen verschillende combinaties van flens- en lijfafmetingen worden gebruikt om een plaatligger te maken, waarbij elke combinatie een momentcapaciteit heeft, maar er is slechts één combinatie van flens- en lijfafmetingen die de maximale momentcapaciteit geeft.

De nadruk is gelegd op de optimale verdeling van een bepaalde hoeveelheid staal over de flenzen en het lijf om de maximale momentcapaciteit te bewerkstelligen. Het onderzoek omvat een literatuurstudie, laboratoriumonderzoek, de analyse van de proefresultaten, numerieke simulaties van de experimenten, een parameteronderzoek en een ontwerpstrategie.

De toepassing van geoptimaliseerde plaatliggers is gelegen in dak- en vloerconstructies in gebouwen. Uitgangspunt is dat de flens op druk volledig is gesteund om kippen van de plaatligger te voorkomen. Dit betekent dat de gedrukte flens horizontaal is gesteund door een dak- of vloersysteem. Idealiter wordt, om de maximale momentcapaciteit te verkrijgen, zoveel mogelijk staal in de flenzen geplaatst en zo min mogelijk staal in het lijf. De hoogte van de plaatligger dient zo groot mogelijk te zijn, hetgeen inhoudt dat het lijf zo slank mogelijk dient te zijn.

In de meeste staalconstructies, opgebouwd uit standaard warmgevormde walsprofielen tot en met doorsnedeklasse 3, is de stijfheid het maatgevende criterium voor de afmetingen van de doorsnede en niet de sterkte. Naast stijfheid kan ook instabiliteit de afmetingen bepalen. Die instabiliteit

betreft het knikken van de flens in de richting van het lijf en het plooien van het lijf. In de literatuurstudie is aandacht besteed aan beide instabiliteitsvormen. Verticaal knikken van de gedrukte flens in het lijf bepaalt de maximale lijfslankheid, overeenkomstig één laboratoriumproef door Basler e.a. op de Lehigh University in Amerika aan het eind van de jaren vijftig, begin jaren zestig.

De momentcapaciteit van een plaatligger met een bijzonder slank lijf, een doorsnedeklasse 4 lijf, is gebaseerd op de effectieve breedtemethode conform EN1993-1-5 [30]. Deze methode is ontwikkeld na de meer conservatieve lineair elastische plooitheorie, waarin de maximale spanning beperkt is tot de plooispanning, dit om plooien te voorkomen, terwijl dit plooien bij de effectieve breedtemethode wordt geaccepteerd. Iteratieve berekeningen zijn noodzakelijk om de effectieve momentcapaciteit te bepalen, hetgeen wordt veroorzaakt door het verschuiven van de neutrale lijn ten gevolge van het niet effectieve deel van het lijf op druk.

In de literatuurstudie is ook aandacht besteed aan methoden, ontwikkeld door verscheidene onderzoekers, om de effectieve momentcapaciteit te bepalen, zonder iteratieve berekeningen. Geen van deze methoden leidt tot de maximale momentcapaciteit voor een bepaalde hoeveelheid staal. De proefligger, die volgens Basler is bezwaken door verticaal knikken van de gedrukte flens in het lijf, is met een FEM-model gesimuleerd. Diens resultaat is gevalideerd op de proefresultaten, zodat dit FEM-model gebruikt kan worden in het parameteronderzoek. Verschillende restspanningsverdelingen zijn gebruikt in de simulatie en de FEM-resultaten zijn vergeleken met de proefresultaten.

In verband met het beperkt aantal laboratoriumproeven naar het verticaal knikken van de gedrukte flens in het lijf, zijn 10 aanvullende laboratoriumproeven uitgevoerd op proefliggers op schaal met verschillende oppervlakteverhoudingen en verschillende lijfslankheden in het Stevin 2 laboratorium van de Technische Universiteit Delft. Deze laboratoriumproeven worden eveneens gebruikt om het normartikel m.b.t. het verticaal knikken van de gedrukte flens in het lijf te verifiëren en om de momentcapaciteiten te vergelijken met theoretische momentcapaciteiten van plaatliggers met dergelijke bijzonder slanke lijven.

Naast deze vergelijking, zijn de testliggers ook gesimuleerd met FEM-modellen. De restspanningsverdeling die bij de validatie van de FEM-resultaten op de resultaten van de door Basler beproefde ligger tot het beste resultaat leidde, is gebruikt bij de simulaties van de Delftse proefliggers.

Een parameteronderzoek is uitgevoerd, met gebruik van de FEM-modellen, om de maximale momentcapaciteit te bepalen voor een bepaalde hoeveelheid staal van de staalsoorten S235 en

S460. De afmetingen van de flenzen en het lijf zijn op verschillende wijze gevarieerd, terwijl het totale oppervlak van de doorsnede gelijk is gehouden. De auteur heeft een model ontwikkeld om de momentcapaciteit te berekenen, gebaseerd op een vereenvoudigde effectieve breedte methode, zonder daarbij iteratieve berekeningen te moeten maken. Deze methode houdt rekening met het vakwerklijggerachtige gedrag van een dubbelsymmetrische plaatlijgger met een bijzonder slank lijf en enkel de flenzen en een klein deel van het lijf dragen bij aan de momentcapaciteit. Dit betekent dat, naast een effectief deel van het lijf op druk, er ook een effectief deel van het lijf op trek is. Dit model is gebaseerd op de resultaten van de laboratoriumproeven en op de resultaten van de FEM-simulaties. Aanvullend parameteronderzoek is uitgevoerd met behulp van deze vereenvoudigde effectieve breedte methode. Dit aanvullende parameteronderzoek resulteert in een ontwerpmethode om de minimale doorsnede van een plaatlijgger en de daarbij behorende optimale afmetingen van het lijf en de flenzen te bepalen, zodanig, dat het maximaal buigend moment ten gevolge van de rekenwaarden van de belasting kan worden opgenomen.

Geconcludeerd kan worden dat de maximale lijfslankheid fors kan worden verhoogd ten opzichte van hetgeen op dit moment in internationale normen, gebaseerd op het onderzoek van Basler, wordt vereist. Door deze toename van de maximale lijfslankheid, zal de stijfheid niet langer het maatgevende criterium zijn, afhankelijk van het statisch systeem, waardoor het gebruik van hogere staalsoorten ten opzichte van de in het laboratorium gebruikte staalsoorten S235 en S355, interessant wordt om verder laboratoriumonderzoek te doen. Desondanks kan nu reeds voor een plaatlijgger belast op zuivere buiging een reductie van 50% op het materiaalgebruik worden gerealiseerd bij gebruik van staalsoorten tot en met S355.

LIST OF SYMBOLS AND ABBREVIATIONS

The list below includes the symbols and abbreviations as they are used in this thesis. In the text symbols are *italicised*. In some cases, the same symbol is used to describe two parameters. However, the explanation in the text and the context in which the symbols are used will make the meaning of all symbols unambiguous.

Symbol	Description	Units
a	length of a stiffened or unstiffened plate panel	[mm]
a	throat thickness	[mm]
b	width of a stiffened or unstiffened plate	[mm]
b_{eff}	effective width	[mm]
$b_{eff,i}$	effective width at iteration i	[mm]
$b_{e1,i}$	effective width at the top of a compressive web at iteration i	[mm]
$b_{e2,i}$	effective width at the bottom of compressive web at iteration i	[mm]
$e_{1,i}$	distance neutral axis to the bottom of section, iteration i	[mm]
$e_{2,i}$	distance neutral axis to the bottom of section, iteration i	[mm]
f_y	yield strength	[MPa]
$f_{y,bf}$	yield strength of a bottom flange	[MPa]
$f_{y,w}$	yield strength of a web	[MPa]
$f_{y,tf}$	yield strength of a top flange	[MPa]
f_u	ultimate strength	[MPa]
h	depth of a cross-section	[mm]
h_w	web depth between the flanges	[mm]
i	number of iterations	[-]
j	number of iterations	[-]
k	spring stiffness	[kN/m]
k_σ	plate buckling coefficient	[-]
l	length	[mm]
t	thickness of a plate	[mm]
t_{bf}	bottom flange thickness	[mm]
t_w	web thickness	[mm]
$t_{w,ep}$	web thickness of an end panel of a plate girder	[mm]
$t_{w,tp}$	web thickness of a test panel of a plate girder	[mm]
t_{tf}	top flange thickness	[mm]

Symbol	Description	Units
A	cross-sectional area	$[\text{mm}^2]$
A_{bf}	area of a bottom flange	$[\text{mm}^2]$
A_f	area of a flange	$[\text{mm}^2]$
A_{tf}	area of a top flange	$[\text{mm}^2]$
A_{tot}	total area cross-section	$[\text{mm}^2]$
A_w	area of a web	$[\text{mm}^2]$
D	flexural rigidity	$[\text{Nmm}]$
E	modulus of elasticity (Young's modulus)	$[\text{MPa}]$
G	shear modulus	$[\text{MPa}]$
I_{eff}	effective second moment of area	$[\text{mm}^4]$
I_x	second moment of area around x - x axis	$[\text{mm}^4]$
I_y	second moment of area around the y - y axis	$[\text{mm}^4]$
I_z	second moment of area around the z - z axis	$[\text{mm}^4]$
M	bending moment	$[\text{kNm}]$
M_u	ultimate bending moment resistance	$[\text{kNm}]$
M_{cr}	elastic critical bending moment resistance	$[\text{kNm}]$
M_{el}	elastic bending moment resistance	$[\text{kNm}]$
M_{eff}	effective bending moment resistance	$[\text{kNm}]$
M_f	bending moment resistance of a cross-section consisting of the flanges only	$[\text{kNm}]$
M_{pl}	plastic bending moment resistance	$[\text{kNm}]$
N	axial force	$[\text{N}]$
P	load	$[\text{N}]$
P_{cr}	load that leads to critical bending moment resistance	$[\text{N}]$
P_{el}	load that leads to elastic bending moment resistance	$[\text{N}]$
P_{eff}	load that leads to effective bending moment resistance	$[\text{N}]$
P_f	load that leads to the bending moment resistance of a cross-section consisting of the flanges only	$[\text{N}]$
P_{pl}	load that leads to the plastic bending moment resistance	$[\text{N}]$
W	first moment of area	$[\text{mm}^3]$
W_y	first moment of area around y - y axis	$[\text{mm}^3]$
W_{ef}	effective first moment of area	$[\text{mm}^3]$

Symbol	Description	Units
α	aspect ratio	[-]
β	plate slenderness	[-]
β_w	web slenderness	[-]
δ	deflection	[mm]
ε	strain	[-]
ε_y	yield strain	[-]
ϕ	angle	[-]
γ_{M0}	partial factor for resistance of cross-sections	[-]
γ_{M1}	partial factor for resistance of members to instability	[-]
φ	angle	[-]
κ	curvature	[1/mm]
χ	column buckling factor	[-]
λ	slenderness	[-]
$\bar{\lambda}_p$	relative plate slenderness	[-]
ν	Poisson's ratio in elastic stage	[-]
θ	angle	[°]
ρ	reduction factor for plate buckling	[-]
ρ	ratio between areas web and compressive flange	[-]
ρ_{steel}	density of steel	[kg/m ³]
σ	stress	[MPa]
σ_{cr}	critical stress	[MPa]
σ_e	engineering stress	[MPa]
$\sigma_{i,j}$	stress at location i at iteration j	[MPa]
σ_n	normal stress	[MPa]
σ_r	residual stress	[MPa]
σ_t	true stress	[MPa]
σ_1	maximum compressive stress (positive)	[MPa]
σ_2	minimum compressive stress (positive) or tensile stress (negative)	[MPa]
τ	shear stress	[MPa]
ψ	stress ratio	[-]

TABLE OF CONTENTS

ACKNOWLEDGEMENTS	v
SUMMARY	vii
SAMENVATTING	xi
LIST OF SYMBOLS AND ABBREVIATIONS	xv
1 INTRODUCTION.....	1
1.1 General	1
1.2 Research motivation	1
1.2.1 Problem description	1
1.2.2 State-of-the-art	3
1.2.3 Aim of the research	4
1.3 Thesis	4
2 LITERATURE REVIEW.....	7
2.1 General	7
2.2 Plate Buckling in the web.....	7
2.3 Effective width method	15
2.3.1 Derivation of the effective width	15
2.4 Maximum web slenderness of a plate girder according to basler	18
2.4.1 General	18
2.4.2 Lehigh test specimen G4.....	18
2.4.3 Model for vertical buckling of the compressive flange into the web	25
2.5 Bending moment restistance of plate girders	29
2.5.1 According to Basler	29
2.5.2 According to Höglund.....	36
2.5.3 According to Herzog.....	38
2.5.4 According to Stark	40
2.5.5 According to Veljkovic and Johansson	42
2.6 Requirements in international codes	43
2.6.1 EN1993-1-5	43
2.6.2 ANSI/AISC 360-10 [5].....	46
2.7 Remarks and elaborations on the studied literature	47

2.7.1	Remarks on the maximum web slenderness according to Basler.....	47
2.7.2	Elaborations on the bending moment resistance according to Basler.....	49
2.7.3	Elaborations on the bending moment resistance according to Höglund	53
2.7.4	Elaborations on the bending moment resistance according to Herzog.....	56
2.7.5	Elaborations on the bending moment resistance according to Stark.....	60
2.7.6	Elaborations on the bending moment resistance according to Veljkovic and Johansson.....	62
2.7.7	Comparison of ultimate bending moment resistances.....	65
2.8	Conclusions	72
3	VALIDATION FEM-MODEL ON BASLER EXPERIMENT	77
3.1	General.....	77
3.2	Modelling of the Basler test specimen G4 for tests T1 and T2	77
3.2.1	Geometry of the FEM-model.....	77
3.2.2	Material properties used in the FEM-model	79
3.2.3	Imperfections used in the FEM-model.....	84
3.3	Accuracy related to the number of elements.....	97
3.4	Solution procedures for nonlinear systems	98
3.5	Theoretical bending moment resistances of test specimen g4.....	102
3.5.1	General.....	102
3.5.2	Elastic bending moment resistance	105
3.5.3	Plastic bending moment resistance	107
3.5.4	Bending moment resistance based on the cross-section consisting of the flanges only	108
3.5.5	Critical bending moment resistance	109
3.5.6	Effective bending moment resistance	109
3.5.7	Overview of the theoretical bending moment resistances.....	116
3.6	Theoretical deflections	117
3.7	Comparison FEM results on experimental and theoretical results.....	125
3.7.1	FEM-model with residual stresses according to NEN6771 and test T1.....	128
3.7.2	FEM-model with residual stresses according to NEN6771 and test T2.....	136
3.7.3	FEM-model with residual stresses according to BSK99 and test T1	143
3.7.4	FEM-model with residual stresses according to BSK99 and test T2	149
3.7.5	Comparison laboratory specimen G4 and FEM-calculations.....	154
3.8	Conclusions on the validation of the FEM-models on the basler test girder	155

4	DESCRIPTION OF THE TEST SPECIMENS, TEST RIG AND INSTRUMENTATION OF THE DELFT EXPERIMENTS	159
4.1	General	159
4.2	Geometry	160
4.2.1	Nominal dimensions	160
4.2.2	Actual dimensions	162
4.3	Actual material properties	164
4.4	Test rig including the supports and the instrumentation	165
4.4.1	Test rig	165
4.4.2	Instrumentation	167
4.5	Fabrication and the initial imperfections	170
5	RESULTS OF THE DELFT EXPERIMENTS	173
5.1	General	173
5.2	Measurements	173
5.2.1	Load-deformation behaviour	173
5.2.2	Reaction forces versus the actuator forces	176
5.2.3	The out-of-plane displacements of the web of the test panel	178
5.2.4	Vertical deflections of the test girder	182
5.2.5	Rotation of the compressive flange around the longitudinal axis	184
5.2.6	Rotation of the tensile flange determined from the vertical deflections of the tips of test girder 9, 800x80, and test girder 3, 400x80(2), divided by the distance between the measured locations	185
5.2.7	Strain measured with strain gauges	187
5.3	Elaborations on the measurements of the experiments	190
5.3.1	Reaction forces versus the actuator force	190
5.3.2	The load deformation behaviour	206
5.3.3	The out-of-plane deflections of the web in the test panel	208
5.3.4	The rotation of the compressive flange	216
5.3.5	The rotation of the tensile flange	218
5.3.6	The strains	221
5.4	Overview of the location of the final collapse mode	232
5.5	The bending moment resistance of the test girders	235
5.6	Conclusions	235

6	VALIDATION OF THE FEM-MODEL ON THE DELFT EXPERIMENTS	237
6.1	General	237
6.2	Modelling of the Delft experiments	237
6.2.1	Geometry of the FEM-models	237
6.2.2	Material properties used in the FEM-models	239
6.2.3	Imperfections used in the FEM-model	240
6.3	Theoretical resistances of the Delft test specimens	245
6.3.1	General	245
6.3.2	Effective bending moment resistance	245
6.3.3	Theoretical deflections	259
6.4	Comparison results Delft experiments with results FEM	264
6.4.1	General	264
6.4.2	Test girder 9, 800x80	264
6.4.3	Test girder 3, 400x80(2)	266
6.4.4	Overview results	267
6.5	Conclusions	269
7	PARAMETRIC STUDY	271
7.1	General	271
7.2	Most influential geometrical parameter	280
7.3	Parametric study based on FEM-models	283
7.3.1	Approach 1: constant A_f and t_w , varying A_{tot} , A_w and h_w	283
7.3.2	Approach 2: constant A_{tot} , A_w and A_f , varying h_w and t_w	286
7.3.3	Approach 3: constant A_{tot} and t_w and , varying A_w , A_f and h_w	290
7.3.4	Comparison of the results of the approaches used	296
7.4	Parametric research based on the simplified effective width method according to Abspoel	301
7.4.1	The ratio of area	301
7.4.2	The maximum web slenderness	304
7.4.3	The minimum flange slenderness	306
7.4.4	The steel grade	306
7.5	Strategy to design the cross-section for a plate girder	315
7.6	Conclusions	318

8	DESIGN PROCEDURE FOR PLATE GIRDERS MADE OF S235 AND S355	321
8.1	Procedure to determine the minimal cross-sectional area	321
8.2	Examples	323
8.2.1	Example 1 Plate girder without any limitation of the height.....	323
8.2.2	Example 2 Plate girder with a web height based on the adapted web thickness and maximum web slenderness	325
8.2.3	Example 3: Plate girder with web height close to the optimal web height.....	327
8.2.4	Example 4: Plate girder with a limited web height	328
8.2.5	Comparison with a hot-rolled section	329
8.3	Conclusions	329
9	CONCLUSIONS AND RECOMMENDATIONS	331
9.1	Conclusions	331
9.2	Recommendations.....	332
10	REFERENCES.....	333
APPENDIX A:	Actuator force versus deformations of the piston	339
APPENDIX B:	Half of the actuator force versus the deformation at the load introductions.....	345
APPENDIX C:	Reaction forces versus the actuator force.....	351
APPENDIX D:	Out-of-plane deflections.....	357
APPENDIX E:	Vertical deflections of the bottom flange over the span of the test panel.....	389
APPENDIX F:	Rotation of the top flange over the span of the test panel.....	395
APPENDIX G:	Vertical deformation of the tips of the bottom flange over the span of the test panel.....	399
APPENDIX H:	Vertical deformation of the tips of the top flange over the span of the test panel.....	401
APPENDIX I:	Strains in the cross-section.....	407
APPENDIX J:	Half of the actuator force versus the longitudinal deformations.....	427
APPENDIX K:	Static schemes with the location of the point of action of the resulting friction force.....	433
APPENDIX L:	Out-of-plane deformations as function of the load.....	435
APPENDIX M:	Incremental out-of-plane deflections.....	465
APPENDIX N:	Rotation of the bottom flange as a results of the deflections of the tips	495
APPENDIX O:	Rotation of the top flange as a results of the vertical deflections of the tips of this flange.....	501

APPENDIX P: Strains over the height of the cross-section at midspan.....	507
APPENDIX Q: Sum of the reaction forces versus the vertical deflections left load introduction of the FEM-models and the laboratory tests.....	531
Curriculum Vitae.....	537

1 INTRODUCTION

1.1 GENERAL

In this thesis, a model is developed for the distribution of a certain amount of steel over the flanges and the web of a plate girder to achieve the maximum ultimate bending moment resistance. This model is based on a parametric study using the FEM method. The results of FEM models are validated with an test performed by Basler [6 to 16] at the Fritz Laboratory of the Lehigh University and with ten tests on plate girders performed at the Stevin II Laboratory of the Delft University of Technology. The model predicts the strength and local stability behaviour of laterally supported plate girders.

1.2 RESEARCH MOTIVATION

1.2.1 PROBLEM DESCRIPTION

In many steel structures like buildings, industrial halls and bridges, standardized hot-rolled sections are used. These sections are divided into specific types, such as IPE, HEA, HEB, HEM, HED and UNP in Europe and similar profiles in the USA. The range of hot-rolled sections is limited and therefore fabricated plate girders are used when the standard hot-rolled sections do not meet the requirements for stiffness, strength, stability and economy.

Such a plate girder is built up from steel plates for the top and bottom flange and for the web, welded together to an I-shape cross-section, single or double symmetric. Using this type of plate girders, a high degree of optimisation of material use is achieved by using different plate thickness and width for the flanges, and thickness and height for the web over the span of the girder adapted to the distribution of bending moments and the shear forces.

Optimisations can be carried out for many aspects, but in this thesis the ultimate bending moment resistance of a plate girder, given a certain weight per unit length, is the main topic for optimisation. For a long time, this was not or hardly of interest at all in Western countries, especially because the cost of structures was mainly determined by labour cost and hardly by material cost. Due to the increasing automation in the production of plate girders, the material cost becomes more important than the labour cost. However, for nowadays structures, life cycle costs and the environmental impact of structures become of greater influence on the design, beside to the increasing cost of steel by expanding demand by booming economies like China, Brazil, India and other upcoming economies. So, optimisation for minimal use of materials has become highly important.

Using higher steel grades, applying most material in the flanges and increasing the lever arm between both flanges are the main possibilities to maximise the bending moment resistance of a plate girder under pure bending given a certain amount of steel.

In many cases, when using hot-rolled sections, the deflections is the decisive design criterion and therefore using high steel grades seems not useful. For plate girders with the same cross-sectional area as hot-rolled sections, the stiffness is much higher and the strengths of the material can be better exploited, so using higher steel grades can be useful.

In case of a fixed cross-sectional area, by increasing the lever arm, more material is placed in the web, reducing the remaining material for the flanges. However, the lever arm can also be increased without using more material in the web by increasing the web height and decreasing the web thickness. This process is restricted by a limit for a practical thickness of the web, to enable welding of the section and also the handling of the plate girder.

The slenderness of the flanges, expressed in the width to thickness ratio of the flange plate, is restricted such that at least yielding of the outer fibre is possible to ensure that the plate girder exhibits at least a “not brittle-like” post-critical behaviour.

In terms of cross-sectional classification, as given in Eurocode 3, EN 1993-1-1 [29] based on local instability of plate girder elements, the compressive flange may be either elastic (class 3), semi-compact (class 2) or compact, plastic (class 1), but not slender (class 4).

The web slenderness, expressed in the height to thickness ratio of the web plate, needs not be restricted. Reaching the elastic critical plate buckling stress in the web is hardly of influence on the bending behaviour of the plate girder. The post-critical plate buckling behaviour of the web plate can be easily exploited using the effective width theory.

However, EN1993-1-5 [30] limits the web slenderness by a specific phenomenon called “flange induced buckling”. This phenomenon has been studied by Basler [6 to 16] and described as “vertical buckling of the compressive flange into the web”, see Figure 1-1.

Basler based this maximum web slenderness only on one laboratory test result and so it was considered of interest to perform additional research on this limitation to investigate whether this phenomenon really limits the bending moment resistance of a plate girder and to see if it is possible to increase this maximum web slenderness.

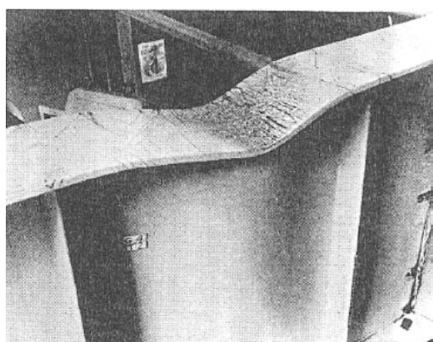


Figure 1-1 Vertical buckling of the compressive flange into the web of test specimen G4, Basler [12]

1.2.2 STATE-OF-THE-ART

For many decades, plated structures have been used, especially for long span girders for buildings, industrial halls and bridges. Plate buckling is one of the criteria to check the structural safety of this kind of structures. For bridges, besides plate buckling, fatigue is one of the governing criteria, which means that the web slenderness may be restricted to prevent fatigue cracks caused by web breathing. In building structures, fatigue is hardly a criterion, so girders with very slender webs are in principle possible.

The critical stress for a perfectly straight column buckling is used to determine the slenderness of such a column. As a result of geometrical imperfections, the fact that steel yields at a certain stress level and because of the presence of residual stresses, the real resistance of columns is lower than the critical column buckling stress.

Unlike column buckling, the critical stress for plate buckling does not determine the resistance, but determines the stress level where a perfectly flat plate will initially buckle. A rectangular plate with all edges simply supported and loaded under pure compression in one direction, will buckle at a certain stress level, called critical plate buckling stress, and withdraw itself from the loading. The areas close to the supporting edges react stiffer than in the area in the middle of the plate and so the in-plane stresses will redistribute from the middle part of the plate towards the edges. This redistribution of stresses is taken into account in the so called “effective width” method developed by Von Kármán [46, 47]. Winter [74, 75] fine tuned the effective width method based on experiments, especially for cold formed sections taking into account the influence of geometrical imperfections, the fact that steel yields at a certain stress level and the presence of residual stresses. The use of this effective width method by Winter exploits the post buckling behaviour of compressive plates.

By the end of the 1950's, early 1960's, a lot of research was carried out to apply slender welded plate girders, based on the effective width method, especially by Basler and Thürliman [6 to 16] at Lehigh University.

By using this effective width method, the bending moment and shear resistances were considerably increased in comparison to these resistances based on the initial plate buckling theory. Yielding, lateral torsional buckling, torsional buckling and combinations of these phenomena, or vertical buckling of the compressive flange into the web, determine the bending moment resistance of a plate girder.

1.2.3 AIM OF THE RESEARCH

The main goal of this thesis is to investigate the bending moment of double symmetric welded plate girders with very slender webs and laterally restrained compressive flanges, how to maximise this resistance and to what extent this maximum resistance is influenced by vertical buckling of the compressive flange into the web (flange induced buckling). In addition a method is developed for the distribution of a certain amount of steel area over the flanges and the web to find the maximum bending moment resistance.

Because the compressive flange is assumed to be laterally restrained, lateral torsional buckling is not taken into account.

1.3 THESIS

Chapter 1 describes the Introduction.

Chapter 2 comprises the literature survey, divided into a part about the theory on plate buckling and effective width, followed by torsional buckling and the phenomenon of flange induced buckling and a part about the calculation of the bending moment resistance of plate girders and by code based information about these subjects. This survey ends with a part on remarks and elaborations on the studied literature.

Chapter 3 describes the FEM-model used to simulate the Basler experiment.

In Chapter 4, information about the Delft experiments is given, including the geometrical dimensions, material properties, fabrication of the test specimens, information about the test rig and the instrumentation.

In Chapter 5, the results of the Delft experiments are shown.

FEM-models of the Delft experiments are described in Chapter 6. The results of the FEM-calculations are compared with the results of the experiments.

A parametric study was performed with additional FEM-calculations and described in Chapter 7.

Finally, a design strategy for plate girders is presented in Chapter 8 and the thesis ends with Conclusions and Recommendations in Chapter 9.

2 LITERATURE REVIEW

2.1 GENERAL

The literature review is related to topics that are most influential on the bending moment resistance of plate girders. These topics are plate buckling and effective width describing the behaviour of the web plate of the girder, followed by torsional buckling and the phenomenon flange induced buckling describing the behaviour of the compressive flange. Attention is paid to literature on the calculation of the bending moment resistance and code-based information about these topics. This survey ends with remarks and elaborations on the studied literature.

The bending moment resistance M_u of plate girders is based mainly on the behaviour of the flanges. The dimensions of the flanges are selected such that local plate buckling will not occur. The web of the plate girder is mainly to provide the lever arm to the flanges. The behaviour of the web plate is of less importance for the bending moment resistance of the plate girder. To maximise this lever arm, the height of the web needs to be maximised and the web thickness minimised. Such slender webs will buckle under bending.

2.2 PLATE BUCKLING IN THE WEB

Webs of plate girders in bending are loaded by in-plane stresses, which may result in plate buckling of these webs. It is of interest to study the phenomenon of plate buckling in more detail.

The differential equation describing the initial buckling of the plate is given by Timoshenko [73], see Eq.(2.1). Here w is the out-of-plane deflection and N_x , N_y and N_{xy} are loads ($N_{yx} = -N_{xy}$) in the plane, the x - y plane, of the plate.

$$\frac{\partial^4 w}{\partial x^4} + 2 \frac{\partial^4 w}{\partial x^2 \partial y^2} + \frac{\partial^4 w}{\partial y^4} = \frac{1}{D} \left(N_x \frac{\partial^2 w}{\partial x^2} + N_y \frac{\partial^2 w}{\partial y^2} + 2 N_{xy} \frac{\partial^2 w}{\partial x \partial y} \right) \quad (2.1)$$

The solution of this differential equation Eq.(2.1) depends on the type of the load and the boundary conditions.

For the web of a plate girder under pure bending, the load N_x acts in the plane of the web. To illustrate the behaviour of a web plate, some examples are given in which the loading and boundary conditions are varied.

For a plate, simply supported at the edges perpendicular to the load N_x (for $x=0$ and $x=a$) and free at the edges in the direction of the load N_x (for $y=0$ and $y=b$), see Figure 2-1, the resistance based on plate buckling can be compared with the resistance based on column buckling.

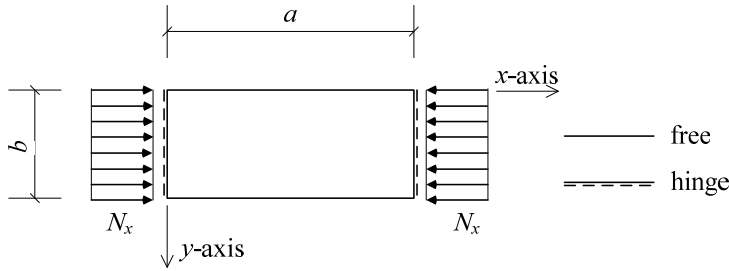


Figure 2-1 A plate under pure compression, simply supported at $x=0$ and $x=a$ along $y=0$ to $y=b$ and free at $y=0$ and $y=b$ along $x=0$ to $x=a$

The deflection w perpendicular to the plane of the plate represents the plate buckling shape which is assumed to be a sine:

$$w = A \cdot \sin\left(\frac{\pi x}{a}\right) \quad (2.2)$$

The derivatives are:

$$\begin{aligned} \frac{\partial w}{\partial x} &= A \cdot \left(\frac{\pi}{a}\right) \cdot \cos\left(\frac{\pi x}{a}\right) & \frac{\partial^2 w}{\partial x^2} &= -A \cdot \left(\frac{\pi}{a}\right)^2 \cdot \sin\left(\frac{\pi x}{a}\right) \\ \frac{\partial^3 w}{\partial x^3} &= -A \cdot \left(\frac{\pi}{a}\right)^3 \cdot \cos\left(\frac{\pi x}{a}\right) & \frac{\partial^4 w}{\partial x^4} &= A \cdot \left(\frac{\pi}{a}\right)^4 \cdot \sin\left(\frac{\pi x}{a}\right) \end{aligned}$$

Here, A is the amplitude of the out-of-plane deflection w . All derivatives to y are zero because the variable y is not present in Eq.(2.2). Substitution of the derivatives into Eq.(2.1) leads to:

$$\begin{aligned} A \cdot \left(\frac{\pi}{a}\right)^4 \cdot \sin\left(\frac{\pi x}{a}\right) + 2 \underbrace{\frac{\partial^4 w}{\partial x^2 \partial y^2}}_0 + \underbrace{\frac{\partial^4 w}{\partial y^4}}_0 &= \\ &= \frac{1}{D} \left(-N_x \cdot A \cdot \left(\frac{\pi}{a}\right)^2 \cdot \sin\left(\frac{\pi x}{a}\right) + \underbrace{N_y \frac{\partial^2 w}{\partial y^2}}_0 + 2 \underbrace{N_{xy} \frac{\partial^2 w}{\partial x \partial y}}_0 \right) \\ \Rightarrow -\cancel{A} \cdot \left(\frac{\pi}{a}\right)^4 \cdot \cancel{\sin\left(\frac{\pi x}{a}\right)} &= \frac{N_x}{D} \cdot \cancel{A} \cdot \left(\frac{\pi}{a}\right)^2 \cdot \cancel{\sin\left(\frac{\pi x}{a}\right)} \\ \Rightarrow N_x = N_{cr} &= - \left(\frac{\pi^2}{a^2} \frac{Et^3}{12(1-\nu^2)} \right) = -k_\sigma \cdot \left(\frac{\pi^2}{b^2} \frac{Et^3}{12(1-\nu^2)} \right) \end{aligned} \quad (2.3)$$

By using $D = \frac{Et^3}{12(1-\nu^2)}$, called the flexural rigidity of the plate, the solution given in Eq.(2.3)

changes into:

$$N_x = N_{cr} = -k_\sigma \cdot \left(\frac{\pi^2 D}{b^2} \right) \quad (2.4)$$

Where k_σ is the plate buckling factor. In the example, the plate simply supported at $x=0$ and $x=a$, and free for $y=0$ and $y=b$ and so the plate buckling factor k_σ is equal to:

$$k_\sigma = \left(\frac{b}{a} \right)^2 \quad (2.5)$$

Because it is assumed that the compressive force has a positive sign, the $-$ in Eq.(2.4) is not used anymore. The critical stress σ_{cr} can be determined with:

$$\sigma_{cr} = \frac{N_{cr}}{t} = k_\sigma \cdot \frac{\pi^2 E}{12(1-\nu^2) \left(\frac{b}{t} \right)^2} \quad (2.6)$$

The Euler buckling load F_E of a column with the dimensions b and t (with $b \gg t$), simply supported at both ends and a buckling length ℓ_{buc} is:

$$F_E = \frac{\pi^2 EI}{\ell_{buc}^2} \quad (2.7)$$

From substitution of $I = \frac{bt^3}{12}$ and $\ell_{buc} = a$ into Eq.(2.7) follows:

$$F_E = \frac{\pi^2 E \cdot b \cdot t^3}{12a^2} \quad (2.8)$$

This Euler column buckling load can be compared with the plate buckling load of the plate. The plate buckling force is determined by multiplying the critical stress σ_{cr} , as given in Eq.(2.6), by the dimensions of the plate. This leads to:

$$F_{cr} = b \cdot t \cdot \sigma_{cr} = b \cdot t \cdot k_\sigma \cdot \frac{\pi^2 E}{12(1-\nu^2) \left(\frac{b}{t} \right)^2} = b \cdot t \cdot \left(\frac{b}{a} \right)^2 \cdot \frac{\pi^2 E}{12(1-\nu^2) \left(\frac{b}{t} \right)^2} =$$

$$= \frac{\pi^2 E \cdot b \cdot t^3}{12 \cdot a^2} \cdot \frac{1}{(1-\nu^2)} \quad (2.9)$$

As can be seen, the only difference between Eq.(2.8) and Eq.(2.9) is the positive influence of the Poisson ratio ν . It is possible that more buckles appear in the x -direction. The number of buckles m can be taken into account by changing the plate buckling factor k_σ into $k_\sigma = \left(\frac{mb}{a}\right)^2$. The aspect ratio α is based on the plate dimensions, namely $\alpha = \frac{a}{b}$. In Figure 2-2, the plate buckling factor k_σ is presented versus the aspect ratio α .

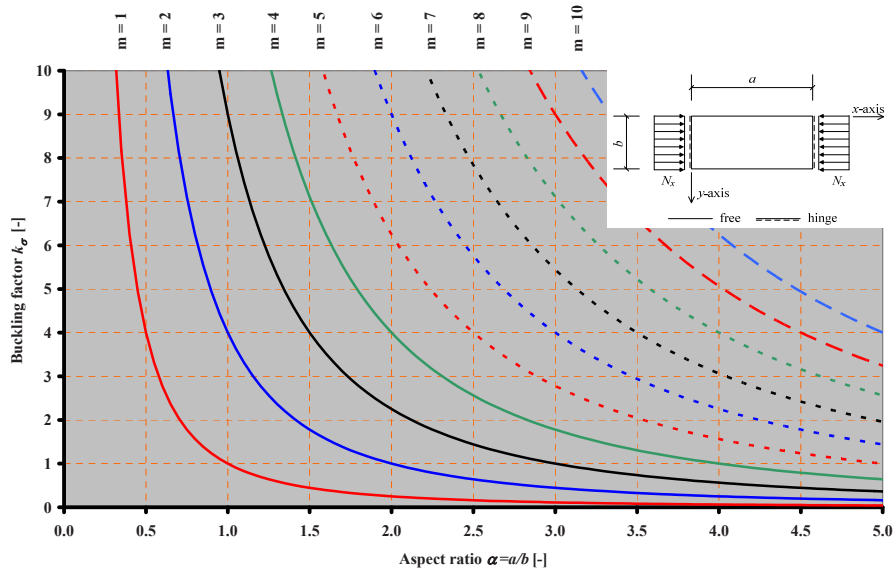


Figure 2-2 Plate buckling factor k_σ for a plate under compression, simply supported at $x=0$ and $x=a$

From this graph, it can be seen that the buckling factor k_σ is the smallest for every aspect ratio α for $m=1$.

The second example concerns a plate under a uniformly distributed load N_x , simply supported at all four edges, as shown in Figure 2-3.

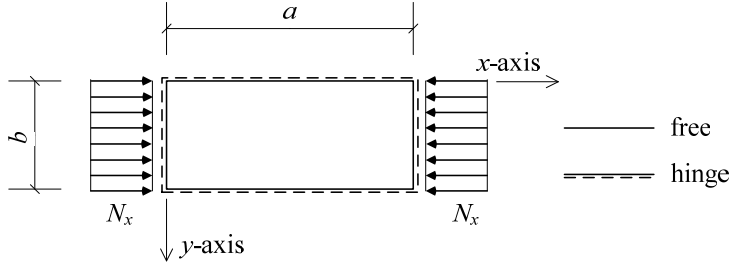


Figure 2-3 A plate under pure compression, simply supported at all four edges

The deflection w can be written as:

$$w = A \cdot \sin\left(\frac{\pi x}{a}\right) \cdot \sin\left(\frac{\pi y}{b}\right) \quad (2.10)$$

The derivatives to x are determined as follows:

$$\begin{aligned} \frac{\partial w}{\partial x} &= A \cdot \left(\frac{\pi}{a}\right) \cdot \cos\left(\frac{\pi x}{a}\right) \cdot \sin\left(\frac{\pi y}{b}\right) & \frac{\partial^2 w}{\partial x^2} &= -A \cdot \left(\frac{\pi}{a}\right)^2 \cdot \sin\left(\frac{\pi x}{a}\right) \cdot \sin\left(\frac{\pi y}{b}\right) \\ \frac{\partial^3 w}{\partial x^3} &= -A \cdot \left(\frac{\pi}{a}\right)^3 \cdot \cos\left(\frac{\pi x}{a}\right) \cdot \sin\left(\frac{\pi y}{b}\right) & \frac{\partial^4 w}{\partial x^4} &= A \cdot \left(\frac{\pi}{a}\right)^4 \cdot \sin\left(\frac{\pi x}{a}\right) \cdot \sin\left(\frac{\pi y}{b}\right) \end{aligned}$$

The derivatives to y are determined as follows:

$$\begin{aligned} \frac{\partial^3 w}{\partial x^2 \partial y} &= -A \cdot \left(\frac{\pi}{a}\right)^2 \cdot \left(\frac{\pi}{b}\right) \cdot \sin\left(\frac{\pi x}{a}\right) \cdot \cos\left(\frac{\pi y}{b}\right) \\ \frac{\partial^4 w}{\partial x^2 \partial y^2} &= A \cdot \left(\frac{\pi}{a}\right)^2 \cdot \left(\frac{\pi}{b}\right)^2 \cdot \sin\left(\frac{\pi x}{a}\right) \cdot \sin\left(\frac{\pi y}{b}\right) \\ \frac{\partial w}{\partial y} &= A \cdot \frac{\pi}{b} \cdot \sin\left(\frac{\pi x}{a}\right) \cdot \cos\left(\frac{\pi y}{b}\right) \\ \frac{\partial^2 w}{\partial y^2} &= -A \cdot \left(\frac{\pi}{b}\right)^2 \cdot \sin\left(\frac{\pi x}{a}\right) \cdot \sin\left(\frac{\pi y}{b}\right) \\ \frac{\partial^3 w}{\partial y^3} &= -A \cdot \left(\frac{\pi}{b}\right)^3 \cdot \sin\left(\frac{\pi x}{a}\right) \cdot \cos\left(\frac{\pi y}{b}\right) \\ \frac{\partial^4 w}{\partial y^4} &= A \cdot \left(\frac{\pi}{b}\right)^4 \cdot \sin\left(\frac{\pi x}{a}\right) \cdot \sin\left(\frac{\pi y}{b}\right) \end{aligned}$$

Substitution of these derivatives into Eq.(2.1) leads to:

$$\begin{aligned}
& A \cdot \left(\frac{\pi}{a}\right)^4 \cdot \sin\left(\frac{\pi x}{a}\right) \cdot \sin\left(\frac{\pi y}{b}\right) + 2A \cdot \left(\frac{\pi}{a}\right)^2 \cdot \left(\frac{\pi}{b}\right)^2 \cdot \sin\left(\frac{\pi x}{a}\right) \cdot \sin\left(\frac{\pi y}{b}\right) + \\
& + A \cdot \left(\frac{\pi}{b}\right)^4 \cdot \sin\left(\frac{\pi x}{a}\right) \cdot \sin\left(\frac{\pi y}{b}\right) = \frac{1}{D} \left[-N_x \cdot A \cdot \left(\frac{\pi}{a}\right)^2 \cdot \sin\left(\frac{\pi x}{a}\right) \cdot \sin\left(\frac{\pi y}{b}\right) \right] \\
\Rightarrow & \cancel{A \cdot \left(\frac{\pi}{a}\right)^4 \cdot \sin\left(\frac{\pi x}{a}\right) \cdot \sin\left(\frac{\pi y}{b}\right)} + 2\cancel{A \cdot \left(\frac{\pi}{a}\right)^2 \cdot \left(\frac{\pi}{b}\right)^2 \cdot \sin\left(\frac{\pi x}{a}\right) \cdot \sin\left(\frac{\pi y}{b}\right)} + \\
& + \cancel{A \cdot \left(\frac{\pi}{b}\right)^4 \cdot \sin\left(\frac{\pi x}{a}\right) \cdot \sin\left(\frac{\pi y}{b}\right)} = -\frac{1}{D} N_x \cdot \cancel{A \cdot \left(\frac{\pi}{a}\right)^2 \cdot \sin\left(\frac{\pi x}{a}\right) \cdot \sin\left(\frac{\pi y}{b}\right)} \\
\Rightarrow & \left(\frac{\pi}{a}\right)^4 + 2 \cdot \left(\frac{\pi}{a}\right)^2 \cdot \left(\frac{\pi}{b}\right)^2 + \left(\frac{\pi}{b}\right)^4 = -\frac{1}{D} N_x \cdot \left(\frac{\pi}{a}\right)^2
\end{aligned}$$

Assuming compression is a positive sign, this results into:

$$\begin{aligned}
N_x = N_{cr} &= D \cdot \frac{\left(\frac{\pi}{a}\right)^4 + 2 \cdot \left(\frac{\pi}{a}\right)^2 \cdot \left(\frac{\pi}{b}\right)^2 + \left(\frac{\pi}{b}\right)^4}{\left(\frac{\pi}{a}\right)^2} = D \cdot \left\{ \left(\frac{\pi}{a}\right)^2 + 2 \cdot \left(\frac{\pi}{b}\right)^2 + \left(\frac{\pi}{b}\right)^4 \left(\frac{a}{\pi}\right)^2 \right\} = \\
&= D \cdot \left\{ \left(\frac{\pi}{a}\right)^2 \cdot \left(\frac{b}{\pi}\right)^2 + 2 + \left(\frac{a}{\pi}\right)^2 \cdot \left(\frac{\pi}{b}\right)^2 \right\} \cdot \left(\frac{\pi}{b}\right)^2 = \\
&= D \cdot \left\{ \left(\frac{b}{a}\right)^2 + 2 + \left(\frac{a}{b}\right)^2 \right\} \cdot \left(\frac{\pi}{b}\right)^2 = k_\sigma \cdot \left(\frac{\pi^2 D}{b^2}\right) \tag{2.11}
\end{aligned}$$

Where the plate buckling factor k_σ is:

$$k_\sigma = \left(\frac{b}{a}\right)^2 + 2 + \left(\frac{a}{b}\right)^2 = \left(\frac{a}{b} + \frac{b}{a}\right)^2 \tag{2.12}$$

The critical stress σ_{cr} is determined with:

$$\sigma_{cr} = \frac{N_{cr}}{t} = k_\sigma \cdot \frac{\pi^2 E}{12(1-\nu^2) \left(\frac{b}{t}\right)^2} \tag{2.13}$$

A more general solution of the deflection function w can be obtained by including the number of buckles m and n , which represent the number of half sine waves in the x -direction and in the y -direction respectively. In the y -direction it is assumed that the plate buckles only in one half sine

wave, so $n = 1$. The number of buckles m can be taken into account by changing equation Eq.(2.12)

for the plate buckling factor k_σ into $k_\sigma = \left(\frac{a}{mb} + \frac{mb}{a} \right)^2$.

Figure 2-4 presents the plate buckling factor k_σ versus the aspect ratio α .

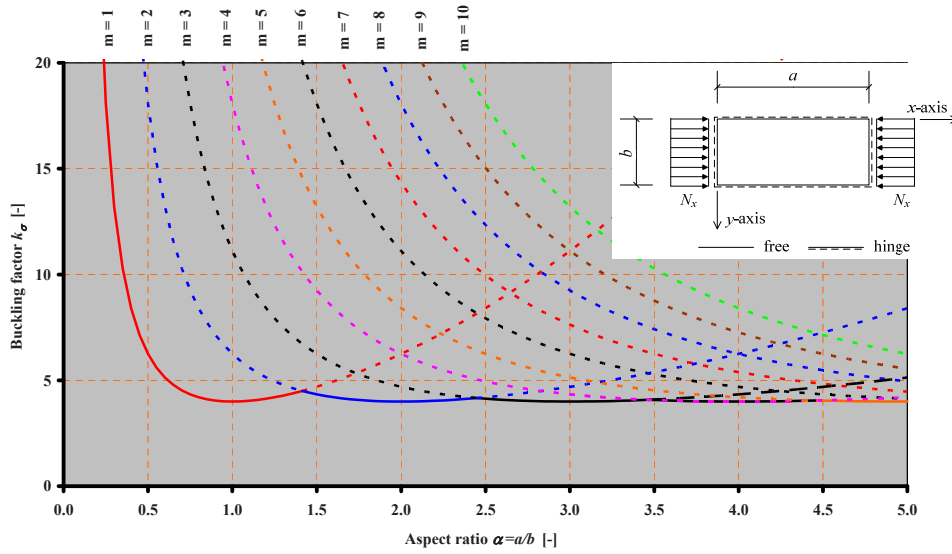


Figure 2-4 Plate buckling factor k_σ for a plate under compression, all four edges simply supported

For a specific aspect ratio α the critical stress σ_{cr} , determined by the minimum value for the plate buckling factor k_σ , is found for different numbers of buckles m in the x -direction. For example, for $\alpha = 1$ the minimum value for k_σ is found for $m = 1$, but for $\alpha = 2$ this minimum is found for $m = 2$. In general, the minimum value for the plate buckling factor k_σ is found for $\alpha = m$, so the minimum plate buckling factor is $k_\alpha = 4$.

For a plate under bending, see Figure 2-5, the same method is used to determine the critical stress.

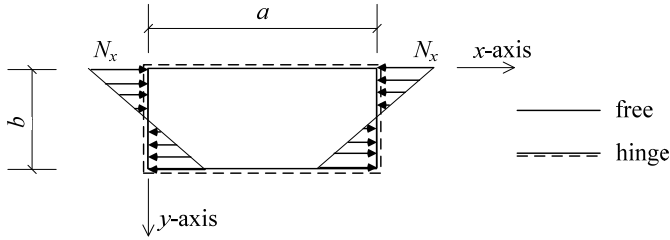


Figure 2-5 A plate simply supported at all four edges, under bending

The critical stress σ_{cr} is:

$$\sigma_{cr} = k_{\sigma} \frac{\pi^2 E}{12(1-\nu^2)} \left(\frac{t}{b} \right)^2 \quad (2.14)$$

The buckling factor k_{σ} is shown in Eq.(2.15):

$$k_{\sigma} = \frac{\pi^2}{\left(\frac{a}{b} \right)^2} \cdot \frac{\left(m^2 + \frac{a^2}{b^2} \right) \cdot \left(m^2 + 4 \frac{a^2}{b^2} \right) \cdot \left(m^2 + 9 \frac{a^2}{b^2} \right)}{\sqrt{\left(m^2 + \frac{a^2}{b^2} \right)^2 \cdot \left(16m^2 \frac{6}{25} \right)^2 + \left(m^2 + 9 \frac{a^2}{b^2} \right) \cdot \left(16m^2 \frac{2}{9} \right)^2}} \quad (2.15)$$

Figure 2-6 shows the buckling factor k_{σ} for certain values of m versus the aspect ratio α .

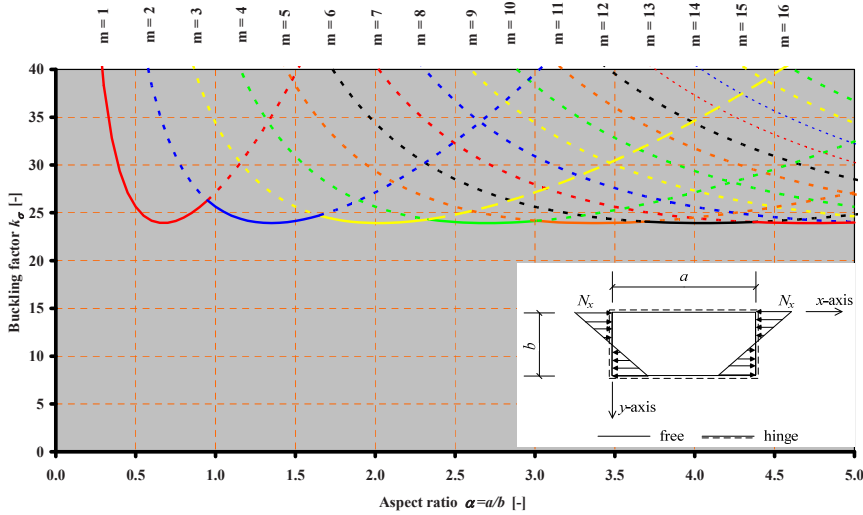


Figure 2-6 Plate buckling factor k_{σ} for a plate simply supported at all edges under pure bending

2.3 EFFECTIVE WIDTH METHOD

2.3.1 DERIVATION OF THE EFFECTIVE WIDTH

The stress is uniformly distributed over the cross-section of the plate up to the critical stress σ_{cr} , see the stress distribution at the left-hand side of Figure 2-7. When the stress level reaches the critical stress σ_{cr} the plate buckles and redistribution of stresses takes place. The distribution of stresses is shown in the middle of Figure 2-7. The stresses close to the edges increase and in the middle of the plate decrease because of the buckling of the plate.

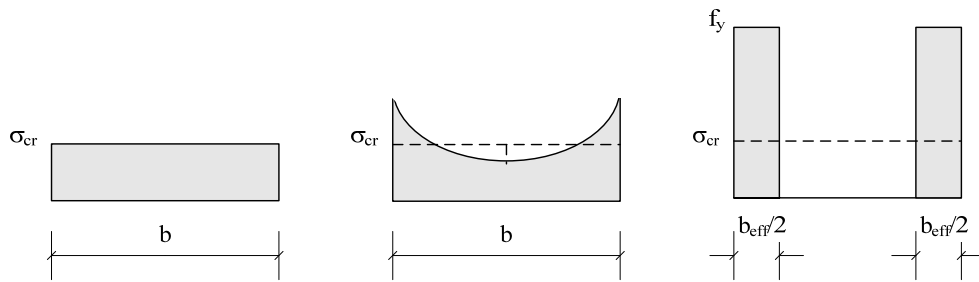


Figure 2-7 Stress distributions just before reaching the critical stress, just at reaching the critical and the effective stress distribution

Von Kármán [46] determined an effective width b_{eff} , see the right-hand side of Figure 2-7, with:

$$\sigma_{cr} \cdot b \cdot t = f_y \cdot b_{eff} \cdot t \quad (2.16)$$

$$\Rightarrow \frac{b_{eff}}{b} = \frac{\sigma_{cr}}{f_y} \quad (2.17)$$

The product of stress and cross-sectional area for all three stress distributions in Figure 2-7 is the same and so the resistance is exactly the same. When the load further increases, this non-linear stress distribution enhances up to the maximum stress, the yield strength f_y , at the edges, see the left-hand side in Figure 2-8.

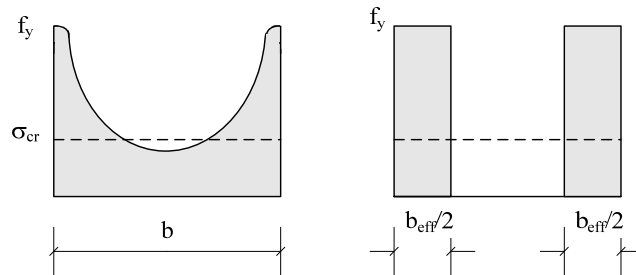


Figure 2-8 Stress distributions beyond the critical stress and the effective stress distribution

The effective width b_{eff} is determined by substitution $\sigma_{cr} = f_y$ in Eq.(2.13), while $b = b_{eff}$. This gives the following relations, see Eq.(2.18) and Eq.(2.19):

$$\sigma_{cr} = k_\sigma \frac{\pi^2 E}{12(1-\nu^2)} \left(\frac{t}{b} \right)^2 \quad (2.18)$$

And:

$$f_y = k_\sigma \frac{\pi^2 E}{12(1-\nu^2)} \left(\frac{t}{b_{eff}} \right)^2 \quad (2.19)$$

The effective width b_{eff} is determined from Eq.(2.18) and Eq.(2.19):

$$\frac{b_{eff}}{b} = \sqrt{\frac{\sigma_{cr}}{f_y}} \quad (2.20)$$

For example, the axial resistance based on the critical stress σ_{cr} for a plate under pure compression is equal to:

$$N_{cr} = \sigma_{cr} \cdot b \cdot t \quad (2.21)$$

The axial resistance based on the effective width b_{eff} for a plate under pure compression is equal to:

$$N_u = f_y \cdot b_{eff} \cdot t \quad (2.22)$$

It can be shown that for slender plates ($\sigma_{cr} \leq f_y$) that $N_u > N_{cr}$ by substitution of Eq.(2.20) for the effective width b_{eff} into Eq.(2.22):

$$N_u = f_y \cdot b_{eff} \cdot t = f_y \cdot b \cdot \sqrt{\frac{\sigma_{cr}}{f_y}} \cdot t = \sqrt{\sigma_{cr} \cdot f_y} \cdot b \cdot t > N_{cr} = \sigma_{cr} \cdot b \cdot t \quad (2.23)$$

This is evident while $\sqrt{\frac{\sigma_{cr}}{f_y}} \geq \frac{\sigma_{cr}}{f_y}$ for $\frac{\sigma_{cr}}{f_y} \leq 1$.

Von Kármán [43, 44] substitutes Eq.(2.18) for the critical stress σ_{cr} into Eq.(2.20) for the effective width $\frac{b_{eff}}{b}$ and so the effective width b_{eff} is related to the thickness t of the plate:

$$\frac{b_{eff}}{b} = \sqrt{\frac{\sigma_{cr}}{f_y}} = \sqrt{\frac{k_\sigma \frac{\pi^2 E}{12(1-\nu^2)} \left(\frac{t}{b}\right)^2}{f_y}}$$

$$\Rightarrow \frac{b_{eff}}{t} = \frac{\pi \sqrt{k_\sigma}}{\sqrt{12(1-\nu^2)}} \sqrt{\frac{E}{f_y}} \quad (2.24)$$

For a constant compressive stress, the buckling factor is $k_\sigma = 4$ and so Eq.(2.24) simplifies to:

$$\frac{b_{eff}}{t} = 1,901 \sqrt{\frac{E}{f_y}} \quad (2.25)$$

Test results did not correspond with this theory. Sechler [69] introduced a factor C instead of this constant value 1.901:

$$\frac{b_{eff}}{t} = C \sqrt{\frac{E}{f_y}} \quad \text{with} \quad C = 1.9 - 1.09 \frac{t}{b} \sqrt{\frac{E}{f_y}}$$

$$\Rightarrow \frac{b_{eff}}{t} = 1.9 \sqrt{\frac{E}{f_y}} \left(1 - 0.574 \frac{t}{b} \sqrt{\frac{E}{f_y}} \right) \quad (2.26)$$

The factor C is related to $\frac{b}{t}$ and the yield stress f_y . The reduction factor 0.574 in Eq.(2.26) was reduced by Winter [76] and [77] to 0.475 and so Eq.(2.26) changes into:

$$\frac{b_{eff}}{t} = 1.9 \sqrt{\frac{E}{f_y}} \left(1 - 0.475 \frac{t}{b} \sqrt{\frac{E}{f_y}} \right) \quad (2.27)$$

This formula can be rewritten, but now into the ratio $\frac{b_{eff}}{b}$ as follows:

$$\frac{b_{eff}}{b} = \underbrace{\frac{1.9}{\frac{t}{b}} \sqrt{E}}_{\sqrt{\sigma_{cr}}} \underbrace{\sqrt{\frac{1}{f_y}}}_{\sqrt{\frac{1}{f_y}}} \left(1 - 0.25 \cdot \underbrace{\frac{1.9}{\frac{t}{b}} \sqrt{E}}_{\sqrt{\sigma_{cr}}} \underbrace{\sqrt{\frac{1}{f_y}}}_{\sqrt{\frac{1}{f_y}}} \right) = \sqrt{\frac{\sigma_{cr}}{f_y}} \left(1 - 0.25 \sqrt{\frac{\sigma_{cr}}{f_y}} \right) \quad (2.28)$$

Later, the factor 0.25 was reduced to 0.22 by Winter to fit better with additional laboratory test results:

$$\frac{b_{eff}}{b} = \sqrt{\frac{\sigma_{cr}}{f_y}} \left(1 - 0.22 \sqrt{\frac{\sigma_{cr}}{f_y}} \right) \quad (2.29)$$

2.4 MAXIMUM WEB SLENDERNESS OF A PLATE GIRDER ACCORDING TO BASLER

2.4.1 GENERAL

The maximum bending moment resistance is strongly influenced by the lever arm in-between both flanges and the area of the flanges. The web should be as slender as possible. According to Basler [10] this web slenderness is limited by vertical buckling of the compressive flange into the web. From 1958 up to 1964, a huge research program on the behaviour of plate girders was carried out at the Lehigh University [6] to [16] and [78] to [80]. The maximum web slenderness is based on the result of one of the test specimens of this program.

In this chapter, the model for vertical buckling of the compressive flange into the web is described. The properties of this specific test specimen are described for use of this information for the validation of the FEM-model to describe the behaviour of plate girders.

2.4.2 LEHIGH TEST SPECIMEN G4

The research program is divided into three parts: welded unstiffened plate girders and welded longitudinally stiffened plate girders under bending, shear and the combinations of bending and shear, and the fatigue strength of welded plate girders. The research on unstiffened plate girders under bending is of interest, test specimens G1 to G5, see Figure 2-9.

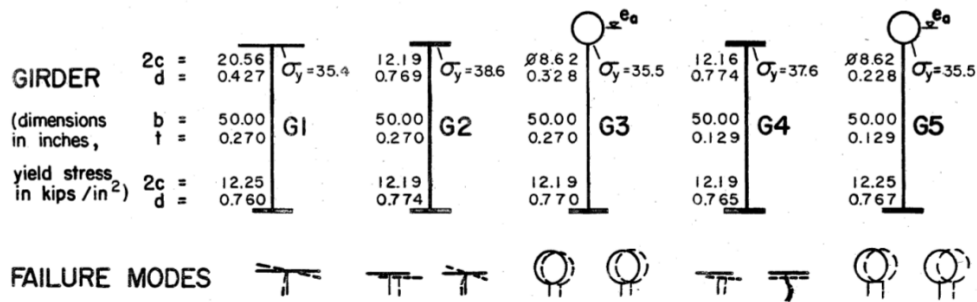


Figure 2-9 Overview by Basler [12] of test specimens G1 to G5 under bending

2.4.2.1 Dimensions of the Basler test girder G4-T1 and G4-T2

These girders were tested to investigate the stability of the web and the compressive flange, and to investigate the bending moment resistance of plate girders with a very slender web. Test specimen G4 was tested twice, indicated by T1 and T2, and in the second test vertical buckling of the com-

pressive flange into the web occurred. As shown in Figure 2-9, the dimensions are given in inches according to the American Standards, the stresses in psi, the forces in kips and the bending moments in k-in. In this thesis these dimensions are presented in the metric system.

Test girder G4 is a double symmetric I-shaped plate girder, built up from plate elements welded together. The span of the girder is 13716 mm, see Figure 2-10. The girder is simply supported at both ends and loaded by two concentrated loads, located at 3810 mm from the supports. Between these two concentrated loads, there is a test area where only bending stresses occur. The test area has a length of 3810 mm, indicated by the shaded area in Figure 2-10. The test area is transversely stiffened at the edges of the three panels of the test area, as indicated by numbers 1, 2 and 3 in Figure 2-10. The length of the test panels 1 and 2 is 952.5 mm and the length of test panel 3 is 1905 mm. There are also transverse stiffeners located at the supports and at the concentrated loads. A transverse stiffener is added between the support and the concentrated load to prevent shear instability.

The compressive flange is laterally supported at the transverse stiffeners. Both end stiffeners and the stiffeners at the concentrated forces are laterally supported at the bottom as well. The actual dimensions of the top flange, the bottom flange and the web are given in Table 2-1.

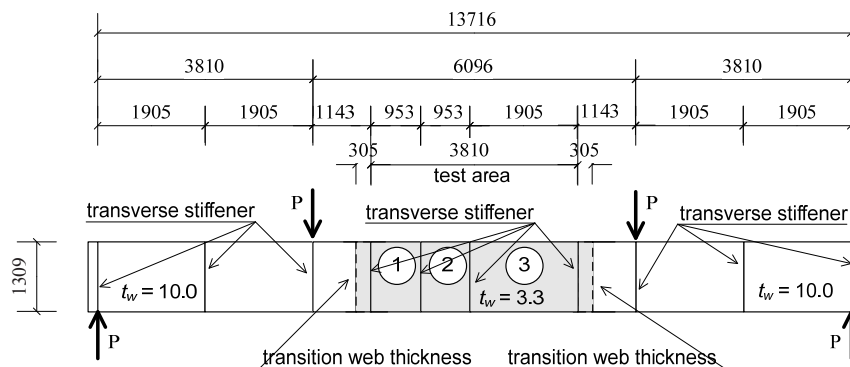


Figure 2-10 Length and depth of the panels of test specimen G4, Basler [12]

Table 2-1 Dimensions of the test girder G4

Element	Width [mm]	Thickness [mm]
Top flange	308.9	19.7
Bottom flange	309.6	19.4
Web test panel	1270.0	3.3
Web	1270.0	10.0

The sum of the throat thickness of both filled welds connecting the web plate to the flanges is equal to the web thickness.

2.4.2.2 Material properties

Tensile tests were conducted to determine the yield strength of the material, unless the elements of the cross-section were from the same steel slab. For test girder G4, four tensile tests were conducted, namely coupon CP22 for the web of the end panels, CP23 and CP23B for the web of the test panels and CP27 for the top flange. The B indicates that the tensile test specimen was taken in addition to the original one. All these test specimens were made in longitudinal direction of the test girder, so in the direction of the stresses due to bending moments.

Although a coupon for the bottom flange was not conducted, the yield stress for this bottom flange is given. It was based on a tensile test on the bottom flange of one of the other test girders. According to Basler [12], this yield strength is 37.0 ksi and this is shown for the bottom flange of test girder G5. 37.0 ksi is equal to 255 MPa.

Stress-strain diagrams were not published, but a force – strain diagram was published, namely for coupon CP27 for the compressive flange of test girder G4, see Figure 2-11. The graph is presented to a maximum strain of 4%.

The graph includes the upper yield point u , the lower yield point l , the dynamic yield point d and the static yield level st . The static yield level st is the yield stress obtained under a zero strain rate. After reaching obvious yielding, the test was stopped and the load settled at the static yield level st . After 5 minutes, the test was continued with the original speed of 2.54 mm per minute. For this coupon CP27, a static stress level was found for a load of 193053 N. The original area A_0 of the coupon was 743 mm² and so the yield stress was $f_y = 259.2$ MPa. The ultimate stress was based on the ultimate load of 326944 N. Based on the original area A_0 of the coupon, the ultimate stress was

$$f_u = \frac{F_u}{A_0} = \frac{326944}{743} = 439.9 \text{ MPa} .$$

The rupture stress was based on the load 250.9 kN. The current

area A was given by Basler [12] as a reduction of 60.9% on the original area $A_0 = 743 \text{ mm}^2$, so the current area of the coupon CP27 is $A = (1.000 - 0.609) \cdot 743 = 290.3 \text{ mm}^2$. The rupture stress is

$$f_r = \frac{F_r}{A} = \frac{250880}{290.3} = 863.9 \text{ MPa} .$$

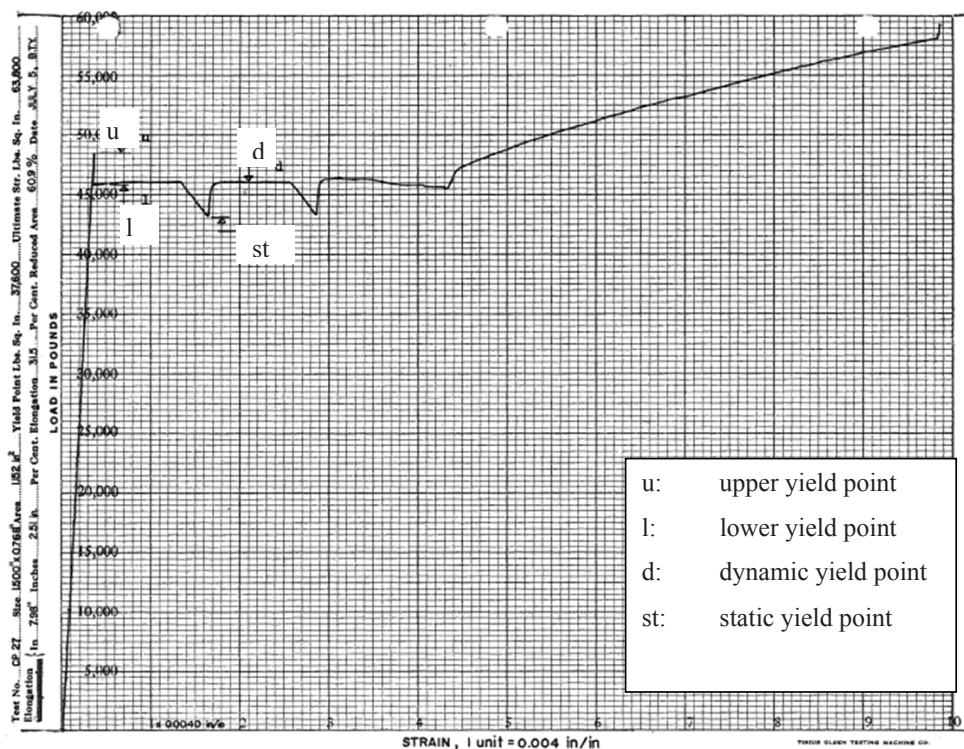


Figure 2-11 Force – Strain curve of coupon CP27, Basler [12]

In Table 2-2, the yield stresses, the ultimate stress and the rupture stress of the flanges and the web in the test panels and the end panels of test specimen G4 are given.

Table 2-2 Yield stresses of the components of test specimen G4

Element	Yield stress [MPa]	Ultimate stress [MPa]	Rupture stress [MPa]
Top flange (CP27)	259	440	864
Bottom flange (CP51)	255	462	728
Web test panel (CP23/CP23B)	(300/298) 299	(419/420) 419	(722/920) 821
Web end panel (CP22)	276	462	728

The remarkable difference in rupture stress of CP23 and CP23B was caused by a big difference between the actual areas.

2.4.2.3 Bending moment resistances

Depending on the actual dimensions and the actual yield stresses of the components, the theoretical geometrical properties of the girder were determined. Basler gives the forces that lead to a specific theoretical bending moment, such as the critical load P_{cr} , the elastic load P_{el} and the plastic load P_{pl} . Also given is a flange load P_f which causes a bending moment resistance of the cross-section consisting of the flanges only.

The critical bending moment M_{cr} is based on the critical stress σ_{cr} of the slender web and the section modulus W_{tf} related to the top flange, the compressive flange.

The elastic bending moment M_{el} depends on the section moduli W_{tf} and W_{bf} , and the accompanying yield stresses of the flanges, $f_{y,tf}$ and $f_{y,bf}$. The yield stress $f_{y,w}$ of the web is larger than the yield stresses of both flanges and therefore this is not relevant in the determination of the elastic bending moment resistance M_{el} . The area of the top flange A_{tf} is larger than the area of the bottom flange A_{bf} and so the neutral axis is positioned closer to the top flange. This means that the stress at the extreme fibre of the bottom flange is higher than the stress at the extreme fibre of the top flange. While the yield stress of the bottom flange $f_{y,bf}$ is smaller than the yield stress of the top flange $f_{y,tf}$, the elastic bending moment resistance is based on the bottom flange $M_{el} = W_{bf} \cdot f_{y,bf}$.

The plastic bending moment resistance M_{pl} is based on the areas and yield stresses of the flanges and web. The location of the plastic neutral axis is determined by equilibrium of the compressive and tensile forces, as a result of the stresses by bending.

Basler also presented a method to determine the theoretical ultimate load P_u , based on an effective width method. This method will be described in 2.5.1.

2.4.2.4 Imperfections

Basler measured the imperfections in the test area at 11 cross-sections, measured from the centre of the girder (midspan) located at -1587.5, -1270, -952.5, -635, -317.5, 0, +317.5, +635, +952.5, +1270 and +1587.5 mm. The vertical positions from the horizontal centre of the web of the girder are -381, 0, +228.6, +381 and 533.4 mm. This means that the imperfections and, during the test, the deflections, are measured at 55 locations of the web, see Figure 2-12.

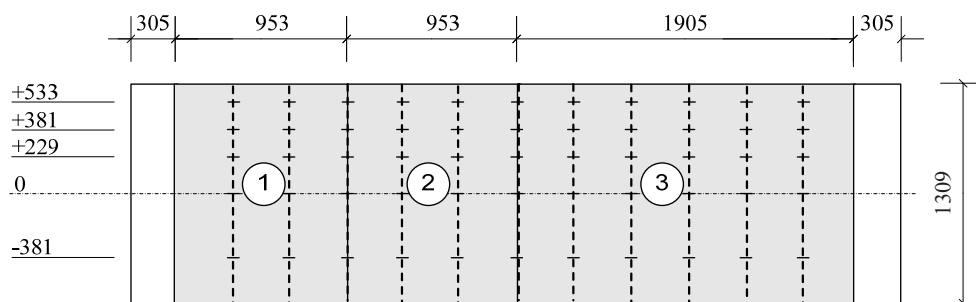


Figure 2-12 Position dial rigs for web deflections and position measurements at test panel

Figure 2-13 shows the web deflections of the test panels of girder G4. The scale is shown at the left-hand side bottom part. The initial imperfections are presented in Table 2-3.

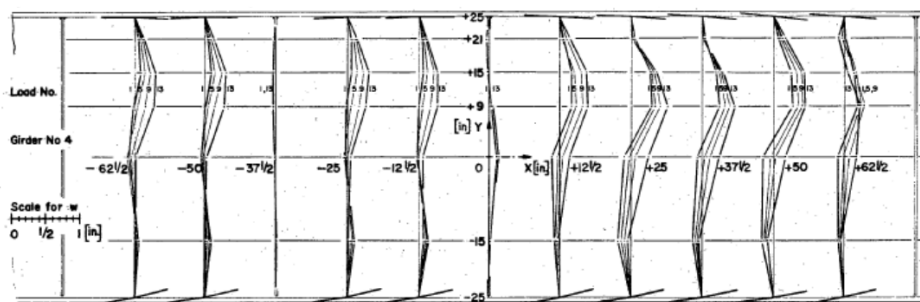


Figure 2-13 Web deflection of girder G4, Basler [10]

Table 2-3 Initial imperfections of test specimen G4

Hor./vert	-1587.5	-1270	-952.5	-635	-317.5	0	+317.5	+635	+952.5	+1270	+1587.5
position	(-62.5")	(-50")	(-37.5")	(-25")	(-12.5")	(0")	(+12.5")	(+25")	(+37.5")	(+50")	(+62.5")
+533	+1.40	+1.21	-0.28	+1.40	+1.58	-0.93	+1.21	+0.28	+0.28	+1.86	-2.79
+381	+2.33	+2.51	-0.93	+1.58	+1.40	-0.28	+4.65	+6.51	+5.12	+6.51	+1.40
+229	-0.70	+0.00	-1.21	-0.56	0.00	+0.93	+4.19	+7.44	+6.51	+6.98	+4.93
0	-2.79	-1.49	-0.28	-0.28	-0.93	+2.79	-3.07	-3.26	-1.86	-4.19	-2.33
-381	+0.47	+0.28	-0.28	+0.47	+1.58	+0.28	-2.14	-5.12	-3.72	-4.19	-1.86

2.4.2.5 Experimental results

The tests on girder G4 were as follows:

- Test specimen G4 was tested twice, namely test T1 and test T2;

- The girder of test T1 collapsed after “pronounced yielding set in”, by lateral buckling of the compressive flange of the test panel 3, column buckling of this flange;
- The buckled part of the compressive flange of panel 3 was reinforced and the second test T2 was started;
- The compressive flange of test panel 1 collapsed by vertical buckling of the compressive flange into the web (flange induced buckling);
- The bending moment resistance of a plate girder is essentially governed by the stability of the compressive flange;
- The web exhibits initial buckling due to bending of the plate girder, which had no significant influence on the bending moment resistance of the plate girder

Table 2-4 shows the loads P based on theoretical resistances, based on actual properties and actual yield stresses and the corresponding bending moments. The load P in the table is one of the loads shown in Figure 2-10. Besides to these theoretical resistances, also the resistance of the experiments is shown.

Table 2-4 Moment capacities of plate girder G4

	Girder G4-T1				Girder G4-T2	
	Elastic	Plastic	Critical	Ultimate	Experiment	Experiment
Load P [kN]	578.3	618.3	68.1	524.9	564.0	556.0
Moment M [kNm]	2203.2	2355.7	259.3	1999.8	2149.0	2118.5

The load as found for the experiment of test T1 is exactly than predicted for lateral buckling of the compressive flange in test panel 3.

The load as found for the experiment of test T2 is 4% higher as predicted. The prediction was based on an effective width method and did not take vertical buckling of the compressive flange into the web into account.

Basler mentioned that the web slenderness $\beta_w = \frac{h_w}{t_w}$ is the most influential of all parameters.

The tests have demonstrated that the initial linear buckling theory on which, up to 1960, all specifications were based, is very conservative and the effective width method respects the reality much better.

2.4.3 MODEL FOR VERTICAL BUCKLING OF THE COMPRESSIVE FLANGE INTO THE WEB

Test G4-T2 failed by vertical buckling of the compressive flange into the web. This failure, described by Basler, occurred "with a tremendous noise and in an explosive manner, the compressive flange pushed into the web of this panel".

Basler mentioned that the tendency is to arrange as much material as possible in the extreme fibres. The web area has to be kept as small as possible, while the lever arm of the internal forces is maximised and with that the bending moment resistance. Vertical buckling of the compressive flange is the only criterion to limit the web slenderness.

Basler described this limitation as follows. Because of the curvature κ of the plate girder in bending, the curved compressive flange alone is not in equilibrium. This also holds for the tension flange. Both flanges are in equilibrium because of the uniformly distributed compressive stress σ_n acting on the web, see Figure 2-14.

Basler ignored the bending stresses in the web and considered the web as a perfect column which will fail at a stress level σ_n , taking into account that the cross-section of this "column" is in fact a plate:

$$\sigma_n \leq \sigma_{cr} = \frac{\pi^2 E}{12 \cdot (1 - \nu^2) \cdot \left(\frac{h_w}{t_w}\right)^2} \quad (2.30)$$

He ignored the bending stresses because he assumed that "the negative influence of the compressive longitudinal stresses is offset by the positive influence of the tensile stresses in longitudinal direction". Basler also assumed that "the influence of the yield penetration into the web at high flange strains is offset by the restraint offered to the thin web by the flange" and so Eq.(2.30) can be considered as an estimate for the resistance of the web against vertical buckling of the flange".

The transverse component F_n of the flange force F_{ff} is dependent on the rate of change of angle φ , see Figure 2-14. This rate of change of angle φ is determined by the curvature κ :

$$\kappa = \frac{d\varphi}{dx} \quad \Rightarrow \quad d\varphi = \kappa \cdot dx \quad (2.31)$$

The flange force F_{ff} is dependent on the compressive flange area A_{ff} and the yield strength $f_{y,ff}$:

$$F_{ff} = A_{ff} \cdot f_{y,ff} \quad (2.32)$$

The curvature κ of the test area is constant because the bending moment is constant, and depends on the strain ε_{ff} in the compressive flange as well:

$$\kappa = \frac{\varepsilon_{yf}}{\frac{h}{2}} \quad (2.33)$$

The transverse component F_n is:

$$F_n = F_{yf} \cdot d\varphi = F_{yf} \cdot \kappa \cdot dx = A_{yf} \cdot f_{y,yf} \cdot \frac{\varepsilon_{yf}}{\frac{h}{2}} \cdot dx \quad (2.34)$$

In this Figure 2-14, Basler used another notation and assumed the girder to be symmetric. In the equations the following notations are used: $b=h$ the height of the plate girder, $A_f = A_{yf}$ the area of the top flange, $\sigma_f = \sigma_{yf}$ stress in the top flange, $\sigma_y = f_{y,yf}$ the yield strength of the top flange and $\varepsilon_f = \varepsilon_{yf}$ the strain in the top flange.

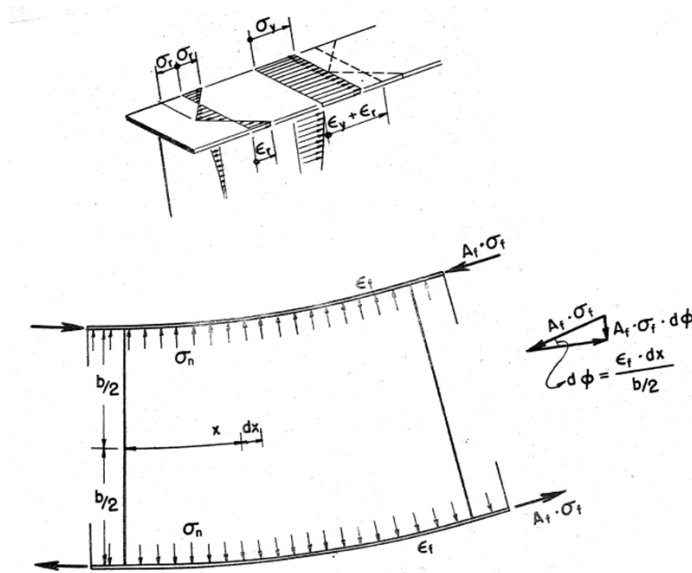


Figure 2-14 Determination of the maximum web slenderness according to Basler [12]

Dividing this transverse component F_n by the thickness of the web t_w and dx for the length, results in the compressive stress σ_n acting transversely on the edges of the web and this stress can not become higher than the critical stress σ_{cr} of the web. At failure of the web $\sigma_n = \sigma_{cr}$. The criterion for the maximum web slenderness $\beta_{w,max}$ was derived by using the simplification for $A_w = h_w \cdot t_w \approx h \cdot t_w$, as follows:

$$\sigma_n = A_{yf} \cdot f_{y,yf} \cdot \frac{2 \cdot \varepsilon_{yf}}{h \cdot t_w} \approx \frac{A_{yf}}{A_w} \cdot 2 f_{y,yf} \cdot \varepsilon_{yf} = \sigma_{cr} = \frac{\pi^2 E}{12 \cdot (1 - \nu^2) \cdot \left(\frac{h_w}{t_w}\right)^2}$$

$$\beta_{w,\max} = \sqrt{\frac{\pi^2 E}{24 \cdot (1 - \nu^2)} \cdot \frac{A_w}{A_{yf}} \cdot \frac{1}{f_{y,yf} \cdot \varepsilon_{yf}}} \quad (2.35)$$

The strain of the flange is assumed to be larger than the yield strain, $\varepsilon_{yf} \geq \varepsilon_{y,yf} = \frac{f_{y,yf}}{E}$, because it is required that the flange fully yields to obtain some deformation capacity to guarantee that the compressive flange will fully yield. To be sure $\varepsilon_{yf} \geq \varepsilon_{y,yf}$, the strain ε_{yf} of the top flange is taken equal to $\varepsilon_{yf} = \frac{f_{y,yf} + \sigma_r}{E}$, where σ_r is the residual stress in the compressive flange.

$$\beta_{w,\max,I} = \sqrt{\frac{\pi^2 E}{24 \cdot (1 - \nu^2)} \cdot \frac{A_w}{A_{yf}} \cdot \frac{1}{f_{y,yf} \cdot \frac{f_{y,yf} + \sigma_r}{E}}} = 0.67 \cdot \sqrt{\frac{A_w}{A_{yf}}} \cdot \sqrt{\frac{E^2}{f_{y,yf} \cdot (f_{y,yf} + \sigma_r)}} \quad (2.36)$$

This is the most general equation for the maximum web slenderness $\beta_{w,\max}$. By assuming minimum values for the ratio of area $\frac{A_w}{A_{yf}}$, but also by assuming a minimum for the residual stress σ_r in the compressive flange, this equation can be simplified.

Basler [12] mentioned that the ratio of area $\rho = \frac{A_w}{A_f}$ shall not be taken smaller than 0.5. Substitution of the ratio of area $\rho = 0.5$ in Eq.(2.36), gives for the maximum web slenderness β_{\max} :

$$\beta_{w,\max,II} = \frac{0.48E}{\sqrt{f_{y,yf} \cdot (f_{y,yf} + \sigma_r)}} \quad (2.37)$$

A second simplification of Eq. (2.36) is found by assuming a residual stress level of $\sigma_r = \frac{f_{y,yf}}{2}$ for mild steel and so the maximum web slenderness $\beta_{w,\max}$ becomes:

$$\beta_{w,\max,III} = \sqrt{\frac{\pi^2}{36 \cdot (1 - \nu^2)}} \cdot \frac{E}{f_{y,yf}} \cdot \sqrt{\frac{A_w}{A_f}} = 0.55 \cdot \frac{E}{f_{y,yf}} \cdot \sqrt{\frac{A_w}{A_f}} \quad (2.38)$$

In EN1993-1-5 [30] this Eq.(2.38) is used. In EN1993-1-5, vertical buckling of the compressive flange into the web is called “flange induced buckling”.

A third simplification of the maximum web slenderness is given by taking into account a ratio of area $\rho = 0.5$ as well as a residual stress level of $\sigma_r = \frac{f_{y,ff}}{2}$. The maximum web slenderness $\beta_{w,max}$ as given in Eq.(2.36), changes into:

$$\beta_{w,max,IV} = \frac{0.40E}{f_{y,ff}} \quad (2.39)$$

In EUR 8849 [34], a draft Eurocode, the equation for the maximum web slenderness $\beta_{w,max}$ is presented as given in Eq.(2.39). For mild steel S235, the maximum web slenderness is 360.

Test specimen G4-T2 failed by vertical buckling of the compressive flange. The actual web slenderness of girder G4 was $\beta_w = \frac{h_w}{t_w} = \frac{1270}{3.3} = 388$ and the actual ratio of area was

$$\rho = \frac{A_w}{A_f} = \frac{h_w \cdot t_w}{b_f \cdot t_{ff}} = \frac{1270 \cdot 3.3}{308.9 \cdot 19.7} = 0.69. \text{ The actual maximum web slenderness } \beta_{w,max} \text{ based on this ratio of area } \rho = \frac{A_w}{A_f} = 0.68 \text{ according to Eq. (2.35) is determined with:}$$

$$\beta_{w,max} = \frac{A_w}{A_f} \cdot \beta_{w,max,IV} = 0.68 \cdot 360 = 244.8$$

$$\beta_{w,max} = 0.55 \cdot \frac{E}{f_{y,ff}} \cdot \sqrt{\frac{A_w}{A_f}} = 0.55 \cdot \frac{206000}{259.2} \cdot 0.68 = 388$$

The web slenderness β_w of test specimen G4-T2 is larger than the maximum web slenderness $\beta_{w,max}$ and so there will be vertical buckling of the flange into the web. The strain was “slightly” higher than the yield strain ε_y .

The actual strengths and areas of test specimen G4-T2 are given in Table 2-5, including the actual web slenderness β_w and the actual maximum web slenderness $\beta_{w,max,III}$ based on Eq.(2.38) and $\beta_{w,max,IV}$ based on Eq.(2.39).

Table 2-5 Maximum web slenderness according to Basler and the actual web slenderness G4-T2

	A_f [mm ²]	$f_{y,ff}$ [N/mm ²]	A_w [mm ²]	$\beta_{w,max,III}$ [-]	$\beta_{w,max,IV}$ [-]	β_w [-]
G4-T2	6072.1	259.2	4161.2	368.3	324.3	387.6

Table 2-5 does not given the maximum web slenderness $\beta_{w,max,I}$ based on Eq.(2.36) and $\beta_{w,max,II}$ based on Eq.(2.37) because these maximum web slenderness's are based on actual residual stresses, but they are not known by Basler.

2.5 BENDING MOMENT RESISTANCE OF PLATE GIRDERS

2.5.1 ACCORDING TO BASLER

Basler [12] concluded that there are four independent parameters that determine the ultimate bending moment resistance for plate girders with a very slender web, namely column buckling slenderness in the lateral direction of the compressive flange between two transverse stiffeners $\frac{\ell}{i}$, the plate slenderness of the compressive flange $\frac{b}{t_{ef}}$, the ratio of area $\rho = \frac{A_w}{A_{ef}}$ and the web slenderness $\beta_w = \frac{h_w}{t_w}$. The first two parameters essentially control lateral (horizontal) and in some cases torsional buckling of the compressive flange, whereas the latter two parameters influence the vertical buckling of the compressive flange into the web.

Basler [12] determined two limits for the web slenderness β_w for S235, namely $\beta_w = 53$ for nowadays so called compact elements of the cross-section, where the plastic bending moment resistance occurs, and $\beta_w = 360$ where the effective width for this web is assumed to be $30t_w$. This effective width is proposed by Von Kármán and was determined for mild steel by using Eq.(2.25) for a plate under a uniformly compressive load, all four edges simply supported, with:

$$\frac{2b_{eff}}{t} = 1.901 \sqrt{\frac{E}{f_y}} \quad \Rightarrow \quad b_{eff} = \frac{1.901}{2} \sqrt{\frac{210000}{235}} \cdot t = 28.4t \quad (2.40)$$

Basler rounded this $b_{eff} = 28.4t$ up to $b_{eff} = 30t$. Between both limits for the web slenderness's $\beta_w = 53$ and $\beta_w = 360$ Basler assumed a linear relationship for the ultimate bending moment resistance M_u and the elastic bending moment resistance M_{el} .

This bending moment resistance predictions can be presented with sufficient accuracy by straight lines in the range of web slenderness $0 < \beta_w < 360$. Basler used the following variables:

$$A_w = h_w \cdot t_w \quad \rho = \frac{A_w}{A_f} \quad \eta_{ef} = \frac{e_{ef}}{h} \quad \eta_{bf} = \frac{e_{bf}}{h} \quad (2.41)$$

Basler assumed that the flange thicknesses t_f for a symmetric girder are infinitely small in relation to the height of the plate girder h and so $h \approx h_w$. The neutral axis is found by assuming a stress distribution as presented in Figure 2-15.

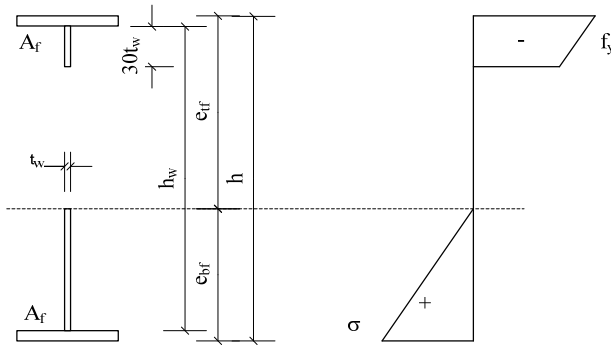


Figure 2-15 Effective cross-section and stress distribution for slenderness 360 according to Basler

The position of the neutral axis is found with:

$$A_f \cdot e_{bf} + t_w \cdot e_{ff} \cdot \frac{e_{ff}}{2} = A_f \cdot (h - e_{ff}) + \frac{h}{12} \cdot t_w \cdot \left(\frac{23}{24} h - e_{bf} \right) \quad (2.42)$$

By substitution of $\eta_{bf} = \frac{e_{bf}}{h}$ and $\rho = \frac{A_f}{A_w}$, this Eq.(2.42) is transformed into:

$$\rho \cdot \left(\frac{23}{288} - \frac{\eta_{bf}}{12} - \frac{\eta_{bf}^2}{2} \right) - (2\eta_{bf} - 1) = 0 \quad (2.43)$$

For a certain ratio of area ρ , this η_{bf} can be solved as follows:

$$\eta_{bf} = \frac{-\left(\frac{\rho}{12} + 2\right) + \sqrt{\frac{1}{6} \cdot (\rho + 2)(\rho + 12)}}{\rho} \quad (2.44)$$

The moment of inertia I_{eff} is found with:

$$I_{eff} = \frac{2}{12} A_f \cdot t_f^2 + \frac{1}{12} t_w \cdot e_{bf}^3 + \frac{1}{12} t_w \cdot \left(\frac{h}{12} \right)^3 + A_f \cdot \left\{ e_{bf}^2 + (h - e_{bf})^2 \right\} + e_{bf} \cdot t_w \cdot \left(\frac{e_{bf}}{2} \right)^2 \quad (2.45)$$

Basler used only the underlined parts of Eq.(2.45):

$$I_{eff} = \frac{1}{12} t_w \cdot e_{bf}^3 + A_f \cdot \left\{ e_{bf}^2 + (h - e_{bf})^2 \right\} + e_{bf} \cdot t_w \cdot \left(\frac{e_{bf}}{2} \right)^2 \quad (2.46)$$

The effective section modulus W_{eff} for the top flange is:

$$W_{eff, yf} = \frac{I_{eff}}{e_{yf}} = \frac{\frac{1}{12} t_w \cdot e_{bf}^3 + A_f \cdot \left\{ e_{bf}^2 + (h - e_{bf})^2 \right\} + e_{bf} \cdot t_w \cdot \left(\frac{e_{bf}}{2} \right)^2}{h - e_{bf}} \quad (2.47)$$

This is rewritten into:

$$W_{eff} = \frac{I_{eff}}{e_{yf}} = \frac{A_f \cdot h}{1 - \eta_{bf}} \cdot \left[\eta_{bf}^2 + \frac{\rho}{3} \cdot \eta_{bf}^3 + (1 - \eta_{bf})^2 + \frac{\rho}{12} \left(\frac{23}{24} - \eta_{bf} \right)^2 \right] \quad (2.48)$$

For a web slenderness $\beta_w = 360$ the ratio $\frac{M_u}{M_{el}}$ of the ultimate bending moment resistance M_u and the elastic bending moment resistance M_{el} is equal to:

$$\frac{M_u}{M_{el}} = \frac{W_{eff} \cdot f_y}{A_f \cdot h \cdot \left(1 + \frac{\rho}{6} \right) \cdot f_y} = \frac{\eta_{bf}^2 + \frac{\rho}{3} \cdot \eta_{bf}^3 + (1 - \eta_{bf})^2 + \frac{\rho}{3} \cdot \left(\frac{23}{24} - \eta_{bf} \right)^2}{(1 - \eta_{bf}) \left(1 + \frac{\rho}{6} \right)} \quad (2.49)$$

Here, the elastic bending moment resistance M_{el} is determined by Basler with:

$$M_{el} = A_f \cdot (h - t_f) \cdot f_y + \frac{1}{6} \cdot t_w \cdot h_w^2 \cdot f_y \quad (2.50)$$

This is a rather rough determination for M_{el} and further simplification, assuming $h - t_f \approx h$, $h_w \approx h$ and $A_w = h_w \cdot t_w \approx h \cdot t_w$, leads to:

$$M_{el} = A_f \cdot (h - t_f) \cdot f_y + \frac{1}{6} \cdot t_w \cdot h_w^2 \cdot f_y \approx A_f \cdot h \cdot f_y + \frac{1}{6} \cdot A_w \cdot h \cdot f_y = A_f \cdot h \cdot \left(1 + \frac{\rho}{6} \right) \cdot f_y \quad (2.51)$$

For a compact web, Basler assumed, according to Haayer and Thürlimann [40], plastic behaviour for a web slenderness of $\beta_w = 53$. Such a relationship for the ratio $\frac{M_u}{M_{el}}$ is:

$$\frac{M_u}{M_{el}} = \frac{M_{pl}}{M_{el}} = \frac{A_f \cdot h \cdot \left(1 + \frac{\rho}{4} \right) \cdot f_y}{A_f \cdot h \cdot \left(1 + \frac{\rho}{6} \right) \cdot f_y} = \frac{\left(1 + \frac{\rho}{4} \right)}{\left(1 + \frac{\rho}{6} \right)} \quad (2.52)$$

Here, M_{pl} is determined in a similar way as shown for M_{el} in Eq.(2.51).

For a certain steel grade and specific values of the ratio of area $\rho = \frac{A_w}{A_f}$, the position of the neutral axis η_{bf} is determined with Eq. (2.44). The ratio $\frac{M_u}{M_{el}}$ based on Eq.(2.52) for a web slenderness's of $\beta_w = 53$ can be determined and the ratio $\frac{M_u}{M_{el}}$ based on Eq.(2.49) for a web slenderness of $\beta_w = 360$, can be determined too, by using the determined η_{bf} . In Table 2-6, this is represented for steel grade S235.

Table 2-6 Ultimate bending moment resistance according to Eq.(2.49) and Eq.(2.52)

$\rho = \frac{A_w}{A_f}$	$\beta_w = 53$ $\frac{M_u}{M_{el}}$ Eq.(2.52)	η_{bf} Eq.(2.44)	$\beta_w = 360$ $\frac{M_u}{M_{el}}$ Eq.(2.49)
0.0	1.000	0.500	1.000
0.5	1.038	0.481	0.940
1.0	1.071	0.466	0.893
1.5	1.100	0.454	0.854
2.0	1.125	0.444	0.821
3.0	1.167	0.429	0.769
4.0	1.200	0.417	0.728
5.0	1.227	0.407	0.696

The values as represented in Table 2-6 are also represented in a graph, see Figure 2-16.

This graph is simplified by the following equation:

$$\frac{M_u}{M_{el}} = 1 - C(\beta - \beta_0) \quad (2.53)$$

with:

$$C = \frac{1}{300 + 1200 \frac{A_f}{A_w}} \quad (2.54)$$

C is an approximation for the slope of the determined lines as represented in Figure 2-16. Basler [12]

stated $\frac{A_w}{A_f} < 2$ and a second simplification is used for the equation for C:

$$C = 0.0005 \frac{A_w}{A_f} \quad (2.55)$$

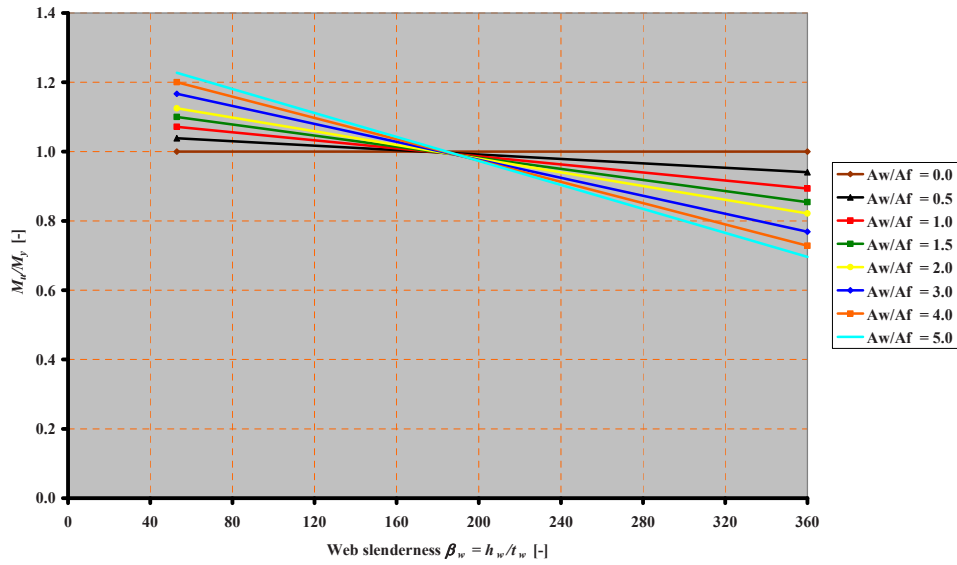


Figure 2-16 Reduction factor M_u / M_{el} depending on the web slenderness according to Basler [12]

The slenderness β_0 in Eq.(2.53) is determined by the intersection abscissa of these graphs with

$\frac{M_u}{M_{el}} = 1$. β_0 is the web slenderness that permits yielding in bending without buckling of the web,

depending on the plate buckling factor k_σ . When there is no rotation stiffness for the connection between flange and web, there will be no flange restraint, so there is a hinge, and the plate buckling

factor $k_\sigma = 23.9$. For full flange restraint, a clamp, the plate buckling factor $k_\sigma = 39.6$. Therefore,

based on the critical stress σ_{cr} , this specific slenderness β_0 can be found with:

$$\sigma_{cr} = k_\sigma \frac{\pi^2 E}{12(1-\nu^2) \left(\frac{h_w}{t_w} \right)^2} = f_y \quad (2.56)$$

$$k_\sigma = 23.9 \Rightarrow \beta_0 = 4.65 \sqrt{\frac{E}{f_y}} \quad (2.57)$$

$$k_\sigma = 39.6 \Rightarrow \beta_0 = 5.98 \sqrt{\frac{E}{f_y}} \quad (2.58)$$

Basler suggested an intermediate value for the restraint and suggested:

$$\beta_0 = 5.7 \sqrt{\frac{E}{f_y}} \quad (2.59)$$

The ratio of the ultimate bending moment resistance and the elastic bending moment resistance, as given in Eq.(2.53), changes into:

$$\frac{M_u}{M_{el}} = 1 - 0.0005 \cdot \frac{A_w}{A_f} \left(\frac{h}{t} - 5.7 \sqrt{\frac{E}{f_y}} \right) \quad (2.60)$$

Eq.(2.60) is represented in graphs for steel grade S235 and S355 in respectively Figure 2-17 and Figure 2-18. For S235 $\beta_0 = 5.7 \sqrt{\frac{210000}{235}} = 170$ and for S355 $\beta_0 = 5.7 \sqrt{\frac{210000}{355}} = 139$. To check Basler's statement that the reduction factor C , as given in Eq.(2.55), fits very well with factor C as given in Eq.(2.54), the effects of these reduction factors C on the reduction factor $\frac{M_u}{M_{el}}$ as given in Eq.(2.53), are represented in Figure 2-19 for S235 and in Figure 2-20 for S355. The web slenderness in these two graphs is according to the determination of the maximum web slenderness $\beta_{w,max,III}$ according to Eq.(2.38).

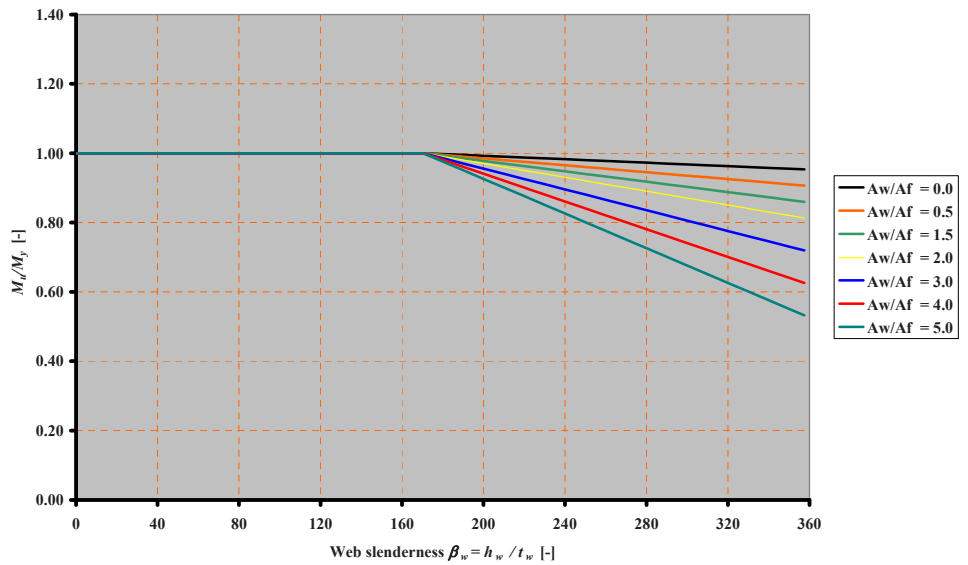


Figure 2-17 Reduction factor M_u / M_{el} according to Basler Eq.(2.60) for S235

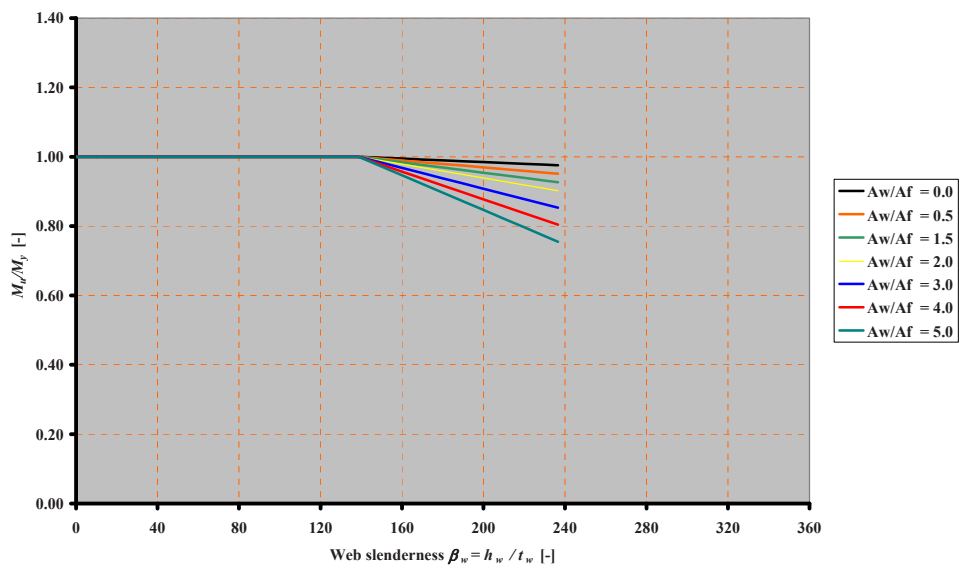


Figure 2-18 Reduction factor M_u / M_{el} according to Basler Eq.(2.60) for S355

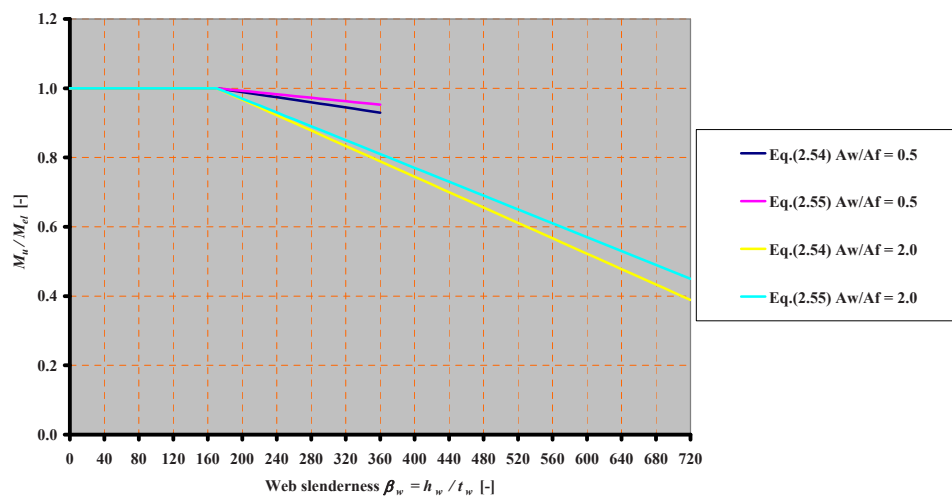


Figure 2-19 Influence of the factor C as given by Eq.(2.54) and as given by Eq.(2.55) on M_u / M_{el} as given by Eq.(2.53), S235

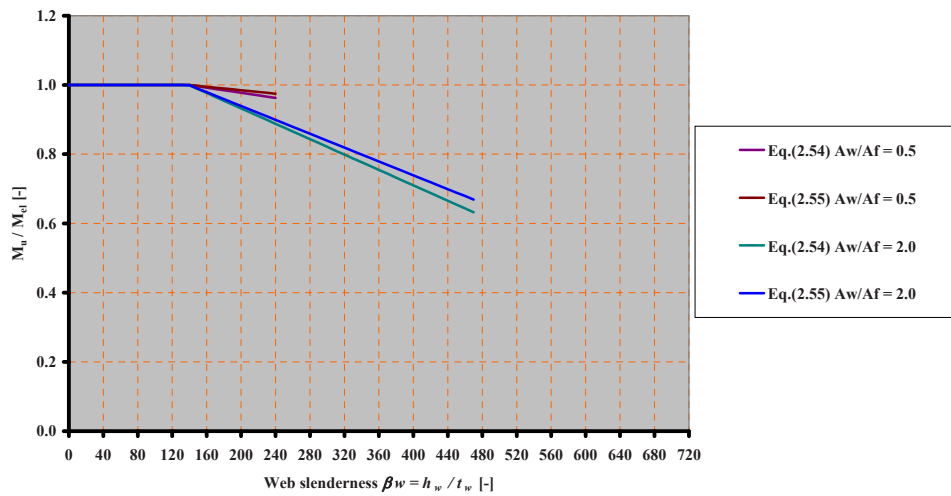


Figure 2-20 Influence of the factor C as given by Eq.(2.54) and as given by Eq.(2.55) on M_u / M_{el} as given by Eq.(2.53), S355

In both graphs, the maximum web slenderness $\beta_{w,max}$ is related to the ratio of area $\rho = \frac{A_w}{A_f}$ used. It

is shown that Basler's statement fits for small web slenderness's β_w , but especially for the ratio of

area $\rho = \frac{A_w}{A_f} = 2$, the difference increases for higher web slenderness's β_w .

2.5.2 ACCORDING TO HÖGLUND

Höglund [42] determined effective widths of $b_{e1} = 0.76 \cdot t_w \cdot \sqrt{\frac{E}{f_y}}$ and $b_{e2} = 1.64 \cdot t_w \cdot \sqrt{\frac{E}{f_y}}$, see Figure 2-21.

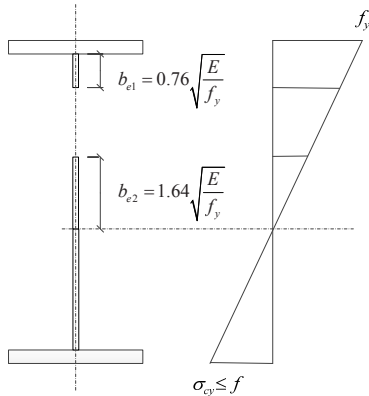


Figure 2-21 Effective cross-section and stress distribution

The effective section modulus W_{eff} is derived and in his paper related to the elastic section modulus W_{el} and thus comparable to the Basler's formula Eq.(2.60):

$$\frac{M_u}{M_{el}} = \frac{W_{eff} \cdot f_y}{W_{el} \cdot f_y} = 1 - 0.15 \cdot \frac{A_w}{A_f} \cdot \left(1 - 4.8 \cdot \frac{t_w}{h_w} \cdot \sqrt{\frac{E}{f_y}} \right) \quad (2.61)$$

$$\text{for } \beta_w = \frac{h_w}{t_w} \geq 4.8 \cdot \sqrt{\frac{E}{f_y}}$$

This limitation leads to a slenderness of $\beta_w = 144$ for S235 and $\beta_w = 117$ for S355.

The reduction in the second part of the Basler formula, see Eq.(2.60), is linear, while the reduction in the second part of the Höglund formula according to Eq.(2.61), is hyperbolic, based on the reciprocal of the web slenderness, $\frac{1}{\beta_w} = \frac{t_w}{h_w}$.

The Höglund formula according to Eq.(2.61), is presented in Figure 2-22 for S235 and in Figure 2-23 for S355.

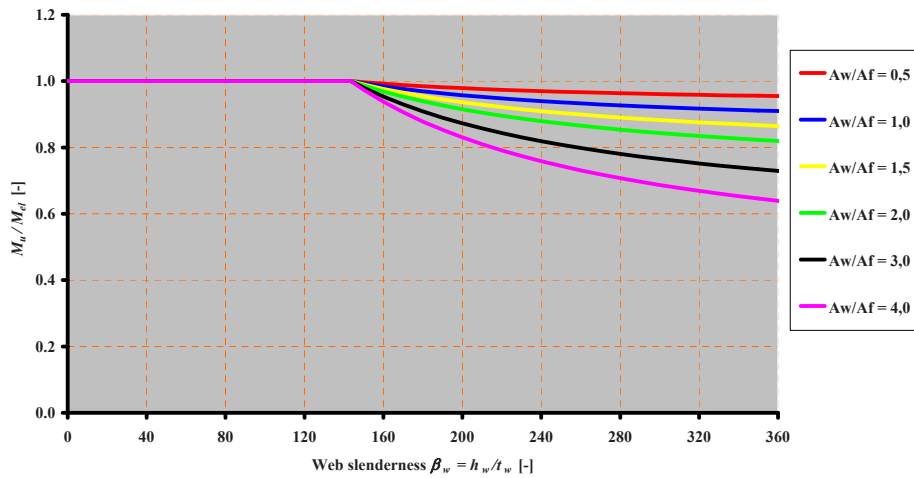


Figure 2-22 Reduction factor M_u / M_{el} according to Höglund Eq.(2.61) for S235

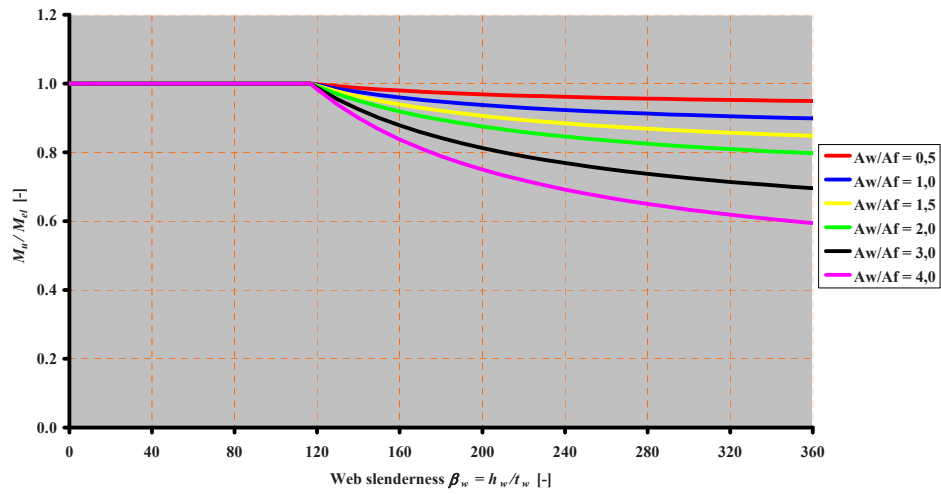


Figure 2-23 Reduction factor M_u / M_{el} according to Höglund Eq.(2.61) for S355

2.5.3 ACCORDING TO HERZOG

Herzog [41] published a different method to determine the ultimate bending moment resistance and took into account the influences of torsional buckling, lateral (horizontal) buckling and vertical buckling of the compressive flange into the web. Herzog [41] took the non-linear behaviour of the web into account by reduction of the maximum stress in the compressive part of the web to half of the yield strength $\frac{f_{y,w}}{2}$, see Figure 2-24.

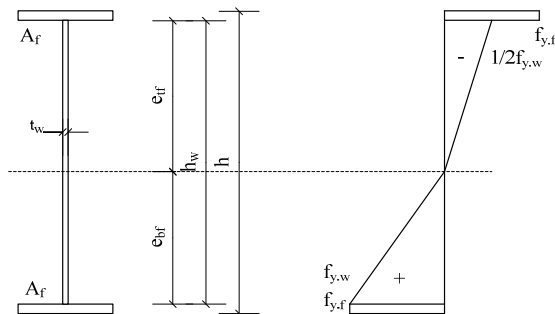


Figure 2-24 Stress distribution according to Herzog

Assuming the yield stress in the top flange is equal to the yield stress of the bottom flange, so $f_{y,tf} = f_{y,bf} = f_{y,f}$, and also the gross areas of these flanges are equal to each other, $A_{tf} = A_{bf} = A_f$, the height e_{tf} of the compressive part of the web can be determined from equilibrium by:

$$\begin{aligned}
\frac{1}{2} \cdot e_{yf} \cdot t_w \cdot \frac{1}{2} \cdot f_{y:w} &= \frac{1}{2} \cdot h_{bf} \cdot t_w \cdot f_{y:w} & \text{and} & \quad e_{bf} = h_w - e_{yf} \\
\Rightarrow e_{yf} \cdot \frac{1}{2} &= (h_w - e_{yf}) \\
\Rightarrow e_{yf} &= \frac{2}{3} \cdot h_w
\end{aligned} \tag{2.62}$$

The bending moment according to this stress distribution, the so called unmodified bending moment resistance M_{Uo}^o , is determined by:

$$\begin{aligned}
M_{Uo}^o &= A_f \cdot f_{y,f} \cdot \left(e_{yf} + \frac{t_f}{2} \right) + A_f \cdot f_{y,f} \cdot \left(e_{bf} + \frac{t_f}{2} \right) + \frac{1}{2} \cdot e_{yf} \cdot t_w \cdot \frac{f_{y:w}}{2} \cdot \frac{2}{3} \cdot e_{yf} + \frac{1}{2} \cdot e_{bf} \cdot t_w \cdot f_{y:w} \cdot \frac{2}{3} \cdot e_{bf} = \\
&= A_f \cdot f_{y,f} \cdot \left(e_{yf} + \frac{t_f}{2} \right) + A_f \cdot f_{y,f} \cdot \left(e_{bf} + \frac{t_f}{2} \right) + \frac{1}{6} \cdot t_w \cdot e_{yf}^2 \cdot f_{y:w} + \frac{1}{3} \cdot t_w \cdot e_{bf}^2 \cdot f_{y:w} = \\
&= A_f \cdot f_{y,f} \cdot (h_w + t_f) + \frac{1}{9} \cdot A_w \cdot f_{y:w} \cdot h_w
\end{aligned} \tag{2.63}$$

To take the influence of torsional buckling of the compressive flange into account, this unmodified bending moment resistance M_{Uo}^o has to be multiplied by the factor K_1 :

$$K_1 = \sqrt{\frac{16 \cdot t_f}{b}} < 1.0 \tag{2.64}$$

This means that for flange slenderness's $\frac{b}{t_f} \leq 16$ Herzog did not reduce the unmodified bending moment resistance for torsional buckling.

To take the horizontal buckling into account, the unmodified ultimate bending moment M_{Uo}^o has to be multiplied by the factor K_2 :

$$K_2 = \sqrt{1 - \left(\frac{\lambda_y}{70} \right)^2} < 1.0 \tag{2.65}$$

For this study, the horizontal buckling will not occur because of the horizontal supports.

To take into account the vertical buckling of the compressive flange into the web, the unmodified bending moment resistance M_{Uo}^o has to be multiplied by the factor K_3 :

$$K_3 = 1.17 - \frac{d'}{2000 \cdot t_w} \tag{2.66}$$

Because of the absence of a longitudinal stiffener $d' = h_w$, Eq.(2.66) changes into:

$$K_3 = 1.17 - \frac{h_w}{2000 \cdot t_w} = 1.17 - \frac{\beta_w}{2000} \quad (2.67)$$

For a web slenderness $\beta_w \leq 340$ the factor $K_3 = 1.0$ and so vertical buckling of the compressive flange into the web has not been taken into account. This is more or less according to Eq.(2.39) for $\beta_{w,max,III}$ according to Basler.

The ultimate bending moment resistance M_u according to Herzog is not directly related to the web slenderness β_w and so it is not presented in graphs, like it is for the models of Basler and Höglund.

2.5.4 ACCORDING TO STARK

Stark [70] developed a method to design an optimal plate girder based on the effective width method too, based on a draft Eurocode 3 [34] and on the previous Dutch code NEN6771. The formula to determine the effective width as given in this draft Eurocode 3 is strongly related to the Winter formula [76], but at that time, 1988, adapted to:

$$\frac{b_e}{b} = \sqrt{\frac{\sigma_{cr}}{f_y}} \cdot \left(1 - 0.20 \cdot \sqrt{\frac{\sigma_{cr}}{f_y}} \right) \quad (2.68)$$

The value of 0.22 in the Winter formula is herein adapted to 0.20, which means that the effective width b_e is a little bit larger than based on the Winter formula. The distribution of this effective width b_e over the compressive part of the web was not given in this draft Eurocode 3. The effective width b_{el} , see Figure 2-21, at the top of the web of a plate girder is defined to be half of the effective width based on pure compression. The critical stress σ_{cr} is determined with a buckling factor $k = 4$:

$$\sqrt{\frac{\sigma_{cr}}{f_y}} = \sqrt{k \cdot \frac{\pi^2 \cdot \frac{E}{f_y}}{12 \cdot (1-\nu^2) \cdot \left(\frac{b}{t}\right)^2}} = \sqrt{4.0 \cdot \frac{\pi^2 \cdot \frac{E}{f_y}}{12 \cdot (1-\nu^2) \cdot \left(\frac{b}{t}\right)^2}} = 1.90 \cdot \frac{\sqrt{\frac{E}{f_y}}}{\frac{b}{t}} \quad (2.69)$$

Substitution of Eq.(2.69) into Eq.(2.68) results by taking into account the defined factor $\frac{1}{2}$ into:

$$\Rightarrow b_{el} = 0.95 \cdot t \cdot \sqrt{\frac{E}{f_y}} \cdot \left(1 - 0.38 \cdot \frac{\sqrt{\frac{E}{f_y}}}{\frac{b}{t}} \right) \quad (2.70)$$

The total effective width b_{eff} of the web of a plate girder under pure bending is determined based on a critical stress σ_{cr} with a buckling factor $k_\sigma = 23.9$. This leads to:

$$\sqrt{\frac{\sigma_{cr}}{f_y}} = \sqrt{k_\sigma \cdot \frac{\pi^2 \cdot \frac{E}{f_y}}{12 \cdot (1-\nu^2) \cdot \left(\frac{b}{t}\right)^2}} = \sqrt{23.9 \cdot \frac{\pi^2 \cdot \frac{E}{f_y}}{12 \cdot (1-\nu^2) \cdot \left(\frac{b}{t}\right)^2}} = 4.65 \cdot \frac{\sqrt{\frac{E}{f_y}}}{\frac{b}{t}} \quad (2.71)$$

Substitution of Eq.(2.71) into Eq.(2.68) leads to:

$$b_{eff} = 4.65 \cdot t \cdot \sqrt{\frac{E}{f_y}} \cdot \left(1 - 0.93 \cdot \frac{\sqrt{\frac{E}{f_y}}}{\frac{b}{t}} \right) \quad (2.72)$$

The effective part from the bottom part of the web is determined with $b_{e2} = b_{eff} - b_{e1}$:

$$b_{e2} = 3.69 \cdot t \cdot \sqrt{\frac{E}{f_y}} \cdot \left(1 - 1.07 \cdot \frac{\sqrt{\frac{E}{f_y}}}{\frac{b}{t}} \right) \quad (2.73)$$

Stark suggested to use a simplified effective width model, see Figure 2-25, with:

$$b_{e1} = 0.85 \cdot t_w \cdot \sqrt{\frac{E}{f_y}} \quad (2.74)$$

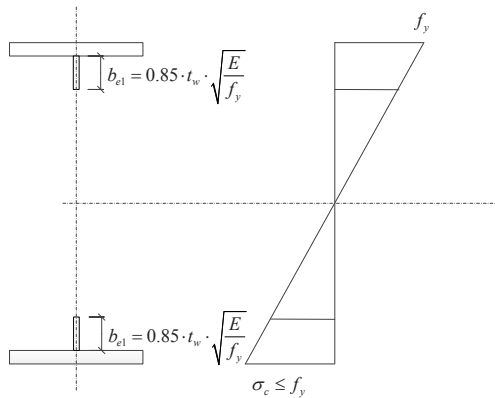


Figure 2-25 Simplified effective width model and stress distribution according to Stark [70]

2.5.5 ACCORDING TO VELJKOVIC AND JOHANSSON

Veljkovic and Johansson [74] refer to Höglund and adjusted Eq.(2.61) and presented the ultimate bending moment resistance M_{Rk} for a hybrid I-girder with equal flanges as follows:

$$M_{Rk} = f_{y,f} \cdot (W_{eff} - \Delta W) \quad (2.75)$$

with:

$$f_{y,f} \quad \text{yield stress of the flange}$$

$$W_{eff} = W \left[1 - 0.1 \frac{A_w}{A_f} \left(1 - 124 \varepsilon \cdot \frac{t_w}{h_w} \right) \right] \quad \text{when } \beta_w = \frac{h_w}{t_w} > 124 \varepsilon$$

$$\varepsilon = \sqrt{\frac{235}{f_{y,f}}}$$

$$\Delta W = \frac{h_w \cdot A_w}{12} \cdot \left(1 - \frac{f_{y,w}}{f_{y,f}} \right)^2 \cdot \left(2 + \frac{f_{y,w}}{f_{y,f}} \right)$$

M_{Rk} is the bending moment resistance without partial safety factor. To enable comparison of this ultimate bending moment resistance to the other mentioned researchers, it is assumed that the material factor is equal to 1.

The factor for ΔW is 0 for $f_{y,w} = f_{y,f}$. Eq.(2.75) is rewritten into the following equation:

$$M_{Rk} = W \cdot f_{y,f} \left[1 - 0.1 \frac{A_w}{A_f} \left(1 - 124 \varepsilon \cdot \frac{t_w}{h_w} \right) \right] \quad (2.76)$$

The effective section modulus W_{eff} divided by the section modulus W corresponds with the reduction factor $\frac{M_u}{M_{el}}$ as given by other authors.

$$\frac{M_u}{M_{el}} = \frac{M_{Rk}}{W \cdot f_{y,f}} = \left[1 - 0.1 \frac{A_w}{A_f} \left(1 - 124 \varepsilon \cdot \frac{t_w}{h_w} \right) \right] \quad (2.77)$$

This reduction factor can be presented in a graph, like Basler did, see Figure 2-26 for S235 and Figure 2-27 for S355. The effective width is based on EN1993-1-5 [30], see Chapter 2.6.1.

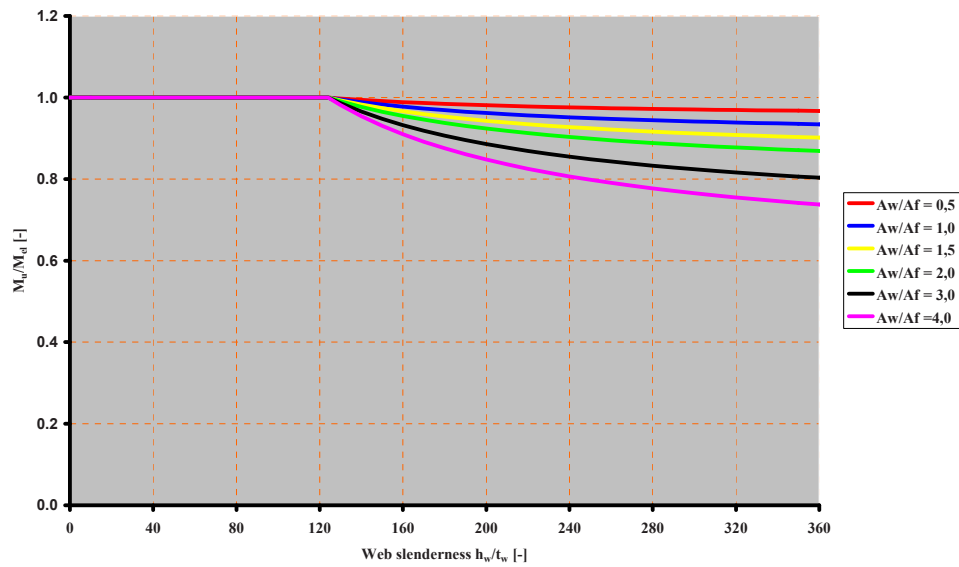


Figure 2-26 Reduction factor M_u / M_{el} according to Veljkovic Eq.(2.75) for S235

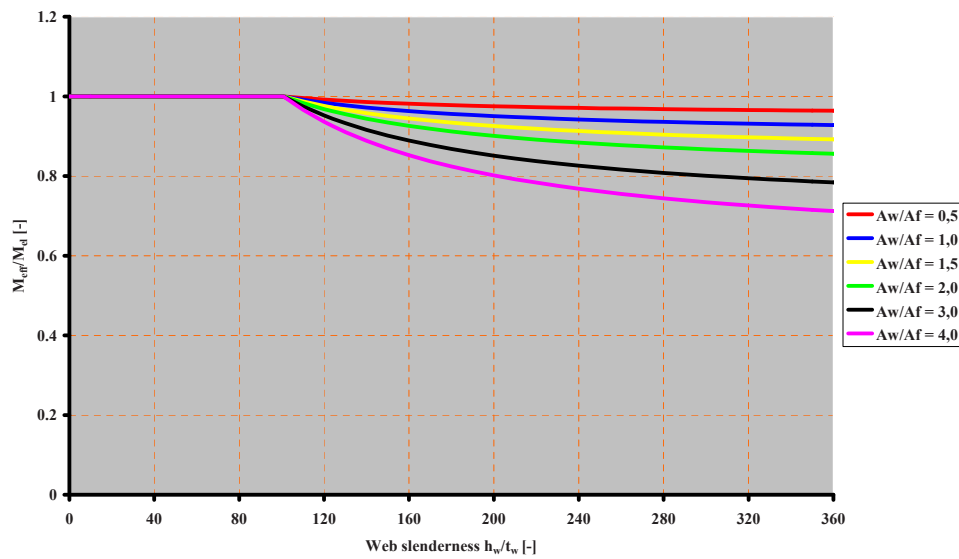


Figure 2-27 Reduction factor M_u / M_{el} according to Veljkovic Eq.(2.75) for S355

2.6 REQUIREMENTS IN INTERNATIONAL CODES

2.6.1 EN1993-1-5

Eurocode 3 [30], EN1993-1-5, gives two applications for effective width, namely related to shear lag, which is not of interest in this thesis, and related to plate buckling. In this Eurocode, the effec-

tive width method is recommended and the reduced stress method is available. Internal and outstand compression elements are considered. The effective width b_{eff} is dependent on the relative plate slenderness $\bar{\lambda}_p$. For internal elements the following equations are available:

$$A_{c,eff} = \rho \cdot A_c$$

Here, A_c is the area under compression and $A_{c,eff}$ the effective area under compression. The reduction factor ρ depends on the relative plate slenderness $\bar{\lambda}_p$ and is determined by:

$$\rho = \frac{\bar{\lambda}_p - 0.055(3 + \psi)}{\bar{\lambda}_p^2} \quad \bar{\lambda}_p > 0.673 \text{ and } (3 + \psi) \geq 0 \quad (2.78)$$

$$\bar{\lambda}_p = \sqrt{\frac{f_y}{\sigma_{cr}}} = \frac{\bar{b}}{28.4\epsilon\sqrt{k_\sigma}} \quad (2.79)$$

$$\rho = 1.0 \quad \bar{\lambda}_p \leq 0.673 \quad (2.80)$$

The Winter formula can be recognised when $\psi = \frac{\sigma_2}{\sigma_1} = +1$ for pure compression is substituted in Eq.(2.78). The reduction factor $0.055(3 + \psi) = 0.22$. This factor $0.055(3 + \psi)$ in Eq.(2.78) becomes smaller than 0.22 for the combination compression or tension and bending.

Eq.(2.79) can be found by substitution of the critical stress σ_{cr} , see Eq.(2.14), into $\bar{\lambda}_p = \sqrt{\frac{f_y}{\sigma_{cr}}}$:

$$\bar{\lambda}_p = \sqrt{\frac{f_y}{\sigma_{cr}}} = \sqrt{\frac{f_y}{k_\sigma \cdot \frac{\pi^2 E}{12(1-\nu^2) \left(\frac{\bar{b}}{t}\right)^2}}} = \frac{\bar{b}}{t} \sqrt{\frac{12(1-\nu^2) \cdot 235}{\pi^2 \cdot 210000}} \frac{1}{\sqrt{\frac{235}{f_y} \cdot k_\sigma}} = \frac{\bar{b}}{28.4\epsilon\sqrt{k_\sigma}} \quad (2.81)$$

The limit $\bar{\lambda}_p = 0.673$ is found for the situation that the effective width b_{eff} is equal to the width b of

the plate and the plate is under pure bending, $\psi = \frac{\sigma_2}{\sigma_1} = -1$:

$$\begin{aligned} \rho = \frac{b}{b_{eff}} = \frac{\bar{\lambda}_p - 0.22}{\bar{\lambda}_p^2} = 1 & \quad \Rightarrow \bar{\lambda}_p^2 - \bar{\lambda}_p + 0.22 = 0 \\ \Rightarrow \bar{\lambda}_{p,1/p,2} = \frac{1 \mp \sqrt{(-1)^2 - 4 \cdot 1 \cdot 0.22}}{2 \cdot 1} = \frac{1}{2} \mp \frac{1}{2} \sqrt{0.12} & \quad (2.82) \end{aligned}$$

This means $\bar{\lambda}_{p,1} = 0.327$ and $\bar{\lambda}_{p,2} = 0.673$. The first solution does not have any physical meaning and the second solution is given in EN1993-1-5 [30] and other codes, such as the previous Dutch code NEN6771 [62].

The plate buckling factor k_σ depends on the stress distribution $\psi = \frac{\sigma_2}{\sigma_1}$ in the cross-section and is

determined with:

$$\begin{aligned} \text{If } 1 > \psi > 0 \quad k_\sigma &= \frac{8.2}{1.05 + \psi} \\ \text{If } 0 > \psi > -1 \quad k_\sigma &= 7.81 - 6.29 \cdot \psi + 9.78 \cdot \psi^2 \\ \text{If } -1 > \psi > -2 \quad k_\sigma &= 5.98 \cdot (1 - \psi)^2 \end{aligned} \quad (2.83)$$

The effective width b_{eff} is dependent also on the stress distribution expressed by $\psi = \frac{\sigma_2}{\sigma_1}$, but also

on the width \bar{b} :

$$\begin{aligned} \text{If } 1 \geq \psi \geq 0 \quad b_{eff} &= \rho \bar{b} \quad b_{e1} = \frac{2}{5 - \psi} b_{eff} \quad b_{e2} = b_{eff} - b_{e1} \\ \text{If } \psi < 0 \quad b_{eff} &= \rho b_c = \frac{\rho \bar{b}}{1 - \psi} \end{aligned} \quad (2.84)$$

$$b_{e1} = 0.4 b_{eff} \quad b_{e2} = 0.6 b_{eff} \quad (2.85)$$

For outstand elements the requirements differ a little:

$$\rho = \frac{\bar{\lambda}_p - 0.188}{\bar{\lambda}_p^2} \leq 1, 0 \quad \bar{\lambda}_p > 0.748 \quad (2.86)$$

$$\rho = 1.0 \quad \bar{\lambda}_p \leq 0.748 \quad (2.87)$$

The limit for the relative plate slenderness $\bar{\lambda}_p = 0.748$ can be found as shown before for internal elements. The plate buckling factor k_σ depends on the stress ratio $\psi = \frac{\sigma_2}{\sigma_1}$:

$$\begin{aligned} \text{If } 1 > \psi > 0 \quad k_\sigma &= \frac{0.578}{\psi + 0.34} \\ \text{If } 0 > \psi > -1 \quad k_\sigma &= 1.70 - 5.0 \cdot \psi + 17.1 \cdot \psi^2 \end{aligned} \quad (2.88)$$

The effective width b_{eff} depends on the stress ratio $\psi = \frac{\sigma_2}{\sigma_1}$ and depends on the location of the maximum compressive stress. The following is required:

$$\text{If } 1 \geq \psi \geq 0 \quad b_{eff} = \rho c$$

$$\text{If } \psi < 0 \quad b_{eff} = \rho b_c = \frac{\rho c}{1 - \psi} \quad (2.89)$$

For the situation where the maximum stress, this is the tensile stress or the minimum compressive stress, is located at the support, so $\sigma_1 \leq \sigma_2$, the following is required:

$$\text{If } 1 \geq \psi \geq 0 \quad b_{eff} = \rho c$$

$$\text{If } \psi < 0 \quad b_{eff} = \rho b_c = \frac{\rho c}{1 - \psi} \quad (2.90)$$

The relative plate slenderness based on the yield stress f_y can be replaced by a equation based on the actual stress $\sigma_{com.Ed}$:

$$\bar{\lambda}_{p,rel} = \bar{\lambda}_p \sqrt{\frac{\sigma_{com.Ed}}{\left(\frac{f_y}{\gamma_{M0}}\right)}} \quad (2.91)$$

Vertical buckling of the compressive flange into the web, or flange induced buckling, as it is called in EN1993-1-5, is given by:

$$\beta_w = \frac{h}{t_w} \leq \beta_{w,max} = k \frac{E}{f_{yf}} \cdot \sqrt{\frac{A_w}{A_f}} \quad (2.92)$$

With $k = 0.55$ for cross-section class 4.

The factor k is determined with $k = \sqrt{\frac{\pi^2}{36 \cdot (1 - \nu^2)}} = 0.55$ is given by Basler, see Eq.(2.38).

2.6.2 ANSI/AISC 360-10 [5]

The American National Standard Institute and the American Institute of Steel Construction published the Specification for Structural Steel Buildings, ANSI/AISC 360-10 [5].

The requirements related to the ultimate bending moment resistance of a plate girder with a very slender web are:

$$M_u = R_{pg} \cdot f_y \cdot W \quad (2.93)$$

with:

$$R_{pg} = 1 - \frac{a_w}{1200 + 300a_w} \left(\frac{h_w}{t_w} - 5.7 \sqrt{\frac{E}{f_y}} \right) \leq 1 \quad (2.94)$$

wherein:

$$a_w = \frac{h_w \cdot t_w}{b \cdot t_f} \quad (2.95)$$

This is exactly according to Basler, see Chapter 2.5.1, by using the reduction factor $\frac{M_u}{M_{el}}$ based on Eq.(2.53), Eq.(2.54) for the reduction factor C and Eq.(2.59) for the web slenderness β_0 .

The determination of the maximum web slenderness $\beta_{w,max}$ is also based on Basler, see Chapter 2.4.3. The residual stress σ_r is reduced to $\sigma_r = 0.3f_y$ instead of $\sigma_r = 0.5f_y$ as used by Basler. The influence of this reduced residual stress σ_r on the maximum web slenderness $\beta_{w,max}$ according to (2.39), $\beta_{w,max,IV}$, is rather small. AISI 310 gives:

$$\beta_{w,max} = \frac{0.42E}{f_{y,tf}} \quad (2.96)$$

2.7 REMARKS AND ELABORATIONS ON THE STUDIED LITERATURE

2.7.1 REMARKS ON THE MAXIMUM WEB SLENDERNESS ACCORDING TO BASLER

In his publication [12], Basler mentioned that the method to determine the maximum web slenderness $\beta_{w,max}$ is rather rough and so it is of interest to comment on this:

1. To fulfil the requirement that every fibre of the compressive flange yields before vertical buckling of the compressive flange into the web occurs, the strain of the top flange ε_{tf}

should be at least the yield strain plus the strain caused by the residual stress $\varepsilon_{tf} = \frac{f_{y,tf} + \sigma_r}{E}$.

For S235, Basler [12] assumed a residual compressive and tensile stress of $\sigma_r = 0.5 \cdot f_{y,tf}$. EN1993-1-1 [29] and EN1993-1-5 [30] do not explicitly give patterns for residual stresses in plate girders, but in Eq.(2.38) the maximum web slenderness $\beta_{w,max}$ according to EN1993-1-5 [30] a level of $\sigma_r = 0.5 \cdot f_{y,tf}$ for the residual tensile stress is taken into account. The previous Dutch code NEN6771 [62] and the previous Swedish code BSK99 [24] gave patterns and both consider the yield stress $f_{y,tf}$ as maximum residual tensile stress. This means that the maximum web slenderness $\beta_{w,max}$ will decrease compared with the maximum web slenderness $\beta_{w,max,III}$ as determined by Basler and by EN1993-1-5, see Eq. (2.38);

2. For steel grades higher than S355, the residual stress σ_r becomes smaller than the yield stress $f_{y,ff}$ as indicated in the previous Dutch code NEN6771 [62] and the previous Swedish code BSK99 [24]. This means that maximum web slenderness $\beta_{w,max}$ will increase;
3. The curvature κ is based on the strain ε_{ff} in the top flange and the position of the neutral axis. Basler assumed that the position of the neutral axis is at half of the web height. However, for a cross-section of class 4 the position of the neutral axis is based on the effective cross-section and so the position of the neutral axis shifts downwards towards the tensile (bottom) flange. Because of this shift of the neutral axis, the curvature κ compared with Eq.(2.33) decreases and thus the compressive stress σ_n . Therefore, the maximum web slenderness $\beta_{w,max}$ will increase compared with the one calculated by Basler;
4. Basler [12] assumed that the web is simply supported by the flanges and the column buckling length of the web is therefore taken equal to the web height h_w . However, the web edges are welded to the flanges and therefore these boundaries are actually no hinges. There will be some rotational stiffness caused by the flanges, as a result of which the buckling length is smaller than the web height h_w . The buckling length will be in-between $0.5h_w$ and h_w and so the maximum web slenderness $\beta_{w,max}$ will increase considerably compared with the one calculated by Basler;
5. Basler [12] checked the compressive stress σ_n against the Euler critical column buckling stress σ_{cr} and thus did not taking the influences of the geometrical and physical imperfections into account. This aspect affects the maximum web slenderness $\beta_{w,max}$ negatively and therefore the maximum slenderness $\beta_{w,max}$ decreases;
6. Basler [12] based vertical buckling of the compressive flange into the web on column buckling of the web only, but next to compressive stress σ_n there are stresses in longitudinal direction of the web, caused by the bending moment. These bending stresses are much larger than the compressive stress σ_n , but are completely neglected. Basler [12] justified this neglect by assuming that the negative influence of these compressive stresses due to bending will be balanced by the positive influence of the tensile stresses due to bending in the lower part of the web near the tension flange. The check on column buckling of the web should be replaced by a check on plate buckling taking the actual stresses into account, such as the

compressive stress σ_n and the stresses due to bending of the girder. This will positively affect the maximum web slenderness $\beta_{w,max}$.

The above mentioned remarks form sufficient reason to further research the influence of the web slenderness β_w on the maximum bending moment resistance.

2.7.2 ELABORATIONS ON THE BENDING MOMENT RESISTANCE ACCORDING TO BASLER

The maximum bending moment resistance M_u of the plate girder depends on the product of the reduction factor $\left(\frac{M_u}{M_{el}}\right)$, described by Eq.(2.60), and the elastic bending moment resistance $M_{el} = W_{el} \cdot f_y$. Here, W_{el} is the elastic section modulus of the cross-section. In this thesis, the reduction factor $\left(\frac{M_u}{M_{el}}\right)$ is presented by the symbol ξ and so $M_u = \left(\frac{M_u}{M_{el}}\right) \cdot W_{el} \cdot f_y = \xi \cdot W_{el} \cdot f_y$. To determine the maximum bending moment resistance M_u the product $\xi \cdot W_{el}$ has to be maximised. The product $\xi \cdot W_{el}$ follows from multiplying Eq.(2.60) with the section modulus W_{el} :

$$M_u = \xi \cdot M_{el} = \xi \cdot W_{el} \cdot f_y \quad (2.97)$$

$$M_u = \xi \cdot W_{el} \cdot f_y = \left[1 - 0.0005 \cdot \frac{A_w}{A_{ff}} \left(\frac{h}{t} - 5.7 \sqrt{\frac{E}{f_{y,ff}}} \right) \right] \cdot \left[\frac{b(h_w + 2t_f)^3 - (b - t_w)h_w^3}{12 \left(\frac{h_w}{2} + t_f \right)} \right] f_y \quad (2.98)$$

The dependent variables, such as the web slenderness β_w , the ratio of area ρ and the cross-sectional area A_{tot} are related to the independent variable b for the flange width, t_f for the flange thickness, h_w for the web height and t_w for the web thickness and are related as follows:

$$\beta_w = \frac{h_w}{t_w} \quad (2.99)$$

$$\rho = \frac{A_w}{A_f} = \frac{h_w \cdot t_w}{b \cdot t_f} \quad (2.100)$$

$$A_{tot} = A_w + 2A_f = h_w \cdot t_w + 2 \cdot b \cdot t_f \quad (2.101)$$

The flange slenderness $\frac{b}{t_f}$ is taken such that the flange is fully effective for steel grades up to S460:

$$\frac{b}{t_f} = 24\varepsilon = 24\sqrt{\frac{235}{f_y}} \quad (2.102)$$

Based on these equations, the flange area A_f can be expressed in the cross-sectional area A_{tot} and the ratio of area ρ :

$$A_f = \frac{A_{tot}}{2 + \rho} \quad (2.103)$$

The dimensions of the flange, the flange width b and the flange thickness t_f can be expressed in the cross-sectional area A_{tot} and the ratio of area ρ :

$$t_f = \sqrt{\frac{A_{tot}}{24\varepsilon \cdot (2 + \rho)}} \quad (2.104)$$

$$b = \sqrt{\frac{24\varepsilon \cdot A_{tot}}{(2 + \rho)}} \quad (2.105)$$

The web area A_w is also expressed in the cross-sectional area A_{tot} and the ratio of area ρ :

$$A_w = \rho \cdot A_f = \frac{\rho \cdot A_{tot}}{2 + \rho} \quad (2.106)$$

The web dimensions, the web height h_w and the web thickness t_w , are expressed in these depending variables, the cross-sectional area A_{tot} and the ratio of area ρ , but also on the web slenderness β_w :

$$t_w = \sqrt{\frac{\rho \cdot A_{tot}}{(2 + \rho) \cdot \beta_w}} \quad (2.107)$$

$$h_w = \sqrt{\frac{\rho \cdot A_{tot} \cdot \beta_w}{(2 + \rho)}} \quad (2.108)$$

For specific values for the web slenderness's β_w and the total cross-sectional area A_{tot} , the ratio ρ is varied to determine the maximum bending moment resistance M_u .

For steel grades S235, S355 and S460 the elastic and maximum bending moment resistance, M_{el} and M_u , are presented in Figure 2-28, Figure 2-29 and Figure 2-30 respectively, for $A_{tot} = 1200 \text{ mm}^2$. The steel grade for the flanges is the same as the steel grade for the web.

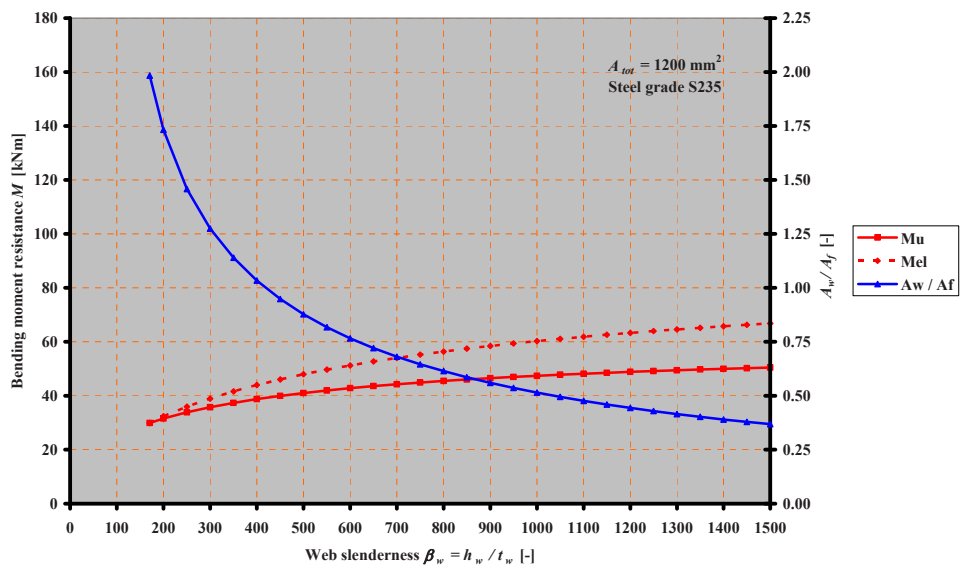


Figure 2-28 Bending moment resistance M_u and the ratio of area ρ dependent on the web slenderness β_w

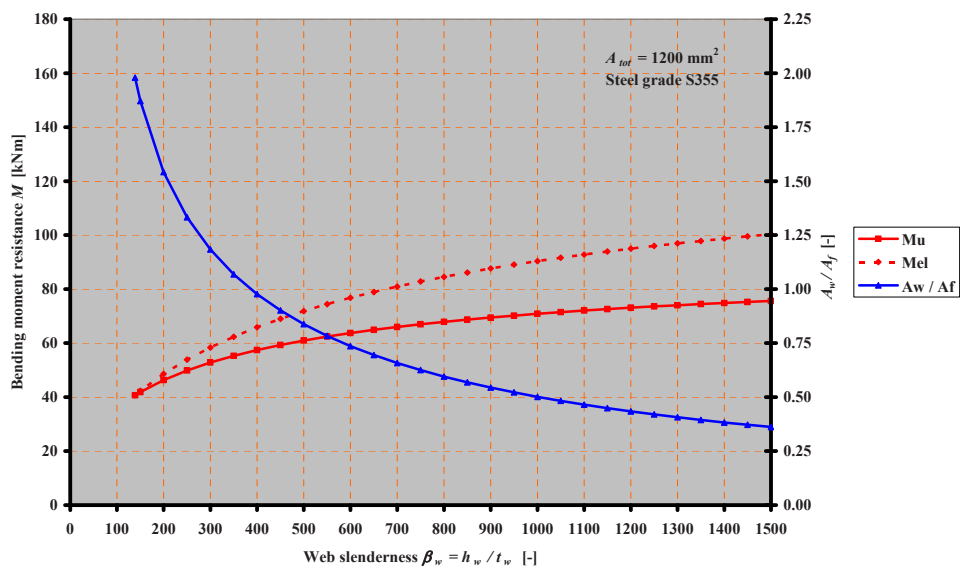


Figure 2-29 Bending moment resistance M_u and the ratio of area ρ dependent on the web slenderness β_w

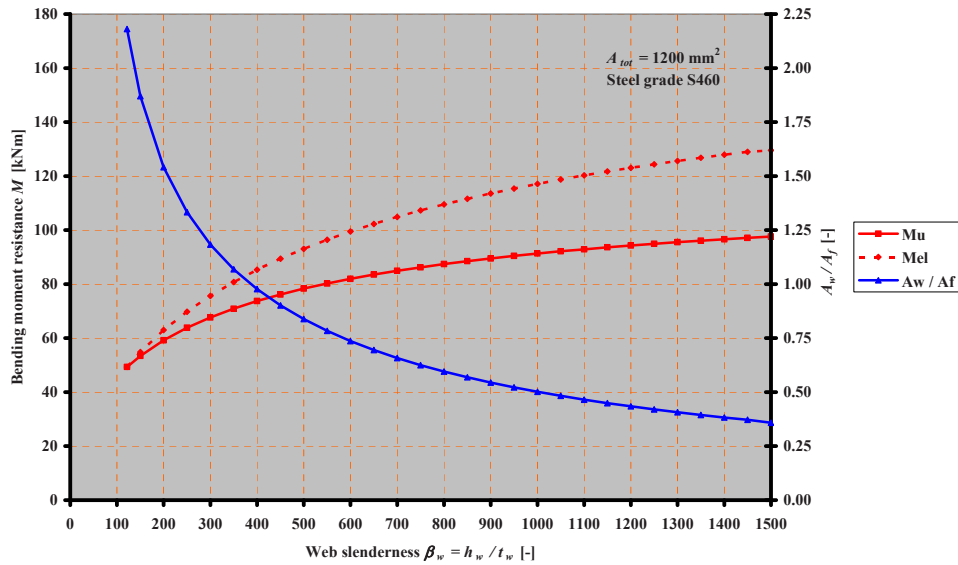


Figure 2-30 Bending moment resistance M_u and the ratio of area ρ dependent on the web slenderness β_w

The graphs start at a web slenderness $\beta_0 = 5.7 \sqrt{\frac{E}{f_y}}$, so for steel grade S235 $\beta_0 = 170$, for S355

$\beta_0 = 139$ and for S460 $\beta_0 = 122$. In none of these graphs a top is found for the maximum bending moment resistance and so for practical reasons the graph stops at $\beta_w = 1500$.

From these graphs it can be seen that the elastic bending moment resistance M_{el} (the red dotted lines) and the maximum bending moment resistance M_u (the red solid lines) increase with increasing web slenderness β_w .

According to Basler [12], the ratio of area ρ is important and in the graphs as shown in Figure 2-28, Figure 2-29 and Figure 2-30 this ratio is represented by the solid blue line and can be read from the vertical axis on the right-hand side. It can be seen that these blue lines are descending for all steel grades.

For web slenderness $\beta_w = \beta_0$, the bending moment resistance M_u is found for a ratio of area ρ of approximately 2. For higher web slenderness's β_w the ratio of area ρ decreases. For every ratio of area ρ and the yield strength f_y , the maximum web slenderness $\beta_{w,max}$ according to Basler, see Eq.(2.36), can be determined.

The ultimate bending moment resistances for S235, S355 and S460 are represented in Figure 2-31, including the ratios between the ultimate bending moment resistances for steel grades S355 and S235, $M_{u.S355}/M_{u.S235}$ and between S460 and S235, $M_{u.S460}/M_{u.S235}$. These ratios are more or less constant and exactly the ratio between the yield strengths $f_{y.S355}/f_{y.S235}$ and $f_{y.S460}/f_{y.S235}$. This means that by changing the dimensions of the plate girder, 100% of the advantage of higher yield strengths can be utilised by modifying the dimensions. The total area is the same for all steel grades.

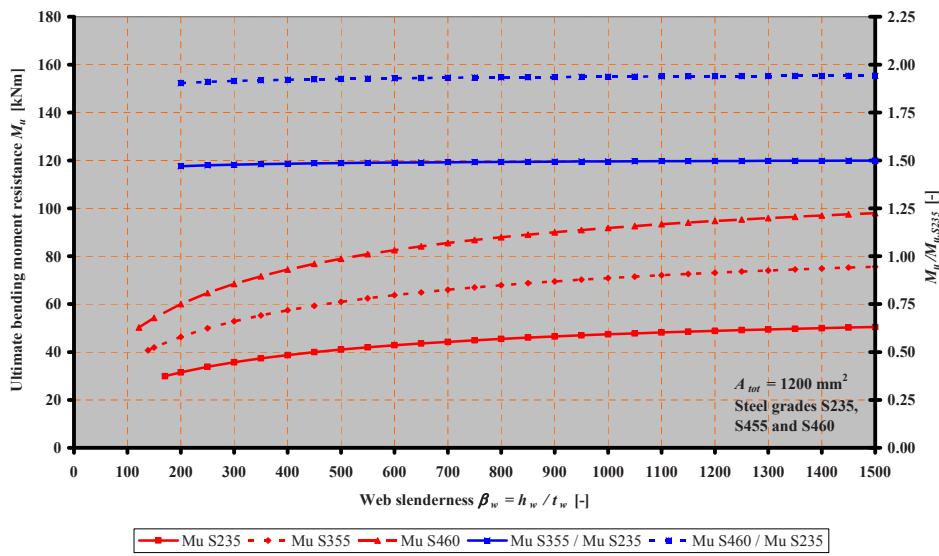


Figure 2-31 Comparison effective bending moment resistances for S235, S355 and S460

2.7.3 ELABORATIONS ON THE BENDING MOMENT RESISTANCE ACCORDING TO HÖGLUND

Höglund [42] gives also the ratio $\xi = \left(\frac{M_u}{M_{el}} \right)$ between the ultimate bending moment resistance M_u

and the elastic bending moment resistance M_{el} , see Eq.(2.61). By using the same approach as described in Chapter 2.7.2, the same kind of graphs can be made to see the difference for different steel grades, see Figure 2-32, Figure 2-33 and Figure 2-34 for respectively S235, S355 and S460. In these graphs, the same kind of results for the ultimate bending moment resistance are seen as for the Basler model. The ultimate bending moment resistance M_u is bigger than according to Basler.

The ratio of area $\rho = \frac{A_w}{A_f}$ is going to a limit close to 1, while in the Basler model this ratio was continuously going down.

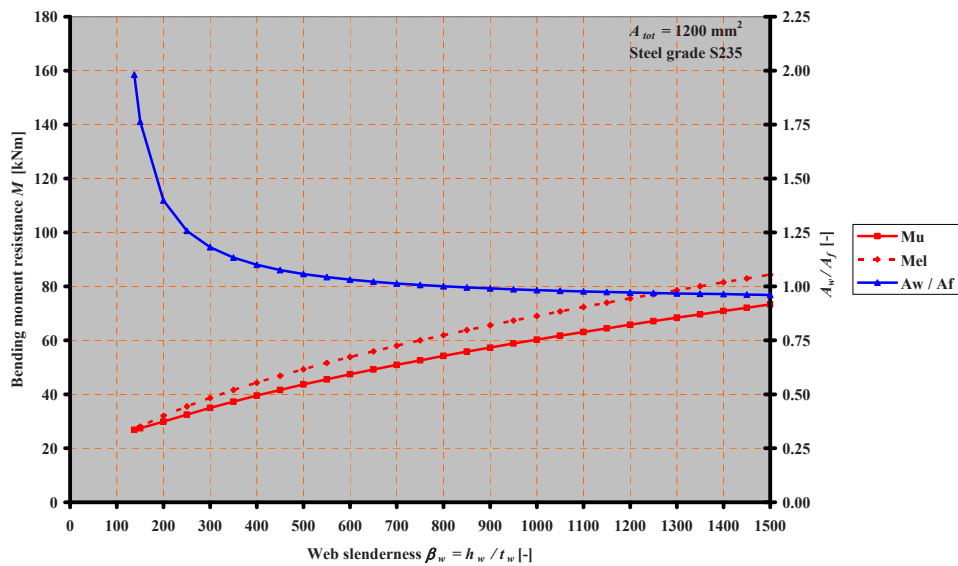


Figure 2-32 Bending moment resistance and ratio of area related to the web slenderness, S235

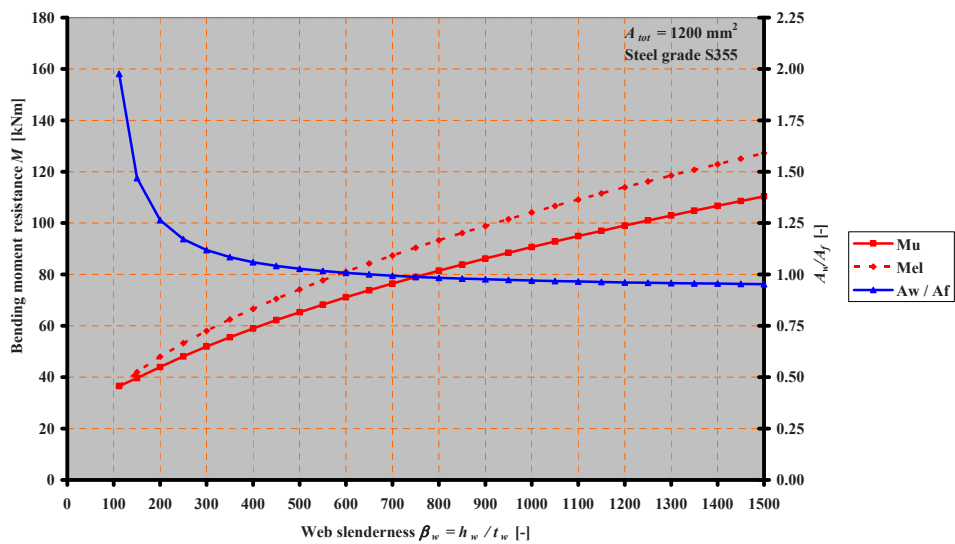


Figure 2-33 Bending moment resistance and ratio of area related to the web slenderness, S355

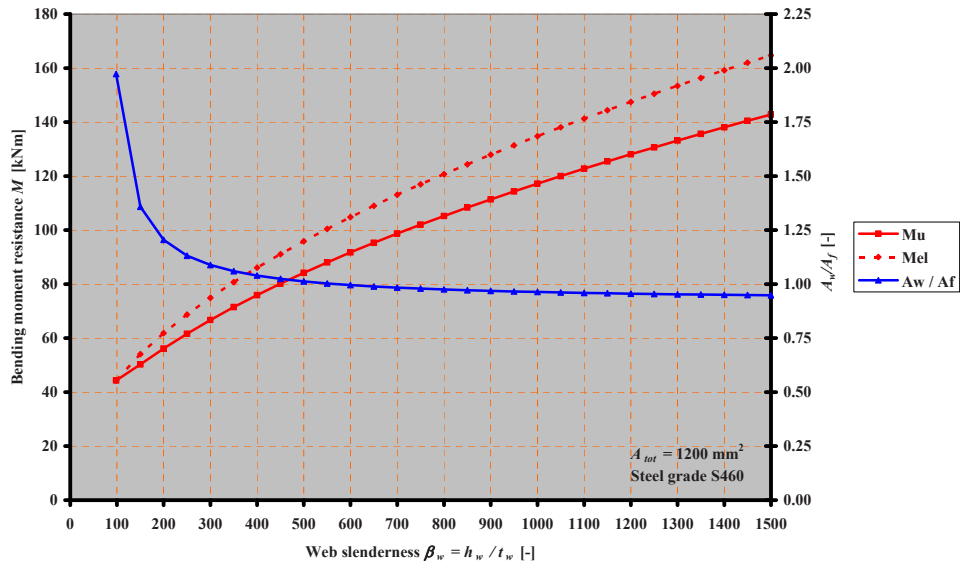


Figure 2-34 Bending moment resistance and ratio of area related to the web slenderness, S460

In Figure 2-35 a comparison is made for M_u for S235, S355 and S460, including the ratios of the ultimate bending moment resistance of S355 and S235, $M_{u.S355}/M_{u.S235}$, and between S460 and S235, $M_{u.S460}/M_{u.S235}$. This graph shows that the increase in ultimate bending moment resistance is equal to the ratio of the yield strengths $f_{y.S355}/f_{y.S235}$ and $f_{y.S460}/f_{y.S235}$.

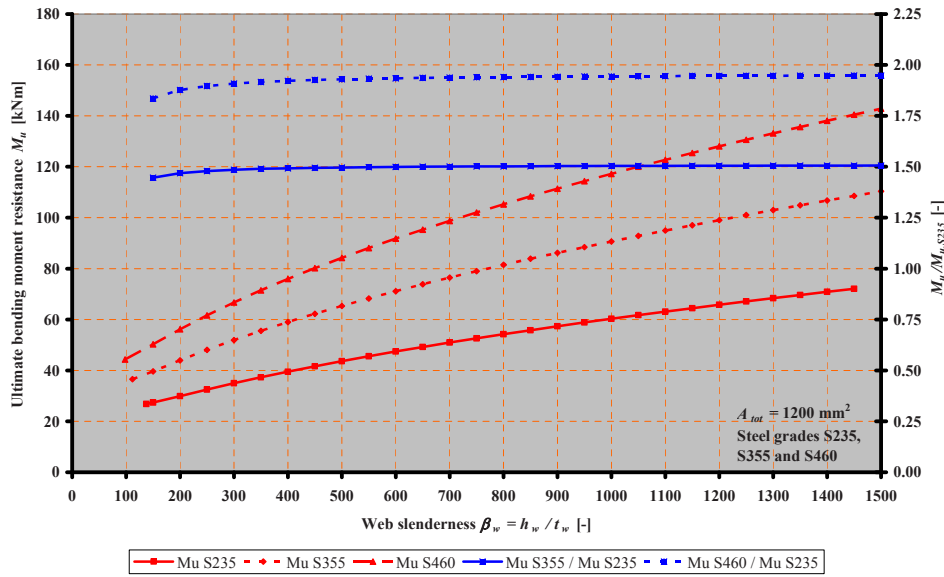


Figure 2-35 Comparison bending moment resistance Höglund steel grades S235, S355 and S460

2.7.4 ELABORATIONS ON THE BENDING MOMENT RESISTANCE ACCORDING TO HERZOG

As mentioned in Chapter 2.5.3, the unmodified bending moment M_{Uo}^o has to be multiplied by factors K_i related to specific collapse modes. While the compressive flange is laterally supported, there are two collapse modes that have to be taken into account, namely K_1 for torsional buckling and K_3 for vertical buckling of the compressive flange into the web:

$$\begin{aligned} \frac{K_1 \cdot K_3 \cdot M_{Uo}^o}{M_{el}} &= \left(1.17 - \frac{h_w}{2000 \cdot t_w} \right) \sqrt{\frac{16 \cdot t_c}{b_c}} \cdot \\ &\quad \frac{\left\{ A_f \cdot \left(\frac{2h_w}{3} + \frac{t_f}{2} \right) + A_f \cdot \left(\frac{h_w}{3} + \frac{t_f}{2} \right) + \frac{1}{6} \cdot t_w \cdot \left(\frac{2h_w}{3} \right)^2 + \frac{1}{3} \cdot t_w \cdot \left(\frac{h_w}{3} \right)^2 \right\}}{\left\{ A_f \cdot h_w \left(1 + \frac{\rho}{6} \right) \right\}} = \\ &\approx \frac{\left(2340 - \frac{h_w}{t_w} \right) \sqrt{\frac{16 \cdot t_c}{b_c}} \left\{ A_f \cdot h_w \left(1 + \frac{\rho}{9} \right) \right\}}{2000 \left\{ A_f \cdot h_w \left(1 + \frac{\rho}{6} \right) \right\}} = \frac{\left(2340 - \frac{h_w}{t_w} \right) \sqrt{\frac{16 \cdot t_c}{b_c}} \left(1 + \frac{\rho}{9} \right)}{2000 \left(1 + \frac{\rho}{6} \right)} \end{aligned} \quad (2.109)$$

with: $\rho = \frac{A_w}{A_f}$

In Eq.(2.109) the simplified equation according to Basler is used for the elastic bending moment resistance M_{el} . This equation is used to optimize the ultimate bending moment resistance $M_u = K_1 \cdot K_3 \cdot M_{Uo}^0$ and the results are represented in graphs, see Figure 2-36, Figure 2-37 and Figure 2-38 for respectively S235, S355 and S460:

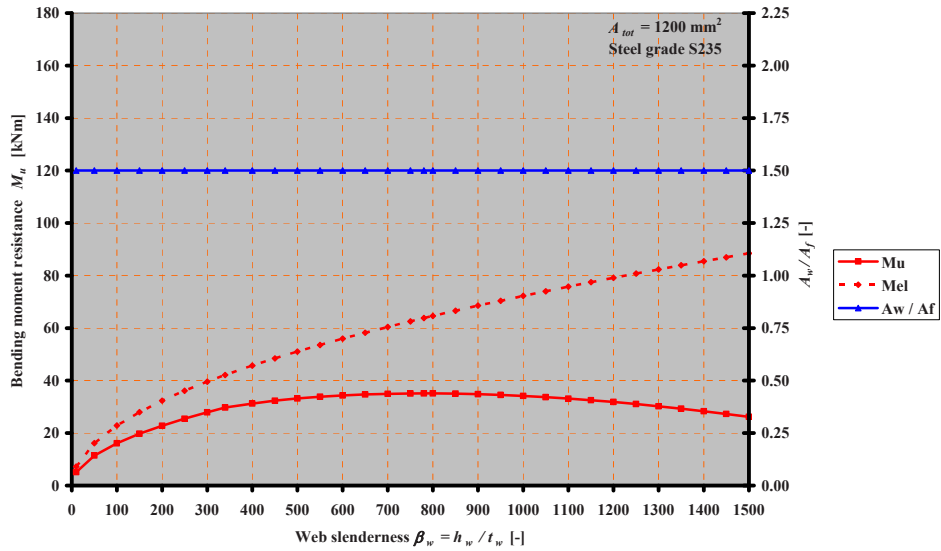


Figure 2-36 Bending moment resistance and ratio of area related to the web slenderness, S235

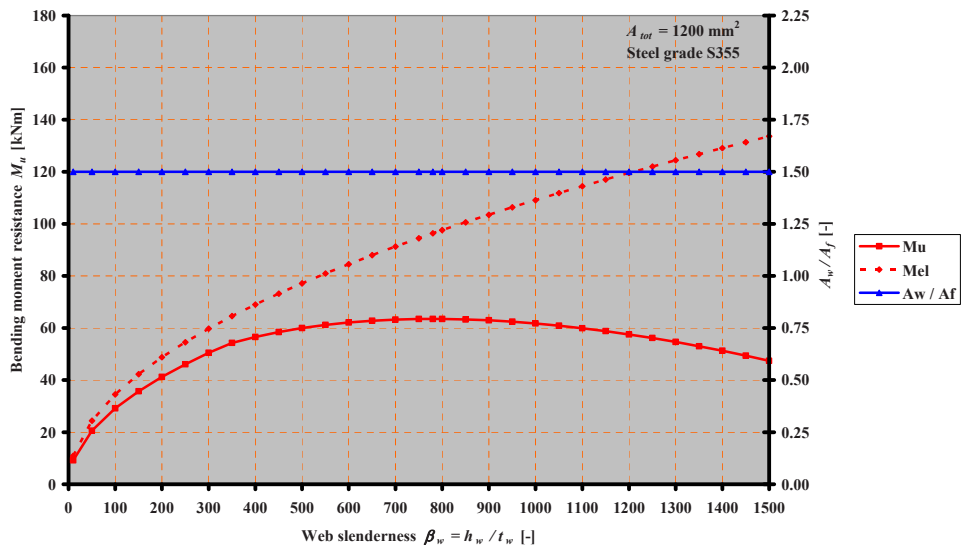


Figure 2-37 Bending moment resistance and ratio of area related to the web slenderness, S355

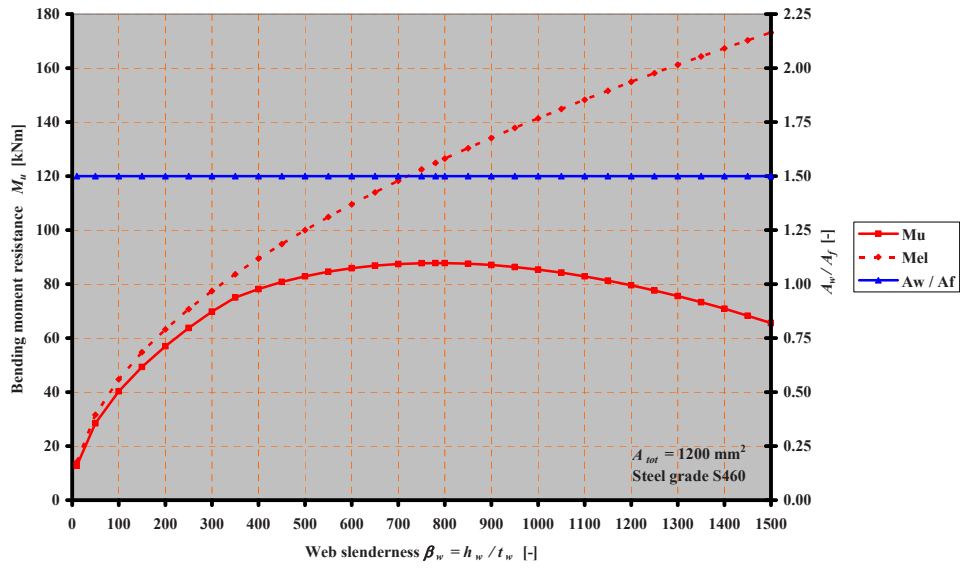


Figure 2-38 Bending moment resistance and ratio of area related to the web slenderness, S460

Because of the influence of factor K_3 , there is a maximum for the ultimate bending moment resistance M_u for all three steel grades close to a web slenderness $\beta_w \approx 800$. This is caused by the following:

$$\rho = \frac{A_w}{A_f} \quad A_w = h_w \cdot t_w \quad \beta_w = \frac{h_w}{t_w}$$

$$\Rightarrow A_f = \frac{A_w}{\rho} = \frac{h_w \cdot t_w}{\rho} = \frac{\beta_w \cdot t_w^2}{\rho} \quad (2.110)$$

Substitution of these variables in Eq.(2.109) gives:

$$M_u = \frac{M_u^0}{M_{el}} \cdot M_{el} = \frac{\left(2340 - \frac{h_w}{t_w}\right) \sqrt{\frac{16 \cdot t_c}{b_c}} \left(1 + \frac{\rho}{9}\right) \cdot A_f \cdot h_w \cdot \left(1 + \frac{\rho}{6}\right) \cdot f_y}{2000 \left(1 + \frac{\rho}{6}\right)}$$

$$= \frac{(2340 - \beta_w) \sqrt{\frac{16 \cdot t_c}{b_c}} \left(1 + \frac{\rho}{9}\right) \frac{\beta_w \cdot t_w^2}{\rho} \cdot h_w \cdot f_y}{2000} =$$

$$= \frac{(2340 \beta_w - \beta_w^2) \sqrt{\frac{16 \cdot t_c}{b_c}} \left(1 + \frac{\rho}{9}\right) \frac{t_w^2}{\rho} \cdot h_w \cdot f_y}{2000} \quad (2.111)$$

In this equation $-\beta_w^2$ leads to an upward opening parabola, according to the graph. In the models for the ultimate bending moment resistance M_u of Basler [12], Höglund [42] and Veljkovic and Johansson [74], this factor K_3 is not taken into account.

The ratio of area $\rho = \frac{A_w}{A_f}$ is constant for every steel strength f_y and for every web slenderness β_w , namely 1.5.

In Figure 2-39 the ultimate bending moment resistance M_u is shown for S235, S355 and S460, with a total area $A_{tot} = 1200 \text{ mm}^2$.

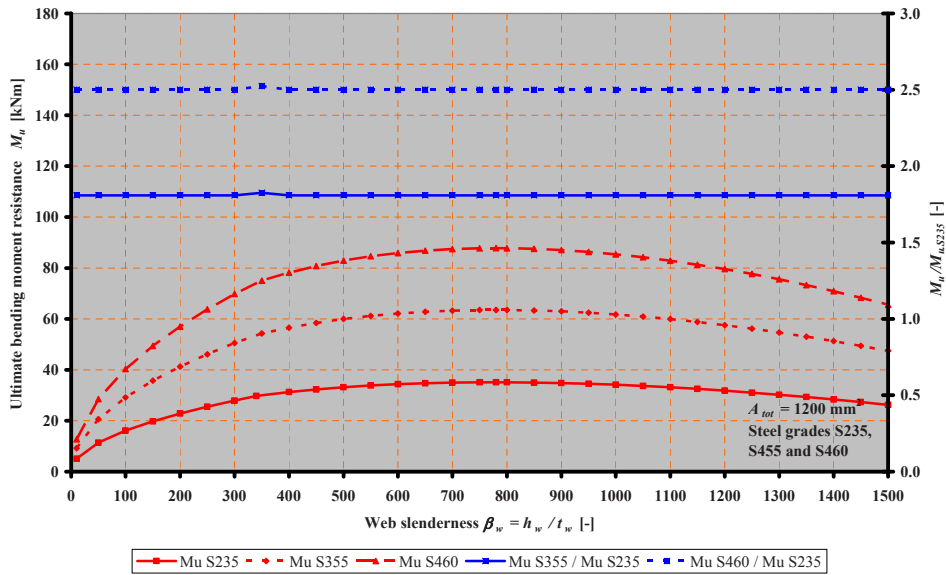


Figure 2-39 Comparison bending moment resistances according to Herzog, S235, S355 and S460

From this graph it can be seen that the ratio between the ultimate bending moment resistance for steel grade S355 and S460 and the ultimate bending moment resistance of steel grade S235,

$\frac{M_{u,S355}}{M_{u,S235}}$ and $\frac{M_{u,S460}}{M_{u,S235}}$, are constant and higher than the ratio between the relevant yield strengths.

The ratios $\frac{M_{u,S355}}{M_{u,S235}}$ and $\frac{M_{u,S460}}{M_{u,S235}}$ are much higher than determined by the other researchers.

2.7.5 ELABORATIONS ON THE BENDING MOMENT RESISTANCE ACCORDING TO STARK

Stark [70] did not give an explicit equation to determine the ultimate bending moment resistance, but it can be determined iteratively based on the effective width's b_{e1} , Eq.(2.72), and b_{e2} , Eq.(2.73) see Figure 2-21, or based on the effective width b_{e1} , Eq.(2.74), see Figure 2-25, for the simplified effective width model. Figure 2-40 shows the graphs for these ultimate bending moment resistances for S235, Figure 2-41 for S355 and Figure 2-42 for S460 related to the web slenderness β_w .

Next to the ultimate bending moment resistances, the elastic bending moment resistance is shown and the ratios of area ρ for the optimised cross-sections with a specific web slenderness β_w , see the blue lines in these figures. It can be seen that the differences between the effective width method according to Stark and the simplified effective width method according to Stark are very small, especially when the web slenderness is rather large or the steel grade is S460.

The ratio of area ρ decreases with increasing web slenderness β_w to a value just larger than 1.0.

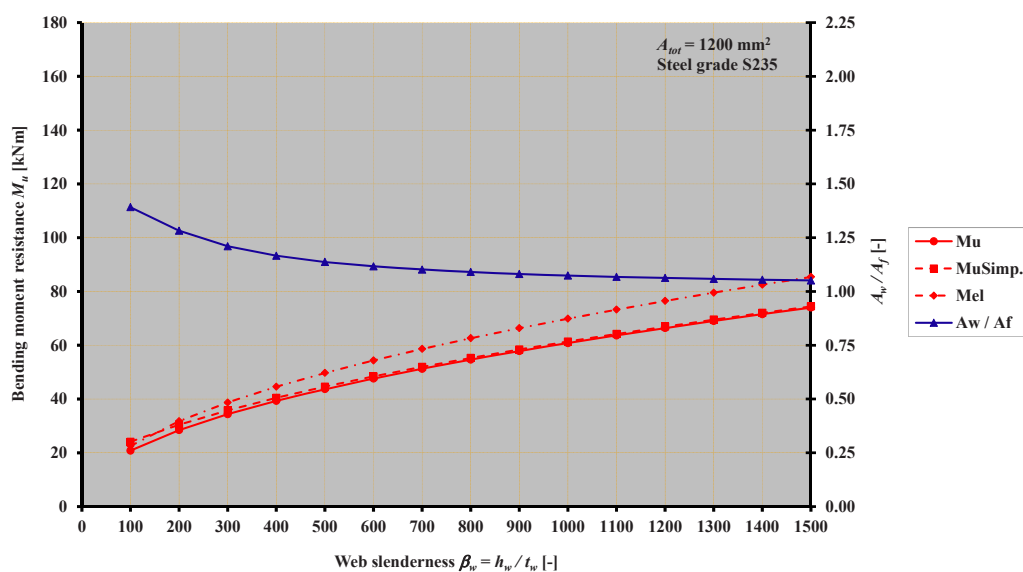


Figure 2-40 Bending moment resistance and ratio of area related to the web slenderness, S235

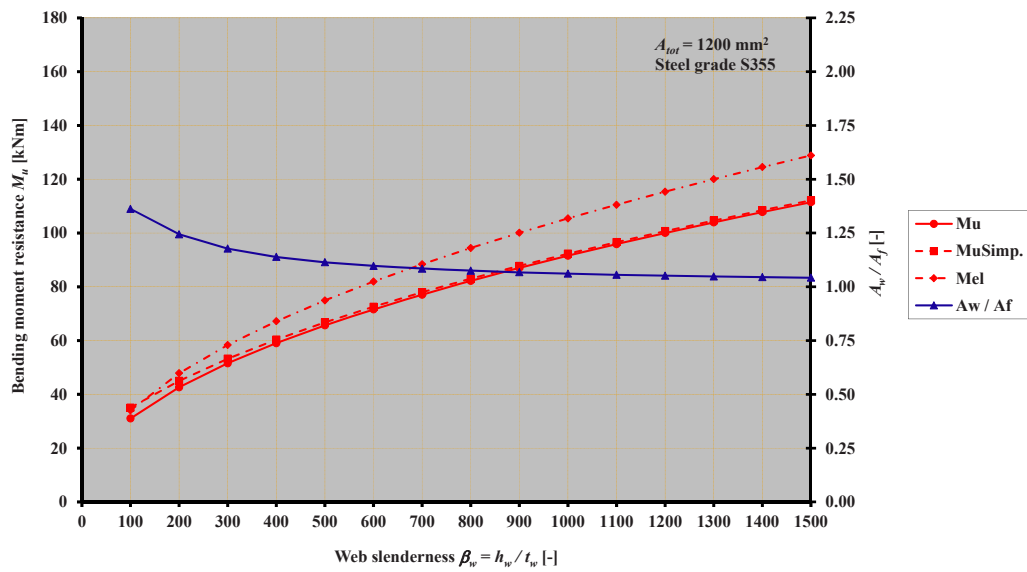


Figure 2-41 Bending moment resistance and ratio of area related to the web slenderness, S355

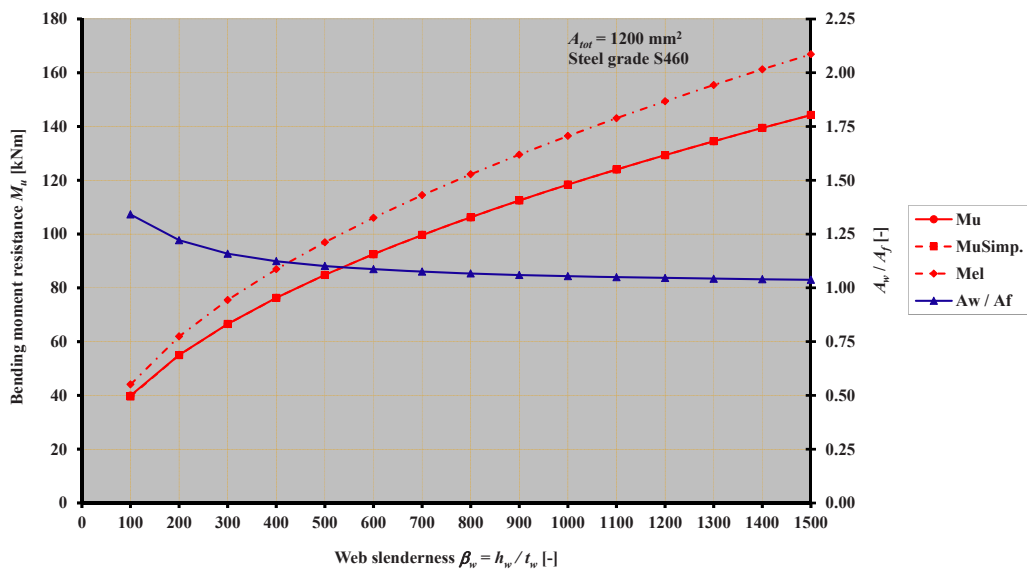


Figure 2-42 Bending moment resistance and ratio of area related to the web slenderness, S460

These bending moment resistances for different steel grades are summarised in Figure 2-43

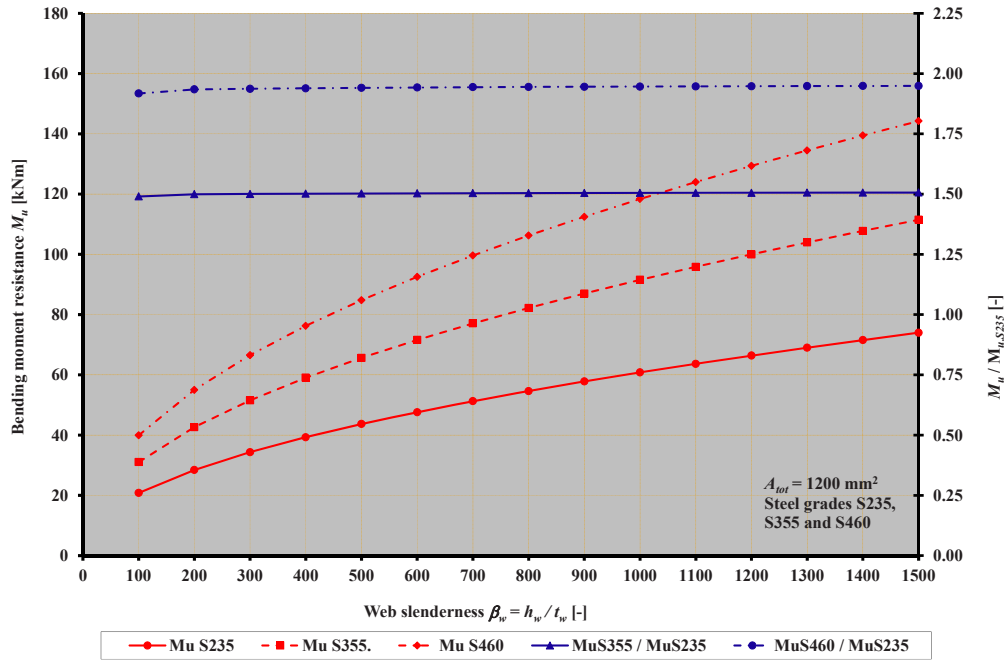


Figure 2-43 Comparison of the bending moment resistances, S235, S355 and S460

The ratio between the ultimate bending moment resistances M_u of steel grades S355 and S235

$$\frac{M_{u,S355}}{M_{u,S235}} \quad \text{and the ratio between the resistance of steel grades S460 and S235 } \frac{M_{u,S460}}{M_{u,S235}}$$

are represented by the blue lines. The ultimate bending moment resistance, based on the effective width of the web, is more or less related to the ratios between the yield strengths.

2.7.6 ELABORATIONS ON THE BENDING MOMENT RESISTANCE ACCORDING TO VELJKOVIC AND JOHANSSON

The ultimate bending moment resistance M_u of the plate girder depends on the product of the pre-

sented reduction factor $\xi = \left(\frac{M_u}{M_{el}} \right) \left[1 - 0.1 \frac{A_w}{A_f} \left(1 - 124 \varepsilon \cdot \frac{t_w}{h_w} \right) \right]$ and the elastic section modulus W .

The ultimate bending moment resistance M_u is determined with:

$$M_u = \xi \cdot M_{el} = \left(\frac{M_u}{M_{el}} \right) \cdot M_{el} =$$

$$= \left[1 - 0.1 \cdot \frac{h_w \cdot t_w}{b \cdot t_f} \cdot \left(1 - 124 \frac{\varepsilon}{\left(\frac{h_w}{t_w} \right)} \right) \right] \cdot \left[\frac{b(h_w + 2t_f)^3 - (b - t_w)h_w^3}{12 \left(\frac{h_w}{2} + t_f \right)} \right] f_y \quad (2.112)$$

The results for the optimum M_u based on Eq. (2.112) are presented in Figure 2-44, Figure 2-45 and Figure 2-46 for respectively S235, S355 and S460, in the same way as shown for the Basler, Herzog Stark and Höglund models.

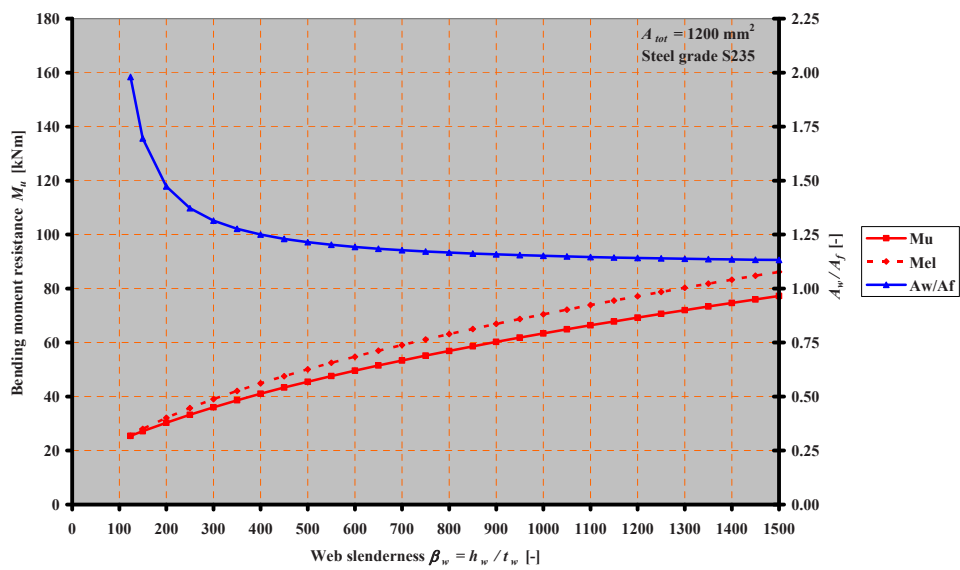


Figure 2-44 Bending moment resistance and ratio of area related to the web slenderness, S235

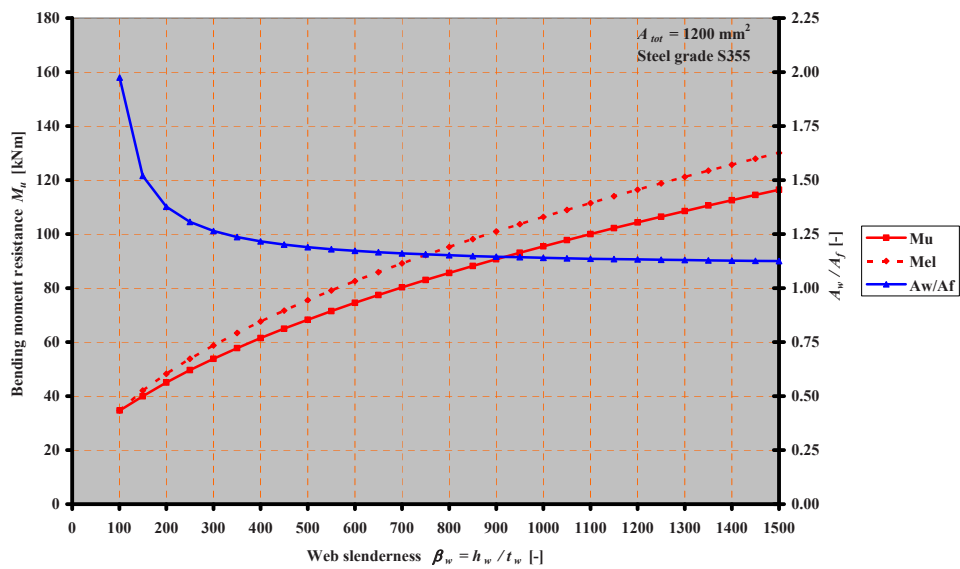


Figure 2-45 Bending moment resistance and ratio of area related to the web slenderness, S355

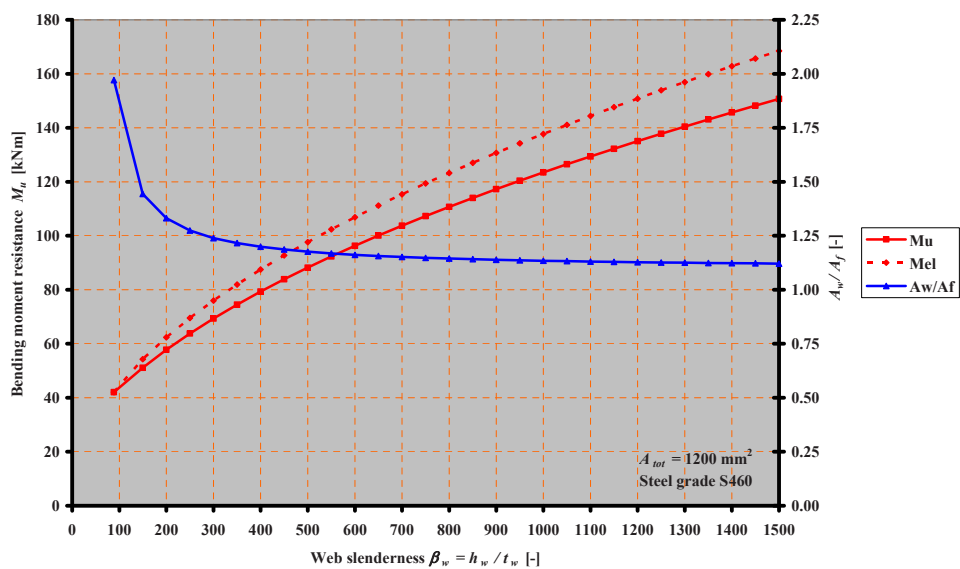


Figure 2-46 Bending moment resistance and ratio of area related to the web slenderness, S460

The ratio between the ultimate bending moment resistances M_u of steel grades S355 and S235

$$\frac{M_{u,S355}}{M_{u,S235}} \text{ and the ratio between the resistance of steel grades S460 and S235 } \frac{M_{u,S460}}{M_{u,S235}}$$

are represented by the blue lines. The ultimate bending moment resistance, based on the effective width of the web, is more or less related to the ratios between the yield strengths.

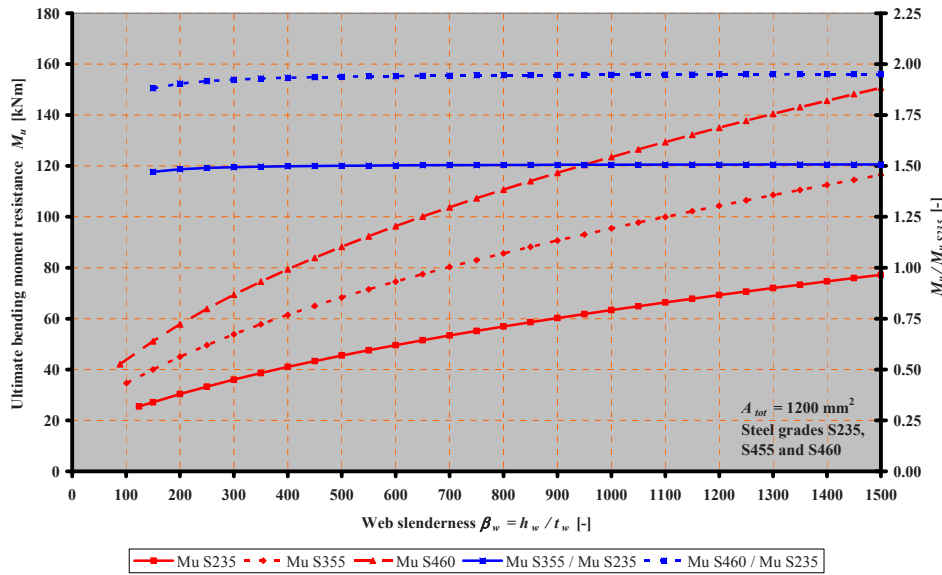


Figure 2-47 Comparison of the bending moment resistances, S235, S355 and S460

2.7.7 COMPARISON OF ULTIMATE BENDING MOMENT RESISTANCES

Basler [12], Höglund [42] and Veljkovic and Johansson [74] more or less follow the same approach to determine the ultimate bending moment resistance M_u and so it is of interest to compare the results of the elaborations. Although Herzog [41] has a different approach to determine the ultimate bending moment resistance M_u , it is of interest to compare the results of the elaboration as well. The comparison is made for steel grades S235, S355 and S460, as shown in Figure 2-48, Figure 2-49 and Figure 2-50 respectively. The tendency between the models by Basler, Höglund and Veljkovic and Johansson is the same for the three steel grades. The Basler model gives the smallest ultimate bending moment resistance M_u and the Veljkovic and Johansson model gives the highest values for all steel grades. The curves based on these models increase continuously. The Herzog [41] model is the only model with a maximum for the ultimate bending moment resistance M_u at a web slenderness of about 800 for all steel grades. For S235 the difference between the Herzog model and the other models is rather great, but for S355 and S460 the Herzog model gives more or less similar results for the ultimate bending moment resistance M_u up to a web slenderness $\beta_w \approx 500$.

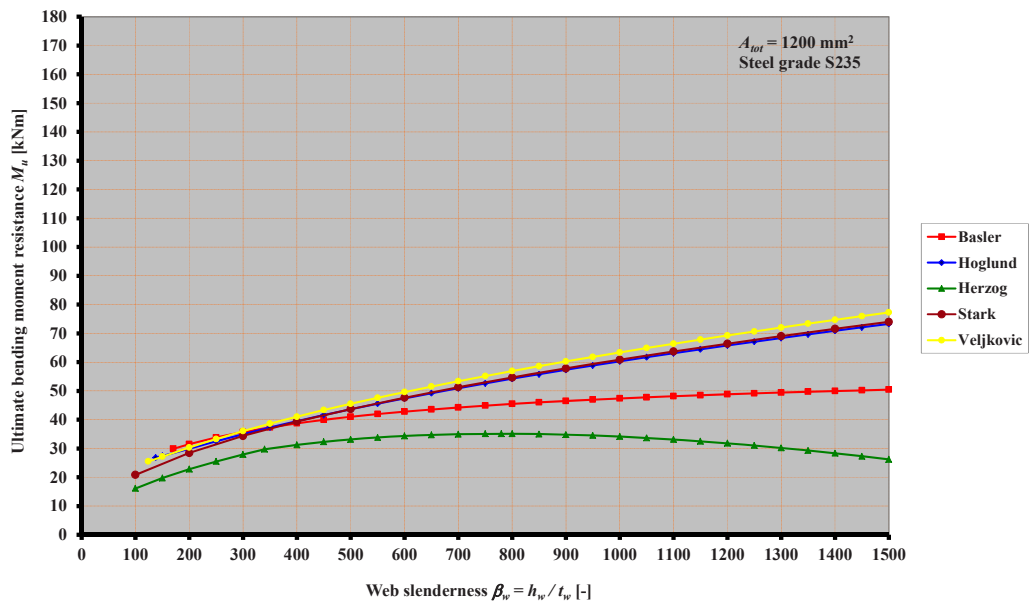


Figure 2-48 Comparison ultimate bending moment resistances based on models according to Basler, Höglund, Herzog, Stark and Veljkovic and Johansson, S235

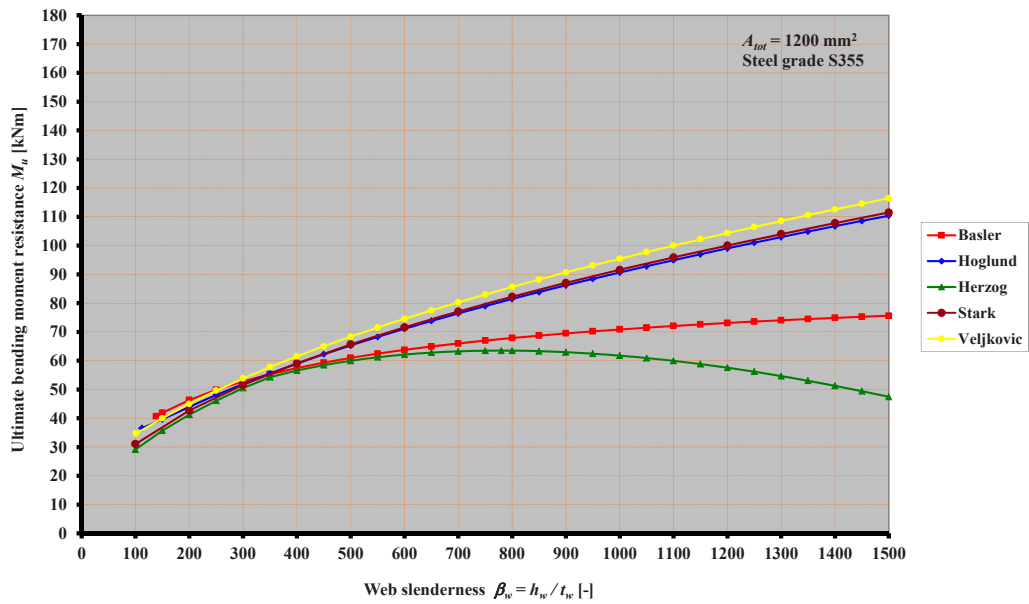


Figure 2-49 Comparison ultimate bending moment resistances based on models according to Basler, Höglund, Herzog, Stark and Veljkovic and Johansson, S355

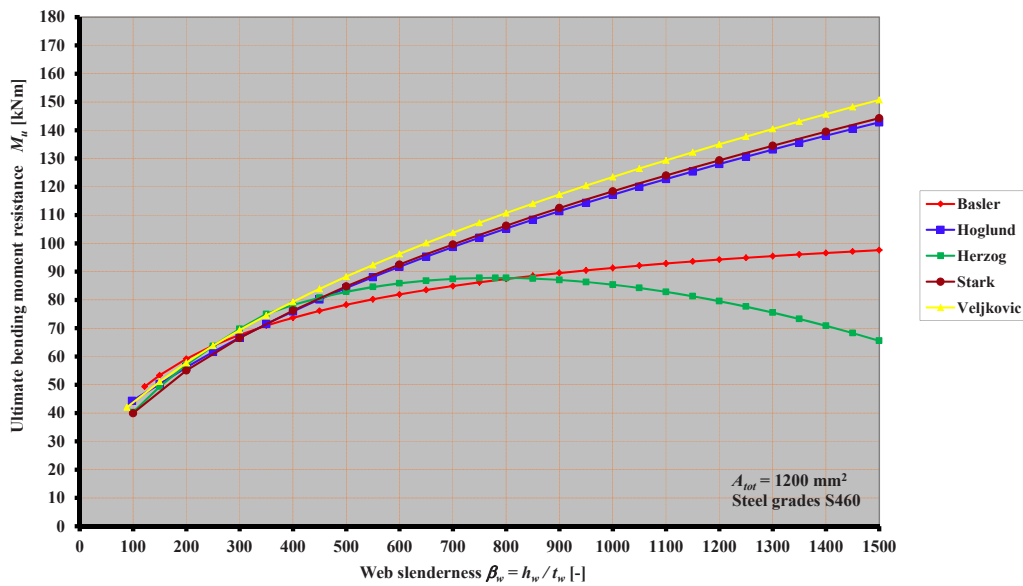


Figure 2-50 Comparison ultimate bending moment resistances based on the models according to Basler, Höglund and Veljkovic and Johansson, S460

In the elaborations given in Chapter 2.7.2 to 2.7.6, the maximum bending moment resistances are presented, based on $M_u = \xi \cdot M_{el}$ which depends on the ratio of area ρ and the maximum web slenderness $\beta_{w,max}$. The reduction factor ξ is determined based on publications of several researchers. Other values of the ratio of area ρ result in smaller bending moment resistances M_u . To prove the maximum bending moment resistance as determined in Chapter 2.7.2 to 2.7.6, additional graphs are presented in Figure 2-51, Figure 2-52 and Figure 2-53 for some specific values of the web slenderness's β_w for steel grades S235, S355 and S460 respectively, according to Veljkovic and Johansson. The web slenderness's β_w are 124ε , 300ε , 600ε , 900ε , 1200ε and 1500ε .

The highest bending moment resistances M_u are found for higher web slenderness's β_w , but for a smaller ratio of area ρ . The top of every curve of specific web slenderness's β_w , is similar to the maximum moment resistances M_u at the Veljkovic and Johansson curve of Figure 2-48 for steel grade S235, Figure 2-49 for steel grade S355 and Figure 2-50 for steel grade S460.

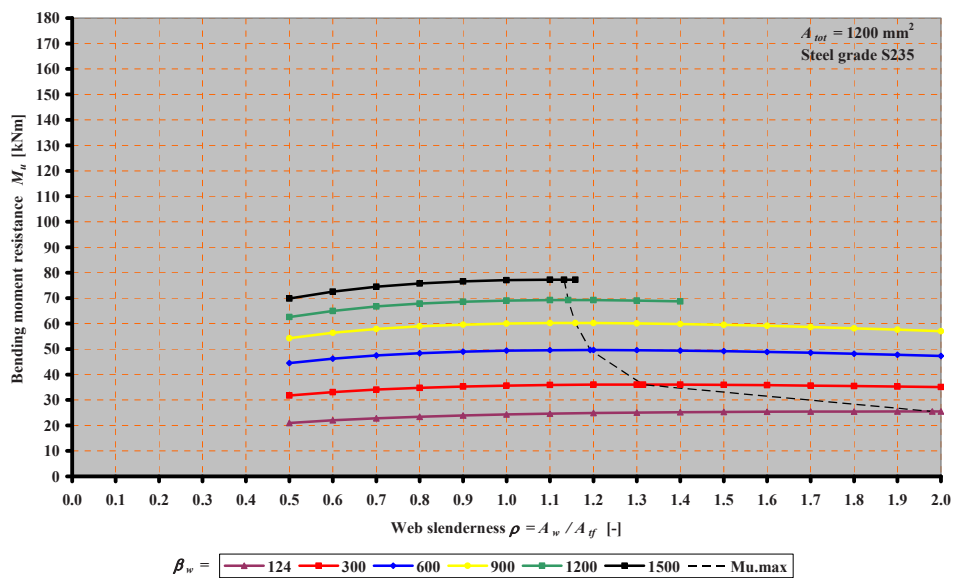


Figure 2-51 Bending moment resistance M_u dependent on the ratio of area ρ for specific web slenderness's β_w

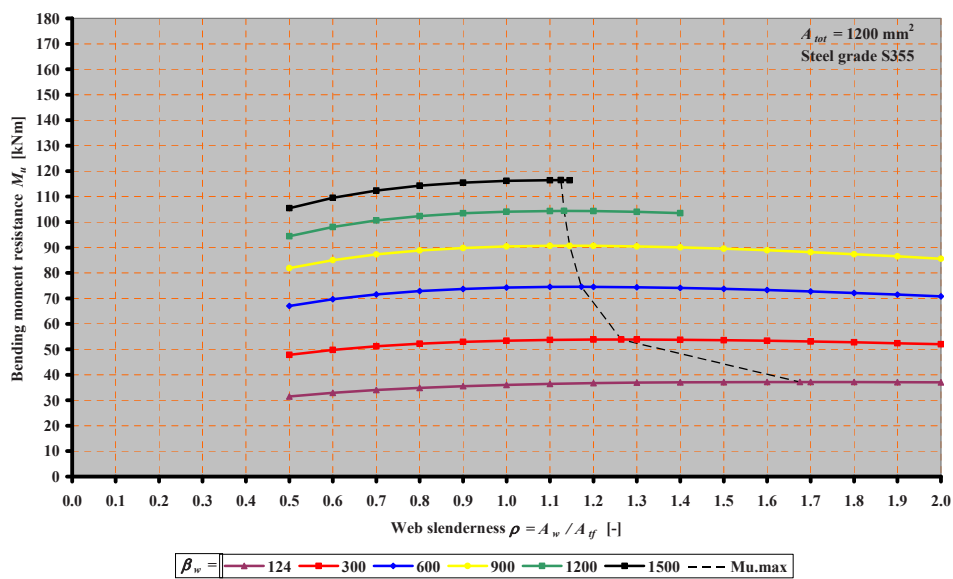


Figure 2-52 Bending moment resistance M_u dependent on the ratio of area ρ for specific web slenderness's β_w

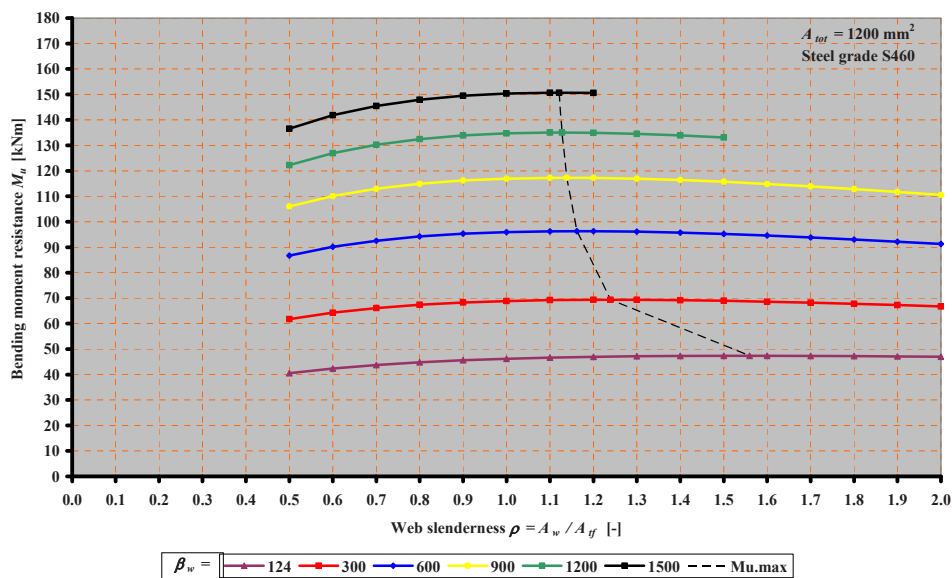


Figure 2-53 Bending moment resistance M_u dependent on the ratio of area ρ for specific web slenderness's β_w

In every graph, the maximum bending moment resistance is also represented, as well as the tops for every web slenderness, by black dotted lines. From these lines, it can be seen the ratio of area ρ decreases for higher web slenderness's.

Up to now, it is not clear which aspect determines the maximum bending moment resistance M_u , the reduction factor ξ or the elastic bending moment resistance M_{el} . For several ratios of area ρ the accompanying dimensions are presented in Table 2-7 for steel grade S235, Table 2-8 for steel grade S355 and Table 2-9 for steel grade S460.

Table 2-7 Dimensions of cross-sections, reduction factor ζ , the elastic and the ultimate bending moment resistance for steel grade S235 and $A_{tot} = 1200 \text{ mm}^2$ according to Veljkovic and Johansson

	h_w [mm]	t_w [mm]	β_w [-]	b [mm]	t_f [mm]	ρ [-]	(M_u/M_{el}) [-]	M_{el} [kNm]	M_u [kNm]
	h_w	t_w	β_w	b	t_f	ρ	(M_u/M_{el})	M_{el}	M_u
$\rho = 1.000$	346.4	1.15	300	98.0	4.08	1.000	0.941	37.87	35.65
Maximum	377.8	1.275	300	93.2	3.88	1.275	0.923	39.05	36.04
$\rho = 1.314$									
$\rho = 1.500$	392.8	1.31	300	90.7	3.78	1.500	0.912	39.41	35.95
$\rho = 1.000$	489.9	0.82	600	98.0	4.08	1.000	0.921	53.60	49.35
Maximum	518.6	0.86	600	95.0	3.96	1.193	0.905	54.78	49.60
$\rho = 1.193$									
$\rho = 1.500$	555.5	0.93	600	90.7	3.78	1.500	0.881	55.80	49.16
$\rho = 1.000$	629.3	0.67	900	98.0	4.08	1.000	0.914	65.68	60.01
Maximum	680.3	0.70	900	95.5	3.98	1.158	0.900	66.91	60.23
$\rho = 1.158$									
$\rho = 1.500$	692.8	0.76	900	90.7	3.78	1.500	0.871	68.37	59.53
$\rho = 1.000$	723.4	0.58	1200	98.0	4.08	1.000	0.910	75.86	69.05
Maximum	785.6	0.60	1200	95.7	3.99	1.142	0.898	77.16	69.26
$\rho = 1.142$									
$\rho = 1.500$	774.6	0.65	1200	90.7	3.78	1.500	0.866	78.97	68.35
$\rho = 1.000$	806.7	0.52	1500	98.0	4.08	1.000	0.908	84.82	77.04
Maximum	878.3	0.54	1500	95.9	4.00	1.132	0.896	86.20	77.24
$\rho = 1.132$									
$\rho = 1.500$	774.6	0.59	1500	90.7	3.78	1.500	0.862	88.31	76.16

Table 2-8 Dimensions of cross-sections, reduction factor ζ , the elastic and the ultimate bending moment resistance for steel grade S355 and $A_{tot} = 1200 \text{ mm}^2$ according to Veljkovic and Johansson

	h_w [mm]	t_w [mm]	β_w [-]	b [mm]	t_f [mm]	ρ [-]	(M_u/M_{el}) [-]	M_{el} [kNm]	M_u [kNm]
	h_w	t_w	β_w	b	t_f	ρ	(M_u/M_{el})	M_{el}	M_u
$\rho = 1.000$	346.4	1.15	300	88.4	4.53	1.000	0.933	57.2	53.39
Maximum	373.4	1.24	300	84.7	4.33	1.264	0.916	58.77	53.84
$\rho = 1.264$									
$\rho = 1.500$	392.8	1.31	300	81.8	4.19	1.500	0.900	59.52	53.59
$\rho = 1.000$	489.9	0.82	600	88.4	4.53	1.000	0.917	80.96	74.22
Maximum	515.8	0.74	600	85.9	4.40	1.172	0.860	82.58	74.53
$\rho = 1.172$									
$\rho = 1.500$	555.5	0.93	600	81.8	4.19	1.500	0.875	84.27	73.75
$\rho = 1.000$	600.0	0.67	900	88.4	4.53	1.000	0.911	99.20	90.39
Maximum	627.1	0.70	900	86.3	4.42	1.145	0.898	100.93	90.66
$\rho = 1.145$									
$\rho = 1.500$	680.3	0.76	900	81.8	4.19	1.500	0.867	103.26	89.51
$\rho = 1.000$	692.8	0.58	1200	88.4	4.53	1.000	0.908	114.57	104.08
Maximum	721.6	0.60	1200	86.5	4.43	1.133	0.896	116.43	104.35
$\rho = 1.133$									
$\rho = 1.500$	785.6	0.65	1200	81.8	4.19	1.500	0.863	119.27	102.89
$\rho = 1.000$	774.6	0.52	1500	88.4	4.53	1.000	0.907	128.12	116.17
Maximum	834.9	0.56	1500	84.7	4.34	1.264	0.882	131.69	116.16
$\rho = 1.264$									
$\rho = 1.500$	878.3	0.59	1500	81.8	4.19	1.500	0.860	133.38	114.72

Table 2-9 Dimensions of cross-sections, reduction factor ξ , the elastic and the ultimate bending moment resistance for steel grade S460 and $A_{tot} = 1200 \text{ mm}^2$ according to Veljkovic and Johansson

	h_w [mm]	t_w [mm]	β_v [-]	b [mm]	t_f [mm]	ρ [-]	(M_u/M_{el}) [-]	M_{el} [kNm]	M_u [kNm]
$\rho = 1.000$	346.4	1.15	300	82.8	4.83	1.000	0.935	37.87	35.42
Maximum	371.1	1.24	300	79.7	4.65	1.239	0.917	38.95	35.73
$\rho = 1.275$									
$\rho = 1.500$	392.8	1.31	300	76.7	4.47	1.500	0.903	39.41	35.58
$\rho = 1.000$	489.9	0.82	600	82.8	4.83	1.000	0.871	48.55	42.29
Maximum	514.4	0.86	600	80.7	4.70	1.162	0.835	51.23	42.80
$\rho = 1.162$									
$\rho = 1.500$	555.5	0.93	600	76.7	4.47	1.500	0.785	53.60	42.09
$\rho = 1.000$	600.0	0.67	900	82.8	4.83	1.000	0.891	48.27	42.99
Maximum	626.0	0.70	900	89.0	4.72	1.139	0.796	58.45	46.51
$\rho = 1.139$									
$\rho = 1.500$	680.3	0.76	900	76.7	4.47	1.500	0.635	65.68	41.72
$\rho = 1.000$	692.8	0.58	1200	82.8	4.83	1.000	0.846	55.75	47.14
Maximum	720.5	0.60	1200	81.1	4.73	1.128	0.772	63.30	48.84
$\rho = 1.128$									
$\rho = 1.500$	785.6	0.65	1200	76.7	4.47	1.500	0.485	75.86	36.80
$\rho = 1.000$	774.6	0.52	1500	82.8	4.83	1.000	0.801	62.33	49.90
Maximum	804.1	0.53	1500	81.2	4.73	1.121	0.755	66.80	50.45
$\rho = 1.121$									
$\rho = 1.500$	878.3	0.59	1500	76.7	4.47	1.500	0.335	84.82	28.43

From these tables it can be seen that the maximum bending moment resistance $M_u = \xi \cdot M_{el}$ is found when the product $\xi \cdot M_{el}$ is maximised.

2.8 CONCLUSIONS

From the above described literature and the elaborations, the following conclusions can be made:

1. Related to vertical buckling of the compressive flange into the web the following is concluded:

- a. Basler is the only one who derived a model to determine the maximum web slenderness based on vertical buckling of the compressive flange into the web;
- b. The model of Basler for vertical buckling of the compressive flange into the web is adopted in the EN-1993-1-5 and in the AISI 310;
- c. To fulfil the requirement that every flange fibre yields before vertical buckling of the compressive flange into the web occurs, the strain in the flange should be more than the yield strain plus the strain caused by a residual stress $\varepsilon = \frac{f_{yf} + \sigma_{res}}{E}$. For S235 Basler assumed a residual stress of $\sigma_{res} = 0.50 \cdot f_{yf}$. EN1993 does not give a pattern for residual stresses in plate girders. The previous Dutch code NEN6771 and the previous Swedish code BSK99 give patterns and both have the yield strength as maximum tensile residual stress. This means that maximum web slenderness $\beta_{w,max}$ according to Basler will decrease;
- d. For higher steel grades the residual stress σ_{res} is smaller than half of the yield stress. This means that the maximum web slenderness $\beta_{w,max}$ according to Basler will increase;
- e. The curvature κ is based on the strain as mentioned in the conclusion c and the position of the neutral axis. Basler assumed that this position is half of the height of a symmetric girder, but for a class 4 cross-section the position of the neutral axis is based on the asymmetric effective cross-section and so the position of the neutral axis shifts downwards to the tensile bottom flange. The curvature κ decreases and so the normal stress σ_n perpendicular to the flanges. The maximum web slenderness $\beta_{w,max}$ according to Basler will increase;
- f. Basler assumed that the web is simply supported by the flanges and so the column buckling length of the web is equal to the web height h_w . However, the web edges are welded to the flanges and these boundaries are actually no hinges. There will be some rotational stiffness caused by the flanges and as a result the buckling length is smaller than the web height h_w . The buckling length will be in between $0.5h_w$ and h_w and so the maximum web slenderness $\beta_{w,max}$ according to Basler will increase considerably;

- g. Basler checked the compressive stress σ_n against the Euler critical column buckling stress σ_{cr} . This is not correct because it does not take into account the geometrical and physical imperfections. This aspect influences the maximum web slenderness $\beta_{w,max}$ according to Basler negatively, so the maximum web slenderness $\beta_{w,max}$ decreases;
 - h. Vertical buckling of the compressive flange into the web according to Basler is based on Euler column buckling of the web. But next to these normal stresses σ_n in transverse direction there are stresses σ_x in longitudinal direction, caused by the bending moment in the girder. These stresses σ_x are much larger than the stresses σ_n , but are neglected completely by Basler. Basler justified this neglect by assuming that the negative influences of the compressive stresses σ_x on the Euler column buckling of the web in transverse direction will be balanced by the positive influence of the tensile stresses σ_x in the lower part of the web near the tensile flange. The check on column buckling of the web should be replaced by a check on plate buckling and taking the normal stresses σ_n and the bending stresses σ_x in longitudinal direction of the web into account. This will influence the maximum web slenderness $\beta_{w,max}$, but it is not clear beforehand if this influence is positive or negative;
2. Related to the maximum bending moment resistance M_u , based on models of different researchers, the following is concluded:
- a. The models of Basler, Höglund, Stark and Veljkovic and Johansson are all based on an effective width method;
 - b. The models by Basler, Höglund, Stark and Veljkovic and Johansson lead to continuously increasing bending moment resistances;
 - c. The model of Herzog is based on a method using a reduced stress in the compressive part of the web;
 - d. The model by Herzog leads to a maximum ultimate bending moment resistance at around $\beta_w = 800$ for all steel grades used. This is due to additional reduction factors to take additional influences into account, namely torsional buckling and vertical buckling of the compressive flange (beyond a web slenderness of $\beta_w = 340$);

- e. The model of Veljkovic and Johansson leads, for all used steel grades, S235, S355 and S460, to the highest ultimate bending moment resistance M_u ;
 - f. The models by Basler, Höglund, Stark and Veljkovic and Johansson give for S235 more or less the same results up to a slenderness of around $\beta_w = 400$;
 - g. The yield strength can be fully utilised by adaptation of the dimensions of the cross-section;
3. Related to the elaborations of the maximum bending moment resistance M_u the following is concluded:
- a. The maximum bending moment resistance is found for a maximum of the product $\xi \cdot M_{el}$;
 - b. For higher steel grades the reduction factor ξ decreases and the elastic bending moment resistance M_{el} increases;
 - c. The reduction factor ξ decreases and the elastic bending moment resistance M_{el} increases for higher ratio of area ρ for all steel grades;
 - d. The maximum bending moment resistance M_u is found for smaller ratios of area ρ when the web slenderness β_w increases.

Based on these conclusions, it is expected that the Basler model for the maximum web slenderness, based on vertical buckling of the compressive flange into the web, is rather conservative. Additional experiments are conducted to verify whether vertical buckling of the compressive flange into the web determines the ultimate bending moment resistance.

3 VALIDATION FEM-MODEL ON BASLER EXPERIMENT

3.1 GENERAL

Before FEM-models can be used to do parametric research on the behaviour of plate girders with a very slender web, these models have to be validated against test results. Because the requirements for the maximum web slenderness in EN1993-1-5 [30] and ASCI [5] are based on the results of the experiments on test specimen G4, this girder is simulated with a FEM-model.

In Chapter 2.4, all data relevant for the FEM-modelling of test specimen G4 are specified, for test T1 as well as for test T2.

3.2 MODELLING OF THE BASLER TEST SPECIMEN G4 FOR TESTS T1 AND T2

3.2.1 GEOMETRY OF THE FEM-MODEL

The FEM program Msc Marc Mentat 2005r3 is used to simulate the Basler test specimen G4. The dimensions of the web panels of the specimen G4 are presented in Figure 3-1.

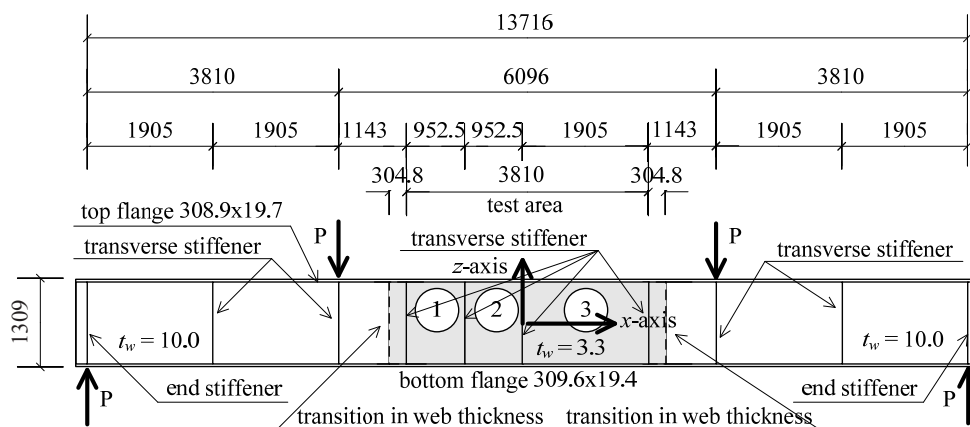


Figure 3-1 Geometry of test specimen G4 (dimensions in mm)

The FEM-model is built up with four nodes shell elements, element 75, a bilinear thick-shell element with six degrees of freedom per node, three global translations and three global rotations, which are accurate enough to simulate plate girders with a very slender web subjected to large deflections.

Another shell element with eight nodes could also be used, but because of modelling the initial imperfections of the web in the test panels by moving the nodes, it is easier to use the four nodes shell elements. The number of elements increases compared with eight nodes elements.

Test girder G4 is divided into FEM-elements as shown in Figure 3-2.

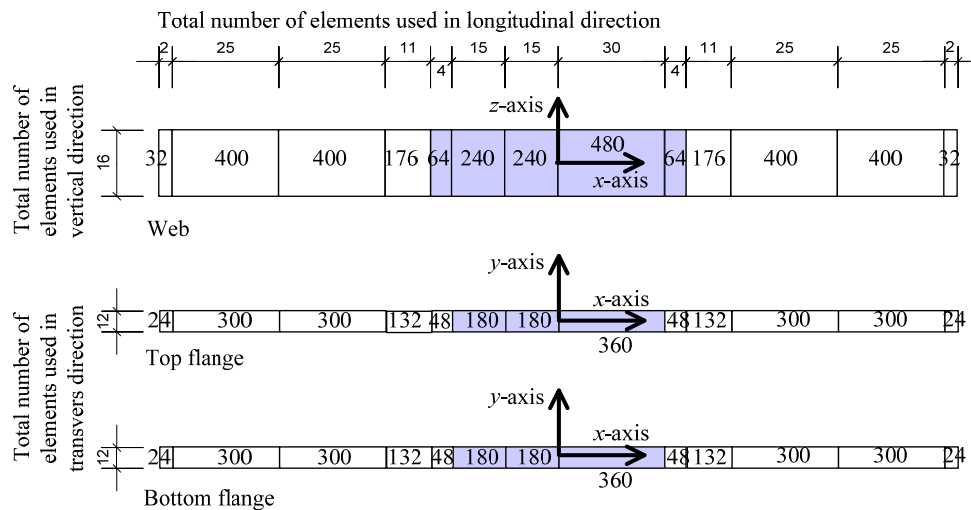


Figure 3-2 Number of elements used in the web and both flanges of test specimen G4

Later on, the number of elements is doubled to check the accuracy of this FEM-model. This will be discussed in Chapter 3.7.4.

The transverse end stiffeners at both supports, also called the bearing transverse stiffeners, are connected to the web and the tensile (bottom) flange to transfer the shear forces to the vertical supports, but are not connected to the compressive (top) flange. The intermediate transverse stiffeners are connected to the web and to the compressive (top) flange. The intermediate transverse stiffeners under the concentrated loads transfer these loads into the web, see Figure 3-3.

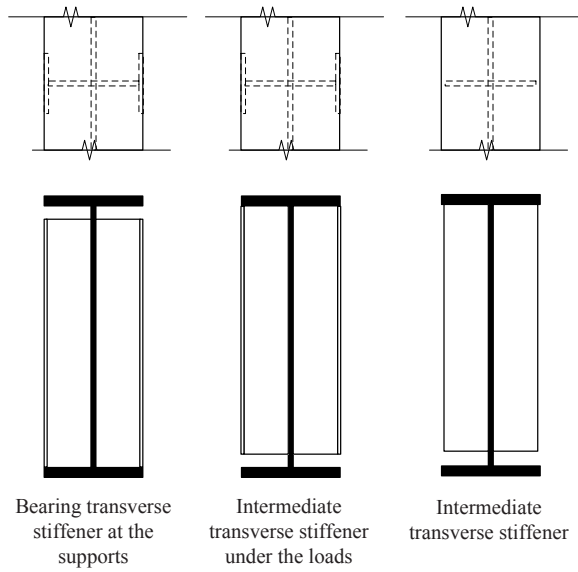


Figure 3-3 Transverse stiffeners of test specimen G4 as in the test

The x -axis is located in the centre of the web. The z -ordinates of the nodes in the centre of the top and the bottom flanges are respectively:

$$z_{top} = \frac{h_w}{2} + \frac{t_{tf}}{2} = \frac{1309 - 19.7 - 19.4}{2} + \frac{19.7}{2} = +644.8 \text{ mm} \quad (3.1)$$

$$z_{bottom} = -\frac{h_w}{2} - \frac{t_{bf}}{2} = -\frac{1309 - 19.7 - 19.4}{2} - \frac{19.4}{2} = -644.7 \text{ mm} \quad (3.2)$$

The other 15 nodes are uniformly distributed between these two nodes.

3.2.2 MATERIAL PROPERTIES USED IN THE FEM-MODEL

3.2.2.1 Yield stresses

The actual yield stresses of the material used for the web plates and both flanges in test specimen G4 are mentioned in Table 2-2 and are repeated here:

1. The yield stress of the web in the test panels 1, 2 and 3 is $f_{y.w.tp} = 299 \text{ MPa}$
2. The yield stress of the web in the other panels is $f_{y.w.ep} = 276 \text{ MPa}$
3. The yield stress of the top flange is $f_{y.tf} = 259 \text{ MPa}$
4. The yield stress of the bottom flange is $f_{y.bf} = 255 \text{ MPa}$

5. The yield strength of the stiffeners is not described by Basler, but in this analysis it is assumed to be equal to $f_{y,st} = 300 \text{ MPa}$.

3.2.2.2 Strain hardening

Basler presented only one force-strain curve for all his tests, see Figure 3-4 (earlier presented in Figure 2-11), namely for coupon CP27 as mentioned in Chapter 2.4. This coupon is taken from the top flange of test specimen G4. This specimen is of interest because of the failure mode in the second test, T2, which was vertical buckling of the compressive flange into the web.

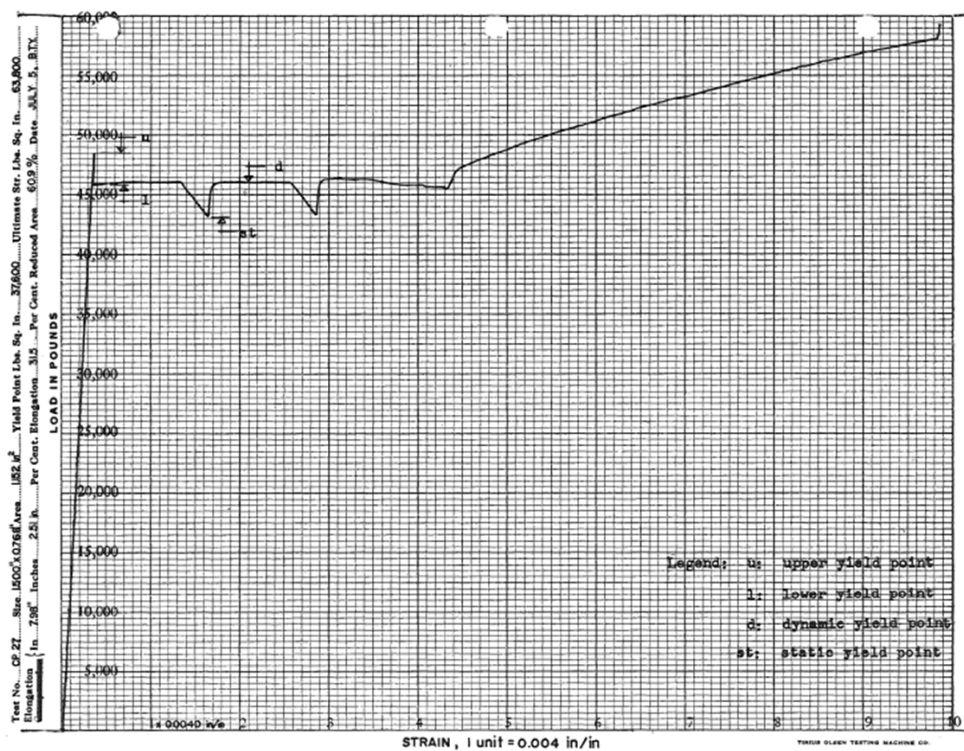


Figure 3-4 Stress – Strain curve of coupon CP27, Basler [9]

In most calculations, the engineering or the so called conventional stress-strain relationship satisfies the required accuracy, but in specific calculation cases, where large strains occur, the true stress-strain relationship is required.

The engineering strain is defined by:

$$\varepsilon_e = \frac{\ell - \ell_0}{\ell_0} \quad (3.3)$$

For such a situation, the incremental change in strain is determined by the incremental change in length divided by the length at the beginning of that increment:

$$d\varepsilon = \frac{d\ell}{\ell} \quad (3.4)$$

The total strain, the so called true strain ε_t , also called the logarithmic strain, can be determined by integration of $d\varepsilon$ from the original length ℓ_0 to the final length ℓ of the test specimen :

$$\varepsilon_t = \int_{\ell_0}^{\ell} \frac{d\ell}{\ell} = \ln \ell - \ln \ell_0 = \ln \frac{\ell}{\ell_0} \quad (3.5)$$

The engineering stress σ_e is based on the original cross-sectional area A_0 :

$$\sigma_e = \frac{P}{A_0} \quad (3.6)$$

The true stress σ_t is based on the actual cross-sectional area A at that stress level:

$$\sigma_t = \frac{P}{A} \quad (3.7)$$

After yielding of the material the initial cross-sectional area A_0 decreases, but the volume does not change and so the change in volume $dV=0$. This leads to:

$$A \cdot \ell = A_0 \cdot \ell_0 \quad (3.8)$$

Eq.(3.8) can be rewritten into:

$$\frac{\ell}{\ell_0} = \frac{A_0}{A} \quad (3.9)$$

The engineering strain ε_e is determined as follows:

$$\varepsilon_e = \frac{\Delta \ell}{\ell_0} = \frac{\ell - \ell_0}{\ell_0} = \frac{\ell}{\ell_0} - 1 \quad (3.10)$$

This results in:

$$\frac{\ell}{\ell_0} = 1 + \varepsilon_e \quad (3.11)$$

From Eq.(3.9) it follows that:

$$A = \frac{A_0 \cdot \ell_0}{\ell} \quad (3.12)$$

The relationship between the true stress σ_t and the engineering stress σ_e can be determined. First, Eq.(3.12) is substituted into Eq.(3.7):

$$\sigma_t = \frac{P}{A} = \frac{P}{A_0} \frac{\ell}{\ell_0} \quad (3.13)$$

Eq.(3.11) is substituted into Eq.(3.13):

$$\sigma_t = \frac{P}{A_0} \frac{\ell}{\ell_0} = \frac{P}{A_0} (1 + \varepsilon_e) \quad (3.14)$$

And finally, Eq. (3.6) is substituted into Eq.(3.14):

$$\sigma_t = \frac{P}{A_0} (1 + \varepsilon_e) = \sigma_e (1 + \varepsilon_e) \quad (3.15)$$

A relationship for the true strain ε_t and the engineering strain ε_e is determined by substitution of Eq.(3.11) into Eq.(3.5):

$$\varepsilon_t = \ln \frac{\ell}{\ell_0} = \ln(1 + \varepsilon_e) \quad (3.16)$$

Figure 3-5 shows the engineering stress-strain relationship, presented by Basler in Figure 3-4, based on coupon CP27. In addition, the true stress-strain relationship computed from the engineering stress-strain relationship by Basler using Eq.(3.15) and Eq.(3.16) is shown in this Figure 3-5.

As mentioned in Chapter 2.4.2.2, the static yield stress has to be used and so the stress-strain relationship as shown in Figure 3-4 is adapted, shifted downwards.

The input of this true stress-strain relationship for the FEM-model depends on the specific FEM-program. For the input of the true stress-strain relationship as presented in Figure 3-5 in a FEM-model of Msc Marc Mentat 2005 r3, the true stresses σ_t , starting from $\sigma_t = f_y$, have to be divided by the yield strength f_y and the true strains ε_t have to be transformed into plastic strains ε_{pl} as follows:

$$\bar{\sigma}_{pl} = \frac{\sigma_t}{f_y} \quad (3.17)$$

$$\varepsilon_{pl} = \varepsilon_t - \frac{\sigma_t}{E} \quad (3.18)$$

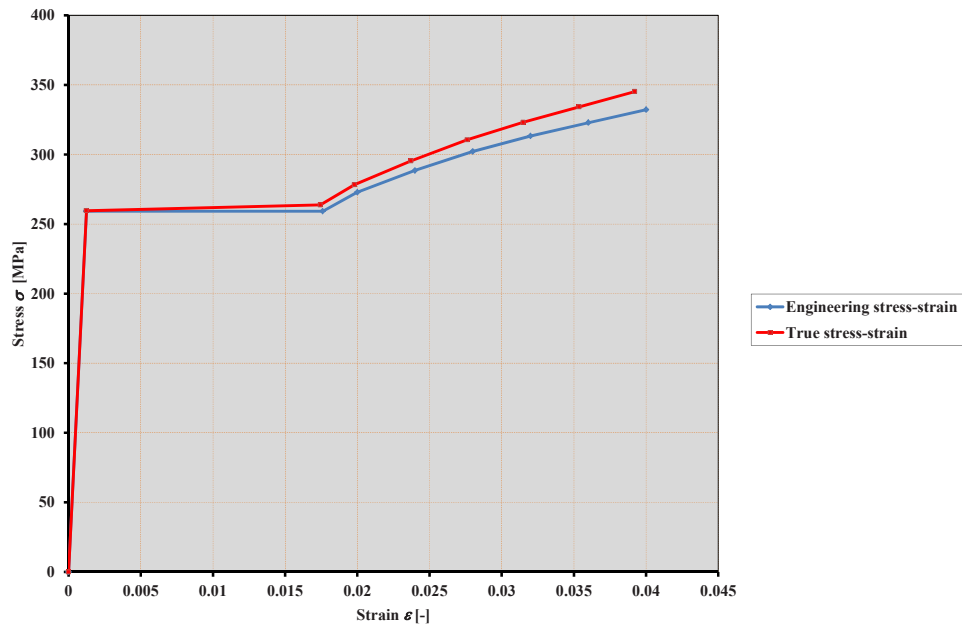


Figure 3-5 Engineering and true stress-strain relationships based on coupon CP27

The results are shown in Table 3-1.

Table 3-1 Overview of the true stress strain relationship and the stress ratio

Stress	Strain	True stress	True strain	Stress ratio	Plastic strain
σ_e	ε_e	σ_t	ε_t	$\bar{\sigma}_{pl}$	ε_p
[MPa]	[-]	[MPa]	[-]	[-]	[-]
0	0.0000	0	0		
258.9	0.0012	259.3	0.0012	<u>1.0000</u>	<u>0.0000</u>
258.9	0.0174	263.4	0.0173	<u>1.0174</u>	<u>0.0160</u>
277.5	0.0200	283.1	0.0198	<u>1.0933</u>	<u>0.0185</u>
292.3	0.0240	299.3	0.0237	<u>1.1561</u>	<u>0.0223</u>
303.1	0.0280	311.6	0.0276	<u>1.2035</u>	<u>0.0261</u>
316.3	0.0320	326.4	0.0315	<u>1.2608</u>	<u>0.0299</u>
326.4	0.0360	338.1	0.0354	<u>1.3061</u>	<u>0.0338</u>
332.6	0.0400	345.9	0.0392	<u>1.3361</u>	<u>0.0376</u>

For the FEM-model, the above determined true stress-strain relationship for the top flange is also used for the bottom flange and the web of the test panels 1, 2 and 3 and the end panels, but with the corresponding yield stresses.

The Von Mises yield surface and isotropic strain hardening have been used in the FEM-model.

3.2.3 IMPERFECTIONS USED IN THE FEM-MODEL

3.2.3.1 Geometrical (initial) imperfections

Basler [10] measured the initial imperfections of the web in the test area at specific points as shown in Figure 3-6 (the same as Figure 2-12).

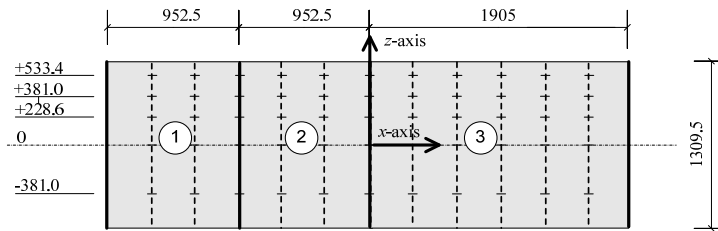


Figure 3-6 Position where the initial imperfections and the deflections of the webs are measured

This means that some of the nodes has to be shifted to the position where the imperfections were measured during the experiment, see Figure 3-7.

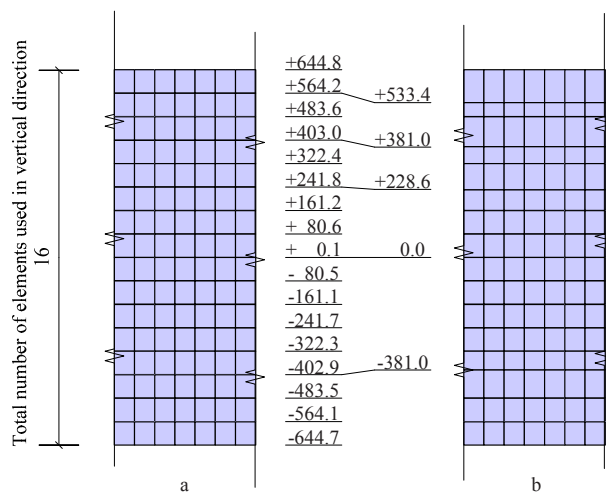


Figure 3-7 Initial z-ordinates of the nodes for the test panels 1, 2, and 3 (a) and z-ordinates after shifting (b)

The aspect ratio of an element, defined as the ratio between its largest and smallest dimension, influences the accuracy of the FEM-results and should not exceed 10, but depending on loading and boundary conditions it is preferred that the ratio should preferable not exceed 3 [22]. The length of an element of the web of the test panels in x-direction is:

$$\ell_{element} = \frac{\ell_1}{n_{x,1}} = \frac{\ell_2}{n_{x,2}} = \frac{\ell_3}{n_{x,3}} = \frac{952.5}{15} = \frac{952.5}{15} = \frac{1905}{30} = 63.5 \text{ mm} \quad (3.19)$$

The maximum height of an element of the web in z -direction is found for the top element of the web in the test panels, see Figure 3-7b:

$$h_{element,max} = 644.8 - 533.0 = 111.8 \text{ mm} \quad (3.20)$$

The maximum aspect ratio of these elements of the web is $\frac{111.8}{63.5} = 1.8$.

The minimum height of an element of the web in z -direction is found for the second element from the top of the web in the test panels, see Figure 3-7b:

$$h_{element,min} = 533.4 - 483.6 = 49.8 \text{ mm} \quad (3.21)$$

The minimum aspect ratio of these elements of the web is $\frac{63.5}{49.8} = 1.3$.

The length of a FEM-element in the flange is the same as the length of a FEM-element in the web, $\ell_{elem} = 63.5 \text{ mm}$. The width of a FEM-element in the flange depends on the width of the flanges and the number of elements used in the y -direction, $n_{elem} = 12$. The minimum width for an element in the flange, the bottom flange in the case of the Basler experiment G4, is:

$$h_{elem,min} = \frac{b_{bf}}{n_{elem}} = \frac{308.9}{12} = 25.7 \text{ mm} \quad (3.22)$$

The maximum aspect ratio for the FEM-elements in the flanges is $\frac{\ell_{elem}}{h_{elem,min}} = \frac{63.5}{25.7} = 2.5$.

3.2.3.2 Physical (initial) imperfections

The physical imperfections, the so called residual stresses, are not measured by Basler. To take the influence of the residual stresses in the x -direction of the girder into account, two models given in different codes are used, namely a model based on the previous Dutch code NEN6771 [62] and a model based on previous Swedish code BSK99 [24]. The models look similar, but there are differences. The model as given by NEN6771 is purely based on the influence of the width of the flange or the web, while the model as given by BSK99 also takes the influence of the thickness into account. The residual stresses are constant over the thickness of the flanges and the web. The used FEM-program only allows the input of a uniformly distributed initial stress. Consequently, the model uses a piece-wise constant residual stress field. A very fine element mesh over the width of

the flanges and the height of the web gives more accuracy, but because of the aspect ratio of the elements, this means that the number of elements over the span of the girder will increase enormously. It is assumed that the resulting compressive force F_r^- , based on the dimensions of the flange and the model for residual stresses, is in equilibrium with the resulting tensile force F_r^+ , within the flange, so $F_r^- = -F_r^+$. Based on these resulting forces, the initial stress distribution for the FEM-model is determined, related to the number of elements over the width of a flange. For the web the resulting residual forces, based on the compressive and tensile stresses, are determined as well and these resulting forces are in equilibrium, so $F_{r,w}^- = -F_{r,w}^+$. The height of the web h_w differs from the height of the web in the FEM-model $h_{w,FEM}$, because in the FEM-model the web height is from the centre of the top flange to the centre of the bottom flange. The heights of the FEM-elements of the web are not all equal. Because of the shift of the nodes to the location, the initial imperfections and the deflections of the web were measured by Basler. The height of the FEM-elements at the top and at the bottom of the web are not the same. Because of this, the first row of nodes at the bottom of the web in the test panels is shifted as well, the same shift as at the top of the web and so the heights of the first two rows of elements at both edges of the web are the same, which makes it easy to simulate the residual tensile stresses at the edges of the web.

Residual stresses of the FEM-model according to NEN6771

The previous Dutch code NEN6771 [62] gave a residual stress distribution for the flanges and the web of a welded girder. The residual compressive stress in a flange plate is $0.25f_y$ and the residual tensile stress is f_y , see Figure 3-8. The width of the area over which the residual tensile stresses are acting, is $0.1b$, where b is the width of the flange plate. The complete residual stress pattern can be determined based on equilibrium of that flange plate.

The lengths x_1 and x_2 are not given in the NEN6771, but are necessary to determine the resulting residual compressive and tensile force, respectively F_r^- and F_r^+ . x_1 can be determined by balancing the residual tensile stresses and the residual compressive stresses, see Figure 3-9.

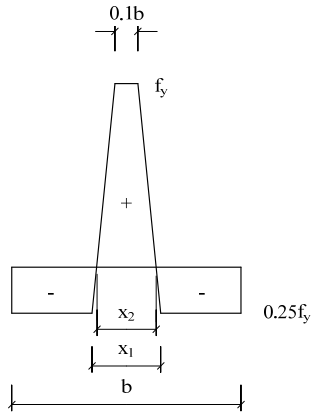


Figure 3-8 Residual stress distribution in a flange plate according to NEN6771 [62]

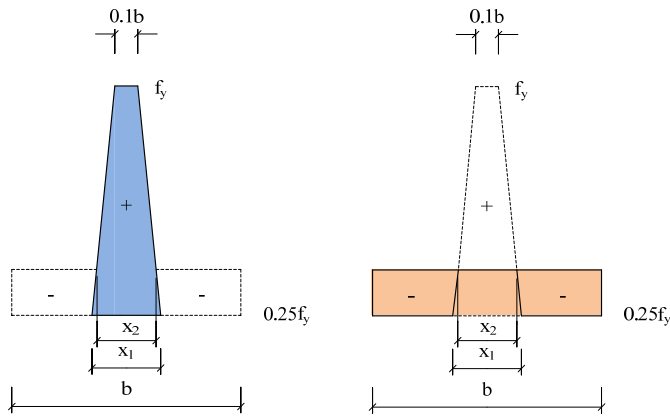


Figure 3-9 Determination of x_1 of the residual stress distribution of a flange according to NEN6771

$$\frac{(0.1b + x_1)}{2} \cdot t_f \cdot (f_y + 0.25f_y) = b \cdot t_f \cdot 0.25f_y$$

$$x_1 = \frac{2 \cdot b \cdot t_f \cdot 0.25f_y}{t_f \cdot (f_y + 0.25f_y)} - 0.1b = 0.3b \quad (3.23)$$

x_2 is determined by linear interpolation and by substitution of x_1 as determined in Eq.(3.23) :

$$\frac{x_1 - 0.1b}{1.25f_y} = \frac{x_2 - 0.1b}{f_y}$$

$$x_2 = \frac{x_1 - 0.1b}{1.25} + 0.1b = \frac{0.3b - 0.1b}{1.25} + 0.1b = 0.26b \quad (3.24)$$

The residual stress distribution according to Figure 3-8 has to be transformed into an initial stress distribution suitable for the FEM-element distribution used for the flanges. To transform the residual stress distribution into an initial stress distribution, uniformly distributed within one element, the resulting tensile force F_r^+ has to be determined:

$$F_r^+ = \frac{0.26b + 0.1b}{2} \cdot t_f \cdot f_y = 0.18 \cdot b \cdot t_f \cdot f_y \quad (3.25)$$

The resulting compressive force F_r^- is determined as well:

$$F_r^- = \frac{(b - 0.3b) + (b - 0.26b)}{2} \cdot t_f \cdot 0.25f_y = 0.18 \cdot b \cdot t_f \cdot f_y \quad (3.26)$$

For the top flange, this resulting tensile or compressive force is:

$$F_{r,tf}^+ = -F_{r,tf}^- = 0.18 \cdot b_{tf} \cdot t_{tf} \cdot f_{y,tf} = 0.18 \cdot 308.9 \cdot 19,7 \cdot 259 = 283083.3 \text{ N} \quad (3.27)$$

And for the bottom flange:

$$F_{r,bf}^+ = -F_{r,bf}^- = 0.18 \cdot b_{bf} \cdot t_{bf} \cdot f_{y,bf} = 0.18 \cdot 309.6 \cdot 19.4 \cdot 255 = 276150.1 \text{ N} \quad (3.28)$$

The number of FEM-elements in the width of the flanges is 12. The two most centrally located elements have an initial tensile stress of $\sigma_{r,f,1}^+ = c_1 \cdot f_y = f_y$ and based on the dimensions of both elements the resulting initial tensile force $F_{r,elem}^+$ of these two FEM-elements is equal to:

$$F_{r,elem}^+ = \frac{2}{12} \cdot b \cdot t_f \cdot f_y = 0.167 \cdot b \cdot t_f \cdot f_y \quad (3.29)$$

This is smaller than $F_r^+ = 0.18 \cdot b \cdot t_f \cdot f_y$ as determined with Eq.(3.25) and therefore two adjacent elements have a reduced initial tensile stress $\sigma_{r,2}^+ = c_2 \cdot f_y$:

$$\sigma_{r,f,2}^+ = c_2 \cdot f_y = \frac{(F_r^+ - F_{r,elem}^+) \cdot f_y}{2 \cdot \frac{1}{12} \cdot b \cdot t_f} = \frac{(0.18 - 0.167) \cdot b \cdot t_f \cdot f_y}{2 \cdot \frac{1}{12} \cdot b \cdot t_f} = 0.08 \cdot f_y \quad (3.30)$$

Eight elements have an initial compressive stress $\sigma_{r,1}^- = c_3 \cdot f_y$, determined as follows:

$$\sigma_{r,f,1}^- = c_3 \cdot f_y = \frac{0.18 \cdot b \cdot t_f \cdot f_y}{8 \cdot \frac{1}{12} \cdot b \cdot t_f} = 0.27 \cdot f_y \quad (3.31)$$

The compressive stress $\sigma_{r,f,1}^- = 0.27f_y$ is a little bit higher than $\sigma_c = 0.25f_y$ as given in NEN6771, due to the smaller available flange width, on which the initial stress $\sigma_{r,f,1}^-$ is acting. The initial stress distribution of both flanges is given in Figure 3-10.

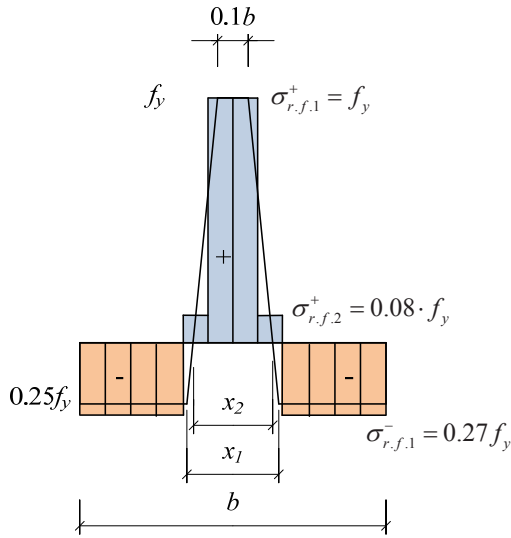


Figure 3-10 Initial stress distribution in the FEM-elements of the flanges compared with the residual stress distribution according to NEN6771

The residual stress distribution for the web is also given in NEN6771, see Figure 3-11.

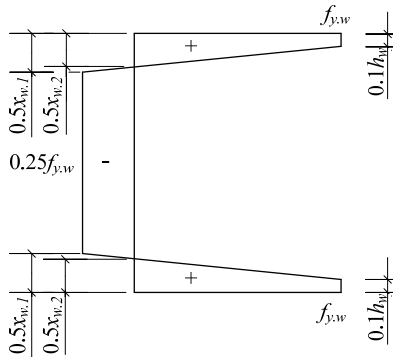


Figure 3-11 Residual stress distribution in the web according to NEN6771 [62]

In the same way as for the flanges, the value for $x_{w,1}$ can be determined, based on equilibrium:

$$2 \cdot \frac{(0.1h_w + 0.5x_{w,1})}{2} \cdot (f_{y,w} + 0.25f_{y,w}) = h_w \cdot 0.25f_{y,w}$$

$$x_{w,1} = 2 \cdot \left\{ \frac{h_w \cdot 0.25f_{y,w}}{(f_{y,w} + 0.25f_{y,w})} - 0.1h_w \right\} = 0.2h_w \quad (3.32)$$

This means that the stress distribution is rectangular and hence $x_{w,2} = x_{w,1}$.

The resulting tensile force $F_{r,w}^+$ in the web caused by the tensile residual stresses is:

$$\begin{aligned} F_{r,w}^+ &= 2 \cdot 0.1 \cdot h_w \cdot t_w \cdot f_{y,w} = 0.2 \cdot h_w \cdot t_w \cdot f_{y,w} = \\ &= 0.2 \cdot 1270 \cdot 3.3 \cdot 299 = 248844.7 \text{ N} \end{aligned} \quad (3.33)$$

And the resulting compressive force $F_{r,w}^-$ is:

$$\begin{aligned} F_{r,w}^- &= 0.8 h_w \cdot t_w \cdot 0.25 f_{y,w} = 0.2 \cdot h_w \cdot t_w \cdot f_{y,w} = \\ &= 0.2 \cdot 1270 \cdot 3.3 \cdot 299 = 248844.7 \text{ N} \end{aligned} \quad (3.34)$$

The height of the web of the FEM-model $h_{w,FEM}$ is different from the height of the web h_w of the test specimen, because of the use of shell elements. The height of the web of the FEM-model $h_{w,FEM}$ is the distance between the centres of both flanges:

$$h_{w,FEM} = h_w + \frac{t_f + t_{bf}}{2} = 1270 + \frac{19.7 + 19.4}{2} = 1289.5 \text{ mm} \quad (3.35)$$

The web in the FEM-model is divided into 16 elements in vertical direction. One element at each edge of the web has an initial tensile stress equal to the yield stress $\sigma_{r,w,1}^+ = c_{w,1} \cdot f_{y,w} = f_{y,w}$ and for the adjacent elements the initial stress has to be reduced, $\sigma_{r,w,2}^+ = c_{w,2} \cdot f_{y,w}$, based on Eq.(3.33) and the height of the FEM-element:

$$F_{r,w}^+ = 2 \cdot (644.8 - 533.4) \cdot t_w \cdot \sigma_{r,w,1}^+ + 2 \cdot (533.4 - 483.6) \cdot t_w \cdot \sigma_{r,w,2}^+ = 248844.7 \text{ N} \quad (3.36)$$

$$\sigma_{r,w,2}^+ = c_{w,2} \cdot f_{y,w} = \frac{248844.7 \cdot t_w \cdot f_{y,w} - 2 \cdot (644.8 - 533.4) \cdot t_w \cdot f_{y,w}}{2 \cdot (533.4 - 483.6) \cdot t_w} = 0.6258 \cdot f_{y,w} \quad (3.37)$$

Because of the tensile residual stresses at the top and bottom in the web, it is preferable that the first two rows of elements at the bottom of the web has the same dimensions as the first two rows of elements at the top of the web. This means that the second row of nodes at the bottom part of the web also has to be shifted, see Figure 3-12.

There are 12 elements available for the initial compressive stress in the web. The average initial compressive stress $\sigma_{r,w,1}^- = c_{w,3} \cdot f_{y,w}$ for these 12 elements is:

$$F_{r,w}^- = \Delta h_{w,FEM} \cdot t_w \cdot \sigma_{r,w,1}^- = 0.2 \cdot h_w \cdot t_w \cdot f_{y,w}$$

$$\sigma_{r,1}^- = c_{w,3} \cdot f_{y,w} = \frac{0.2 \cdot h_w \cdot t_w \cdot f_{y,w}}{\Delta h_{w,FEM} \cdot t_w} = \frac{0.2 \cdot 1270}{\{483.6 - (483.5)\}} \cdot f_{y,w} = 0.2626 \cdot f_{y,w} \quad (3.38)$$

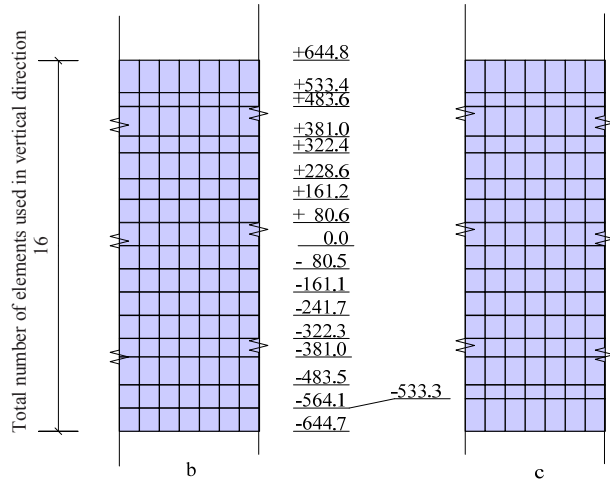


Figure 3-12 z-ordinate of the nodes for test panels 1, 2, and 3 (b) and z-ordinate after shifting (c)

The given residual stress distribution in the code and the initial stress distribution are shown in Figure 3-13. There, it can be seen that there are some differences in the required residual stress distribution according to the code and the initial stress distribution of the web of the FEM-model. With a finer FEM-element mesh it is easier to model the residual stress distribution according to NEN6771, but it takes many more elements in the height of the web as well as in the longitudinal direction. It is expected that the influence on the results of the FEM-model is small.

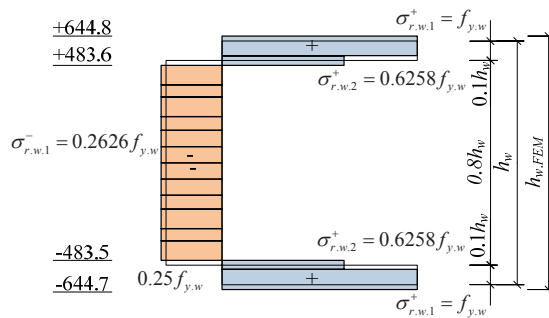


Figure 3-13 Initial stress distribution in the FEM-elements of the web compared with the residual stress distribution according to NEN6771

Residual stresses of the FEM-model according to BSK99

Besides to this residual stress distribution according to the previous Dutch code NEN6771, the previous Swedish code BSK99 [24] gave another residual stress distribution, see Figure 3-14, and it is of interest to look at the differences of the results of the FEM-models with those distributions, compared with the results of the laboratory test specimen G4. This residual stress distribution based on BSK99 looks like the distribution according to NEN6771, but there are differences. The width of the area the tensile residual stress is working on is given, $x_1 = 3t_f$, however, not related to the width b of the flange, but related to the flange thickness t_f . The residual compressive stress σ_c had to be determined, this in contradiction to the distribution according to NEN6771 in which this stress was given $\sigma_c = 0.25f_y$.

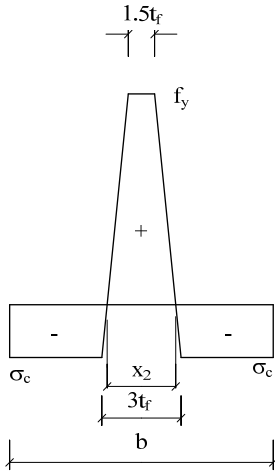


Figure 3-14 Residual stress distribution in a flange plate according to BSK99 [24]

In this residual stress distribution, the compressive residual stress σ_c is not known and has to be determined by balancing the resulting forces caused by the compressive and the tensile residual stresses. Equilibrium is found with:

$$\frac{(1.5t_f + 3.0t_f)}{2} \cdot (f_y + \sigma_c) \cdot t_f = b \cdot t_f \cdot \sigma_c$$

And thus:

$$\sigma_c = \frac{2.25 \cdot t_f \cdot f_y}{b - 2.25 \cdot t_f} \quad (3.39)$$

To compare this compressive residual stress σ_c with the compressive residual stress $0.25f_y$ based on the residual stress distribution given by NEN6771, the actual dimensions of the top flange and the bottom flange have to be used. The compressive stress $\sigma_{c.tf}$ of the top flange is:

$$\sigma_{c.tf} = \frac{2.25 \cdot t_{tf} \cdot f_{y.tf}}{b_{tf} - 2.25 \cdot t_{tf}} = \frac{2.25 \cdot 19.7 \cdot f_{y.tf}}{308.9 - 2.25 \cdot 19.7} = 0.1675 f_{y.tf} \quad (3.40)$$

And for the bottom flange:

$$\sigma_{c.bf} = \frac{2.25 \cdot t_{bf} \cdot f_{y.bf}}{b_{bf} - 2.25 \cdot t_{bf}} = \frac{2.25 \cdot 19.4 \cdot f_{y.bf}}{309.6 - 2.25 \cdot 19.4} = 0.1641 f_{y.bf} \quad (3.41)$$

The residual compressive stress according to BSK99 is about 65% of the residual compressive stress $\sigma_c = 0.25 \cdot f_y$ according to NEN6771, both for the top flange and for the bottom flange.

The distance x_2 has to be determined and so the resulting compressive and tensile force, respectively F_r^- and F_r^+ :

$$\begin{aligned} \frac{3t_f - 1.5t_f}{f_y + \sigma_c} &= \frac{x_2 - 1.5t_f}{f_y} \\ x_2 &= \frac{(3t_f - 1.5t_f) \cdot f_y}{f_y + \sigma_c} + 1.5t_f = \frac{1.5t_f \cdot \cancel{f_y}}{\cancel{f_y} + \frac{2.25 \cdot t_f \cdot \cancel{f_y}}{b - 2.25 \cdot t_f}} + 1.5t_f = \left\{ \frac{(b - 2.25 \cdot t_f)}{b} + 1 \right\} \cdot 1.5t_f = \\ &= \left\{ \frac{(2b - 2.25 \cdot t_f)}{b} \right\} \cdot 1.5t_f = \left(3b - \frac{27}{8} \cdot t_f \right) \frac{t_f}{b} \end{aligned} \quad (3.42)$$

The resulting force F_r^+ is:

$$\begin{aligned} F_r^+ &= \frac{x_2 + 1.5t_f}{2} \cdot t_f \cdot f_y = \frac{\left(3b - \frac{27}{8} \cdot t_f \right) \frac{t_f}{b} + 1.5t_f}{2} \cdot t_f \cdot f_y = \\ &= \left(2.25b - \frac{27}{16} \cdot t_f \right) \cdot \frac{t_f^2}{b} \cdot f_y \end{aligned} \quad (3.43)$$

From this F_r^+ , the actual residual stresses in the FEM-elements of the top and bottom flange can be determined, see Figure 3-15.

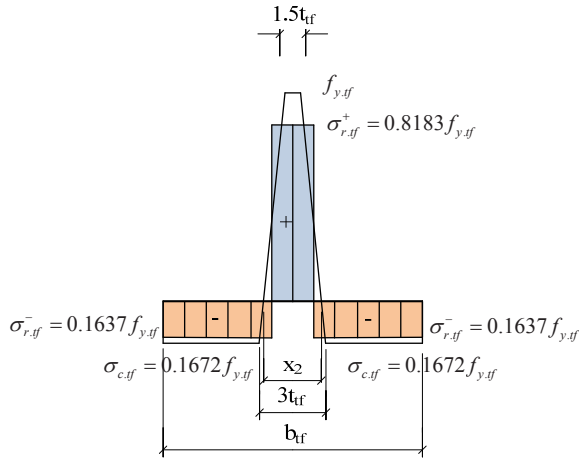


Figure 3-15 Initial stress distribution in the FEM-elements of the top flange compared with the residual stress distribution according to BSK99

The elements of the top flange have a width of $h_{elem,tf} = \frac{308.9}{12} = 25.7 \text{ mm}$. $F_{r,tf}^+$ is determined with:

$$F_{r,tf}^+ = \left(2.25b_{tf} - \frac{27}{16} \cdot t_{tf} \right) \cdot \frac{t_{tf}^2}{b_{tf}} \cdot f_{y,tf} =$$

$$= \left(2.25 \cdot 308.9 - \frac{27}{16} \cdot 19.7 \right) \cdot \frac{19.6^2}{308.9} \cdot 259 = 214480.5 \text{ N} \quad (3.44)$$

The initial tensile stress $\sigma_{r,tf}^+$ in the two FEM-elements in the centre of the top flange is:

$$\sigma_{r,tf}^+ = c_1 \cdot f_{y,tf} = \frac{F_{r,tf}^+}{2 \cdot h_{elem,tf} \cdot t_{tf}} = \frac{214480.5}{2 \cdot 25.7 \cdot 19.7} = 0.8183 \cdot 259 = 211.9 \text{ N / mm}^2 \quad (3.45)$$

This is smaller than the yield stress $f_{y,tf}$ because of the width $h_{elem,tf}$ of the elements in the top flange.

The compressive initial stress, $\sigma_{r,tf}^-$, is determined by:

$$\sigma_{r,tf}^- = c_2 \cdot f_{y,tf} = \frac{F_{r,tf}^+}{10 \cdot h_{elem,tf} \cdot t_{tf}} = \frac{214480.5}{10 \cdot 25.7 \cdot 19.7} = 0.1637 \cdot 259 = 42.4 \text{ N / mm}^2 \quad (3.46)$$

This stress $\sigma_{r,tf}^-$ is slightly smaller than $\sigma_{c,tf} = \sigma_c$ based on Eq.(3.39):

$$\sigma_{c,tf} = \frac{2.25 \cdot t_{tf} \cdot f_{y,tf}}{b - 2.25 \cdot t_{tf}} = \frac{2.25 \cdot 19.7 \cdot 259}{308.9 - 2.25 \cdot 19.7} = 0.1672 \cdot 259 = 43.3 \text{ N / mm}^2 \quad (3.47)$$

This difference is caused by the available area for compressive and tensile initial stresses, based on the dimensions of the FEM-elements. The same procedure can be followed for the bottom flange.

The elements of the bottom flange have a width of $h_{elem.bf} = \frac{309.6}{12} = 25.8 \text{ mm}$. The resulting tensile force $F_{r.bf}^+$, based on the residual stresses, is determined with:

$$F_{r.bf}^+ = \left(2.25b_{bf} - \frac{27}{16} \cdot t_{bf} \right) \cdot \frac{t_{bf}^2}{b_{bf}} \cdot f_{y.bf} =$$

$$= \left(2.25 \cdot 309.6 - \frac{27}{16} \cdot 19.4 \right) \cdot \frac{19.4^2}{309.6} \cdot 255 = 206431.2 \text{ N} \quad (3.48)$$

The tensile initial stress $\sigma_{r.bf}^+$ in the two elements in the centre of the bottom flange is:

$$\sigma_{r.bf}^+ = c_1 \cdot f_{y.bf} = \frac{F_{r.bf}^+}{2 \cdot h_{elem.bf} \cdot t_{bf}} = \frac{206431.2}{2 \cdot 25.8 \cdot 19.4} = 0.8073 \cdot 255 = 205.9 \text{ N/mm}^2 \quad (3.49)$$

The compressive initial stress $\sigma_{r.bf}^-$ is determined by:

$$\sigma_{r.bf}^- = c_2 \cdot f_{y.bf} = \frac{F_{r.bf}^+}{10 \cdot h_{elem.bf} \cdot t_{bf}} = \frac{206431.2}{10 \cdot 25.8 \cdot 19.4} = 0.1615 \cdot 255 = 41.2 \text{ N/mm}^2 \quad (3.50)$$

This stress $\sigma_{r.bf}^-$ is smaller than the residual stress $\sigma_c = \sigma_{c.bf}$ according to BSK99, see Eq.(3.39):

$$\sigma_{c.bf} = \frac{2.25 \cdot t_{bf} \cdot f_{y.bf}}{b_{bf} - 2.25 \cdot t_{bf}} = \frac{2.25 \cdot 19.4 \cdot 255}{309.6 - 2.25 \cdot 19.4} = 0.1644 \cdot 255 = 41.9 \text{ N/mm}^2 \quad (3.51)$$

This difference is caused by the area available for compressive and tensile initial stresses. Figure 3-16 shows the initial stress distribution for the FEM-model and the residual stress distribution.

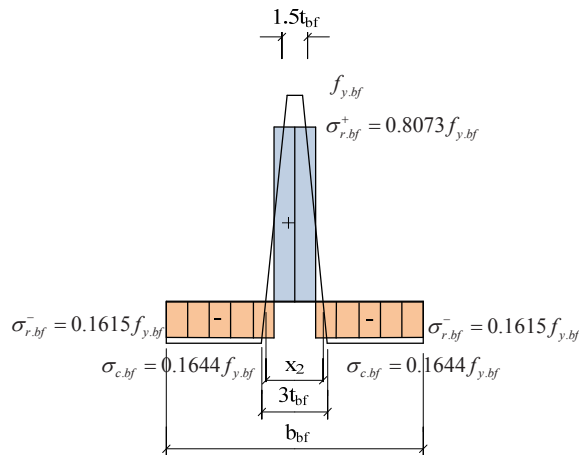


Figure 3-16 Initial stress distribution in the FEM-elements of the bottom flange representing the residual stress distribution according to BSK99

For the web, the same procedure is used to determine the initial stresses in each element of the web in the test panels 1, 2 and 3, see Figure 3-17.

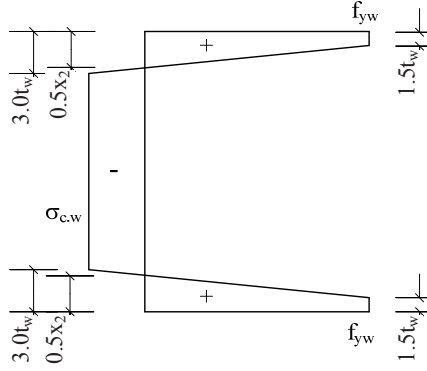


Figure 3-17 Residual stress distribution in the web according to BSK99

From equilibrium, the compressive stress $\sigma_{c,w}$ of the web is found:

$$\cancel{2} \cdot \frac{(1.5t_w + 3.0t_w)}{\cancel{2}} \cdot (f_{y,w} + \sigma_{c,w}) \cdot \cancel{t_w} = b \cdot \cancel{t_w} \cdot \sigma_{c,w}$$

$$\sigma_{c,w} = \frac{4.5 \cdot t_w \cdot f_{y,w}}{b - 4.5 \cdot t_w} \quad (3.52)$$

For the actual dimensions and actual yield strength this results in:

$$\sigma_{c,w} = \frac{4.5 \cdot t_w \cdot f_{y,w}}{b - 4.5 \cdot t_w} = \frac{4.5 \cdot 3.3 \cdot 299}{1270 - 4.5 \cdot 3.3} = 0.0117 \cdot 299 = 3.5 \text{ N/mm}^2 \quad (3.53)$$

The distance $x_{2,w}$ is determined:

$$\frac{(3.0 \cdot t_w - 1.5 \cdot t_w) \cdot f_{y,w}}{f_{y,w} + \sigma_{c,w}} = \frac{(0.5x_{2,w} - 1.5 \cdot t_w) \cdot f_{y,w}}{f_{y,w}}$$

$$x_{2,w} = 2 \cdot \left(\frac{1.5t_w \cdot f_{y,w}}{f_{y,w} + \sigma_{c,w}} + 1.5t_w \right) = 2 \cdot \left(\frac{1.5 \cdot 3.3 \cdot 255}{255 + 3.5} + 1.5 \cdot 3.3 \right) = 19.5 \text{ mm} \quad (3.54)$$

The resulting force $F_{r,w}^+$ is:

$$F_{r,w}^+ = 2 \cdot \frac{\frac{x_{2,w}}{2} + 1.5 \cdot t_w}{2} \cdot t_w \cdot f_{y,w} = 2 \cdot \frac{\frac{19.5}{2} + 1.5 \cdot 3.3}{2} \cdot 3.3 \cdot 299 = 14389.5 \text{ N} \quad (3.55)$$

This is a considerable reduction of 94% compared with $F_{r,w}^+$ based on NEN6771 [62], see (3.33).

The two elements located at the edges of the web have an initial tensile stress $\sigma_{r,w}^+ = c_{w,1} \cdot f_{y,w}$ equal to:

$$\sigma_{r,w}^+ = c_{w,1} \cdot f_{y,w} = \frac{F_{r,w}^+}{2 \cdot h_{elem,1} \cdot t_w} = \frac{14389.5}{2 \cdot (644.8 - 533.4) \cdot 3.3} = 0.0659 f_{y,w} = 19.7 \text{ MPa} \quad (3.56)$$

The compressive residual stress $\sigma_{r,w}^- = c_{w,2} \cdot f_{y,w}$ is:

$$\sigma_{r,w}^- = c_{w,2} \cdot f_{y,w} = \frac{F_{r,w}^+}{(h_{w,FEM} - 2h_{elem,1}) \cdot t_w} = \frac{14389.5}{(1289.5 - 2 \cdot 111.4) \cdot 3.3} = 0.0138 f_{y,w} = 4.1 \text{ MPa} \quad (3.57)$$

These initial stress distribution is compared with the residual stress distribution according to BSK99 as shown in Figure 3-18. Because of the dimensions of the elements, the stresses are different from the residual stress distribution.

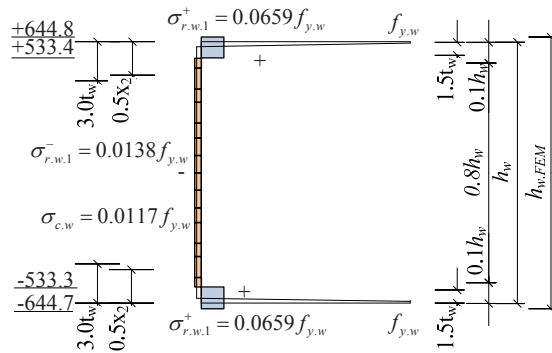


Figure 3-18 Initial stress distribution in the FEM-elements of the web representing the residual stress distribution according to BSK99

3.3 ACCURACY RELATED TO THE NUMBER OF ELEMENTS

The number of elements influences the accuracy of the results of the FEM-models. To check this accuracy, the number of elements for the FEM-model for test specimen G4-T2 with residual stresses according to BSK99 is doubled in horizontal as well as in vertical direction. Figure 3-19 shows

the P - δ diagrams for the model with the initial number of elements, denoted FEM1, and the model with four times the number of elements, FEM4. For each model there are shown two P - δ diagrams, namely for one node at the top of the web and one node at the bottom of the web, both at midspan. From these P - δ diagrams, it is concluded that the mesh is accurate to simulate test specimen G4.

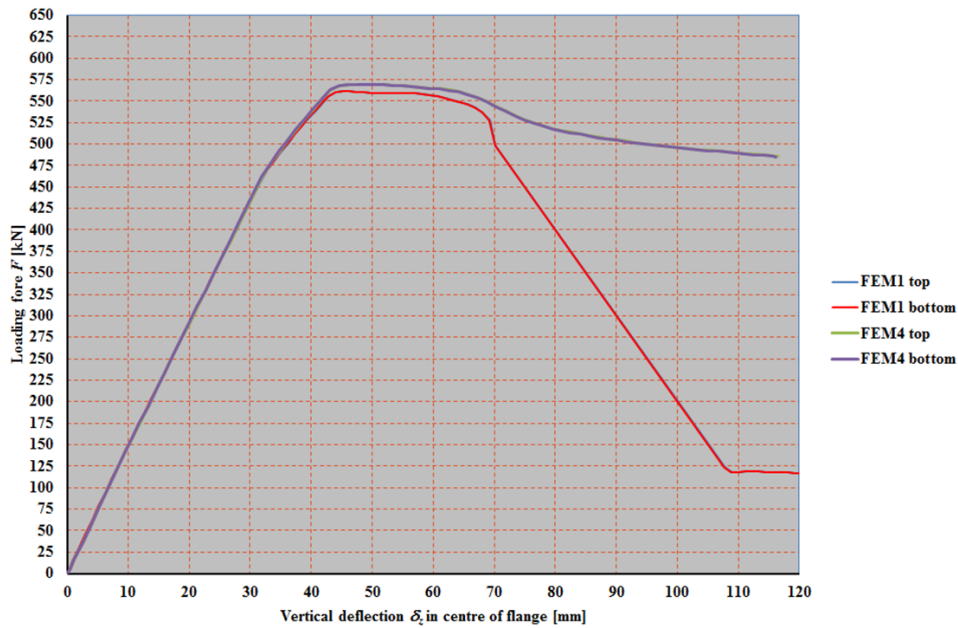


Figure 3-19 Comparison FEM-results of models with 5432 (FEM1) and 21728 (FEM4) elements

3.4 SOLUTION PROCEDURES FOR NONLINEAR SYSTEMS

One of the results of the FEM calculation, but also the laboratory test, is a so-called equilibrium path, a P - δ diagram, see the exact paths in Figure 3-20 up to Figure 3-23. At the horizontal axis, the deflections δ are presented and at the vertical axis the load P . Each point at this equilibrium path represents an equilibrium configuration. The reference state, most of the time the unstressed state, in the case that the residual stresses are not taken into account, and undeformed configuration, is the origin of the diagram.

The upgoing path is called the fundamental or primary path, up to a critical point. This critical point is caused by instability and another path, the secondary path, starts where the load decreases while the deflections increase or decrease. Most of the time, the first part of the primary path for this type of structures, is linear, but later on the behaviour is non-linear as a result of geometrical and physical nonlinearities influenced by geometrical imperfections, the initial imperfections, and physical imperfections, the residual stresses. Several types of several points can be considered, namely:

1. Limit points, points at which the tangent is horizontal;
2. Bifurcation points, points where two or more equilibrium paths cross;
3. Turning points, points where the tangent is vertical;
4. Failure points, points where the path suddenly stops because of physical failure.

The structural element behaves in different ways at these specific points, namely snap-through for limit points and snap-back for turning points. This means that at some deflections there is equilibrium for at least one or more loads, as opposed to linear behaviour. To find critical points for stability analysis as for the plate girders with a very slender web, non-linear finite element analysis has to be executed. The P - δ diagram is found using an incremental iterative solution scheme. The global equilibrium equations are discretized as follows:

$$\{R^{res}\} = \{R^{ext}\} - \{R^{int}\} = \{0\} \quad (3.58)$$

Where, $\{R^{ext}\}$ and $\{R^{int}\}$ are the sum of externally applied loads, respectively the sum of internal element nodal forces. For equilibrium, the sum of the residual forces has to be zero $\{R^{res}\} = \{0\}$, the sum of externally applied loads and the sum of internal element nodal forces are balanced.

The FEM-model has to be such that the sum of the residual forces is acceptably small. An incremental method is used and later on the basic incremental method is improved, especially focused on the speed. The solution error, the difference between the exact results and the FEM results, cumulates for a pure incremental scheme without iterations. To reduce this solution error a large number of small incremental steps has to be realised, which is inefficient.

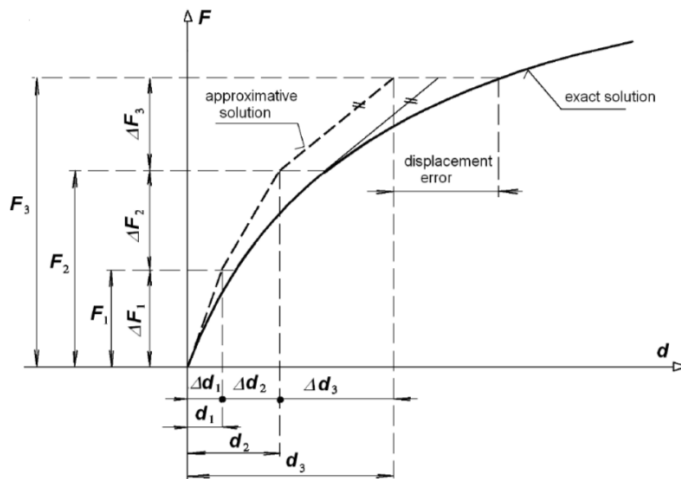


Figure 3-20 Incremental iterative solution [Ivanco (2011)]

The Standard Newton-Raphson method and Modified Newton-Raphson method are methods to improve the speed and are commonly used in FEM-calculations, see for these methods Figure 3-21 and Figure 3-22. In the Standard Newton-Raphson method the stiffness matrix is formed every cycle, while in the Modified Newton-Rahson method this is only updated every increment. The number of iterations increases, but without forming a new stiffness matrix.

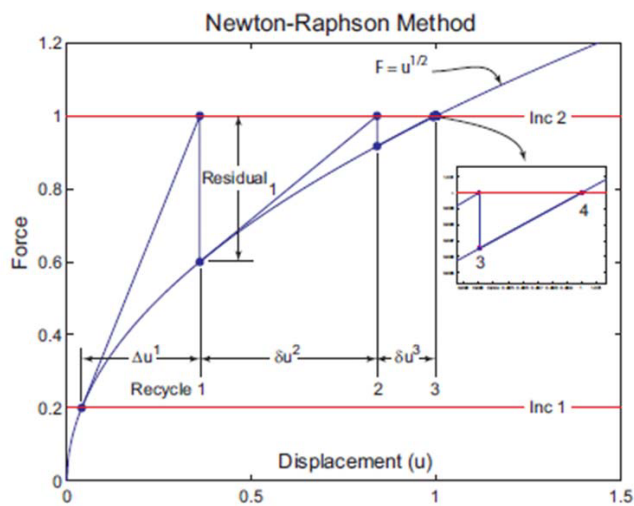


Figure 3-21 Standard Newton-Raphson iterations [57]

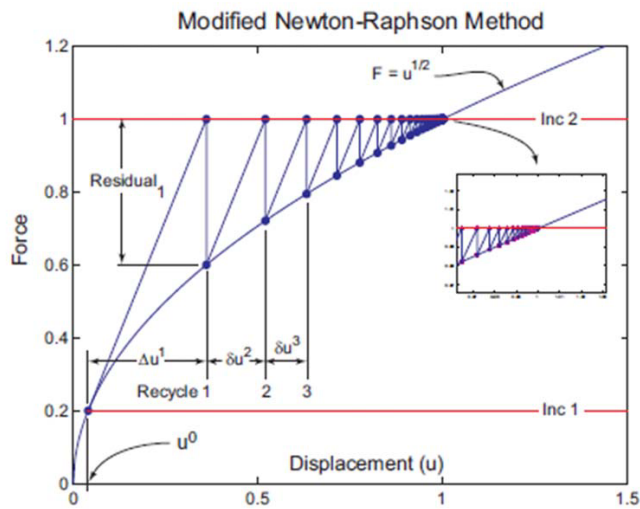


Figure 3-22 Modified Newton-Raphson iterations [57]

A load controlled problem will jump from a limit point in horizontal direction to a next point on the P - δ diagram where the load increases. Snap-through and snap-back will be neglected, when above methods are used. For a displacement controlled problem, the solution jumps in vertical direction and snap-back is neglected.

Nowadays, the Arc-Length method is used. Besides, incremental steps, cycles are used to iterate to an accurate solution. By using the Arc-Length method, these disadvantages are avoided by using the combination of incremental control strategy. Displacement and load increments are controlled simultaneously, see Figure 3-23.

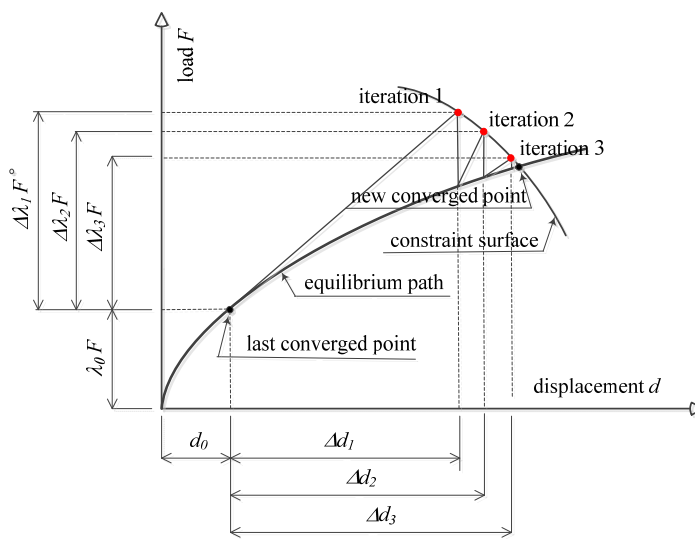


Figure 3-23 The Arc-length method [22]

Related to the Arc-Length, several methods have been developed. For the FEM-models in this thesis the solution method by Crisfield is used. The solution procedure is shown in Figure 3-24.

As mentioned, the sum of the residual force has to be acceptable small, the relative residual force, moments and displacements have to be smaller than 0.05.

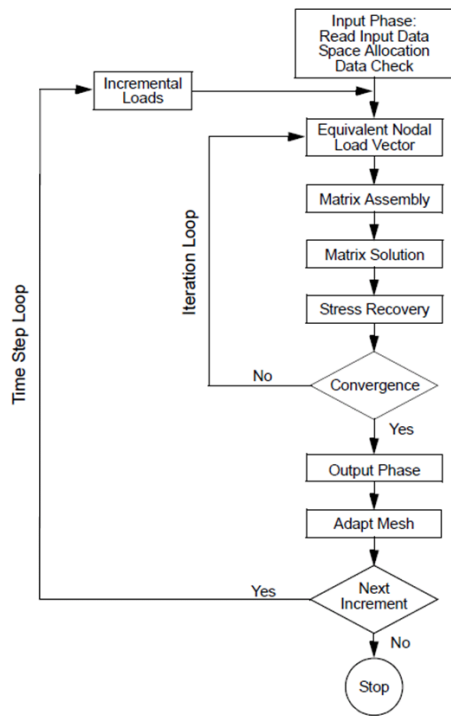


Figure 3-24 Marc flow diagram [57]

3.5 THEORETICAL BENDING MOMENT RESISTANCES OF TEST SPECIMEN G4

3.5.1 GENERAL

The theoretical bending moment resistances are determined based on actual dimensions and actual material properties as described in EN1993-1-5 [30].

The following bending moment resistances are of interest to compare with the bending moment resistance of the experiments:

1. Based on the gross cross-section:
 - a. The critical bending moment resistance M_{cr} , based on the critical stress and the elastic section modulus $M_{cr} = \sigma_{cr} \cdot W_{el}$;
 - b. The elastic bending moment resistance M_{el} , based on the yield stress and the elastic section modulus $M_{el} = f_y \cdot W_{el}$;

- c. The plastic bending moment resistance M_{pl} , based on the yield stress and the plastic section modulus $M_{pl} = f_y \cdot W_{pl}$;
2. Based on a reduced cross-section:
 - a. The bending moment based on the cross-section consisting of the flanges only M_{fl} , based on the yield stress, the area of the flange and the level arm in-between both flanges $M_{pl} = f_y \cdot A_f \cdot (h - t_f)$;
 - b. The effective bending moment resistance M_{eff} , based on the yield stress and the effective section modulus $M_{eff} = f_y \cdot W_{eff}$.

The determination of the bending moment resistances is slightly more complicated, because of the actual yield stresses of the flanges and the web and the actual dimensions. This will be described later on. The critical bending moment resistance M_{cr} and the effective bending moment resistance M_{eff} are based on plate buckling. The effective bending moment resistance M_{eff} is based on the effective width method. The determination of the effective bending moment resistance M_{eff} has to be determined by iterative calculations based on the cross-sections and stress distributions as shown in Figure 3-25. This is caused by changing of the position of the neutral axis and the stress ratio, determined by the compressive stress divided by the tensile stress working on the edges of the web.

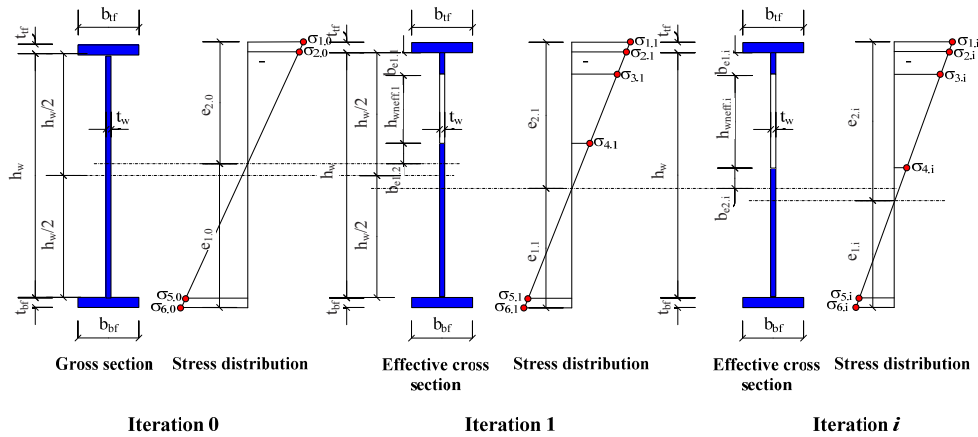


Figure 3-25 Cross-sections and accompanying stress distributions of the gross and effective cross-sections

The symbols used in Figure 3-25 have indices. The first index j of the stresses $\sigma_{j,i}$ as shown in these stress distributions indicates the location of the stresses:

- $j = 1$ indicates the location at the top of the top flange;
- $j = 2$ the bottom of the top flange;
- $j = 3$ the bottom of the effective width b_{e1} , close to the top flange;
- $j = 4$ the top of the effective width b_{e2} beyond the neutral axis;
- $j = 5$ the top of the bottom flange;
- $j = 6$ the bottom of the bottom flange.

The second index i of the stresses $\sigma_{j,i}$ indicates the number of the iteration. $i=0$ is iteration 0, based on the gross cross-section, $i=1,2,3,\dots$ concerns an iteration related to the effective width method.

For iteration 0, based on the gross cross-section, the stresses $\sigma_{3,0}$ and $\sigma_{4,0}$ are missing in Figure 3-25, because these stresses are used for specific locations of interest for the effective width method. The procedure to determine the effective bending moment resistance M_{eff} starts with the determination of the elastic stress distribution of the gross cross-section, iteration 0. For a hybrid girder, a girder with different yield stresses for both flanges and the web, the determination of the elastic stress distribution is more complex than described on the previous page. The stresses as shown by the stress distribution for iteration 0 in Figure 3-25 are limited as follows:

- $\sigma_{1,i} \leq f_{y,tf}$
- $\sigma_{2,i} \leq f_{y,wb}$
- $\sigma_{5,i} \leq f_{y,wb}$
- $\sigma_{6,i} \leq f_{y,bf}$

The sectional constants can be determined, based on the actual dimensions of the girder G4. The location of the neutral axis has to be determined and based on this location the moment of inertia I is determined.

For the Basler test specimen G4, the yield stress of the web is much larger than that of the flanges and so the section moduli and the yield strengths of the flanges determine which flange yields.

The stresses $\sigma_{2,0}$ and $\sigma_{5,0}$ can be determined by using the moment of inertia I and the distance of a specific fibre to the neutral axis, see also the stress distribution of the gross section indicated by Iteration 0 in Figure 3-25.

The following items have to be calculated for the next iterations, iterations 1, 2, ... i , according to EN1993-1-5:

- The stress ratio ψ_i , depending on the stresses $\sigma_{2,i-1}$ and $\sigma_{5,i-1}$, so based on the previous iteration $i-1$, so $\psi_i = \frac{\sigma_{2,i-1}}{\sigma_{1,i-1}}$;
- The plate buckling factor $k_{\sigma,i}$, based on this stress ratio ψ_i ;
- The critical stress $\sigma_{cr,i}$ according to the plate theory;
- The relative plate buckling slenderness $\bar{\lambda}_{p,i}$, related to this critical stress $\sigma_{cr,i}$ and the actual stress $\sigma_{2,i-1}$ of the previous iteration $i-1$. This actual stress $\sigma_{2,i-1} \leq f_{y,w}$
- The ratio ρ_i , based on the equation based on the Winter formula;
- The effective width $b_{eff,i}$ is based on this ratio ρ_i and the stress ratio ψ_i ;
- The effective width $b_{eff,i}$ is divided into an effective width $b_{e1,i}$ close to the top flange and an effective width $b_{e2,i}$ beyond the neutral axis of the effective area of the previous iteration $i-1$;
- The position of the neutral axis of the effective cross-section $A_{eff,i}$ is determined;
- The moment of inertia $I_{eff,i}$ of the effective cross-section $A_{eff,i}$ is determined;
- The stresses $\sigma_{j,i}$ for location $j=1$ to $j=6$ for iteration i are determined. For $j=1$ the stress is checked on the yield stress of the top flange $\sigma_{1,i} \leq f_{y,tf}$, for $j=2$ and $j=4$ the stress is checked on the yield stress of the web $\sigma_{j,i} \leq f_{y,w}$ and for $j=6$ is checked on the yield stress of the bottom flange $\sigma_{6,i} \leq f_{y,bf}$;
- The effective bending moment resistance $M_{eff,i}$ is determined, based on the moment of inertia $I_{eff,i}$ and the governing stress $\sigma_{j,i} = f_y$ as determined in the previous item;
- The next iteration is started as long as the difference for $\frac{M_{eff,i} - M_{eff,i-1}}{M_{eff,i-1}} \cdot 100\% > 0.1\%$.

3.5.2 ELASTIC BENDING MOMENT RESISTANCE

The properties of the gross cross-section of girder G4 are determined.

$$A_{tf} = b_{tf} \cdot t_{tf} = 308.9 \cdot 19.7 = 6072 \text{ mm}^2$$

$$A_w = h_w \cdot t_w = 1270 \cdot 3.3 = 4161 \text{ mm}^2$$

$$A_{bf} = b_{bf} \cdot t_{bf} = 309.6 \cdot 19.3 = 6016 \text{ mm}^2$$

$$A_{tot} = A_{gross} = A_{tf} + A_w + A_{bf} = 6072 + 4161 + 6016 = 16250 \text{ mm}^2 \quad (3.59)$$

The contribution of the flanges to determine the location of the neutral axis is in every iteration the same and therefore this is determined once:

$$\begin{aligned} \sum A_f e_f &= A_{tf} \cdot \left(h - \frac{t_{tf}}{2} \right) + A_{bf} \cdot \frac{t_{bf}}{2} = \\ &= 6072 \cdot \left(1309 - \frac{19.7}{2} \right) + 6016 \cdot \frac{19.4}{2} = 7947749 \text{ mm}^3 \end{aligned} \quad (3.60)$$

The position of the neutral axis from the bottom of the bottom flange, see also Figure 3-25, is:

$$e_{1.0} = \frac{\sum A_f \cdot e_f + A_w \cdot \left(\frac{h_w}{2} + t_{bf} \right)}{A_{tot}} = \frac{7947749 + 4161 \cdot \left(\frac{1270}{2} + 19.4 \right)}{16250} = 656.7 \text{ mm} \quad (3.61)$$

The distance to the other extreme fibre is:

$$e_{2.0} = h - e_{1.0} = 1309.1 - 656.7 = 652.4 \text{ mm} \quad (3.62)$$

The moment of inertia I_{gross} and the elastic section moduli W are:

$$\begin{aligned} I_{gross} &= \frac{1}{12} \cdot \left(A_{tf} \cdot t_{tf}^2 + A_{bf} \cdot t_{bf}^2 + A_w \cdot h_w^2 \right) + A_{tf} \cdot \left(h - \frac{t_{tf}}{2} - e_{1.0} \right)^2 + \\ &\quad + A_{bf} \cdot \left(\frac{t_{bf}}{2} - e_{1.0} \right)^2 + A_w \cdot \left(\frac{h_w}{2} + t_{bf} - e_{1.0} \right)^2 = \\ &= \frac{1}{12} \cdot \left(6072 \cdot 19.7^2 + 6016 \cdot 19.4^2 + 4161 \cdot 3.3^2 \right) + 6072 \cdot \left(1309.1 - \frac{19.7}{2} - 656.7 \right)^2 + \\ &\quad + 6016 \cdot \left(\frac{19.4}{2} - 656.7 \right)^2 + 4161 \cdot \left(\frac{1270}{2} + 19.4 - 656.7 \right)^2 = \\ &= 558518 \cdot 10^4 \text{ mm}^4 \end{aligned} \quad (3.63)$$

$$W_{tf} = \frac{I_{gross}}{e_{2.0}} = \frac{558518 \cdot 10^4}{652.4} = 8560.9 \cdot 10^3 \text{ mm}^3$$

$$W_{bf} = \frac{I_{gross}}{e_{1.0}} = \frac{558518 \cdot 10^4}{656.9} = 8505.1 \cdot 10^3 \text{ mm}^3 \quad (3.64)$$

Based on these properties, the elastic bending moment resistance can be determined:

$$\begin{aligned} M_{el} &= \min(W_{tf} \cdot f_{y,tf}; W_{bf} \cdot f_{y,bf}) = \\ &= \min(8560.9 \cdot 10^3 \cdot 259; 8505.1 \cdot 10^3 \cdot 255) \cdot 10^{-6} = \\ &= \min(2217.3; 2168.8) = 2168.8 \text{ kNm} \end{aligned} \quad (3.65)$$

The elastic bending moment resistance M_{el} is based on yielding of the bottom flange because of the position of the neutral axis and the yield strengths of the flanges. In the case of the Basler experiment G4, the stresses at the edge of the web are not of interest because of the rather high yield stress of the web related to the yield stresses of the flanges.

The stress distribution is presented on the left-hand side of Figure 3-25, iteration 0. The stress can be determined, namely σ_{01} and σ_{06} based on the section moduli W_{tf} and W_{bf} , and the latter stress is governing for the elastic bending moment resistance, $\sigma_{6,0} = f_{y,bf} = 255 \text{ MPa}$.

The other stresses are:

$$\begin{aligned}\sigma_{1,0} &= -\frac{M_{el}}{W_{tf}} = -\frac{2168.80 \cdot 10^6}{8560.9 \cdot 10^6} = -253.3 \text{ MPa} \leq f_{y,tf} = 259 \text{ MPa} \\ \sigma_{2,0} &= \frac{\sigma_{1,0}}{e_{2,0}} \cdot (e_{2,0} - t_{tf}) = \frac{-253.3}{652.4} \cdot (652.4 - 19.7) = -245.7 \text{ MPa} \leq f_{y,w} = 299 \text{ MPa} \\ \sigma_{5,0} &= -\frac{\sigma_{1,0}}{e_{2,0}} \cdot (e_{1,0} - t_{bf}) = \frac{253.3}{652.4} \cdot (656.7 - 19.4) = 247.5 \text{ MPa} \leq f_{y,w} = 299 \text{ MPa}\end{aligned}\quad (3.66)$$

Because of the rather high web slenderness, $\beta_w = \frac{h_w}{t_w} = \frac{1270}{3.28} = 387.6$, plate buckling has to be taken into account.

3.5.3 PLASTIC BENDING MOMENT RESISTANCE

The plastic bending moment resistance M_{pl} has to be determined, based on the actual dimensions, see Table 2-1 and Table 2-5, and the actual yield strengths, see Table 2-2. The plastic stress distribution is shown in Figure 3-26.

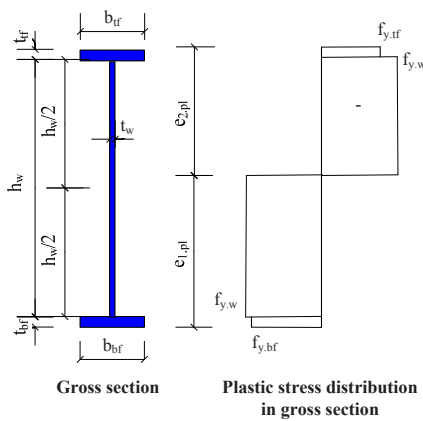


Figure 3-26 Cross-section with plastic stress distribution

The location of the plastic neutral axis is determined, based on equilibrium:

$$A_{yf} \cdot f_{y,yf} + (h_w + t_{bf} - e_{1,pl}) \cdot t_w \cdot f_{y,w} = A_{bf} \cdot f_{y,bf} + (e_{1,pl} - t_{bf}) \cdot t_w \cdot f_{y,w} \quad (3.67)$$

$$\text{So: } A_{yf} \cdot f_{y,yf} - A_{bf} \cdot f_{y,bf} + \{(h_w + t_{bf} - e_{1,pl}) - (e_{1,pl} - t_{bf})\} \cdot t_w \cdot f_{y,w} = 0 \quad (3.68)$$

$$\text{And: } e_{1,pl} = \frac{A_{yf} \cdot f_{y,yf} - A_{bf} \cdot f_{y,bf} + A_w \cdot f_{y,w} + 2t_{bf} \cdot t_w \cdot f_{y,w}}{2 \cdot t_w \cdot f_{y,w}} \quad (3.69)$$

The location of the plastic neutral axis $e_{1,pl}$ is measured from the bottom of the bottom flange:

$$e_{1,pl} = \frac{6072.1 \cdot 259 - 6016.3 \cdot 255 + 4161.3 \cdot 299 + 2 \cdot 19.4 \cdot 3.3 \cdot 299}{2 \cdot 3.3 \cdot 299} = 674.1 \text{ mm}$$

The plastic bending moment resistance is M_{pl} is:

$$\begin{aligned} M_{pl} &= A_{yf} \cdot f_{y,yf} \cdot \left(h_w + t_{bf} - e_{1,pl} + \frac{t_{yf}}{2} \right) + A_{bf} \cdot f_{y,bf} (e_{1,pl} - t_{bf}) + \frac{1}{2} (h_w + t_{bf} - e_{1,pl})^2 \cdot t_w \cdot f_{y,w} + \\ &+ \frac{1}{2} (e_{1,pl} - t_{bf})^2 \cdot t_w \cdot f_{y,w} = 6072.1 \cdot 259 \cdot \left(1270 + 19.4 - 674.1 + \frac{19.7}{2} \right) + \\ &+ 6016.3 \cdot 255 (674.1 - 19.4) + \frac{1}{2} (1270 + 19.4 - 674.1)^2 \cdot 3.3 \cdot 299 + \\ &+ \frac{1}{2} (674.1 - 19.4)^2 \cdot 3.3 \cdot 299 = 2383.0 \cdot 10^6 \text{ Nmm} \end{aligned} \quad (3.70)$$

3.5.4 BENDING MOMENT RESISTANCE BASED ON THE CROSS-SECTION CONSISTING OF THE FLANGES ONLY

The bending moment resistance of a plate girder with a slender web will be between the elastic bending moment resistance and the bending moment resistance based on the cross-section consisting of the flanges only. The web fully contributes in the elastic bending moment resistance and is totally neglected in the bending moment resistance based on the cross-section consisting of the flanges only.

This bending moment resistance M_{fl} is determined by the different flange areas and the different yield strengths. Because the area of the top flange of girder G4 as well as the yield strength of the top flange is higher than that of the bottom flange, the bending moment resistance is determined by the bottom flange:

$$M_{fl} = A_{yf} \cdot \left(h_w + \frac{t_{yf} + t_{bf}}{2} \right) \cdot f_{y,yf} = 6016.1 \cdot \left(1270.0 + \frac{19.7 + 19.4}{2} \right) \cdot 255 = 1978.4 \cdot 10^6 \text{ Nmm}$$

3.5.5 CRITICAL BENDING MOMENT RESISTANCE

The critical bending moment resistance is determined based on the section modulus of the gross cross-section and the buckling stress. The buckling stress is determined as follows. The stress ratio ψ_1 is based on the stresses $\sigma_{2,0}$ and $\sigma_{5,0}$ on the edges of the web:

$$\psi_1 = \frac{\sigma_{5,0}}{\sigma_{2,0}} = \frac{247.5}{-245.7} = -\frac{e_{1,0} - t_{bf}}{e_{2,0} - t_{bf}} = -\frac{656.7 - 19.7}{652.4 - 19.4} = -1.01 \quad (3.71)$$

The buckling factor $k_{\sigma,1}$ is based on the stress ratio ψ_1 :

$$k_{\sigma,1} = 7.81 - 6.29\psi_1 + 9.78\psi_1^2 = 7.81 - 6.29 \cdot (-1.01) + 9.78 \cdot (-1.01)^2 = 24.1 \quad (3.72)$$

The critical stress $\sigma_{cr,1}$, based on the initial buckling theory, can be determined as follows:

$$\sigma_{cr,1} = \frac{k_{\sigma,1} \cdot \pi^2 E}{12(1-\nu^2) \left(\frac{h_w}{t_w} \right)^2} = \frac{24.1 \cdot \pi^2 \cdot 2.1 \cdot 10^5}{12(1-0.3^2) \left(\frac{1270}{3.3} \right)^2} = 30.4 \text{ MPa} \quad (3.73)$$

The bending moment related to the critical stress at the top of the web is determined by:

$$\frac{M_{cr}}{I_0} \cdot (h_w + t_{bf} - e_{1,0}) = \frac{M_{cr}}{I_0} \cdot (e_{2,0} - t_{bf}) = \sigma_{cr} \quad (3.74)$$

$$M_{cr} = \frac{I_0}{(h_w + t_{bf} - e_{0,1})} \cdot \sigma_{cr} = \frac{558518 \cdot 10^4}{(1270 + 19.4 - 652.4)} \cdot 30.4 = 268.4 \cdot 10^6 \text{ Nmm}$$

3.5.6 EFFECTIVE BENDING MOMENT RESISTANCE

The effective bending moment resistance has to be determined iteratively because of the shift of the neutral axis and the change of the stress ratio $\psi_i = \frac{\sigma_{2,i-1}}{\sigma_{5,i-1}}$. The iterations are stopped when the difference in the effective bending moment resistance from the last iteration i and the second last iteration $i-1$ is less than 0.1%.

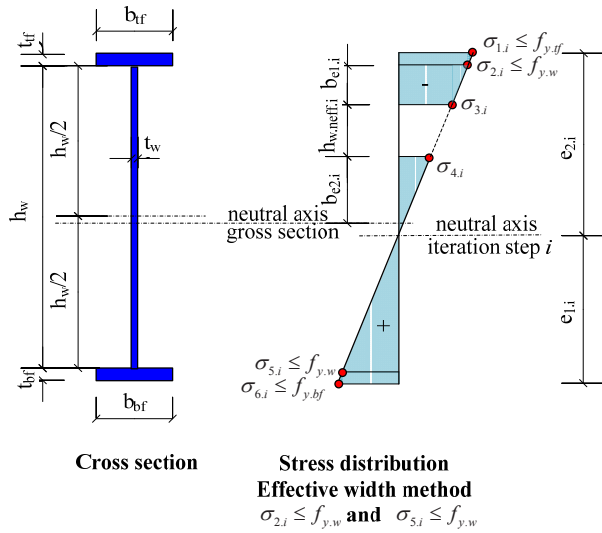


Figure 3-27 Cross-section with effective stress distribution

Iteration 1

Beyond the critical stress $\sigma_{cr,1}$ the effective width method is used to determine the effective bending moment resistance M_{eff} . In the general formula to determine the relative slenderness, the yield strength $f_{y,w}$ of the web is taken into account, but EN1993-1-5 offers the possibility to take the actual, smaller, stress $\sigma_{2,i}$ into account. When the actual stress $\sigma_{2,i}$ is used instead of the yield strength $f_{y,w}$, the effective width $b_{eff,i}$ increases.

$$\bar{\lambda}_{p,1} = \sqrt{\frac{\sigma_{2,0}}{\sigma_{cr,1}}} = \sqrt{\frac{245.7}{30.4}} = 2.84 \quad (3.75)$$

The effective width $b_{eff,1}$ is determined by using the factor ρ_1 , more or less according to the Winter formula:

$$\rho_1 = \frac{1}{\bar{\lambda}_{p,1}^2} \cdot \left\{ \bar{\lambda}_{p,1} - 0.055 \cdot (3 + \psi_1) \right\} = \frac{1}{2.84^2} \cdot \left\{ 2.84 - 0.055 \cdot (3 - 1.01) \right\} = 0.34$$

$$b_{eff,1} = \frac{\rho_1 \cdot h_w}{1 - \psi_1} = \frac{0.34 \cdot 1.270}{1 - (-1.01)} = 214.0 \text{ mm} \quad (3.76)$$

This effective width $b_{eff,1}$ is distributed over $b_{e1,1}$ close to the top flange and over $b_{e2,1}$ beyond the neutral axis of the previous iteration, so beyond $e_{1,0}$, see the second cross-section of Figure 3-25.

$$b_{e1,1} = 0.4b_{eff,1} = 0.4 \cdot 214.0 = 85.6 \text{ mm}$$

$$b_{e2.1} = 0.6b_{eff.1} = 0.6 \cdot 214.0 = 128.4 \text{ mm} \quad (3.77)$$

Because of a non effective part of the compressive web, the position of the neutral axis will shift downwards to the tensile flange. The shift is determined by the effective widths of the web and by the contribution of the flanges.

The effective web area $A_{w,eff.1}$ based on the effective widths in this first iteration is:

$$A_{w,eff.1} = (e_{1.0} - t_{bf} + b_{eff.1}) \cdot t_w = (656.7 - 19.4 + 214.0) \cdot 3.3 = 2289.2 \text{ mm}^2 \quad (3.78)$$

The total effective cross area $A_{eff.1}$ becomes:

$$A_{eff.1} = A_{fl} + A_{w,eff.1} + A_{bf} = 6072 + 2289 + 6016 = 14878 \text{ mm}^2 \quad (3.79)$$

The point of gravity of this effective web area $A_{w,eff.1}$ is determined, see Figure 3-28.

$$\begin{aligned} e_{w,eff.1} &= \left[(e_{1.0} - t_{bf}) \cdot \left\{ \frac{(e_{1.0} - t_{bf})}{2} + t_{bf} \right\} + b_{e2.1} \left(e_{1.0} + \frac{b_{e2.1}}{2} \right) + b_{e1.1} \left(h - t_{bf} - \frac{b_{e1.1}}{2} \right) \right] \cdot \frac{t_w}{A_{w,eff.1}} = \\ &= \left[(656.7 - 19.4) \cdot \left\{ \frac{(656.7 - 19.4)}{2} + 19.4 \right\} + 128.4 \cdot \left(652.4 + \frac{128.4}{2} \right) + \right. \\ &\quad \left. + 85.6 \cdot \left(1.309.1 - 19.7 - \frac{85.6}{2} \right) \right] \cdot \frac{3.3}{2289.2} = 487.2 \text{ mm} \end{aligned} \quad (3.80)$$

This $e_{w,eff.1}$ is from the bottom of the bottom flange. The position of the neutral axis of the effective cross-section $A_{w,eff.1}$ can be determined with:

$$e_{1.1} = \frac{\sum A_{fl} \cdot e_f + A_{w,eff.1} \cdot e_{w,eff.1}}{A_{eff.1}} = \frac{7947748 + 487.2 \cdot 2289.2}{14878} = 625.5 \text{ mm} \quad (3.81)$$

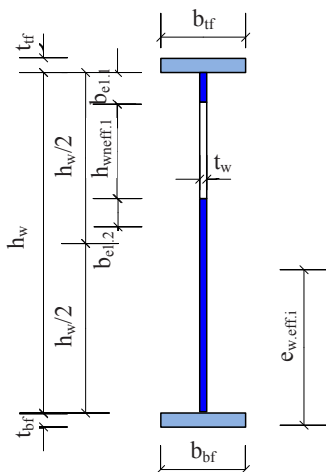


Figure 3-28 Point of gravity of all effective parts of the web

This eccentricity $e_{1,1}$ is from the bottom of the bottom flange of the gross cross-section:

$$e_{2,1} = h - e_{1,1} = 1309.1 - 625.5 = 683.6 \text{ mm} \quad (3.82)$$

Based on this, the effective moment of inertia $I_{eff,1}$ for this first iteration is determined as follows:

$$\begin{aligned} I_{eff,1} &= \frac{1}{12} \left\{ A_{tf} \cdot t_{tf}^2 + A_{bf} \cdot t_{bf}^2 + t_w \cdot b_{e1,1}^3 + t_w \cdot (e_{z0,1} - t_{bf} + b_{e1,2})^3 \right\} + A_{tf} \cdot \left(e_{z1,2} - \frac{t_{tf}}{2} \right)^2 + \\ &\quad + b_{e1,1} \cdot t_w \cdot \left(e_{z1,2} - t_{tf} - \frac{b_{e1,1}}{2} \right)^2 + (e_{z0,1} - t_{bf} + b_{e1,2}) \cdot t_w \cdot \left\{ \left(\frac{e_{z0,1} - t_{bf} + b_{e1,2}}{2} \right) + t_{bf} - e_{z1,1} \right\}^2 + \\ &\quad + A_{bf} \cdot \left(\frac{t_{bf}}{2} - e_{z1,1} \right)^2 = \\ &= \frac{1}{12} \left\{ 6072 \cdot 13.7^2 + 6016 \cdot 13.4^2 + 3.3 \cdot 85.6^3 + 3.3 \cdot (656.7 - 13.4 + 128.4)^3 \right\} + \\ &\quad + 6072 \cdot \left(683.6 - \frac{19.7}{2} \right)^2 + 85.6 \cdot 3.3 \cdot \left(683.6 - 13.7 - \frac{85.6}{2} \right)^2 + \\ &\quad + (656.7 - 13.4 + 128.4) \cdot 3.3 \cdot \left\{ \left(\frac{656.7 - 13.4 + 128.4}{2} \right) + 19.4 - 625.5 \right\}^2 + \\ &\quad + 6016 \cdot \left(\frac{19.4}{2} - 625.5 \right)^2 = 539416 \cdot 10^4 \text{ mm}^4 \end{aligned} \quad (3.83)$$

Based on this effective moment of inertia $I_{eff,1}$, the effective bending moment resistance $M_{eff,1}$ can be determined, based on yielding of one of the flanges:

$$\begin{aligned} M_{eff,1} &= \min \left(\frac{I_{eff,1}}{e_{2,1}} \cdot f_{y,tf}, \frac{I_{eff,1}}{e_{1,1}} \cdot f_{y,bf} \right) = \min \left(\frac{539416 \cdot 10^4}{683.6 \cdot 10^3} \cdot 259; \frac{539416 \cdot 10^4}{625.5 \cdot 10^3} \cdot 255 \right) \cdot 10^{-6} = \\ &= \min(2043.9; 2198.9) = 2043.9 \text{ kNm} \end{aligned} \quad (3.84)$$

$$\frac{M_{el} - M_{eff,1}}{M_{el}} = \frac{2168.8 - 2043.9}{2168.8} \cdot 100\% = 5.76\% > 0.1\%.$$

The linear stress distribution is changed because of the shift of the neutral axis and the moment of inertia of the effective cross-section. The calculation has to be repeated. The stresses at specific points, see Figure 3-25, are determined

$$\sigma_{1,1} = f_{y,tf} = 259 \text{ MPa}$$

$$\begin{aligned}
\sigma_{2,1} &= \frac{\sigma_{1,1}}{e_{2,1}} \cdot (e_{2,1} - t_{ff}) = \frac{-259.0}{683.6} \cdot (683.6 - 19.7) = -251.6 \text{ MPa} \leq f_{y,w} = 299 \text{ MPa} \\
\sigma_{3,1} &= \frac{\sigma_{1,1}}{e_{2,1}} \cdot (e_{2,1} - t_{ff} - b_{e1,1}) = \frac{-259.0}{683.6} \cdot (683.6 - 19.7 - 85.6) = -219.1 \text{ MPa} \\
\sigma_{4,1} &= \frac{\sigma_{1,1}}{e_{2,1}} \cdot (e_{1,0} - e_{1,1} + b_{e2,1}) = \frac{-259}{683.6} \cdot (656.7 - 625.5 + 128.4) = -60.4 \text{ MPa} \\
\sigma_{5,1} &= -\frac{\sigma_{1,1}}{e_{2,1}} \cdot (e_{1,1} - t_{bf}) = \frac{259.0}{683.6} \cdot (625.5 - 19.4) = 229.7 \text{ MPa} \leq f_{y,w} = 299 \text{ MPa} \\
\sigma_{6,1} &= -\frac{\sigma_{1,1}}{e_{2,1}} \cdot e_{1,1} = \frac{259.0}{683.6} \cdot 625.5 = 237.0 \text{ MPa} \leq f_{y,bf} = 259 \text{ MPa}
\end{aligned} \tag{3.85}$$

Iteration 2

$$\psi_2 = \frac{\sigma_{5,1}}{\sigma_{2,1}} = \frac{229.7}{-251.6} = -0.913 \tag{3.86}$$

$$k_2 = 7.81 - 6.29\psi_2 + 9.78\psi_2^2 = 7.81 - 6.29(-0.913) + 9.78(-0.913)^2 = 21.704 \tag{3.87}$$

$$\sigma_{cr,2} = \frac{k_{\sigma,2} \cdot \pi^2 E}{12(1-\nu^2) \left(\frac{h_w}{t_w} \right)^2} = \frac{21.704 \cdot \pi^2 \cdot 2.1 \cdot 10^5}{12(1-0.3^2) \left(\frac{1270}{3.3} \right)^2} = 27.4 \text{ MPa} \tag{3.88}$$

$$\bar{\lambda}_{p,2} = \sqrt{\frac{\sigma_{2,1}}{\sigma_{cr,2}}} = \sqrt{\frac{251.6}{27.4}} = 3.029$$

$$\rho_2 = \frac{1}{\bar{\lambda}_{p,2}^2} \cdot \left\{ \bar{\lambda}_{p,2} - 0.055 \cdot (3 + \psi_2) \right\} = \frac{1}{3.029^2} \cdot \{ 3.029 - 0.055 \cdot (3 - 0.913) \} = 0.318$$

$$b_{eff,2} = \frac{\rho_2 \cdot h_w}{1 - \psi_{\sigma,2}} = \frac{0.318 \cdot 1279}{1 - (-0.913)} = 210.9 \text{ mm} \tag{3.89}$$

$$b_{e1,2} = 0.4b_{eff,2} = 0.4 \cdot 210.9 = 84.4 \text{ mm}$$

$$b_{e2,2} = 0.6b_{eff,2} = 0.6 \cdot 210.9 = 126.5 \text{ mm}$$

$$A_{w,eff,2} = (e_{1,1} - t_{bf} + b_{eff,2}) \cdot t_w = (625.5 - 19.4 + 210.9) \cdot 3.3 = 2676.9 \text{ mm}^2 \tag{3.90}$$

$$A_{eff,2} = A_{ff} + A_{w,eff,2} + A_{bf} = 6072 + 2677 + 6016 = 14765 \text{ mm}^2 \tag{3.91}$$

$$\begin{aligned}
e_{w,eff,2} &= \left[(e_{1,1} - t_{bf}) \cdot \left\{ \frac{(e_{1,1} - t_{bf})}{2} + t_{bf} \right\} + b_{e2,2} \left(e_{1,1} + \frac{b_{e2,2}}{2} \right) + b_{e1,2} \left(h - t_{ff} - \frac{b_{e1,2}}{2} \right) \right] \cdot \frac{t_w}{A_{w,eff,2}} = \\
&= \left[(625.2 - 19.4) \cdot \left\{ \frac{(625.2 - 19.4)}{2} + 19.4 \right\} + 126.5 \cdot \left(625.2 + \frac{126.5}{2} \right) + \right.
\end{aligned}$$

$$+85.6 \cdot \left(1309.1 - 19.7 - \frac{85.6}{2} \right) \cdot \frac{3.3}{2677} = 474.7 \text{ mm} \quad (3.92)$$

$$e_{1.2} = \frac{\sum A_{fl} \cdot e_i + A_{w,eff.2} \cdot e_{w,eff.2}}{A_{eff.2}} = \frac{7947749 + 2677 \cdot 474.7}{14765.4} = 624.3 \text{ mm}$$

$$e_{2.2} = h - e_{1.2} = 1309.1 - 624.3 = 684.8 \text{ mm} \quad (3.93)$$

$$\begin{aligned} I_{eff.2} &= \frac{1}{12} \left\{ A_{yf} \cdot t_{yf}^2 + A_{bf} \cdot t_{bf}^2 + t_w \cdot b_{e1.2}^3 + t_w \cdot (e_{1.1} - t_{bf} + b_{e2.2})^3 \right\} + A_{yf} \cdot \left(e_{2.2} - \frac{t_{yf}}{2} \right)^2 + \\ &+ b_{e1.2} \cdot t_w \cdot \left(e_{2.2} - t_{yf} - \frac{b_{e1.2}}{2} \right)^2 + (e_{1.1} - t_{bf} + b_{e2.2}) \cdot t_w \cdot \left\{ \left(\frac{e_{1.1} - t_{bf} + b_{e2.2}}{2} \right) + t_{bf} - e_{1.2} \right\}^2 + \\ &+ A_{bf} \cdot \left(\frac{t_{bf}}{2} - e_{1.2} \right)^2 = \\ &= \frac{1}{12} \left\{ 6072 \cdot 13.7^2 + 6016 \cdot 13.4^2 + 3.3 \cdot 84.4^3 + 3.3 \cdot (625.5 - 13.4 + 126.5)^3 \right\} + \\ &+ 6072 \cdot \left(684.8 - \frac{19.7}{2} \right)^2 + 84.4 \cdot 3.3 \cdot \left(684.8 - 13.7 - \frac{84.4}{2} \right)^2 + \\ &+ (625.5 - 13.4 + 126.5) \cdot 3.3 \cdot \left\{ \left(\frac{625.5 - 13.4 + 126.5}{2} \right) + 19.4 - 624.3 \right\}^2 + \\ &+ 6016 \cdot \left(\frac{19.4}{2} - 624.3 \right)^2 = 539055 \cdot 10^4 \text{ mm}^4 \quad (3.94) \end{aligned}$$

$$\begin{aligned} M_{eff.2} &= \min \left(\frac{I_{eff.2}}{e_{2.2}} \cdot f_{y,yf}, \frac{I_{eff.2}}{e_{1.2}} \cdot f_{y,bf} \right) = \min \left(\frac{539055 \cdot 10^4}{684.8 \cdot 10^3} \cdot 259, \frac{539055 \cdot 10^4}{624.3 \cdot 10^3} \cdot 255 \right) \cdot 10^{-6} = \\ &= \min(2038.9; 2201.7) = 2038.9 \text{ kNm} \quad (3.95) \end{aligned}$$

$$\frac{M_{eff.1} - M_{eff.2}}{M_{eff.1}} \cdot 100\% = \frac{2043.9 - 2038.9}{2043.9} \cdot 100\% = 0.24\% > 0.1\%$$

The stresses are:

$$\sigma_{1.2} = f_{y,yf} = 259 \text{ MPa}$$

$$\sigma_{2.2} = \frac{\sigma_{1.2}}{e_{2.2}} \cdot (e_{2.2} - t_{yf}) = \frac{-259.0}{684.8} \cdot (684.8 - 19.7) = -251.6 \text{ MPa}$$

$$\sigma_{3.2} = \frac{\sigma_{1.2}}{e_{2.2}} \cdot (e_{2.2} - t_{yf} - b_{e1.2}) = \frac{-259.0}{684.8} \cdot (684.8 - 19.7 - 84.4) = -219.7 \text{ MPa}$$

$$\sigma_{4.2} = \frac{\sigma_{1.2}}{e_{2.2}} \cdot (e_{1.1} - e_{1.2} + b_{e2.2}) = \frac{-259}{684.8} \cdot (625.5 - 624.3 + 126.5) = -47.9 \text{ MPa}$$

$$\sigma_{5.2} = -\frac{\sigma_{1.2}}{e_{2.2}} \cdot (e_{1.2} - t_{bf}) = \frac{259.0}{684.8} \cdot (624.3 - 19.4) = 228.8 \text{ MPa}$$

$$\sigma_{6.2} = -\frac{\sigma_{1.2}}{e_{2.2}} \cdot e_{1.2} = \frac{259.0}{684.8} \cdot 624.3 = 236.1 \text{ MPa} \quad (3.96)$$

Iteration 3

$$\psi_3 = \frac{\sigma_{5.2}}{\sigma_{2.2}} = \frac{228.8}{-251.6} = -0.909 \quad (3.97)$$

$$k_{\sigma.3} = 7.81 - 6.29\psi_3 + 9.78\psi_3^2 = 7.81 - 6.29(-0.909) + 9.78(-0.909)^2 = 21.620 \quad (3.98)$$

$$\sigma_{cr.3} = \frac{k_{\sigma.3} \cdot \pi^2 E}{12(1-\nu^2) \left(\frac{h_w}{t_w} \right)^2} = \frac{21.620 \cdot \pi^2 \cdot 2.1 \cdot 10^5}{12(1-0.3^2) \left(\frac{1270}{3.3} \right)^2} = 27.3 \text{ MPa} \quad (3.99)$$

$$\bar{\lambda}_{p.3} = \sqrt{\frac{\sigma_{2.2}}{\sigma_{cr.2}}} = \sqrt{\frac{251.6}{27.3}} = 3.035$$

$$\rho_3 = \frac{1}{\bar{\lambda}_{p.3}^2} \cdot \left\{ \bar{\lambda}_{p.3} - 0.055 \cdot (3 + \psi_3) \right\} = \frac{1}{3.035^2} \cdot \{3.035 - 0.055 \cdot (3 - 0.935)\} = 0.317$$

$$b_{eff.3} = \frac{\rho_3 \cdot h_w}{1 - \psi_3} = \frac{0.317 \cdot 1270}{1 - (-0.909)} = 210.9 \text{ mm} \quad (3.100)$$

$$b_{e1.3} = 0.4b_{eff.3} = 0.4 \cdot 210.9 = 84.3 \text{ mm}$$

$$b_{e2.3} = 0.6b_{eff.3} = 0.6 \cdot 210.9 = 126.5 \text{ mm}$$

$$A_{w,eff.3} = (e_{1.2} - t_{bf} + b_{eff.3}) \cdot t_w = (624.3 - 19.4 + 210.9) \cdot 3.3 = 2672.9 \text{ mm}^2 \quad (3.101)$$

$$A_{eff.3} = A_f + A_{w,eff.3} + A_{bf} = 6072 + 2673 + 6016 = 14761 \text{ mm}^2 \quad (3.102)$$

$$\begin{aligned} e_{w,eff.3} &= \left[(e_{1.2} - t_{bf}) \cdot \left\{ \frac{(e_{1.2} - t_{bf})}{2} + t_{bf} \right\} + b_{e2.3} \left(e_{1.2} + \frac{b_{e2.3}}{2} \right) + b_{e1.3} \left(h - t_{bf} - \frac{b_{e1.3}}{2} \right) \right] \cdot \frac{t_w}{A_{w,eff.3}} = \\ &= \left[(624.3 - 19.4) \cdot \left\{ \frac{(624.3 - 19.4)}{2} + 19.4 \right\} + 126.5 \cdot \left(624.3 + \frac{126.5}{2} \right) + \right. \\ &\quad \left. + 84.3 \cdot \left(1309.1 - 19.7 - \frac{84.3}{2} \right) \right] \cdot \frac{3.3}{2673} = 474.3 \text{ mm} \end{aligned} \quad (3.103)$$

$$e_{1.3} = \frac{\sum A_{fl} \cdot e_f + A_{w,eff.3} \cdot e_{w,eff.3}}{A_{eff.3}} = \frac{7947749 + 2673 \cdot 474.3}{14761.4} = 624.3 \text{ mm}$$

$$e_{2.3} = h - e_{1.3} = 1309.1 - 624.3 = 684.8 \text{ mm} \quad (3.104)$$

$$\begin{aligned}
I_{eff.3} &= \frac{1}{12} \left\{ A_{yf} \cdot t_{yf}^2 + A_{bf} \cdot t_{bf}^2 + t_w \cdot b_{e1.3}^3 + t_w \cdot (e_{1.2} - t_{bf} + b_{e2.3})^3 \right\} + A_{yf} \cdot \left(e_{2.3} - \frac{t_{yf}}{2} \right)^2 + \\
&+ b_{e1.3} \cdot t_w \cdot \left(e_{2.3} - t_{yf} - \frac{b_{e1.3}}{2} \right)^2 + (e_{1.2} - t_{bf} + b_{e2.3}) \cdot t_w \cdot \left\{ \left(\frac{e_{1.2} - t_{bf} + b_{e2.3}}{2} \right) + t_{bf} - e_{1.3} \right\}^2 + \\
&+ A_{bf} \cdot \left(\frac{t_{bf}}{2} - e_{1.3} \right)^2 = \\
&= \frac{1}{12} \left\{ 6072 \cdot 13.7^2 + 6016 \cdot 13.4^2 + 3.3 \cdot 84.3^3 + 3.3 \cdot (624.3 - 13.4 + 126.5)^3 \right\} + \\
&+ 6072 \cdot \left(684.8 - \frac{19.7}{2} \right)^2 + 84.3 \cdot 3.3 \cdot \left(684.8 - 13.7 - \frac{84.3}{2} \right)^2 + \\
&+ (624.3 - 13.4 + 126.5) \cdot 3.3 \cdot \left\{ \left(\frac{624.3 - 13.4 + 126.5}{2} \right) + 19.4 - 624.3 \right\}^2 + \\
&+ 6016 \cdot \left(\frac{19.4}{2} - 624.3 \right)^2 = 539047 \cdot 10^4 \text{ mm}^4
\end{aligned} \tag{3.105}$$

$$\begin{aligned}
M_{eff.3} &= \min \left(\frac{I_{eff.3}}{e_{2.3}} \cdot f_{y.yf}, \frac{I_{eff.3}}{e_{1.3}} \cdot f_{y.bf} \right) = \min \left(\frac{539047 \cdot 10^4}{684.3 \cdot 10^3} \cdot 259, \frac{539047 \cdot 10^4}{624.3 \cdot 10^3} \cdot 255 \right) \cdot 10^{-6} = \\
&= \min(2038.8; 2201.8) = 2038.8 \text{ kNm}
\end{aligned} \tag{3.106}$$

$$\frac{M_{eff.2} - M_{eff.3}}{M_{eff.2}} \cdot 100\% = \frac{2038.9 - 2038.8}{2038.9} \cdot 100\% = 0.007\% < 0.1\% .$$

The stresses are:

$$\begin{aligned}
\sigma_{1.3} &= f_{y.yf} = 259 \text{ MPa} \\
\sigma_{2.3} &= \frac{\sigma_{1.3}}{e_{2.3}} \cdot (e_{2.3} - t_{yf}) = \frac{-259.0}{684.3} \cdot (684.3 - 19.7) = -251.6 \text{ MPa} \\
\sigma_{3.3} &= \frac{\sigma_{1.3}}{e_{2.3}} \cdot (e_{2.3} - t_{yf} - b_{e1.3}) = \frac{-259.0}{684.3} \cdot (684.3 - 19.7 - 84.3) = -219.7 \text{ MPa} \\
\sigma_{4.3} &= \frac{\sigma_{1.3}}{e_{2.3}} \cdot (e_{1.2} - e_{1.3} + b_{e2.3}) = \frac{-259.0}{684.3} \cdot (624.3 - 624.3 + 126.5) = -47.9 \text{ MPa} \\
\sigma_{5.3} &= -\frac{\sigma_{1.3}}{e_{2.3}} \cdot (e_{1.3} - t_{bf}) = \frac{259.0}{684.3} \cdot (624.3 - 19.4) = 228.8 \text{ MPa} \\
\sigma_{6.3} &= -\frac{\sigma_{1.3}}{e_{2.3}} \cdot e_{1.3} = \frac{259.0}{684.3} \cdot 624.3 = 236.1 \text{ MPa}
\end{aligned} \tag{3.107}$$

3.5.7 OVERVIEW OF THE THEORETICAL BENDING MOMENT RESISTANCES

The theoretical bending moment resistances are presented in Table 3-2 and compared with the theoretical bending moment resistances as published by Basler. The differences between these theoretical resistances are caused by the more accurate determination in this thesis. For example, Basler determined the elastic bending moment resistance as follows:

$$M_{el} = A_{yf} \cdot f_{y,tf} \cdot h_w \cdot \left(1 + \frac{\rho}{6}\right) \quad (3.108)$$

With:

$$\rho = \frac{A_w}{A_f} = \frac{4161}{6072} = 0.69 \quad (3.109)$$

And so:

$$M_{el} = A_{yf} \cdot f_{y,tf} \cdot h_w \cdot \left(1 + \frac{\rho}{6}\right) = 6072 \cdot 259 \cdot 1270 \cdot \left(1 + \frac{0.69}{6}\right) \cdot 10^{-6} = 2203.2 \text{ kNm} \quad (3.110)$$

This calculation is less accurate because of full plastic yielding of the compressive flange and because of neglecting the shift of the neutral axis. The lever arm in-between both flanges is taken equal to the web height.

Table 3-2 Theoretical bending moment resistances of Basler test specimen G4 tests T1 and T2 based on actual dimensions and actual material properties

	M_{el}	M_{pl}	M_f	M_{cr}	M_{eff}	
	[kNm]	[kNm]	[kNm]	[kNm]	[kNm]	
					G4-T1	G4-T2
Basler	2203.2	2355.7		259.3	2033.1	2050.7
EN-1993-1-5	2168.8	2383.0	1978.4	268.4	2038.7	2038.7

3.6 THEORETICAL DEFLECTIONS

For girders with high span to height ratios $\frac{\ell}{h}$ the beam theory can be used because the deflections caused by shear deformation can be fully neglected. For plate girders with a very slender web the span to height ratio $\frac{\ell}{h}$ is rather small and the shear deformation has to be taken into account.

The four-points-bending Lehigh experiment leads to a shear distribution and a bending moment distribution as presented in Figure 3-29.

The Unit Virtual Load Method gives the following equation to determine the deflection:

$$\delta = \int \frac{Mm}{EI} dx + \int \frac{Vv}{GA_w} dx \quad (3.111)$$

In this formula M is the bending moment distribution and V the shear force distribution based on the actual load. The variables m and v represent respectively the bending moment and shear force distribution based on the Unit Virtual Load of 1 kN at the location on the span of the girder where the deflection is determined.

The second integral of Eq.(3.111) is neglected in beam theory, because the contribution to the deflection by shear is very small in relation to the contribution by bending moments as determined by the first integral. For plate girders it is expected that there can be a significant contribution to the deflection by shear, like it is for trusses and castellated beams.

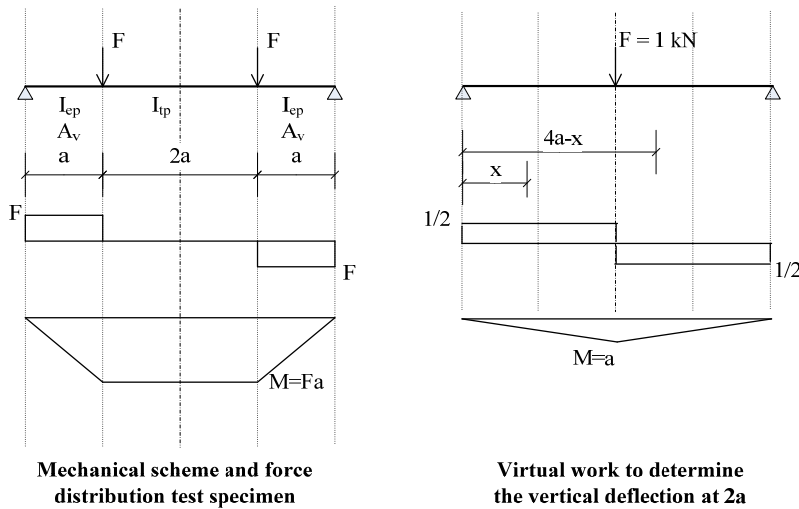


Figure 3-29 Analytical determination of the deflections

Eq.(3.111) is divided into more integrals because of different geometrical properties over the span of test girder G4, so for the end panels and the test panel. In Chapter 3.5, the bending moment resistances of test specimens are determined including the moments of inertia $I_{eff.3}$, the second moment of area, at the third iteration.

Up to the critical load P_{cr} the deflection δ_z is determined with the second moment of area of the gross sections of the end panels I_{ep} and the test panels I_{tp} . Beyond the critical load P_{cr} the second moment of area of the test panels I_{tp} will be reduced by buckling of the web and using the effective second moment of area $I_{tp,ef}$.

The minimum effective second moment of area $I_{tp,ef}$ is determined when the compressive stress is equal to the yield stress f_y . Because the yield stress of the web $f_{y,w}$ of test girder G4 is much higher than the yield strengths of the flanges, $f_{y,w} > f_{y,tf}$ and $f_{y,w} > f_{y,bf}$ while $f_{y,tf} \approx f_{y,bf}$, and because of the shift of the neutral axis in the direction of the bottom flange, the minimum effective width is determined by yielding of the top flange in the case of the test girder G4.

For the end panels the properties have to be determined. The gross area is:

$$A_{gross,ep} = A_{tf,ep} + A_{bf,ep} + A_{w,ep} = \underbrace{308.9 \cdot 19.7}_{6072.1} + \underbrace{309.6 \cdot 19.4}_{6016.3} + \underbrace{1270 \cdot 10.0}_{12645.1} = 24733.6 \text{ mm}^2 \quad (3.112)$$

The position of the neutral axis of the gross section is determined with:

$$e_{1.0} = \frac{\sum A_f \cdot e_f + A_w \cdot \left(\frac{h_w}{2} + t_{bf} \right)}{A_{tot}} = \frac{7947749 + 12645 \cdot \left(\frac{1270}{2} + 19.4 \right)}{24734} = 655.9 \text{ mm} \quad (3.113)$$

The moment of inertia I_{ep} for the end panels is determined as follows:

$$\begin{aligned} I_{ep} &= \frac{1}{12} \cdot (A_{tf} \cdot t_{tf}^2 + A_{bf} \cdot t_{bf}^2 + A_w \cdot h_w^2) + A_{tf} \cdot \left(h - \frac{t_{tf}}{2} - e_{1.0} \right)^2 + \\ &\quad + A_{bf} \cdot \left(\frac{t_{bf}}{2} - e_{1.0} \right)^2 + A_w \cdot \left(\frac{h_w}{2} + t_{bf} - e_{1.0} \right)^2 = \\ &= \frac{1}{12} \cdot (6072 \cdot 19.7^2 + 6016 \cdot 19.4^2 + 12645 \cdot 10.0^2) + 6072 \cdot \left(1309.1 - \frac{19.7}{2} - 655.9 \right)^2 + \\ &\quad + 6016 \cdot \left(\frac{19.4}{2} - 655.9 \right)^2 + 12645 \cdot \left(\frac{1270}{2} + 19.4 - 655.9 \right)^2 = 672551 \cdot 10^4 \text{ mm}^4 \end{aligned} \quad (3.114)$$

The web slenderness of the end panel $\beta_{w,ep}$ is, because of its yield strength $f_{y,ep}$, close to the limit of a class 4 cross-section:

$$\beta_{w,ep} = \frac{h_{w,ep}}{t_{w,ep}} = \frac{1270}{10.0} = 127.6 \leq 124 \sqrt{\frac{235}{f_{y,ep}}} = 124 \sqrt{\frac{235}{276}} = 114.2 \quad (3.115)$$

The effective second moment of area is $I_{eff,ep} = 665868 \cdot 10^4 \text{ mm}^4$ based on additional calculations.

The difference between the second moment of area of the gross cross-section I_{ep} and the effective one, $I_{eff,ep}$, is very small, namely 1.0%. In reality, the stresses at the edges of the web in the end panel are smaller than the yield stress $f_{y,ep}$ and that the limit of $\beta_{w,ep}$ becomes higher and the section is fully effective.

3.6.1.1 The theoretical deflection for test girder G4-T1

According to Basler, the geometrical properties of the cross-section changed at 4648.2 mm from the supports, see Figure 3-1. The deflection at midspan δ_z is determined as follows:

$$\begin{aligned}
 \delta_z &= 2 \cdot \left\{ \int_0^{3810} \frac{M(x)m(x)}{EI_{ep}} dx + \int_{3810}^{4648.2} \frac{M(x)m(x)}{EI_{ep}} dx + \int_{4648.2}^{6858} \frac{M(x)m(x)}{EI_{tp}} dx + \right. \\
 &\quad \left. + \int_0^{3810} \frac{V(x)v(x)}{GA_{w,ep}} dx + \int_{3810}^{4648.2} \frac{V(x)v(x)}{GA_{w,ep}} dx + \int_{4648.2}^{6858} \frac{V(x)v(x)}{GA_w} dx \right\} = \\
 &= \left\{ \int_0^{3810} \frac{P \cdot x \cdot \frac{x}{2}}{EI_{ep}} dx + \int_{3810}^{4648.2} \frac{P \cdot 3810 \cdot \frac{x}{2}}{EI_{ep}} dx + \int_{4648.2}^{6858} \frac{P \cdot 3810 \cdot \frac{x}{2}}{EI_{tp}} dx + \right. \\
 &\quad \left. + \int_0^{3810} \frac{P \cdot \frac{1}{2}}{GA_{w,ep}} dx + \int_{3810}^{4648.2} \frac{0 \cdot \frac{1}{2}}{GA_{w,ep}} dx + \int_{4648.2}^{6858} \frac{0 \cdot \frac{1}{2}}{GA_w} dx \right\} = \\
 &= 2 \cdot \left\{ \left[\frac{P \cdot x^3}{6EI_{ep}} \right]_0^{3810} + \left[\frac{3810 \cdot P \cdot x^2}{4EI_{ep}} \right]_{3810}^{4648.2} + \left[\frac{3810 \cdot P \cdot x^2}{4EI_{tp}} \right]_{4648.2}^{6858} + \left[\frac{P \cdot x}{2GA_{w,ep}} \right]_0^{3810} \right\} = \\
 &= 2 \cdot \left\{ \frac{P \cdot 3810^3}{6EI_{ep}} + \frac{3810 \cdot P \cdot 4648.2^2}{4EI_{ep}} - \frac{3810 \cdot P \cdot 3810^2}{4EI_{ep}} + \right. \\
 &\quad \left. + \frac{3810 \cdot P \cdot 6858^2}{4EI_{tp}} - \frac{3810 \cdot P \cdot 4648.2^2}{4EI_{tp}} + \frac{P \cdot 3810}{2GA_{w,ep}} \right\} = \\
 &= 2 \cdot \left\{ 16.0 \cdot 10^9 \cdot \frac{P}{EI_{ep}} + 24.2 \cdot 10^9 \cdot \frac{P}{EI_{tp}} + 1905 \cdot \frac{P}{GA_{w,ep}} \right\} \quad (3.116)
 \end{aligned}$$

Based on the critical bending moment resistance $M_{cr} = 268.4 \text{ kNm}$, the critical load P_{cr} is:

$$F = P_{cr} = \frac{M_{cr}}{a} = \frac{268.4}{3.81} = 70.4 \text{ kN}$$

The second moment of area is equal to $I_{tp} = I_y = 558518 \cdot 10^4 \text{ mm}^4$, see Eq.(3.63). The deflection

$\delta_{z,cr}$ is based on the critical load $P_{cr} = 70.4 \text{ kN}$ is:

$$\begin{aligned}\delta_{z,cr} &= 2 \cdot \left\{ 16.0 \cdot 10^9 \cdot \frac{P_{cr}}{EI_{ep}} + 24.2 \cdot 10^9 \cdot \frac{P_{cr}}{EI_{tp}} + 1905 \cdot \frac{P_{cr}}{GA_{w,ep}} \right\} = \\ &= 2 \cdot \left\{ 16.0 \cdot 10^9 \cdot \frac{70.4 \cdot 10^3}{2.1 \cdot 10^5 \cdot 672551 \cdot 10^4} + 24.2 \cdot 10^9 \cdot \frac{70.4 \cdot 10^3}{2.1 \cdot 10^5 \cdot 558518 \cdot 10^4} + \right. \\ &\quad \left. + 1905 \cdot \frac{70.4 \cdot 10^3}{0.81 \cdot 10^5 \cdot 12645} \right\} = 1.59 + 2.91 + 0.26 = 4.77 \text{ mm}\end{aligned}$$

The effective load P_{eff} is based on the effective bending moment resistance of the test panels

$$M_{eff} = 2038.8 \text{ kNm} :$$

$$F = P_{eff} = \frac{M_{eff}}{a} = \frac{2038.8}{3.81} = 535.1 \text{ kN}$$

The effective deflection $\delta_{z,eff}$, based on the effective load $P_{eff} = 535.1 \text{ kN}$, is:

$$\begin{aligned}\delta_{z,eff} &= \delta_{z,cr} + 2 \cdot \left\{ 16.0 \cdot 10^9 \cdot \frac{P_{eff} - P_{cr}}{EI_{ep}} + 24.2 \cdot 10^9 \cdot \frac{P_{eff} - P_{cr}}{EI_{eff}} + 1905 \cdot \frac{P_{eff} - P_{cr}}{GA_{w,ep}} \right\} = \\ &= 4.77 + 2 \cdot \left\{ 16.0 \cdot 10^9 \cdot \frac{(535.1 - 70.4) \cdot 10^3}{2.1 \cdot 10^5 \cdot 672551 \cdot 10^4} + 24.2 \cdot 10^9 \cdot \frac{(535.1 - 70.4) \cdot 10^3}{2.1 \cdot 10^5 \cdot 539048 \cdot 10^4} + \right. \\ &\quad \left. + 1905 \cdot \frac{(535.1 - 70.4) \cdot 10^3}{0.81 \cdot 10^5 \cdot 12645} \right\} = 4.77 + 10.51 + 19.88 + 1.73 = 36.89 \text{ mm} \quad (3.117)\end{aligned}$$

This means that deflection $\delta_{z,cr}$ for the critical load $P_{cr} = 70.4 \text{ kN}$ is $\delta_{z,cr} = 4.77 \text{ mm}$ and for the effective load $P_{eff} = 535.1 \text{ kN}$ the deflection is $\delta_{z,eff} = 36.89 \text{ mm}$, see Figure 3-30.

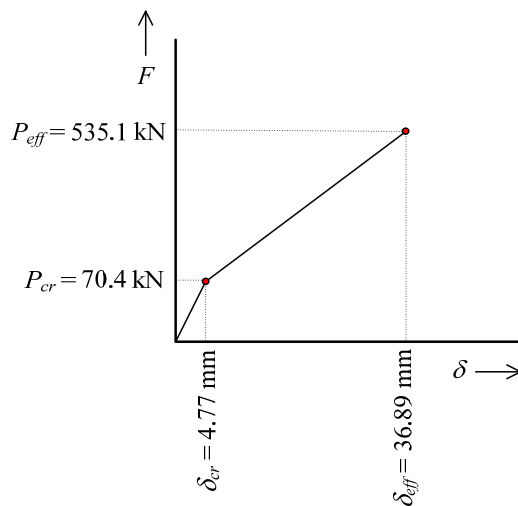


Figure 3-30 Deflections bilinear relation

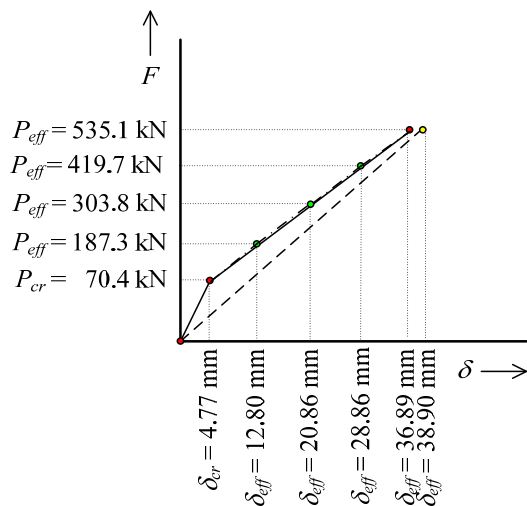


Figure 3-31 Comparison deflections

The deflections δ_z between these two points of the P - δ diagram can be determined. The effective second moments of area have to be adapted according to the current load level. Intermediate points on the graph are determined by using intermediate stress levels, between the critical stress $\sigma_{cr} = 30.4 \text{ MPa}$, see Eq.(3.73), and the maximum stress in the top of the web $\sigma_{2,3}$ in case the top of the top flange yields, so for $\sigma_{1,3} = f_{y,ff} = 259 \text{ MPa}$ and $\sigma_{2,3} = f_{y,ff} = 251.6 \text{ MPa}$, see Eq.(3.107).

For these intermediate stress levels are taken: $\sigma_{2,3} = 85.7 \text{ MPa}$, $\sigma_{2,3} = 141.0 \text{ MPa}$ and $\sigma_{2,3} = 196.3 \text{ MPa}$. The iterations shown in Chapter 3.5.6 are repeated, but for the yield stress of the web such intermediate stress level is taken. The effective moment is determined and so the effective load corresponding with the mentioned stresses is $P_{eff, \sigma_{2,3}}$. Also, the effective second moments of area is determined.

For $\sigma_{2,3} = 85.7 \text{ MPa}$ this means an effective load $P_{eff} = 187.3 \text{ kN}$ and the effective second moment of area $I_{eff} = 545480 \cdot 10^4 \text{ mm}^4$. The corresponding deflection is:

$$\delta_{z, eff} = 4.77 + 2.64 + 4.94 + 0.44 = 12.79 \text{ mm}.$$

For $\sigma_{2,3} = 141.0 \text{ MPa}$ is $F = 303.8 \text{ kN}$ and $I_{eff} = 542178 \cdot 10^4 \text{ mm}^4$. The corresponding deflection is:

$$\delta_{z, eff} = 4.77 + 5.28 + 9.93 + 0.87 = 20.84 \text{ mm}.$$

For $\sigma_{2,3} = 196.3 \text{ MPa}$ is $F = 419.7 \text{ kN}$ and $I_{eff} = 540306 \cdot 10^4 \text{ mm}^4$. The corresponding deflection is:

$$\delta_{z, eff} = 4.77 + 7.90 + 14.91 + 1.30 = 28.87 \text{ mm}.$$

These points are shown in Figure 3-31. This graph is out of scale to show that the influence of the actual effective second moment of area on the deflections is negligibly small. When these intermediate points are determined based on linear interpolation between the critical load level and the effective load level, these intermediate deflections are respectively 12.80 mm, 20.83 mm and 28.86 mm. This is very close to the deflections based on the adapted effective second moments of area, see Figure 3-31 too.

Looking at the kink in this P - δ diagram, the deflection is also determined by using only the effective stiffness based on the effective width determined by the yield stress of the top flange:

$$\begin{aligned} \delta_{z, eff} &= 2 \cdot \left\{ 16.0 \cdot 10^9 \cdot \frac{P_{eff}}{EI_{ep}} + 24.2 \cdot 10^9 \cdot \frac{P_{eff}}{EI_{eff}} + 1905 \cdot \frac{P_{eff}}{GA_{w, ep}} \right\} = \\ &= 2 \cdot \left\{ 16.0 \cdot 10^9 \cdot \frac{535.1 \cdot 10^3}{2.1 \cdot 10^5 \cdot 672551 \cdot 10^4} + 24.2 \cdot 10^9 \cdot \frac{535.1 \cdot 10^3}{2.1 \cdot 10^5 \cdot 539048 \cdot 10^4} + \right. \\ &\quad \left. + 1905 \cdot \frac{535.1 \cdot 10^3}{0.81 \cdot 10^5 \cdot 12645} \right\} = 12.10 + 22.90 + 2.05 = 38.90 \text{ mm} \end{aligned} \quad (3.118)$$

The difference in deflection is 5.5%. The difference in stiffness of the gross section EI_{gross} of the test panels and EI_{eff} of the effective section is shown explicitly in Figure 3-31 by scaling up the deflections, the deflection by the critical force P_{cr} and the deflection by the effective force P_{eff} in Figure 3-30. In Figure 3-31 it is shown that the influence of the stiffness EI_{gross} of the gross section of the test panels is negligibly small.

3.6.1.2 The theoretical deflection for test girder G4-T2

The deflections of test specimen G4 in test T2 were different from the deflections in test T1. The failure mode of the girder in test T1 was lateral deflection of the top flange of test panel 3 and so this flange was stiffened and the second moment of area changed. So did the deflections. The flange was stiffened by two plates with a total cross-sectional area of $A_{st,lf,ip3} = 2 \cdot 101.6 \cdot 6.4 = 1290 \text{ mm}^2$, but it is not clear where they were placed. Basler mentioned that the plates did not influence the point of gravity of the top flange and therefore the thickness of this part of the flange was adapted to 23.8 mm in the FEM-model for the second test T2. The total cross-sectional area of test panel 3 was changed into:

$$A_{lf,ip3,st} = A_{lf} + A_{st,lf,ip3} = 6072 + 1290 = 7362 \text{ mm}^2$$

The position of the neutral axis of the gross cross-section changed. The influence of the flanges on the position of the neutral axis is:

$$\begin{aligned} \sum A_f e_f &= A_{lf,ip3,st} \cdot \left(h - \frac{t_{lf}}{2} \right) + A_{bf} \cdot \frac{t_{bf}}{2} = \\ &= 7362 \cdot \left(1309 - \frac{19.7}{2} \right) + 6016 \cdot \frac{19.4}{2} = 9624212 \text{ mm}^3 \end{aligned} \quad (3.119)$$

The position of the neutral axis from the bottom of the bottom flange, see also Figure 3-25, is:

$$e_{1,0} = \frac{\sum A_f \cdot e_f + A_w \cdot \left(\frac{h_w}{2} + t_{bf} \right)}{A_{tot}} = \frac{9624212 + 4161 \cdot \left(\frac{1270}{2} + 19.4 \right)}{16250 + 1290} = 704.0 \text{ mm} \quad (3.120)$$

The distance to the other extreme fibre is:

$$e_{2,0} = h - e_{1,0} = 1309.1 - 704.0 = 605.1 \text{ mm} \quad (3.121)$$

The moment of inertia I_{gross} and the deflections δ are:

$$I_{gross} = \frac{1}{12} \cdot \left(A_{lf} \cdot t_{lf}^2 + A_{bf} \cdot t_{bf}^2 + A_w \cdot h_w^2 \right) + A_{lf} \cdot \left(h - \frac{t_{lf}}{2} - e_{1,0} \right)^2 +$$

$$\begin{aligned}
& + A_{bf} \cdot \left(\frac{t_{bf}}{2} - e_{1.0} \right)^2 + A_w \cdot \left(\frac{h_w}{2} + t_{bf} - e_{1.0} \right)^2 = \\
& = \frac{1}{12} \cdot (7362 \cdot 19.7^2 + 6016 \cdot 19.4^2 + 4161 \cdot 3.3^2) + 7362 \cdot \left(1309.1 - \frac{19.7}{2} - 704.0 \right)^2 + \\
& + 6016 \cdot \left(\frac{19.4}{2} - 605.1 \right)^2 + 4161 \cdot \left(\frac{1270}{2} + 19.4 - 605.1 \right)^2 = 607881 \cdot 10^4 \text{ mm}^4 \quad (3.122)
\end{aligned}$$

The deflection as given in Eq.(3.116) changes:

$$\begin{aligned}
\delta_z &= 2 \cdot \left\{ \int_0^{3810} \frac{M(x)m(x)}{EI_{ep}} dx + \int_{3810}^{4648.2} \frac{M(x)m(x)}{EI_{ep}} dx + \right. \\
& + \int_0^{3810} \frac{V(x)v(x)}{GA_{w,ep}} dx + \int_{3810}^{4648.2} \frac{V(x)v(x)}{GA_{w,ep}} dx + \int_{4648.2}^{6858} \frac{V(x)v(x)}{GA_w} dx \Bigg\} + \\
& + \int_{4648.2}^{6858} \frac{M(x)m(x)}{EI_{tp}} dx + \int_{4648.2}^{6858} \frac{M(x)m(x)}{EI_{tp3.st}} dx = \\
& = 2 \cdot \left\{ \int_0^{3810} \frac{P \cdot x \cdot \frac{x}{2}}{EI_{ep}} dx + \int_{3810}^{4648.2} \frac{P \cdot 3810 \cdot \frac{x}{2}}{EI_{ep}} dx + \int_0^{3810} \frac{P \cdot \frac{1}{2}}{GA_{w,ep}} dx + \int_{3810}^{4648.2} \frac{0 \cdot \frac{1}{2}}{GA_{w,ep}} dx + \int_{4648.2}^{6858} \frac{0 \cdot \frac{1}{2}}{GA_w} dx \right\} + \\
& + \int_{4648.2}^{6858} \frac{P \cdot 3810 \cdot \frac{x}{2}}{EI_{tp}} dx + \int_{4648.2}^{6858} \frac{P \cdot 3810 \cdot \frac{x}{2}}{EI_{tp3.st}} dx = \\
& = 2 \cdot \left\{ \left[\frac{P \cdot x^3}{6EI_{ep}} \right]_0^{3810} + \left[\frac{3810 \cdot P \cdot x^2}{4EI_{ep}} \right]_{3810}^{4648.2} + \left[\frac{P \cdot x}{2GA_{w,ep}} \right]_0^{3810} \right\} + \\
& + \left[\frac{3810 \cdot P \cdot x^2}{4EI_{tp}} \right]_{4648.2}^{6858} + \left[\frac{3810 \cdot P \cdot x^2}{4EI_{tp3.st}} \right]_{4648.2}^{6858} = \\
& = 2 \cdot \left\{ \frac{P \cdot 3810^3}{6EI_{ep}} + \frac{3810 \cdot P \cdot 4648.2^2}{4EI_{ep}} - \frac{3810 \cdot P \cdot 3810^2}{4EI_{ep}} + \frac{P \cdot 3810}{2GA_{w,ep}} \right\} + \\
& + \frac{3810 \cdot P \cdot 6858^2}{4EI_{tp}} - \frac{3810 \cdot P \cdot 4648.2^2}{4EI_{tp}} + \frac{3810 \cdot P \cdot 6858^2}{4EI_{tp3.st}} - \frac{3810 \cdot P \cdot 4648.2^2}{4EI_{tp3.st}} = \\
& = 31.9 \cdot 10^9 \cdot \frac{P}{EI_{ep}} + 24.2 \cdot 10^9 \cdot \frac{P}{EI_{tp}} + 24.2 \cdot 10^9 \cdot \frac{P}{EI_{tp3.st}} + 3810 \cdot \frac{P}{GA_{w,ep}} \quad (3.123)
\end{aligned}$$

The deflection $\delta_{z,cr}$ based on the critical load $P_{cr} = 70.4 \text{ kN}$ is:

$$\delta_{z,cr} = 31.9 \cdot 10^9 \cdot \frac{P}{EI_{ep}} + 24.2 \cdot 10^9 \cdot \frac{P}{EI_{tp}} + 24.2 \cdot 10^9 \cdot \frac{P}{EI_{tp3.st}} + 3810 \cdot \frac{P}{GA_{w,ep}} =$$

$$\begin{aligned}
&= 31.9 \cdot 10^9 \cdot \frac{70.4 \cdot 10^3}{2.1 \cdot 10^5 \cdot 672551 \cdot 10^4} + 24.2 \cdot 10^9 \cdot \frac{70.4 \cdot 10^3}{2.1 \cdot 10^5 \cdot 558518 \cdot 10^4} + \\
&\quad + 24.2 \cdot 10^9 \cdot \frac{70.4 \cdot 10^3}{2.1 \cdot 10^5 \cdot 607881 \cdot 10^4} + 3810 \cdot \frac{70.4 \cdot 10^3}{0.81 \cdot 10^5 \cdot 12645} = \\
&= 1.59 + 1.45 + 1.34 + 0.26 = 4.65 \text{ mm}
\end{aligned}$$

The effective second moment of area of test panel 3 is $I_{eff.tp3} = 593751 \cdot 10^4 \text{ mm}^4$. The effective deflection $\delta_{z,eff}$ based on the effective load $P_{eff} = 535.1 \text{ kN}$ of test panels 1 and 2 is:

$$\begin{aligned}
\delta_{z,eff} &= \delta_{z,cr} + 31.9 \cdot 10^9 \cdot \frac{P_{eff} - P_{cr}}{EI_{ep}} + 24.2 \cdot 10^9 \cdot \frac{P_{eff} - P_{cr}}{EI_{eff}} + 24.2 \cdot 10^9 \cdot \frac{P_{eff} - P_{cr}}{EI_{eff.tp3}} + 3810 \cdot \frac{P_{eff} - P_{cr}}{GA_{w,ep}} = \\
&= 4.77 + 31.9 \cdot 10^9 \cdot \frac{(535.1 - 70.4) \cdot 10^3}{2.1 \cdot 10^5 \cdot 672551 \cdot 10^4} + 24.2 \cdot 10^9 \cdot \frac{(535.1 - 70.4) \cdot 10^3}{2.1 \cdot 10^5 \cdot 539048 \cdot 10^4} + \\
&\quad + 24.2 \cdot 10^9 \cdot \frac{(535.1 - 70.4) \cdot 10^3}{2.1 \cdot 10^5 \cdot 593751 \cdot 10^4} + 3810 \cdot \frac{(535.1 - 70.4) \cdot 10^3}{0.81 \cdot 10^5 \cdot 12645} \Bigg\} = \\
&= 4.77 + 10.51 + 9.94 + 9.03 + 1.73 = 35.97 \text{ mm}
\end{aligned} \tag{3.124}$$

The difference in deflection of the test girder with a stiffened top flange of test panel 3 and with an unstiffened top flange is 2.5%. This is based on $\delta_{z,eff} = 36.89 \text{ mm}$, see Eq.(3.117), of the unstiffened girder and $\delta_{z,eff} = 35.97 \text{ mm}$, see Eq.(3.124), of the stiffened girder.

3.7 COMPARISON FEM RESULTS ON EXPERIMENTAL AND THEORETICAL RESULTS

The results of the laboratory tests G4-T1 and G4-T2 were given by Basler [12] in a $P - \delta$ diagram, see Figure 3-32. On the vertical axis the stress was given in ksi, kips per square inch, but also the total force in kip, kilopounds. On the horizontal axis the vertical deflection was presented in inches.

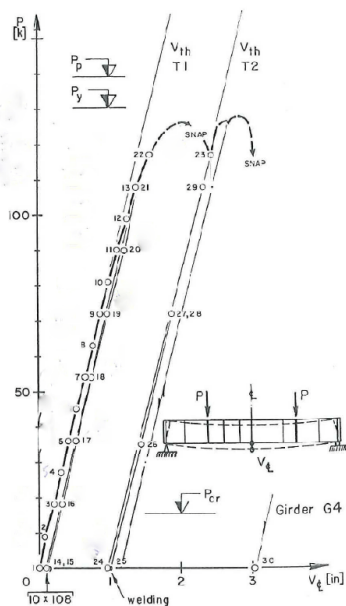


Figure 3-32 $P - \delta$ diagram of the laboratory tests on girder G4 in tests T1 and T2, Basler [12]

With a view to this graph, it is of interest to explain the testing procedure. The graph shows the results of tests T1 and T2 of girder G4. At zero load, load No. 1, a complete set of data was recorded. The load increment was 9 kips, corresponding with 40.0 kN, up to the point where the behaviour became inelastic, point 13, shown by the deviation of the load-deflection curve at a load level of 108 kips, 480.4 kN.

After recording another complete set of data, the girder was completely unloaded to point 14. The girder was reloaded 10 times up to this point 13 and unloaded to point 15 to prove that repeated loads would not lead to additional distortions. The girder was loaded again in steps of 9 kips up to point 21, which is equal to point 13. After a new increase of the load to 117 kips, 520.4 kN, point 22, another set of data was recorded.

From this point “a very low strain rate was imposed on the girder and the deflection at each kip was recorded by means of the centreline dial gauge”, according to the publication by Basler [12]. A dynamic ultimate load of 128 kips, 569.4 kN, was reached and from this the curve began to drop.

According to Basler, the imposed deflection was kept constant and the load stabilised at 117 kips, 569.4 kN, point 23 in the graph of Figure 3-32. The description is in contradiction with the curve, because the curve shows an increase of the deflection, the dotted line between points 22 and 23. The girder was unloaded, point 24.

The top flange of the longer panel, panel 3, failed by lateral buckling and so this flange was reinforced by welding two steel plates along this failed top flange. The deflection increased a little by welding of these strips, point 25, and test T2 started. According to the $P - \delta$ diagram as shown in Figure 3-32 the deformation steps of the second test T2 were 36 kips, 160.1 kN, up to point 27, 72 kips corresponding to 320.3 kN. Basler did not describe what happened at this point, but another point is shown, point 28, at the same load level, without unloading the girder in the second test T2. Another load step of 36 kips, kN, was made and after that the load also increased up to a dynamic ultimate load of 128 kips, 569.4 kN. It looks like the girder was unloaded close to the maximum load of the girder in test T2, but additional points are given. The last point of test T2, point 30, was given by Basler, for the situation after failure and unloading. The plastic deformation was 3 inch, 76.2 mm.

In this chapter, the results of the FEM-models for tests T1 and T2 are compared with the results of the experiments. For test T1 as well as for test T2, two FEM-models are used, namely one with an initial stress distribution based on the residual stress distribution according to the previous Dutch code NEN6771 and one based on the residual stress distribution according to the previous Swedish code BSK99 as mentioned in Chapter 3.2.3.2.

To compare both results, the American dimensions in Figure 3-32 have to be transformed into metric dimensions, 100 kips correspond with 444.82216 kN and 1 inch corresponds with 25.4 mm.

The following results are compared:

1. The $P - \delta$ diagrams of tests T1 and T2
 - a. The stiffness of the girder;
 - b. The maximum load;
2. The failure mode of tests T1 and T2;
3. The ultimate bending moment resistance related to reference resistances, the elastic, plastic bending moment resistance, the bending moment resistance based on the cross-section consisting of both flanges only, the critical bending moment resistance and the effective bending moment resistance as determined in Chapter 3.5.6.

The results of the FEM-model of girder G4-T1 with initial stresses based on the residual stress according to the previous Dutch code NEN6771 are compared in Chapter 3.7.1 with the topics mentioned and results of test T2 in Chapter 3.7.2. In Chapters 3.7.3 and 3.7.4, this comparison is de-

scribed for the model with initial stresses according to the previous Swedish code BSK99 with the topics mentioned. $P - \delta$ diagrams are presented for the vertical deflections of nodes 1255 and 1751, see Figure 3-33, and also $P - \delta$ diagrams for the lateral deflections. In the centre of test panels 1 and 2 no node is situated and the average of the deflection of nodes 2031 and 2032 for test panel 1 is used and the average of nodes 1759 and 1760 for test panel 2. The lateral deflection of node 1240, which is located in the centre of test panel 3, is also shown for all four FEM-models.

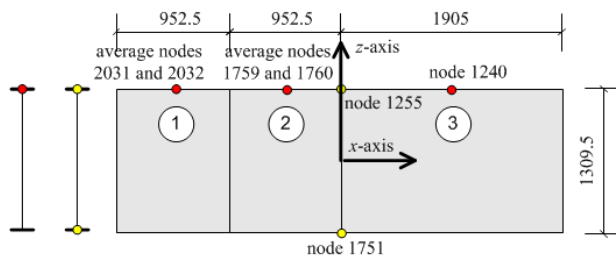


Figure 3-33 The locations of vertical ● and horizontal ● deflections, used in the $P - \delta$ diagrams

3.7.1 FEM-MODEL WITH RESIDUAL STRESSES ACCORDING TO NEN6771, TEST T1

In Figure 3-34, the $P - \delta$ diagrams of the Basler experiment G4-T1 and the result of the FEM-model of this girder are represented, including the theoretical resistances mentioned as determined in Chapter 3.5.

From this $P - \delta$ diagram, the following can be seen:

1. The maximum load of $P_{FEM.NEN.G4-T1} = 565.0 \text{ kN}$ is very close to the dynamic ultimate load of the experiment $P_{G4-T1} = 565.5 \text{ kN}$. Both forces lead to bending moment resistances, determined by $M_u = P_u \cdot a$, namely $M_{FEM.G4-T1} = 2152.8 \text{ kNm}$ and $M_{Basler.G4-T1} = 2154.6 \text{ kNm}$. The difference is 0.09 %;
2. The top of the $P - \delta$ is found for a deflection of $\delta_{FEM.G4-T1} = 58.3 \text{ mm}$ in the FEM-model and of $\delta_{Basler.G4-T1} = 50.8 \text{ mm}$ in the experiment. The difference is 14.81%;
3. The stiffness of the FEM-model is up to a load of $P = 425.0 \text{ kN}$ according to the theoretical stiffness as determined in Chapter 3.6 and from around $P = 450.0 \text{ kN}$ the FEM-model behaves much more flexibly. This is due to the assumed residual stresses and the rather roughly measured imperfections from the Basler's graphs;

4. The stiffness of the experiment is close to the theoretical stiffness. This means that dimensions of the FEM-model correspond very well to the actual dimensions;
5. The stiffness of the FEM-model is smaller than the stiffness of the experiments. This means that the assumed geometrical and physical imperfections are too large;
6. The ultimate force is between the force related to the effective bending moment resistance and the elastic bending moment resistance, but very close to the elastic bending moment resistance. This is strange, because it means that plate buckling did not influence the bending moment resistance, although the web slenderness is $\beta_w = 388$. This is caused by the different yield strengths of the elements of the plate girder, both flanges and the web. The yield stress of the web was considerably higher than the yield stresses of both flanges, being respectively $f_{y,w} = 299 \text{ MPa}$, $f_{y,tf} = 259 \text{ MPa}$ and $f_{y,bf} = 255 \text{ MPa}$. Related to the effective width, first the top flange yielded and thus the top of the web participated more and more. The strains in the top flange became higher than the yield strain, while the top of the web was not yielding.

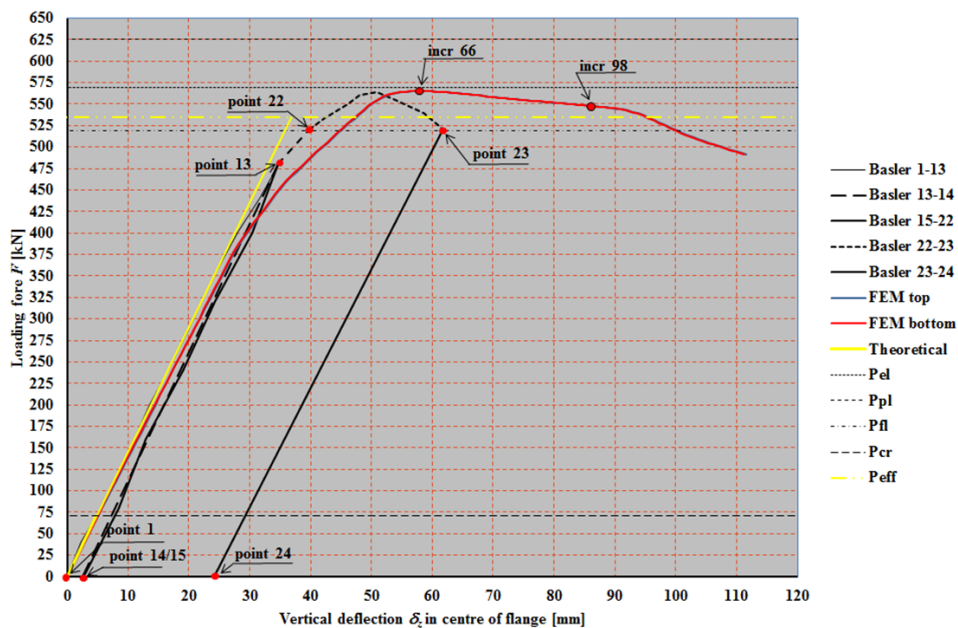


Figure 3-34 $P - \delta$ diagram of experiment G4-T1 and FEM-model with residual stress according to NEN6771

The elastic forces representing the elastic bending moment resistance as determined in Chapter 3.5.2 and presented by Basler in the P - δ diagram as shown in Figure 3-34 are different. This is caused by the rather rough method Basler used. Basler determined the elastic bending moment resistance by assuming full yielding of the top flange plus an elastic contribution of the web:

$$P_{el.Basler.G4} = \frac{M_{el.Basler.G4}}{a} = \frac{A_{tf} \cdot f_{y,tf} \cdot h \cdot \left(1 + \frac{\rho}{6}\right)}{a} =$$

$$= \frac{6072 \cdot 259 \cdot 1309.1 \cdot \left(1 + \frac{4161}{6 \cdot 6072}\right)}{3810} \cdot 10^{-3} = 602.1 \text{ kN}$$

The difference in elastic bending moment resistance according to Basler and according to the EN1993 is 5.77 %.

The plastic forces representing the plastic bending moment resistance as determined in Chapter 3.5.3 and presented by Basler in the P - δ diagram as shown in Figure 3-34 are also different. The plastic moment is determined in the same way as the elastic moment, but taking the plastic contribution of the web into account and so $P_{pl.Basler.G4} = 632.9 \text{ kN}$. The difference is smaller than that for elastic force, namely 1.20 %. The failure mode of the FEM-model is compared with the failure mode of the experiment. The failure mode of test specimen G4-T1 is described by Basler as lateral deflection of the compressive flange in the longest panel of the test panels, panel 3. Basler published pictures of the collapse mode of G4-T1, see Figure 3-35. The horizontal deflections of test panel 3 are shown in Table 3-3 and Figure 3-36.

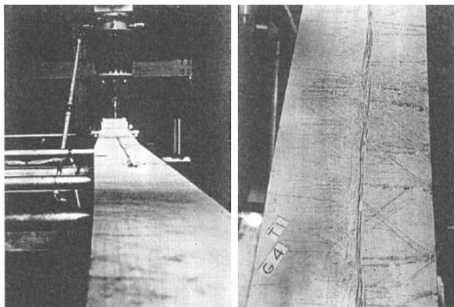


Figure 3-35 Lateral buckling of the compressive flange in test panel 3, girder G4-T1, Basler [12]

Table 3-3 Horizontal deflection δ_y top flange of specimen G4-T1, test panel 3

	Incr. 50	Incr. 55	Incr. 60	Incr. 66	Incr. 70	Incr. 75	Incr. 80	Incr. 85	Incr. 90	Incr. 95
δ_y [mm]	+1.40	+2.15	+3.25	+4.77	+6.52	+8.35	+10.28	+12.09	+13.83	+15.49

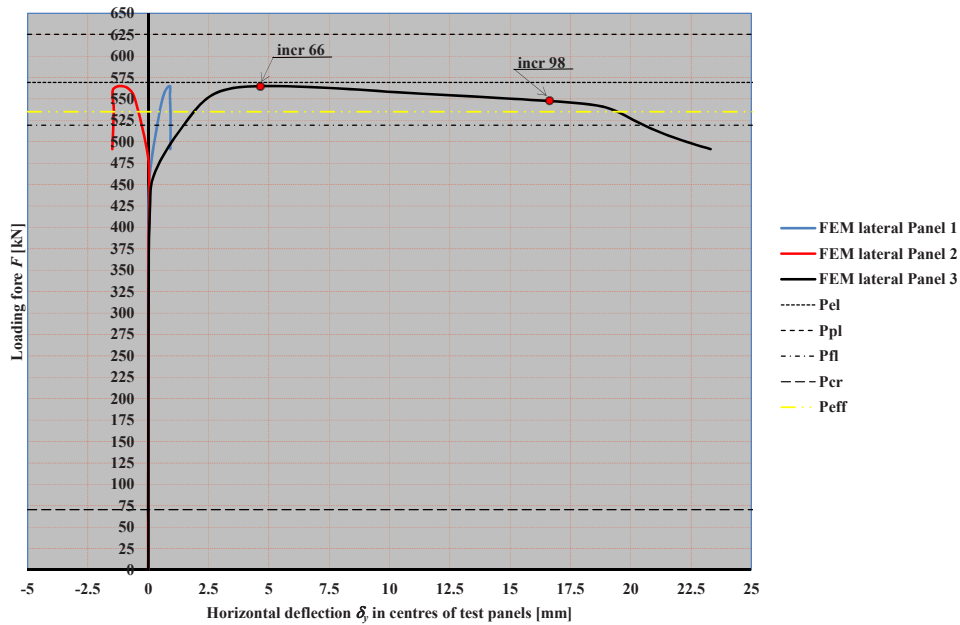


Figure 3-36 Horizontal deflection of the compressive flange of test panels 1 to 3 of experiment G4-T1, residual stresses according to NEN6771

The lateral deflection, the one in y -direction, of test panel 3 slowly increases from around $P_{FEM} = 450.0 \text{ kN}$, while the deflections of the small test panels 1 and 2 are rather small.

These lateral deflections of the top flange of the test panels are presented in the top views in Figure 3-37. The yellow colour indicates a lateral deflection $\delta_y = +15 \text{ mm}$ and the blue colour indicates a deflection of $\delta_y = -15 \text{ mm}$. The red colour indicates a deflection between $\delta_y = +4 \text{ mm}$ and $\delta_y = -4 \text{ mm}$. These deflections are presented in Figure 3-38 in perspective view.

Figure 3-39 shows in perspective view the Von Mises stresses of the panels in the test areas. In the test panel, these Von Mises stresses are equal to the normal stress because of constant moment in the test panels, but later on other stresses will be seen depending on the failure mode. In these figures, the yellow colour indicates a stress of 259 MPa, based on the yield stress of the top flange and the blue one indicates 0 MPa. The total strains are presented in a perspective view in Figure 3-40. Yellow indicates a strain of +0.0015 and blue -0.0015, which is close to the yield strain ϵ_y of the top flange. The maximum load in the FEM-model of girder G4-T1 is found for increment 66. Above mentioned figures are presented for increment 66 and for higher increments as indicated in the titles.

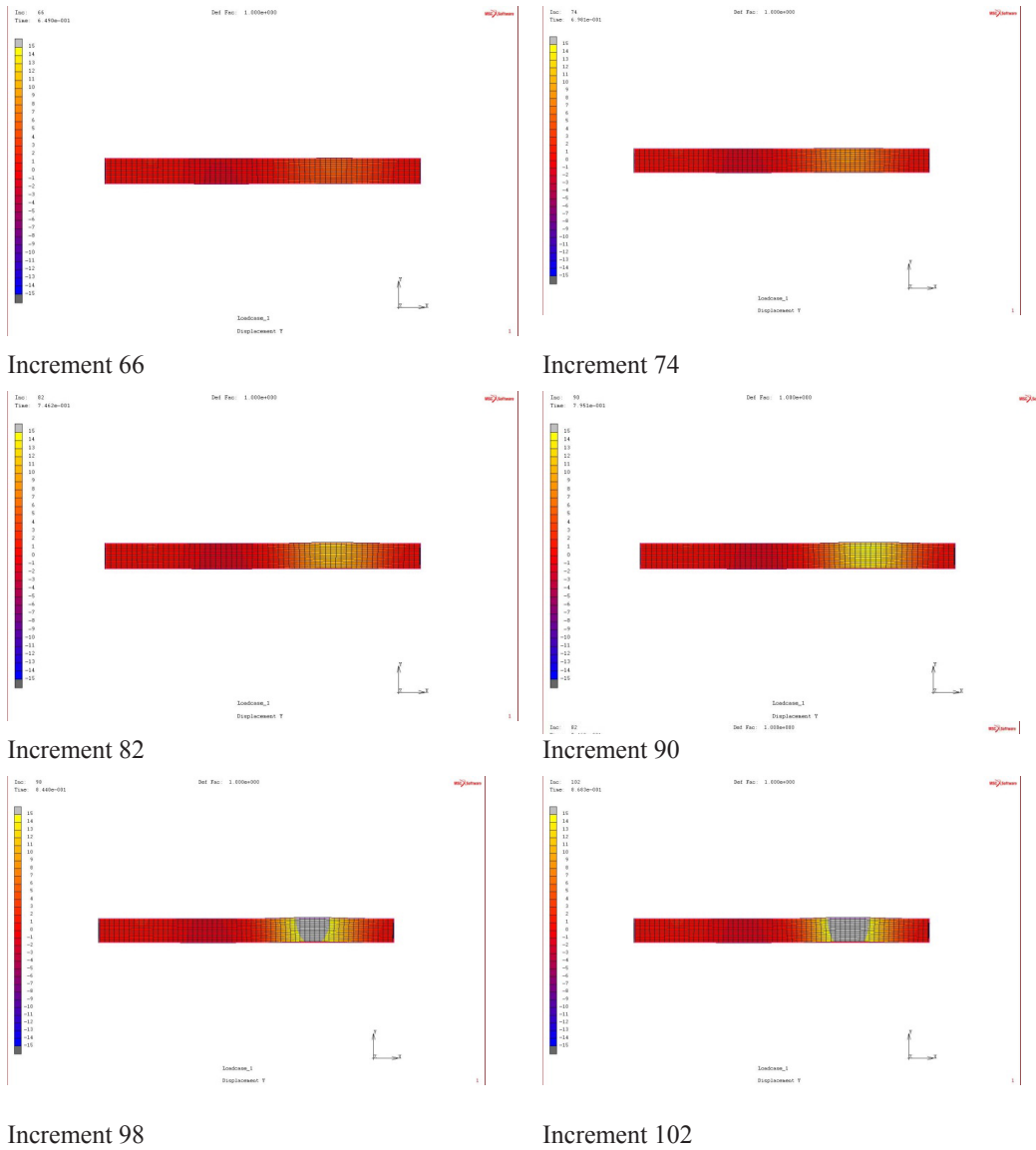


Figure 3-37 Top views of the lateral deflection δ_y of the top flange of the test area of girder G4-T1, residual stresses according to NEN6771 for different load steps

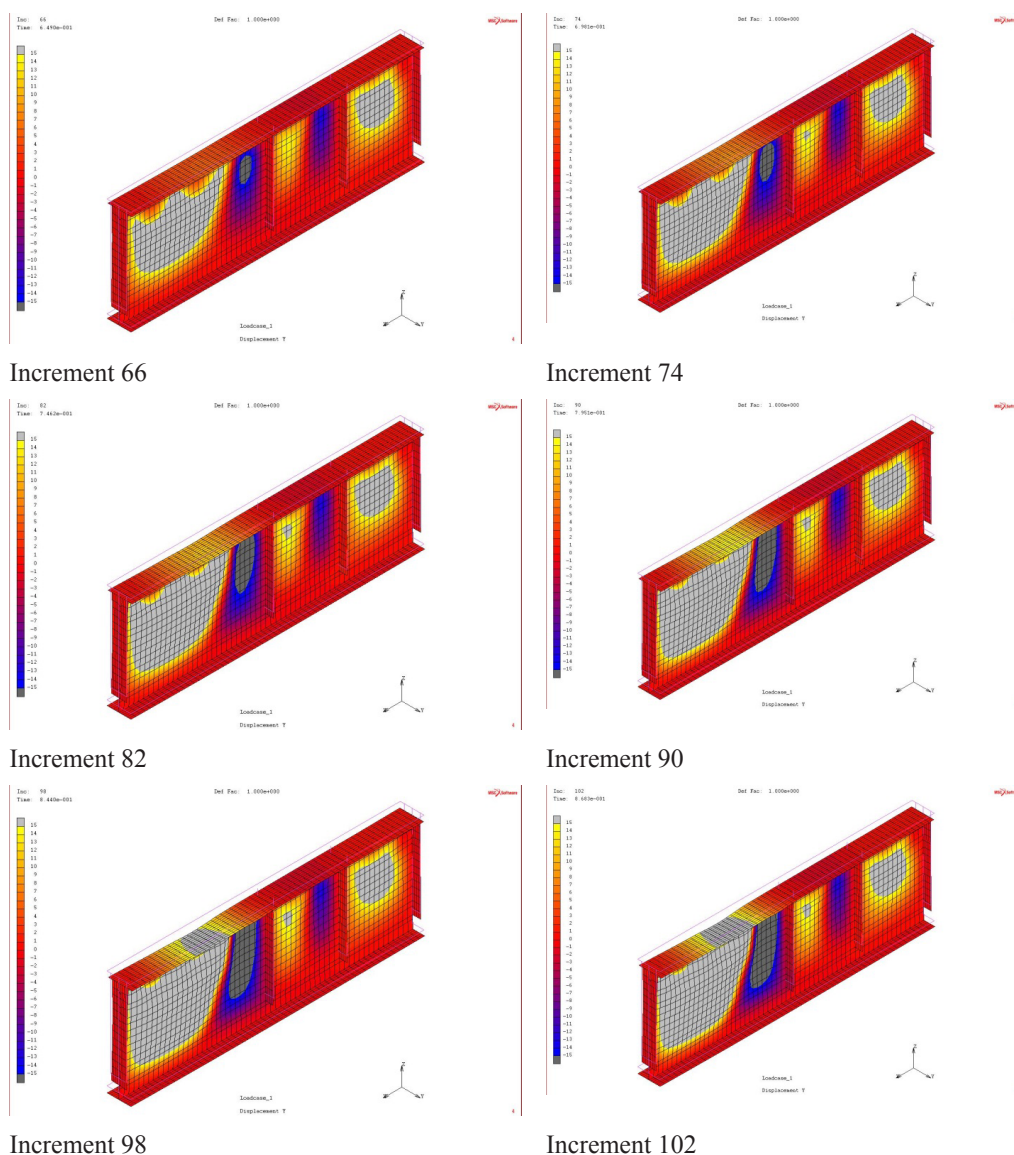
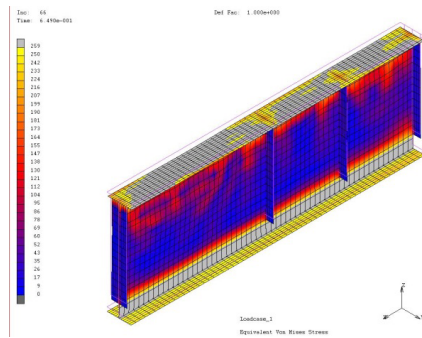
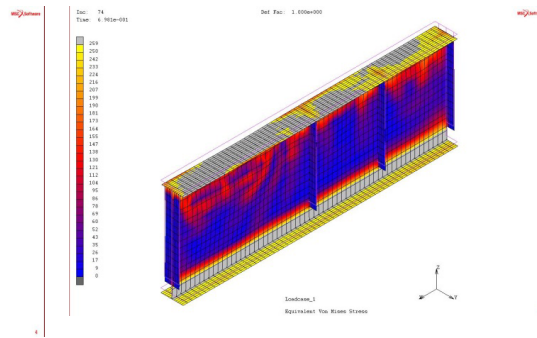


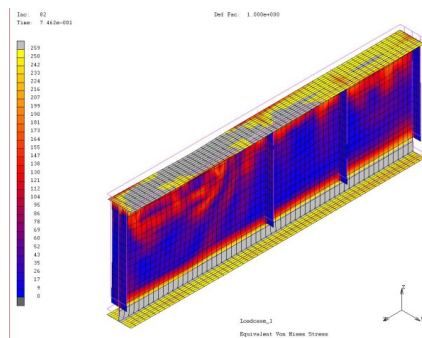
Figure 3-38 3-D views of the lateral deflection δ_y of the test panels of girder G4-T1, residual stresses according to NEN6771 for different load steps



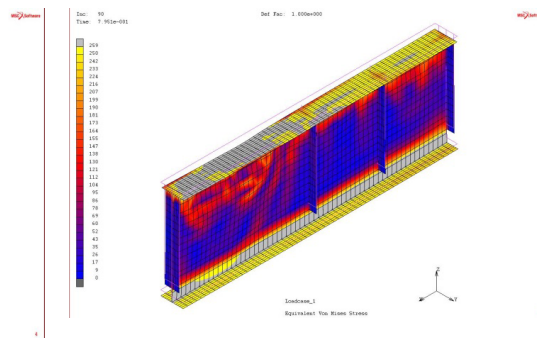
Increment 66



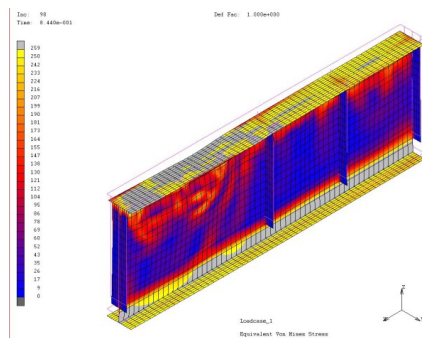
Increment 74



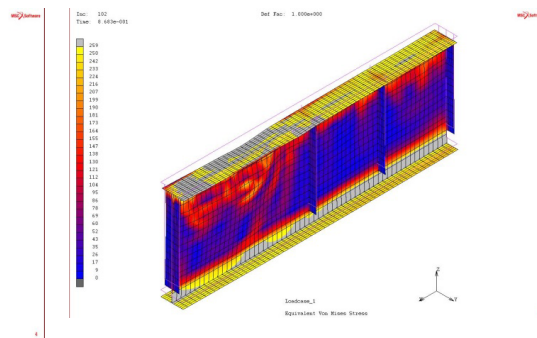
Increment 82



Increment 90

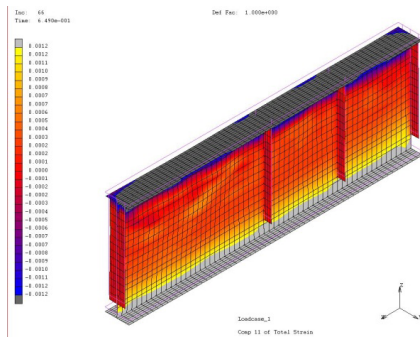


Increment 98

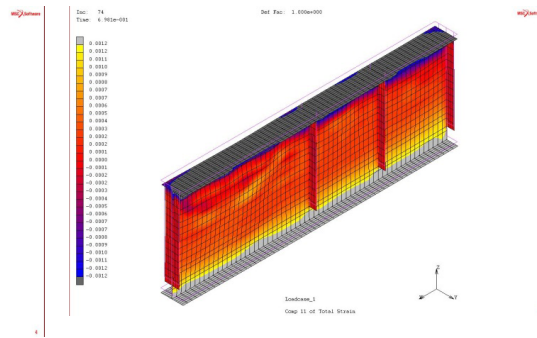


Increment 102

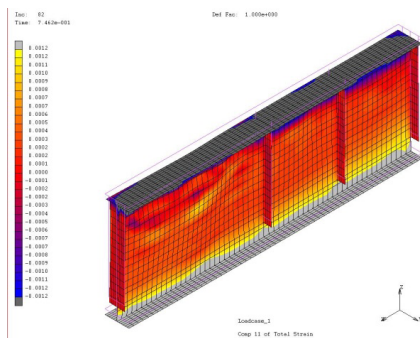
Figure 3-39 3-D views of the Von Mises stresses $\sigma_{Von Mises}$ in the test area of girder G4-T1, residual stresses according to NEN6771 for different increments



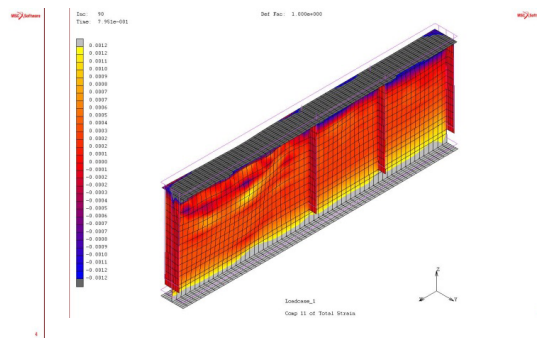
Increment 66



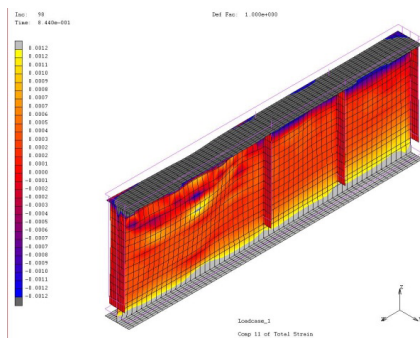
Increment 74



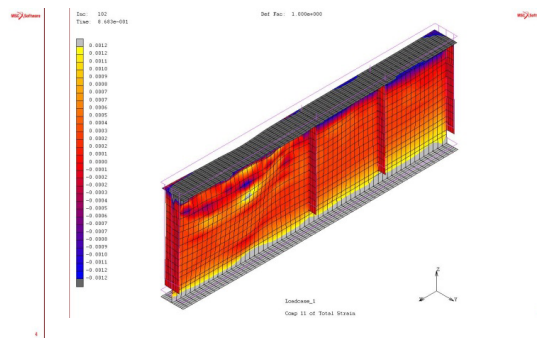
Increment 82



Increment 90



Increment 98



Increment 102

Figure 3-40 3-D views of the strains ε in the test area of girder G4-T1, residual stresses according to NEN6771 for different load steps

3.7.2 FEM-MODEL WITH RESIDUAL STRESSES ACCORDING TO NEN6771, TEST T2

The compressive top flange of test panel 3 was stiffened, reinforced, in the experiment and so it is in the FEM-model. As mentioned, the initial imperfections of the test panel and the residual stresses in this FEM-model of G4-T2 are the same as in the FEM-model of G4-T1. The P - δ diagram of this specimen G4-T2 is shown in Figure 3-41.

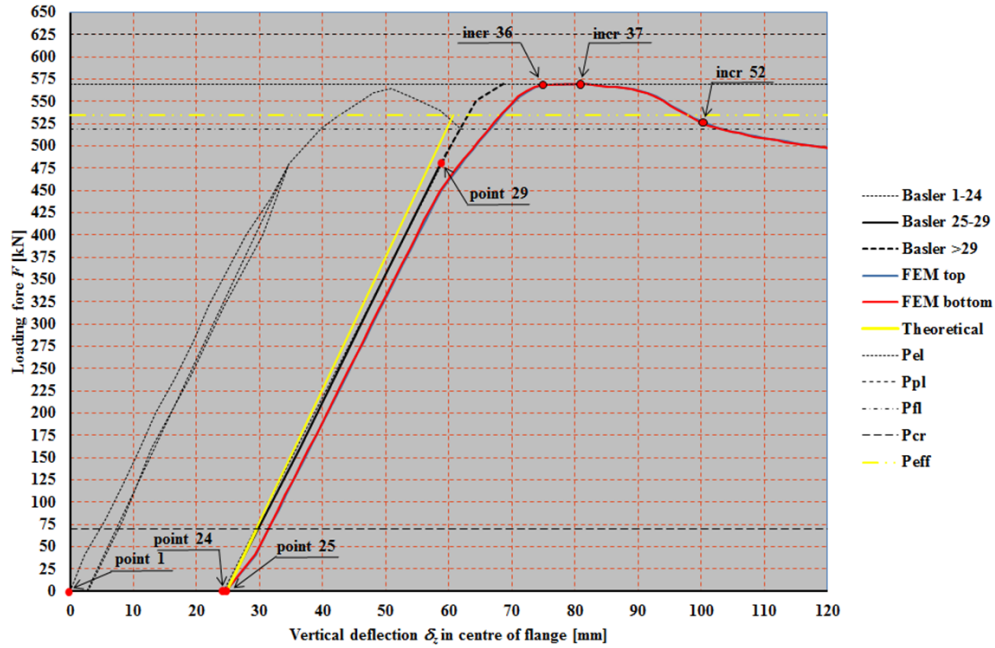


Figure 3-41 P - δ diagram of experiment G4-T2 and FEM-model with residual stress according to NEN6771

From this P - δ diagram, the following can be seen:

The maximum load of $P_{FEM, NEN, G4-T2} = 569.6 \text{ kN}$ is very close to the dynamic ultimate load of the experiment $P_{G4-T2} = 569.4 \text{ kN}$. Both forces lead to bending moment resistances, determined by $M_u = P_u \cdot a$, namely $M_{FEM, G4-T2} = 2170.2 \text{ kNm}$ and $M_{Basler, G4-T2} = 2169.4 \text{ kNm}$. The difference is 0.04 %;

The top of the P - δ is found for a deflection of $\delta_{FEM, G4-T2} = 81.7 \text{ mm}$ for increment 37 in the FEM-model and $\delta_{Basler, G4-T2} = 68.0 \text{ mm}$ in the experiment. The difference is 20.15%. The load for incre-

ment 36 is very close to this maximum and the relevant deflection at this load level is $\delta_{FEM,G4-T1} = 75.1 \text{ mm}$ and the difference is 10.44 %;

The stiffness of the FEM-model up to a load of $P=450.0 \text{ kN}$ is according to the theoretical stiffness as determined in Chapter 3.6 and for higher loads the FEM-model behaves more flexibly. This is caused by the assumed residual stresses and the rather roughly measured imperfections. Apart from this, the girder is of course influenced by the first test, test T1. Basler presented the deflection up to point 13 in his $P - \delta$ diagram, so the initial imperfections at the start of the second test, test T2, so at point 24, is not known. It could be expected that the residual stresses were smaller and the geometrical imperfections were larger than in test T1;

The stiffness of the experiment is close to the theoretical stiffness. The small difference can be explained by the influence of the actual geometrical imperfections;

The stiffness of the FEM-model is smaller than the stiffness of the experiments. As pointed out in 3, the assumed initial imperfections are too small and the residual stresses are too high, while it is shown that the girder dimensions of the FEM-model correspond with these of the experiment, see Chapter 3.7.1;

The ultimate force is very close to the theoretical elastic bending moment resistance as determined in Chapter 3.5, namely $P_{el} = 569.2 \text{ kN}$ with a difference of only 0.04 %. This is explained in Chapter 3.7.1.

In Figure 3-42, the vertical buckling of the compressive flange into the web of Basler's test specimen G4-T2 can be seen. This specific collapse mode occurs more or less in the FEM-model G4-T2 too.

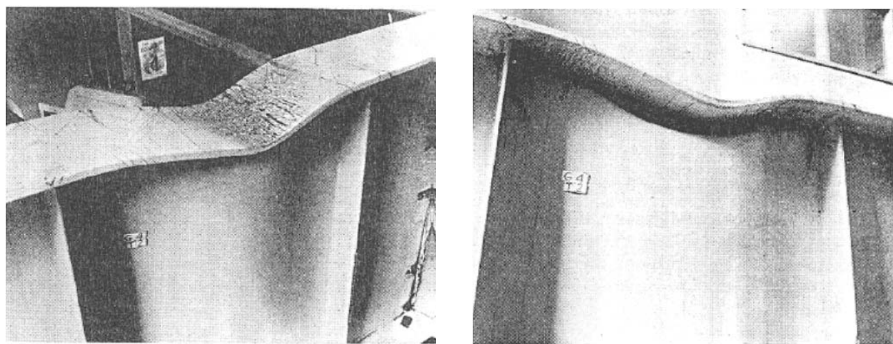


Figure 3-42 Vertical buckling of the compressive flange into the web, Basler test G4-T2 [10]

In Table 3-4, the lateral deflections of the centre of the top flange of test panel 1 for several iterations (load steps) are shown. See Figure 3-43 for the lateral deflections of the centres of the top flanges of all three test panels.

Table 3-4 Horizontal deflection δ_y top flange of specimen G4-T2, test panel 1

	Incr. 10	Incr. 20	Incr. 30	Incr. 37	Incr. 40	Incr. 50	Incr. 55	Incr. 60
δ_y [mm]	-0.02	-0.02	+0.19	+1.87	+2.54	+4.22	+5.33	+6.57

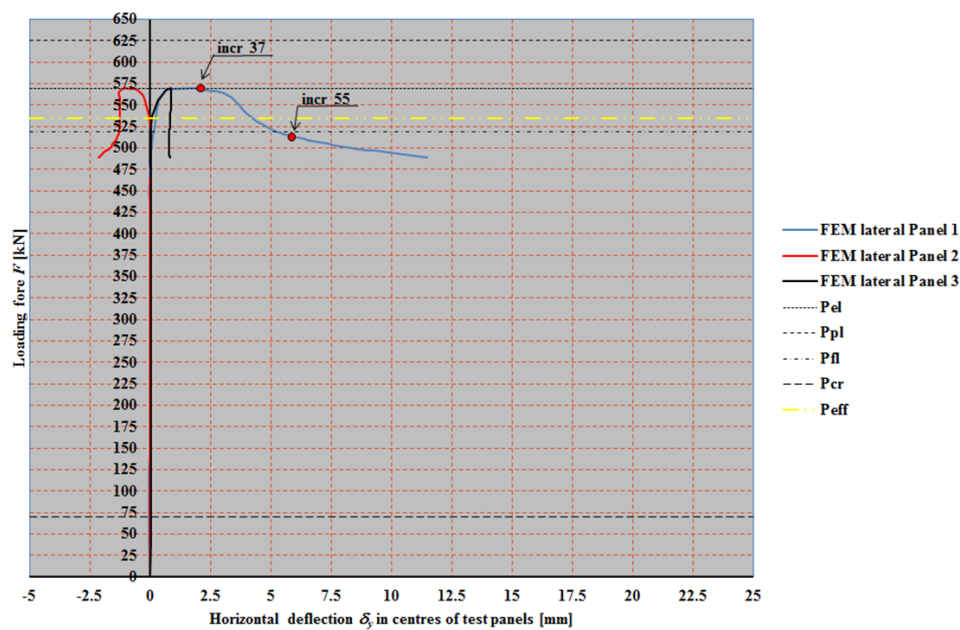
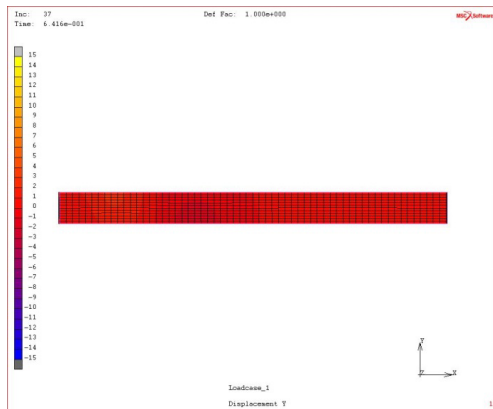
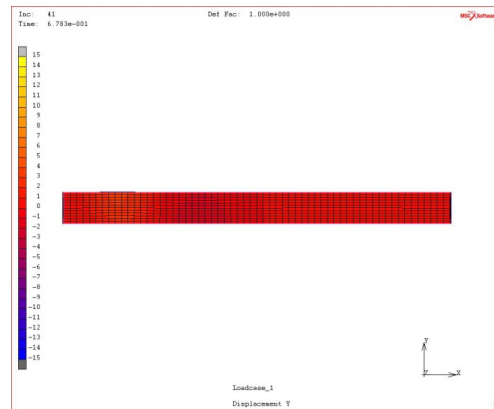


Figure 3-43 Horizontal deflections of the compressive flange of test panels 1 to 3 of experiment G4-T2, residual stresses according to NEN6771

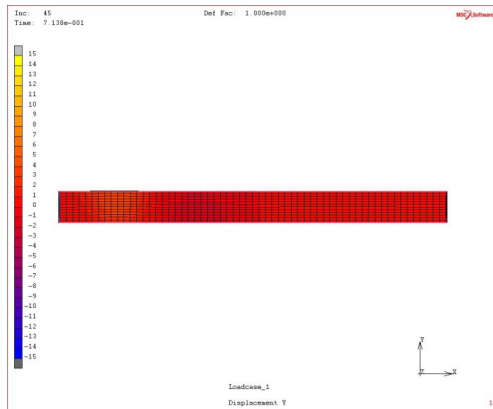
In above graph, three lines show the lateral deflections of the centres of the three test panels of this FEM-model of test specimen G4-T2 with residual stresses according to NEN6771. The external small test panel, panel 1, deflects approximately +1.9 mm. From this graph it can be seen that test panel 1 tends to buckle horizontally and so it can not be concluded that the girder collapses by vertical buckling of the compressive flange into the web of test panel 1, as concluded by Basler. Figure 3-44 and Figure 3-45 show the horizontal deflections of the test panels for different load levels in top view and in perspective view. Figure 3-46 shows the Von Mises stresses of the test panels of girder G4 for different load levels in perspective view. Figure 3-47 presents the total strains of test panels of the girder G4 for different load levels in perspective view.



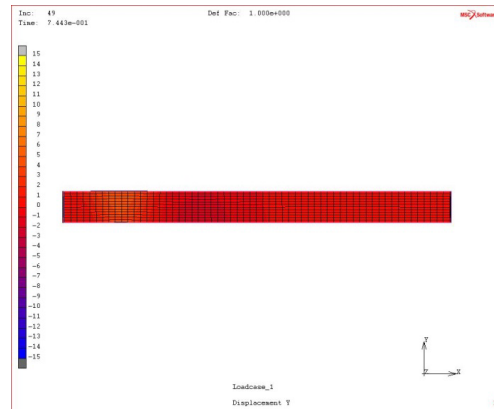
Increment 37



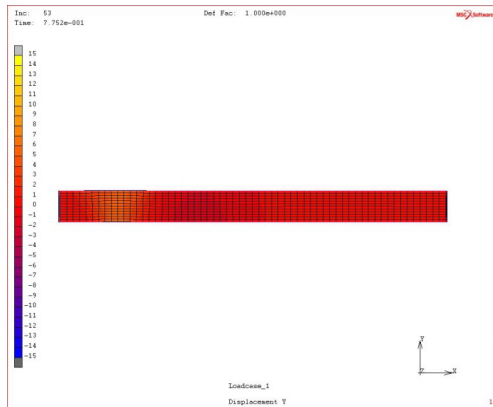
Increment 41



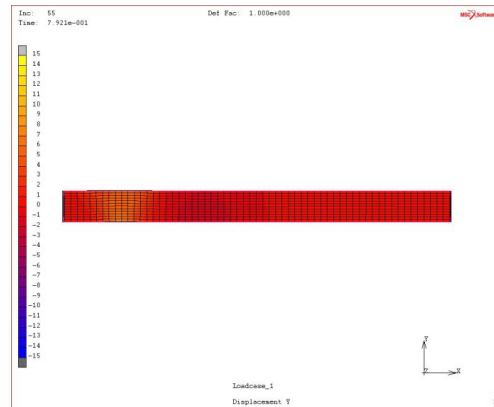
Increment 45



Increment 49

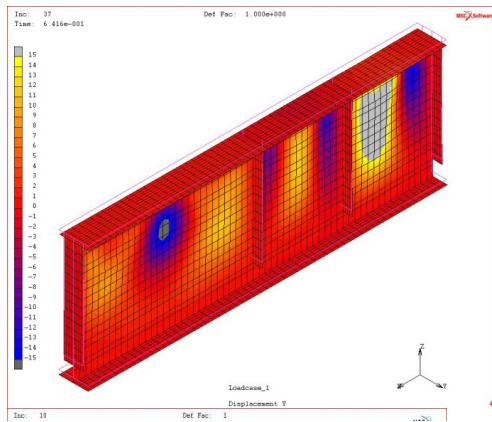


Increment 53

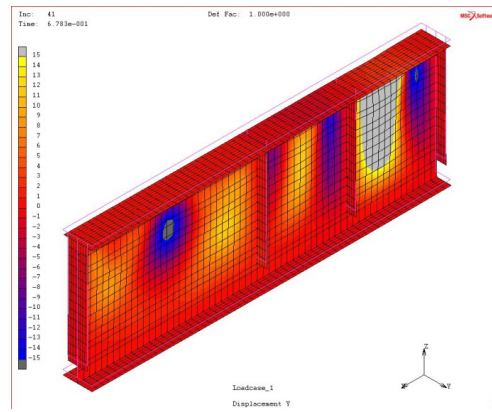


Increment 55

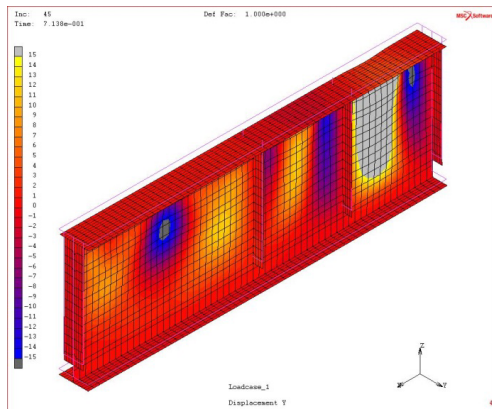
Figure 3-44 The lateral deflection δ_y of the top flange of the test area of girder G4-T2, residual stresses according to NEN6771 for different load levels



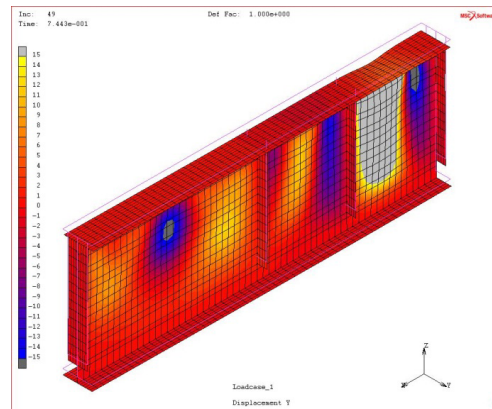
Increment 37



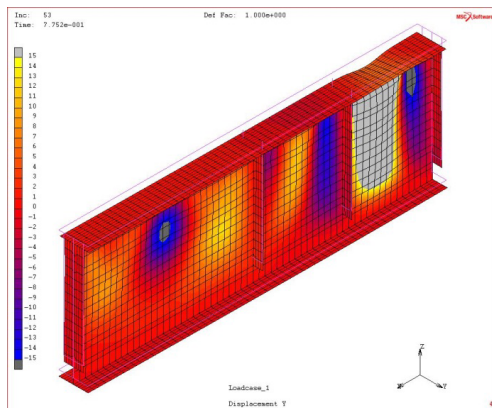
Increment 41



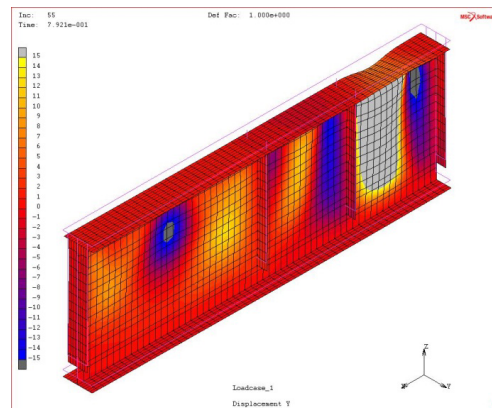
Increment 45



Increment 13

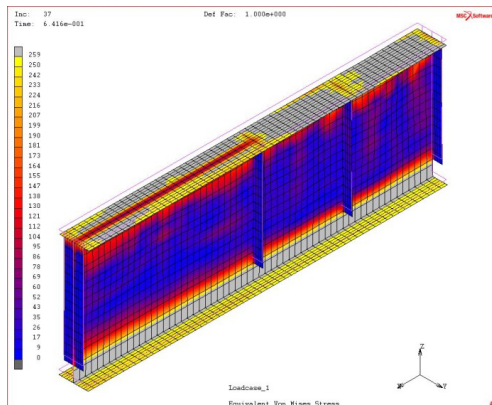


Increment 53

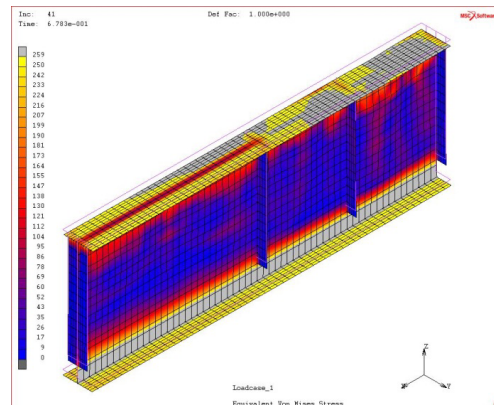


Increment 55

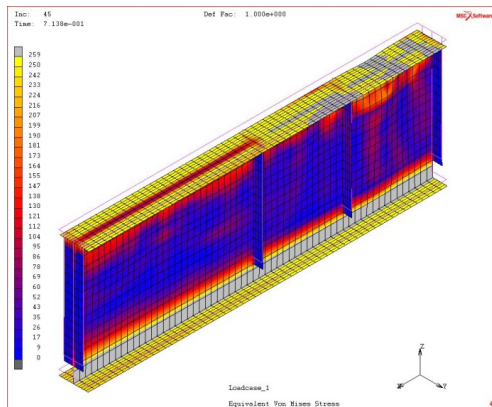
Figure 3-45 3-D views of the lateral deflection δ_y of the test area of girder G4-T2, residual stresses according to NEN6771 for different load levels



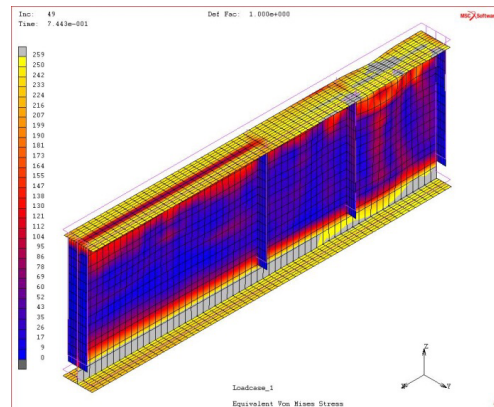
Increment 37



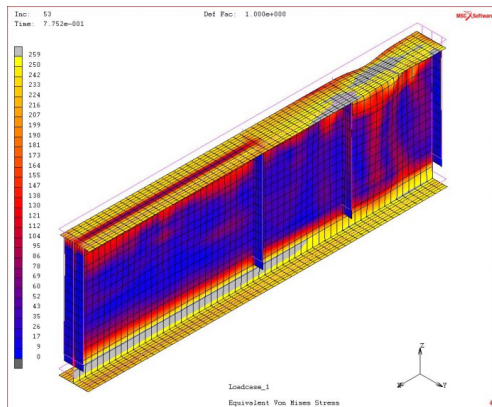
Increment 41



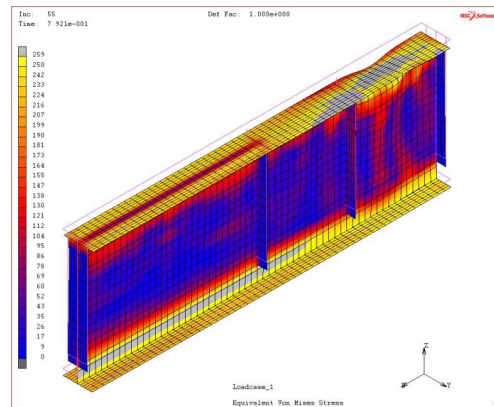
Increment 45



Increment 49

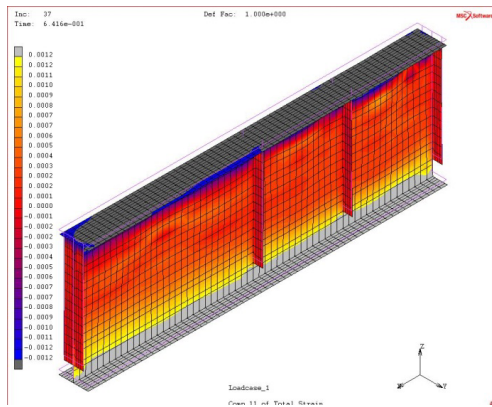


Increment 53

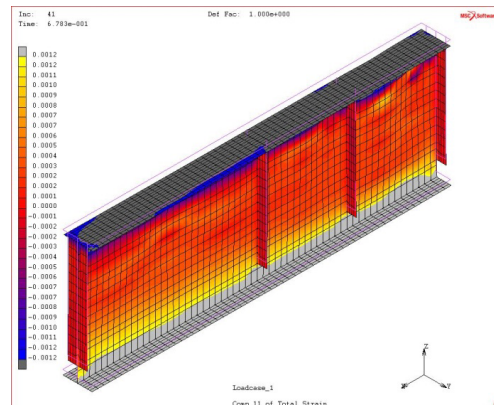


Increment 55

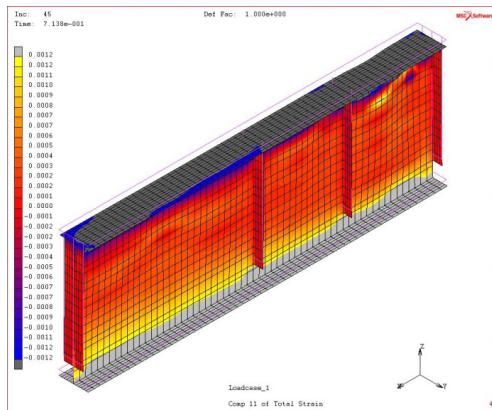
Figure 3-46 3-D views of the Von Mises stresses $\sigma_{Von Mises}$ in the test area of girder G4-T2, residual stresses according to NEN6771 for different load levels



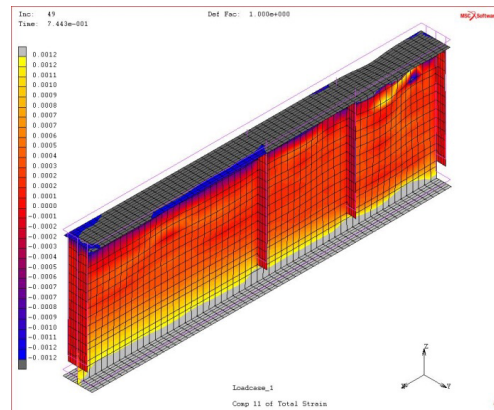
Increment 37



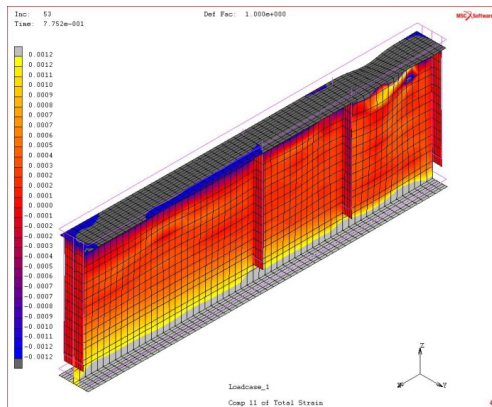
Increment 41



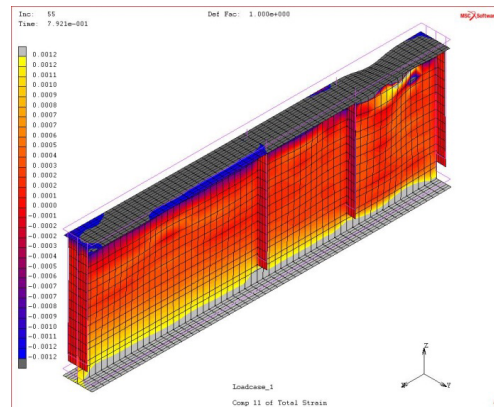
Increment 45



Increment 49



Increment 53



Increment 55

Figure 3-47 3-D views of the strains ε in the test area of girder G4-T2, residual stresses according to NEN6771 for different load levels

Based on Figure 3-44 and Figure 3-45 it looks like lateral buckling of the flange of test panel 1 occurs.

3.7.3 FEM-MODEL WITH RESIDUAL STRESSES ACCORDING TO BSK99, TEST T1

The same kind of results is presented for the FEM-models G4-T1 with initial stresses representing the residual stress distribution according to the previous Swedish code BSK99. The P - δ diagrams of experiment and of the FEM-model of specimen G4-T1 are presented in Figure 3-48.

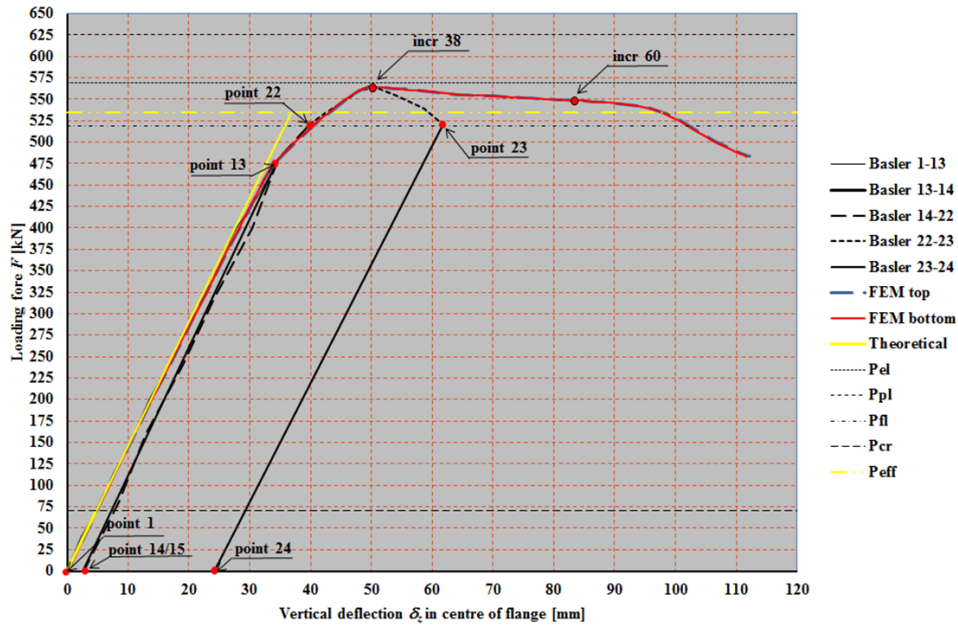


Figure 3-48 P - δ diagram of experiment G4-T1 and FEM with residual stress according to BSK99

From this P - δ diagram the following can be seen:

1. The maximum load of $P_{FEM,BSK,G4-T1} = 564.0 \text{ kN}$ is very close to the dynamic ultimate load of the experiment $P_{G4-T1} = 565.5 \text{ kN}$. Both forces lead to bending moment resistances, determined by $M_u = P_u \cdot a$, namely $M_{FEM,G4-T1} = 2148.9 \text{ kNm}$ and $M_{Basler,G4-T1} = 2154.6 \text{ kNm}$. The difference is 0.27 %;
2. The top of the P - δ is found for a deflection of $\delta_{FEM,G4-T1} = 50.9 \text{ mm}$ for increment 38 in the FEM-model and $\delta_{Basler,G4-T1} = 50.8 \text{ mm}$ in the experiment. The difference is 0.20%;

3. The stiffness of the FEM-model is very close to the actual stiffness of the experiment. This means that the deflections are more or less the same. This is due to a good assumption of the residual stresses related to the roughly determined initial imperfections based on the measurements of Basler;
4. The stiffness of both, the FEM-model and the experiment, is according to the theoretical stiffness as determined in Chapter 3.6;
5. The ultimate force is very close to the theoretical elastic bending moment resistance as determined in Chapter 3.5.2, namely $P_{el}=569.2\text{ kN}$ with a difference of only 0.65 %. This is explained in Chapter 3.7.1.

The lateral deflections presented in Table 3-5 for test panel 3 In Figure 3-49 show the lateral deflections of the top flange in the centre of the three test panels.

Table 3-5 Horizontal deflection δ_y top flange of specimen G4-T1, test panel 3

	Incr. 10	Incr. 20	Incr. 30	Incr. 38	Incr. 40	Incr. 50	Incr. 60	Incr. 70	Incr. 80
δ_y [mm]	+0.02	+0.03	+0.91	+3.73	+5.09	+12.02	+18.64	+24.13	+28.25

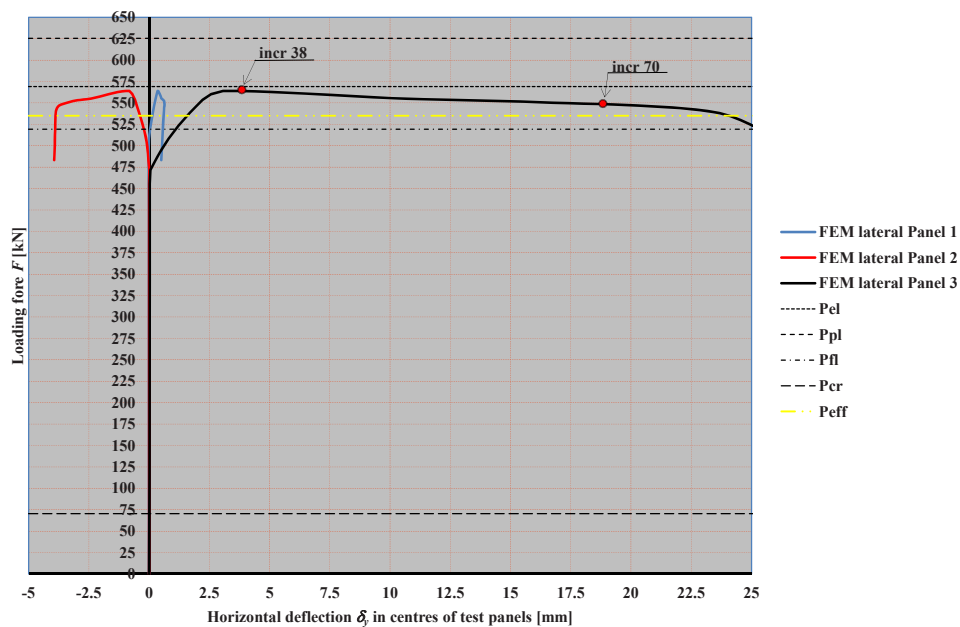
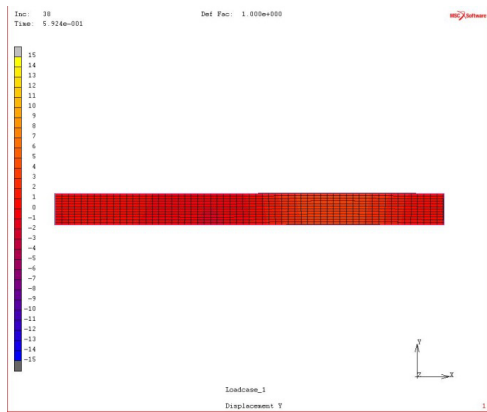
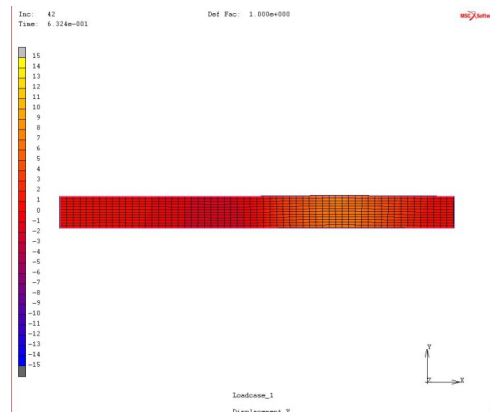


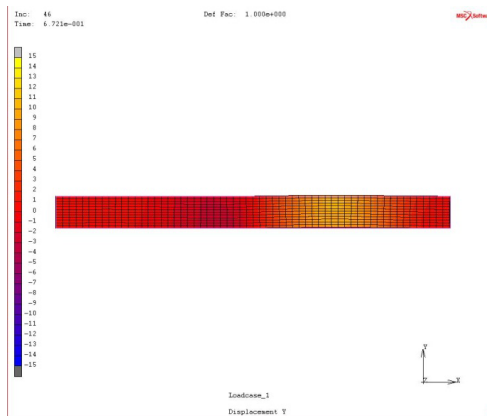
Figure 3-49 P - δ diagram horizontal deflections of the compressive flange of test panels 1 to 3 of experiment G4-T1, residual stress according to BSK99



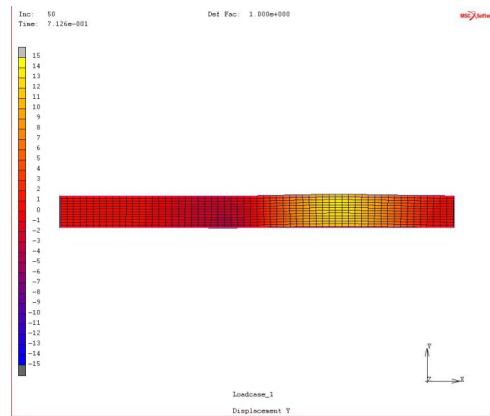
Increment 38



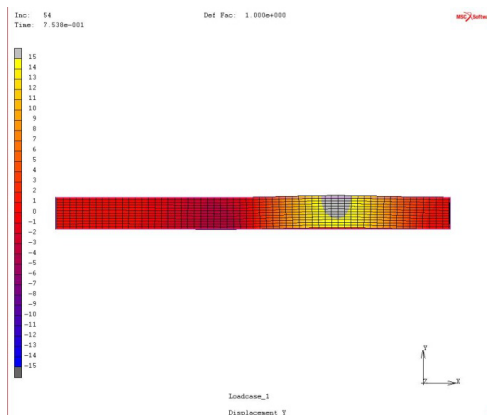
Increment 42



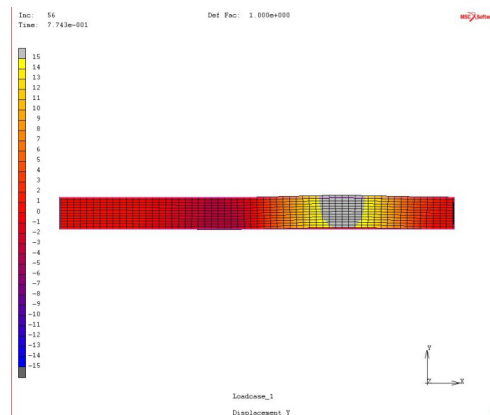
Increment 46



Increment 50

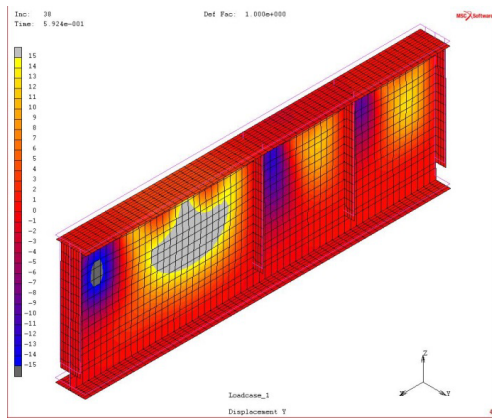


Increment 54

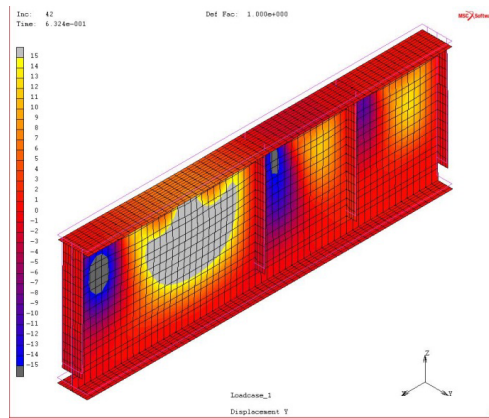


Increment 56

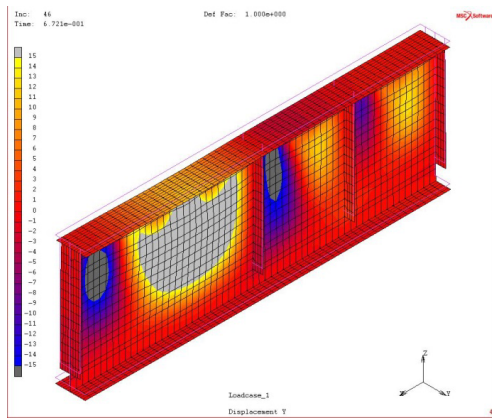
Figure 3-50 Top views of the lateral deflection δ_y of the top flange of the test area of girder G4-T1, residual stresses according to BSK99 for different load levels



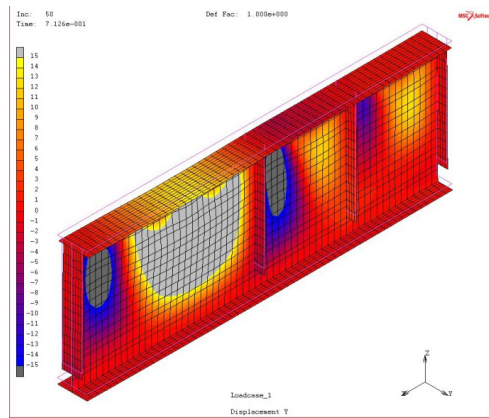
Increment 38



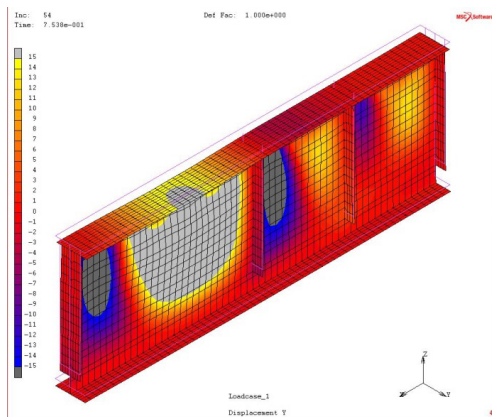
Increment 42



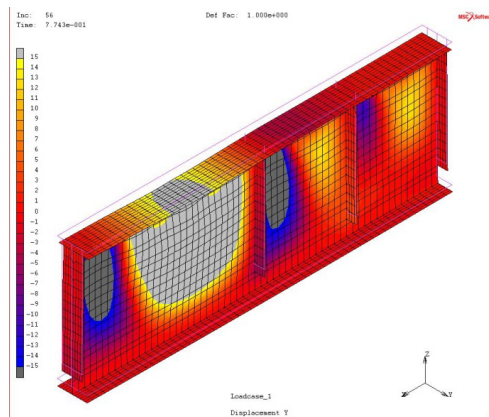
Increment 46



Increment 50

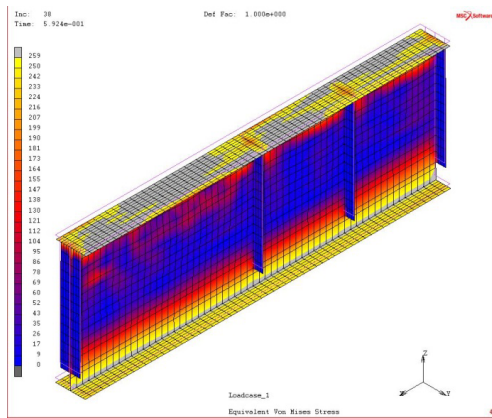


Increment 54

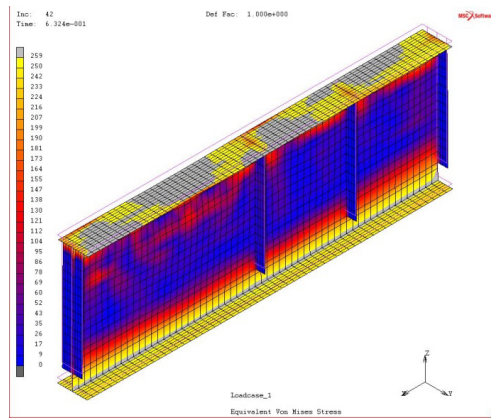


Increment 56

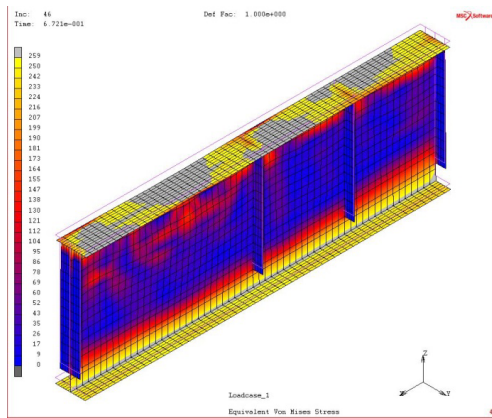
Figure 3-51 3-D views of the lateral deflection δ_y of the test area of girder G4-T1, residual stress-
es according to BSK99 for different increments



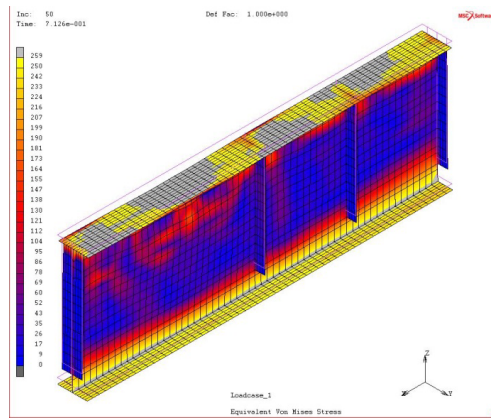
Increment 38



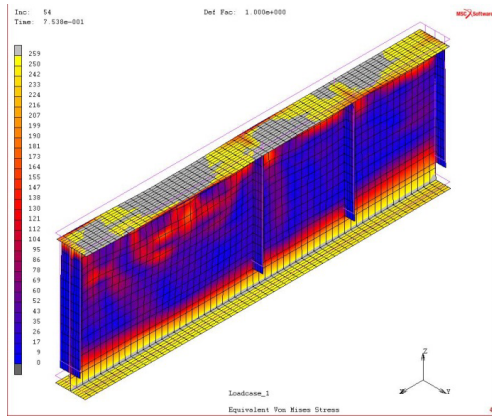
Increment 42



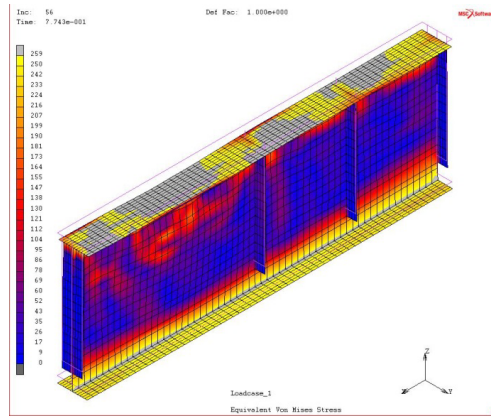
Increment 46



Increment 50

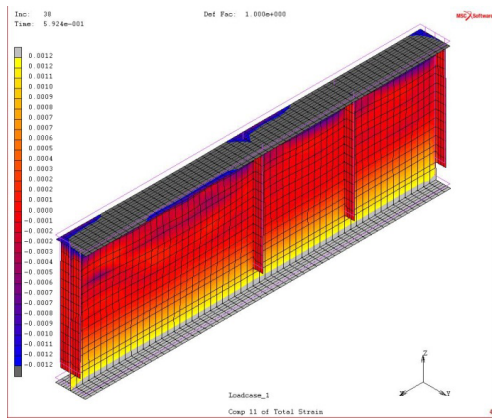


Increment 54

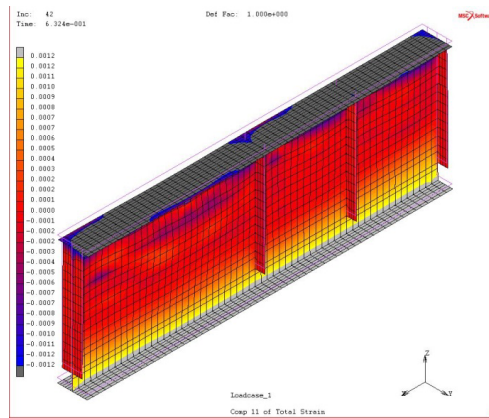


Increment 56

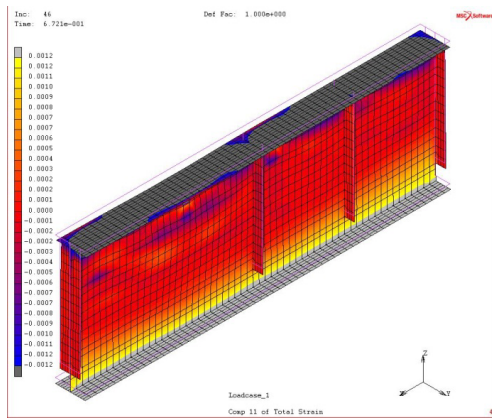
Figure 3-52 3-D views of the Von Mises stresses $\sigma_{Von Mises}$ in the test area of girder G4-T1, residual stresses according to BSK99 for different load levels



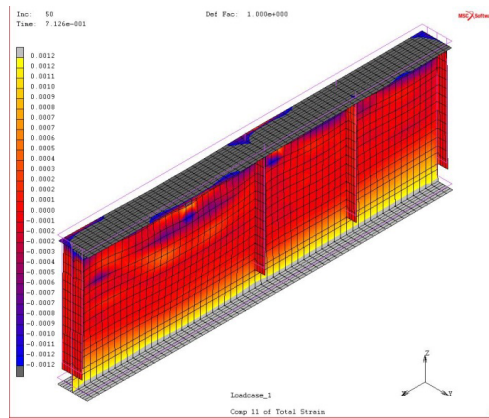
Increment 38



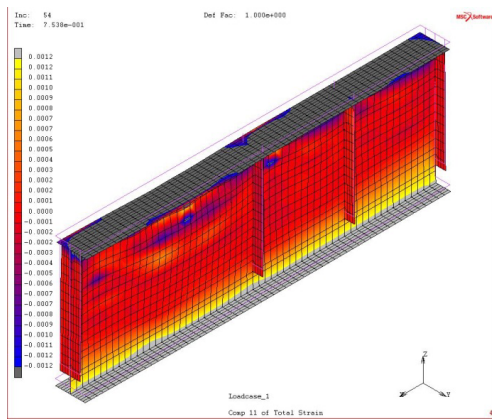
Increment 42



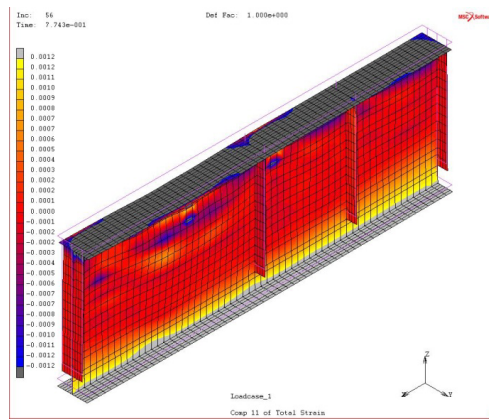
Increment 46



Increment 50



Increment 54



Increment 56

Figure 3-53 3-D views of the strains ε in the test area of girder G4-T1, residual stresses according to BSK99 for different load levels

3.7.4 FEM-MODEL WITH RESIDUAL STRESSES ACCORDING TO BSK99, TEST T2

Finally, the results of FEM-model G4-T2 with an assumed residual stress according to BSK99 are compared with the results of the laboratory test of Basler. In Figure 3-54 the P - δ diagram is shown.

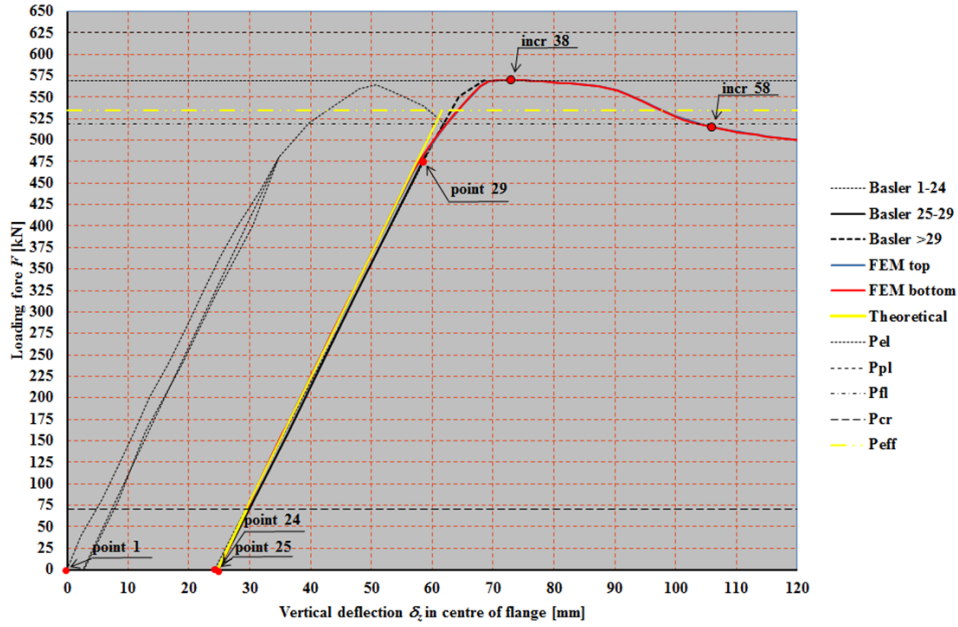


Figure 3-54 P - δ diagram of experiment G4-T2 and FEM with residual stress according to BSK99

From this P - δ diagram the following can be seen:

1. The maximum load of $P_{FEM.NEN.G4-T2} = 569.3 \text{ kN}$ is very close to the dynamic ultimate load of the experiment $P_{G4-T2} = 569.4 \text{ kN}$. Both forces lead to bending moment resistances, determined by $M_u = P_u \cdot a$, namely $M_{FEM.G4-T1} = 2169.1 \text{ kNm}$ and $M_{Basler.G4-T2} = 2169.4 \text{ kNm}$. The difference is 0.02 %;
2. The top of the P - δ is found for a deflection of $\delta_{FEM.G4-T1} = 75.3 \text{ mm}$ for increment 38 in the FEM-model and $\delta_{Basler.G4-T1} = 68.0 \text{ mm}$ in the experiment. The difference is 10.74%;
3. The stiffness of the FEM-model is up to a load of $P = 500.0 \text{ kN}$ according to the theoretical stiffness as determined in Chapter 3.6 and for higher loads the FEM-model behaves more flexible. This is due to the assumed residual stresses and the rather roughly determined im-

perfections based on the measurements of Basler. Further, the girder is influenced by the first test, test T1. Basler presented the deflection up to point 13 in his $P - \delta$ diagram, so the initial imperfections at the start of the second test, test T2, that is at point 24, is not known. It can be expected that the residual stresses were smaller and the geometrical imperfections were larger than in test T1;

4. The stiffness of the experiment is very close to the theoretical stiffness;
5. The stiffness of the FEM-model is also very close to the stiffness of the experiments. As pointed out in 3, the assumed initial imperfections are too small and the residual stresses are too high, while it is shown that the girder dimensions of the FEM-model correspond to those of the experiment, see Chapter 3.7.1;

Table 3-6 presents the horizontal deflections of panel 2. Figure 3-55 shows the horizontal deflections for all three test panels.

Table 3-6 Horizontal deflection δ_y top flange of specimen G4-T2 test panel 2

	Incr. 10	Incr. 20	Incr. 30	Incr. 38	Incr. 40	Incr. 50	Incr. 60	Incr. 70
δ_y [mm]	+0.00	+0.00	+0.30	+1.68	+2.17	+4.16	+6.74	+9.77

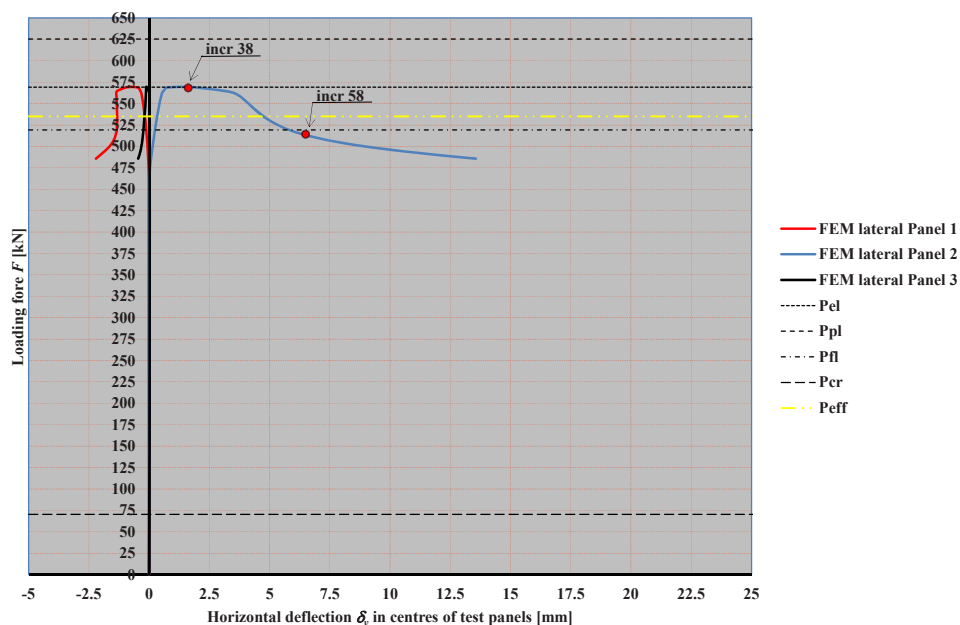


Figure 3-55 $P - \delta$ diagram horizontal deflections of the compressive flange of test panels 1 to 3 experiment G4-T2, residual stress according to BSK99

Just as in the previous FEM-models, the lateral deflection is presented from the top view of the compressive flange in Figure 3-56 and Figure 3-57. Both other test panels hardly deflect laterally.

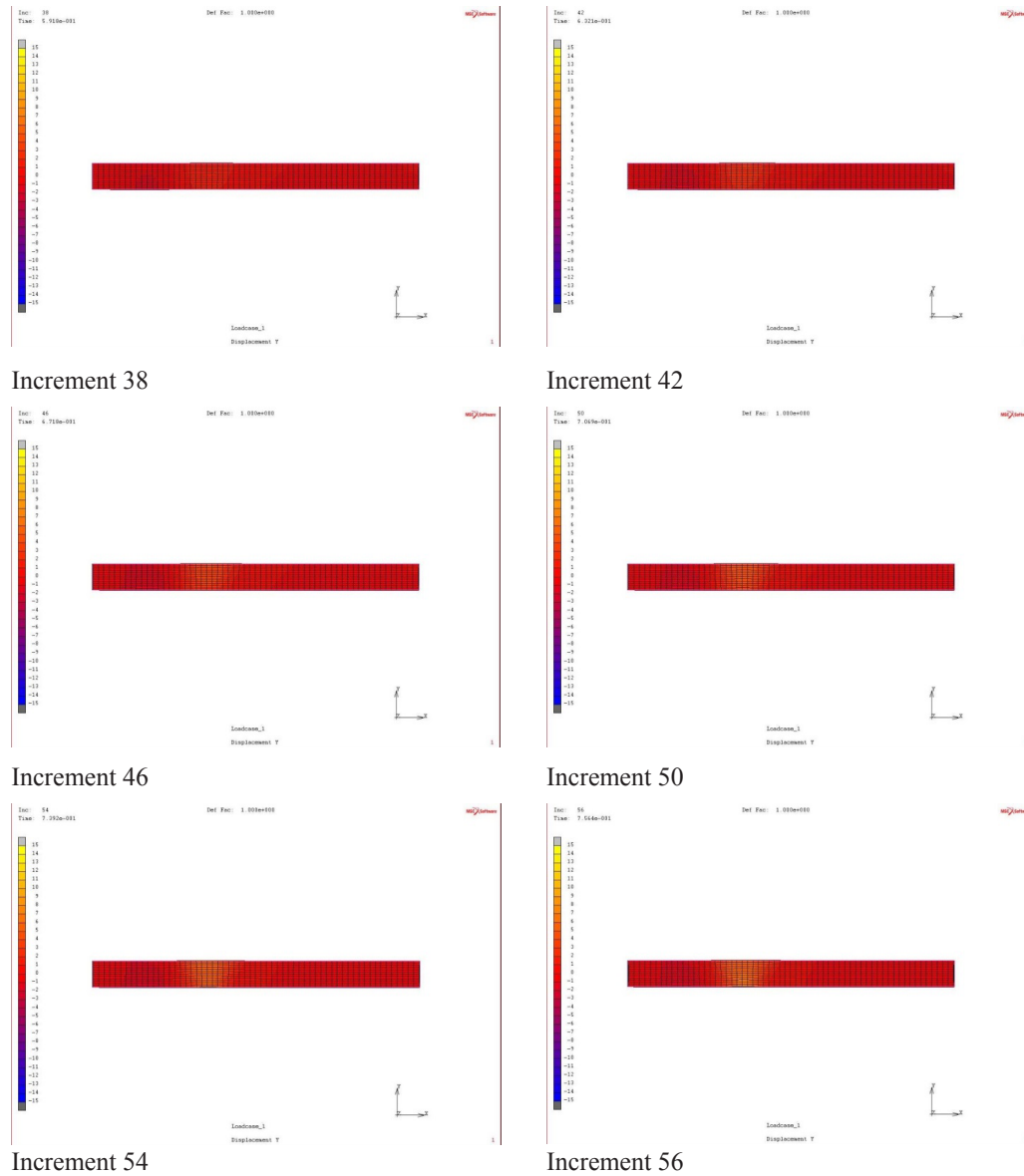


Figure 3-56 Top views of the lateral deflection δ_y of the top flange of the test area of girder G4-T2, residual stresses according to BSK99 for different increments

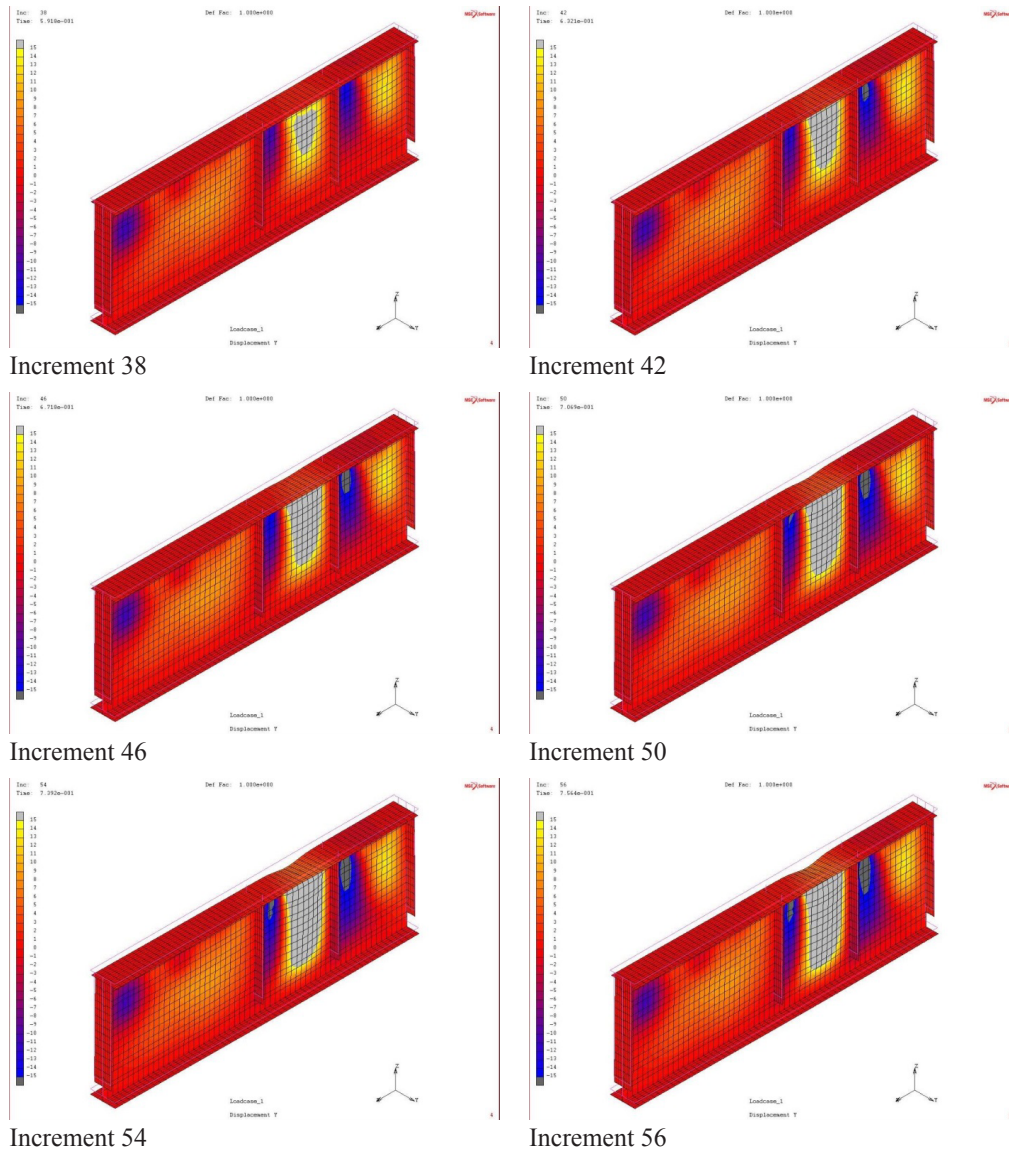
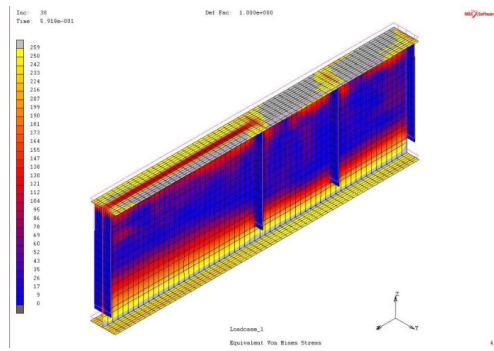
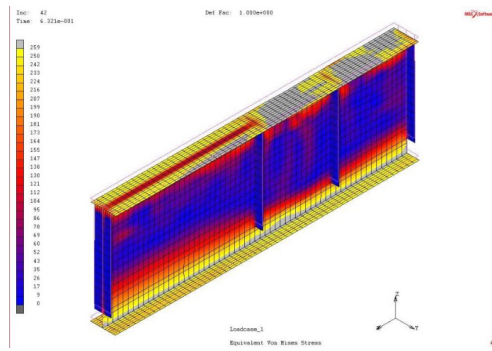


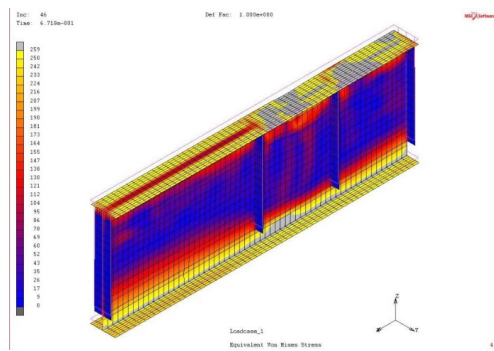
Figure 3-57 3-D views of the lateral deflection δ_y of the test area of girder G4-T2, residual stresses according to BSK99 for different load levels



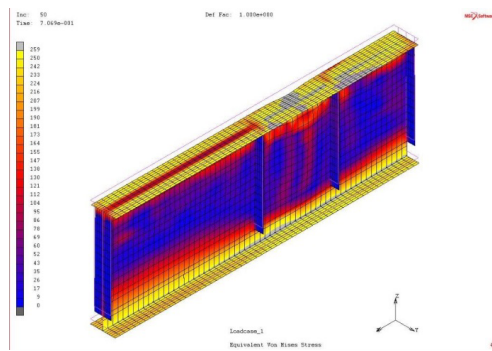
Increment 38



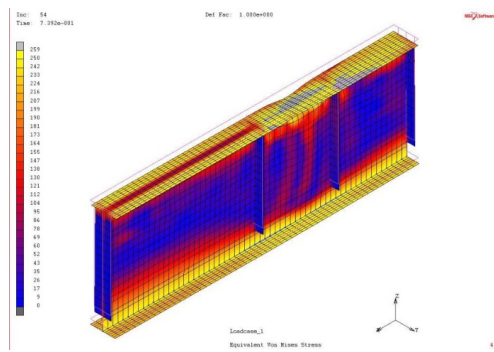
Increment 42



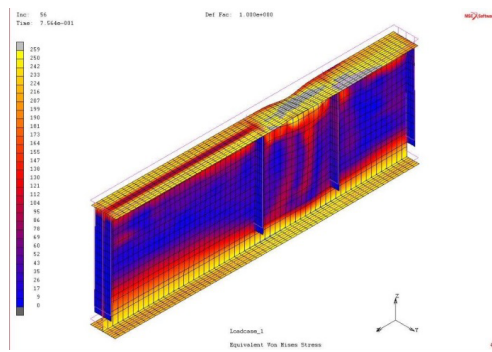
Increment 46



Increment 50



Increment 54



Increment 56

Figure 3-58 3-D views of the Von Mises stresses $\sigma_{Von Mises}$ in the test area of girder G4-T2, residual stresses according to BSK99 for different increments

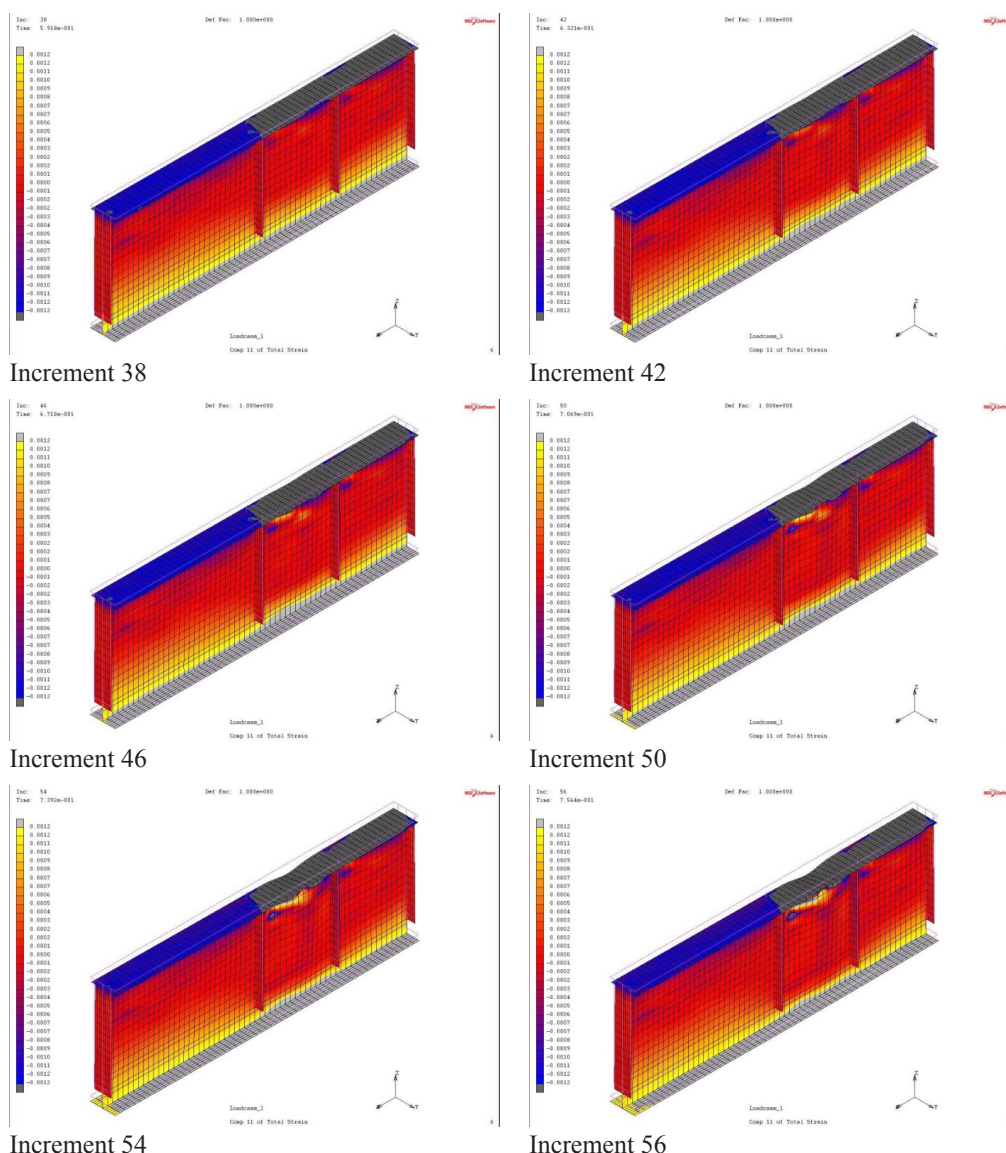


Figure 3-59 3-D views of the strains ε in the test area of girder G4-T2, residual stresses according to BSK99 for different increments

3.7.5 COMPARISON LABORATORY SPECIMEN G4 AND FEM-CALCULATIONS

The theoretical resistances are shown in Table 3-7, based on Basler as well as based on EN1993-1-5. Table 3-8 shows the bending moment resistance determined with FEM-calculations and the differences compared with the bending moment resistance based on the laboratory tests by Basler. Table 3-9 shows the deflections according to the FEM-calculations and the laboratory tests by Basler.

Table 3-7 Theoretical bending moment resistances of Basler test specimen G4 test T1 and T2 based on actual dimensions and actual material properties

	M_{el}	M_{pl}	M_f	M_{cr}	M_{eff}	$M_{test} (M_{max})$	
	[kNm]	[kNm]	[kNm]	[kNm]	[kNm]	[kNm]	
					G4-T1	G4-T2	
Basler	2203.2	2355.7		259.3	2033.1	2050.7	2154.6
EN-1993-1-5	2168.8	2383.0	1978.4	268.4	2038.7	2038.7	-

Table 3-8 Bending moment resistances according to FEM-models

	FEM-models		FEM-models	
	Residual stresses according to NEN6771		Residual stresses according to BSK99	
	G4-T1	G4-T2	G4-T1	G4-T2
M_u [kNm]	2152.8	2170.2	2148.9	2169.1
Difference	-0.09 %	+0.04 %	-0.26 %	-0.00 %

Table 3-9 Deflections according to FEM-models and according to Basler

	FEM-models		FEM-models		Experiment	
	Residual stresses according to NEN6771		Residual stresses according to BSK99			
	G4-T1	G4-T2	G4-T1	G4-T2	G4-T1	G4-T2
δ [mm]	58.3	81.7	50.9	75.3	50.8	68.0
Difference	+14.76 %	20.15 %	+0.20 %	+10.74 %		

The difference in elastic and plastic bending moment resistance based on Basler and based on EN-1993-1-5 is explained in Chapter 3.7.1. The difference in effective moment resistance according to Basler for girder G4-T1 and G4-T2 is caused by the reduced stress due to lateral buckling of the compressive flange in panel 3.

3.8 CONCLUSIONS ON THE VALIDATION OF THE FEM-MODELS ON THE BASLER TEST GIRDER

The following can be concluded about the validation of the four FEM-models on the experiments:

1. The bending moment resistances of the FEM-model for test girder G4, as well for test T1 as for test T2, fit very well with the bending moment resistances based on the test results;
2. The bending moment resistance of experiment G4-T1 is $M_{Basler.G4-T1} = 2154.6 \text{ kNm}$ is higher than the effective bending moment resistance $M_{eff} = 2038.7 \text{ kNm}$ according to EN1993-1-5, a difference of -5.38 %;
3. The bending moment resistance of experiment G4-T2 is $M_{Basler.G4-T2} = 2169.3 \text{ kNm}$ is higher than the effective bending moment resistance $M_{eff} = 2038.7 \text{ kNm}$ according to EN1993-1-5, a difference -6.02 %;
4. The bending moment resistances of experiment G4-T1 as well as experiment G4-T2, respectively $M_{Basler.G4-T1} = 2154.6 \text{ kNm}$ and $M_{Basler.G4-T2} = 2169.3 \text{ kNm}$, are very close to the elastic bending moment $M_{el} = 2168.8 \text{ kNm}$ according to EN-1993-1-5, with differences of only -0.65 % and +0.02 %. Of course this is strange, because girder G4 had a very slender web and so the effective resistance should be the ultimate resistance;
5. The differences in bending moment resistance according to the four FEM-models and the bending moment resistances of the experiments are very small, less than 0.17 %;
6. The differences in the resistances based on the FEM-models with initial stresses based on the residual stress distribution according to the previous Swedish code BSK99 compared with the resistances of both experiments, so G4-T1 and G4-T2, are smaller than the FEM-models with initial stresses based on the residual stress distribution according to the previous Dutch code NEN6771;
7. The differences in deflection vary between 0.20 % and 20.15 %, so rather great differences. This is due to the rather rough measuring of the initial imperfections based on graphs of Basler, but also on the assumption of the residual stress distribution;
8. The FEM-models with initial stresses based on the residual stress distribution based on the previous Swedish code BSK99 give smaller differences in deflections than the FEM-models with initial stresses based on the residual stress distribution based on the previous Dutch code NEN6771;
9. The failure mode of both models for experiment G4-T1 is lateral buckling of the compressive flange in test panel 3, the same as in the experiment;

10. The failure mode of the FEM-model for experiment G4-T2 with initial stresses based on the residual stress distribution according to the previous Dutch code NEN6771 is torsional buckling of the compressive flange in test panel 1. When the load is increased the failure mode is vertical buckling of the compressive flange into the web, the same as in experiment G4-T2;
11. The failure mode of the FEM-model for experiment G4-T2 with initial stressed based on the residual stress distribution according to the previous Swedish code is torsional buckling of the compressive flange in test panel 2, instead of in vertical buckling of the compressive flange into the web in test panel 1 in experiment G4-T2.

In further FEM-models the initial stresses are based on the residual stress distribution of the previous Swedish code BSK99, because of the FEM-results are very similar to the results of the experiments,.

4 DESCRIPTION OF THE TEST SPECIMENS, TEST RIG AND INSTRUMENTATION OF THE DELFT EXPERIMENTS

4.1 GENERAL

At the Stevin II Laboratory of the Delft University of Technology 10 model-scale plate girders are subjected to a four point bending test, similar to the test specimen G4 of Basler [12]. In Figure 4-1 a schematic presentation of the test setup is given.

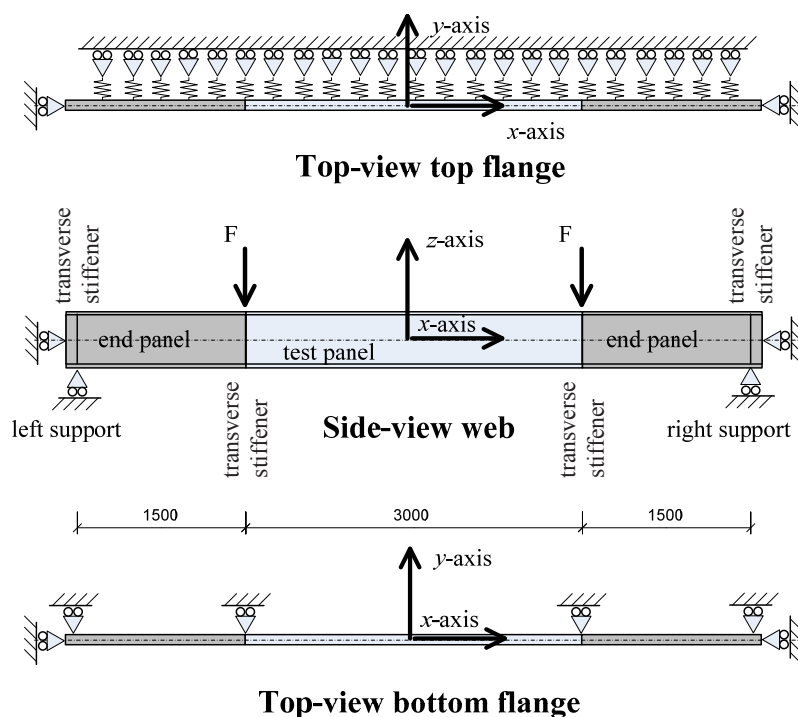


Figure 4-1 Schematic presentation of a test specimen and the test rig

The focus is put on the part of the girder under pure bending. The web of that part of the girder under pure bending, called test panel, is an unstiffened plate. The geometry of the test specimens is described in Chapter 4.2.

The actual material properties are determined by performing standard tensile tests and presented in Chapter 4.3. In that chapter also the theoretical resistances of the girder under pure bending based on actual dimensions and actual material strengths are presented.

The test rig including the supports and the instrumentation of the test specimen are presented in Chapter 4.4. The fabrication and the initial imperfections of the plate girders are described in Chapter 4.5.

4.2 GEOMETRY

4.2.1 NOMINAL DIMENSIONS

The test specimens are double symmetric I-shaped plate girders, see Figure 4-2.

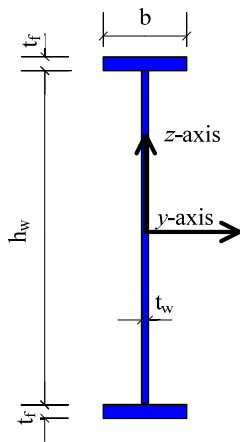


Figure 4-2 Cross-section of the test specimen

The design of the test specimens is based on the ratio of area $\rho = \frac{A_w}{A_f}$ and the web slenderness

$\beta_w = \frac{h_w}{t_w}$, as discussed in Chapter 2, which is based on the dimensions of the plate girder, the flange thickness t_f , the flange width b , the web thickness t_w and the web height h_w .

The web slenderness β_w of interest lies between 400 and 800, related to commonly used ratios of areas ρ , between $\frac{1}{2}$ and 2 according to Basler [12]. Based on Basler's formula for the maximum web slenderness $\beta_{w, \max}$, see Eq.(2.38), the web slenderness β_w lies between 360 and 720. Because of the shift of the neutral axis due to the use of the effective width method, these web slenderness's are taken higher than described by Basler, namely between 400 and 800.

The smallest plate thickness for a web to be welded to flanges is approximately 3 mm. To realise a web slenderness $\beta_w = 800$, starting with a web thickness of 3 mm, leads to a web height of 2400 mm. Slender beams made of rolled sections have a beam slenderness $\frac{\ell}{h}$ between 20 and 40. How-

ever, plate girders commonly have a beam slenderness ℓ/h in the range between 7.5-20, comparable to that of trusses. Using a beam slenderness of $\frac{\ell}{h} \approx 10$, would lead to a span ℓ of 24 m. To make these relatively large objects more suitable for testing in a laboratory, the dimensions are scaled down to a web thickness of 1 mm and a span of 6000 mm for all 10 test specimens. Based on this web thickness $t_w = 1 \text{ mm}$, web heights of 400 mm, 600 mm and 800 mm are used, which leads to a web slenderness β_w of 400, 600 and 800 respectively and so the beam slenderness's ℓ/h are 15, 10 and 7.5.

Related to the limitation of the ratios of area $\frac{1}{2} \leq \rho \leq 2.0$, the cross-sectional area of the flanges is taken 200 mm^2 and 400 mm^2 . Based on the flange slenderness of cross-section class 3 according to EN1993-1-1 [30], the following flange dimensions are taken: $50 \times 4 \text{ mm}^2$, $80 \times 5 \text{ mm}^2$ and $100 \times 4 \text{ mm}^2$. The last two flanges have the same flange area A_f , but different flange dimensions. Especially, because of the difference in flange thicknesses t_f , the torsional stiffnesses EI_t differ, based on $b \cdot t_f^3$. The nominal geometrical dimensions of the test specimens are given in Table 4-1.

Table 4-1 Nominal dimensions of test girders

No.	Test specimen	h_w [mm]	t_w [mm]	b [mm]	t_f [mm]	$\beta_w = \frac{h_w}{t_w}$	$\rho = \frac{A_w}{A_f}$
1	400x50	400	1.0	50	4	400	2.0
2	400x80(1)	400	1.0	80	5	400	1.0
3	400x80(2)	400	1.0	80	5	400	1.0
4	400x100	400	1.0	100	4	400	1.0
5	600x50	600	1.0	50	4	600	3.0
6	600x80	600	1.0	80	5	600	1.5
7	600x100	600	1.0	100	4	600	1.5
8	800x50	800	1.0	50	4	800	4.0
9	800x80	800	1.0	80	5	800	2.0
10	800x100	800	1.0	100	4	800	2.0

As can be seen in this table, the ratio of area ρ varies between $1.0 \leq \rho \leq 4.0$ for the combinations of web areas and flange areas. According to Basler's equation for the maximum web slenderness, see Eq.(2.38), the ratio of area ρ has to be as big as possible to find the ultimate bending moment resistance for a certain amount of steel. On the other hand, in Chapter 2.7 it is shown that this ratio

of area ρ will be close to 1.0 to determine the maximum bending moment resistance based on the elaborations on several researches, see Chapter 2.7.

Starting point in the design of plate girders is that the flanges are not susceptible to plate buckling and consequently they need to be of cross-sectional class 1, 2 and 3 at the utmost. The $\frac{b}{t}$ ratio for a

flange for cross-sectional class 3 is $\frac{c}{t_f} \leq 14\varepsilon$, which roughly corresponds with $\frac{b}{2t_f} \leq 14\varepsilon$ when the

web thickness t_w and the dimensions of the weld are not taken into account. The factor $\varepsilon = \sqrt{\frac{235}{f_y}}$

takes the influence into account of the yield strength f_y . For yield strengths higher than S235, this

cross-sectional limit $\frac{b}{2t_f} \leq 14\varepsilon$ will be smaller than 14.

The flanges are continuous over the whole span of the test specimen. To reduce the influence of the panels that are loaded in the combination of bending and shear, the so called end panels, the nominal web thickness taken is 4 mm.

4.2.2 ACTUAL DIMENSIONS

The actual dimensions of these test girders are different from the nominal dimensions due to tolerances and geometrical imperfections. The dimensions of each element, the top flange, the bottom flange and the web, are measured at five specific locations, I to V, over the span of the test specimen, at the front as well as the reverse side of the girder, see Figure 4-3.

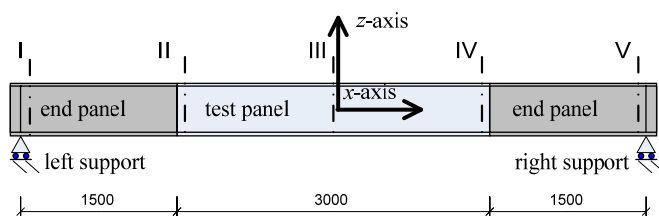


Figure 4-3 Locations of the measurements of the dimensions of the test specimens

In each of the cross-sections I to V, the following dimensions are measured, see also Figure 4-4:

- The thickness of the top flange as well as the bottom flange at the front and the back side of the girder, respectively $t_{tf,1}$, $t_{tf,2}$, $t_{bf,1}$ and $t_{bf,2}$. Here, 1 is the index for the front and 2 for the back;

- The width of top and bottom flange, respectively b_{tf} and b_{bf} ;
- The distances of the edges of the top as well as at the bottom flange to the web, at the front as well as at the reverse side of the test specimen, respectively $b_{tf.e1}$, $b_{tf.e2}$, $b_{bf.e1}$ and $b_{bf.e2}$
- The total height of the test specimen, at the front as well as at reverse side, respectively h_1 and h_2 ;
- The thickness t_w of the web of the test panels;
- The thickness $t_{w.ep}$ of the web of the test panels is measured once.

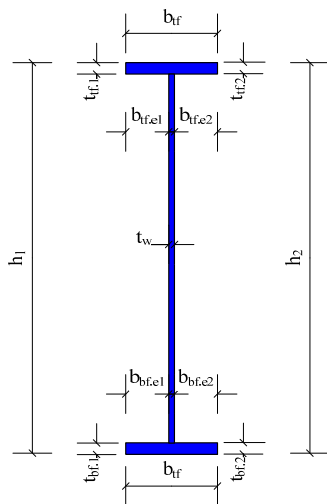


Figure 4-4 Locations of the measurements of the dimensions of the test specimens

The average dimensions are shown in Table 4-2. This table includes the maximum web slenderness and the ratio of area.

Table 4-2 Actual average dimensions of test girders

Test girder	h_w [mm]	$t_{w,tp}$ [mm]	$t_{w,ep}$ [mm]	b_{tf} [mm]	t_{tf} [mm]	b_{bf} [mm]	t_{bf} [mm]	β_w [-]	$\beta_{w,max}$ [-]	ρ [-]
1, 400x50	400.0	1.01	3.99	49.7	4.36	49.8	4.33	396.1	471.2	1.87
2, 400x80(1)	399.3	1.00	4.00	80.0	5.40	80.0	5.29	399.3	344.7	0.92
3, 400x80(2)	399.8	1.02	4.07	80.1	5.57	79.8	5.53	392.0	349.6	0.91
4, 400x100	400.1	0.93	4.05	98.7	4.29	98.9	4.37	430.2	315.7	0.88
5, 600x50	601.6	1.02	3.99	49.6	4.48	49.9	4.47	589.8	585.0	2.76
6, 600x80	600.2	0.97	4.01	79.9	5.53	79.9	5.66	618.7	403.1	1.32
7, 600x100	600.1	0.97	4.00	99.1	4.31	98.7	4.33	618.7	395.5	1.36
8, 800x50	801.0	0.97	3.98	50.2	4.40	49.5	4.37	825.8	664.2	3.51
9, 800x80	799.4	0.98	4.01	80.2	5.60	80.1	5.60	815.7	476.8	1.75
10, 800x100	799.4	1.00	3.99	98.8	4.24	98.7	4.24	799.4	470.7	1.91

4.3 ACTUAL MATERIAL PROPERTIES

For the test specimens, the steel grade S235 is selected. To determine the actual strength of the web and flanges, tensile tests are performed. The plates for the webs are cut out of two plates of 6 x 3 m², one with a nominal thickness of 1 mm for the test panels and another plate with a nominal thickness of 4 mm for the end panels.

The actual yield strengths of the flanges and web of the plate girders, these are the $\sigma_{0.2}$ of the tensile tests, are shown in Table 4-3.

Table 4-3 Actual yield strengths of the elements of test specimens in [MPa]

No.	1	2	3	4	5	6	7	8	9	10
Test girder	400x50	400x80(1)	400x80(2)	400x100	600x50	600x80	600x100	800x50	800x80	800x100
Top flange	335	322	316	343	328	329	341	326	320	339
Bottom flange	319	331	315	342	309	314	344	310	317	350
Web test panel	288	284	278	208	240	287	286	292	296	290

From this table it can be seen that two values are rather strange, compared with the other values of the $\sigma_{0.2}$ strengths, namely for the web of girders 4 and 5. This is due to the strange web thicknesses of these test specimens. These strengths are changed into the average value $\sigma_{0.2}$ of the tensile test specimens of the webs.

4.4 TEST RIG INCLUDING THE SUPPORTS AND THE INSTRUMENTATION

4.4.1 TEST RIG

Test specimens are subjected to a four-point bending test as presented in Figure 4-1. The test rig is built up from standard hot-rolled sections, see Figure 4-5. The loading is introduced by a hydraulic jack at the top flange of the plate girder at two locations via the spreader beam. A fixed roll is located on one side of the spreader beam. This fixed roll is fixed by two angles that are welded on each test specimen. Another roll is located at the other end of the spreader beam. The test specimen in longitudinal direction is supported at both ends with threaded rods in the centre of the web.

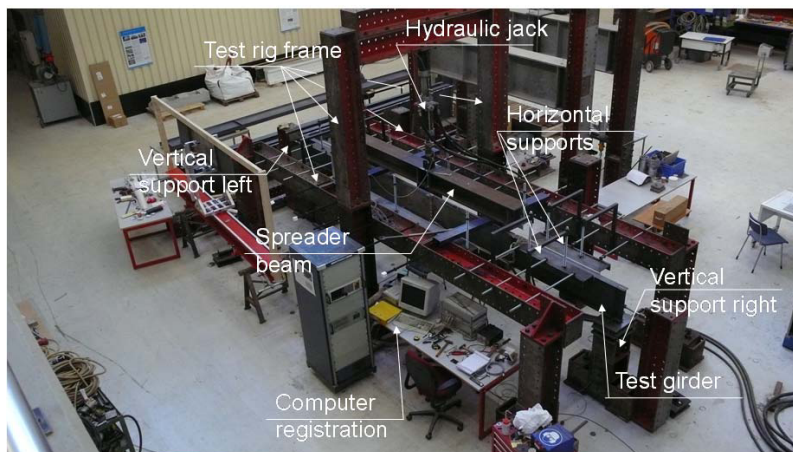


Figure 4-5 Test rig

The girders are simply supported in vertical direction at both ends. Rollers are placed between a package of plates at these supports, so the test specimen can elongate in longitudinal direction, see Figure 4-6 and Figure 4-7.

It is decided to place this package of plates at the top of the load cell because this simplified the way to install in the test specimen. Small elongations are expected and the load cells are calibrated on an eccentric load force.

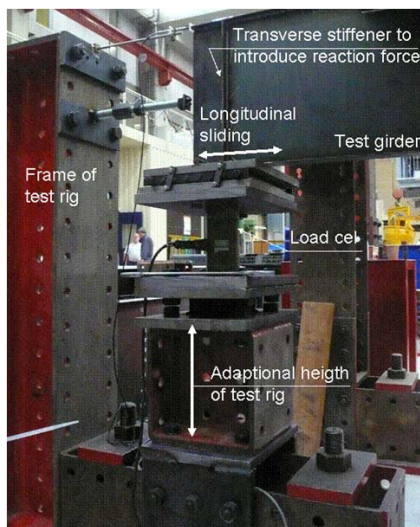


Figure 4-6 Left-hand side vertical support



Figure 4-7 Right-hand side vertical support

To prevent lateral torsional buckling, the top flange is laterally supported over the whole span of the girder, only interrupted by the equipment to transfer the loading from the spreader beam to the test specimen, see Figure 4-8. To reduce the friction between the edges of the top flange and the lateral supports, Teflon strips are glued to these lateral supports.

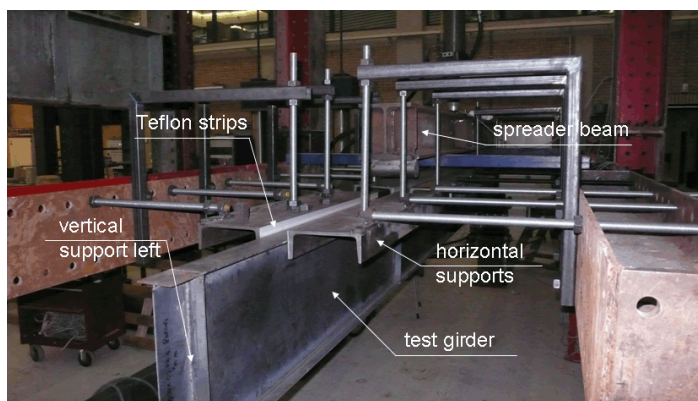


Figure 4-8 Horizontal supports of the top flange, including Teflon strips

Besides these lateral supports at the top flange, also lateral supports are placed at the bottom flange, close to the intermediate transverse stiffeners.

4.4.2 INSTRUMENTATION

To register the deformations at various load levels and to register these levels of forces during the experiments, the test specimen is equipped with instrumentation, see Figure 4-9.

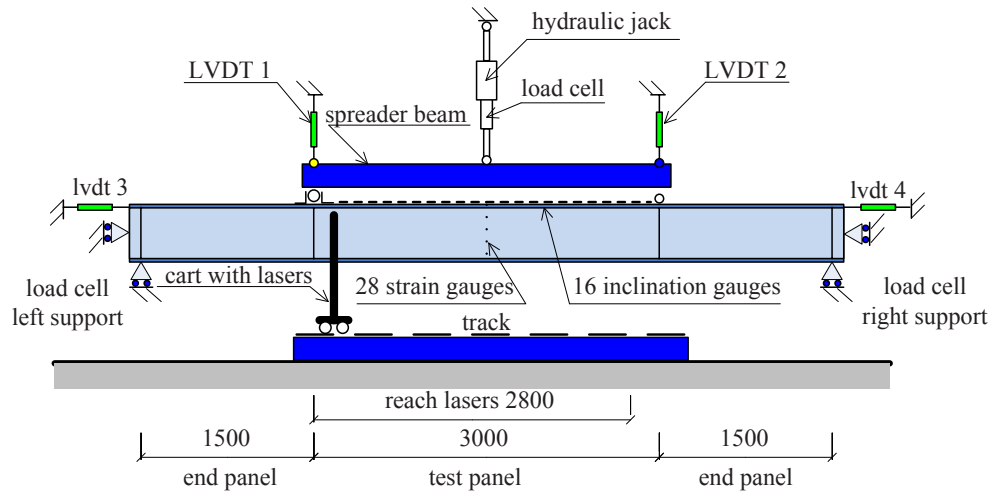


Figure 4-9 Overview of the instrumentation

The following data is measured:

- The loading caused by the actuator is measured with a load cell in-between this actuator and the spreader beam;
- The reaction forces are measured with a load cell at both vertical supports;
- The vertical deflection is measured by Lvd1 and Lvd2 at the top of the spreader beam at the location where the force is introduced into the test specimen. These Lvd's are positioned at the top flange of the spreader beam, because of the limited space in-between the top flange of the test specimen and the bottom of the spreader beam. At the bottom flange of the test specimen, the vertical displacement is measured using lasers and so it is not possible to place Lvd's under the test specimen;
- The longitudinal deflection at both sides of the edges of the test specimen is measured by Lvd3 and Lvd4, positioned at the top flange;
- The horizontal deflections of the web of the test panel is measured by several lasers. These lasers are positioned in a special cart on a track in longitudinal direction of the test panel, the x -direction, see Figure 4-10 and Figure 4-11.

During driving of the cart over the track, the vertical position of the horizontal lasers is adapted to the vertical deflection of the test specimen by the measurements of the vertical

laser in the centre of the bottom flange, to make sure that the horizontal deflections of the web are measured every time at the same material points of the web.

The geometrical imperfections and the lateral deflections of the whole web of the test panels are measured using these lasers. After every load step, these lasers scan the whole web, from the left-hand side intermediate transverse stiffener to about 200 mm before the right-hand intermediate transverse stiffener. The position of the cart with lasers in the longitudinal direction of the beam is measured with a steel rope, see Figure 4-12 and Figure 4-13.

- The vertical deflection of the tips of the top flange is measured using lasers. Based on this data, the deflections as well as the rotation are determined. The vertical deflections of the tips of the top flange are measured by two horizontal lasers, placed at the top of the cart. The horizontal infrared rays from the lasers are reflected by two mirrors, one on each side of the web, in the vertical direction. During testing of the first test specimen with a flange width of 50 mm, the mirrors broke and this measurement was not continued for the remaining test specimens;
- The rotation of the top flange of the test panel is measured by inclination gauges. The position of these inclination gauges are presented in Figure 4-14;
- The strain of the cross-section in the centre of the beam is measured by strain gauges. The positions of these strain gauges are shown in Figure 4-15 and the strain gauges are shown in Figure 4-16. Strain gauges 11 and 21 are always glued halfway the web height of the test specimen.

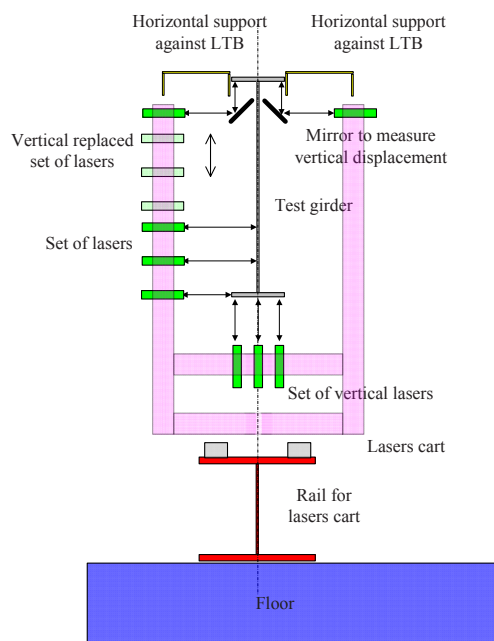


Figure 4-10 Cart with lasers



Figure 4-11 Horizontal and vertical lasers

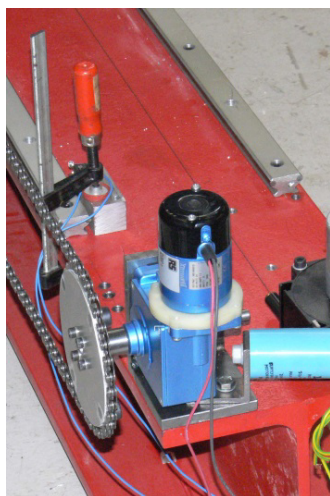


Figure 4-12 Motor for the cart

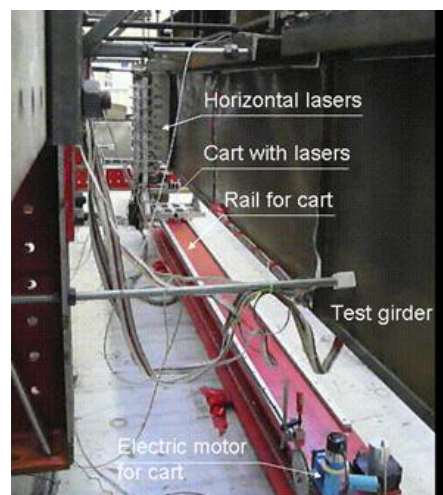


Figure 4-13 Laser equipment

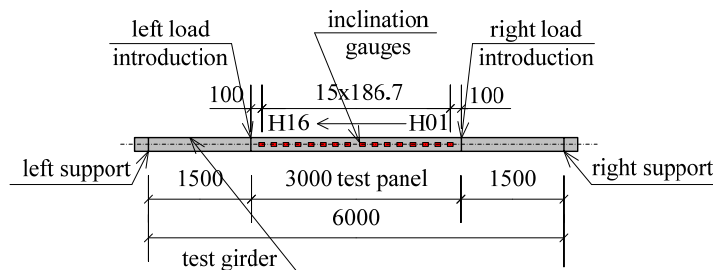


Figure 4-14 Location of 16 inclination gauges at the top of the compressive flange

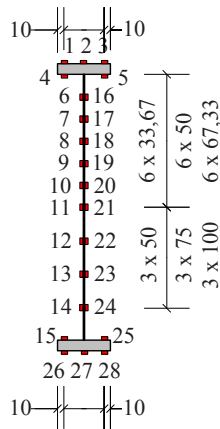


Figure 4-15 Numeration of strain gauges

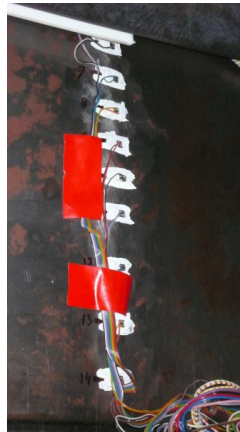


Figure 4-16 Strain gauges

4.5 FABRICATION AND THE INITIAL IMPERFECTIONS

The test specimens are fabricated in the Stevin II Laboratory of the Delft University of Technology.

The flanges with dimensions $50 \times 4 \text{ mm}^2$, $80 \times 5 \text{ mm}^2$ and $100 \times 4 \text{ mm}^2$ are cut from strips. The length of the flanges is 6.0 m, being the whole span of the test girder. The flange is tag-welded on one side of the web of the test panel, see Figure 4-18, and on the other side the web is continuously welded by automatic welding equipment, see Figure 4-19. A CO_2 -welding process is used. The thickness of the weld, because of the web thickness of 1 mm, is very small.

After welding of the web of the test area to the flange, the web of the end panels is welded to this flange. The intermediate transverse stiffeners are positioned between the web of the end panels and

the web of the test panel and connected to the webs and the flange by welding. The whole welded part is rotated 180° and the webs and the stiffeners are welded to the other flange.

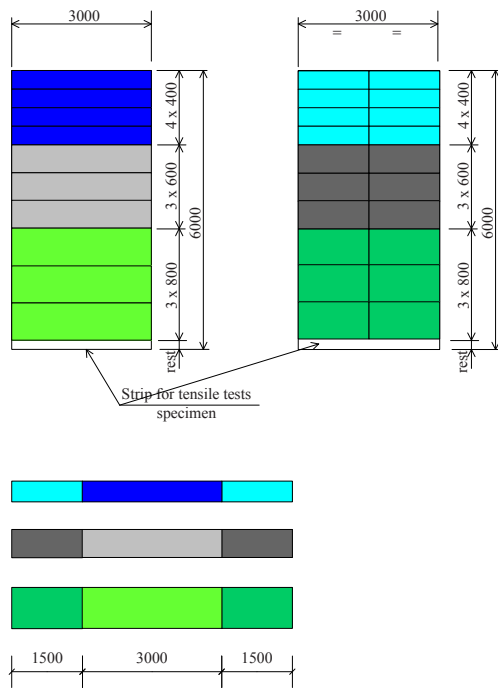


Figure 4-17 Overview of the web plates for the test and the end panels



Figure 4-18 Web of the end panel is tag welded to the flange after the web of the test panel



Figure 4-19 Welding of test girder

5 RESULTS OF THE DELFT EXPERIMENTS

5.1 GENERAL

The measured data of the forces, displacements, rotations and strains of two test girders are presented in several diagrams and tables in Chapter 5.2, namely for the relatively rigid test girder 9, 800x80, and for the relatively flexible test girder 3, 400x80(2). The results of all test girders are presented in Appendix A to Appendix Q. Chapter 5.3 shows the elaborations on these test results, including the failure modes of each test girder. The bending moment resistance for all test girders is determined in Chapter 5.5 and finally the conclusions of the experiments are given in Chapter 5.6.

5.2 MEASUREMENTS

5.2.1 LOAD-DEFORMATION BEHAVIOUR

The actuator force F_{act} and the displacement at the location of the piston δ_{piston} are used to perform the experiment in a deformation controlled manner. The displacement at the location of the piston of the actuator δ_{piston} is influenced by the displacement of the test girder δ_{ig} at the load introduction, but also by the displacements of the spreader beam δ_{sb} , see Figure 5-1, and the test rig itself.

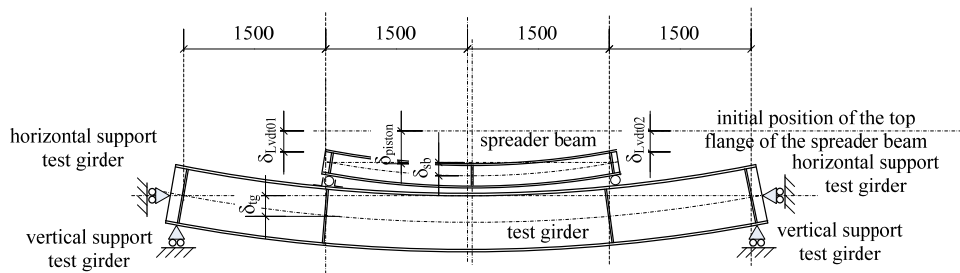


Figure 5-1 The displacements at specific locations as used in the P - δ diagrams of the test girders

In Figure 5-2, the actuator force going along with the prescribed displacement is shown for test girder 9, 800x80, see Appendix A too. To concentrate on the behaviour of the test girder itself, the relationship between the forces at the load introductions (li) of the girder and the displacements at these load introductions, δ_{Lvd01} and δ_{Lvd02} at the left-hand side and right-hand side load introduction respectively, are used. These forces at the load introductions are equal to each other $F_{li} = 0.5F_{act}$. Figure 5-3 presents the forces at the load introductions versus the displacements at both load introductions for test girder 9, 800x80.



Figure 5-2 The actuator force as a result of the prescribed displacements of the piston for test girder 9, 800x80

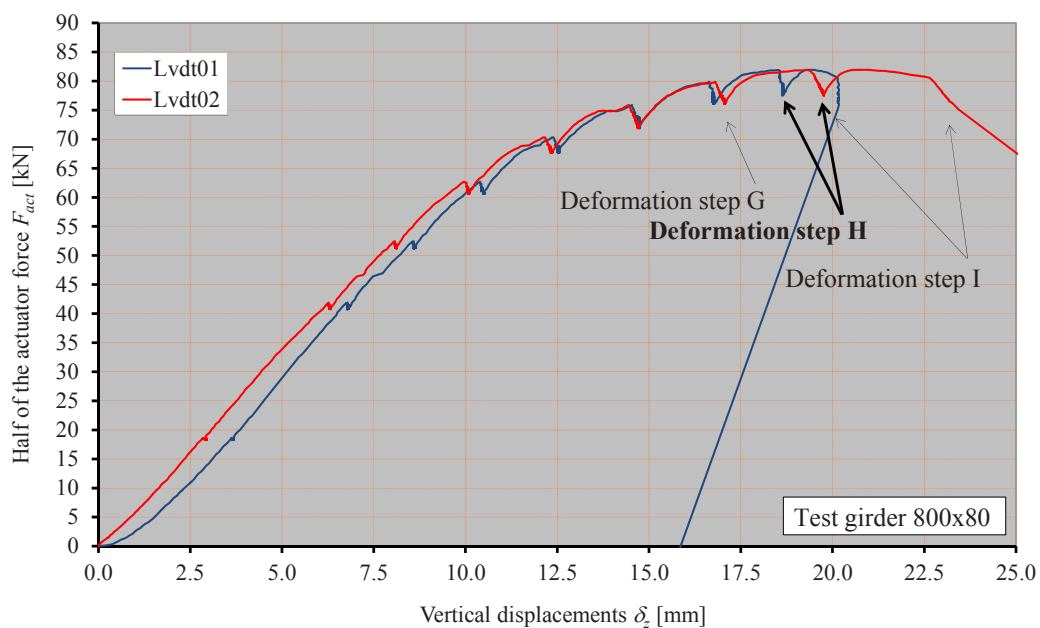


Figure 5-3 The forces at the load introductions versus the displacements at both load introductions for test girder 9, 800x80

Figure 5-4 presents the actuator force going along with the prescribed displacement for test girder 3, 400x80(2). Figure 5-5 shows the forces at the load introductions versus the displacements at both load introductions for test girder 3, 400x80(2).

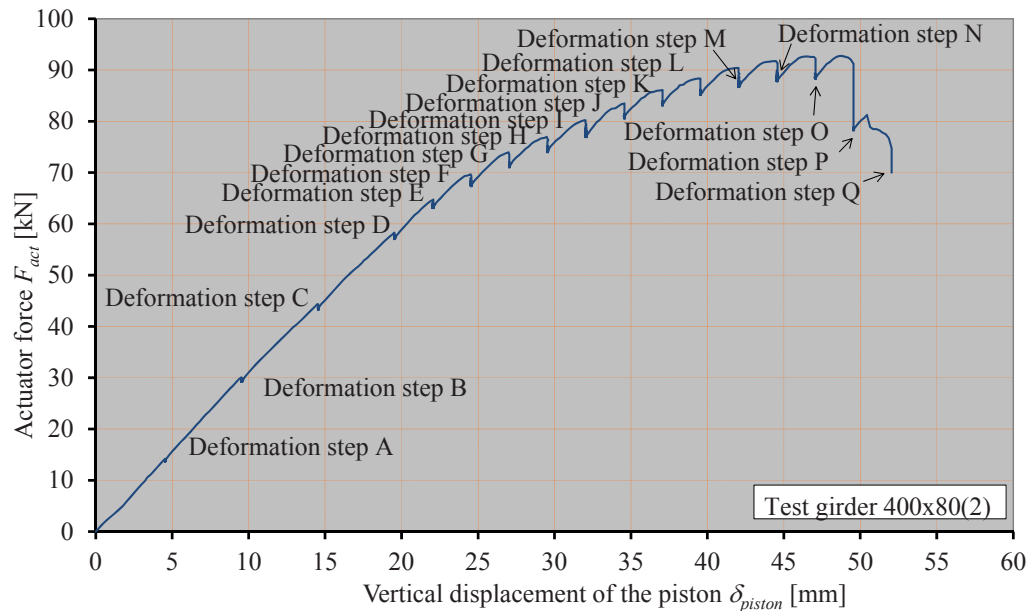


Figure 5-4 The actuator force as a result of the prescribed displacements of the piston for test girder 3, 400x80(2)

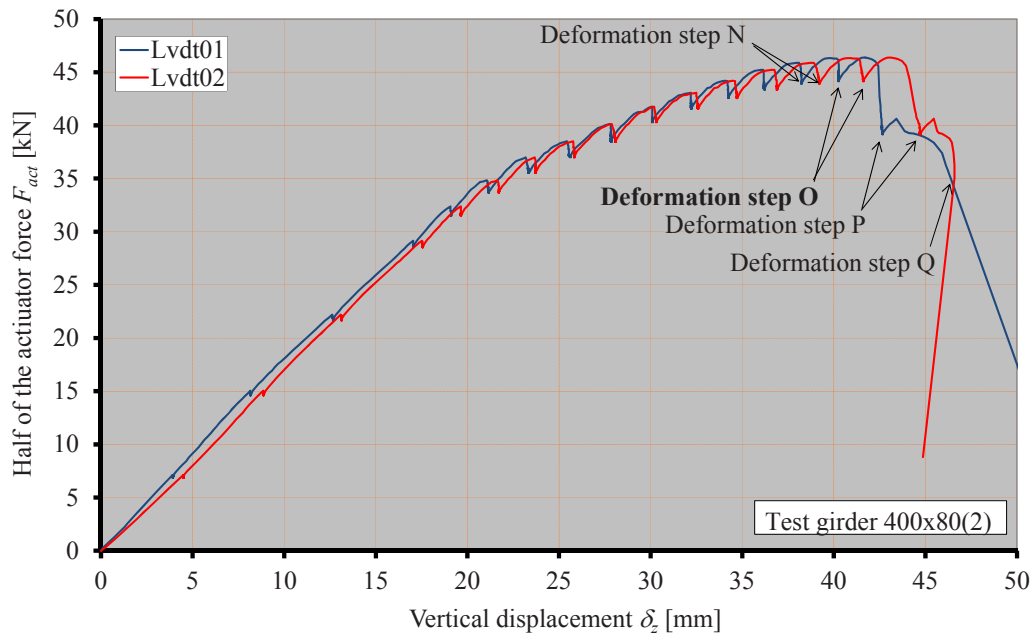


Figure 5-5 The forces at the load introductions versus the displacements at both load introductions for test girder 3, 400x80(2)

5.2.2 REACTION FORCES VERSUS THE ACTUATOR FORCES

The actuator force F_{act} and, based on that, the forces at the load introductions and the reaction forces R_L and R_R at respectively the left-hand side and right-hand side supports, are continuously measured by load cells, see Appendix C. The individual reaction forces R_L and R_R and the sum of these reaction forces $\sum R$ of test girder 9, 800x80, versus to the actuator force F_{act} are shown in Figure 5-6. The yellow line represents the sum of the reaction forces $\sum R$ and this is compared with the actuator force F_{act} , represented by the dotted black line indicated as '100% Actuator force'. The left-hand side reaction force R_L is represented by the blue line in the graph and the right-hand side reaction force R_R is represented by the red line. Both reaction forces are compared with half of the actuator force $0.5F_{act}$, represented by the black dotted line indicated as the '50% Actuator force'. For test girder 3, 400x80(2) the same type of graph is shown in Figure 5-7. Please note that the scales of both axes are different from those of the graph presented in Figure 5-6 because of the difference in strength and stiffness of these test girders.

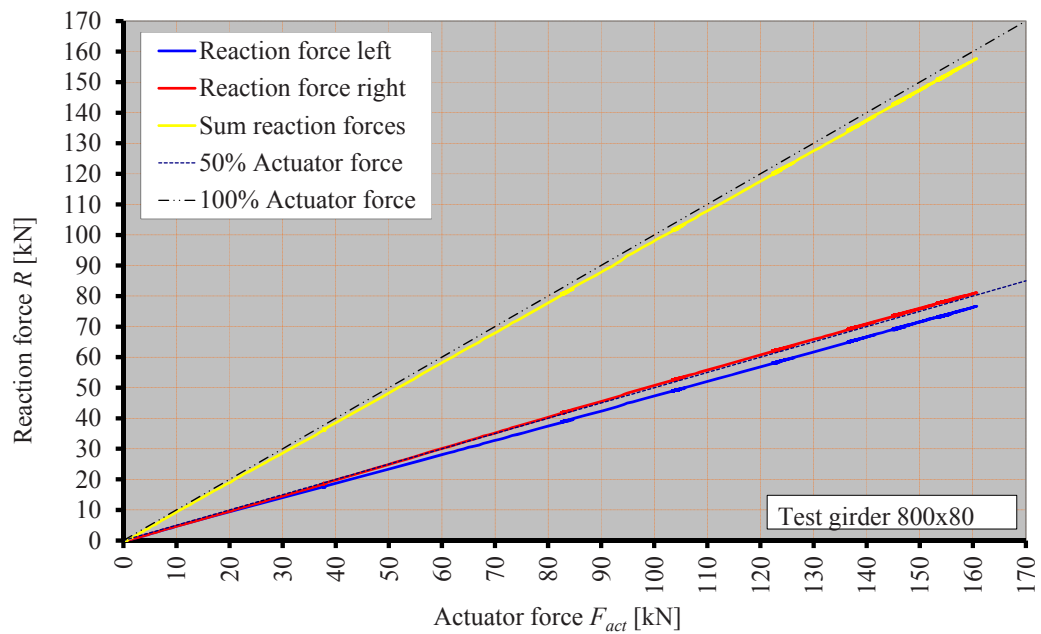


Figure 5-6 The reaction forces versus the actuator force, test girder 9, 800x80

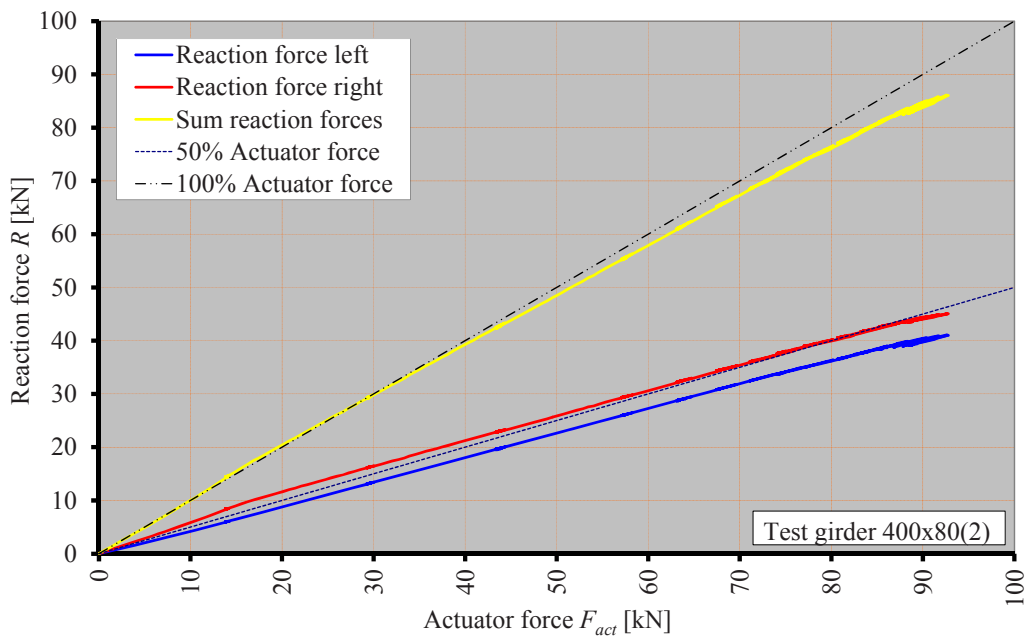


Figure 5-7 The reaction forces versus the actuator force for test girder 3, 400x80(2)

5.2.3 THE OUT-OF-PLANE DISPLACEMENTS OF THE WEB OF THE TEST PANEL

Horizontal lasers are used to measure the out-of-plane displacements of the web of the test panel after each deformation step, see Appendix D. These lasers have to be moved in the longitudinal x -direction, but also in the vertical z -direction to scan the whole web of the test panel using a limited number of lasers. The vertical position of the lasers is compensated for the deflection of the test girders in order to arrive at the original grid points. For test girder 9, 800x80, the initial out-of-plane displacements, the imperfections, are shown in Figure 5-8. The total out-of-plane displacements, the initial displacements plus the displacements of the web of the test panel as a result of the loading on the girder, are presented in Figure 5-9 for deformation step A up to Figure 5-17 for deformation step I. These deformation steps A up to I are shown in Figure 5-2.

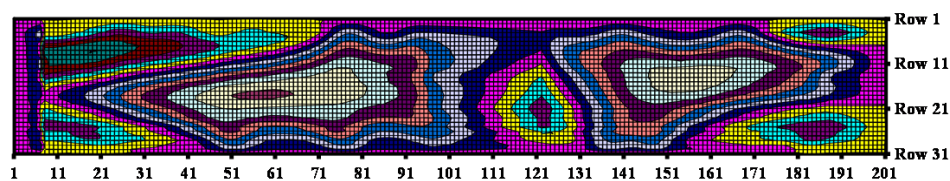


Figure 5-8 Initial out-of-plane displacements of the test panel of test girder 9, 800x80, deformation step 0

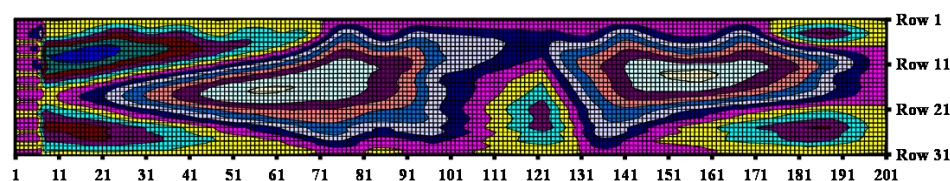


Figure 5-9 Total out-of-plane displacements of the test panel of test girder 9, 800x80 deformation step A

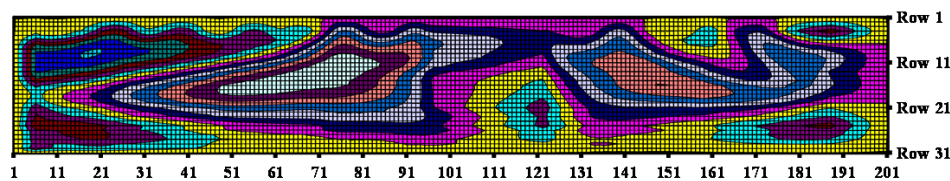


Figure 5-10 Total out-of-plane displacements of the test panel of test girder 9, 800x80 deformation step B

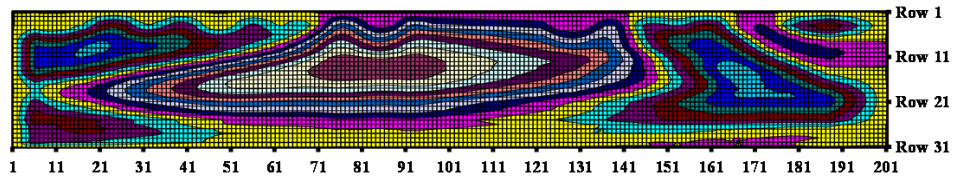


Figure 5-11 Total out-of-plane displacements of the test panel of test girder 9, 800x80 deformation step C

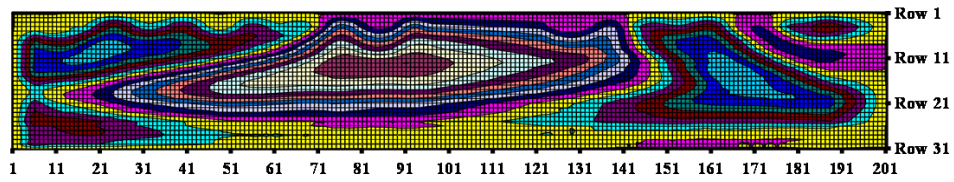


Figure 5-12 Total out-of-plane displacements of the test panel of test girder 9, 800x80 deformation step D

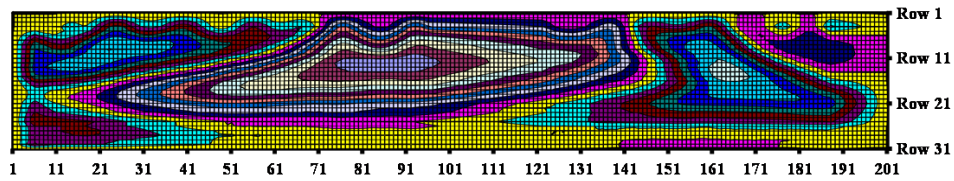


Figure 5-13 Total out-of-plane displacements of the test panel of test girder 9, 800x80 deformation step E

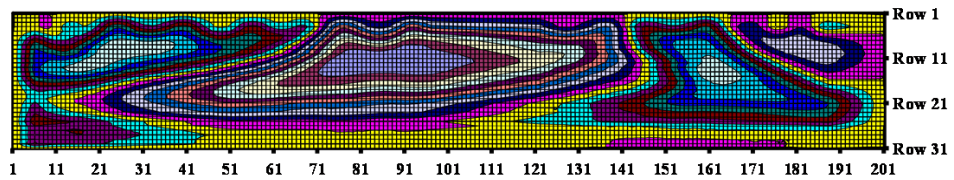


Figure 5-14 Total out-of-plane displacements of the test panel of test girder 9, 800x80 deformation step F

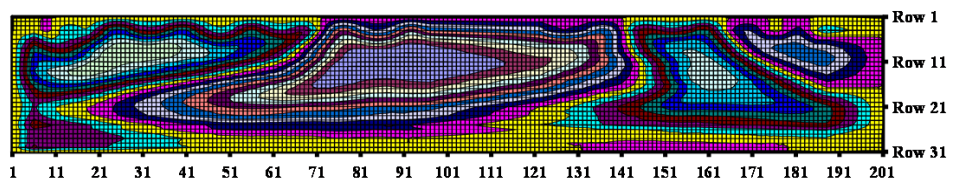


Figure 5-15 Total out-of-plane displacements of the test panel of test girder 9, 800x80 deformation step G

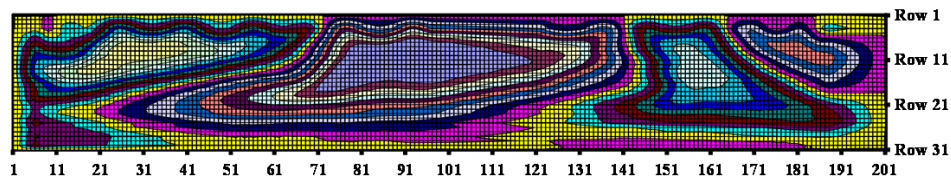


Figure 5-16 Total out-of-plane displacements of the test panel of test girder 9, 800x80 deformation step H

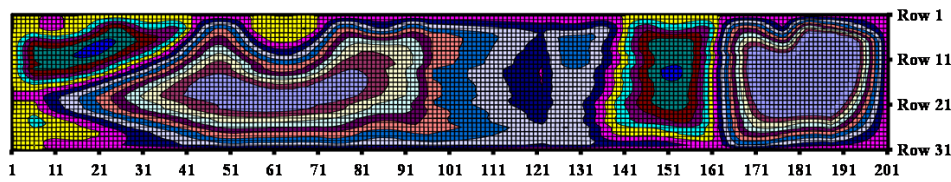


Figure 5-17 Total out-of-plane displacements of the test panel of test girder 9, 800x80 deformation step I

For test girder 3, 400x80(2), these out-of-plane displacements are presented for a limited number of deformation steps in Figure 5-18 for the initial deformation step 0, up to Figure 5-26 for deformation step P. These deformation steps are shown in Figure 5-4.

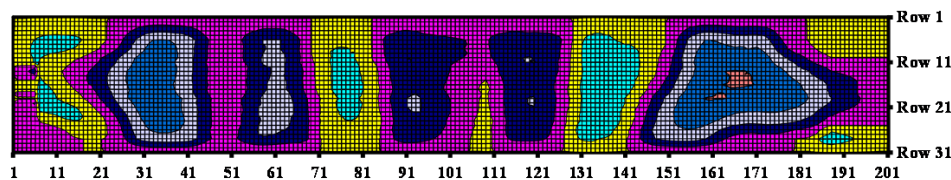


Figure 5-18 Total out-of-plane displacements of the test panel of test girder 3, 400x80(2), deformation step 0

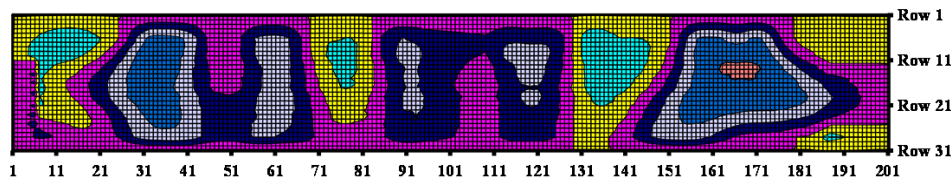


Figure 5-19 Total out-of-plane displacements of the test panel of test girder 3, 400x80(2), deformation step B

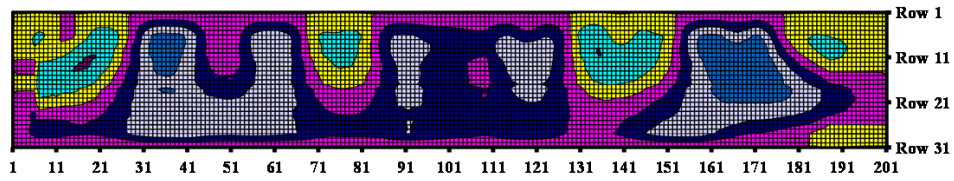


Figure 5-20 Total out-of-plane displacements of the test panel of test girder 3, 400x80(2), deformation step D

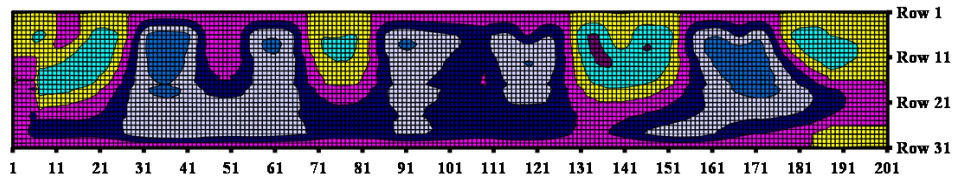


Figure 5-21 Total out-of-plane displacements of the test panel of test girder 3, 400x80(2), deformation step F

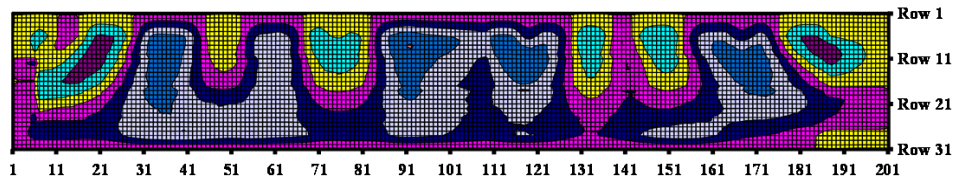


Figure 5-22 Total out-of-plane displacements of the test panel of test girder 3, 400x80(2), deformation step H

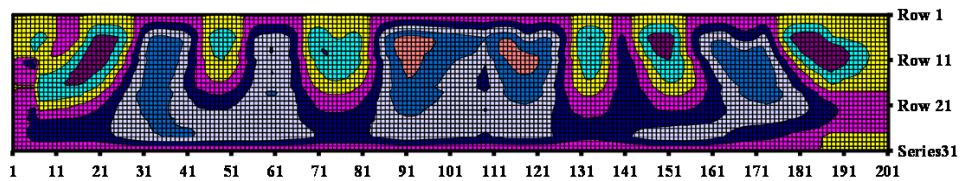


Figure 5-23 Total out-of-plane displacements of the test panel of test girder 3, 400x80(2), deformation step J

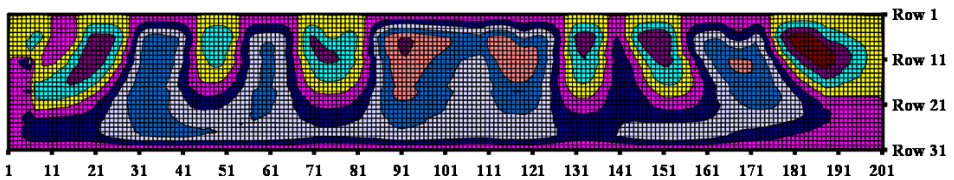


Figure 5-24 Total out-of-plane displacements of the test panel of test girder 3, 400x80(2), deformation step L

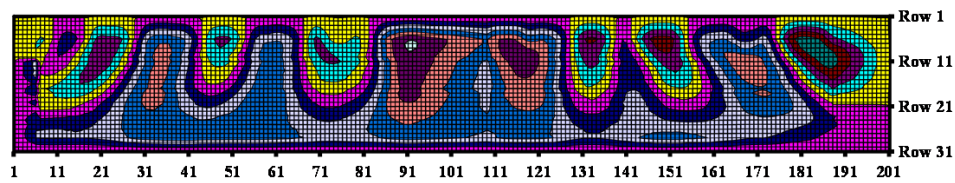


Figure 5-25 Total out-of-plane displacements of the test panel of test girder 3, 400x80(2), deformation step N

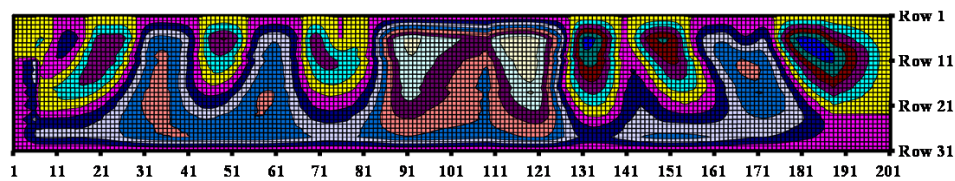


Figure 5-26 Total out-of-plane displacements of the test panel test girder 3, 400x80(2), deformation step P

5.2.4 VERTICAL DEFLECTIONS OF THE TEST GIRDER

The vertical deformations at the centre of the bottom flange of test girder 9, 800x80, and test girder 3, 400x80(2), are shown in Figure 5-27 and Figure 5-28, see also Appendix E for the vertical deformations of all test girders. The vertical lines in the centre of the test panel are caused by the presence of the strain gauges and the connected cables.

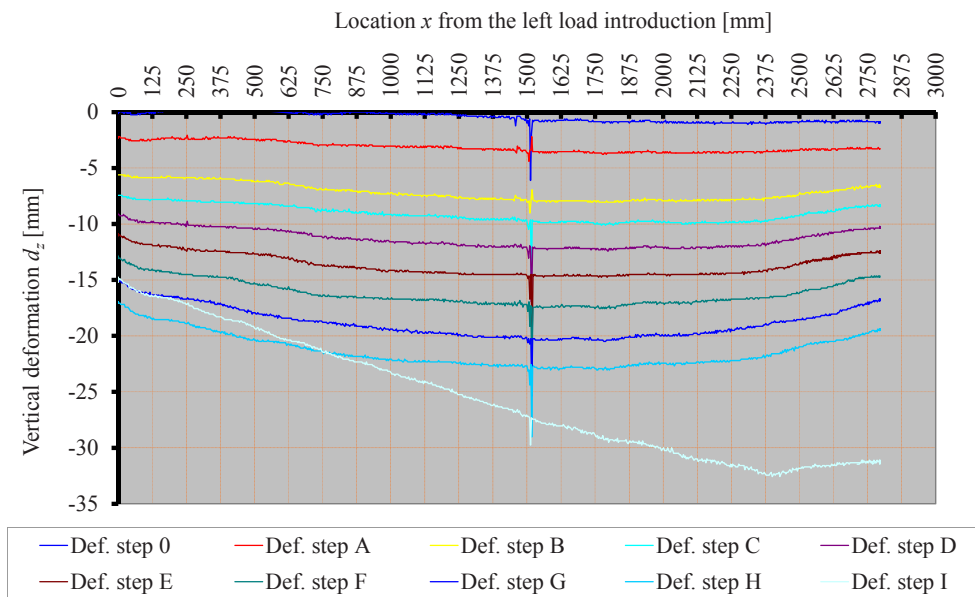


Figure 5-27 Vertical deformations of the test panel of test girder 9, 800x80

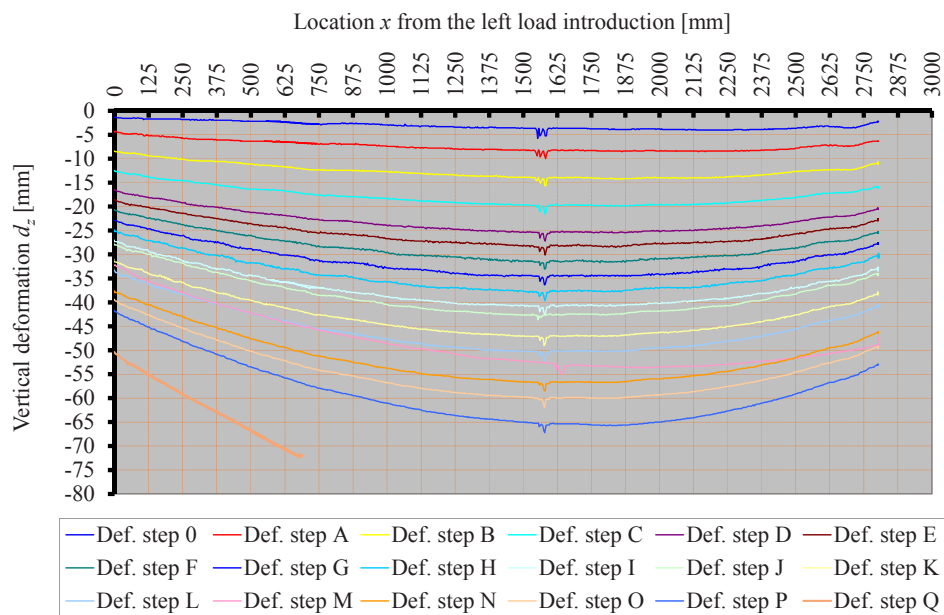


Figure 5-28 Vertical deformations of the test panel of test girder 3, 400x80(2)

5.2.5 Rotation of the compressive flange around the longitudinal axis

5.2.5.1 Rotation of the compressive flange measured by inclination gauges

The difference in deflections of the tips of the compressive flange is an indication for the rotation of that flange, see Appendix F. As described in Chapter 4.4.2, two horizontal lasers, laser 03 and 04, measure, via two mirrors positioned under 45° , the vertical deflections at the tips of the flange. This method to determine the rotation of the compressive flange is used for test girders 1 to 4, respectively girders 400x50, 400x80(1), 400x80(2) and 400x100. For the fourth experiment in the sequence of tests, the experiment on test girder 1, 400x50, the mirrors broke because of the rather high amplitudes of the buckles in the web and the width of the flange of 50 mm. The rotation of the next test girders, girders 5 to 10, respectively 600x50, 600x80, 600x100, 800x50, 800x80 and 800x100, are measured by inclination gauges.

Figure 5-29 shows the inclinations of test girder 9, 800x80 at the vertical axis, measured by the inclination gauges, versus the x -direction of the test panel. From this figure it can be seen that in deformation step I the rotation at the right-hand side load introduction suddenly increases.

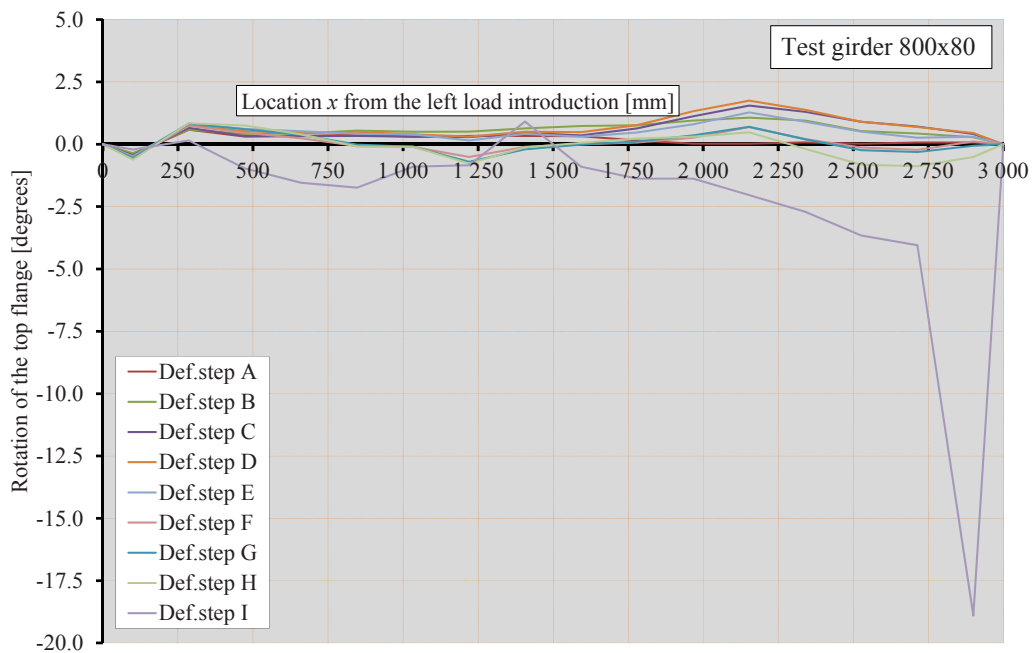


Figure 5-29 Inclinations of the compressive flange of experiment 9, 800x80, deformation steps 0 up to I

5.2.5.2 Rotation of the compressive flange determined from the vertical deflections of the tips of test girder 3, 400x80(2), divided by the distance between the measured locations

Figure 5-30 shows the vertical deflections of the tips of the compressive flange for deformation steps 0, C, F, L, M, N and O of experiment 3, 400x80(2), see also Appendix G. For the readability of the figure some intermediate deformation steps are not shown in it.

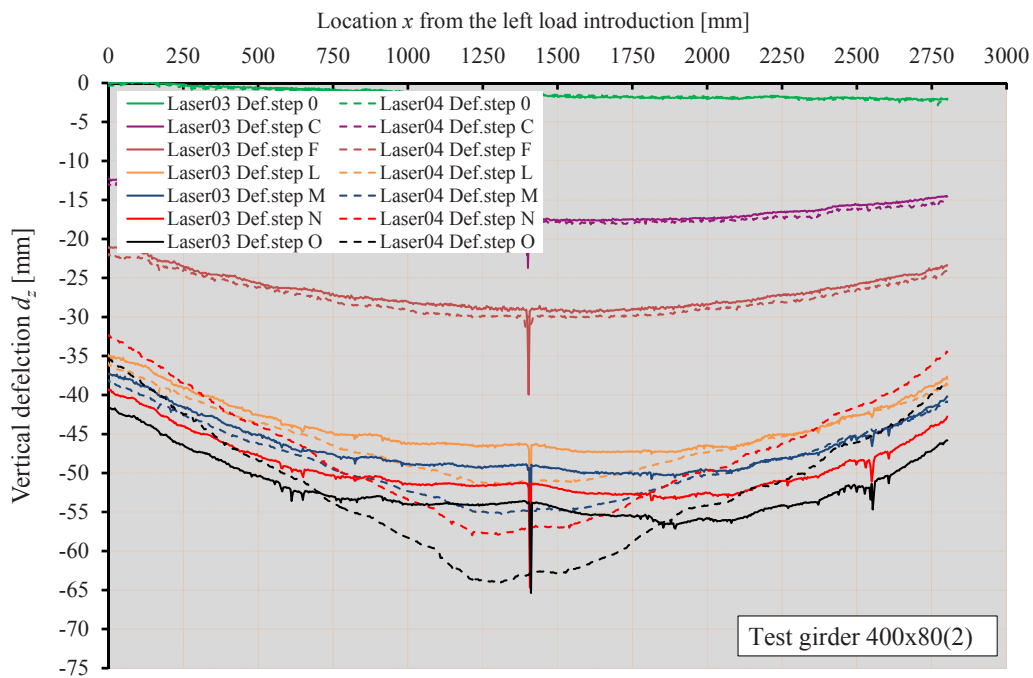


Figure 5-30 Vertical deflections of the compressive flange of test girder 3, 400x80(2), deformation steps 0, C, F, L, M, N and O

5.2.6 ROTATION OF THE TENSILE FLANGE DETERMINED FROM THE VERTICAL DEFLECTIONS OF THE TIPS OF TEST GIRDER 9, 800x80, AND TEST GIRDER 3, 400x80(2), DIVIDED BY THE DISTANCE BETWEEN THE MEASURED LOCATIONS

From the rotations in the compressive flange it can be seen that there is a sudden increase in rotation in a specific deformation step. From the out-of-plane deflections it can be seen that the amplitudes of the initial buckles increase during testing of the test girders.

Basler assumed that the web will column buckle with a buckling length equal to the web height. This means that the flanges won't rotate due to the increase of the amplitudes of the buckles. The

rotation of the compressive flange is caused by the compressive stresses in this flange and it is expected that the rotation of the tensile flange is very limited. For test girders 9, 800x80 and 3, 400x80(2) the vertical deformations of the tips of the tensile flange, solid lines in the front and dotted lines in the back are shown in Figure 5-31 and Figure 5-32 respectively for a limited number of deformation steps, see also Appendix H. The number of deformation steps is limited to clearly show the increments in rotation, especially because the rotations of both flanges are very similar for the first deformation steps.

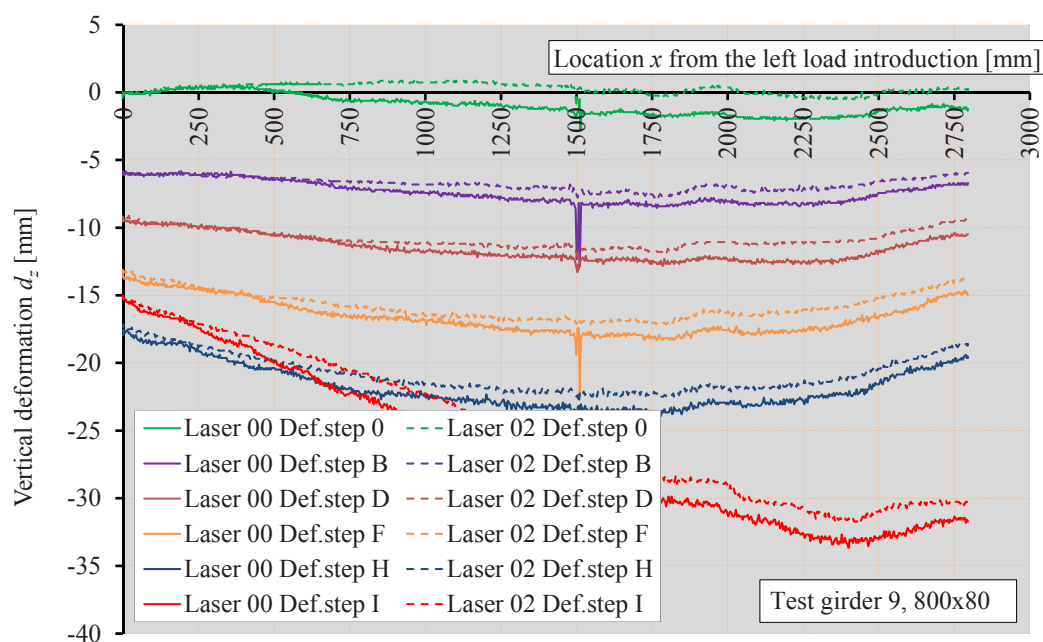


Figure 5-31 Vertical deformation of the tips of the tensile flange of test girder 9, 800x80 for deformation steps 0, B, D, F, H and I

The difference in deformation as shown by the solid and the dotted lines in one colour is an identification of the rotation. Chapter 5.3.5 shows the rotations based on these differences in vertical deformations.

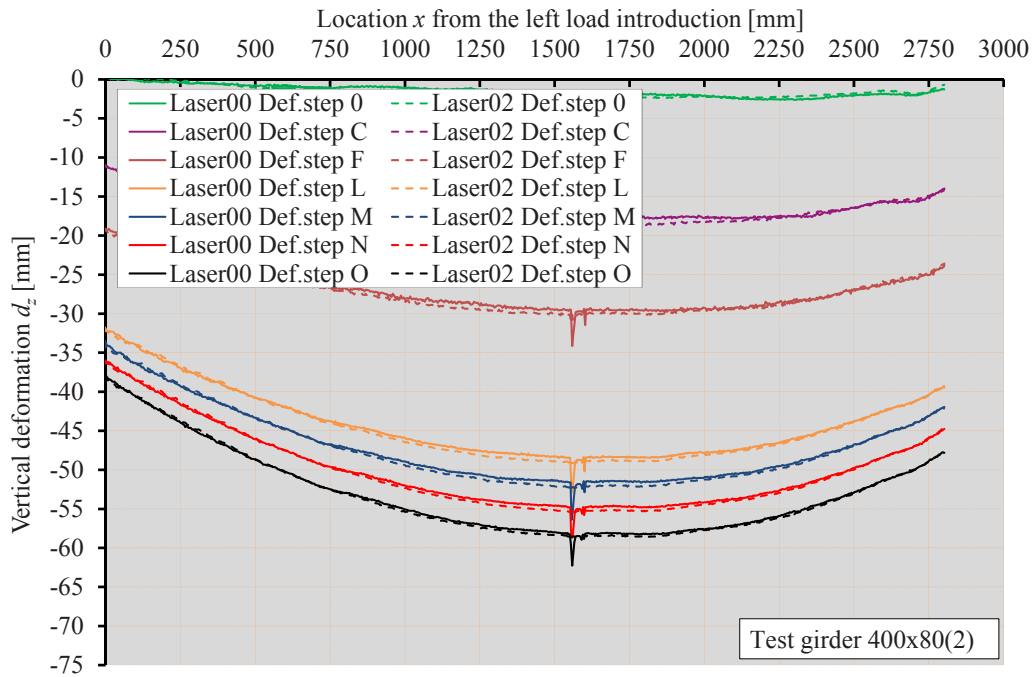


Figure 5-32 Vertical deformation of the tips of the tensile flange of test girder 3, 400x80(2) for deformation steps 0, C, F, L, M, N and O

5.2.7 STRAIN MEASURED WITH STRAIN GAUGES

The positions of the strain gauges are presented in Figure 4-15. The strain gauges measured the strains of the test girders in the midspan cross-section. The measured strains are shown in the cross-section for each deformation step, see Appendix I.

For test girder 9, 800x80, these cross-sections including the measured strains are presented in Figure 5-33. The reason why some strains are printed in bold will be explained in Chapter 5.3.6. For girder 3, 400x80(2), these strains are presented in Figure 5-34 and Figure 5-35.

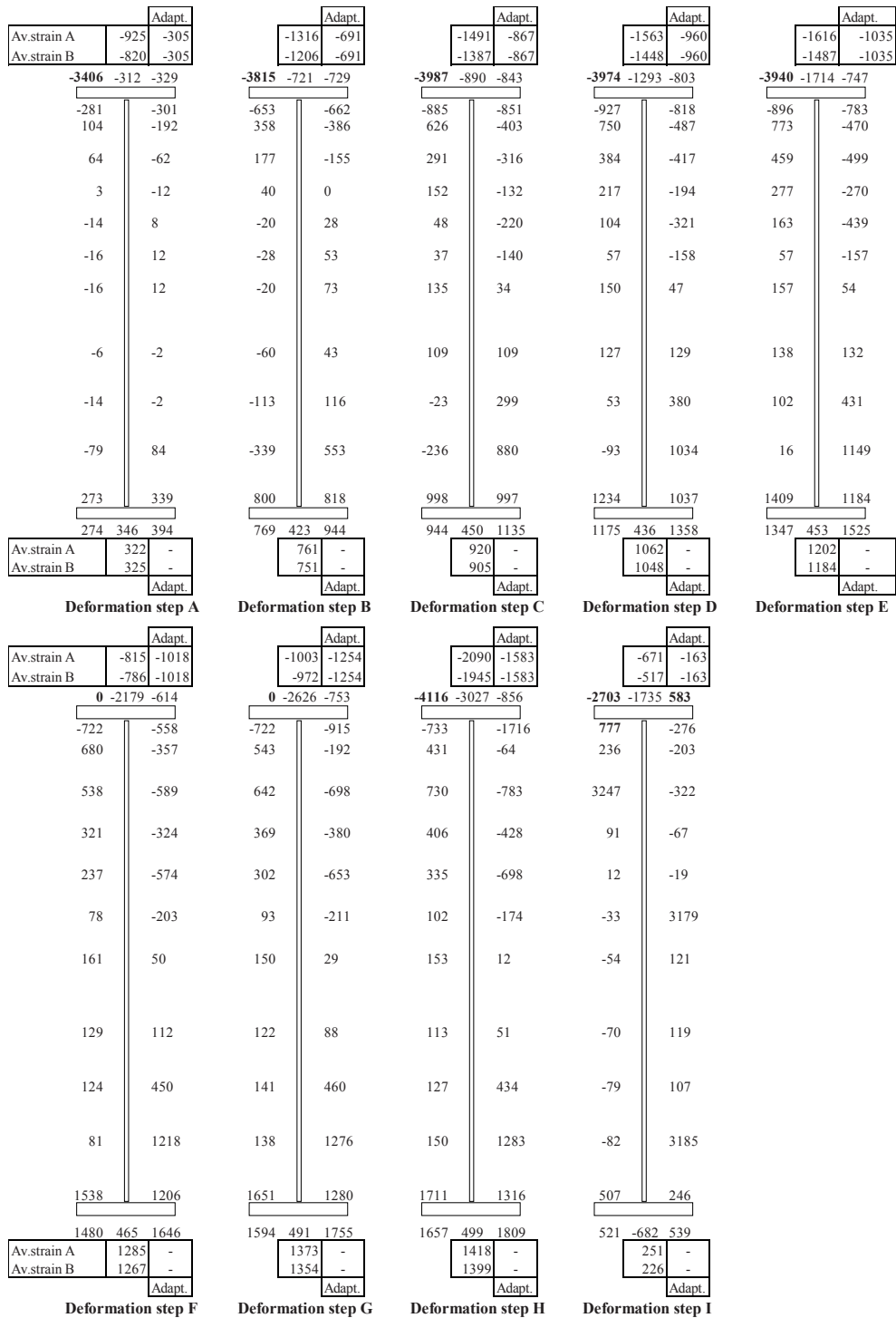


Figure 5-33 Strains per deformation step for test girder 9, 800 x 80

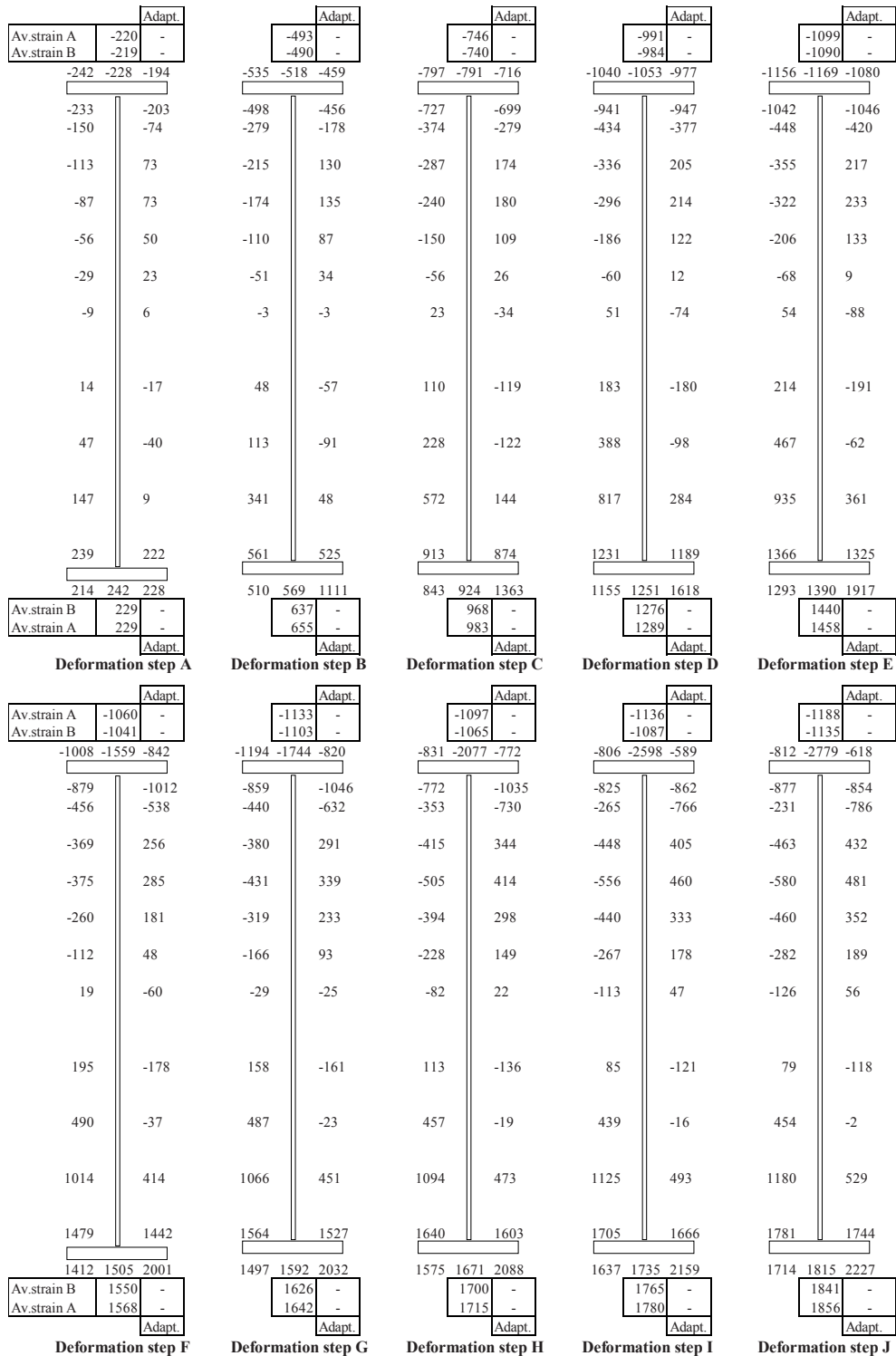


Figure 5-34 Strains per deformation step for test girder 3, 400 x 80 (2), steps A up to J

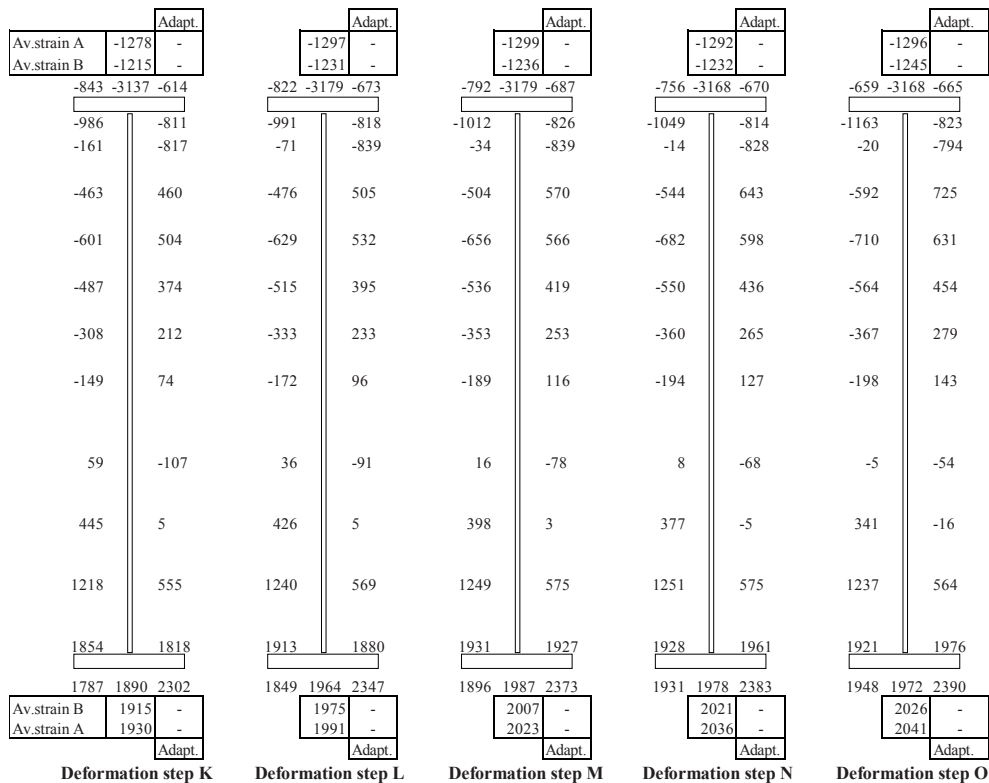


Figure 5-35 Strains per deformation step for test girder 3, 400 x 80 (2), steps K up to O

5.3 ELABORATIONS ON THE MEASUREMENTS OF THE EXPERIMENTS

5.3.1 REACTION FORCES VERSUS THE ACTUATOR FORCE

From Figure 5-6 for test girder 9, 800x80, and Figure 5-7 for test girder 3, 400x80(2), and from the Appendix C giving the same information for all the other experiments, it can be seen that the right-hand side reaction force is almost always higher than the left-hand side reaction force. Table 5-1 shows an overview of the actuator force and the reaction forces of all tests at the deformation step in which the maximum load appears.

It is of interest to look in more detail what influences this unbalance in reaction forces. This phenomenon is caused by the fact that the test rig is not completely symmetric. Also, the actuator force F_{act} is always greater than the sum of the reaction forces. This is because of friction forces between the compressive flange and the lateral supports.

Table 5-1 The actuator force and the reaction forces of the test girders, including related results

Test girder	F_{act} [kN]	$R_{L,max}$ [kN]	$R_{R,max}$ [kN]	ΣR [kN]	F_{fric} [kN]	ΔR [kN]	$\Sigma R/F_{act}$ [%]	F_{fric}/F_{act} [%]	$\Delta R/F_{act}$ [%]
1, 400x50	47.66	20.89	<u>22.57</u>	43.46	4.19	+1.68	91.20	8.80	+3.53
2, 400x80(1)	81.20	36.40	34.73	71.13	10.07	-1.66	87.60	12.40	-2.05
3, 400x80(2)	88.43	39.17	<u>43.54</u>	82.71	5.72	+4.37	93.53	6.47	+4.94
4, 400x100	84.13	37.56	<u>39.53</u>	77.09	7.05	+1.97	91.62	8.38	+2.34
5, 600x50	71.29	32.02	<u>34.79</u>	66.81	4.48	+2.77	93.72	6.28	+3.88
6, 600x80	125.39	56.16	<u>60.11</u>	116.27	9.11	+3.95	92.73	7.27	+3.15
7, 600x100	122.07	59.25	<u>61.57</u>	120.82	1.25	+2.32	98.97	1.03	+1.90
8, 800x50	90.62	41.61	<u>45.31</u>	86.92	3.71	+3.50	95.91	4.04	+4.08
9, 800x80	155.27	74.23	<u>79.05</u>	153.27	2.00	+4.82	98.71	1.29	+3.10
10, 800x100	154.10	74.40	<u>78.65</u>	153.05	1.14	+4.16	99.26	0.74	+2.70

5.3.1.1 The offset of the spreader beam relative to the test girder

First, the influence of the test rig on the difference in reaction forces is discussed. The test rig is described in Chapter 4.4 and shown in Figure 5-36 for the loaded and deformed situation. The test girder is vertically supported by rollers at both ends of the girder. To prevent horizontal displacement of the test girder in longitudinal direction, the test girder is restrained in this direction by threaded rods in the centre line of the girder at both ends. The vertical supports of the spreader beam as well as the vertical supports of the test girder itself are positioned under the bottom flange of the sections of the spreader beam and the test girder. This means that during loading the centre-to-centre distances of the vertical supports under the spreader beam as well as under the test girder increase because of the curvature of both beams. The left-hand side vertical support of the spreader beam is a hinge and this means that the spreader beam moves to the right-hand side. Because of the offset of the position of the spreader beam relative to the test girder in deformed situation the actuator force can be subdivided into a vertical and a horizontal component. The influence of both components on the reaction forces is shown in Figure 5-36.

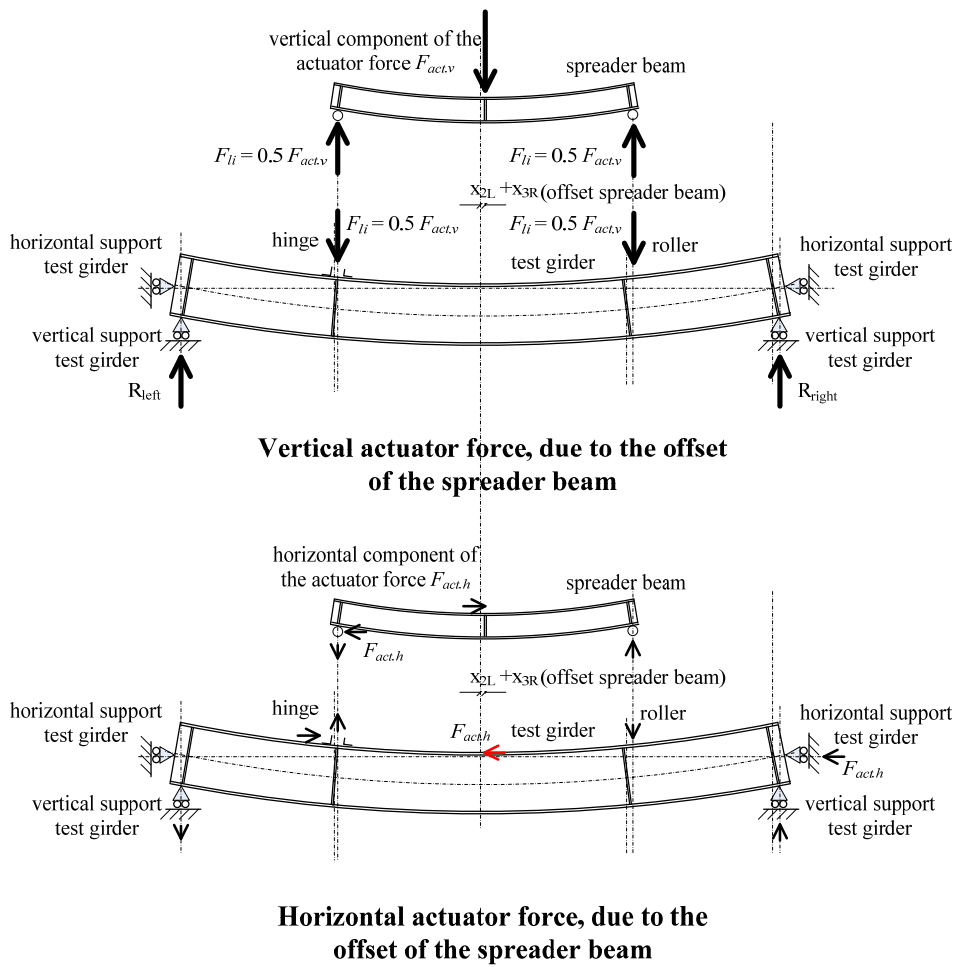


Figure 5-36 Internal force distribution due to the offset of the spreader beam

Vertical component:

The actual centre-to-centre distance of the vertical supports of the test girder (tg) increases due to the curvature of the test girder from the initial unloaded situation with $\ell_{tg} = 6000 \text{ mm}$ to the loaded situation with $\ell_{tg} + x_{1L} + x_{1R}$, where the longitudinal displacements are x_{1L} at the left-hand side support and x_{1R} at the right-hand side support, see Figure 5-37.

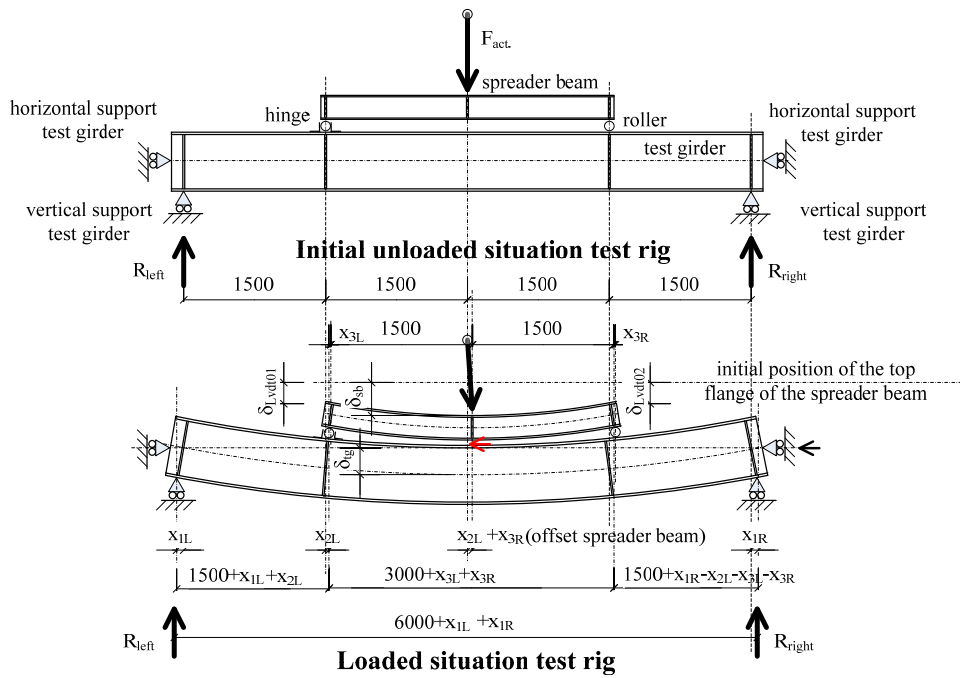


Figure 5-37 Displacements due to the curvature of the spreader beam and the test girder

The actual centre-to-centre distance of the vertical supports of the spreader beam (sb) also increases, but now because of the curvature of the spreader beam. The centre-to-centre distance of the vertical supports under the spreader beam increases from $\ell_{sb} = 3000 \text{ mm}$ in the initial unloaded situation to $\ell_{sb} + x_{3L} + x_{3R}$ in the loaded situation, where the longitudinal displacements due to the curvature of the spreader beam are x_{3L} at the left-hand side support, the hinge, and x_{3R} at the right-hand side support, the roller. The distance between the left-hand side support of the test girder and the left-hand side support of the spreader beam changes. This is caused to the longitudinal displacement x_{1L} due to the curvature of the test girder and because of the longitudinal displacement x_{2L} due to the curvature of the spreader beam, it increases from 1500 mm in the initial unloaded situation to $1500 + x_{1L} + x_{2L}$ in the loaded situation, see Figure 5-37.

The actual location of the right-hand side support under the spreader beam, compared with the actual location of the left-hand side support under the test girder, is determined by the actual location of the left-hand side support under the spreader beam and the actual centre-to-centre distance between both supports under the spreader beam. This means that the actual location of the right-hand side

support under the spreader beam, related to the position of the left-hand side support of the test girder, becomes $(1500 + x_{1L} + x_{2L})$ plus $(3000 + x_{3L} + x_{3R})$, so this location increases from 4500 mm in the unloaded situation to $(4500 + x_{1L} + x_{2L} + x_{3L} + x_{3R})$ in the loaded situation. The distance between the right-hand side support under the spreader beam and the right-hand side support under the test girder increases from 1500 mm in the unloaded situation to $\{6000 + x_{1L} + x_{1R} -$

$(4500 + x_{1L} + x_{2L} + x_{3L} + x_{3R})\} = (1500 + x_{1R} - x_{2L} - x_{3L} - x_{3R})$ in the loaded situation.

The midspan of the spreader beam moves to the right-hand side related to the midspan of the test girder, namely $\{(1500 + x_{1L} + x_{2L}) - x_{1L}\} + (x_{2L} + 1500) - 3000 = (x_{2L} + x_{3L})$, see Figure 5-37. When these displacements are taken into account, the reaction forces of the test girders are as follows:

$$\begin{aligned} R_R &= \frac{(1500 + x_{1L} + x_{2L}) \cdot \frac{F_{act}}{2} + \{(1500 + x_{1L} + x_{2L}) + (3000 + x_{3L} + x_{3R})\} \cdot \frac{F_{act}}{2}}{(6000 + x_{1L} + x_{1R})} = \\ &= \frac{(6000 + 2x_{1L} + 2x_{2L} + x_{3L} + x_{3R}) \cdot \frac{F_{act}}{2}}{(6000 + x_{1L} + x_{1R})} \end{aligned} \quad (5.1)$$

$$\begin{aligned} R_L &= \frac{(1500 + x_{1R} - x_{2L} - x_{3L} - x_{3R}) \cdot \frac{F_{act}}{2} + \{(1500 + x_{1R} - x_{2L} - x_{3L} - x_{3R}) + (3000 + x_{3L} + x_{3R})\} \cdot \frac{F_{act}}{2}}{(6000 + x_{1L} + x_{1R})} = \\ &= \frac{(6000 + 2x_{1R} - 2x_{2L} - x_{3L} - x_{3R}) \cdot \frac{F_{act}}{2}}{(6000 + x_{1L} + x_{1R})} \end{aligned} \quad (5.2)$$

It is clear that the left-hand side reaction force R_L is always smaller than the right-hand side reaction force R_R , irrespective of the values of the longitudinal deformations of the spreader beam and the test girder. The sum of both reaction forces $\sum R$ has to be equal to the force F_{act} produced by the actuator:

$$\begin{aligned} \sum R = R_L + R_R &= \frac{(6000 + 2x_{1L} + 2x_{2L} + x_{3L} + x_{3R}) \cdot \frac{F_{act}}{2}}{(6000 + x_{1L} + x_{1R})} + \frac{(6000 + 2x_{1R} - 2x_{2L} - x_{3L} - x_{3R}) \cdot \frac{F_{act}}{2}}{(6000 + x_{1L} + x_{1R})} = \\ &= \frac{(12000 + 2x_{1L} + 2x_{1R}) \cdot \frac{F_{act}}{2}}{(6000 + x_{1L} + x_{1R})} = F_{act} \end{aligned} \quad (5.3)$$

All influences of the offset of the position of the spreader beam relative to the test girder can be calculated. The rotation $\varphi_{L.sb}$ of the end of the spreader beam depends on the actuator force $F_{act.}$ and the stiffness of the spreader beam, a hot-rolled section HEB240, so EI_{HEB240} . Based on this rotation $\varphi_{L.sb}$ the displacement x_{3L} in longitudinal direction for test girder 9, 800x80, is, based on the maximum actuator force:

$$\varphi_{L.sb} = \frac{F \ell_{sb}^2}{16EI_{HEB240}} = \frac{155.27 \cdot 10^3 \cdot 3000^2}{16 \cdot 210000 \cdot 11259 \cdot 10^4} = 0.00369$$

$$x_{3L} = \sin(\varphi_{L.sb}) \cdot \left(\frac{h_{HEB240}}{2} + \frac{d_{roll}}{2} \right) = \sin(0.00369) \cdot \left(\frac{240}{2} + \frac{100}{2} \right) = 0.63 \text{ mm} \quad (5.4)$$

This displacement of the spreader beam is very small. For every experiment the same spreader beam is used and so this displacement x_{3L} is a maximum for the maximum actuator force of 155.27 kN for this test girder 9, 800x80. The rotation of the left (L) end of the test girder $\varphi_{L.ig}$ is:

$$\varphi_{L.ig} = \frac{F/2 \cdot \ell_{ep}^2}{2EI_{ep}} + \frac{F/2 \cdot \ell_{ep} \cdot \ell_{tp}/2}{EI_{tp}} = \frac{153.27 \cdot 10^3 / 2 \cdot 1500^2}{2 \cdot 210000 \cdot 26618.2 \cdot 10^4} + \frac{155.27 \cdot 10^3 / 2 \cdot 1500 \cdot 3000 / 2}{210000 \cdot 16694.5 \cdot 10^4} =$$

$$= 0.00655$$

The moments of inertia of the end panel (ep) and the test panel (tp) are determined in Chapter 4. The longitudinal deflection x_{1L} is determined as follows:

$$x_{1L} = \sin(\varphi_{L.ig}) \cdot \left(\frac{h_w}{2} + t_{gf} + \frac{d_{rod}}{2} \right) = \sin(0.00655) \cdot \left(\frac{799.4}{2} + 5.60 + \frac{12}{2} \right) = 2.69 \text{ mm} \quad (5.5)$$

The rotation $\varphi_{li.ig}$ of the test girder at the load introduction (li) is:

$$\varphi_{li.ig} = \frac{F/2 \cdot \ell_{ep} \cdot \ell_{tp}/2}{EI_{tp}} = \frac{153.27 \cdot 10^3 / 2 \cdot 1500 \cdot 3000 / 2}{210000 \cdot 16695.5 \cdot 10^4} = 0.00498$$

The longitudinal deflection x_{2L} is determined as follows:

$$x_{2L} = \sin(\varphi_{li.ig}) \cdot \left(\frac{h_w}{2} + t_{gf} + \frac{d_{roll}}{2} \right) = \sin(0.00498) \cdot \left(\frac{799.4}{2} + 5.60 + \frac{100}{2} \right) = 2.27 \text{ mm} \quad (5.6)$$

The longitudinal deflection x_{1L} is measured by Lvd03 and x_{1R} by Lvd04, see Figure 5-38 and Appendix J.

The moment the maximum load occurs, the longitudinal deflection at the left-hand side support is equal to $x_{1L} = 4.99 \text{ mm}$ and at the right-hand side support it is $x_{1R} = 6.13 \text{ mm}$, see Figure 5-38. These measured longitudinal deformations are based on non-linear behaviour, while the calculated deformations are based on the linear elastic theory. It can be seen that both measured deformations are much greater than the calculated 2.69 mm.

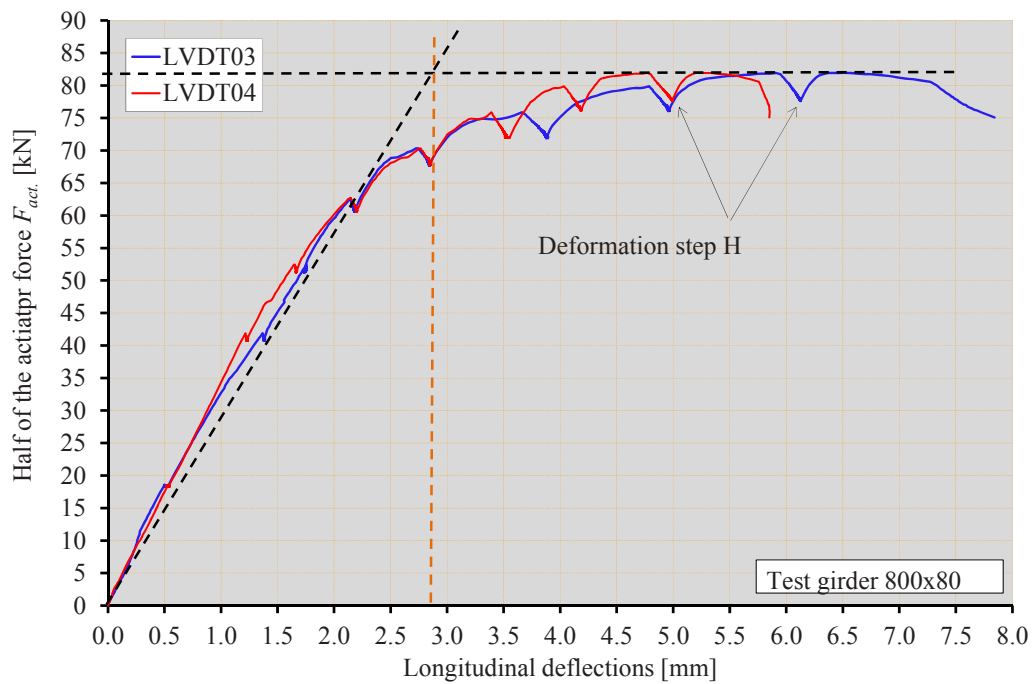


Figure 5-38 P - δ diagram test girder 9, 800x80, based on half of the actuator force $F_{act.}$ and the longitudinal deformations x_{1L} and x_{1R} measured by LVDT03 and 04

Based on the measured horizontal displacements, it can be seen that the calculated horizontal displacements x_{1L} , x_{1R} , x_{2L} and x_{2R} based on linear elastic theory have to be doubled to take the non-linear displacements into account. The ratio between the maximum horizontal displacement, measured by Lvd03 or Lvd04, and the calculated horizontal displacement x_{1L} is used to adapt the horizontal displacement x_{2L} of the test girder as well. The horizontal displacements of test girder 9, 800x80, are adapted to $x_{1L} = x_{1R} = 6.13 \text{ mm}$ and $x_{2L} = x_{2R} = \frac{6.13}{2.69} \cdot 2.27 = 5.16 \text{ mm}$ and for the

spreader beam $x_{3L} = x_{3R} = 0.63 \text{ mm}$. The influence of the horizontal displacements on the difference in reaction forces is determined by substitution of the adapted horizontal displacements of the test girder based on linear elastic theory and the horizontal displacements of the spreader beam based on linear elastic theory into Eq.(5.1) and Eq.(5.2), see Eq.(5.7) and Eq.(5.8):

$$R_R = \frac{(6000 + 2x_{1L} + 2x_{2L} + 2x_{3L}) \cdot \frac{F_{act}}{2}}{(6000 + x_{1L} + x_{1R})} = \frac{(6000 + 2 \cdot 6.13 + 2 \cdot 5.16 + 2 \cdot 0.63) \cdot \frac{F_{act}}{2}}{(6000 + 2 \cdot 6.13)} = 0.5010 \cdot F_{act} \quad (5.7)$$

$$R_L = \frac{(6000 + 2x_{1R} - 2x_{2L} - 2x_{3L}) \cdot \frac{F_{act}}{2}}{(6000 + x_{1L} + x_{1R})} = \frac{(6000 + 2 \cdot 6.13 - 2 \cdot 5.16 - 2 \cdot 0.63) \cdot \frac{F_{act}}{2}}{(6000 + 2 \cdot 6.13)} = 0.4990 \cdot F_{act} \quad (5.8)$$

The influence of the longitudinal deformations on the difference in reaction forces is determined

$$\text{with } \Delta R_{th,rel} = \frac{\Delta R_{th}}{\sum R} \cdot 100\% = \frac{R_R - R_L}{R_R + R_L} \cdot 100\% = \frac{0.5010 \cdot F_{act} - 0.4990 \cdot F_{act}}{0.5010 \cdot F_{act} + 0.4990 \cdot F_{act}} \cdot 100\% = 0.19\%.$$

For the flexible test girder 3, 400x80(2), similar calculations are made. The rotation $\varphi_{L, sb}$ of the left end of the spreader beam is:

$$\varphi_{L, sb} = \frac{F \ell_{sb}^2}{16EI_{HEB240}} = \frac{88.43 \cdot 10^3 \cdot 3000^2}{16 \cdot 210000 \cdot 11259 \cdot 10^4} = 0.00210$$

The horizontal displacement x_{3L} is calculated by using this rotation $\varphi_{L, sb}$:

$$x_{3L} = \sin(\varphi_{L, sb}) \cdot \left(\frac{h_{HEB240}}{2} + \frac{d_{roll}}{2} \right) = \sin(0.00210) \cdot \left(\frac{240}{2} + \frac{100}{2} \right) = 0.36 \text{ mm} \quad (5.9)$$

The rotation of the left end of the test girder $\varphi_{L, ig}$ is:

$$\varphi_{L, ig} = \frac{F/2 \cdot \ell_{ep}^2}{2EI_{ep}} + \frac{F/2 \cdot \ell_{ep} \cdot \ell_{ip}}{EI_{ip}} = \frac{88.43 \cdot 10^3 / 2 \cdot 1500^2}{2 \cdot 210000 \cdot 5855.2 \cdot 10^4} + \frac{88.43 \cdot 10^3 / 2 \cdot 1500 \cdot 3000 / 2}{210000 \cdot 3987.3 \cdot 10^4} = 0.01593$$

The horizontal displacement x_{1L} of the test girder is determined as follows:

$$x_{1L} = \sin(\varphi_{L, ig}) \cdot \left(\frac{h_w}{2} + t_{yf} + \frac{d_{rod}}{2} \right) = \sin(0.01593) \cdot \left(\frac{399.8}{2} + 5.57 + \frac{12}{2} \right) = 3.37 \text{ mm} \quad (5.10)$$

The rotation $\varphi_{li, ig}$ of the test girder at the left-hand side load introduction is:

$$\varphi_{li,lg} = \frac{F/2 \cdot \ell_{ep} \cdot \ell_{ip}/2}{EI_{ip}} = \frac{88.43 \cdot 10^3/2 \cdot 1500 \cdot 3000/2}{210000 \cdot 3987.3 \cdot 10^4} = 0.01188$$

The horizontal displacement x_{2L} is determined as follows:

$$x_{2L} = \sin(\varphi_{is,sb}) \cdot \left(\frac{h_w}{2} + t_{ef} + \frac{d_{roll}}{2} \right) = \sin(0.01188) \cdot \left(\frac{399.8}{2} + 5.57 + \frac{100}{2} \right) = 3.04 \text{ mm} \quad (5.11)$$

The horizontal displacement x_{1L} is measured by Lvdt03 and x_{1R} by Lvdt04, see Figure 5-39. The moment the maximum load occurs in deformation step O, the horizontal displacements are $x_{1L} = 6.81 \text{ mm}$ and $x_{1R} = 8.83 \text{ mm}$.

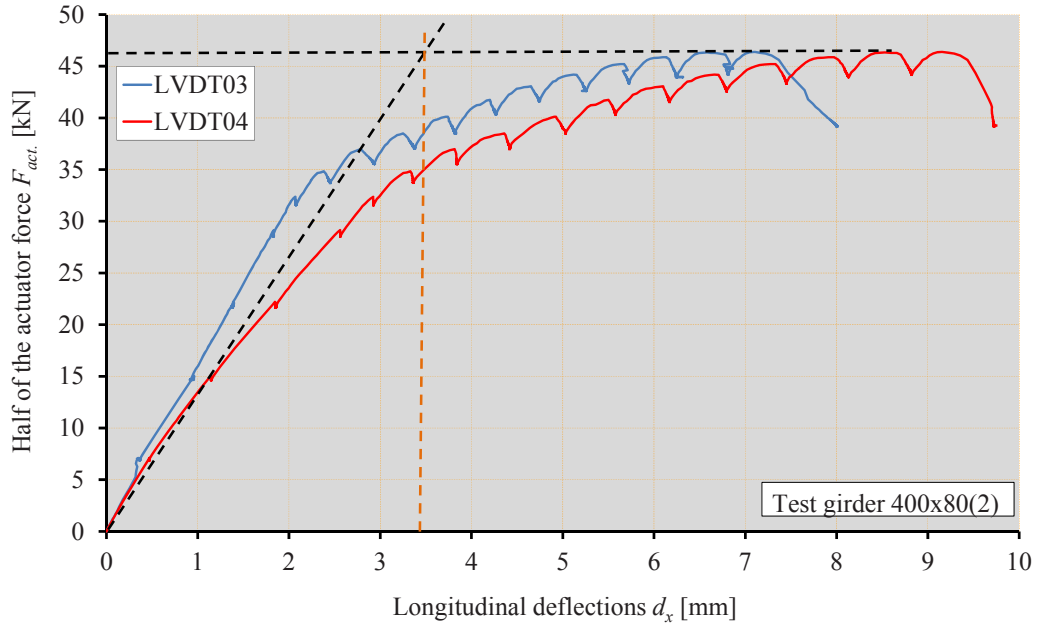


Figure 5-39 P - δ diagram test girder 3, 400x80(2), based on half of the actuator force F_{act} and the longitudinal deformations x_{1L} and x_{1R} measured by Lvdt3 and Lvdt4

The ratio between the maximum horizontal displacement, measured by Lvdt03 or Lvdt04, and the calculated horizontal displacement x_{1L} is used to adapt the horizontal displacement x_{2L} of the test girder as well. The horizontal displacements of test girder 3, 400x80(2), are $x_{1L} = x_{1R} = 8.83 \text{ mm}$

and $x_{2L} = x_{2R} = \frac{8.83}{3.37} \cdot 3.04 = 7.95 \text{ mm}$ and for the spreader beam $x_{3L} = x_{3R} = 0.36 \text{ mm}$. The influence of the horizontal displacements on the difference in reaction forces are determined by substitution of the adapted horizontal displacements of the test girder based on linear elastic theory and the horizontal displacements of the spreader beam based on linear elastic theory into Eq.(5.1) and Eq.(5.2), see Eq.(5.12) and Eq.(5.13).

$$R_R = \frac{(6000 + 2x_{1L} + 2x_{2L} + 2x_{3L}) \cdot \frac{F_{act.}}{2}}{(6000 + x_{1L} + x_{1R})} = \frac{(6000 + 2 \cdot 8.83 + 2 \cdot 7.95 + 2 \cdot 0.36) \cdot \frac{F_{act.}}{2}}{(6000 + 2 \cdot 8.83)} = 0.5014 \cdot F_{act.} \quad (5.12)$$

$$R_L = \frac{(6000 + 2x_{1R} - 2x_{2L} - 2x_{3L}) \cdot \frac{F_{act.}}{2}}{(6000 + x_{1L} + x_{1R})} = \frac{(6000 + 2 \cdot 8.83 - 2 \cdot 7.95 - 2 \cdot 0.36) \cdot \frac{F_{act.}}{2}}{(6000 + 2 \cdot 8.83)} = 0.4986 \cdot F_{act.} \quad (5.13)$$

The influence of the longitudinal deformations on the difference in reaction forces is determined with $\Delta R_{th,rel} = \frac{\Delta R_{th}}{F_{act.}} \cdot 100\% = \frac{R_R - R_L}{F_{act.}} \cdot 100\% = \frac{0.5014 \cdot F_{act.} - 0.4986 \cdot F_{act.}}{F_{act.}} \cdot 100\% = 0.28\%$.

These differences in the calculated reaction forces related to the sum of the reaction forces of all test girders in percentage terms are shown in the first column of Table 5-2. The table shows that the influence of the offset of the position of the spreader beam relative to the test girders on the differences in reaction forces is only minor, namely between 0.09% and 0.28 %.

Horizontal component:

The vertical component is smaller than the measured actuator force $F_{act.v} < F_{act.}$ and the horizontal component is a very small fraction of the actuator force $F_{act.h} \ll F_{act.}$. The horizontal component $F_{act.h}$ introduced in the spreader beam is restrained by the hinge at the left-hand side under the spreader beam. Couples of forces are introduced into the spreader beam as well as into the test girder, see Figure 5-36. The horizontal actuator force may be (partly) restrained by longitudinal friction between the compressive flange of the test girder and the lateral supports, see red arrow in Figure 5-36, or by the longitudinal support in the centre of the web, see black arrow in Figure 5-36.

Based on the small influence of the vertical component due to the offset of the spreader beam on the reaction forces, it is clear that the influence of the horizontal component of the actuator force $F_{act,h}$ on the vertical reaction force is negligibly small.

The conclusion of this calculation is that the difference in reaction forces is partly explained by the offset of the position of the spreader beam relative to the test girder due to curvature of these beams. The second issue related to this difference in reaction forces, the friction force, is discussed in Chapter 5.3.1.2.

5.3.1.2 The friction forces

The difference between the actuator force F_{act} and the sum of the reaction forces $\sum R$ is the resultant of the friction forces, the so called resulting friction force F_{fric} , see Eq.(5.14).

$$F_{fric} = F_{act} - R_L - R_R \quad (5.14)$$

The locations at which the friction forces act on the test girder are different for each test girder, depending on the out-of-plane initial imperfections of the compressive flange and those of the lateral supports. The location x of the point of action of the resulting friction force F_{fric} , see Figure 5-40, can be calculated with Eq. (5.15).

$$x = \frac{3.0 \cdot F_{act} - 6.0 \cdot R_R}{F_{fric}} \quad (5.15)$$

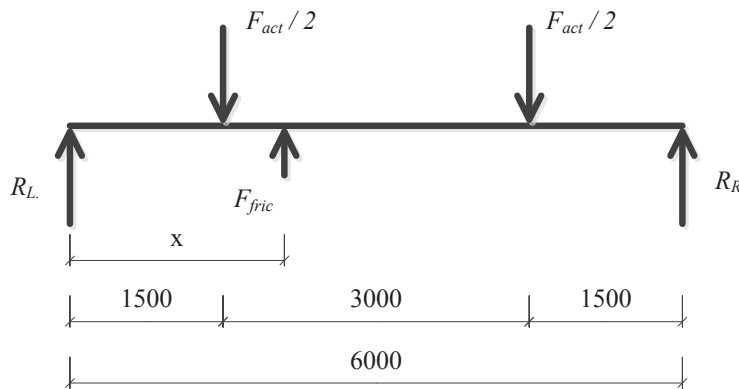


Figure 5-40 Static scheme of the test girder including the loads at the load introductions, the reaction forces and the resulting friction force

For almost all test girders the maximum right-hand side reaction force $R_{R,max}$ is greater than the maximum left-hand side reaction force $R_{L,max}$, see the underlined maximum right-hand side reaction forces $R_{R,max}$ in Table 5-2. The maximum left-hand side reaction force $R_{L,max}$ of test girder 2, 400x80(1) is the only one that is greater than the maximum right-hand side reaction force $R_{R,max}$.

Table 5-2 shows that for test girders 1, 400x50, to 6, 600x80, the maximum right-hand side reaction force $R_{R,max}$ is smaller than half of the actuator force F_{act} . This means that the numerator of Eq.(5.15) is always a positive value and so the location x of the point of action of the resulting friction force F_{fric} will be located in-between both supports of the test girder.

Table 5-2 shows also that for test girders 7, 600x50, 9, 800x80, and 10, 800x 100, the maximum right-hand side reaction force $R_{R,max}$ is greater than half of the actuator force F_{act} , see the values printed in bold in Table 5-2. This means that in these cases the numerator in Eq. (5.15) is negative and the location x of the point of action of the friction force F_{fric} is located outside the test girder, which is physically impossible.

For test girder 8, 800x50, the maximum right-hand side reaction force $R_{R,max}$ is equal to half of the actuator force F_{act} . The numerator becomes zero and the location x of the point of action of the friction force F_{fric} is located at the left-hand side support and this is also physically impossible.

Table 5-2 Influence of the offset of the spreader beam relative to the test girder on the unbalance ΔR in reaction forces

Test girder	$\Delta R_{th,rel}$ [%]	F_{act} [kN]	$R_{L,max}$ [kN]	$R_{R,max}$ [kN]	ΔR [kN]	$\sum R$ [kN]	F_{frict} [kN]	ΔR_{rel} [%]	$\Delta R_{rel}-\Delta R_{th,rel}$ [%]
1, 400x50	0.18	47.66	20.89	<u>22.57</u>	1.68	43.46	4.19	3.87	3.59
2, 400x80(1)	0.22	81.20	36.40	34.73	-1.67	71.13	10.07	2.35	2.13
3, 400x80(2)	0.28	88.43	39.17	<u>43.54</u>	4.37	82.71	5.72	5.28	5.28
4, 400x100	0.21	84.13	37.56	<u>39.53</u>	1.97	77.09	7.05	2.56	2.35
5, 600x50	0.25	71.29	32.02	<u>34.79</u>	2.77	66.81	4.48	4.15	3.90
6, 600x80	0.24	125.39	56.16	<u>60.11</u>	3.95	116.27	9.11	3.40	3.16
7, 600x100	0.20	122.07	59.25	61.57	2.32	120.82	1.25	1.92	1.72
8, 800x50	0.22	90.62	41.61	<u>45.31</u>	3.70	86.92	3.71	4.26	4.04
9, 800x80	0.19	155.27	74.23	79.05	4.82	153.27	2.00	3.14	2.95
10, 800x100	0.09	154.10	74.40	78.65	4.25	153.05	1.14	2.72	2.69

5.3.1.3 The accuracy of the measurement

From Eq.(5.15) it can be seen that the location x of the point of action of the resulting friction force F_{fric} is situated outside the span of the test girder when the numerator is smaller than zero. This is the case for the four most rigid test girders and hence the difference in reaction force can not be explained by this location, because such location is physically impossible.

In general one can say that the end result of a laboratory test is combined of k measured independent quantities. This can be expressed by Eq.(5.16):

$$E = E(x_1, x_2, x_3, \dots, x_k) \quad (5.16)$$

The absolute error Δx_i in the measured quantities has to be taken into account to determine the absolute error ΔE in this end result E . The error propagation is determined based on:

$$(\Delta E)^2 = \sum_{i=1}^k \left(\frac{\partial E}{\partial x_i} \cdot \Delta x_i \right)^2 \quad (5.17)$$

A distinction is made between the absolute error Δx_i and a relative error $\frac{\Delta x_i}{x}$.

The distances 3.0 and 6.0 for respectively the distance from the left-handed support to the actuator force F_{act} and the distance from the left-handed support to the right-handed support as given in Eq.(5.15), are assumed to be exact, but in reality there will be an error in the measurements of these distances too, which will affect the location x of the point of action of the friction force F_{fric} . The derivations of x are as follows:

$$\begin{aligned} \frac{\partial E}{\partial x_i} = \frac{\partial x}{\partial F_{act}} &= \frac{3.0 \cdot (F_{act} - R_L - R_R) - 1.0 \cdot (3.0 \cdot F_{act} - 6.0 \cdot R_R)}{(F_{act} - R_L - R_R)^2} = \frac{3.0 \cdot (-R_L + R_R)}{(F_{act} - R_L - R_R)^2} \\ \frac{\partial E}{\partial x_i} = \frac{\partial x}{\partial R_L} &= \frac{0.0 \cdot (F_{act} - R_L - R_R) - (-1.0) \cdot (3.0 \cdot F_{act} - 6.0 \cdot R_R)}{(F_{act} - R_L - R_R)^2} = \frac{3.0 \cdot (F_{act} - 2.0 R_R)}{(F_{act} - R_L - R_R)^2} \\ \frac{\partial E}{\partial x_i} = \frac{\partial x}{\partial R_R} &= \frac{-6.0 \cdot (F_{act} - R_L - R_R) - (-1.0) \cdot (3.0 \cdot F_{act} - 6.0 \cdot R_R)}{(F_{act} - R_L - R_R)^2} = \frac{3.0 \cdot (-F_{act} + 2.0 R_L)}{(F_{act} - R_L - R_R)^2} \end{aligned} \quad (5.18)$$

And the absolute errors are:

$$\begin{aligned} \Delta x_i = \Delta F_{act} &= 0.01 \cdot F_{act} \\ \Delta x_i = \Delta R_L &= 0.02 \cdot R_L \\ \Delta x_i = \Delta R_R &= 0.02 \cdot R_R \end{aligned} \quad (5.19)$$

For test girder 800x80 the following is measured:

$$F_{act} = 155.27 \text{ kN}$$

$$\Delta x_i = \Delta F_{act} = 0.01 \cdot 155.27 = 1.55 \text{ kN}$$

$$R_L = 74.23 \text{ kN}$$

$$\Delta x_i = \Delta R_L = 0.02 \cdot 74.23 = 1.48 \text{ kN}$$

$$R_R = 79.05 \text{ kN}$$

$$\Delta x_i = \Delta R_R = 0.02 \cdot 79.05 = 1.58 \text{ kN}$$

$$\frac{\partial x}{\partial F_{act}} = \frac{3.0 \cdot (-R_L + R_R)}{(F_{act} - R_L - R_R)^2} = \frac{3.0 \cdot (-74.23 + 79.05)}{(155.27 - 74.23 - 79.05)^2} = +3.651 \text{ m}$$

$$\frac{\partial x}{\partial R_L} = \frac{3.0 \cdot (F_{act} - 2.0 R_R)}{(F_{act} - R_L - R_R)^2} = \frac{3.0 \cdot (155.27 - 2.0 \cdot 79.05)}{(155.27 - 74.23 - 79.05)^2} = -2.144 \text{ m}$$

$$\frac{\partial x}{\partial R_R} = \frac{3.0 \cdot (-F_{act} + 2.0 \cdot R_L)}{(F_{act} - R_L - R_R)^2} = \frac{3.0 \cdot (-155.27 + 2.0 \cdot 74.23)}{(155.27 - 74.23 - 79.05)^2} = -5.159 \text{ m} \quad (5.20)$$

The absolute error for the distance x of the point of action of the resulting friction force F_{fric} can be calculated with:

$$\begin{aligned} (\Delta E)^2 &= \sum_{i=1}^k \left(\frac{\partial E}{\partial x_i} \cdot \Delta x_i \right)^2 \\ \Rightarrow \Delta E &= \Delta x = \sqrt{\sum \left\{ \left(\frac{\partial x}{\partial F_{act}} \cdot \Delta F_{act} \right)^2 + \left(\frac{\partial x}{\partial R_L} \cdot \Delta R_L \right)^2 + \left(\frac{\partial x}{\partial R_R} \cdot \Delta R_R \right)^2 \right\}} = \\ &= \sqrt{\sum \left\{ (3.651 \cdot 1.55)^2 + (-2.144 \cdot 1.48)^2 + (-5.159 \cdot 1.81)^2 \right\}} = 10.431 \text{ m} \end{aligned} \quad (5.21)$$

The location x of the point of action is determined:

$$x = \frac{3.0 \cdot F_{act} - 6.0 \cdot R_R}{F_{act} - R_L - R_R} = \frac{3.0 \cdot 155.27 - 6.0 \cdot 79.05}{155.27 - 74.23 - 79.05} = -4.266 \text{ m} \quad (5.22)$$

Based on the error propagation, the location of the point of action will be positioned between:

$$-4.266 - 10.431 = -14.697 \text{ m} \leq x \mp \Delta x \leq -4.266 + 10.431 = +6.164 \text{ m} \quad (5.23)$$

Figure 5-41 shows the realistic positions of the location of the point of action of the friction force.

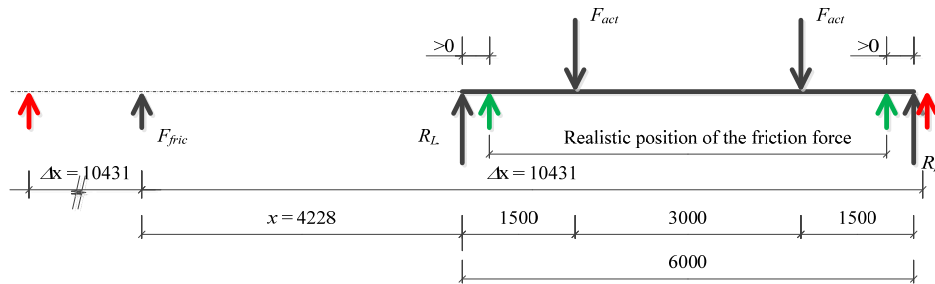


Figure 5-41 Static scheme of test girder 9, 800x80, including the realistic position of the friction force F_{fric} based on the error propagation

This means that, because of the error of 1% in the measuring of the actuator force F_{act} and 2% of the errors of the reaction forces R , the location of the point of the action of the resulting friction force F_{fric} can be at any position of the span of the test girder.

For test girder 3, 400x80(2) the same calculations are made:

$$\begin{aligned}
 F_{act} &= 88.43 \text{ kN} & \Delta x_i &= \Delta F_{act} = 0.01 \cdot 88.43 = 0.88 \text{ kN} \\
 R_L &= 39.17 \text{ kN} & \Delta x_i &= \Delta R_L = 0.02 \cdot 39.17 = 0.78 \text{ kN} \\
 R_R &= 43.54 \text{ kN} & \Delta x_i &= \Delta R_R = 0.02 \cdot 43.54 = 0.87 \text{ kN} \\
 \frac{\partial x}{\partial F_{act}} &= \frac{3.0 \cdot (-R_L + R_R)}{(F_{act} - R_L - R_R)^2} = \frac{3.0 \cdot (-39.17 + 43.54)}{(88.43 - 39.17 - 43.54)^2} = +0.401 \text{ m} \\
 \frac{\partial x}{\partial R_L} &= \frac{3.0 \cdot (F_{act} - 2.0 R_R)}{(F_{act} - R_L - R_R)^2} = \frac{3.0 \cdot (88.43 - 2.0 \cdot 39.17)}{(88.43 - 39.17 - 43.54)^2} = +0.124 \text{ m} \\
 \frac{\partial x}{\partial R_R} &= \frac{3.0 \cdot (-F_{act} + 2.0 \cdot R_L)}{(F_{act} - R_L - R_R)^2} = \frac{3.0 \cdot (-88.43 + 2.0 \cdot 39.17)}{(88.43 - 39.17 - 43.54)^2} = -0.925 \text{ m}
 \end{aligned} \tag{5.24}$$

The absolute error for the distance x of the point of action of the resulting friction force F_{fric} can be calculated with:

$$\begin{aligned}
 \Delta E = \Delta x &= \sqrt{\sum \left\{ \left(\frac{\partial x}{\partial F_{act}} \cdot \Delta F_{act} \right)^2 + \left(\frac{\partial x}{\partial R_L} \cdot \Delta R_L \right)^2 + \left(\frac{\partial x}{\partial R_R} \cdot \Delta R_R \right)^2 \right\}} = \\
 &= \sqrt{\sum \left\{ (0.401 \cdot 0.88)^2 + (+0.124 \cdot 0.78)^2 + (-0.925 \cdot 0.87)^2 \right\}} = 0.885 \text{ m}
 \end{aligned} \tag{5.25}$$

The location x of the point of action is determined:

$$x = \frac{3.0 \cdot F_{act} - 6.0 \cdot R_R}{F_{act} - R_L - R_R} = \frac{3.0 \cdot 88.43 - 6.0 \cdot 39.17}{88.43 - 39.17 - 43.54} = +0.708 \text{ m} \tag{5.26}$$

Based on the error propagation, the location x of the point of action will be positioned in-between:

$$+0.708 - 0.885 = -0.177 \text{ m} \leq x \mp \Delta x \leq +0.708 + 0.885 = +1.593 \text{ m} \tag{5.27}$$

Figure 5-41 shows the realistic position of the location x of the point of action of the friction force F_{fric} .

Table 5-3 shows for all test girders the range of the location x of the point of action of the friction force F_{fric} , based on the error propagations of the measurements of the load cells for the actuator force F_{act} and the reaction forces R , see Appendix K too.

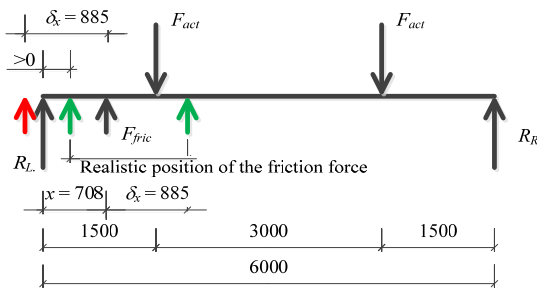


Figure 5-42 Static scheme of test girder 3, 400x80(2), including the realistic position of the friction force F_{fric} based on the accuracies of the measurements

Table 5-3 The range $x \pm \Delta x$ of the location x of the point of action of the resulting friction force

F_{fric} based on error propagation of the measurements of the load cells

	$\frac{\Delta F_{act}}{F_{act}} = 0.01$		$\frac{\Delta R_i}{R_i} = 0.02$		$\frac{\Delta F_{act}}{F_{act}} = 0.005$		$\frac{\Delta R_i}{R_i} = 0.01$	
Test girder	x_{min}	x_{max}	x	Δx	x_{min}	x_{max}	x	Δx
	[m]	[m]	[m]	[m]	[m]	[m]	[m]	[m]
1, 400x50	+0.863	+2.044	+1.454	+0.590	+1.159	+1.749	+1.454	+0.295
2, 400x80(1)	+3.189	+3.806	+3.498	+0.309	+3.343	+3.652	+3.498	+0.154
3, 400x80(2)	-0.177	+1.593	+0.708	+0.885	+0.265	+1.151	+0.708	+0.443
4, 400x100	+1.661	+2.660	+2.161	+0.499	+1.911	+2.410	+2.161	+0.250
5, 600x50	+0.319	+1.971	+1.145	+0.826	+0.732	+1.558	+1.145	+0.413
6, 600x80	+1.071	+2.331	+1.701	+0.630	+1.386	+2.016	+1.701	+0.315
7, 600x100	-12.899	+7.763	-2.568	+10.331	-7.734	+2.598	-2.568	+5.166
8, 800x50	-1.643	+1.643	+0.000	+1.643	-0.821	+0.821	+0.000	+0.821
9, 800x80	-14.697	+6.164	-4.266	+10.431	-9.482	+0.949	-4.266	+5.215
10, 800x100	-40.767	+22.481	-9.143	+31.624	-24.955	+6.669	-9.143	+15.812

5.3.1.4 Conclusions

The following is concluded about the elaborations of the reaction forces versus the actuator force:

1. The right-hand side reaction force $R_{R,max}$ is always greater than the left-hand side reaction force $R_{L,max}$, except for test girder 2, 400x80(1), which was the first girder tested with Teflon instead of Teflon between the compressive flange and the lateral supports;
2. For test girder 2, 400x80(1), the resulting friction force is a maximum, namely 12.40% of the actuator force F_{act} . This maximum is due to using PVDF (Teflon or polyvinylidene

difluoride) with a friction coefficient (static) of 0.2-0.4, instead of PTFE (Teflon or polytetrafluoroethylene) with a friction coefficient (static) of 0.08 between the compressive flange and the lateral supports;

3. The resulting friction force F_{fric} for test girders 1, 400x50, and 3, 400x80(2), 4, 400x100, 5, 600x50 and 6, 600x80, is less than 8.80% of the actuator force F_{act} ;
4. For test girders 7, 9 and 10, respectively 600x100, 800x80 and 800x100, the resulting friction force F_{fric} is less than 1.29% of the actuator force F_{act} ;
5. For test girder 8, 800x50, the resulting friction force is 4.09% of the actuator force F_{act} ;
6. The difference in reaction forces is hardly influenced by the offset of the spreader beam relative to the test girder;
7. The resulting friction force is the main cause of the unbalance of the reaction forces;
8. All reaction forces are smaller than half of the actuator force F_{act} , except for the right-hand side reaction forces $R_{R,max}$ of the test girders 7, 600x100, 8, 800x50, 9, 800x80 and 10, 800x100;
9. For these four most rigid test girders, the right-hand side reaction force $R_{R,max}$ is greater than or equal to half of the actuator force F_{act} and the friction force F_{fric} is smaller than the difference in reaction forces ΔR . The offset of the spreader beam relative to the test girder and the location x of the point of action of the resulting friction force F_{fric} do not explain the difference in the reaction force of these test girders. By taking into account the uncertainties in measurements of the actuator force F_{act} and the reaction forces $R_{L,max}$ and $R_{R,max}$, this unbalance is fully explained.

5.3.2 THE LOAD DEFORMATION BEHAVIOUR

The maximum actuator force F_{act} that occurs in a test is based on the P - δ diagram as presented in Figure 5-3 for test girder 9, 800x80 and Figure 5-5 for 3, 400x80(2), see also Appendix A. The experiments are deformation driven and in the diagrams it can be seen that after every deformation step a time lapse is introduced to allow for relaxation of the test rig and test girder to stabilise. During the time lapse, the actuator force F_{act} reduces to a stable level. These stable values of the actuator forces are taken to be the actuator force F_{act} due to a certain deformation step. The time lapse is also used to take all the measurements.

The bending moment resistance of the test girder should be based on the maximum actuator force F_{act} , which can be determined from the load-deformation curves shown in Figure 5-3 and Figure 5-5 and the other curves from Appendix A. The bending moment resistance can be calculated by multiplying the load at the load introduction, equal to half of the actuator force F_{act} , times the distance between load introduction and the nearby support. This should be equal to the reaction force multiplied by the same distance. From Chapter 5.3.1 Table 5-2 it can be seen that the reaction force is a bit lower than the force at the nearby load introduction due to unbalance in the test rig and friction. Multiplying the reaction force times the distance of that reaction force and the nearby load introduction leads to a safe sided calculation of the bending moment resistance because of ignoring the contribution of the friction when it is located in the end panels.

Now the remaining question is which of both reaction forces is to be taken to calculate the bending moment resistance. An option is to take the lowest of both reaction forces to calculate the bending moment resistance. From Figure 5-3 and Figure 5-5 and the corresponding figures of the other test girders given in Appendix B, it can be observed that after reaching the maximum actuator force F_{act} it was always possible to apply one or more deformation steps going along with decreasing forces. At the end of these additional deformation steps, “final” collapse of the test girders took place. Figure 5-3 and Figure 5-5 show the maximum load for test girder 9, 800x80 and 3, 400x80(2) respectively, but also the vertical displacements of the test girder at the load introduction, measured by Lvdt01 on the left-hand side load introduction and Lvdt02 on the right-hand side load introduction. Table 5-4 shows the difference in deformations based on the measurements by Lvdt01 and Lvdt02 for the deformation step in which the maximum load occurs for all test girders. These differences in vertical deformation are very small. The maximum difference in deformation is 5.86 mm for test girder 5, 600x50. By taking into account that this difference is over the length of the test panel of 3000 mm, this difference of 5.86 mm is relatively small.

Although the beam is behaving symmetrically up to reaching the maximum actuator force F_{act} at final collapse, an asymmetric mechanism occurs in the girder. From Figure 5-3 and Figure 5-5 and the corresponding Figures of the other test girders given in Appendix B this can be seen from the difference in displacements of the girder sections at the load introductions in the descending parts of the graphs. Only a few girders, namely test girder 1, 400x50 and test girder 3, 400x80(2), remained symmetric in the final collapse mode. Observing this behaviour of the test girders, it was decided to determine the bending moment resistance on the reaction force at that support which was most nearby to the final “plastic hinge” in the failure mechanism of the test girder.

Table 5-4 Difference in vertical deflections $\Delta\delta_z$ based on measurements by Lvdt01 and Lvdt02

Test specimen	$\delta_{z,Lvdt01}$ [mm]	$\delta_{z,Lvdt02}$ [mm]	$\Delta\delta_z$ [mm]	$\delta_{z,act.}$ [mm]	$F_{act.}$ [kN]
1, 400x50	27.14	26.59	-0.55	28.32	47.66
2, 400x80(1)	31.86	32.59	+0.73	38.43	81.20
3, 400x80(2)	40.27	41.61	+1.34	47.07	88.43
4, 400x100	37.28	36.41	-0.87	41.85	84.13
5, 600x50	31.30	25.44	-5.86	29.05	71.29
6, 600x80	22.25	22.29	+0.04	26.37	125.39
7, 600x100	23.55	23.90	+0.35	28.22	122.07
8, 800x50	20.87	22.29	+1.40	24.17	90.62
9, 800x80	18.63	19.76	+2.13	24.90	155.27
10, 800x100	18.63	20.97	+2.61	24.56	154.10

5.3.3 THE OUT-OF-PLANE DEFLECTIONS OF THE WEB IN THE TEST PANEL

5.3.3.1 The out-of-plane deflections as function of the loading

In Chapter 5.2.3, the total out-of-plane deflections of the test panels are shown. Based on these total out-of-plane deflections at every deformation step, the out-of-plane deflections as function of the loading are determined, defined as the total out-of-plane deflections of deformation step i minus the initial out-of-plane deflections of deformation step 0, see Figure 5-43 up to Figure 5-51 for test girder 9, 800x80 and see Appendix L for all test girders.

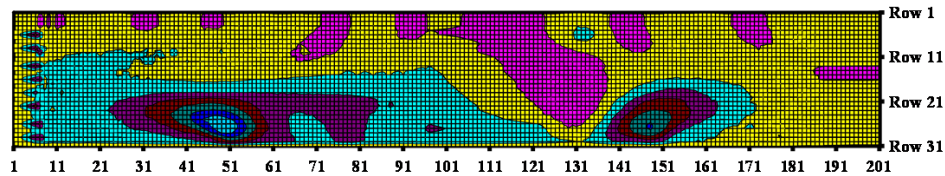


Figure 5-43 The out-of-plane deflections of the test panel of test girder 9, 800x80, as function of the loading in deformation step A

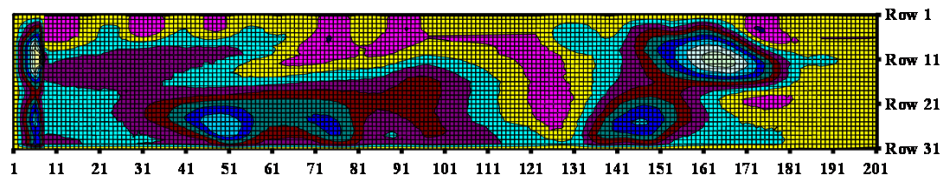


Figure 5-44 The out-of-plane deflections of the test panel of test girder 9, 800x80, as function of the loading in deformation step B

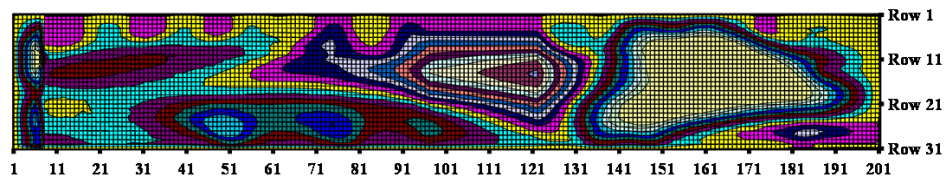


Figure 5-45 The out-of-plane deflections of the test panel of test girder 9, 800x80, as function of the loading in deformation step C

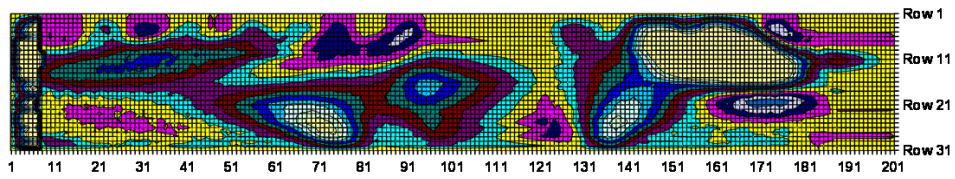


Figure 5-46 The out-of-plane deflections of the test panel of test girder 9, 800x80, as function of the loading in deformation step D

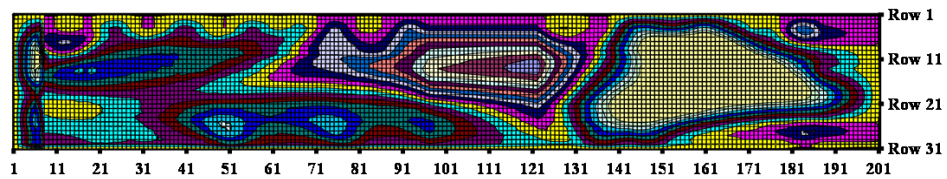


Figure 5-47 The out-of-plane deflections of the test panel of test girder 9, 800x80, as function of the loading in deformation step E

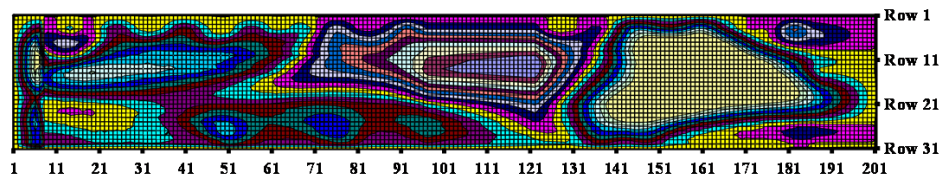


Figure 5-48 The out-of-plane deflections of the test panel of test girder 9, 800x80, as function of the loading in deformation step F

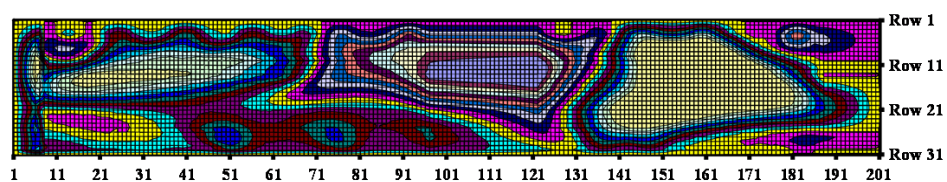


Figure 5-49 The out-of-plane deflections of the test panel of test girder 9, 800x80, as function of the loading in deformation step G

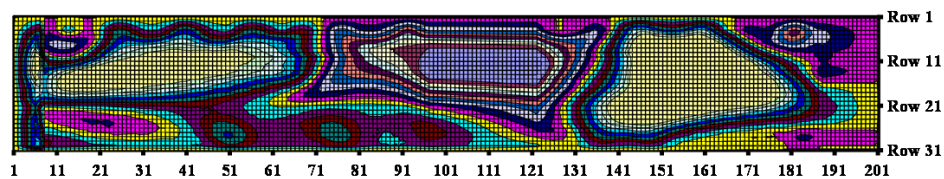


Figure 5-50 The out-of-plane deflections of the test panel of test girder 9, 800x80, as function of the loading in deformation step H

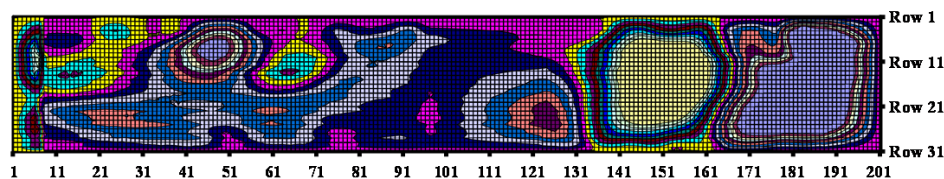


Figure 5-51 The out-of-plane deflections of the test panel of test girder 9, 800x80, as function of the loading in deformation step I

From these graphs, it can be seen that the out-of-plane deflections as function of the loading, suddenly change on the right-hand side of the test panel between points 135 and 201, corresponding with the location 3525 mm-4500 mm from the left-hand side support, from deformation step B to C, but also from deformation step H to I. The maximum actuator force F_{act} appears in deformation step H and in deformation step I the big buckle changes into two smaller buckles with different signs for the amplitudes, the web snaps through in the descending part of the $P-\delta$ diagram as shown in Figure 5-3. These out-of-plane deflections of the web confirm the previous observations about the location of the “plastic hinge” formed due to vertical buckling of the compressive flange into the web.

For test girder 3, 400x80(2), these out-of-plane deflections as function of the loading are shown in Figure 5-52 up to Figure 5-59 for several deformation steps.

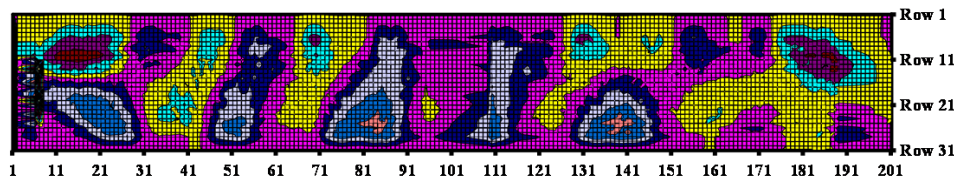


Figure 5-52 The out-of-plane deflections of the test panel of test girder 3, 400x80(2), as function of the loading in deformation step B

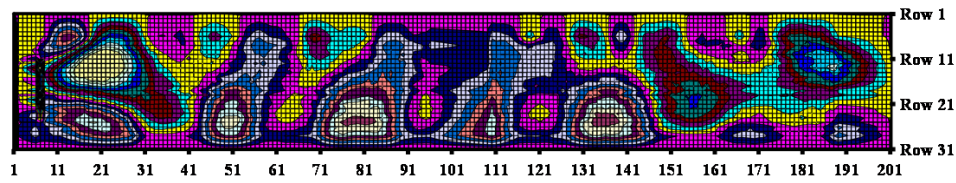


Figure 5-53 The out-of-plane deflections of the test panel of test girder 3, 400x80(2), as function of the loading in deformation step D

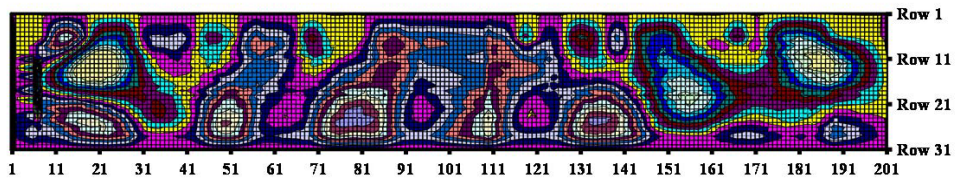


Figure 5-54 The out-of-plane deflections of the test panel of test girder 3, 400x80(2), as function of the loading in deformation step F

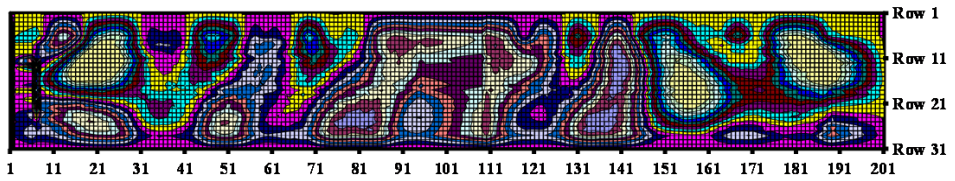


Figure 5-55 The out-of-plane deflections of the test panel of test girder 3, 400x80(2), as function of the loading in deformation step H

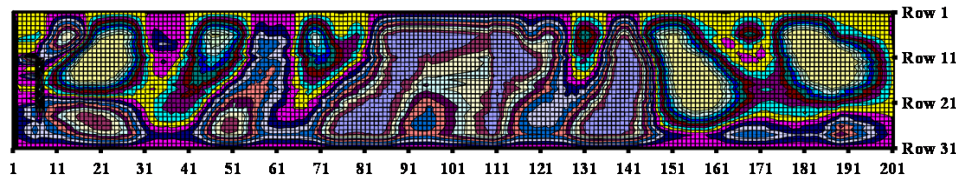


Figure 5-56 The out-of-plane deflections of the test panel of test girder 3, 400x80(2), as function of the loading in deformation step J

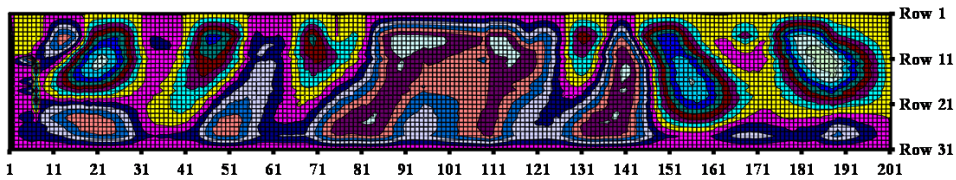


Figure 5-57 The out-of-plane deflections of the test panel of test girder 3, 400x80(2), as function of the loading in deformation step L

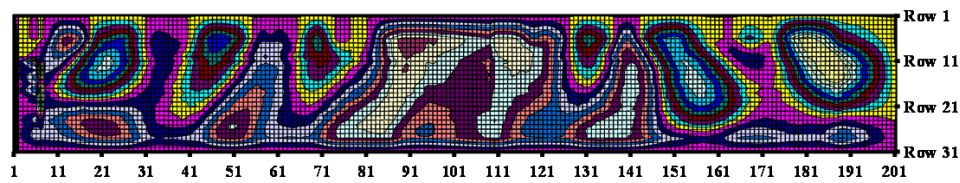


Figure 5-58 The out-of-plane deflections of the test panel of test girder 3, 400x80(2), as function of the loading in deformation step N

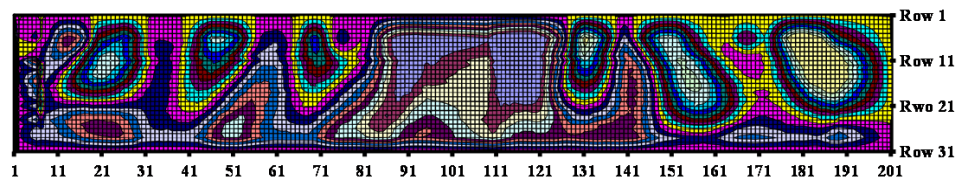


Figure 5-59 The out-of-plane deflections of the test panel of test girder 3, 400x80(2), as function of the loading in deformation step P

From these out-of-plane deflections of the web as function of the loading, it can be seen that the location of the final collapse mode of the compressive flange, between number points 80-120, corresponding to 2700-3300 mm from the left-hand side support, can also be seen from these web deformations. These out-of-plane deflections confirm the symmetric behaviour and for this test girder 3, 400x80(2), also in the deformation steps after the deformation step in which the maximum actual force F_{act} occurs. Appendix L shows the out-of-plane deflections for all test girders

5.3.3.2 Increments in the out-of-plane deflections as function of the loading

Apart from these out-of-plane deflections as function of the load, the increment in the out-of-plane deflections, so the deflections in deformation step i minus the deflections of the previous deformation step $i-1$, are determined. For test girder 9, 800x80, the increment in the out-of-plane deflections of the web as function of the loading for every deformation step is shown in Figure 5-60 up to Figure 5-67 and see Appendix M for all test girders.

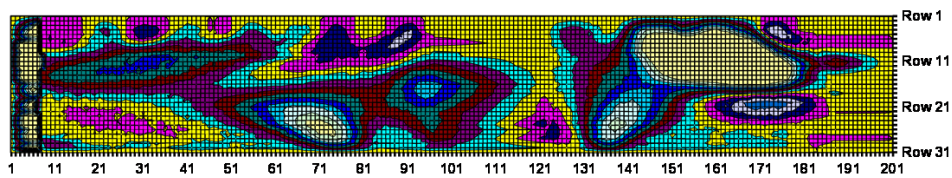


Figure 5-60 The increment in the out-of-plane deflections of the web of test girder 9, 800x80, deformation step B

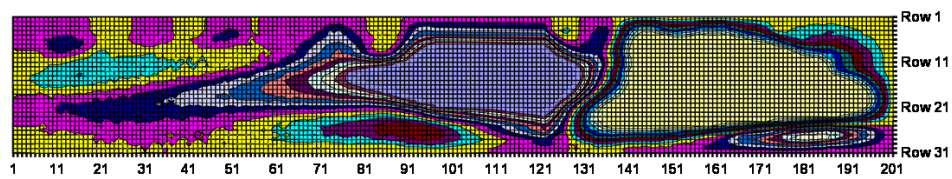


Figure 5-61 The increment in the out-of-plane deflections of the web of test girder 9, 800x80, deformation step C

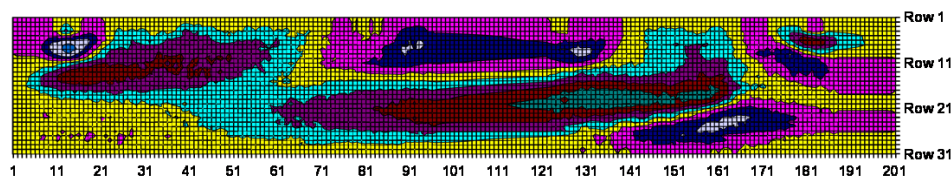


Figure 5-62 The increment in the out-of-plane deflections of the web of test girder 9, 800x80, deformation step D

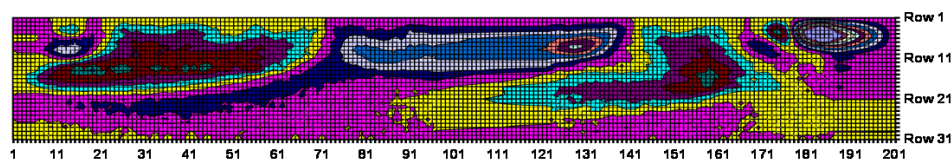


Figure 5-63 The increment in the out-of-plane deflections of the web of test girder 9, 800x80, deformation step E

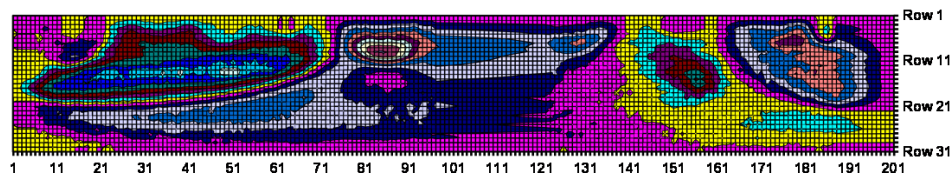


Figure 5-64 The increment in the out-of-plane deflections of the web of test girder 9, 800x80, deformation step F

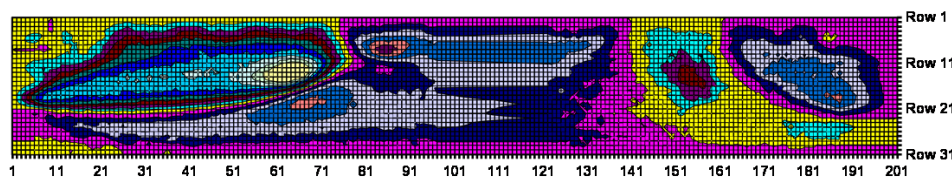


Figure 5-65 The increment in the out-of-plane deflections of the web of test girder 9, 800x80, deformation step G

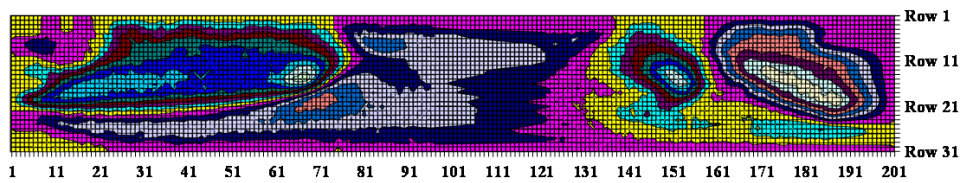


Figure 5-66 The increment in the out-of-plane deflections of the web of test girder 9, 800x80, deformation step H

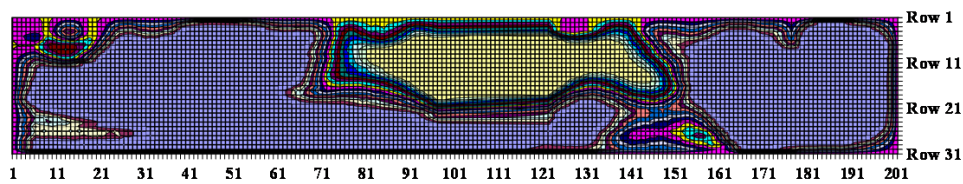


Figure 5-67 The increment in the out-of-plane deflections of the web of test girder 9, 800x80, deformation step I

The increments in the out-of-plane deflections also show the big change in deflections in deformation step C. The increments in the next deformation steps show the same development in the out-of-plane deflections, up to deformation step H, in which the maximum actuator force F_{act} appears. In deformation step I, the final collapse mode occurs for test girder 9, 800x80.

Figure 5-68 up to Figure 5-75 show the increments in the out-of-plane deflections as function of the loading for test girder 3, 400x80(2). The increments in the out-of-plane deflections of test girder 3, 400x80(2), are rather small up to deformation O. In deformation step P, the increment increases in the centre of the test panel.

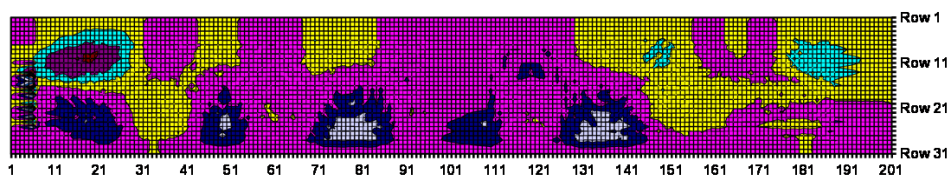


Figure 5-68 The increment in the out-of-plane deflections of the web of test girder 3, 400x80(2) deformation step B

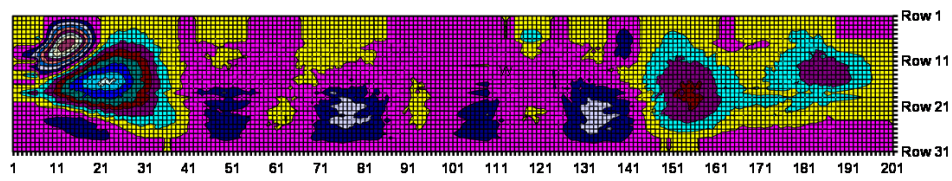


Figure 5-69 The increment in the out-of-plane deflections of the web of test girder 3, 400x80(2), deformation step D

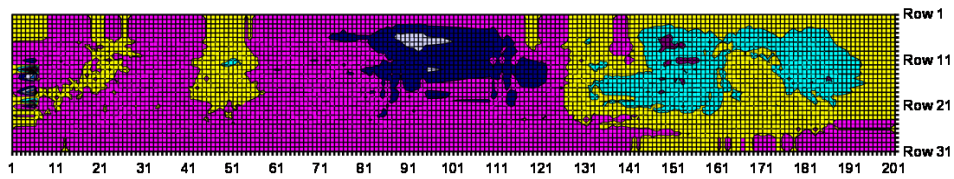


Figure 5-70 The increment in the out-of-plane deflections of the web of test girder 3, 400x80(2), deformation step F

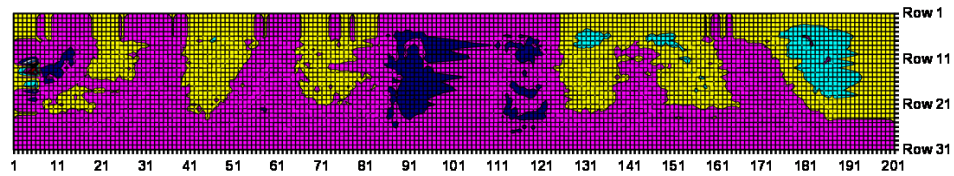


Figure 5-71 The increment in the out-of-plane deflections of the web of test girder 3, 400x80(2), deformation step H

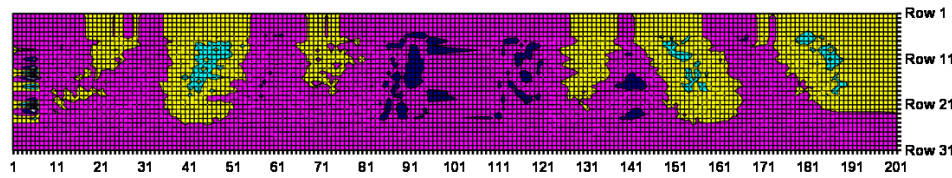


Figure 5-72 The increment in the out-of-plane deflections of the web of test girder 3, 400x80(2), deformation step J

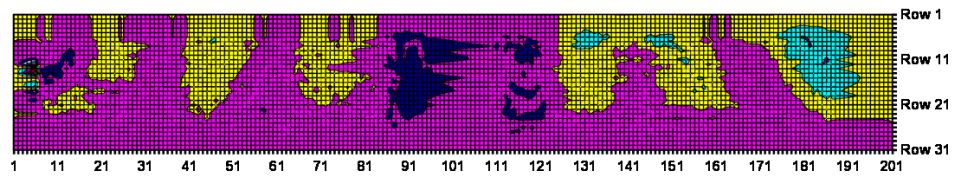


Figure 5-73 The increment in the out-of-plane deflections of the web of test girder 3, 400x80(2), deformation step L

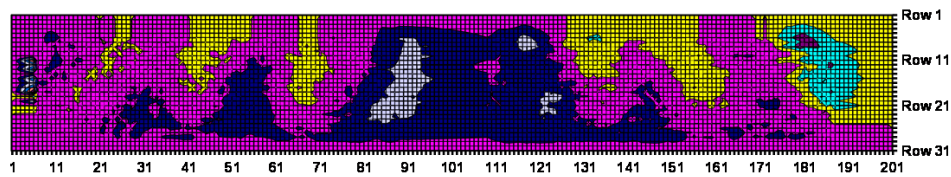


Figure 5-74 The increment in the out-of-plane deflections of the web of test girder 3, 400x80(2), deformation step N

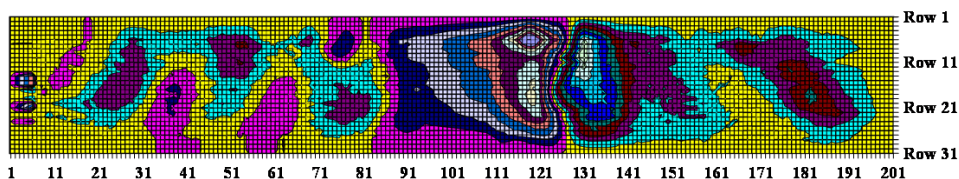


Figure 5-75 The increment in the out-of-plane deflections of the web of test girder 3, 400x80(2), deformation step P

5.3.4 THE ROTATION OF THE COMPRESSIVE FLANGE

As mentioned in Chapter 5.2.5, the rotations are indirectly determined by measuring the vertical deformations of the tips of the compressive flange by lasers for the test girders 1 to 4, respectively 400x50, 400x80(1), 400x80(2) and 400x100, and directly by the inclination gauges for the remaining test girders. The vertical deformations of the first group of test girders have to be transformed into rotations. Figure 5-30 shows the vertical deformations of the tips of the compressive flange of test girder 3, 400x80(2) and Figure 5-76 shows the corresponding rotations for specific steps, see also Appendix N for test girders 1, 400x50, 2, 400x80(1) and 4, 400x100.

Initially, the compressive flange rotates slightly in one direction over the whole length of the test panel. The parts of the compressive flange at the edges of the test panel rotate in the opposite direction from the part of the flange in the centre of the test panel in deformation step N, the step in which the maximum actuator force appears according to Figure 5-4. In deformation step O, these rotations of the compressive flange increase up to -10° over a large part in the centre of the test panel.

Table 5-5 shows the rotations of all experiments for the maximum loads, measured by lasers for test girders 2 to 4 and by the inclination gauges for test girders 5 to 10. This table shows the maximum rotation in the deformation step i in which the maximum load occurs, but also the rotations in the previous deformation step, step $i-1$, and the next deformation step, step $i+1$.

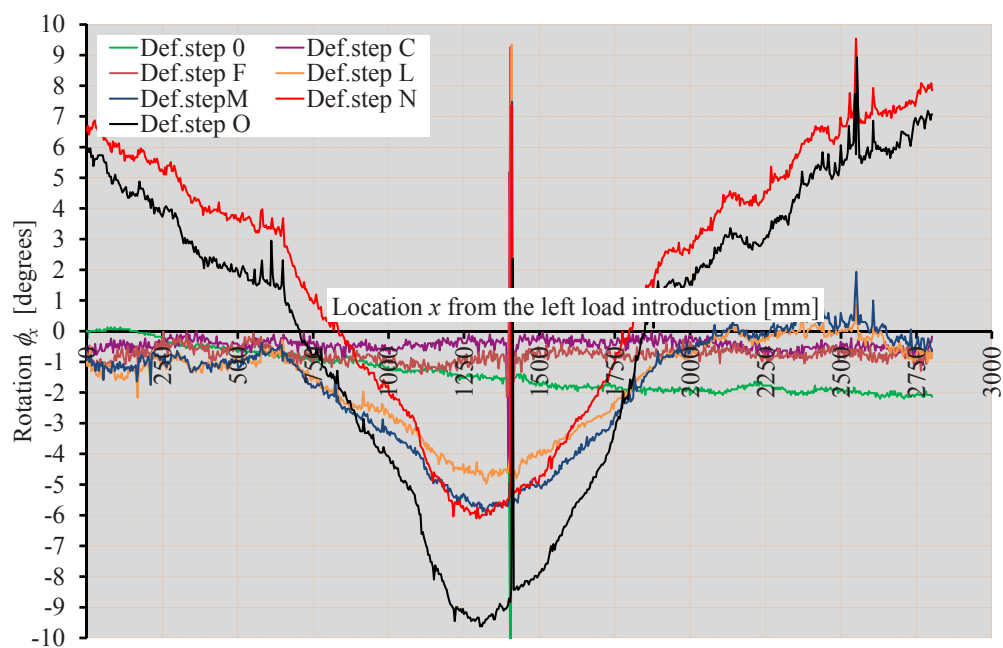


Figure 5-76 Rotation of the compressive flange of test girder 3, 400x80(2) for deformation steps 0, C, F, L, M, N and O

Table 5-5 Rotations of the top flange of all test girders for deformation step i , in which the maximum actuator force appears, for the previous step $i-1$ and for the next step $i+1$

No.	Test specimen	$\alpha_{f,max}$ $= \alpha_{f,i}$ [°]	Gauge/ dist. x [mm]	Deformation step [-]	$\alpha_{f,i-1}$ [°]	Gauge/ dist. x [mm]	$\alpha_{f,i+1}$ [°]	Gauge/ dist. x [mm]
1	400x50	-	-	-	-	-	-	-
2	400x80(1)	-5.16	2310	L	-3.05	2310	+8.79	2310
3	400x80(2)	+8.70	2490	O	-4.54	2490	-	-
4	400x100	+9.14	1860	M	-4.32	1860	-0.21	1860
5	600x50	+12.13	H14	N	+6.99	H14	+38.25	H14
6	600x80	+4.42	H03	I	+3.06	H03	+13.68	H03
7	600x100	+4.02	H03	H	+3.24	H03	+3.86	H03
8	800x50	-0.61	H15		-0.82	H15	+1.18	H15
9	800x80	-0.51	H01	H	-0.44	H01	-18.91	H01
10	800x100	+4.05	H14	M	+2.89	H14	+17.44	H14

The rotation of the compressive flange of experiment 1, 400x50, is not measured at all, because the mirrors to bow the infrared rays break rather soon after the start of the test and inclination gauges are used for the next experiments.

Table 5-5 shows that the rotation in the deformation step in which the maximum load appears, is smaller than 5.16° for the experiments 2 and 6 to 10. For experiments 3 to 5, the rotations are rather high, especially related to the rotation of the flange in the previous deformation step.

For experiments 2, 4 and 8, the sign of the rotation changes in the deformation step after the deformation step in which the maximum load appears. For experiments 5, 6, 9 and 10 the rotation in the next deformation step, step $i+1$, is at least three times the rotation in deformation step i .

5.3.5 THE ROTATION OF THE TENSILE FLANGE

The vertical deformations of the tips of the tensile flange as shown in Chapter 5.2.6 are also transformed in rotations. These rotations are of interest to verify conclusion 1d as given in Chapter 2.8. This conclusion states that the model by Basler completely neglects the influence of the rotational stiffness of the web to flange connections that affect the buckling length of the web.

Figure 5-77 and Figure 5-78 show the rotations of the tensile flange of test girder 9, 800x80, and 3, 400x80(2) respectively, see also Appendix O for the rotations of all test girders.

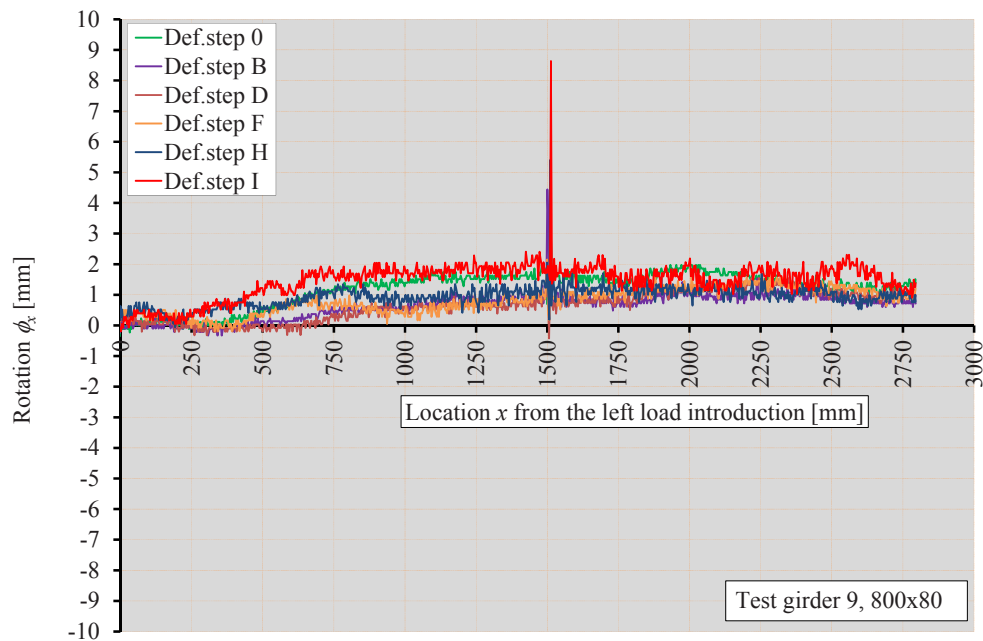


Figure 5-77 Rotation of the tensile flange of test girder 9, 800x80

The rotations of the tensile flanges of these test girders are rather small, less than 2° .

The test girders with a nominal flange width of 50 mm show more irregular rotations. For test girder 5, 600x50, Figure 5-79 shows these rotations of the tensile flange.

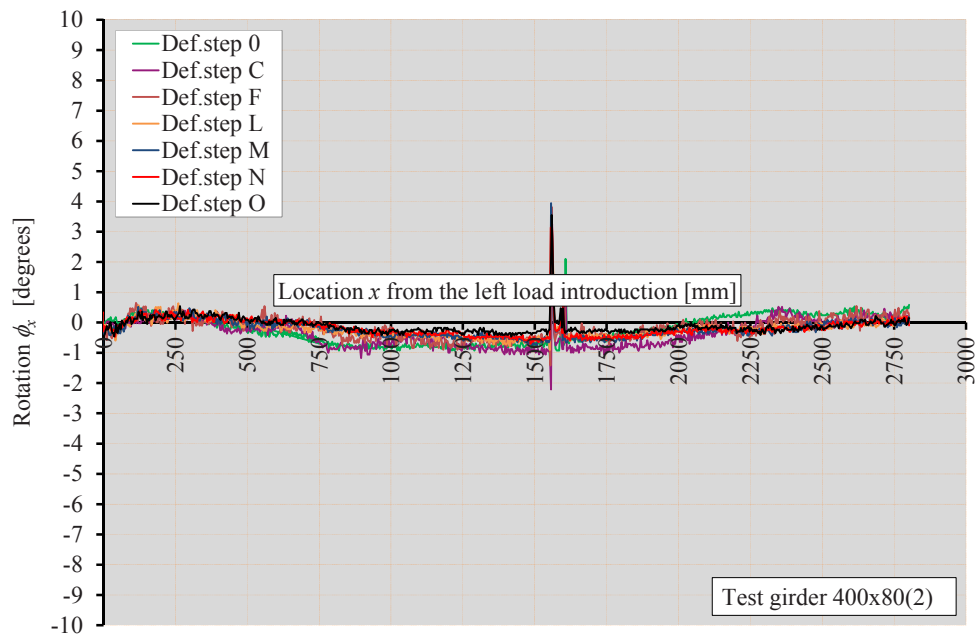


Figure 5-78 Rotation of the tensile flange of test girder 3, 400x80(2)

The rotation of the tensile flange of test girder 10, 800x100, differs from the rotations of the other test girders as well, see Figure 5-80. From the start of the experiment, the whole tensile flange in the test panel rotates in one direction. In deformation step N, the step after deformation step M in which the maximum force appears, the rotations change in sign, the web snaps through over the whole span of the test panel.

It is clear that the rotations of the tensile flange of all test girders are rather small as compared with the rotations of the compressive flange. It is concluded that these rotations of the compressive flanges are caused by the compressive stresses in the flange and not by the increasing buckling amplitudes of the web. Combining the information of the out-of-plane deflections and these rotations of the flanges, it can be concluded that conclusion 1d as presented in Chapter 2.8 is confirmed, implying that the rotational stiffness of the flanges will influence the buckling length of the web in vertical direction under vertical compression due to curvature of the test girder.

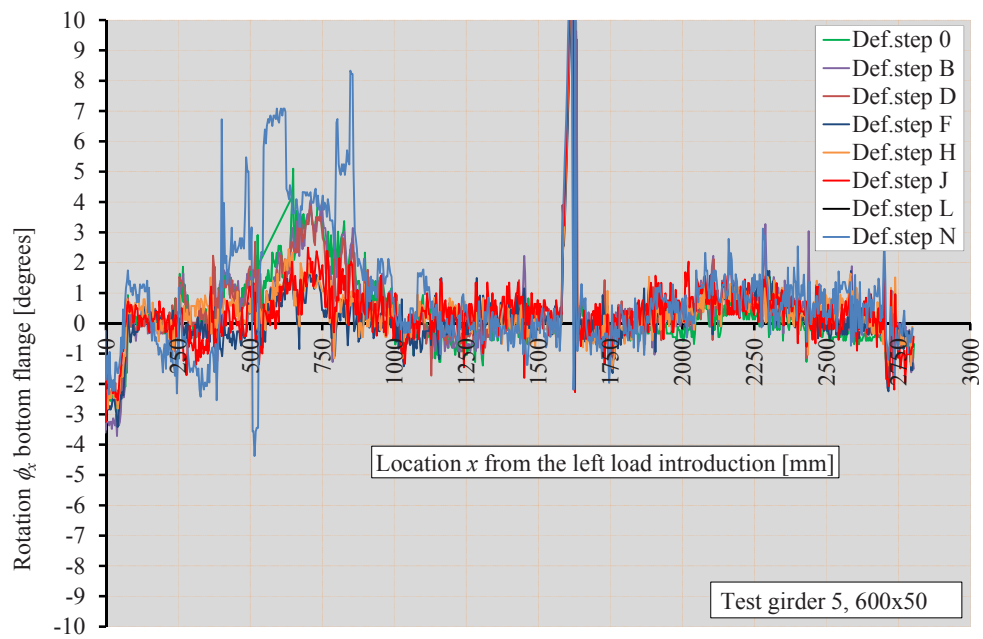


Figure 5-79 Rotation of the tensile flange of test girder 5, 600x50

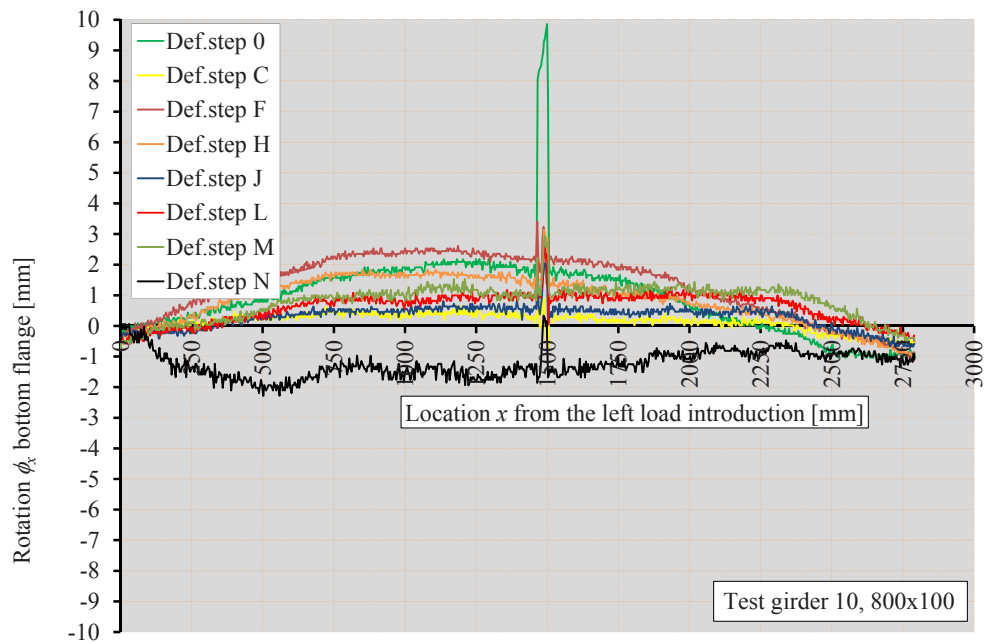


Figure 5-80 Rotation of the tensile flange of test girder 10, 800x100

5.3.6 THE STRAINS

5.3.6.1 Average strains in the cross-sections

Table 5-6 shows the actual yield strains ε_y of the flanges and the web of all test girders.

Table 5-6 Actual yield stress of flanges and web and the accompanying yield strains

Test speci- men	Top flange		Web		Bottom flange	
	f_y [MPa]	ε_y [10 ⁻⁶]	f_y [MPa]	ε_y [10 ⁻⁶]	f_y [MPa]	ε_y [10 ⁻⁶]
1, 400x50	335	1595	288	1371	319	1519
2, 400x80(1)	322	1533	284	1352	331	1576
3, 400x80(2)	316	1505	278	1324	315	1500
4, 400x100	343	1633	288	1371	342	1629
5, 600x50	328	1562	288	1371	309	1471
6, 600x80	329	1567	287	1367	314	1495
7, 600x100	341	1624	286	1362	344	1638
8, 800x50	326	1552	292	1390	310	1476
9, 800x80	320	1524	296	1410	317	1510
10, 800x100	339	1614	290	1381	350	1667

Figure 5-33 and Figure 5-34 and Figure 5-35 show the measured strains in the cross-section at mid-span of test girders 9, 800x80 and 3, 400x80(2), respectively, in each deformation step, see Appendix P for all test girders. Average strains are determined and presented in graphs. The average strains at a specific location of the web are determined by the average of the strains on the front side and on the back side of the web at that location.

The average of the flanges is determined in two different ways. Figure 5-81 shows four groups of strain gauges. Group A is formed by the measurements of strain gauges 1, 2 and 3 and Group B by the measurements of strain gauges 4 and 5 on the compressive flange. Group C is formed by the measurements of strain gauges 15 and 25 and group D by the measurements of strain gauges 26, 27 and 28. A weighted average strain in the compressive flange is determined by the average of the averages of Groups A and B and the average in the tensile flange is determined by the average of the averages of Groups C and D.

The second way to determine the average strain is the mathematical average of the 5 measured strains of groups A and B for the compressive flange and groups C and D for the tensile flange.

From the strains, as shown in these figures, but also from the figures for the remaining test girders as given in the Appendix I, it can be seen that the 5 measured strains of the compressive top flange vary very much, certainly when compared with the 5 strains of the tensile bottom flange. Because of

the four-point bending test it is expected that the bending moment in the test panel is constant and the strains and corresponding stresses should also be constant.

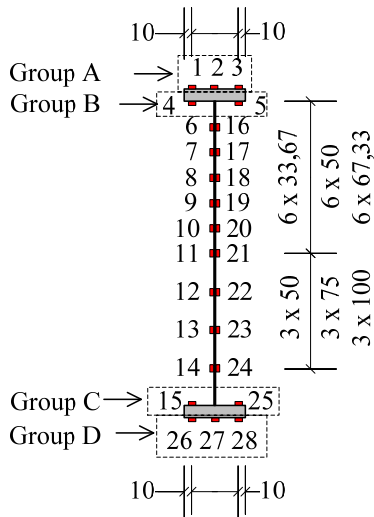
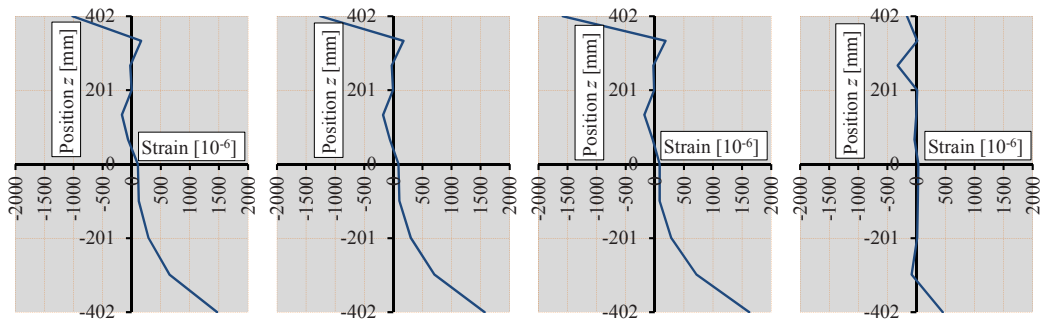


Figure 5-81 Group of strain gauges at the flanges of a test girder

From the figures it can be seen that the average strains in the flanges vary enormously. This is caused by the initial buckles in the compressive part of the web, but it is clear that the interaction between the compressive flange and the lateral supports influences these differences in strains as well. The compressive flange touches the lateral randomly supports, so once at the lateral support on the front side and once at the lateral support in the back side of the test girder. The friction is, because of the deformation driven test, in vertical direction, but also in longitudinal direction because of the offset of the spreader beam relative to the test girder.

Figure 5-82 shows the weighted average strains over the height of test girder 9, 800x80, for some of the deformation steps. From this figure and Figure 5-33, it can be seen that the tensile bottom flange yields in deformation step G, the strain $\varepsilon_{wa,bf} = 1570 \cdot 10^{-6}$ is larger than the yield strain $\varepsilon_{y,bf} = 1524 \cdot 10^{-6}$. The strain of the compressive top flange $\varepsilon_{wa,tf} = 1583 \cdot 10^{-6}$ is larger than the yield strain $\varepsilon_{y,tf} = 1510 \cdot 10^{-6}$ in deformation step H, the load step in which the maximum actuator force appears, so in this deformation step H both flanges yield. In the next deformation step the strain decreases enormously and the final collapse mode occurs.

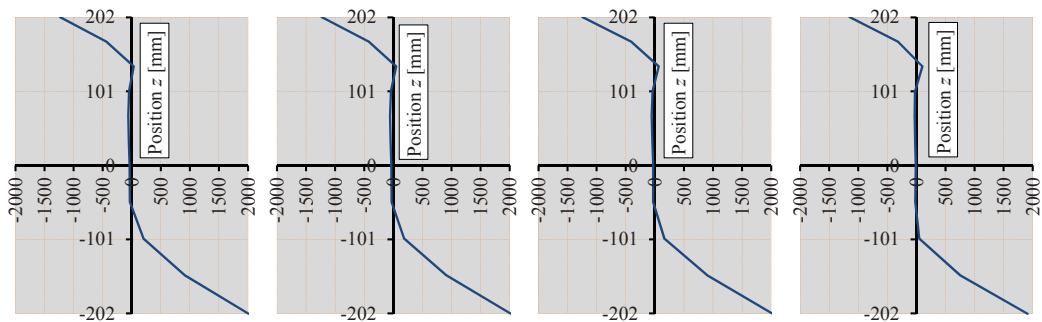


Deformation step F Deformation step G Deformation step H Deformation step I

Figure 5-82 Weighted average strains over the height of test girder 9, 800x80

Figure 5-83 presents the weighted average strains for test girder 3, 400x80(2). From this Figure and from Figure 5-34 and Figure 5-35 it can be seen that the weighted average strain of the tensile bottom flange is larger than the yield strain, $\varepsilon_{wa,bf} = 1568 \cdot 10^{-6} \geq \varepsilon_{y,bf} = 1500 \cdot 10^{-6}$ in deformation step G. The compressive top flange is not yielding in any of the deformation steps.

This is remarkable, because, based on the effective width method, it is expected that the neutral axis of the effective cross-section shifts to the tensile bottom flange and so the strains of this compressive top flange should be larger than the strains in the tensile bottom flange. Related to the measured strain at midspan, it can be seen that for example the weighted average strains in the tensile bottom flange in deformation step M are much larger than the weighted strains of the compressive top flange, $\varepsilon_{wa,bf} = 2007 \cdot 10^{-6} \geq \varepsilon_{wa,tf} = 1236 \cdot 10^{-6}$.



Deformation step M Deformation step N Deformation step O Deformation step P

Figure 5-83 Weighted average strains over the height of test girder 3, 400x80(2)

It is of interest to look at these strains in both flanges in more detail. From Figure 5-34 and Figure 5-35 it can be seen that the weighted average strains are similar up to deformation step E in the compressive flange. In deformation step E the central external strain is equal to $-1559 \cdot 10^{-6}$, while the strains in the tips of the compressive flange are much smaller, namely $-1008 \cdot 10^{-6}$ and $-879 \cdot 10^{-6}$ in the left-hand side tip of the flange and in the other tip the strains are $-842 \cdot 10^{-6}$ and $-1012 \cdot 10^{-6}$. The central external strain increases in the next deformation steps up to $-3179 \cdot 10^{-6}$ in deformation step L, while the strains in the tips hardly change in the next deformation steps. In deformation step O, this central external strain changes in sign and does not change in the next deformation steps and the strain gauge fails.

5.3.6.2 Average strain per deformation step

For each test girder Table 5-7 up to Table 5-16 show the average strains in the compressive top flange and in the tensile bottom flange in each deformation step.

In these tables can be find:

- ε_{wa} weighted average strain, the average of the average strains on the external and internal sides of the flange
- ε_{awa} adapted average strain, equal to average strains, but clearly incorrect strains are ignored
- ε_a average strain of the five strain gauges
- ε_{aa} adapted average strain, clearly incorrect strains are ignored

Table 5-7 Average strains of the top and bottom flange of experiment 9, 800x80

Def. step	Top flange				Bottom flange			
	ε_{wa} [x10 ⁻⁶]	ε_{awa} [x10 ⁻⁶]	ε_a [x10 ⁻⁶]	ε_{aa} [x10 ⁻⁶]	ε_{wa} [x10 ⁻⁶]	ε_{awa} [x10 ⁻⁶]	ε_a [x10 ⁻⁶]	ε_{aa} [x10 ⁻⁶]
A 36.3 kN		-305		-305	+322		+325	
B 80.7 kN		-691		-691		+833		+833
C 101.6 kN		-867		-867		+1018		+1018
D 120.6 kN		-960		-960		+1201		+1201
E 134.2 kN		-1035		-1035		+1366		+1366
F 142.8 kN		-1018		-1018		+1468		+1468
G 150.8 kN		-1254		-1254		<u>+1570</u>		<u>+1570</u>
H 153.7 kN		<u>-1583</u>		<u>-1583</u>		<u>+1623</u>		<u>+1623</u>
I 4.7 kN		-167		-167		+453		+453

Based on the strains as presented in Table 5-7, it can be seen that the maximum sum of the reaction forces occurs after continuing the experiment after deformation step G. The bottom flange yields in

deformation step G, while the top flange does not yield in load G. This looks rather strange, because it is expected, due to of the very slender web, that the effective width describes the behaviour of the test girder best. Based on the effective width theory, the neutral axis shifts in the direction of the bottom flange and so the stresses in the top flange should be larger than the stresses in the bottom flange. The difference in yield strength of the top and bottom flange is rather small and does not justify the yielding of the bottom flange before the yielding of the top flange.

Table 5-8 presents the average strains in the top and bottom flange of experiment 3, 400x80(2). The table shows that the tensile bottom flange yields much quicker than the compressive top flange, but both flanges yield before the maximum load occurs. In the next deformation step, the forces decrease, but the strains increase.

Table 5-8 Average strains of the top and bottom flange of experiment 3, 400x80(2)

Def. step	Top flange				Bottom flange			
	ϵ_{wa}	ϵ_{awa}	ϵ_a	ϵ_{aa}	ϵ_{wa}	ϵ_{awa}	ϵ_a	ϵ_{aa}
	[x10 ⁻⁶]	[x10 ⁻⁶]	[x10 ⁻⁶]	[x10 ⁻⁶]	[x10 ⁻⁶]	[x10 ⁻⁶]	[x10 ⁻⁶]	[x10 ⁻⁶]
A 14.5 kN	-219		-220		+229		+229	
B 29.4 kN	-490		-493		+655		+637	
C 42.6 kN	-740		-746		+983		+968	
D 55.4 kN	-984		-991		+1289		+1276	
E 61.1 kN	-1090		-1090		+1458		+1440	
F 65.3 kN	-1041		-1060		<u>+1568</u>		<u>+1550</u>	
G 68.6 kN	-1103		-1133		<u>+1642</u>		<u>+1626</u>	
H 71.5 kN	-1065		-1097		<u>+1715</u>		<u>+1700</u>	
I 74.0 kN	-1087		-1136		<u>+1780</u>		<u>+1765</u>	
J 77.2 kN	-1135		-1188		<u>+1856</u>		<u>+1841</u>	
K 79.5 kN	-1215		-1278		<u>+1930</u>		<u>+1915</u>	
L 81.1 kN	-1231		-1297		<u>+1991</u>		<u>+1975</u>	
M 82.2 kN	-1236		-1299		<u>+2023</u>		<u>+2007</u>	
N 82.7 kN	-1232		-1292		<u>+2036</u>		<u>+2021</u>	
O 82.8 kN	-1245		-1296		<u>+2041</u>		<u>+2026</u>	
P 75.0 kN	-1149		-1159		<u>+1927</u>		<u>+1911</u>	

From the beginning of the test, it can be seen that the strains over the height of the test girders are rather irregular and far from linear over the height of the cross-section. It can also be seen that the strains in the web are the most fanciful, caused by the buckling pattern of this web, the initial imperfections. The strains in the compressive top flange vary strongly, much more than the strains in the bottom flange.

For an example, this latter average is determined for the bottom flange for the deformation step of test girder 9, 800x80. On the external side of the bottom flange, the strains for deformation step A are: +274, +346 and +394·10⁻⁶ and the strains are +273 and +339·10⁻⁶ on the internal side. The average strain in the centre of the flange ε_{wa} is determined by the average strain on the external side and the average of the internal side of the flange. The weighted average strain ε_{as} is determined as follows:

$$\varepsilon_{as} = \frac{\frac{+274 + 346 + 394}{3} + \frac{273 + 339}{2}}{2} \cdot 10^{-6} = \frac{338.0 + 306.0}{2} \cdot 10^{-6} = 322 \cdot 10^{-6} \quad (5.28)$$

This weighted average strain differs from the average strain ε_a , the average of the five strains measured at each flange. The average strain ε_a is determined as follows:

$$\varepsilon_{wa} = \frac{+274 + 346 + 394 + 273 + 339}{5} \cdot 10^{-6} = 325.2 \cdot 10^{-6} \quad (5.29)$$

It is shown that both averages of the strains are close to each other. The method to determine the average strain is not relevant, but when there are big differences in measurements, both averages differ much more.

When one or more of the measured strains are not correct because they are incorrectly glued to the flange or the strain is out of the range of the strain gauges, the average strains are based only on correct measurements.

Table 5-9 Average strains of the top and bottom flange of test girder 1, 400x50

Def. step	Top flange				Bottom flange			
	ϵ_{wa}	ϵ_{awa}	ϵ_a	ϵ_{aa}	ϵ_{wa}	ϵ_{awa}	ϵ_a	ϵ_{aa}
	[x10 ⁻⁶]	[x10 ⁻⁶]	[x10 ⁻⁶]	[x10 ⁻⁶]	[x10 ⁻⁶]	[x10 ⁻⁶]	[x10 ⁻⁶]	[x10 ⁻⁶]
A 0.9 kN	-21		-21		+24		+24	
B 0.0 kN	-2		-2		-1		-1	
C 0.9 kN	-21		-21		+22		+22	
D 1.9 kN	-45		-46		+49		+49	
E 2.7 kN	-64		-66		+70		+70	
F 3.7 kN	-87		-90		+96		+96	
G 4.7 kN	-110		-114		+124		+124	
H 5.7 kN	-132		-138		+153		+153	
I 7.6 kN	-177		-185		+208		+208	
J 9.5 kN	-216		-228		+274		+274	
K 18.9 kN	-458		-487		+604		+602	
L 28.4 kN	-730		-775		+933		+932	
M 36.0 kN	-977		-1032		+1203		+1202	
N 41.0 kN	-1112		-1175		+1393		+1381	
O 42.7 kN		-1481		-1076	<u>+1541</u>		<u>+1542</u>	
P 43.5 kN		-1545		-1126	<u>+1597</u>		<u>+1602</u>	
Q 43.7 kN		<u>-1626</u>		-1185	<u>+1608</u>		<u>+1614</u>	
R		<u>-1734</u>		-1254	<u>+1619</u>		<u>+1625</u>	
U		<u>-1960</u>		-1445	<u>+1712</u>		<u>+1718</u>	
V		<u>-1634</u>		-1186	+1509		+1515	
W		<u>-1683</u>		-1218	<u>+1575</u>		<u>+1580</u>	
X		<u>-1783</u>		-1250	<u>+1631</u>		<u>+1638</u>	
Y		<u>-1812</u>		-1313	<u>+1653</u>		<u>+1660</u>	
Z		<u>-1866</u>		-1352	<u>+1660</u>		<u>+1666</u>	
AA 49.41		<u>-1913</u>		-1390	<u>+1655</u>		<u>+1661</u>	
AB 49.61		<u>-1944</u>		-1407	<u>+1652</u>		<u>+1657</u>	
AC 49.61		<u>-1961</u>		-1421	<u>+1648</u>		<u>+1654</u>	
AD 49.61		<u>-1976</u>		-1432	<u>+1641</u>		<u>+1647</u>	
AE 49.02		<u>-2000</u>		-1448	<u>+1629</u>		<u>+1634</u>	
AF 48.44		<u>-2018</u>		-1469	<u>+1675</u>		<u>+1680</u>	
AG 8.79		-237		-237	+519		+524	

Table 5-10 Average strains of the top and bottom flange of experiment 2, 400x80(1)

Def. step		Top flange				Bottom flange			
		ε_{wa}	ε_{awa}	ε_a	ε_{aa}	ε_{wa}	ε_{awa}	ε_a	ε_{aa}
		[x10 ⁻⁶]	[x10 ⁻⁶]	[x10 ⁻⁶]	[x10 ⁻⁶]	[x10 ⁻⁶]	[x10 ⁻⁶]	[x10 ⁻⁶]	[x10 ⁻⁶]
A	9.0 kN	-137		-			+167		+169
B	23.5 kN	-375		-386			+452		+454
C	36.3 kN	-636		-653			+768		+773
D	49.0 kN	-913		-929			+1065		+1072
E	54.5 kN		-1183		-1183		+1196		+1204
F	59.9 kN		-1359		-1359		+1325		+1333
G	63.7 kN		-1477		-1477		+1439		+1450
H	66.4 kN		<u>-1585</u>		<u>-1585</u>		+1525		+1540
I	69.1 kN		<u>-1660</u>		<u>-1660</u>		<u>+1609</u>		<u>+1628</u>
J	70.9 kN		<u>-1785</u>		<u>-1785</u>		<u>+1702</u>		<u>+1723</u>
K	71.8 kN		<u>-1854</u>		<u>-1854</u>		<u>+1764</u>		<u>+1789</u>
L	71.4 kN		<u>-1763</u>		<u>-1763</u>		<u>+1624</u>		<u>+1644</u>
M			-760		-760		+311		+327

Table 5-11 Average strains of the top and bottom flange of experiment 4, 400x100

Def. step		Top flange				Bottom flange			
		ε_{wa}	ε_{awa}	ε_a	ε_{aa}	ε_{wa}	ε_{awa}	ε_a	ε_{aa}
		[x10 ⁻⁶]	[x10 ⁻⁶]	[x10 ⁻⁶]	[x10 ⁻⁶]	[x10 ⁻⁶]	[x10 ⁻⁶]	[x10 ⁻⁶]	[x10 ⁻⁶]
A	10.8 kN	-199		-200		+234		+237	
B	23.8 kN	-456		-457		+517		+515	
C	35.8 kN	-693		-695		+876		+864	
D	47.8 kN	-731		-748		+1313		+1280	
E	53.8 kN	-730		-759		+1543		+1497	
F	59.0 kN	-834		-868		<u>+1713</u>		<u>+1776</u>	
G	63.2 kN	-1031		-1044		<u>+1821</u>		<u>+1882</u>	
H	66.8 kN	-1123		-1134		<u>+1895</u>		<u>+1950</u>	
I	69.5 kN	-1206		-1217		<u>+1957</u>		<u>+2008</u>	
J	71.9 kN	-1495		-1461		<u>+2025</u>		<u>+2076</u>	
K	73.8 kN	-1577		-1537		<u>+2071</u>		<u>+2119</u>	
L	76.0 kN	-1556		-1534		<u>+2119</u>		<u>+2166</u>	
M	77.6 kN	-1582		-1570		<u>+2154</u>		<u>+2199</u>	
N	0.9	-487		-388		+657		+697	

Table 5-12 Average strains of the top and bottom flange of experiment 5, 600x50

Def. step		Top flange				Bottom flange			
		ε_{wa}	ε_{awa}	ε_a	ε_{aa}	ε_{wa}	ε_{awa}	ε_a	ε_{aa}
		[x10 ⁻⁶]	[x10 ⁻⁶]	[x10 ⁻⁶]	[x10 ⁻⁶]	[x10 ⁻⁶]	[x10 ⁻⁶]	[x10 ⁻⁶]	[x10 ⁻⁶]
A	3.7 kN	-74		-75		+79		+78	
B	7.5 kN	-153		-155		+160		+159	
C	11.2 kN	-231		-234		+239		+237	
D	15.2 kN	-316		-319		+322		+319	
E	35.2 kN	-758		-765		+722		+715	
F	52.2 kN	-1098		-1116		+1215		+1206	
G	58.2 kN	-1213		-1239		<u>+1501</u>		<u>+1506</u>	
H	62.7 kN	-1303		-1336		<u>+1668</u>		<u>+1678</u>	
I	59.6 kN	-1216		-1250		<u>+1650</u>		<u>+1655</u>	
J	61.8 kN	-1251		-1288		<u>+1689</u>		<u>+1704</u>	
K	63.0 kN	-1264		-1302		<u>+1715</u>		<u>+1729</u>	
L	65.6 kN	-1308		-1348		<u>+1768</u>		<u>+1783</u>	
M	70.1 kN	-1333		-1373		<u>+1807</u>		<u>+1823</u>	
N	67.0 kN	-1328		-1368		<u>+1815</u>		<u>+1832</u>	

Table 5-13 Average strains of the top and bottom flange of experiment 6, 600x80

Def. step		Top flange				Bottom flange			
		ε_{wa}	ε_{awa}	ε_a	ε_{aa}	ε_{wa}	ε_{awa}	ε_a	ε_{aa}
		[x10 ⁻⁶]	[x10 ⁻⁶]	[x10 ⁻⁶]	[x10 ⁻⁶]	[x10 ⁻⁶]	[x10 ⁻⁶]	[x10 ⁻⁶]	[x10 ⁻⁶]
A	8.8 kN	-75		-78		+96		+95	
B	38.6 kN	-442		-442		+449		+446	
C	67.2 kN	-760		-764		+1211		+1272	
D	81.4 kN	-934		-937		+1457		<u>+1524</u>	
E	92.9 kN	-1031		-1040			+1326		+1326
F	102.5 kN		-1078		-1117		<u>+1497</u>		<u>+1497</u>
G	109.1 kN		-1121		-1178		<u>+1620</u>		<u>+1620</u>
H	114.0 kN		<u>-1572</u>		-1464		<u>+1724</u>		<u>+1724</u>
I	119.0 kN		<u>-2156</u>		<u>-1812</u>		<u>+1831</u>		<u>+1831</u>
J	111.4 kN		<u>-1756</u>		<u>-1604</u>		<u>+1761</u>		<u>+1761</u>

Table 5-14 Average strains of the top and bottom flange of experiment 7, 600x100

Def. step	Top flange				Bottom flange			
	ε_{wa}	ε_{awa}	ε_a	ε_{aa}	ε_{wa}	ε_{awa}	ε_a	ε_{aa}
	[x10 ⁻⁶]	[x10 ⁻⁶]	[x10 ⁻⁶]	[x10 ⁻⁶]	[x10 ⁻⁶]	[x10 ⁻⁶]	[x10 ⁻⁶]	[x10 ⁻⁶]
A 30.5 kN		-363		-362	+359		+361	
B 60.3 kN		-714		-717	+760		+762	
C 86.4 kN		-1016		-1038	+1180		+1185	
D 97.8 kN		-1040		-1119	+1332		+1333	
E 106.3 kN		-1150		-1271	+1458		+1456	
F 111.3 kN		-1205		-1375	+1539		+1536	
G 116.4 kN		-1312		-1505	+1636		+1633	
H 120.8 kN		-1370		-1583	<u>+1735</u>		<u>+1734</u>	
I 24.3 kN		-232		-411	+631		+625	

Table 5-15 Average strains of the top and bottom flange of experiment 8, 800x50

Def. step	Top flange				Bottom flange			
	ε_{wa}	ε_{awa}	ε_a	ε_{aa}	ε_{wa}	ε_{awa}	ε_a	ε_{aa}
	[x10 ⁻⁶]	[x10 ⁻⁶]	[x10 ⁻⁶]	[x10 ⁻⁶]	[x10 ⁻⁶]	[x10 ⁻⁶]	[x10 ⁻⁶]	[x10 ⁻⁶]
A 5.7 kN	-75		-76		+90		+91	
B 18.7 kN	-285		-289		+299		+300	
C 33.3 kN	-535		-543		+561		+568	
D 47.5 kN	-782		-793		+874		+875	
E 61.2 kN	-1020		-1032		+1209		+1208	
F 73.4 kN	-1236		-1250		<u>+1559</u>		<u>+1563</u>	
G 82.3 kN	-1396		-1417		<u>+1833</u>		<u>+1845</u>	
H 87.0 kN	-1480		-1503		<u>+1987</u>		<u>+2001</u>	
I 87.4 kN	-1527		<u>-1554</u>		<u>+2022</u>		<u>+2035</u>	
J 91.7 kN	<u>-1629</u>		<u>-1656</u>		<u>+2068</u>		<u>+2081</u>	
K 89.8 kN	<u>-1561</u>		<u>-1589</u>		<u>+1974</u>		<u>+1987</u>	
L 84.8 kN	-1201		-1226		<u>+1634</u>		<u>+1645</u>	

Table 5-16 Average strains of the top and bottom flange of test girder 10, 800x100

Def. step	Top flange				Bottom flange			
	ε_{wa}	ε_{awa}	ε_a	ε_{aa}	ε_{wa}	ε_{awa}	ε_a	ε_{aa}
	[x10 ⁻⁶]	[x10 ⁻⁶]	[x10 ⁻⁶]	[x10 ⁻⁶]	[x10 ⁻⁶]	[x10 ⁻⁶]	[x10 ⁻⁶]	[x10 ⁻⁶]
A 35.2 kN	-317		-319		+328		+330	
B 77.5 kN	-695		-700		+697		+690	
C 97.7 kN	-900		-907		+863		+848	
D 116.9 kN	-935		-960		+1033		+1011	
E 131.1 kN	-1042		-1073		+1167		+1139	
H	-341		-342		+298		+299	
I	-781		-784		+657		+660	
J	-1228		-1234		+1008		+1012	
K	-1536		-1537		+1150		+1151	
L	<u>-1997</u>		<u>-2001</u>		+1251		+1247	
M	<u>-2448</u>		<u>-2429</u>		+1339		+1332	
N	-1438		-1396		+195		+195	

Table 5-17 shows an overview of the deformation steps in which the compressive top flange and the tensile bottom flange are yielding, based on the weighted average strains.

Table 5-17 Overview of yielding in the flanges in all test girders

Test girder	Top flange	Bottom flange	Maximum
1, 400x50	Def. step O	Def. step O	AC
2, 400x80(1)	Def. step H	Def. step J	K
3, 400x80(2)		Def. step F	O
4, 400x100	-1583<-1633	Def. step F	M
5, 600x50	-1333<-1562	Def. step G	N
6, 600x80	Def. step H	Def. step F	I
7, 600x100	-1583<1624	Def. step H	H
8, 800x50	Def. step I	Def. step F	J
9, 800x80	Def. step H	Def. step G	H
10, 800x100	Def. step L		M

From the tables, the following can be seen:

1. Both flanges are yielding in test girder 1, 400x50, 2, 400x80(1), 6, 600x50, 8, 800x50, and 9, 800x80;
2. The top flange yields before the bottom flange in two test girders, namely in girder 2, 400x80(1) and in girder 10, 800x100;
3. In test girder 10, 800x100, only the top flange yields;

4. The top flanges of test girders 3, 400x80(2), 4, 400x100, 5, 600x50, and 7, 600x100, do not yield at all.

5.4 OVERVIEW OF THE LOCATION OF THE FINAL COLLAPSE MODE

The final collapse mode occurs at a location of 74", corresponding with 1880 mm, from the left-hand side load introduction, see Figure 5-84.

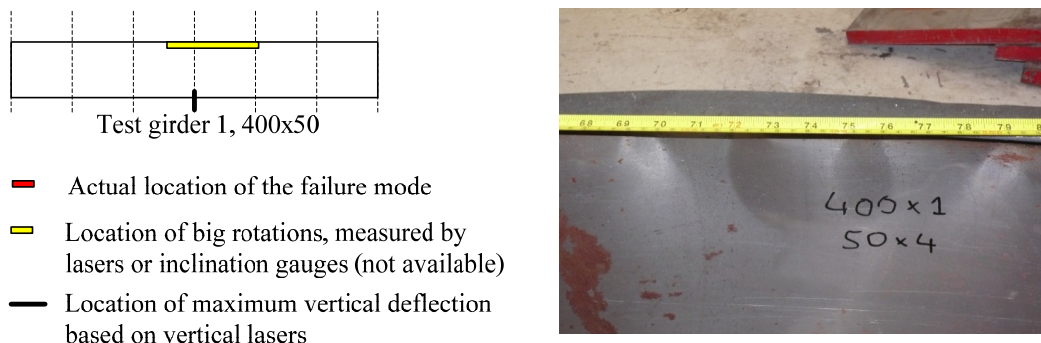


Figure 5-84 Location of final failure mode of test girder 1, 400x50

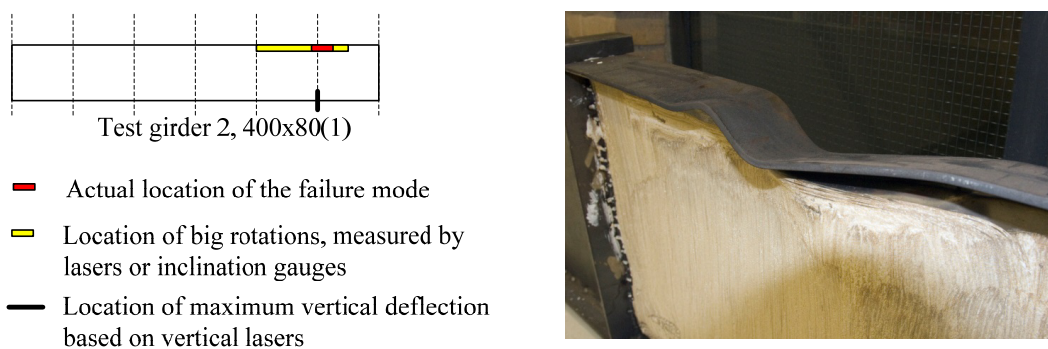


Figure 5-85 Location of the final failure mode of test girder 2, 400x80(1)

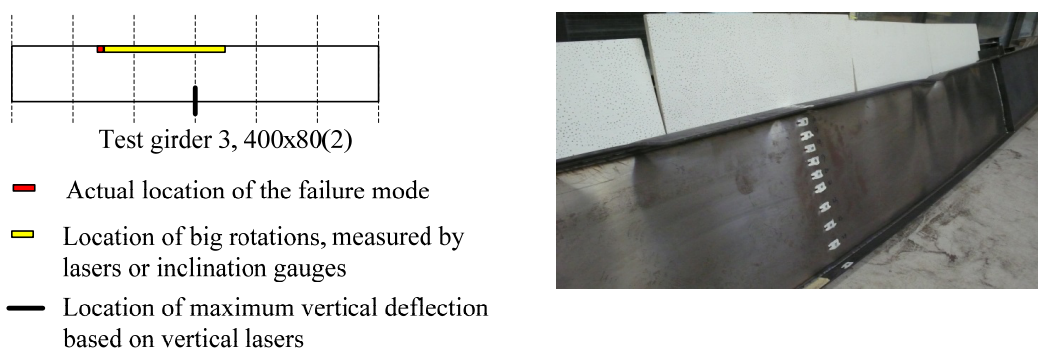


Figure 5-86 Location of the final failure mode of test girder 3, 400x80(2)

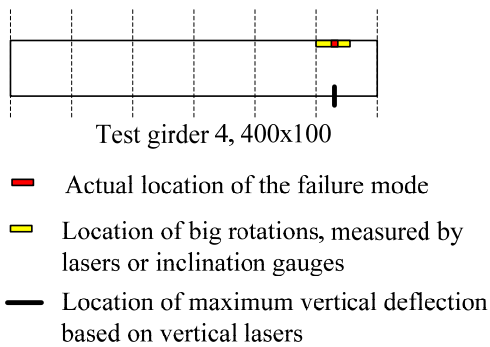


Figure 5-87 Location of the final failure mode of test girder 4, 400x100

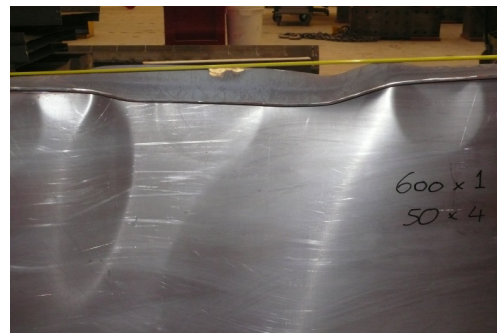
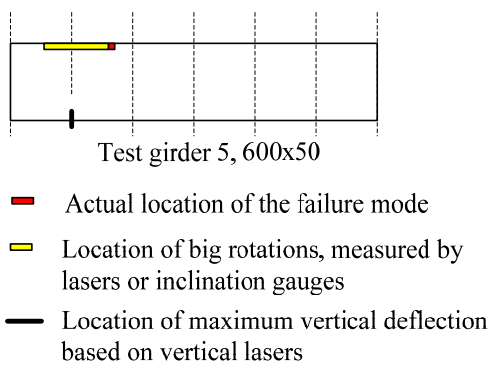


Figure 5-88 Location of the final failure mode of test girder 5, 600x50

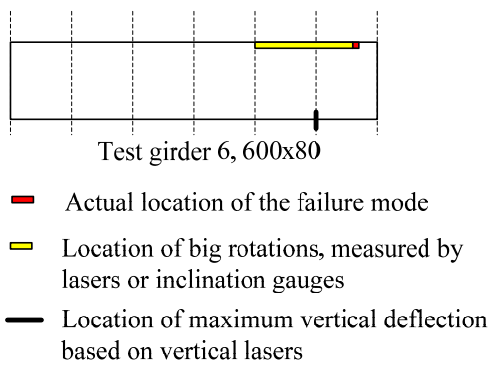
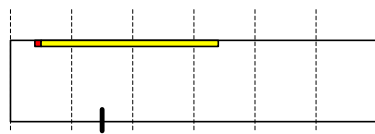


Figure 5-89 Location of the final failure mode of test girder 6, 600x80

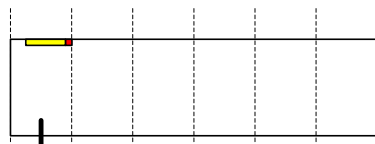


Test girder 7, 600x100

- █ Actual location of the failure mode
- █ Location of big rotations, measured by lasers or inclination gauges
- Location of maximum vertical deflection based on vertical lasers



Figure 5-90 Location of the final failure mode of test girder 7, 600x100

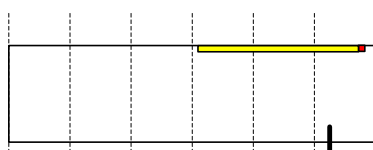


Test girder 8, 800x50

- █ Actual location of the failure mode
- █ Location of big rotations, measured by lasers or inclination gauges
- Location of maximum vertical deflection based on vertical lasers



Figure 5-91 Location of the final failure mode of test girder 8, 800x50

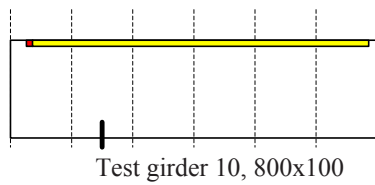


Test girder 9, 800x80

- █ Actual location of the failure mode
- █ Location of big rotations, measured by lasers or inclination gauges
- Location of maximum vertical deflection based on vertical lasers



Figure 5-92 Location of the final failure mode of test girder 9, 800x80



- Actual location of the failure mode
- Location of big rotations, measured by lasers or inclination gauges
- Location of maximum vertical deflection based on vertical lasers



Figure 5-93 Location of the final failure mode of test girder 10, 800x100

5.5 THE BENDING MOMENT RESISTANCE OF THE TEST GIRDERS

The bending moment resistance will be determined by the reaction force at the support that is the closest to the final “plastic hinge” in the final collapse mode of the test girder and the nearby load introduction. Any friction between this reaction force and the nearby load introduction is completely ignored and safesided. Table 5-18 presents the bending moment resistance of the test girders

Table 5-18 Bending moment resistances M_{test} of the test girders

Test specimen	$R_{L,max}$ [kN]	$R_{R,max}$ [kN]	$F_{act,max}$ [kN]	M_{test} [kNm]
1, 400x50	<u>20.89</u>	22.57	47.66	31.34
2, 400x80(1)	36.66	<u>34.69</u>	82.47	52.10
3, 400x80(2)	<u>39.24</u>	43.59	88.57	58.7
4, 400x100	37.96	<u>39.63</u>	84.13	59.30
5, 600x50	<u>32.02</u>	34.87	71.29	48.03
6, 600x80	57.45	<u>61.57</u>	125.39	90.17
7, 600x100	<u>59.25</u>	61.57	122.46	88.88
8, 800x50	41.61	<u>45.31</u>	90.63	67.97
9, 800x80	74.23	<u>79.05</u>	155.27	118.58
10, 800x100	<u>74.40</u>	78.36	154.10	111.60

5.6 CONCLUSIONS

From the experiments, the following is concluded:

1. The initial imperfections of all experiments are relatively large in relation to the web thickness, in some cases by far exceeding $\delta_0 \gg 2 \cdot t_w$;

2. The vertical deformation of the test girder is symmetric at least up to the deformation step in which the maximum load and maximum reaction forces appear;
3. A sudden increase of the rotation of the compressive flange occurs in a deformation step after the deformation step in which the maximum load and reaction forces appear;
4. The bending moment resistances M_u of the test girders were not determined by vertical buckling of the compressive flange into the web, although the web slenderness's β_w was larger than the maximum web slenderness $\beta_{w,max}$ according to Basler;
5. In 9 out of 10 tests vertical buckling of the compressive flange into the web appeared, but after the top of the $P-\delta$ diagram, so in the descending part of this diagram. Vertical buckling of the compressive flange into the web always occurred after strong rotation of the compressive flange. The vertical deformations of the girder at the location where the load was introduced, were no longer symmetric in these final deformation steps of the tests;
6. The rotation of the compressive flange over a large length appeared only in 1 out of 10 tests girders. The vertical deformations of the girder at the location where the load was introduced remained symmetric. Vertical buckling of the compressive flange into the web did not appear at all;
7. For experiments 1, 400x50, 2, 400x80(1), 3, 400x80(2), 4, 400x100, 6, 600x80 and 8, 800x50 both flanges yield before the maximum load is reached and in these situations the bottom flange yields first, except for experiment 1, 400x50. Here both flanges yield in the same deformation step;
8. For experiments 5, 600x50, 7, 600x100 and 9, 800x80 the bottom flange yields before the maximum load is reached;

6 VALIDATION OF THE FEM-MODEL ON THE DELFT EXPERIMENTS

6.1 GENERAL

This chapter describes the validation of the FEM-models used to simulate the Delft experiments by comparing the FEM-results with the test results. These FEM-models are similar to the FEM-models used to simulate the Basler test girders G4-T1 and G4-T2, as described in Chapter 3, but a few adaptations are made, namely the number of elements, the dimensions of all FEM-elements in the flanges or the web are the same and the flanges are connected asymmetric to the web. Chapter 6.2 shows the input for the FEM-models such as geometry, materials, geometrical and physical imperfections and the mesh sizes used for the flanges, the web and the stiffeners. Chapter 6.3 presents the calculation of the theoretical bending moment resistances, such as the elastic and plastic bending moment resistance, but also the effective bending moment resistance and the resistance of the section existing of the flanges only. Also, the calculation of the stiffness of the girders based on the gross cross-section and based on the effective cross-section are presented. Chapter 6.4 shows the validation of the FEM-model of the relatively rigid test girder 9, 800x80, and the relatively flexible test girder 3, 400x80(2), and also gives an overview of the validation of the results of the FEM-models on the results of the test girders, see also Appendix Q. This chapter is finalised with the conclusions presented in Chapter 6.5.

6.2 MODELLING OF THE DELFT EXPERIMENTS

6.2.1 GEOMETRY OF THE FEM-MODELS

The dimensions of the FEM-models are based on the average actual dimensions, measured in five cross-sections of the test girder. Figure 6-1 shows the symbols used for the dimensions of the test girders. Table 6-1 presents the average dimensions of every test girder and is the same as Table 4-2.

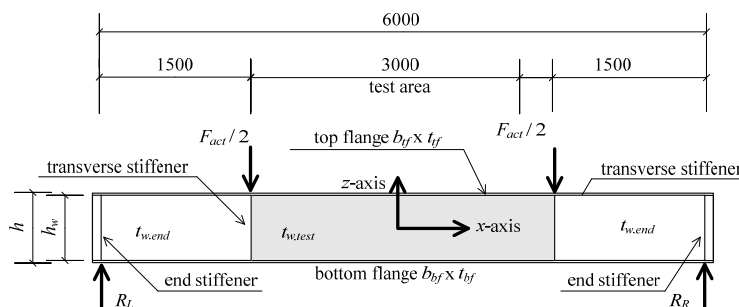


Figure 6-1 Geometry of test specimens

Table 6-1 Actual average dimensions of test girders, web slenderness and ratio of area

Test girder	h_w [mm]	$t_{w,tp}$ [mm]	$t_{w,ep}$ [mm]	b_{tf} [mm]	t_{tf} [mm]	b_{bf} [mm]	t_{bf} [mm]	β_w [-]	$\beta_{w,max}$ [-]	ρ [-]
1, 400x50	400.0	1.01	3.99	49.7	4.36	49.8	4.33	396.1	471.2	1.87
2, 400x80(1)	399.3	1.00	4.00	80.0	5.40	80.0	5.29	399.3	344.7	0.92
3, 400x80(2)	399.8	1.02	4.07	80.1	5.57	79.8	5.53	392.0	349.6	0.91
4, 400x100	400.1	0.93	4.05	98.7	4.29	98.9	4.37	430.2	315.7	0.88
5, 600x50	601.6	1.02	3.99	49.6	4.48	49.9	4.47	589.8	585.0	2.76
6, 600x80	600.2	0.97	4.01	79.9	5.53	79.9	5.66	618.7	403.1	1.32
7, 600x100	600.1	0.97	4.00	99.1	4.31	98.7	4.33	618.7	395.5	1.36
8, 800x50	801.0	0.97	3.98	50.2	4.40	49.5	4.37	825.8	664.2	3.51
9, 800x80	799.4	0.98	4.01	80.2	5.60	80.1	5.60	815.7	476.8	1.75
10, 800x100	799.4	1.00	3.99	98.8	4.24	98.7	4.24	799.4	470.7	1.91

The FEM-model is built up with four nodes shell elements with six degrees of freedom per node, three translations and three rotations, which are accurate to simulate plate girders with a very slender web subjected to large deflections. Although it is already proven that the number of elements used to simulate the Basler test specimen G4 is sufficient, the number of elements is increased for the Delft experiments. The main reason to increase the number of elements and nodes of the FEM-models for the Delft experiments is the more accurate way of measuring of the initial out-of-plane deflections by lasers.

The numbers of the FEM-elements for the flanges and the web of the test girders are:

- 100 elements for the web as well as the flanges over a length of 1500 mm of the end panels;
- 200 elements for the web as well as the flanges over a length of 3000 mm of the test panel;
- 6 elements for the web as well as the flanges over a length of 90 mm of the over lengths at each edge of the girder;
- 30 elements over the height of the web, regardless it's height;
- 10 elements over the width of the flanges, regardless it's width. This is a reduction compared with the number of elements in the flange of the Basler test girder G4 to improve the aspect ratio of the FEM-elements;
- 30 elements over the height of the transverse stiffeners at the supports, regardless the height of the web;
- 30 elements over the height of the transverse stiffeners at the load introductions, regardless the height of the web.

The largest aspect ratio for the flange is found for the smallest flange with a nominal width of 50

mm, $\frac{3000/200}{50/10} = 3$. The largest aspect ratio for the web is found for the highest web,

$\frac{800/30}{3000/200} = 1.78$. The aspect ratios for the web of the test panel and the compressive flange are

smaller or equal to 3, as preferred, and for the other parts they are smaller than 10, as recommended.

6.2.2 MATERIAL PROPERTIES USED IN THE FEM-MODELS

6.2.2.1 Yield stresses

Table 6-2, which is equal to Table 4-3, shows the actual yield stresses f_y of the material used for the web plates and both flanges in the test girders.

Table 6-2 Actual yield strengths of the elements of test specimens in [MPa]

Test girder	1, 400x50	2, 400x80(1)	3, 400x80(2)	4, 400x100	5, 600x50	6, 600x80	7, 600x100	8, 800x50	9, 800x80	10, 800x100
Top flange	335	322	316	343	328	329	341	326	320	339
Bottom flange	319	331	315	342	309	314	344	310	317	350
Web test panel	288	284	278	288	288	287	286	292	296	290

6.2.2.2 Strain hardening

From the FEM-results of the Basler test specimen G4 and from the Delft experiments it can be seen that the strains are just a little more than the yield strain ε_y and so it is decided to determine the yield stress and the ultimate stress from the tensile tests, as described in Chapter 4.2.2, and to use a bilinear diagram for the material properties.

For the Large Deflections Method, the strain-hardening is according to the Adapted Lagrange formula, so using the Cauchy stress tensor and a logarithmic strain tensor. This means that the input for the strain-hardening is a natural logarithm as described in Chapter 3.2.2.2 applied only to the yield plateau.

6.2.3 IMPERFECTIONS USED IN THE FEM-MODEL

6.2.3.1 Initial geometrical imperfections

The initial geometrical imperfections of the webs of the test panels of the Delft experiments, measured by lasers, are used as input for the FEM-model. The measurements by the horizontal lasers are described in Chapter 4.4.2 and the results are shown in Chapter 5.2.3. Figure 6-2 shows the initial out-of-plane deflections for test girder 9, 800x80, repeated from Figure 5-8.

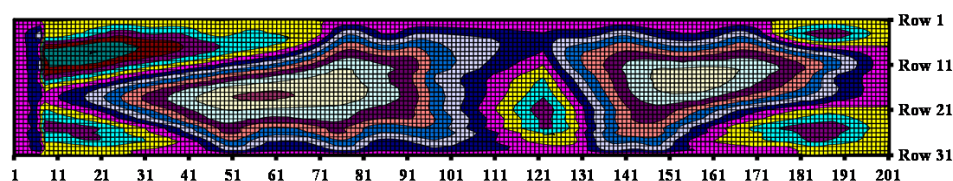


Figure 6-2 Initial out-of-plane deflections of web of the test panel for test girder 9, 800x80, deformation step 0

Table 6-3 shows the maximum and minimum initial out-of-plane deflections, the imperfections, for all Delft test girders.

Table 6-3 Overview of the maximum and minimum imperfections of the test girders

Test girder	1, 400x50	2, 400x80(1)	3, 400x80(2)	4, 400x100	5, 600x50	6, 600x80	7, 600x100	8, 800x50	9, 800x80	10, 800x100
Max.imp.	+17,4	+12,4	+3,9	+6,9	+15,5	+8,7	+10,4	+13,6	+10,0	+76,1
Min.imp	-12,1	-4,6	-8,2	-5,6	-7,8	-15,2	-16,0	-15,4	-16,4	-51,2

From Table 6-3 it is clear that all maximum and minimum geometrical imperfections of the webs are very large values related to the web thickness t_w and extremely large for test girder 10, 800x100. This is due to using a relatively thin plate for the webs creating plate girders at scale, where the welding had a relatively big influence on the distortion of the web plate.

6.2.3.2 Physical (initial) imperfections, residual stresses

The residual stresses for double symmetric plate girders are described in Chapter 3.2.3.2 as assumed to simulate the Basler experiment G4. The residual stress distributions for the web and the flange according to the previous Dutch code NEN6771 and according to the previous Swedish code

BSK99 are transformed into equivalent stress distributions which could be used in the selected element distribution in the FEM-models.

For the validation of the FEM-model on the Delft experiments, only the residual stress distribution according to the previous Swedish code BSK99 is used, justified by the results of the validation of the FEM-results on the Basler experiment G4, see Chapter 3.2.3.2.

Due to the asymmetric position of the web relative to the flanges, the transformed residual stress pattern has to be adapted to create, apart from equilibrium in axial forces, also equilibrium in moments for each of the elements of the test girder, the flanges and the web.

The compressive residual stress is assumed to be uniform, but different for two groups of elements, see Figure 6-3.

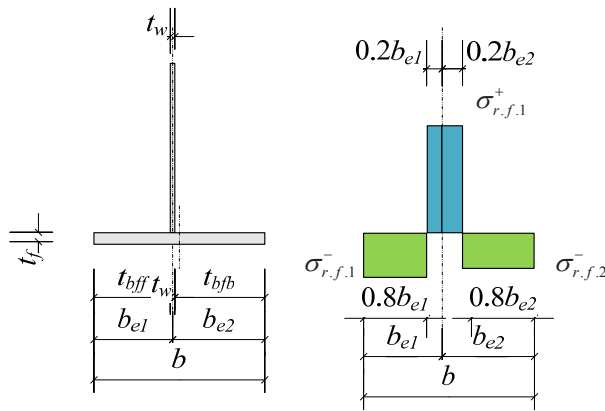


Figure 6-3 Assumed residual stress distribution for an eccentric connection of the web to the flange

These groups of elements are located on each side of the elements with a tensile residual stress, close to the connection of the web to the flange.

The determination of the residual stresses is split up into two steps. First, the determination of the compressive stress for a symmetric girder according to BSK99. In a second step, the compressive residual stresses of both groups of elements are determined, to realise equilibrium in moments.

Centric position of the web relative to the flanges

The compressive residual stress σ_c in the flange according to the Swedish code, BSK99, is shown in Eq.(3.39) and repeated in Eq.(6.1):

$$\sigma_c = \frac{2.25 \cdot t_f \cdot f_{y,f}}{b - 2.25 \cdot t_f} \quad (6.1)$$

The resulting compressive force F_r^- , equal to the resulting tensile force F_r^+ , caused by this residual compressive stress σ_c is determined with Eq.(3.43) and repeated in Eq.(6.2):

$$F_r^- = \left(2.25b - \frac{27}{16} \cdot t_f \right) \cdot \frac{t_f^2}{b} \cdot f_{y,f} \quad (6.2)$$

Eccentric position of the web relative to the flanges

Due to the asymmetric position of the web relative to the flange, the flange width is subdivided into a width b_{e1} and b_{e2} , both consisting of 5 elements with the same width.

Both centrally positioned elements have an initial tensile stress to simulate the tensile residual stress. The number of elements is determined in such a way that the initial tensile stress $\sigma_{r,f,1}^+$ is always smaller than the yield stress $f_{y,f}$ for all test girders. This justifies the reduction in the number of elements from 12 for the simulation of the Basler test girder to 10 for the simulation of the Delft experiments. The initial compressive stress of two elements adjacent to the elements with an initial tensile stress is different from the determined initial compressive stress σ_c according to Eq.(6.1), while the initial compressive stresses for both groups of elements are different from the initial compressive stress $\sigma_{r,f,1}^- = \sigma_c$. The initial tensile stress $\sigma_{r,f,1}^+$ is determined with:

$$\sigma_{r,f,1}^+ = \frac{F_r^-}{0.2b \cdot t_f} = \frac{(b - 0.75 \cdot t_f) \cdot 2.25 \cdot \frac{t_f^2}{b} \cdot f_{y,f}}{0.2 \cdot b \cdot t_f} = (b - 0.75 \cdot t_f) \cdot 11.25 \cdot \frac{t_f}{b^2} \cdot f_{y,f} \quad (6.3)$$

The initial stress distribution has different initial compressive stresses for the parts of the flanges with a width of b_{e1} and b_{e2} , namely respectively $\sigma_{r,f,1}^-$ and $\sigma_{r,f,2}^-$, while the initial tensile residual stress $\sigma_{r,f,1}^+$ is equal Eq.(6.3). Equilibrium in forces gives:

$$F_r^- = 0.8 \cdot b_{e1} \cdot t_f \cdot \sigma_{r,f,1}^- + 0.8 \cdot b_{e2} \cdot t_f \cdot \sigma_{r,f,2}^- = F_r^+ = (b - 0.75 \cdot t_f) \cdot 2.25 \cdot \frac{t_f^2}{b} \cdot f_{y,f}$$

This leads to:

$$\sigma_{r,f,1}^- = \frac{(b - 0.75 \cdot t_f) \cdot 2.25 \cdot \frac{t_f}{b} \cdot f_{y,f} - 0.8 \cdot b_{e2} \cdot \sigma_{r,f,2}^-}{0.8 \cdot b_{e1}} =$$

$$= (b - 0.75 \cdot t_f) \cdot \frac{45}{16} \cdot \frac{t_f}{b \cdot b_{e1}} \cdot f_{y,f} - \frac{b_{e2}}{b_{e1}} \cdot \sigma_{r,f,2}^- \quad (6.4)$$

Equilibrium in moments gives:

$$\begin{aligned} 0.8 \cdot b_{e1} \cdot t_f \cdot 0.6 \cdot b_{e1} \cdot \sigma_{r,f,1}^- - 0.2 \cdot b_{e1} \cdot t_f \cdot 0.1 \cdot b_{e1} \cdot \sigma_{r,f,1}^+ = \\ = 0.8 \cdot b_{e2} \cdot t_f \cdot 0.6 \cdot b_{e1} \cdot \sigma_{r,f,2}^- - 0.2 \cdot b_{e2} \cdot t_f \cdot 0.1 \cdot b_{e2} \cdot \sigma_{r,f,1}^+ \end{aligned}$$

This is rewritten into an expression for $\sigma_{r,f,1}^-$ in $\sigma_{r,f,2}^-$:

$$\begin{aligned} \sigma_{r,f,1}^- = \frac{0.48 \cdot b_{e1} \cdot b_{e2} \cdot \sigma_{r,f,2}^- + 0.02 \cdot (b_{e1}^2 - b_{e2}^2) \cdot \sigma_{r,f,1}^+}{0.48 \cdot b_{e1}^2} = \\ = \frac{b_{e2}}{b_{e1}} \cdot \sigma_{r,f,2}^- + \frac{1}{24} \cdot \left(1 - \frac{b_{e2}^2}{b_{e1}^2} \right) \cdot \sigma_{r,f,1}^+ \end{aligned} \quad (6.5)$$

Balancing Eq.(6.4) and Eq.(6.5) results in:

$$(b - 0.75 \cdot t_f) \cdot \frac{45}{16} \cdot \frac{t_f}{b \cdot b_{e1}} \cdot f_{y,f} - \frac{b_{e2}}{b_{e1}} \cdot \sigma_{r,f,2}^- = \frac{b_{e2}}{b_{e1}} \cdot \sigma_{r,f,2}^- + \frac{1}{24} \cdot \left(1 - \frac{b_{e2}^2}{b_{e1}^2} \right) \cdot \sigma_{r,f,1}^+$$

Stress $\sigma_{r,f,2}^-$ is determined as follows:

$$\begin{aligned} \sigma_{r,f,2}^- = \frac{(b - 0.75 \cdot t_f) \cdot \frac{45}{16} \cdot \frac{t_f}{b \cdot b_{e1}} \cdot f_{y,f} + \frac{1}{24} \cdot \left(1 - \frac{b_{e2}^2}{b_{e1}^2} \right) \cdot \sigma_{r,f,1}^+}{2 \cdot \frac{b_{e2}}{b_{e1}}} = \\ = (b - 0.75 \cdot t_f) \cdot \frac{45}{32} \cdot \frac{t_f}{b \cdot b_{e2}} \cdot f_{y,f} + \frac{1}{48} \cdot \left(\frac{b_{e1}}{b_{e2}} - \frac{b_{e2}}{b_{e1}} \right) \cdot \sigma_{r,f,1}^+ \end{aligned} \quad (6.6)$$

The residual stresses for the web are determined as shown in Chapter 3.2.3.2, based on the actual dimensions of the Delft experiments.

Table 6-4 shows the resulting force caused by the residual compression or tensile stresses $F_r^- = -F_r^+$ in the top and bottom flange and the web of the Delft experiments. Please note that the resulting force caused by the residual stresses in the flanges with a nominal thickness of $t_f = 5\text{mm}$ is around 1.5 times of the flanges with a nominal thickness of $t_f = 4\text{mm}$.

Table 6-4 Resulting compressive and tensile force $F_r^- = -F_r^+$ based on the residual stresses according to BSK99 in [N]

Test specimen	1, 400x50	2, 400x80(1)	3, 400x80(2)	4, 400x100	5, 600x50	6, 600x80	7, 600x100	8, 800x50	9, 800x80	10, 800x100
Top flange	13363	20058	21522	14254	13866	21378	14442	13438	22103	13514
Bottom flange	12579	19793	20852	14483	13096	21893	14537	12914	22279	13662
Web	1334	1321	1334	1279	1313	1378	1475	1397	1393	1360

Table 6-4 shows that the resulting forces in the webs are remarkably small, compared with the resulting force shows in the top and bottom flanges, caused by the rather small web thickness t_w .

Table 6-5 presents the assumed residual stresses for the Delft experiments according to the previous Swedish code BSK99 for all test girders.

Table 6-5 Initial stresses in the web and flanges representing the residual stress distribution [MPa]

	1, 400x50	2, 400x80(1)	3, 400x80(2)	4, 400x100	5, 600x50	6, 600x80	7, 600x100	8, 800x50	9, 800x80	10, 800x100
Top flange										
$\sigma_{r,f,1}^-$	-75.0	-57.2	-59.1	-41.7	-78.7	-61.2	-39.3	-78.0	-60.1	-40.6
$\sigma_{r,f,2}^-$	-79.7	-58.8	-58.2	-39.5	-76.7	-60.3	-38.5	-76.3	-62.3	-39.5
$\sigma_{r,f,1}^+$	+309.1	+232.0	+234.6	+162.2	+310.9	+242.9	+155.6	+308.5	+244.9	+160.3
Bottom flange										
$\sigma_{r,f,1}^-$	-70.4	-59.2	-59.4	-41.2	-70.4	-58.7	-38.2	-73.0	-58.4	-42.6
$\sigma_{r,f,2}^-$	-75.7	-57.8	-57.0	-41.1	-75.0	-59.8	-36.8	-74.9	-58.7	-40.8
$\sigma_{r,f,1}^+$	+291.9	+234.0	+232.6	+164.5	+290.6	+236.9	+150.0	+295.9	+234.2	+166.7
Web										
$\sigma_{r,w}^-$	-3.5	-3.4	-3.3	-3.1	-2.5	-2.2	-2.3	-1.8	-1.8	-1.8

$\sigma_{r,w}^+$	+48.5	+48.0	+46.7	+43.8	+334.5	+31.3	-+31.2	+25.3	+25.4	24.9
------------------	-------	-------	-------	-------	--------	-------	--------	-------	-------	------

6.3 THEORETICAL RESISTANCES OF THE DELFT TEST SPECIMENS

6.3.1 GENERAL

The theoretical bending moment resistances, elastic and plastic bending moment resistance, but also the bending moment resistance based on the flanges only, the critical bending moment resistance and the effective bending moment resistance, are determined based on the actual dimensions and actual material properties as described in EN1993-1-5 and calculated in the same way as for the Basler test specimen G4, see Chapter 3.5.

6.3.2 EFFECTIVE BENDING MOMENT RESISTANCE

6.3.2.1 Cross-section classification based on actual dimensions and material properties

At first the cross-sectional class of the flanges is checked, based on the actual dimensions and actual material properties. The cross-sectional classification for structures is based on nominal dimensions and nominal material properties, but for the Delft experiments the classification is based on actual values. The flange is, at maximum, a cross-sectional class 3 according to EN-1993-1-5. This means that the flange slenderness has to be smaller than:

$$\frac{c}{t} \leq 14 \sqrt{\frac{235}{f_{y,tf}}} \quad (6.7)$$

For the widest flanges with a nominal width of 100 mm, this criterion is roughly checked by neglecting the dimension of the weld on the determination of the slenderness. For test specimen 4, 400x 100, this means:

$$\frac{c}{t} \approx \frac{b_{tf} - t_w}{2 \cdot t_{tf}} = \frac{98.7 - 0.93}{2 \cdot 4.29} = 11.4 \leq 14 \sqrt{\frac{235}{f_{y,tf}}} = 14 \sqrt{\frac{235}{343}} = 11.6 \quad (6.8)$$

$$\frac{c}{t} \approx \frac{b_{bf} - t_w}{2 \cdot t_{bf}} = \frac{98.9 - 0.93}{2 \cdot 4.37} = 11.2 \leq 14 \sqrt{\frac{235}{f_{y,bf}}} = 14 \sqrt{\frac{235}{342}} = 11.6 \quad (6.9)$$

For test specimen 7, 600x100, this means:

$$\frac{c}{t} \approx \frac{b_{tf} - t_w}{2 \cdot t_{tf}} = \frac{99.1 - 0.97}{2 \cdot 4.31} = 11.4 \leq 14 \sqrt{\frac{235}{f_{y,tf}}} = 14 \sqrt{\frac{235}{341}} = 11.6 \quad (6.10)$$

$$\frac{c}{t} \approx \frac{b_{bf} - t_w}{2 \cdot t_{bf}} = \frac{98.7 - 0.97}{2 \cdot 4.33} = 11.4 \leq 14 \sqrt{\frac{235}{f_{y,bf}}} = 14 \sqrt{\frac{235}{344}} = 11.6 \quad (6.11)$$

For test specimen 10, 800x100, this means:

$$\frac{c}{t} \approx \frac{b_{tf} - t_w}{2 \cdot t_{tf}} = \frac{99.1 - 1.00}{2 \cdot 4.24} = 11.5 \leq 14 \sqrt{\frac{235}{f_{y,tf}}} = 14 \sqrt{\frac{235}{339}} = 11.7 \quad (6.12)$$

$$\frac{c}{t} \approx \frac{b_{bf} - t_w}{2 \cdot t_{bf}} = \frac{98.7 - 1.00}{2 \cdot 4.24} = 11.5 \leq 14 \sqrt{\frac{235}{f_{y,bf}}} = 14 \sqrt{\frac{235}{350}} = 11.5 \quad (6.13)$$

The most slender flanges from the test girders are fully effective and so the flanges with a nominal width of 50 mm or 80 mm are fully effective too.

6.3.2.2 Effective bending moment resistance of a hybrid girder

The Delft test girders are so called hybrid girders with different yield stresses for the web and flanges. It is common use for hybrid girders that the yield stress of the flanges is higher than the yield stress of the web.

The Basler test girder G4 is in fact a hybrid girder too, but, for this test girder G4 the yield stress of the web compared with the yield stresses of the flanges is much larger. The influence of this larger yield stress of the web does not affect the effective bending moment resistance very much and is ignored. Further, the flanges have to be of cross-section class 1, so redistribution of forces is possible. Due to larger yield stresses of the flanges compared with the yield stress of the web in the Delft experiments, the effective bending moment resistance can be calculated by using two options. For Option 1, the procedure to determine the effective bending moment resistance M_{eff} as described in Chapter 3.5 is used. Eq.(3.84), repeated as Eq.(6.14), has to be adapted as given in Eq.(6.15) for the Delft experiments to take the smaller yield stress of the webs into account.

$$M_{eff} = \min \left(\frac{I_{eff,i}}{e_{2,i}} \cdot f_{y,tf}, \frac{I_{eff,i}}{e_{1,i}} \cdot f_{y,bf} \right) \quad (6.14)$$

$$M_{eff} = \min \left(\frac{I_{eff,i}}{e_{2,i} - t_{tf}} \cdot f_{y,w}, \frac{I_{eff,i}}{e_{1,i} - t_{bf}} \cdot f_{y,w} \right) \quad (6.15)$$

Figure 6-4 shows at the left-hand side the cross-section and in the centre the stress distribution based on the effective width method as applied in Chapter 3.5. The following requirements related to the stresses have to be satisfied:

- $\sigma_{1,i} \leq f_{y,tf}$
- $\sigma_{2,i} \leq f_{y,w}$
- $|\sigma_{5,i}| \leq f_{y,w}$
- $|\sigma_{6,i}| \leq f_{y,bf}$

For the Basler test specimen G4 the second and third requirement are always met, because the yield stresses of the flanges are smaller than the yield stress of the web, $f_{y,ff} \leq f_{y,w}$ and $f_{y,bf} \leq f_{y,w}$.

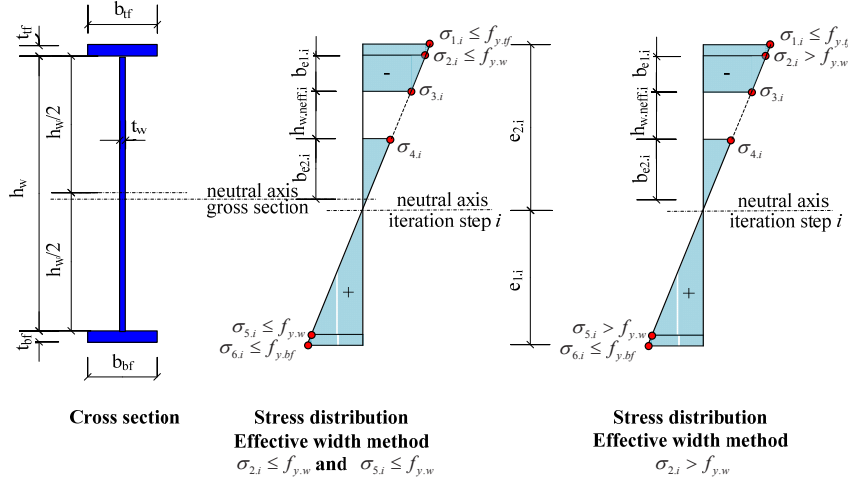


Figure 6-4 Cross-section plus stress distributions according to the effective width method

The yield stress of the web determines the stress distribution, while for the Basler test specimen G4 the yield stress of one of the flanges determines the stress distribution. For the effective bending moment resistance of the Delft test girders this means that $\sigma_{2,i} = f_{y,w}$ or $\sigma_{5,i} = -f_{y,w}$, while the stresses in the flanges are smaller than their yield stresses. For a girder with only one yield stress for all elements of the girder, the web and the flanges, the method as described for the Basler test girder G4 in Chapter 3.5 has to be used.

EN1993-1-5 gives the possibility to take the higher yield strengths of the flanges into account. The web yields at the top or, depending on the difference in the actual yield stresses and the differences in the actual geometry, sometimes at the bottom.

Chapter 3.5.1 presents step by step the procedure to determine the effective bending moment resistance M_{eff} , starting from the stress distribution based on the gross cross-section. This is not repeated in this chapter, but it is extended to determine the effective bending moment resistance of a hybrid girder according to Option 2, called $M_{eff, Opt2}$, by taking into account the higher yield stresses of the flanges, see the linear stress distribution at the right-hand side in Figure 6-4. Partial yielding of the web is ignored. The procedure to determine the intermediate stresses is as follows:

- The linear stress distribution is determined by the yield stresses of the top and the bottom flange, respectively $\sigma_{1,i} = f_{y,ff}$ and $\sigma_{6,i} = -f_{y,bf}$. The intermediate stresses $\sigma_{2,i}$ and $\sigma_{5,i}$ are determined by linear interpolation:

- $\sigma_{2,i} = \sigma_{6,i} + (\sigma_{1,i} - \sigma_{6,i}) \cdot \frac{h - t_{ff}}{h}$
 - $\sigma_{5,i} = \sigma_{6,i} + (\sigma_{1,i} - \sigma_{6,i}) \cdot \frac{t_{bf}}{h}$;
 - Determine the variables related to plate buckling, so $\psi_i = \frac{\sigma_{5,i}}{\sigma_{2,i}}$, $k_i = 7.81 - 6.29\psi_i^2 + 9.78\psi_i$,
- $$\sigma_{cr,i} = k_i \cdot \frac{\pi^2 E}{12(1-\nu^2) \left(\frac{h_w}{t_w} \right)^2} \text{ and } \bar{\lambda}_i = \sqrt{\frac{\sigma_{2,i}}{\sigma_{cr,i}}}, \rho_i = \frac{\{\bar{\lambda}_i - 0.055 \cdot (4 + \psi_i)\}}{\bar{\lambda}_i^2};$$
- The location at which the linear stress distribution is equal to zero, follows from the following equations: $e_{1,i} = \frac{\sigma_{6,i}}{\sigma_{6,i} - \sigma_{1,i}} \cdot h$ and $e_{2,i} = h - e_{1,i}$;
 - The effective width is determined by $b_{eff,i} = \frac{\rho_i \cdot h_w}{(1 - \psi_i)}$ and divided into the part $b_{e1,i} = 0.4 \cdot b_{eff,i}$ at the top of the web and a part $b_{e2,i} = 0.6 \cdot b_{eff,i}$ beyond the neutral axis;
 - The distance x_i from the neutral axis to the locations in the web where the stress is equal to the yield stress, is determined with $x_i = \frac{f_{y,w}}{\sigma_{2,i}} \cdot (e_{2,i} - t_{ff})$, see Figure 6-5;
 - The intermediate stresses σ_{2wi} , $\sigma_{3,i}$, $\sigma_{4,i}$ and σ_{5wi} , see Figure 6-5, are determined:
 - If $\sigma_{2,i} > f_{y,w}$ then $\sigma_{2wi} = f_{y,w}$ else $\sigma_{2wi} = \sigma_{2,i}$
 - If $e_{2,i} - t_{ff} - b_{e1,i} > x_i$ then $\sigma_{3,i} = f_{y,w}$ else $\sigma_{3,i} = \frac{\sigma_{1,i}}{e_{2,i}} \cdot (e_{2,i} - t_{ff} - b_{e1,i})$
 - $\sigma_{4,i} = \frac{\sigma_{1,i}}{e_{2,i}} \cdot b_{e2,i}$
 - If $|\sigma_{5,i}| > f_{y,w}$ then $\sigma_{5wi} = -f_{y,w}$ else $\sigma_{5wi} = \sigma_{5,i}$;

Two stress distributions can be distinguished at the location of $\sigma_{3,i}$, namely for the situation that $\sigma_{3,i} \geq f_{y,w}$ and for the situation that $\sigma_{3,i} < f_{y,w}$, see respectively Figure 6-5 and Figure 6-6. When the yield stresses of the web and the flanges differ very much from each other, it is possible that such a stress distribution occurs at the bottom part of the web. This means that the stress at the top flange is larger than at the bottom flange and in all test girders $|\sigma_{5,i}| \leq f_{y,w}$ and so a triangular stress distribution appears under the neutral axis, see Figure 6-6.

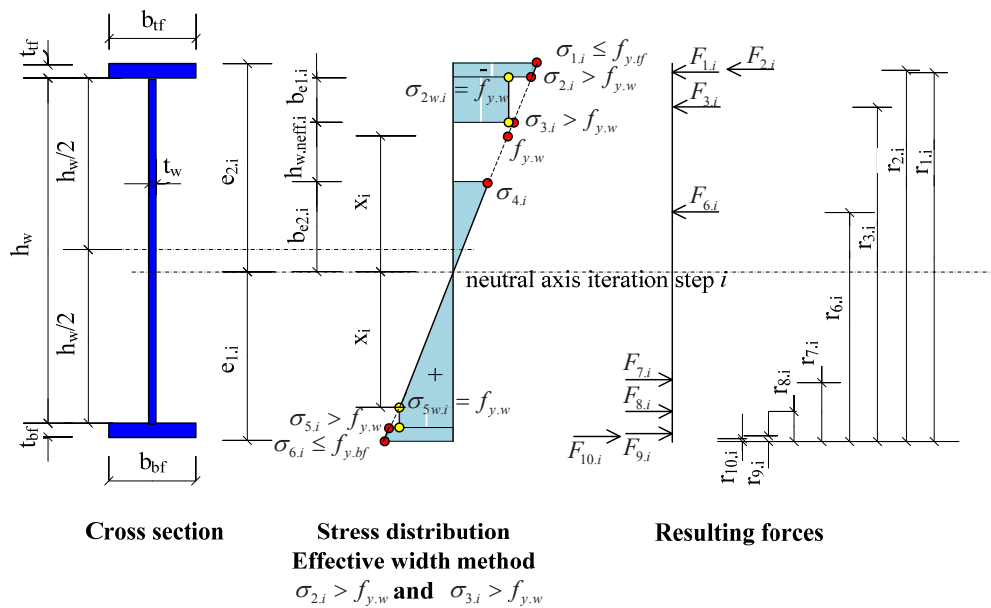


Figure 6-5 Cross-section of the girder including the stress distribution

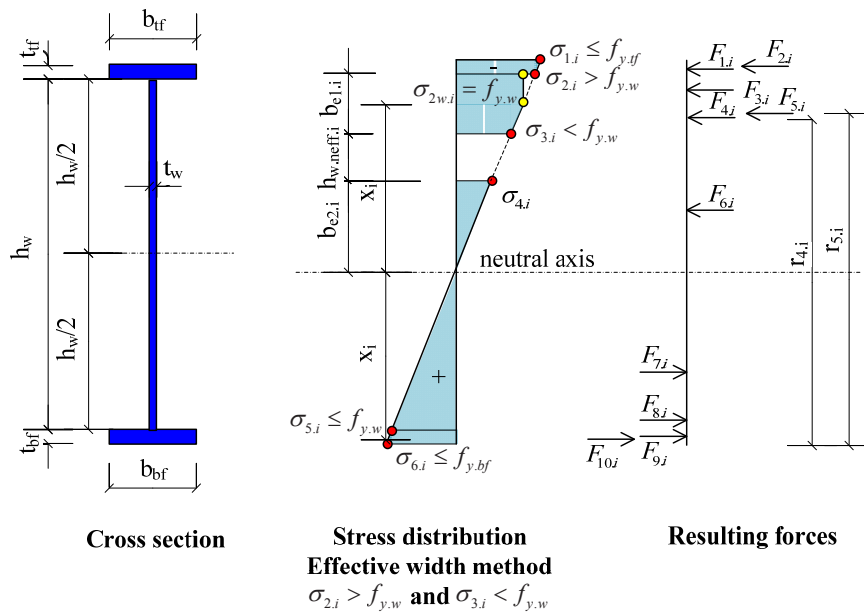


Figure 6-6 Cross-section of the girder including the stress distribution

With these stresses and all effective dimensions, the resulting forces and lever arms are determined:

- The resulting force in the top flange is subdivided into two parts, namely the force with a block stress and a small part with a triangular stress distribution:
 - $F_{1,i} = A_{yf} \cdot \sigma_{2,i}$
 - $F_{2,i} = A_{yf} \cdot (\sigma_{1,i} - \sigma_{2,i}) \cdot \frac{1}{2}$
- The resulting force in the top of the web can be subdivided into three parts, depending on the location of the yield stress of the web and the effective width $b_{e1,i}$:
 - If $e_{2,i} - t_{yf} - b_{e1,i} > x_i$, this can be replaced by $\sigma_{3,i} > f_{y,w}$, then there is a block stress distribution and only one resulting force $F_{3,i} = b_{e1,i} \cdot t_w \cdot f_{y,w}$, see Figure 6-5;
 - If $e_{2,i} - t_{yf} - b_{e1,i} < x_i$, this can be replaced by $\sigma_{3,i} < f_{y,w}$, then there are two resulting forces based on block stress distributions and one based on a triangular stress distribution, see Figure 6-6:
 - $F_{3,i} = (e_{2,i} - t_{yf} - x_i) \cdot t_w \cdot f_{y,w}$;
 - $F_{4,i} = (x_i - e_{2,i} + t_{yf} + b_{e1,i}) \cdot t_w \cdot \sigma_{3,i}$;
 - $F_{5,i} = (x_i - e_{2,i} + t_{yf} + b_{e1,i}) \cdot t_w \cdot (f_{y,w} - \sigma_{3,i}) \cdot \frac{1}{2}$;
- The resulting force of the triangular stress distribution in the area consisting of the effective part $b_{e1,i}$ of the web $F_{6,i} = b_{e1,i} \cdot t_w \cdot \sigma_{4,i} \cdot \frac{1}{2}$;
- The resulting force in the tensile part of the web can be subdivided into two parts, depending on the location x_i where the stress in the web is equal to the yield stress:
 - If $e_{1,i} - t_{bf} > x_i$, this can be replaced by $|\sigma_{5,i}| > f_{y,w}$, then the resulting force is based on a triangular stress distribution and a block stress distribution, see Figure 6-5:
 - $F_{7,i} = x_i \cdot t_w \cdot f_{y,w} \cdot \frac{1}{2}$;
 - $F_{8,i} = (e_{1,i} - t_{bf} - x_i) \cdot t_w \cdot f_{y,w}$;
 - If $e_{1,i} - t_{bf} < x_i$, this can be replaced by $|\sigma_{5,i}| < f_{y,w}$, then the resulting force is based on a triangular stress distribution equal to $F_{7,i} = (e_{1,i} - t_{bf}) \cdot t_w \cdot \sigma_{5,i} \cdot \frac{1}{2}$, see Figure 6-6;
- The resulting force of the bottom flange is subdivided into two forces, one based on a block stress distribution and one based on a triangular stress distribution:

- $F_{9,i} = A_{bf} \cdot \sigma_{5,i}$;
- $F_{10,i} = A_{bf} \cdot (\sigma_{6,i} - \sigma_{5,i}) \cdot \frac{1}{2}$;
- The lever arm $r_{j,i}$ of these resulting forces $F_{j,i}$ has to be determined, in this thesis related to the point of gravity of the specific areas in the cross-sections and the bottom of the bottom flange:
 - Top flange:
 - $r_{1,i} = h - \frac{t_{tf}}{2}$
 - $r_{2,i} = h - \frac{t_{tf}}{3}$
 - Web:
 - If $e_{2,i} - t_{tf} - b_{e1,i} > x_i$, then $r_{3,i} = h - t_{tf} - \frac{b_{e1,i}}{2}$, see Figure 6-5;
 - If $e_{2,i} - t_{tf} - b_{e1,i} < x_i$, see Figure 6-6;
 - $r_{3,i} = h - t_{tf} - \frac{1}{2}(e_{2,i} - t_{tf} - x_i)$;
 - $r_{4,i} = h - t_{tf} - (e_{2,i} - t_{tf} - x_i) - \frac{1}{2}(x_i - e_{2,i} + t_{tf} + b_{e1,i})$;
 - $r_{5,i} = h - t_{tf} - (e_{2,i} - t_{tf} - x_i) - \frac{1}{3}(x_i - e_{2,i} + t_{tf} + b_{e1,i})$;
 - $r_{6,i} = e_{1,i} + \frac{2}{3}b_{e2,i}$
 - If $e_{1,i} - t_{bf} > x_i$, see Figure 6-5:
 - $r_{7,i} = e_{1,i} - \frac{2}{3}x_i$;
 - $r_{8,i} = t_{bf} + \frac{1}{2}(e_{1,i} - t_{bf} - x_i)$;
 - If $e_{1,i} - t_{bf} < x_i$, see Figure 6-6;:
 - $r_{7,i} = t_{bf} + \frac{1}{3}(e_{1,i} - t_{bf})$
 - Bottom flange:
 - $r_{9,i} = t_{bf} \cdot \frac{1}{2}$

$$\blacksquare \quad r_{10,i} = t_{yf} \cdot \frac{1}{3}$$

The sum of the resulting forces $\sum_{j=1}^{10} F_{j,i}$ has to be equal to 0 to realise axial equilibrium. If the sum of

the forces $\sum_{j=1}^{10} F_{j,i} < 0$, the influence of the tensile stresses is too large and so stress $|\sigma_{6,i}|$ has to be decreased and the linear stress distribution has to be adapted.

When the yield stress of the flanges differs very much, it is possible that $\sigma_{1,i} \neq f_{y,yf}$, but $\sigma_{6,i} = -f_{y,bf}$,

or, in other words, the sum of the resulting forces $\sum_{j=1}^{10} F_{j,i} > 0$, the influence of the compressive

stresses is too high and so $\sigma_{1,i}$ has to be decreased. Because of the decrease of the stress in one of the extreme fibres, the effective width is changing too and the whole calculation is repeated again,

up to the sum of the internal forces $\sum_{j=1}^{10} F_{j,i} = 0$. These linear relations are solved by using the Solver

of the spreadsheet Excel. The effective bending moment resistance is determined as follows

$$M_{eff.Opt2,i} = \sum_{j=1}^{10} \Delta M_{j,i} = \sum_{j=1}^{10} F_{j,i} \cdot e_{j,i}.$$

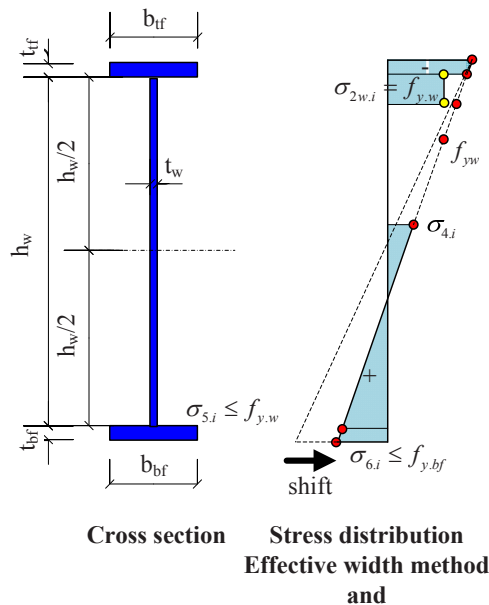


Figure 6-7 Effective bending moment resistance according to Option 2

As an example, this procedure is shown for test specimen 9, 800x80. The actual dimensions of the gross cross-section are given in Table 6-1 and the actual yield strengths are shown in Table 6-2.

$$A_{tf} = b_{tf} \cdot t_{tf} = 80.2 \cdot 5.6 = 448.9 \text{ mm}^2$$

$$A_w = h_w \cdot t_w = 799.4 \cdot 1.0 = 815.4 \text{ mm}^2$$

$$A_{bf} = b_{bf} \cdot t_{bf} = 80.1 \cdot 5.6 = 448.4 \text{ mm}^2$$

$$A_0 = A_{gross} = A_{tf} + A_w + A_{bf} = 448.9 + 815.4 + 448.4 = 1712.7 \text{ mm}^2 \quad (6.16)$$

The gross section is asymmetric, so the position of the neutral axis has to be determined. In all calculations, this position of the neutral axis is related to the bottom of the bottom flange. In this calculation, the contribution of the flanges is the same in every iteration and so this is determined once:

$$\sum A_f e_f = 448.9 \cdot \left(810.6 - \frac{5.6}{2} \right) + 448.4 \cdot \frac{5.6}{2} = 363887.2 \text{ mm}^3 \quad (6.17)$$

The position of the neutral axis of the gross section is:

$$e_{1.0} = \frac{\sum A_f \cdot e_f + A_w \cdot \left(\frac{h_w}{2} + t_{bf} \right)}{A_{tot}} = \frac{363887.2 + 810.6 \cdot \left(\frac{799.4}{2} + 5.6 \right)}{1712.7} = 405.4 \text{ mm} \quad (6.18)$$

The distance to the other extreme fibre is:

$$e_{2.0} = h - e_{1.0} = 810.6 - 405.4 = 405.2 \text{ mm} \quad (6.19)$$

The moment of inertia I_{gross} and the section moduli W_{tf} and W_{bf} are:

$$\begin{aligned} I_{gross} &= \frac{1}{12} \cdot (A_{tf} \cdot t_{tf}^2 + A_{bf} \cdot t_{bf}^2 + A_w \cdot h_w^2) + A_{tf} \cdot \left(h - \frac{t_{tf}}{2} - e_{1.0} \right)^2 + \\ &\quad + A_{bf} \cdot \left(\frac{t_{bf}}{2} - e_{1.0} \right)^2 + A_w \cdot \left(\frac{h_w}{2} + t_{bf} - e_{1.0} \right)^2 = \\ &= \frac{1}{12} \cdot (448.9 \cdot 5.6^2 + 448.4 \cdot 5.6^2 + 783.4 \cdot 799.4^2) + 448.9 \cdot \left(810.6 - \frac{5.6}{2} - 405.4 \right)^2 + \\ &\quad + 448.4 \cdot \left(\frac{5.6}{2} - 405.4 \right)^2 + 783.4 \cdot \left(\frac{799.4}{2} + 5.6 - 405.4 \right)^2 = \\ &= 18710 \cdot 10^4 \text{ mm}^4 \end{aligned} \quad (6.20)$$

$$W_{tf} = \frac{I_{gross}}{e_{2.0}} = \frac{18710 \cdot 10^4}{405.2} = 462 \cdot 10^3 \text{ mm}^3$$

$$W_{bf} = \frac{I_{gross}}{e_{1.0}} = \frac{187106 \cdot 10^4}{405.4} = 461 \cdot 10^3 \text{ mm}^3 \quad (6.21)$$

Based on these properties, the “elastic bending moment resistance $M_{el,R}$ ” is determined. This is the smallest elastic bending moment resistance $M_{el,R}$ based on yielding of the top flange, yielding of the bottom flange or yielding at the top or bottom side of the web:

$$\begin{aligned}
 M_{el} &= \min \left(W_{tf} \cdot f_{y,tf} ; \frac{I_{gross}}{e_{2,0} - t_{tf}} \cdot f_{y,w} ; \frac{I_{gross}}{e_{1,0} - t_{bf}} \cdot f_{y,w} ; W_{bf} \cdot f_{y,bf} \right) = \\
 &= \min \left(462 \cdot 10^3 \cdot 320 ; \frac{18710 \cdot 10^4}{405.2 - 5.6} \cdot 296 ; \frac{18710 \cdot 10^4}{405.4 - 5.6} \cdot 296 ; 461 \cdot 10^3 \cdot 317 \right) \cdot 10^{-6} = \\
 &= \min (147.8 ; 138.6 ; 138.5 ; 146.3) = 138.5 \text{ kNm}
 \end{aligned} \tag{6.22}$$

As can be seen, the elastic bending moment resistance M_{el} is based on yielding of the bottom of the web. The stress distribution to determine the effective width of the hybrid test girder is based on the minimum elastic bending moment resistance $M_{el,R}$ based on yielding of one of the flanges, so based on the bottom flange, $M_{el} = 146.3 \text{ kNm}$. The stresses in the extreme fibres can be determined, namely $\sigma_{1,0}$ and $\sigma_{6,0}$ based on the section moduli, and the stresses $\sigma_{2,0}$ and $\sigma_{5,0}$ are linear related to their locations in the cross-section. This means $\sigma_{6,0} = -f_{y,bf} = -317 \text{ MPa}$, based on the elastic bending moment resistance M_{el} . The other stresses as shown in Figure 6-5 and Figure 6-6 are:

$$\begin{aligned}
 \sigma_{1,0} &= -\frac{\sigma_{6,0}}{e_{1,0}} \cdot e_{2,0} = \frac{317.0}{405.4} \cdot 405.2 = 316.8 \text{ MPa} \leq f_{y,tf} = 320 \text{ MPa} \\
 \sigma_{2,0} &= -\frac{\sigma_{6,0}}{e_{1,0}} \cdot (e_{2,0} - t_{tf}) = \frac{317.0}{405.4} \cdot (405.2 - 5.6) = 312.4 \text{ MPa} \\
 \sigma_{5,0} &= -\frac{\sigma_{1,0}}{e_{2,0}} \cdot (e_{1,0} - t_{bf}) = -\frac{316.8}{405.2} \cdot (405.4 - 5.6) = -312.6 \text{ MPa}
 \end{aligned} \tag{6.23}$$

The stress in the web is limited to its yield strength, so $\sigma_{2w,0} = f_{y,w} = 296 \text{ MPa}$ and $\sigma_{5w,0} = -f_{y,w} = -296 \text{ MPa}$. The distance x_0 in Figure 6-5 and Figure 6-6, is determined as follows:

$$x_0 = \frac{f_{y,w}}{\sigma_{1,0}} \cdot e_{2,0} = \frac{296}{316.8} \cdot 405.2 = 378.6 \text{ mm} \tag{6.24}$$

The internal forces $F_{i,0}$ can be determined, based on these stresses:

$$\begin{aligned}
 F_{1,0} &= \sigma_{2,0} \cdot A_{tf} = 312.4 \cdot 448.9 = 140250 \text{ N} \\
 F_{2,0} &= \frac{\sigma_{1,0} - \sigma_{2,0}}{2} \cdot A_{tf} = \frac{316.8 - 312.4}{2} \cdot 448.9 = 983 \text{ N} \\
 F_{3,0} &= \frac{\sigma_{2w,0} + \sigma_{3,0}}{2} \cdot (e_{2,0} - t_{tf} - x_0) \cdot t_w = \frac{296.0 + 296.0}{2} \cdot (405.2 - 5.6 - 378.6) \cdot 0.98 = 6097 \text{ N}
 \end{aligned}$$

In this gross section, the internal forces $F_{4,0}$ and $F_{5,0}$ do not have a meaning.

$$\begin{aligned}
 F_{6,0} &= \frac{\sigma_{3,0}}{2} \cdot x_0 \cdot t_w = \frac{296.0}{2} \cdot 378.6 \cdot 0.98 = 54909 \text{ N} \\
 F_{7,0} &= \frac{\sigma_{5w,0}}{2} \cdot x_0 \cdot t_w = \frac{-296.0}{2} \cdot 378.6 \cdot 0.98 = -54909 \text{ N} \\
 F_{8,0} &= \sigma_{5w,0} \cdot (e_{1,0} - t_{bf} - x_0) \cdot t_w = -296.0 \cdot (405.4 - 5.6 - 378.6) \cdot 0.98 = -6167 \text{ N} \\
 F_{9,0} &= \frac{\sigma_{6,0} - \sigma_{5,0}}{2} \cdot A_{bf} = \frac{-317.0 + 312.6}{2} \cdot 448.4 = -982 \text{ N} \\
 F_{10,0} &= \sigma_{5,0} \cdot A_{bf} = -312.6 \cdot 448.4 = -140177 \text{ N}
 \end{aligned} \tag{6.25}$$

The sum of these forces $\sum F_{j,0} = +4 \text{ N}$ is very small, due to the adapted stresses in the web.

Because of the rather high web slenderness $\beta_w = \frac{h_w}{t_w} = \frac{799.4}{0.98} = 815.7$ plate buckling has to be taken

into account. The stress ratio ψ_1 is based on the linear stress distribution with acceptance of yielding of the web. The stress ratio ψ_1 is based on $\sigma_{2,0}$ and $\sigma_{5,0}$ instead of on $\sigma_{2w,0}$ and $\sigma_{5w,0}$:

$$\psi_1 = \frac{\sigma_{5,0}}{\sigma_{2,0}} = \frac{-312.6}{312.4} = -1.0 \tag{6.26}$$

The buckling factor $k_{\sigma,0}$ is:

$$k_{\sigma,0} = 7.81 - 6.29\psi_1 + 9.78\psi_1^2 = 7.81 - 6.29 \cdot (-1.0) + 9.78 \cdot (-1.0)^2 = 23.90 \tag{6.27}$$

The critical stress σ_{cr} , based on the initial buckling theory, can be determined:

$$\sigma_{cr,1} = \frac{k_{\sigma,0} \cdot \pi^2 E}{12(1-\nu^2) \left(\frac{h_w}{t_w} \right)^2} = \frac{23.90 \cdot \pi^2 \cdot 2.1 \cdot 10^5}{12(1-0.3^2) \left(\frac{799.4}{0.98} \right)^2} = 6.8 \text{ MPa} \tag{6.28}$$

In the following iteration, the effective width of the compressive web is determined, see Figure 6-7.

Iteration 1

$$\bar{\lambda}_{p,1} = \sqrt{\frac{\sigma_{2,0}}{\sigma_{cr,1}}} = \sqrt{\frac{312.4}{6.8}} = 6.6 \tag{6.29}$$

The effective width $b_{eff,i}$ is determined by using the factor ρ_i for iteration i , more or less according to the Winter formula:

$$\begin{aligned}
 \rho_1 &= \frac{1}{\bar{\lambda}_{p,1}^2} \cdot \left\{ \bar{\lambda}_{p,1} - 0.055 \cdot (4 + \psi_1) \right\} = \frac{1}{6.6^2} \cdot \left\{ 6.6 - 0.055 \cdot (4 - 1.0) \right\} = 0.15 \\
 b_{eff,1} &= \frac{\rho_1 \cdot h_w}{1 - \psi_1} = \frac{0.15 \cdot 799.4}{1 - (-1.00)} = 59.1 \text{ mm}
 \end{aligned} \tag{6.30}$$

This effective width $b_{eff,1}$ is distributed over $b_{e1,i}$ close to the top flange and $b_{e2,i}$ beyond the neutral axis of the previous iteration, so for this iteration beyond $e_{1,0}$, see Figure 6-7.

$$\begin{aligned} b_{e1,1} &= 0.4 \cdot b_{eff,1} = 0.4 \cdot 59.1 = 23.6 \text{ mm} \\ b_{e2,1} &= 0.6 \cdot b_{eff,1} = 0.6 \cdot 59.1 = 35.5 \text{ mm} \end{aligned} \quad (6.31)$$

Because of the non effective part $h_{w,neff,i}$ of the compressive web, the position of the neutral axis will shift downwards to the tensile flange. The position of the neutral axis is determined by the contribution of the effective width of the web and by the fixed contribution of the flanges.

The effective web area $A_{weff,1}$ based on the effective width in this first iteration is:

$$A_{weff,1} = (e_{1,0} - t_{bf} + b_{eff,1}) \cdot t_w = (405.4 - 5.6 + 59.1) \cdot 0.98 = 449.8 \text{ mm}^2 \quad (6.32)$$

The effective cross area becomes:

$$A_{eff,1} = A_{tf} + A_{weff,1} + A_{bf} = 448.9 + 449.8 + 448.4 = 1347.1 \text{ mm}^2 \quad (6.33)$$

The point of gravity $e_{weff,1}$ of this effective web area $A_{weff,1}$ is determined with:

$$\begin{aligned} e_{weff,1} &= \left[(e_{1,0} - t_{bf}) \cdot \left\{ \frac{(e_{1,0} - t_{bf})}{2} + t_{bf} \right\} + b_{e2,1} \left(e_{1,0} + \frac{b_{e2,1}}{2} \right) + b_{e1,1} \left(h - t_{tf} - \frac{b_{e1,1}}{2} \right) \right] \cdot \frac{t_w}{A_{weff,1}} = \\ &= \left[(405.4 - 5.6) \cdot \left\{ \frac{(405.4 - 5.6)}{2} + 5.6 \right\} + 35.5 \cdot \left(405.4 + \frac{35.5}{2} \right) + \right. \\ &\quad \left. + 23.6 \cdot \left(810.6 - 5.6 - \frac{23.6}{2} \right) \right] \cdot \frac{0.98}{1347.1} = 252.6 \text{ mm} \end{aligned} \quad (6.34)$$

This $e_{weff,1}$ is measured from the bottom of the bottom flange. The position of the neutral axis can be determined by:

$$e_{1,1} = \frac{\sum A_{fi} \cdot e_i + A_{weff,1} \cdot e_{weff,1}}{A_{eff,1}} = \frac{363887.2 + 449.8 \cdot 252.6}{1347.1} = 354.5 \text{ mm} \quad (6.35)$$

The distance $e_{2,1}$ of the neutral axis from the bottom of the bottom flange of the gross section is:

$$e_{2,1} = h - e_{1,1} = 810.6 - 354.5 = 456.1 \text{ mm} \quad (6.36)$$

Based on the position of the neutral axis, it is clear that the top flange will yield. The linear stress distribution changes because of this effective cross-section and the shift of the neutral axis. The stresses in this first iteration are:

$$\sigma_{1,1} = f_{y,tf} = 320 \text{ MPa}$$

$$\begin{aligned}
\sigma_{2,1} &= \frac{\sigma_{1,1}}{e_{2,1}} \cdot (e_{2,1} - t_{ff}) = \frac{320.0}{456.1} \cdot (456.1 - 5.6) = 316.1 \text{ MPa} \\
\sigma_{2w,1} &= f_{y,w} = 296.0 \text{ MPa} \\
\sigma_{3,1} &= \frac{\sigma_{1,1}}{e_{2,1}} \cdot (e_{2,1} - t_{ff} - b_{e1,1}) = \frac{320.0}{456.1} \cdot (456.1 - 5.6 - 23.6) = 299.5 \text{ MPa} \geq f_{y,w} = 296 \text{ MPa} \\
\Rightarrow \sigma_{3,1} &= 296 \text{ MPa} \\
\sigma_{4,1} &= \frac{\sigma_{1,1}}{e_{2,1}} \cdot (e_{1,0} - e_{1,1} + b_{e2,1}) = \frac{320}{456.1} \cdot (405.4 - 354.5 + 35.4) = 60.6 \text{ MPa} \\
\sigma_{5,1} &= -\frac{\sigma_{1,1}}{e_{2,1}} \cdot (e_{1,1} - t_{bf}) = -\frac{320.0}{456.1} \cdot (354.5 - 5.6) = -244.7 \text{ MPa} \\
\sigma_{6,1} &= -\frac{\sigma_{1,1}}{e_{2,1}} \cdot e_{1,1} = -\frac{320.0}{456.1} \cdot 354.5 = -248.7 \text{ MPa} \tag{6.37}
\end{aligned}$$

The distance x_1 is:

$$x_1 = \frac{f_{y,w}}{\sigma_{1,1}} \cdot e_{2,1} = \frac{296}{320.0} \cdot 456.1 = 421.9 \text{ mm} \tag{6.38}$$

The resulting forces and lever arms can be determined and again there will be a residual force. A small adaption has to be made, namely:

$$\sigma_{6,1} - \frac{\sigma_{6,1} - f_{y,ff}}{h} \cdot e_{1,1} = 0 \quad \Rightarrow e_{1,1} = \frac{\sigma_{6,1}}{\sigma_{6,1} - f_{y,ff}} h \tag{6.39}$$

Further, the effective part of the web $b_{e2,1}$ is not placed on the position of the neutral axis $e_{1,0}$ of the previous iteration, but directly beyond the position of the neutral axis $e_{1,1}$ of the current iteration. Therefore, all items mentioned are based on the stresses in the same iteration. By using the Solver of the spreadsheet program Excel, the sum of the residual forces $\sum_{j=1}^{10} F_{j,i} = 0$ by varying $\sigma_{6,i}$, see Figure 6-8.

The resulting forces for the specific areas of the cross-section have to be determined again and it is clear that for this effective cross-section the sum of these resulting forces is now positive. To reach equilibrium, the linear stress distribution has to be adapted by reducing stress $\sigma_{6,i}$ and so all the other stresses, except stress $\sigma_{1,i}$. This stress is equal to the yield stress of the top flange $\sigma_{1,i} = f_{y,ff}$. For specific yield stress configurations it is possible that $\sigma_{1,i}$ has to be reduced instead of $\sigma_{6,i}$. The final results for test girder 9, 800x80, are presented in Table 6-6.

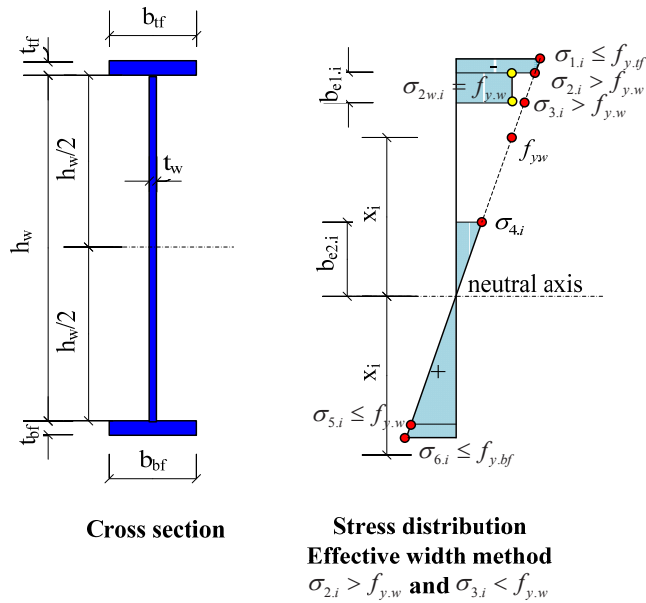


Figure 6-8 Cross-section of the girder including the adaption of the stress distribution

Table 6-6 Forces and moments in the cross-section, final iteration, test girder 9, 800x80

Parameters effective width	Stresses [MPa]	Forces [N]	Lever arm [mm]	$M_{eff,Opt2}$ [kNm]
$\psi = -0.759$	$\sigma_1 = 320.0$	$F_1 = +141898$	$e_1 = 457$	$\Delta M_1 = 64.9$
$k_\sigma = 18.224$	$\sigma_2 = 316.1$	$F_2 = +874$	$e_2 = 458$	$\Delta M_2 = 0.4$
$\sigma_{cr} = 5.198 \text{ MPa}$	$\sigma_{2w} = 296.0$	$F_3 = +6607$	$e_3 = 443$	$\Delta M_3 = 2.9$
$\bar{\lambda}_p = 7.798$	$\sigma_3 = 296.0$	$F_6 = +522$	$e_6 = 23$	$\Delta M_6 = 0.0$
$\rho = 0.125$	$\sigma_4 = 31.2$	$F_7 = -41406$	$e_7 = 230$	$\Delta M_7 = 9.5$
$b_{eff} = 56.9 \text{ mm}$	$\sigma_{5w} = -240.0$	$F_9 = -873$	$e_9 = 349$	$\Delta M_9 = 0.3$
$b_{e1} = 22.8 \text{ mm}$	$\sigma_5 = -240.0$	$F_{10} = -107622$	$e_{10} = 348$	$\Delta M_{10} = 37.4$
$b_{e2} = 34.2 \text{ mm}$	$\sigma_6 = -243.9$	$\sum_{i=1}^{10} F_i = 0$		$\sum_{i=1}^{10} \Delta M_i = 115.5$

The same calculations are made for the other test girders, see the results in Table 6-7. The effective bending moment resistance M_{eff} as determined in Chapter 3.5 is called $M_{eff,Opt1}$ here.

Table 6-7 Bending moment resistances of the test girders, including the moments of inertia

Test girder	M_{pl} [kNm]	M_{el} [kNm]	M_f [kNm]	M_{cr} [kNm]	$M_{eff,Opt1}$ [kNm]	$M_{eff,Opt2}$ [kNm]	I_{gross} [$\times 10^4$ mm ⁴]	I_{eff} [$\times 10^4$ mm ⁴]
1, 400x50	40.2	33.1	27.8	3.3	26.9	30.4	2305	2080
2, 400x80(1)	67.8	56.9	56.3	4.5	51.5	56.3	4031	3831
3, 400x80(2)	68.2	58.0	56.4	4.9	52.1	57.5	4188	3983
4, 400x100	70.0	56.8	58.7	3.7	50.8	58.9	3997	3791
5, 600x50	69.5	59.1	41.8	1.3	41.1	46.1	6173	5009
6, 600x80	112.1	94.4	86.0	2.6	78.6	88.0	9945	9115
7, 600x100	113.4	91.0	88.0	2.5	75.4	88.0	9549	8731
8, 800x50	101.4	81.7	54.0	0.8	<u>54.3</u>	59.4	11245	8946
9, 800x80	161.4	138.5	114.4	1.9	108.5	115.5	18710	16590
10, 800x100	162.2	128.9	114.1	1.8	99.3	114.0	17775	15583

Table 6-7 shows that the effective bending moment resistances according to Option 1 $M_{eff,Opt1}$ are rather small compared with the bending moment resistances based on the cross-section existing of the flanges only M_f , except for test girder 8, 800x50, with a small flange and also with small yield stresses for the flanges, see the underlined bending moment resistances.

The effective bending moment resistances according to Option 2 $M_{eff,Opt2}$ are all larger than or equal to the bending moment resistances based on the cross-section consisting of the flanges only M_f .

6.3.3 THEORETICAL DEFLECTIONS

The results of the Delft experiments are compared with theoretical resistances based on actual dimensions as described in Chapter 6.3.2.2, but also on the theoretical force to displacement diagram. The theoretical deflections are linear up to the critical load P_{cr} , see Chapter 3.6.

Beyond the critical load P_{cr} , the moment of inertia is changing from the moment of inertia I_y based on the gross section into the effective cross-section I_{eff} based on the yield strength $f_{y,w}$ of the web, see the effective section and stress distribution for iteration i in the middle of Figure 6-9, $\sigma_{2,0} = \sigma_{2w,0} = f_{y,w}$.

The effective moment of inertia slowly changes from the moment of inertia based on the gross section I_{gross} to the moment of inertia based on the effective cross-section I_{eff} based on yielding of the web, see the effective cross-section and stress distribution for iteration j at the right-hand side of Figure 6-9, with $\sigma_{cr} < \sigma_{2,j} = \sigma_{2w,j} < f_{y,w}$.

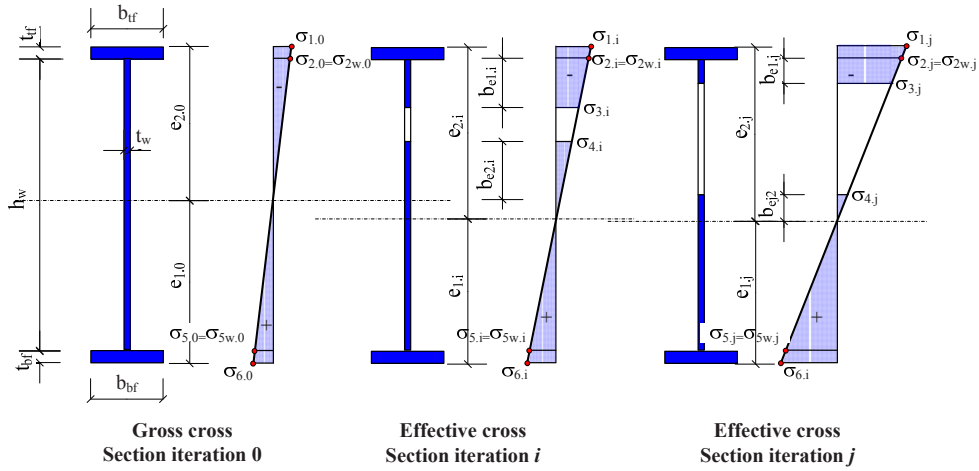


Figure 6-9 Linear stress distribution in the cross-section and effective sections

Chapter 3.6 shows the theoretical deflections for the Basler test specimen G4, a four points bending test, the same type of test as for the Delft experiments. The theoretical deflections are determined for linear elastic behaviour up to the critical load based on plate buckling of the very slender web of the plate girders. Next, the deflection is determined for the effective cross-section, based on yielding of the web at one of the edges of the web. It is based on the yielding of the web, while the yield strength of the web is much smaller than the yield strengths of the flanges and so the web yields before the flanges yield. The properties of the end panel and the test panel of the test specimen are substituted in the general equation as shown in Chapter 3.6 to determine the deflection at the load introduction at $a = \frac{1}{4} \ell$:

$$\delta = \frac{Fa^3}{3EI_{ep}} + \frac{Fa^3}{EI_{ip}} + \frac{Fa}{GA_{ep}} \quad (6.40)$$

From Figure 3-29 it can be seen that the force F in Eq.(6.40) is the reaction force, so half of the actuator force F_{act} .

In this Chapter 6.3.3, the calculation is shown for test specimen 9, 800x80, and the results of the remaining test specimens are given.

6.3.3.1 Determination of the deflection at the load introductions

The moment of inertia of the end panel is determined in the same way as described for the test panel in Chapter 3.6 and Chapter 6.3.2 for the gross section as well as for the effective cross-section. The effective cross-section depends on the stress level too. For a lower stress level than the critical stress,

the moment of inertia of the gross section is used. The critical stress σ_{cr} for the cross-section of the test panel, the panel with the cross-section class 4 web, is determined in Chapter 6.3.2.2 and based on this critical stress σ_{cr} , the critical bending moment is determined.

The deflection according to Eq.(6.40), based on the critical force $P_{cr} = \frac{M_{cr}}{a} = \frac{1.9}{1.5} \cdot 10^3 = 1278 \text{ N}$ is

based on the gross section of the end panel and the gross section of the test panel:

$$\begin{aligned} \delta &= \frac{Fa^3}{3EI_{ep}} + \frac{Fa^3}{EI_{ip}} + \frac{Fa}{GA_{ep}} = \\ &= \frac{1278 \cdot 1500^3}{3 \cdot 210000 \cdot 31611 \cdot 10^4} + \frac{1278 \cdot 1500^3}{210000 \cdot 18710 \cdot 10^4} + \frac{1278 \cdot 1500}{81000 \cdot 799.4 \cdot 4.01} = \\ &= 0.30 + 1.52 + 0.03 = 1.84 \text{ mm} \end{aligned} \quad (6.41)$$

After reaching the critical stress σ_{cr} , the web of the test panel will buckle and from now on the moment of inertia of the test panel is based on the effective width. The maximum concentrated load P_{eff} is based on the effective bending moment resistance M_{eff} , which is based on yielding of the top of the web as determined in Chapter 4:

$$P_{eff} = \frac{M_{eff}}{a} = \frac{108.5}{1.5} \cdot 10^3 = 72325 \text{ N} \quad (6.42)$$

This is the concentrated force P_{eff} that causes yielding in the extreme fibre of the web. The deflection related to this force P_{eff} has to be split up into two parts, namely the deflection up to the critical force P_{cr} and the increase of the deflection based on the difference of the force P_{eff} and the force P_{cr} to reach the effective bending moment resistance $M_{eff.R}$:

$$\Delta P = P_{eff} - P_{cr} = 72325 - 1278 = 71047 \text{ N} \quad (6.43)$$

The deflection is:

$$\begin{aligned} \delta &= \delta_{cr} + \frac{\Delta Fa^3}{3EI_{ep}} + \frac{\Delta Fa^3}{EI_{ip}} + \frac{\Delta Fa}{GA_{ep}} = \\ &= \frac{71047 \cdot 1500^3}{3 \cdot 210000 \cdot 26618 \cdot 10^4} + \frac{71047 \cdot 1500^3}{210000 \cdot 16603 \cdot 10^4} + \frac{71047 \cdot 1500}{81000 \cdot 799.4 \cdot 4.01} = \\ &= 0.14 + 0.12 + 6.88 + 0.41 = 8.85 \text{ mm} \end{aligned} \quad (6.44)$$

These deflections are shown in a graphic, see Figure 6-10. Between the calculated deflections marked by the two red dots, a linear relationship is assumed, while in reality the effective moment of inertia will change for any load level.

Although the bilinear relationship is used, it is hard to see it is bilinear. Up to the critical stress, the cross-section is fully effective. The load belonging to the effective moment, based on yielding of the web, gives the smallest effective width.

This means that small kink in the line as shown in Figure 6-10, is not visible in the comparison with the results of the experiments, it looks like a linear relation.

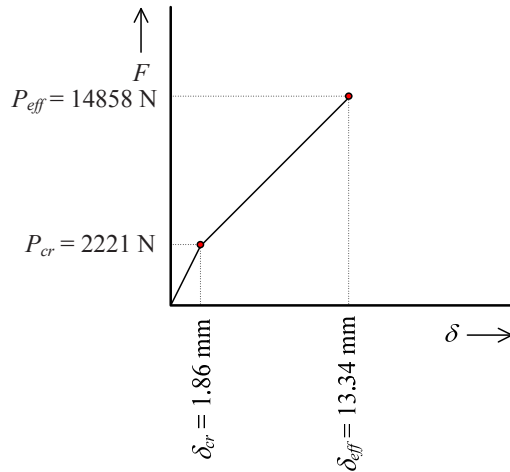


Figure 6-10 Deflections bilinear relation

Figure 6-10 shows the difference in stiffness explicitly by scaling up the deflections, the deflection by the critical force P_{cr} that leads to the critical bending moment resistance M_{cr} , and the deflection by the effective force P_{eff} that leads to the effective bending moment resistance M_{eff} based on the yield stress $f_{y,w}$ of the web.

It is of interest to look at the influence of ignoring the difference in stiffness of the gross section and use only the effective stiffness. This deflection is:

$$\begin{aligned}\delta_{simp} &= \frac{Fa^3}{3EI_{ep}} + \frac{Fa^3}{EI_{tp}} + \frac{Fa}{GA_{ep}} = \\ &= \frac{72325 \cdot 1500^3}{3 \cdot 210000 \cdot 26618 \cdot 10^4} + \frac{72325 \cdot 1500^3}{210000 \cdot 16603 \cdot 10^4} + \frac{72325 \cdot 1500}{81000 \cdot 799.4 \cdot 4.01} = \\ &= 1.46 + 7.00 + 0.42 = 8.88 \text{ mm}\end{aligned}\tag{6.45}$$

The difference in deflection is remarkably small, namely $\delta = 8.85 \text{ mm}$ and $\delta_{simp} = 8.88 \text{ mm}$ and in the P - δ diagram of the test girders, this difference won't be seen.

For all test girders these results are shown in Table 6-8.

Table 6-8 Deflection at the load introduction by the critical load and the effective load (option 1)

Test girder	I_{ep} [x10 ⁴ mm ⁴]	$I_{ep,ef}$ [x10 ⁴ mm ⁴]	P_{cr} [N]	δ [mm]	P_{eff} [N]	δ_{eff} [mm]	δ_{simp} [mm]
1, 400x50	3894	3885	2175	1.84	17965	16.37	16.53
2, 400x80(1)	5622	5622	3030	1.53	34301	17.98	18.04
3, 400x80(2)	5813	5813	3234	1.58	34762	17.55	17.61
4, 400x100	5662	5662	2462	1.25	33868	17.87	17.93
5, 600x50	11328	9930	892	0.29	27395	10.41	10.46
6, 600x80	15421	14099	1729	0.35	52377	11.59	11.62
7, 600x100	15007	13705	1681	0.36	50261	11.56	11.59
8, 800x50	24135	18902	559	0.10	36171	7.69	7.72
9, 800x80	31611	26618	1278	0.14	72325	8.85	8.88
10, 800x100	30503	25539	1225	0.14	66176	8.57	8.58

6.3.3.2 Determination of the deflection at midspan

The deflection at midspan of the girder can be determined in the same way as described before, but now using a Unit Virtual Load in the centre of the span. The determination is as follows:

$$\delta = \frac{Fa^3}{3EI_{ep}} + \frac{3Fa^3}{2EI_{tp}} + \frac{Fa}{GA_{ep}} \quad (6.46)$$

The difference in deflection at $\frac{1}{2}\ell$ with the deflection at $\frac{1}{4}\ell$ of the span is the factor $\frac{3}{2}$ for the second term in Eq.(6.46), thus related to the stiffness of the test panel only. The deflection in the centre is based on the critical load $P_{cr} = 2221 \text{ N}$ and based on the stiffnesses of the gross sections of both the end panel (index ep) $I_{y,ep}$ and the test panels (index tp) $I_{y,tp}$:

$$\begin{aligned} \delta &= \frac{Fa^3}{3EI_{y,ep}} + \frac{3Fa^3}{2EI_{y,tp}} + \frac{F \cdot a}{GA_{v,ep}} = \\ &= \frac{2221 \cdot 1500^3}{3 \cdot 210000 \cdot 4175.0 \cdot 10^4} + \frac{3 \cdot 2221 \cdot 1500^3}{2 \cdot 210000 \cdot 2307.1 \cdot 10^4} + \frac{2221 \cdot 1500}{81000 \cdot 1806.2} = \\ &= 0.3 + 2.3 + 0.0 = 2.6 \text{ mm} \end{aligned} \quad (6.47)$$

The deflection in the centre of the span is based on the following:

- the difference of the maximum effective load and the critical load $\Delta P = 12637 \text{ N}$, which is based on the effective load $P_{eff} = 14858 \text{ N}$ and the critical load $P_{cr} = 2221 \text{ N}$
- the stiffness of the gross section of the end panels $I_{y,ep}$
- the effective stiffness of the test panel $I_{y,eff,tp}$

- the stiffness related to shear

The deflection is:

$$\begin{aligned}
 \delta &= \delta_{cr} + \frac{\Delta F a^3}{3EI_{y,ep}} + \frac{3\Delta F a^3}{2EI_{y,eff,tp}} + \frac{\Delta F \cdot a}{GA_{v,ep}} = \\
 &= 2.6 + \frac{12637 \cdot 1500^3}{3 \cdot 210000 \cdot 4175.0 \cdot 10^4} + \frac{3 \cdot 12637 \cdot 1500^3}{2 \cdot 210000 \cdot 2086.0 \cdot 10^4} + \frac{15637 \cdot 1500}{81000 \cdot 1806.2} = \\
 &= 2.6 + 1.6 + 14.6 + 0.1 = 16.4 \text{ mm}
 \end{aligned} \tag{6.48}$$

The difference in the deflection at $\frac{1}{4}\ell$ and $\frac{1}{2}\ell$ is $16.4 - 13.3 = 3.1$ mm. Although the web of the girder yields, the girder did not collapse and during the experiment the load increased.

6.4 COMPARISON RESULTS DELFT EXPERIMENTS WITH RESULTS FEM

6.4.1 GENERAL

The following results of the experiment and the FEM-models are compared with each other:

1. The $P - \delta$ diagrams:
 - a. The maximum load;
 - b. The stiffness of the girder;
2. The bending moment resistances;
3. The failure mode.

6.4.2 TEST GIRDER 9, 800x80

Figure 6-11 presents the $P - \delta$ diagram of the FEM-model, but also the $P - \delta$ diagram of the actuator force F_{act} and the sum of the reaction forces $\sum R_{test}$ versus the deformation δ_z at the left-hand side load introduction. The theoretical linear elastic deformations, as determined in Chapter 6.3.3, are shown too. The sum of the reaction forces $\sum R_{FEM}$ of the FEM-model is equal to the force F due to the deformation driven load steps, there is no friction. The difference in actuator force F_{act} and the sum of the reaction force of the test $\sum R_{test}$ is equal to the friction force F_{fric} .

Figure 6-11 shows that for the load step the maximum force appears, the sum of the reaction forces of the test is smaller than the maximum force of the FEM-model, namely $\sum R_{test} = 153.3$ kN, while the sum of the reaction forces of the FEM-model is $F = \sum R_{FEM} = 161.9$ kN, which is 105.6% relative to the sum of the reaction force $\sum R_{test}$ of the test. The actuator force is $F_{act} = 155.3$ kN. The

friction force kN and so the friction force is $F_{fric} = 2.0 \text{ kN}$, which is 1.3% relative to the actuator force $F_{act} = 155.3 \text{ kN}$.

Figure 6-11 also shows the results of the experiment, the actuator force and the sum of the reaction force, versus the deformations on the left-hand side of the load introduction δ_{Li} , the dotted red and blue lines. From these lines it can be seen that in the beginning the test rig settles a little bit and because of this, the curves have to be adapted. The dotted red line is adapted to the solid red line and the dotted blue line is adapted to the solid blue line.

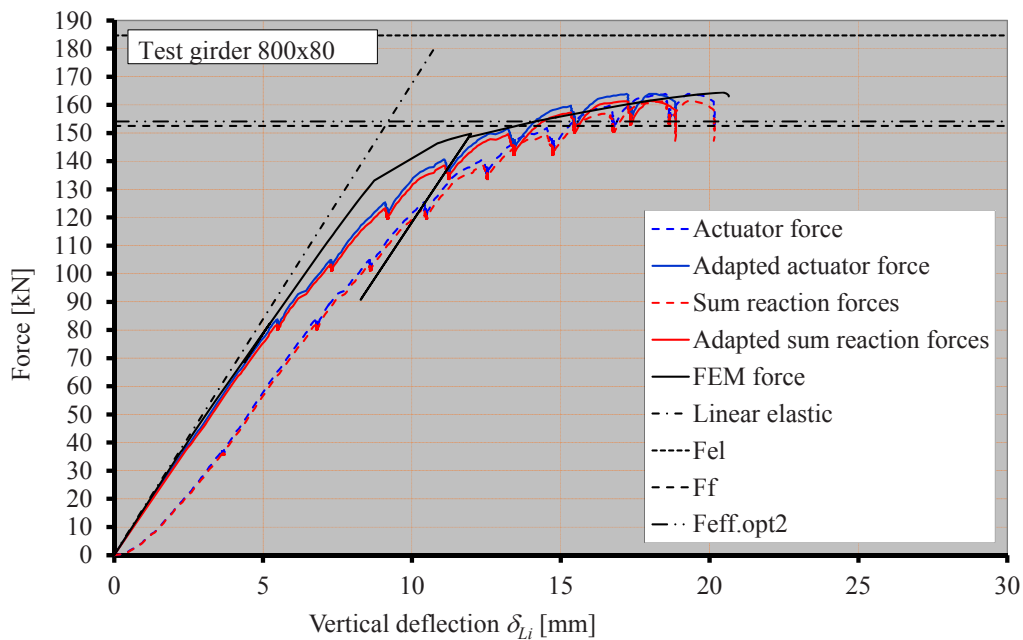


Figure 6-11 P - δ diagram of the experiment and the FEM for test specimen 9, 800x80

The solid lines correspond very well with the theoretical linear elastic deformations and the P - δ diagram of the FEM-model, especially in the beginning. Later on, the deformations of the experiment are larger than the deformations of the FEM-model due to the influence of the residual stresses.

Table 6-9 shows that the reaction forces of the experiment as well as those of the FEM-model, including the accompanying deformations at the location of the load introductions in the deformation step in which the maximum load appears. It can be seen that the reaction forces of the FEM-model are larger than those of the experiment. The deflections at the load introductions of the FEM-model are larger than those deflections of the experiments.

Table 6-9 Maximum load and accompanying deflections at the load introduction, test girder 9, 800x80

Test girder	Reaction forces experiment				Reaction forces FEM-model			
	$R_{max.L}$	δ_{Lvdt1}	$R_{max.R}$	δ_{Lvdt2}	$R_{max.L}$	δ_{Li}	$R_{max.R}$	δ_{Ri}
	[kN]	[mm]	[kN]	[mm]	[kN]	[mm]	[kN]	[mm]
9, 800x80	74.3	18.6	79.1	19.8	82.2	20.3	82.2	20.9

6.4.3 TEST GIRDER 3, 400x80(2)

Figure 6-12 shows the same kind of results for test girder 3, 400x80(2). The maximum sum of the reaction forces of the test is $\sum R_{test} = 82.7 \text{ kN}$, while the sum of the reaction forces of the FEM-model is 80.0 kN, corresponding with 96.7% relative to the sum of the reaction forces of the test. The maximum actuator force is $F_{act} = 88.6 \text{ kN}$ and so the friction force is $F_{fric} = 5.9 \text{ kN}$, which is 7.1% of the sum of the reaction forces $\sum R_{test}$.

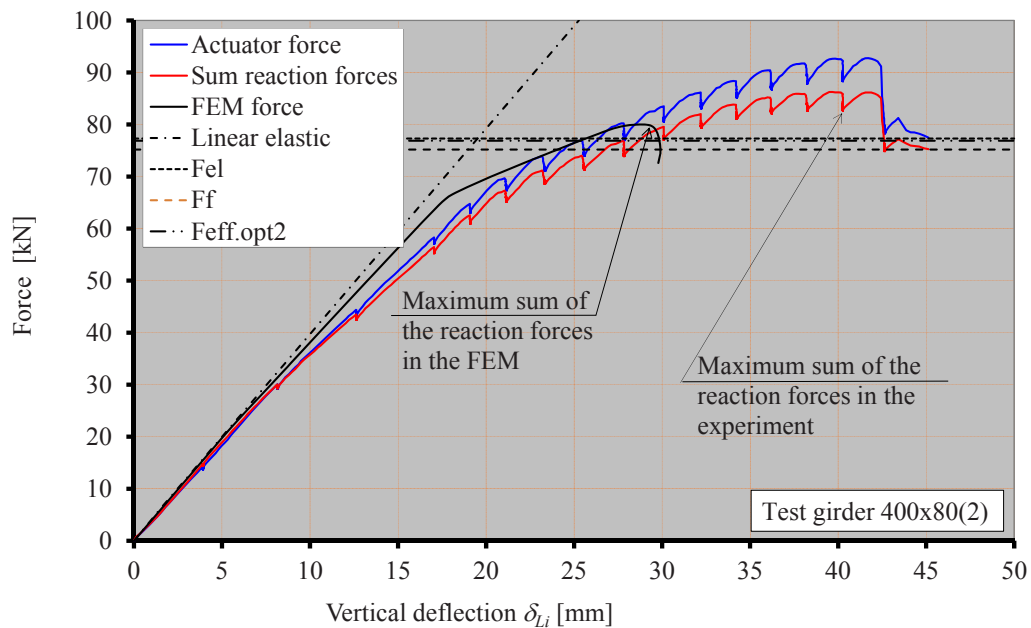


Figure 6-12 P - δ diagram of the experiment and the FEM for test specimen 3, 400x80(2)

Figure 6-12 shows that the sum of the reaction forces of the test girder is very similar to that of the reaction forces of the FEM-model. The deformations are also similar, but for the experiment, the final deformations are larger.

Table 6-10 presents the maximum reaction forces of the experiment as well as those of the FEM-model, including the deformations at the deformation step in which the maximum force occurs. The right-hand side reaction force of the experiment is a little bit larger than both reaction forces of the FEM-model.

Table 6-10 Maximum load and accompanying deflections at the load introduction, test girder 3, 400x80(2)

Test girder	Reaction forces experiment				Reaction forces FEM-model			
	$R_{max.L}$	δ_{Lvd1}	$R_{max.R}$	δ_{Lvd2}	$R_{max.L}$	δ_{Li}	$R_{max.R}$	δ_{Ri}
	[kN]	[mm]	[kN]	[mm]	[kN]	[mm]	[kN]	[mm]
3, 400x80(2)	39.2	39.7	40.3	41.6	40.0	28.9	40.0	29.4

6.4.4 OVERVIEW RESULTS

The reaction forces and the deformations at the load introductions of all test girders and those of the FEM-models are presented in Table 6-11.

Table 6-11 Maximum reaction forces and accompanying deformations at the load introductions

Test girder	Reaction force-displacement test					Reaction force-displacement FEM				
	$R_{max.L}$	$R_{max.R}$	$\sum R_{test}$	$\delta_{z.Lvd101}$	$\delta_{z.Lvd102}$	$R_{max.L}$	$R_{max.R}$	$\sum R_{FEM}$	δ_{Li}	δ_{Ri}
	[kN]	[kN]	[kN]	[mm]	[mm]	[kN]	[kN]	[kN]	[mm]	[mm]
1, 400x50	<u>20.89</u>	22.57	43.46	27.14	26.64	21.48	21.48	42.96	32.72	32.32
2, 400x80(1)	36.66	<u>34.69</u>	71.35	31.86	32.59	39.35	39.35	78.70	28.09	28.08
3, 400x80(2)	<u>39.24</u>	43.59	82.73	40.27	41.61	40.00	40.00	80.00	28.90	29.40
4, 400x100	37.96	<u>39.63</u>	77.59	37.28	36.41	40.27	40.27	80.54	26.52	26.43
5, 600x50	<u>32.02</u>	34.87	66.89	31.30	25.44	32.87	32.87	65.74	19.14	19.35
6, 600x80	57.45	<u>61.57</u>	118.02	22.06	22.72	61.48	61.47	122.95	21.74	20.91
7, 600x100	<u>59.25</u>	61.57	120.82	23.55	2390	56.60	56.60	113.20	15.54	15.60
8, 800x50	<u>41.70</u>	45.39	87.09	20.87	23.71	44.53	44.54	89.07	16.59	17.68
9, 800x80	74.23	<u>79.05</u>	153.28	18.63	19.76	82.20	82.20	164.40	20.44	21.20
10, 800x100	<u>74.40</u>	78.56	152.96	16.36	20.97	70.75	70.75	141.50	10.89	10.48

Table 6-11 shows that the reaction forces of the experiments differ from each other, while those of the FEM-models do not. The reason is that the FEM-model is fully symmetric and there is no friction between the compressive flange and the lateral supports as is the case in the test rig of the experiments. The deformations of the load introductions vary both in the experiments as in the FEM-model, but more in the experiments. The bending moment resistance of the experiments is based on

the reaction force that is close the location of the final failure mode in the test girder. These reaction forces of the experiments are compared with the reaction forces of the FEM-models and presented in terms of percentages in Table 6-12, including those of the sums of the reaction forces.

Table 6-12 The reaction forces and the sum of the reaction forces of the tests compared with those of the FEM-models in terms of percentages

Test girder	R_{FEM}/R_{test} [%]	$\sum R_{FEM} / \sum R_{test}$ [%]	R_{test} [kN]	R_{FEM} [kN]	$\sum R_{test}$ [kN]	$\sum R_{FEM}$ [kN]
1, 400x50	102.8	98.8	<u>20.89</u>	21.48	43.46	42.96
2, 400x80(1)	113.4	110.3	<u>34.69</u>	39.35	71.35	78.70
3, 400x80(2)	101.9	96.7	<u>39.24</u>	40.00	82.73	80.00
4, 400x100	101.6	103.8	<u>39.63</u>	40.27	77.59	80.54
5, 600x50	102.7	98.3	<u>32.02</u>	32.87	66.89	65.74
6, 600x80	99.8	104.2	<u>61.57</u>	61.47	118.02	122.95
7, 600x100	95.5	93.7	<u>59.25</u>	56.60	120.82	113.20
8, 800x50	106.8	102.3	<u>41.70</u>	44.53	87.09	89.07
9, 800x80	104.0	107.3	<u>79.05</u>	82.20	153.28	164.40
10, 800x100	95.1	92.5	<u>74.40</u>	70.75	152.96	141.50

Table 6-12 shows that seven of the reaction forces of the FEM-models are larger than those of the experiments and five times the sum of the reaction forces of the FEM-models.

The bending moment resistances of the experiments and the FEM, beside the theoretical resistances are shown in Table 6-13. The ratios of the bending moment resistance of the FEM-models relative to the resistance of the experiments are exactly the same as those of the reaction forces.

It is expected that the bending moment resistance of the experiments will be between the theoretical bending moment resistance of the section existing of only the flanges and the theoretical effective bending moment resistance. Table 6-14 shows the sequence of these bending moment resistances, including the bending moment resistance of the FEM-model. For seven of the ten test girders the bending moment resistance of the experiment is positioned between the effective bending moment resistance and the bending moment resistance based on the FEM-model, while the bending moment resistance based on the cross-section consisting of only the flange, gives the smallest resistance.

Table 6-13 Bending moment resistances

Test girder	Resistances experiments and FEM			Theoretical resistances				
	M_{test} [kNm]	M_{FEM} [kNm]	M_{FEM} / M_{test} [%]	M_{pl} [kNm]	M_{el} [kNm]	M_f [kNm]	$M_{eff,opt1}$ [kNm]	$M_{eff,opt2}$ [kNm]
1, 400x50	31.34	32.22	102.8	40.2	33.1	27.8	26.9	30.6
2, 400x80(1)	52.10	59.03	113.3	67.8	56.9	56.3	51.5	56.8
3, 400x80(2)	58.76	60.00	102.1	68.2	58.0	56.4	52.1	57.7
4, 400x100	59.30	60.41	101.9	70.0	57.1	56.7	50.8	59.0
5, 600x50	48.03	49.31	102.7	73.0	59.1	41.8	42.0	47.1
6, 600x80	90.17	92.22	102.3	112.1	94.4	86.0	78.6	88.3
7, 600x100	88.88	84.90	95.5	113.4	91.0	88.0	75.4	88.2
8, 800x50	62.55	66.80	106.8	101.4	81.7	54.0	54.3	59.7
9, 800x80	118.58	123.30	104.0	161.4	138.5	114.4	108.5	115.6
10, 800x100	111.60	106.13	95.1	162.2	126.9	114.1	99.3	114.4

Table 6-14 Comparison of the bending moment resistances in the sequence from small to large

1, 400x50	M_f (0.89)	$\underline{M_{eff,opt2}}$ (0.98)	M_{test} (1.00)	M_{FEM} (1.03)
2, 400x80(1)	M_{test} (1.00)	M_f (1.08)	$\underline{M_{eff,opt2}}$ (1.09)	M_{FEM} (1.13)
3, 400x80(2)	M_f (0.96)	$\underline{M_{eff,opt2}}$ (0.98)	M_{test} (1.00)	M_{FEM} (1.02)
4, 400x100	M_f (0.98)	$\underline{M_{eff,opt2}}$ (0.99)	M_{test} (1.00)	M_{FEM} (1.02)
5, 600x50	M_f (0.87)	$\underline{M_{eff,opt2}}$ (0.98)	M_{test} (1.00)	M_{FEM} (1.03)
6, 600x80	M_f (0.93)	$\underline{M_{eff,opt2}}$ (0.96)	M_{test} (1.00)	M_{FEM} (1.00)
7, 600x100	M_{FEM} (0.96)	M_f (0.99)	$\underline{M_{eff,opt2}}$ (0.99)	M_{test} (1.00)
8, 800x50	M_f (0.86)	$\underline{M_{eff,opt2}}$ (0.95)	M_{test} (1.00)	M_{FEM} (1.07)
9, 800x80	M_f (0.96)	$\underline{M_{eff,opt2}}$ (0.97)	M_{test} (1.00)	M_{FEM} (1.04)
10, 800x100	M_{FEM} (0.95)	M_{test} (1.00)	M_f (1.02)	$\underline{M_{eff,opt2}}$ (1.03)

6.5 CONCLUSIONS

From the comparison of the results of the FEM-models with the results of the experiments the following can be concluded:

1. Most of the time the stiffness of the FEM-models is a little bit larger than the stiffness of the test girders;
2. The bending moment resistance M_{test} of seven test girders is larger than the effective bending moment resistance $M_{eff,opt2}$ which takes the larger yield stress of the flange into account, option 2, and so $M_{test} > M_{eff,opt2} > M_{eff,opt1}$;

3. The difference between the bending moment resistance M_{FEM} of the FEM-model and the bending moment resistance M_u of the test girder is considered for three groups of test girders with different nominal web slenderness's, namely:
 - a. The group with a nominal web slenderness $\beta_w = 400$ (4 tests) for which this difference varies in-between +1.9% and +13.3%;
 - b. The group with a nominal web slenderness $\beta_w = 600$ (3 tests) for which this difference varies in-between -4.5% and +2.7%;
 - c. The group with a nominal web slenderness $\beta_w = 800$ (3 tests) for which this difference varies in-between -4.9% and +6.8%;
4. The stiffness of the FEM-models is larger than the stiffness of the test girders, which is caused by the influence of the residual stresses of the scaled test girders with webs of 1 mm only and the influence of the rather big geometrical imperfections;

7 PARAMETRIC STUDY

7.1 GENERAL

The aim of the parametric study is to focus on the following goal:

To find the maximum bending moment resistance M_u for a certain amount of steel A_{tot} , with the following sub-goals:

1. To find the optimal ratio of area ρ_{opt} and the maximum web slenderness $\beta_{w,max}$ to reach this maximum bending moment resistance M_u ;
2. To find the influence of the steel grade on this maximum bending moment resistance M_u .

The parametric research started with a reference plate girder with web dimensions $h_w = 1000 \text{ mm}$ and $t_w = 2 \text{ mm}$ and flange dimensions $b = 200 \text{ mm}$ and $t_f = 10 \text{ mm}$. The steel grade is S235. By using different approaches one or more dimensions are varied and also steel grade S460 is used.

The parametric research is continued by using a theoretical bending moment resistance which fits the bending moment resistances of the FEM-models best. The theoretical resistances used are the plastic M_{pl} and elastic bending moment resistances M_{el} , the effective bending moment resistance M_{eff} and the bending moment resistance $M_{Veljkovic}$, based on the cross-section consisting from only the flanges M_f . The bending moment resistance based on an effective width method by Veljkovic and Johansson is described in Chapter 2.7.6 and is also used to compare the results of the FEM-models.

Besides these different theoretical bending moment resistances, another bending moment resistance is introduced, namely $M_{Abspoel}$, based on a simplified effective width method for the web and a simplified stress model as shown in Figure 7-1. The effective cross-section $A_{Abspoel,eff}$ is a symmetrical cross-section, consisting from both flanges and two small effective widths of the web. The height of these effective parts of the web are equal to b_{e1} , the effective width according to EN1993-1-5. The stress distribution is a full plastic stress distribution for the effective parts of the cross-section. This model is justified by the strain distributions in the Delft experiments as shown in Figure 5-82 and Figure 5-83. The bending moment resistance $M_{Abspoel}$ is determined with Eq.(7.1):

$$M_{Abspoel} = \left\{ b \cdot t_f \cdot (h_w + t_f) + b_{el} \cdot t_w \cdot (h_w - b_{el}) \right\} \cdot f_y \quad (7.1)$$

The effective width b_{el} has to be iteratively determined as described for the effective bending moment resistance M_{eff} , see Chapter 3.5.6.

The parameters that influence the bending moment resistance M_u are the geometrical and material parameters and the geometrical and material imperfections. A distinction can be made between independent and dependent parameters. The latter group of parameters can be composed from the independent parameters and will make it easier to use the specific results of this study more in general.

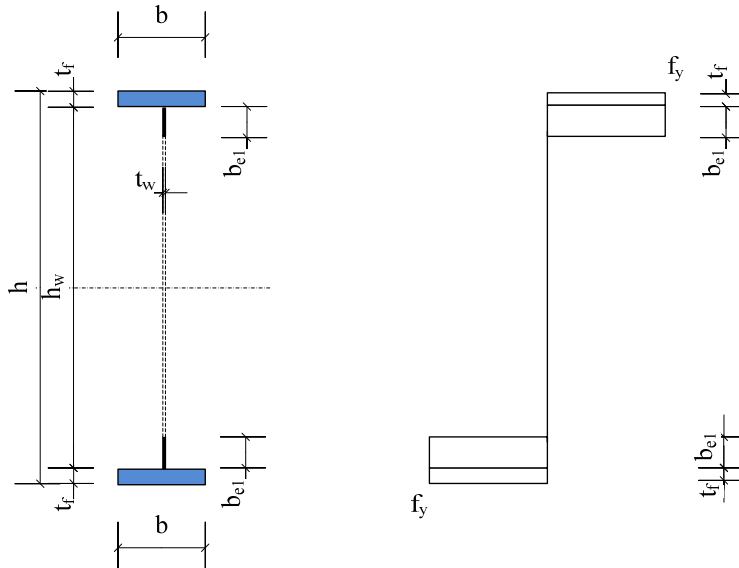


Figure 7-1 Proposed effective cross-section $A_{Abspoel,eff}$ and stress distribution by Abspoel

Geometrical parameters

Independent geometrical parameters are the dimensions of the cross-section: the height of the web h_w , the thickness of the web t_w , the width of the flanges b and the thickness of the flanges t_f , see Figure 7-1. The length dimension of the girder, the span ℓ of the girder, is also a geometrical parameter.

Dependent geometrical parameters are composed from these independent geometrical parameters, such as the total area of the cross-section $A_{tot} = A_w + 2A_f = h_w \cdot t_w + 2 \cdot b \cdot t_f$, the web slenderness

$$\beta_w = \frac{h_w}{t_w} \text{ and the ratio of area } \rho = \frac{A_w}{A_f} = \frac{h_w \cdot t_w}{b \cdot t_f}.$$

Material parameters

The independent material parameter is the steel grade. In this study the steel grades S235 and S460 are used. EN10025-4 gives nominal strengths related to the nominal thicknesses of the elements of the cross-section, the web and the flanges. The nominal yield stresses in this parametric study are 235 MPa for S235 and 460 MPa for S460, because the thickness of all elements of the cross-section is smaller than 16 mm. The Young's modulus is 210000 MPa and the Poisson's ratio is $\nu = 0.3$. The yield strain ε_y can be determined based on the yield stress f_y and the Young's modulus E :

$$\varepsilon_y = \frac{f_y}{E} \quad (7.2)$$

Beyond yielding, a horizontal plateau occurs for the most commonly used steel grades. After a certain strain, usually between 1.5% and 2% depending on the steel grade, the material will harden, caused by changes of the atomic and crystalline structure of the material.

The stress-strain curve is based on so called engineering stress σ_e , the force F divided by the original cross-section A_0 , obtained from a tensile test. In reality, this cross-section A_0 changes after the elastic part of the stress-strain curve. The cross-section becomes significantly smaller by contraction after the proportional limit. This is called necking. Based on the actual cross area A , the true stress σ_t can be determined, which will be higher than the nominal stress, the engineering stress σ_e . Figure 7-2 shows several schematic stress-strain curves according to the EN 1993-1-5, namely a linear diagram and some bilinear diagrams. The first part of all four curves is the linear part, indicated by I, based on the yield strength f_y and the Young's modulus E . The second part of the bilinear diagrams are not similar. The second part can be a horizontal line for pure plastic behaviour, indicated by II in Figure 7-2. To prevent numerical instability in FEM-calculations, a line is shown under a small slope $\arctan\left(\frac{E}{100000}\right)$, indicated by III in Figure 7-2. To take strain-hardening into account, there is a third possibility, namely a line under an angle of $\arctan\left(\frac{E}{100}\right)$, indicated by IV in Figure 7-2. In the diagrams I and IV a horizontal plateau is missing, while in the other two diagrams graphs the strain-hardening is missing.

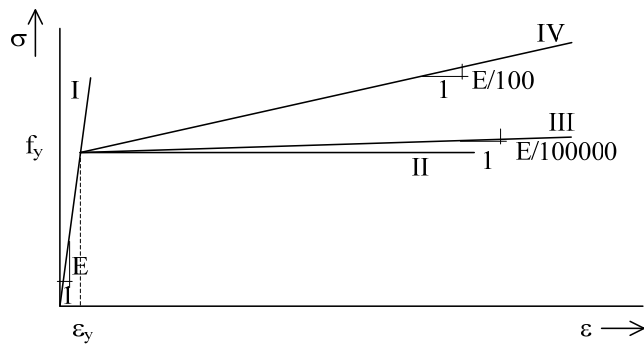


Figure 7-2 Stress-strain relations I to IV according to EN-1993-1-5

EN-1993 does not show a more realistic stress-strain relationship and for this reason it is created. The end of the horizontal plateau, the beginning of the strain hardening, is located at a strain of 1.5% a 2%. A conservative assumption for the beginning of the strain hardening is a strain of 2% (0.020). Two stress-strain relations for the horizontal parts are composed, namely a purely horizontal plateau, see stress-strain relation V in Figure 7-3, and under a small slope of $\arctan\left(\frac{E}{100000}\right)$, see stress-strain relation VI in Figure 7-4. The stress-strain relations V and VI are continued with a strain hardening under a slope of $\arctan\left(\frac{E}{100000}\right)$.

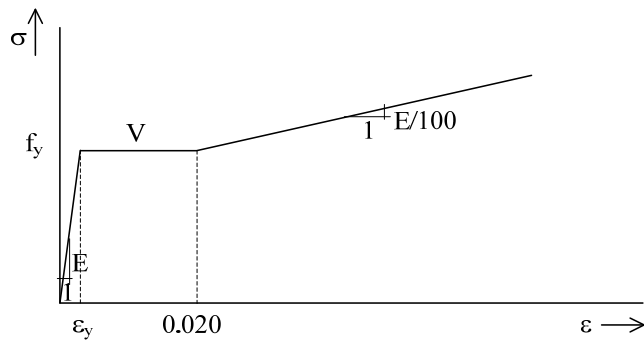


Figure 7-3 Composed Stress-strain relationship V

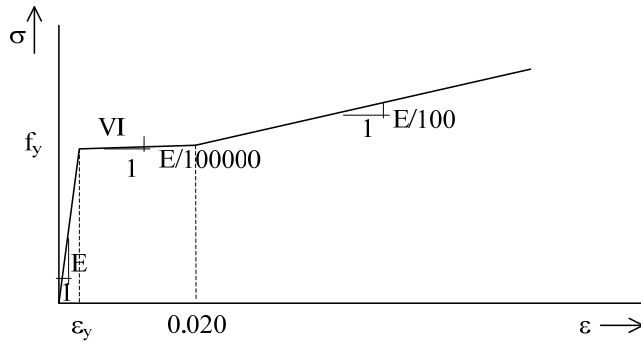


Figure 7-4 Composed Stress-strain relationship VI

The stress-strain relations as presented in Figure 7-2, Figure 7-3 and Figure 7-4 are based on engineering stresses and engineering strains.

The influence of various stress-strain relations on the bending moment resistance M_u is studied by using FEM-models for a reference girder with stress-strain relation III, IV or VI. The stress-strain relation III is very similar to the stress-strain relation II and relation VI is very similar to relation V. The linear elastic stress-strain relation I is not used. The reference girder has the dimensions 1000x2 mm² for the web and 200x10 mm² for the flanges.

The input for the FEM parametric study is divided into a linear part, based on the yield stress f_y and the Young's modulus E and the part after yielding. The input in Msc Marc Mentat 2005r3 for the latter part is the plastic strain ε_p and the ratio between the true stress σ_t and the yield stress f_y . The plastic strain ε_p is determined as follows, see also Chapter 3.2.2:

$$\varepsilon_p = \varepsilon_t - \frac{\sigma_t}{E} \quad (7.3)$$

The input for the true stress σ_t of the FEM-model for this FEM-program is a ratio, determined by the true stress σ_t divided by the yield stress:

$$\frac{\sigma_t}{f_y} \quad (7.4)$$

The FEM results of the models with true stress - true strain relations III, IV and VI are compared with each other. Figure 7-5 shows the input of the stress-strain relations.

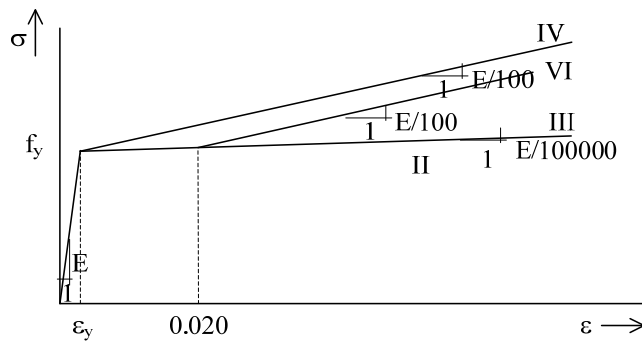


Figure 7-5 Engineering Stress – strain relations for steel grade S235 used as basis for the FEM-models

Table 7-1 and Table 7-2 show the input of the true stress-true strain relations used beyond yielding for steel grades S235 and S460 respectively.

Table 7-1 Input true stress – true strain for FEM program Msc Marc Mentat 2005r3

Pplastic	strain/stress	plastic	strain/stress	plastic	strain/stress
S235 Relationship III		S235 Relationship IV		S235 Relationship VI	
0.000000	1.000000	0.000000	1.000000	0.000000	1.000000
0.013753	1.015126	0.013612	1.140903	0.013753	1.015126
0.018661	1.020172	0.018469	1.192098	0.018661	1.020172
0.023545	1.025219	0.023301	1.243739	0.023494	1.070971
0.028406	1.030266	0.028109	1.295828	0.028303	1.122216
0.033243	1.035313	0.032893	1.348363	0.033088	1.173909
0.038056	1.040361	0.037653	1.401345	0.037849	1.226048
0.042847	1.045410	0.042389	1.454773	0.042586	1.278634
0.047615	1.050459	0.047102	1.508649	0.047300	1.331667
0.052360	1.055508	0.051792	1.562971	0.051991	1.385146
0.057082	1.060558	0.070782	1.790364	0.056659	1.439072
0.059435	1.063083			0.058984	1.466203
0.061782	1.065608			0.061304	1.493446
0.064124	1.068133			0.063618	1.520800
0.066461	1.070659			0.065926	1.548266

Table 7-2 Input true stress – true strain for FEM program Msc Marc Mentat 2005r3

plastic strain/stress S460	plastic strain/stress S460	plastic strain/stress S460	plastic strain/stress S460
Relationship III	Relationship IV	Relationship VI	
0.000000	1.000000	0.000000	1.000000
0.012665	1.015059	0.012535	1.074355
0.017568	1.020083	0.017387	1.102930
0.022447	1.025107	0.022214	1.131734
0.027302	1.030131	0.027016	1.160765
0.032134	1.035155	0.031795	1.190025
0.036942	1.040180	0.036549	1.219513
0.041727	1.045204	0.041280	1.249229
0.046490	1.050229	0.045988	1.279174
0.051229	1.055254	0.050673	1.309347
0.055946	1.060280	0.069641	1.435442
0.058297	1.062793		
0.060641	1.065305		
0.062980	1.067818		
0.065314	1.070331		

The previous Swedish code BSK99 also refers to a composed stress-strain relation. This composed relationship looks like the relationship IV composed by the author, but also shows some differences. While the EN1993-1-5 does not show a maximum strength, the BSK99 does, namely the ultimate stress f_u . Also of interest is the end of the horizontal plateau determined by the strain ε_2 , see Figure 7-6. The slope of the part from yield stress f_y to ultimate stress f_u is different as well, determined by strains ε_2 and ε_3 . The yield strain ε_1 is of course the same as mentioned in EN 1993-1-5. The specific strains ε_1 , ε_2 and ε_3 are determined with:

$$\begin{aligned}
 \varepsilon_1 &= \frac{f_y}{E} \\
 \varepsilon_2 &= 0,025 - 5 \cdot \frac{f_y}{E} \\
 \varepsilon_3 &= 0,02 + 50 \cdot \frac{f_u - f_y}{E}
 \end{aligned} \tag{7.5}$$

For steel grades S235 and S460 these specific strains are shown in Table 7-3.

Table 7-3 Specific strains for S235 and S460 as shown in Figure 7-6

Strain	Steel grade S235	Steel grade S460
ε_1 [-]	0.00112	0.00219
ε_2 [-]	0.01940	0.01405
ε_3 [-]	0.0498	0.04143
f_y [MPa]	235	460
f_u [MPa]	360	550

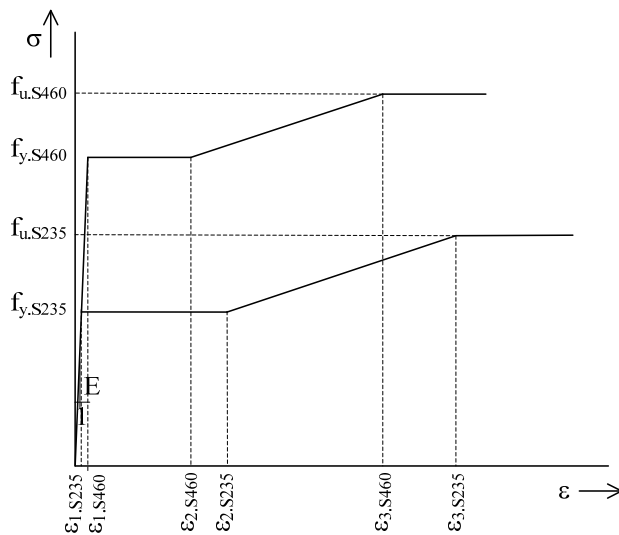


Figure 7-6 Stress-strain diagram according to BSK99 (Swedish code) for S235 and S460

For these three stress-strain relations for steel grades S235 and S460, a limited number of additional FEM-calculations are made to compare the results of the bending moment resistance, see Table 7-4.

Table 7-4 Comparison true stress – true strain relations III, IV and VI for S235 and S460

	S235-III	S235-IV	S235-VI	S460-III	S460-IV	S460-VI
M_u [kNm]	502.30	502.80	502.30	958.21	961.55	958.15

From Table 7-4 it can be seen that the differences in results of the FEM-models with the stress-strain relations III, IV and VI are very small. The smallest difference, for both steel grades, is for relations III and VI and the highest resistance is found for the stress-strain relationship IV. It can be

concluded that the bending moment resistance is reached soon after yielding of the compressive flange, because the various moment resistances are very close to each other.

Based on the results of the FEM-calculations as represented in Table 7-4, it can be concluded that the differences between the stress-strain relationship mentioned in BSK99, the stress-strain relations as given in EN1993-1-5 and the modelled stress-strain relationships will hardly influence the bending moment resistance M_R and so stress-strain relationship III is used for the parametric study.

Geometrical imperfections

The geometrical imperfections used are based on a sine shaped buckling pattern in the length direction with a half sine shape in the transverse direction of the web in the test area. The number of initial buckles depends on the length of the test area. The span ℓ of the FEM-models is constant for the first FEM-calculations in this parametric research, namely 15.0 m, but for very large web slenderness's, the web height h_w increases enormously and the number of initial buckles decreases considerably. A very small number of buckles, less than 3 or 4, influences the results of the FEM-calculations. For this reason, the span ℓ in the next FEM-models is adapted, increased, in such a way that the number of initial buckles in the test panel is always 6.

Additional FEM-calculations were made to look at the influence of the span ℓ on the bending moment resistance M_u . It can be concluded that the bending moment resistance M_u did not change when the span ℓ varied, except, as mentioned, when the number of buckles becomes very small.

The amplitude of the geometrical imperfection is not given in EN1993-1-5, but an equivalent geometrical imperfection is given, which also take the influence of the residual stresses into account.

Material imperfections

The material imperfections, the residual stresses, are taken into account by the equivalent geometrical imperfection. The equivalent geometrical imperfection is, related to the distance a between transverse stiffeners or the height of the web h_w and is according to EN1993-1-5, the smallest of $\frac{h_w}{200}$ and $\frac{a}{200}$. The amplitude of the equivalent geometrical imperfection in this parametric study is always determined by the first requirement $\frac{h_w}{200}$.

7.2 MOST INFLUENTIAL GEOMETRICAL PARAMETER

The first step in this parametric study is to find the independent geometrical parameter that influences the maximum bending moment resistance M_u most. The four independent geometrical parameters are increased by 10% one by one for a reference girder with a web area $1000 \times 2 \text{ mm}^2$ and a flange area $200 \times 10 \text{ mm}^2$.

Table 7-5 shows the bending moment resistances M_u of these four girders, apart from the bending moment resistance relative to the bending moment resistance of the reference girder in terms of a percentage. The increase of the web height h_w , but also the increase of the dimensions of the flange, the width b and the thickness t_f , one by one by 10 %, result in an increase of the bending moment resistance M_u to respectively 109.8%, 109.4% and 109.3% relative to the bending moment resistance M_u of the reference girder. The relative increase of the bending moment resistance M_u of the girder in which the web thickness t_w increased 10% is rather small, 101.5%,

Because of the increase of one of the dimensions of the cross-section of the reference girder, the cross-sectional area A_{tot} increases as well. The increase relative to the total area of the reference girder, is presented in terms of percentage as well, see the 3rd row in Table 7-5. It can be seen that the increase of the dimensions of the web gives a rather small relative increase of the total area, namely to 103.3% and for the increase of the dimensions of the flanges it is 106.7%. The cross-sectional area of the girders with increasing flange dimensions increases much more than the cross-sectional area of the girders with increasing web dimensions, simply because there are two flanges and there is one web only.

It is of interest to compare the increase in relative bending moment resistance, relative to the relative increase of total area A_{tot} , called Q , as follows:

$$Q = \frac{\text{Relative increase in bending moment resistance} \cdot 100\%}{\text{Relative increase in cross sectional area}} \cdot 100\% =$$

$$= \frac{\frac{M_{+10\%}}{M_{ref}} \cdot 100\%}{\frac{A_{tot,+10\%}}{A_{tot.ref}} \cdot 100\%} \cdot 100\% \quad (7.6)$$

For example, the relative increase for the girder with an increased web height to $h_w = 1100 \text{ mm}$ is shown:

$$Q = \frac{\frac{M_{+10\%}}{M_{ref}} \cdot 100\%}{\frac{A_{tot.+10\%}}{A_{tot.ref}} \cdot 100\%} \cdot 100\% = \frac{\frac{551.3}{502.3} \cdot 100\%}{\frac{6200}{6000} \cdot 100\%} \cdot 100\% = \frac{109.8\%}{103.3\%} \cdot 100\% = 106.2\% \quad (7.7)$$

Table 7-5 shows the relative increase Q in terms of percentage.

Table 7-5 Comparison of the bending moment resistances of the FEM-models with an increased independent geometrical parameter with the reference girder with S235

	Reference	$h_w + 10\%$	$t_w + 10\%$	$b + 10\%$	$t_f + 10\%$
M_R [kNm]	502.3	551.3	509.9	549.4	549.2
Relative resistance [%]	100.0	109.8	101.5	109.4	109.3
Relative area [%]	100.0	103.3	103.3	106.7	106.7
Q [%]	100.0	106.2	98.2	102.5	102.5

The bending moment resistance M_u of the girder with a 10% thicker web thickness t_w increases to only 101.5% of the bending moment resistance M_u of the reference girder. Besides, the cross-sectional area increases to 103.3% relative to the cross-sectional area of the reference girder and so there is a relative decrease of 98.2%. The relative increase of the bending moment resistance is smaller than the relative increase of the cross-sectional area.

The bending moment resistance M_u is the most sensitive to an increase of the web height h_w . An increase of the web height of 10% leads to a relative increase of the bending moment resistance of $Q = 106.2\%$. Based on these results, the parametric study was started with the increase of the most influencing parameter on the bending moment resistance, being the height of the web h_w . Further, it appears from Table 7-5 that, contrary to the results for the girder with a 10% increased web thickness, it can be seen that the web thickness should be as low as possible. This means that the web slenderness β_w should be as large as possible. There are three possibilities to increase the web slenderness β_w , namely:

1. Increase the height of the web h_w and keep all other dimensions constant;
2. Decrease the thickness of the web t_w and keep all other dimensions constant;

3. Increase the height of the web h_w and at the same time decrease the thickness of the web t_w .

These possibilities to increase the web slenderness β_w will change the cross-sectional area A_{tot} too. For the parametric research, different approaches are used and for only one approach the cross-sectional area is not constant. The strategies in the three approaches are as follows:

- a. Approach 1. Vary the web height h_w and all other dimensions are kept constant. As a consequence, the total area A_{tot} of the cross-section varies as well;
- b. Approach 2. Vary the web height h_w while the web area A_w and both flange dimensions are kept constant. The ratio of area is taken as $\rho = 1.0$, $\rho = 2.0$ and $\rho = 3.0$. The values for the ratio of area ρ are based on the ratios as mentioned by Basler, see Chapter 2.4.3, on the ratios of areas as found in the elaborations on the bending moment resistance $M_{Veljkovic}$ according to Veljkovic and Johansson, see Chapter 2.7.6, and on the Delft experiments, see Chapter 4.2. The Approaches are called Approach 2 with $\rho = 1.0$, Approach 2 with $\rho = 2.0$ and Approach 2 with $\rho = 3.0$ related to the ratio of area ρ used;
- c. Approach 3. Vary the web height h_w while the web thickness t_w and the total area A_{tot} are kept constant and thus the web area A_w and the flange area A_f interchange material and so the ratio of the area ρ varies as well.

Based on the dimensions of the reference cross-section with a web area of $1000 \times 2 \text{ mm}^2$ and a flange area of $200 \times 10 \text{ mm}^2$, the cross-sectional area is 6000 mm^2 . The ratio of area varies $\frac{1}{2} \leq \rho \leq 4$ based on the Basler recommendations $\frac{1}{2} \leq \rho \leq 2$ and the results of the Delft experiments $1 \leq \rho \leq 4$.

The elaborations of the literature study, see Chapter 2.7, show that according to Veljkovic and Johansson a ratio of area of around $\rho = 1.0$ gives the maximum bending moment resistance M_u and so the distribution of the material over the web and flanges is $A_w = A_f = 2000 \text{ mm}^2$. The parametric study starts with a slenderness $\beta_w = 150$ and is increased up to the maximum web slenderness $\beta_{w,max}$ which is determined by using FEM-models. The Delft experiments proved that a web slenderness $\beta_w = 800$ is possible.

The flange slenderness is based on a maximum slenderness of section class 3 under pure compression, so $\frac{c}{t_f} \approx \frac{b}{2 \cdot t_f} \leq 14\epsilon$. More slender flanges do not have any use because the effective width will be located around the connection of the flange with the web. This means that the edges of such a slender flange are not effective and it is useless to make flanges wider than effective. Because of the effect of the steel grade on the maximum slenderness, the flange slenderness is assumed to be 10 for all girders.

7.3 PARAMETRIC STUDY BASED ON FEM-MODELS

7.3.1 APPROACH 1: CONSTANT A_f AND T_w , VARYING A_{tot} , A_w AND H_w

In Approach 1, the area of the flanges is constant, $A_f = 2000 \text{ mm}^2$, and the web thickness is also constant, $t_w = 2 \text{ mm}$. The web height h_w varies with steps of 100 or 200 mm starting from a web height of $h_w = 300 \text{ mm}$, corresponding to a web slenderness of $\beta_w = 150$. This means that the web area A_w and thus the total area A_{tot} vary for varying web slenderness's β_w .

Figure 7-7 shows the graph of the bending moment resistance M_u versus the web slenderness β_w for steel grade S235. The left-hand side vertical axis presents the bending moment resistance M_u and the horizontal axis shows the web slenderness β_w . The right-hand side vertical axis shows the ratio of the areas ρ .

The bending moment resistance M_u according to the FEM-calculations is compared with specific theoretical bending moment resistances, the plastic bending moment resistance M_{pl} , the elastic bending moment resistance M_{el} , the effective bending moment resistance M_{eff} based on yielding of one of the flanges and the bending moment resistance based on the cross-section consisting of only the flanges M_f . Apart from these resistances, Figure 7-7 shows the bending moment resistances based on the model of Veljkovic $M_{Veljkovic}$ as shown in Chapter 2.7.6 and the model based on Abspoel $M_{Abspoel}$ as shown in Chapter 7.1.

The dashed black line represents the ratio of area ρ related to the vertical axis at the right-hand side of the graph in Figure 7-7.

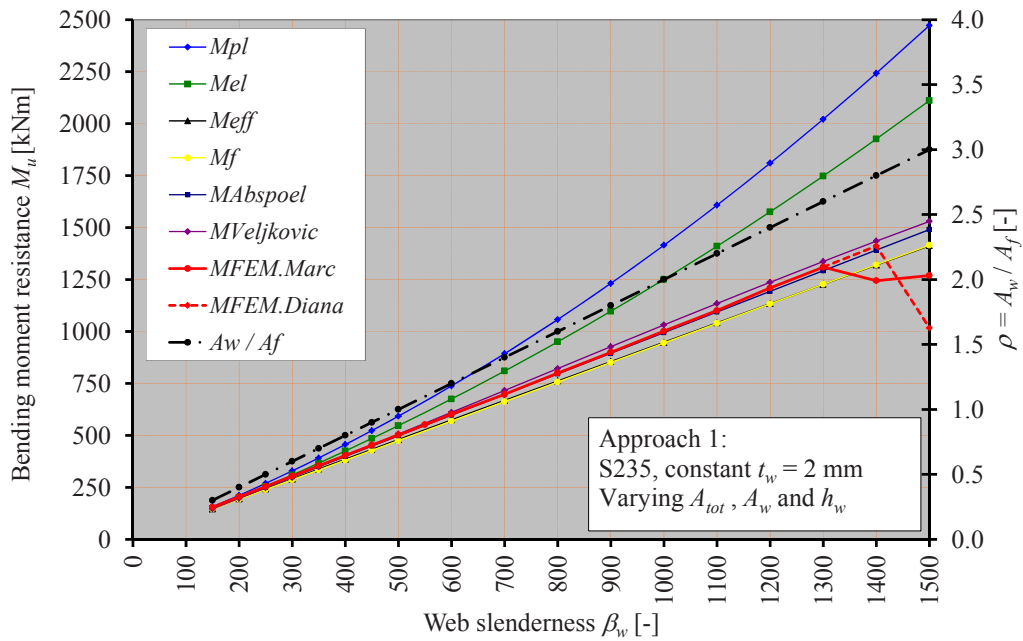


Figure 7-7 Bending moment resistance M_u according to Approach 1 for S235

A linear relationship is found for the bending moment resistance M_R according to the FEM-calculations and the web slenderness β_w , see the red line in the graph in Figure 7-7. This linear relationship is up to a web slenderness $\beta_w = 1300$. To be sure this limit is not based on numerical instability of the FEM-model, a cross-verification of FE-software is performed by doing additional calculations with another FEM program, namely Diana.

Girders with a slenderness of $\beta_w = 600$ and $\beta_w = 1300$ were calculated again and the Diana-results were compared with those of Msc Marc Mentat 2005r3. The results are the same within small margins, less than 0.5% differences. After this first validation, the girder with a web slenderness of $\beta_w = 1400$ was calculated with Diana. The result of the bending moment resistance M_u was positioned on the linear relationship as well. The bending moment resistance M_u of another girder, one with a web slenderness of $\beta_w = 1500$, is no longer linearly related, see the dotted red line in Figure 7-7.

This means that the maximum web slenderness is $\beta_w = 1400$, an incredible slenderness compared with a web slenderness of $\beta_w = 800$ as mentioned in literature and an incredible slenderness compared with current practice of web slenderness's of about $\beta_w = 350$.

For steel grade S460, similar calculations are made and the results are presented in Figure 7-8. With the Diana FEM-program, the same kind of calculations are made for web slenderness's $\beta_w = 500$ and $\beta_w = 1000$ and the same results were found as with Msc Marc Mentat 2005r3. The maximum web slenderness β_w for steel grade S460 was smaller than for steel grade S235, as expected. The maximum bending moment resistances M_u based on the FEM-results for both steel grades are very close to the bending moment resistance $M_{Veljkovic}$ based on Veljkovic and Johansson [74], but also to the suggestion by the author of this thesis, $M_{Abspoel}$, with the difference that the bending moment resistance based on Veljkovic and Johansson is slightly larger than the bending moment resistance $M_{Abspoel}$ and the bending moment resistance based on the FEM-calculations. The resistance $M_{Abspoel}$ based on Abspoel is closer to the results of the FEM.

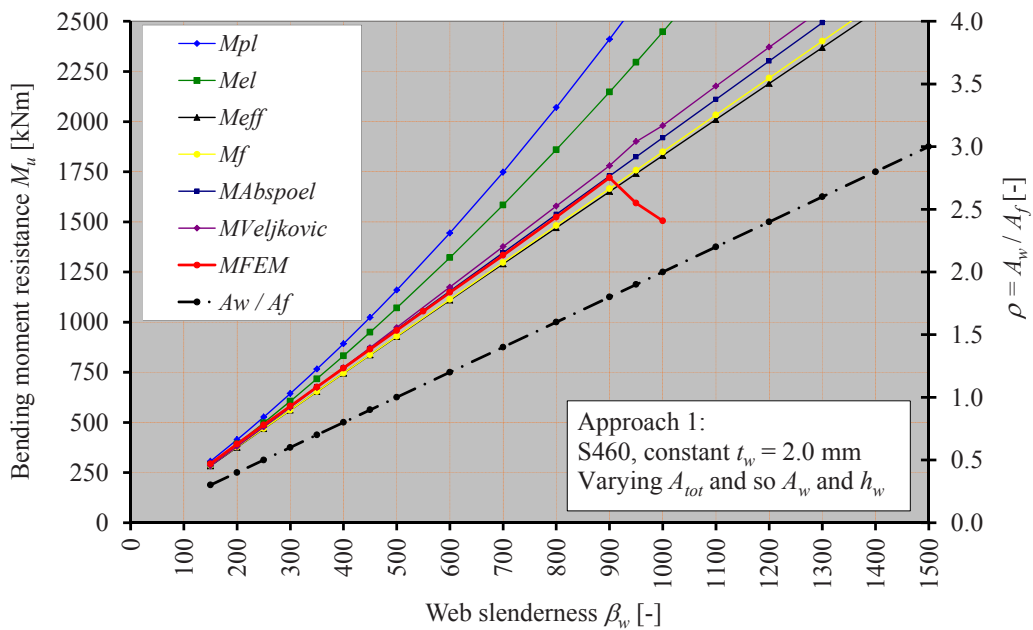


Figure 7-8 Bending moment resistance M_u according to Approach 1 for S460

7.3.2 APPROACH 2: CONSTANT A_{tot} , A_w AND A_f , VARYING H_w AND T_w

In Approach 2, the web height h_w is varied, but A_w is kept constant and so the web thickness t_w has to be varied as well. The total area A_{tot} and the flange area A_f are also kept constant. This means that the web slenderness β_w varies much faster than in Approach 1. The ratio of area ρ is also constant during varying of the web height h_w and web thickness t_w , but this approach is applied for a ratio of area equal to 1, 2 and 3. For a specific total area of the cross-section A_{tot} , for a specific web slenderness β_w and for a specific ratio of area ρ , the web dimensions h_w and t_w can be determined after determination of the web area A_w :

$$\rho = \frac{A_w}{A_f} \Rightarrow A_w = \rho \cdot A_f$$

$$A_{tot} = A_w + 2A_f = (\rho + 2) A_f \Rightarrow A_f = \frac{A_{tot}}{\rho + 2} \quad (7.8)$$

$$\Rightarrow A_w = A_{tot} - 2A_f = A_{tot} - \frac{2A_{tot}}{\rho + 2} = \frac{\rho}{\rho + 2} \cdot A_{tot} \quad (7.9)$$

The web dimensions are based on the web area A_w and a specific value for the web slenderness β_w :

$$\beta_w = \frac{h_w}{t_w} \Rightarrow A_w = \beta_w \cdot t_w^2$$

$$\Rightarrow t_w = \sqrt{\frac{A_w}{\beta_w}} = \sqrt{\frac{\rho}{\rho + 2}} \cdot \sqrt{\frac{1}{\beta_w}} \cdot \sqrt{A_{tot}} \quad (7.10)$$

$$\Rightarrow h_w = \beta_w \cdot t_w = \sqrt{\frac{\rho}{\rho + 2}} \cdot \sqrt{\beta_w} \cdot \sqrt{A_{tot}} \quad (7.11)$$

For the fixed flange slenderness $\frac{b}{2 \cdot t_f} = 10$, which is equal to $\beta_f = \frac{b}{t_f} = 20$, the flange dimensions can be determined as well:

$$A_f = \beta_f \cdot t_f^2 = \frac{A_{tot}}{\rho + 2}$$

$$\Rightarrow t_f = \sqrt{\frac{1}{\rho + 2}} \cdot \sqrt{\frac{1}{\beta_f}} \cdot \sqrt{A_{tot}} \quad (7.12)$$

$$\Rightarrow b = \sqrt{\frac{1}{\rho+2}} \cdot \sqrt{\beta_f} \cdot \sqrt{A_{tot}} \quad (7.13)$$

The web area is $A_w = 2000 \text{ mm}^2$ for $\rho = 1$, $A_w = 1500 \text{ mm}^2$ for $\rho = 2$ and $A_w = 1200 \text{ mm}^2$ for $\rho = 3$.
The flange areas are $A_f = 2000 \text{ mm}^2$ for $\rho = 1$, $A_f = 2250 \text{ mm}^2$ for $\rho = 2$ and $A_f = 2400 \text{ mm}^2$ for $\rho = 3$.

Figure 7-9 shows the bending moment resistances M_u for Approach 2 with $\rho = 1$ for steel grade S235 and Figure 7-10 for steel grade S460.

Figure 7-11 presents the bending moment resistances M_u according to Approach 2 with $\rho = 2$ for steel grade S235 and Figure 7-12 for steel grade S460.

Figure 7-13 and Figure 7-13 show the bending moment resistance M_u according to Approach 2 with $\rho = 3$ for respectively steel grade S235 and S460.

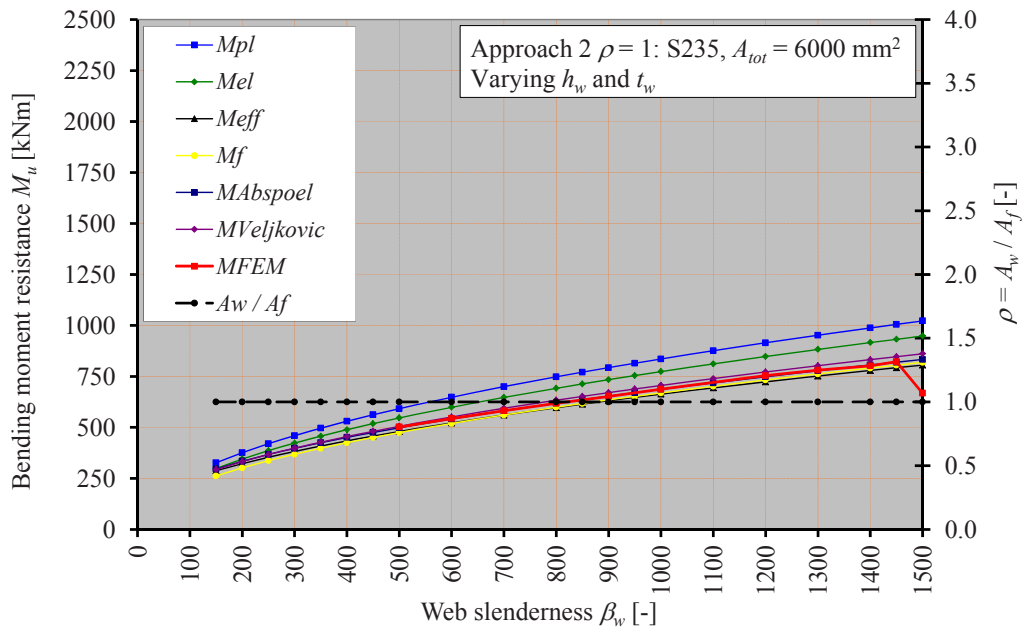


Figure 7-9 Bending moment resistance M_u according to Approach 2 with $\rho = 1.0$ for S235

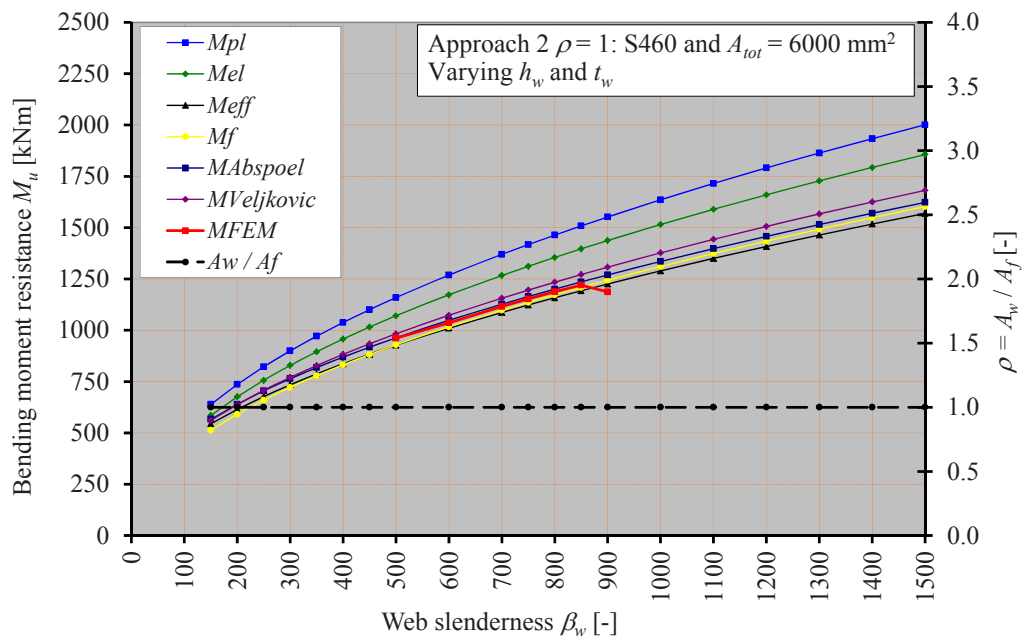


Figure 7-10 Bending moment resistance M_u according to Approach 2 with $\rho = 1.0$ for S460

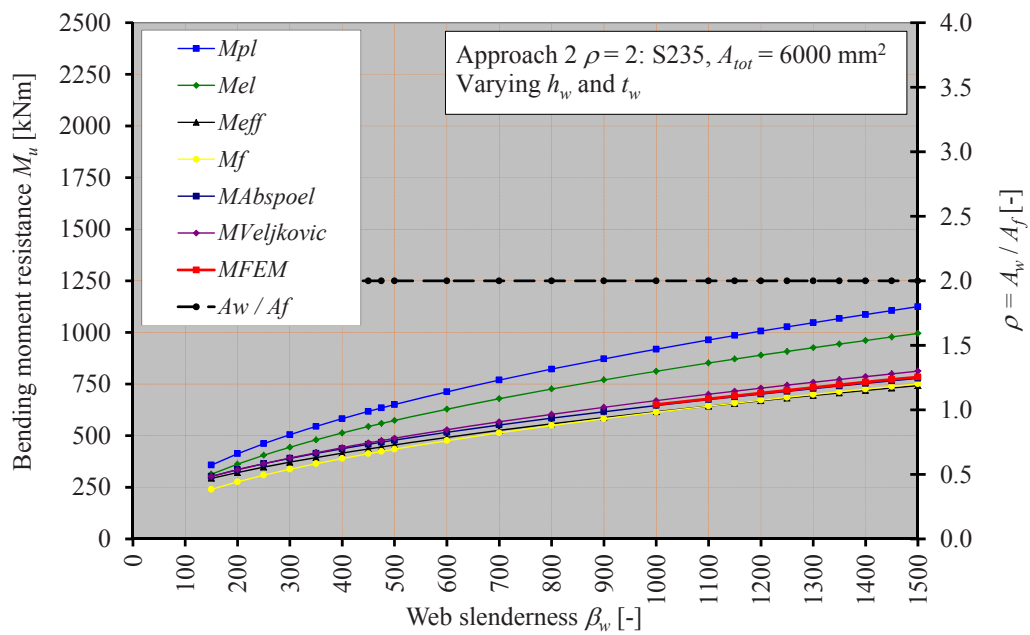


Figure 7-11 Bending moment resistance M_u according to Approach 2 with $\rho = 2.0$ for S235

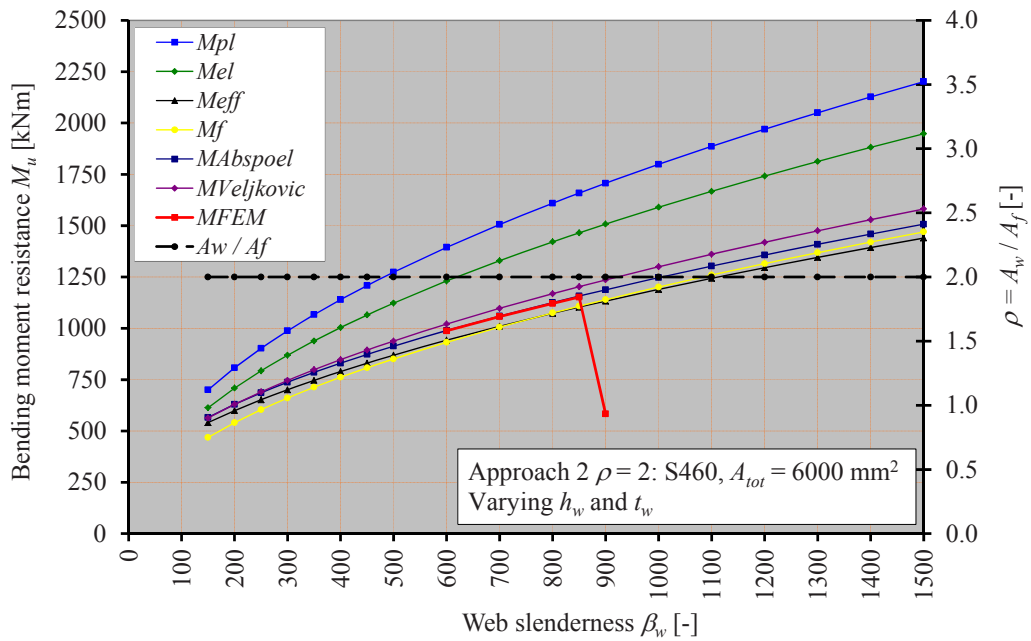


Figure 7-12 Bending moment resistance M_u according to Approach 2 with $\rho = 2.0$ for S460

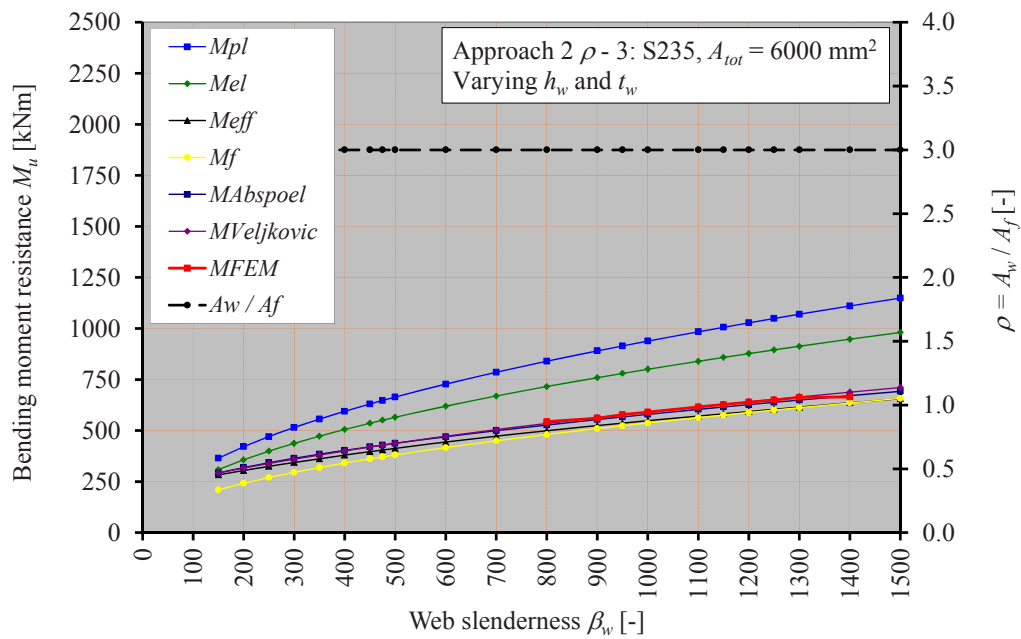


Figure 7-13 Bending moment resistance M_u according to Approach 2 with $\rho = 3.0$ for S235

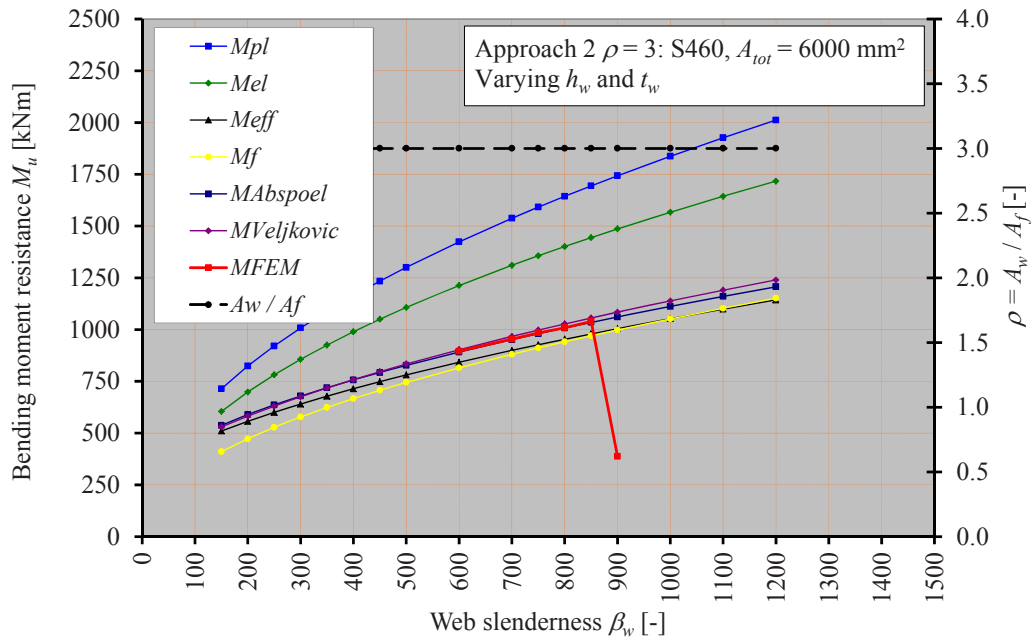


Figure 7-14 Bending moment resistance according to Approach 2 with and $\rho = 3.0$ for S460

The maximum bending moment resistance $M_u = 822 \text{ kNm}$ for steel grade S235 is found for a ratio of area $\rho = 1.0$ and a web slenderness $\beta_w = 1450$.

The maximum bending moment resistance $M_u = 1220 \text{ kNm}$ for steel grade S460 is found for a ratio of area $\rho = 1.0$ and a web slenderness $\beta_w = 850$.

7.3.3 APPROACH 3: CONSTANT A_{TOT} AND T_w AND , VARYING A_w , A_f AND H_w

In Approach 3, the web thickness t_w is kept constant, while the web slenderness β_w increases due to the increasing web height h_w . The total cross-sectional area A_{tot} is also kept constant and thus the flange area A_f has to decrease. The web height h_w can be determined for a specific total area A_{tot} , web slenderness β_w and web thickness t_w and thus the web area A_w and the flange area A_f .

$$\beta_w = \frac{h_w}{t_w} \quad \Rightarrow h_w = \beta_w \cdot t_w \quad \Rightarrow A_w = h_w \cdot t_w = \beta_w \cdot t_w^2$$

$$A_f = \frac{A_{tot} - A_w}{2} = \frac{A_{tot} - \beta_w \cdot t_w^2}{2} \quad (7.14)$$

For the constant flange slenderness $\beta_f = \frac{b}{t_f} = 20$ the flange dimensions can also be determined:

$$t_f = \sqrt{\frac{A_{tot} - A_w}{2 \cdot \beta_f}} = \sqrt{\frac{A_{tot} - \beta_w \cdot t_w^2}{40}} \quad (7.15)$$

$$b = \beta_f \cdot \sqrt{\frac{A_{tot} - A_w}{2 \cdot \beta_f}} = \sqrt{\frac{\beta_f}{2} \cdot (A_{tot} - \beta_w \cdot t_w^2)} \quad (7.16)$$

The bending moment resistances M_u for S235 as a results of the FEM-calculations are presented in Figure 7-15 and for S460 in Figure 7-16.

A top was found about $\beta_w = 750$ for both steel grades S235 and S460. While M_{pl} and M_{el} constantly increase, other theoretical resistances, such as the effective bending moment resistance M_{eff} and the moment of resistance M_f of the cross-section consisting of the flanges only, decrease. The theoretical resistances are strongly related to the product of $A_f \cdot f_y \cdot h_w$ and the decrease of the bending moment resistance M_u means that this product $A_f \cdot f_y$ decreases more than h_w increases.

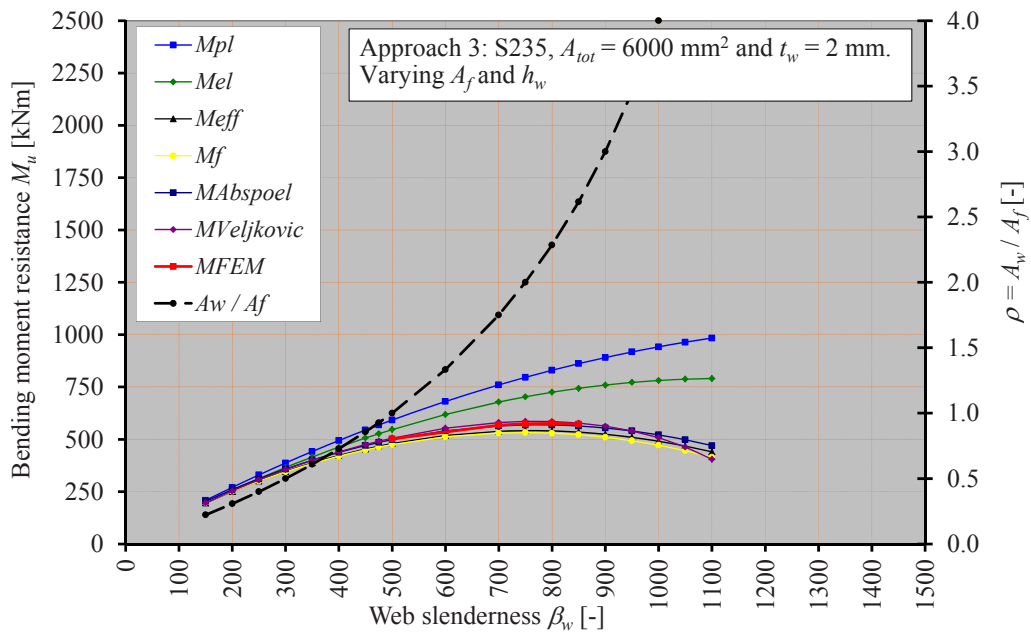


Figure 7-15 Bending moment resistance M_u according to Approach 3 with $t_w = 2.0$ mm for S235

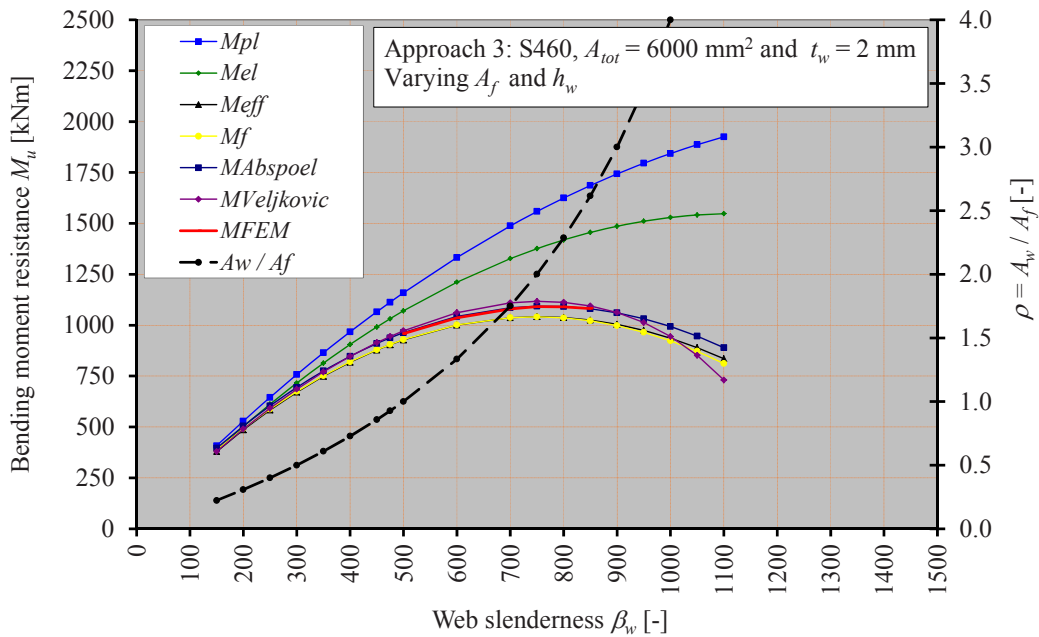


Figure 7-16 Bending moment resistance M_u according to Approach 3 with $t_w = 2.0 \text{ mm}$ for S460

Figure 7-15 and Figure 7-16 show a top for the bending moment resistance M_u for the specific web thickness $t_w = 2 \text{ mm}$ both for steel grade S235 and for S460. The bending moment resistances M_u for test girders with other web thicknesses t_w have to be determined. Because the bending moment resistance based on the simplified effective width method according to Abspoel $M_{Abspoel}$ fits with the bending moment resistance M_{FEM} very well, additional graphs are constructed for other web thicknesses, but now only for the tops of the graphs as shown in Figure 7-15 and Figure 7-16 for steel grades S235 and S460. The tops for each web thickness t_w are determined by using the application Solver of the spreadsheet program Excel to determine the maximum bending moment resistance $M_{Abspoel}$ for a specific total cross-sectional area A_{tot} by varying the web slenderness β_w . The dimensions are determined and the effective width of the web is determined based on EN1993-1-5. Figure 7-17 shows the bending moment resistances $M_{Abspoel}$ for S235 and web thicknesses varying from $t_w = 1.0 \text{ mm}$ up to $t_w = 3.0 \text{ mm}$ and Figure 7-18 presents such curves for S460. The vertical scales of both graphs are different.

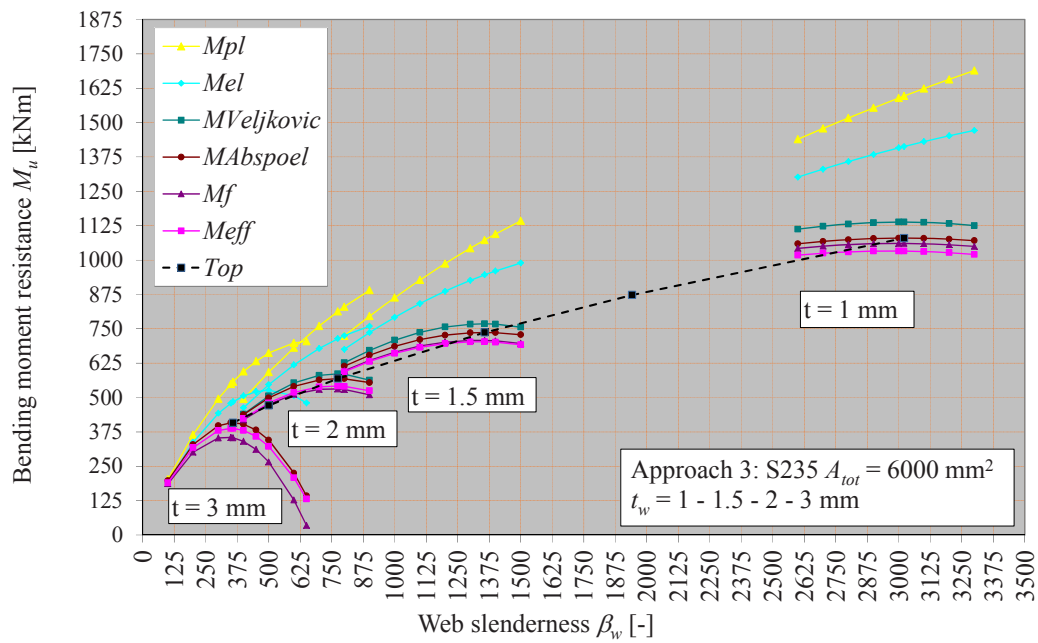


Figure 7-17 Bending moment resistance $M_{Abspoel}$ according to Approach 3 for S235

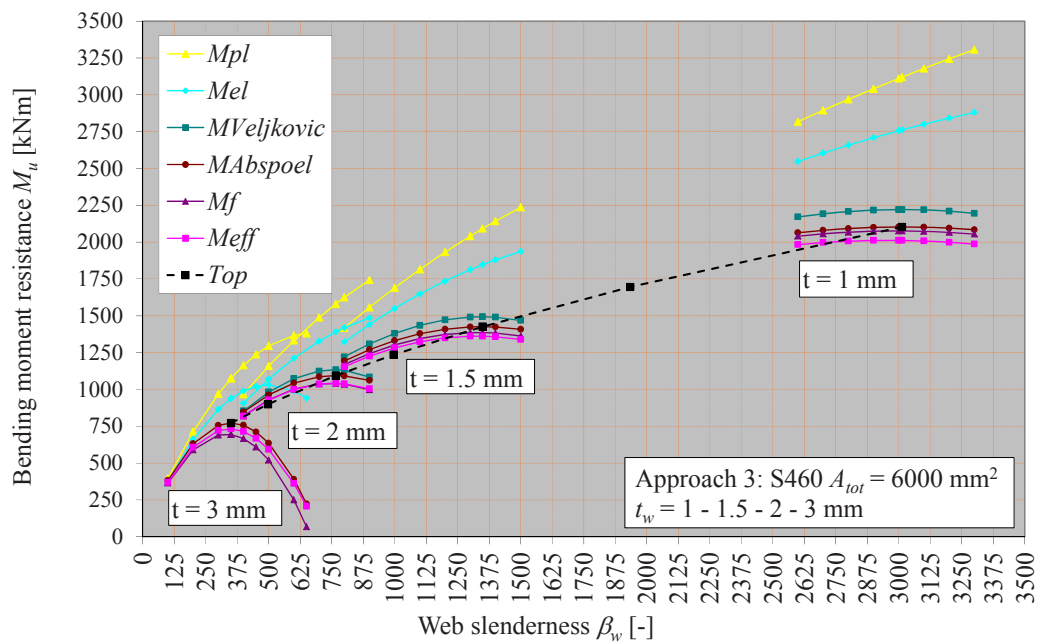


Figure 7-18 Bending moment resistance $M_{Abspoel}$ according to Approach 3 for S460

The top of each curve for a specific web thickness t_w can be connected, see the black dotted line in Figure 7-17 for steel grade S235 and in Figure 7-18 for S460. Table 7-6 shows the bending moment resistances $M_{Abspoel}$, the corresponding web slenderness β_w and the ratio of area ρ .

Table 7-6 Approach 3: bending moment resistance M_u for steel grade S235 and S460

S235				S460			
t_w	$M_{Abspoel}$	$\beta_{w,max}$	$\rho = A_w / A_f$	t_w	$M_{Abspoel}$	$\beta_{w,max}$	$\rho = A_w / A_f$
[mm]	[kNm]	[-]	[-]	[mm]	[kNm]	[-]	[-]
1.5	736.58	1356.5	2.07	1.5	1426.0	1348.7	2.05
1.6	694.2	1195.3	2.08	1.6	1342.4	1187.5	2.05
1.7	657.1	1061.8	2.09	1.7	1268.8	1053.9	2.06
1.8	624.3	949.8	2.11	1.8	1203.7	942.0	2.07
1.9	595.1	855.1	2.12	1.9	1145.6	847.3	2.08
2.0	569.0	774.3	2.07	2.0	1093.6	766.4	2.09

The ratio of area ρ is between 2.0 and 2.1 for steel grade S235 as well as S460. Figure 7-15 shows the top at $\beta_w = 750$ for $t_w = 2.0 \text{ mm}$ for steel grade S235, due to limited number of FEM-models used. The exact maximum web slenderness is $\beta_w = 774.3$, based on the simplified effective width method according to Abspoel. Figure 7-16 shows the top at $\beta_w = 750$ for steel grade S460 and the exact maximum web slenderness is $\beta_w = 766.4$, based on the simplified effective width method according to Abspoel. From Table 7-6 it can be seen that the smaller the web thickness t_w , the larger the maximum bending moment resistance $M_{Abspoel}$ in accordance with the simplified effective width method according to Abspoel. The corresponding girders based on the tops of these curves are simulated in FEM-models. The red line in Figure 7-19 represents the bending moment resistances M_u of these FEM-models. The maximum bending moment resistance for steel grade S235 is $M_u = 699 \text{ kNm}$ and the corresponding maximum web slenderness $\beta_w = 1195$. Figure 7-20 presents the bending moment resistances M_u for steel grade S460. The maximum bending moment resistance is $M_u = 1199 \text{ kNm}$ and the corresponding web slenderness $\beta_w = 942$.

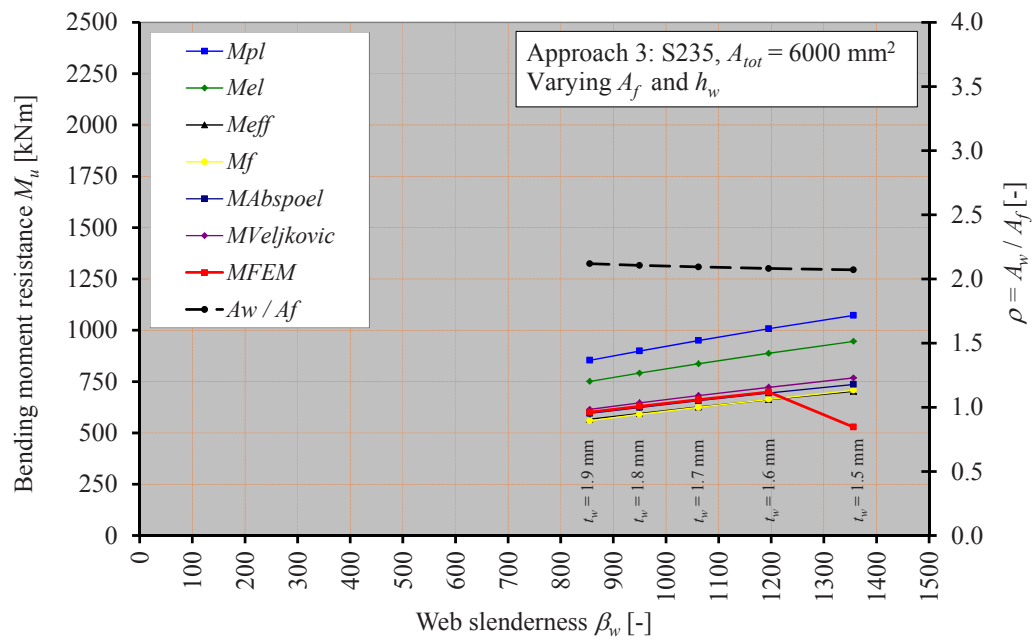


Figure 7-19 Bending moment resistance M_u according to Approach 3 for S235

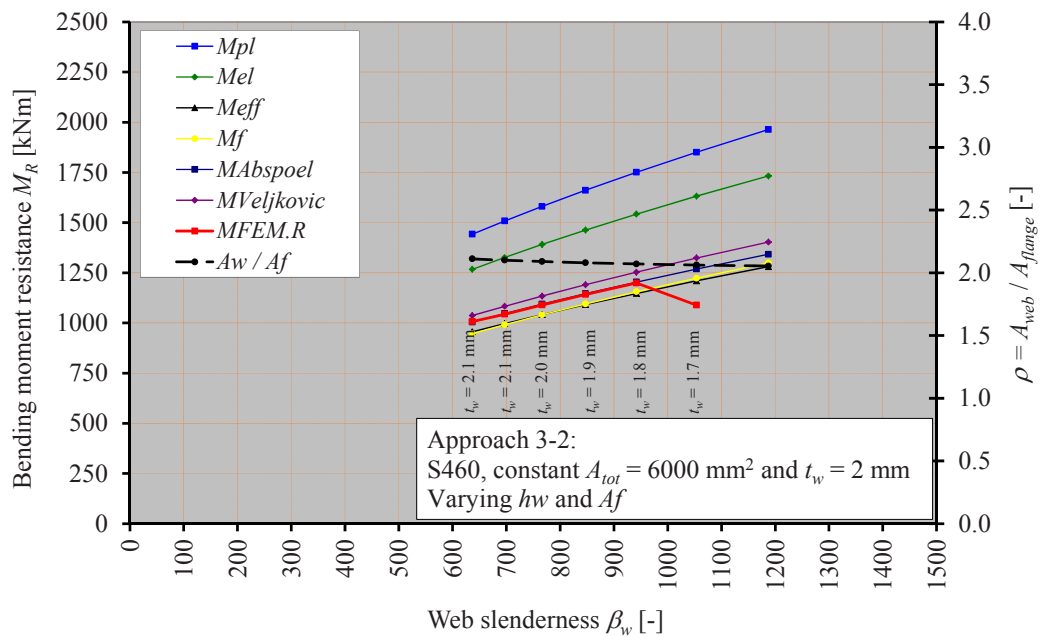


Figure 7-20 Bending moment resistance M_u according to Approach 3 for S460

7.3.4 COMPARISON OF THE RESULTS OF THE APPROACHES USED

The results of all approaches for steel grade S235 are presented in Figure 7-21 and for steel grade S460 in Figure 7-22. The results of Approach 1 can not be compared with the results of the other approaches because the cross-sectional area A_{tot} is not constant and it is clear that larger cross-sectional areas A_{tot} give higher bending moment resistances M_u . The bending moment resistances M_u of Approaches 2 and 3 can be compared with each other and for both steel grades it is concluded that Approach 2 with $\rho = 1.0$ results in the largest bending moment resistance M_u for all web slenderness's up to $\beta_w = 1500$.

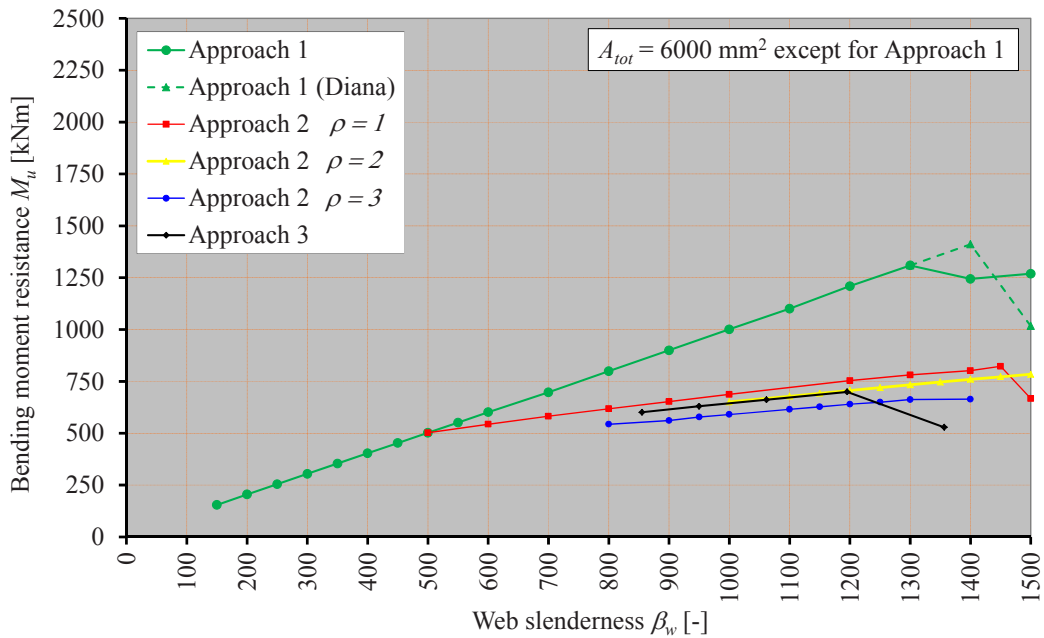


Figure 7-21 Comparison of the bending moment resistances M_u determined by FEM per approach for S235

The only value of M_u , determined with Approach 1 which is comparable to the values of M_u determined with the other approaches, is the one where $A_{tot} = 6000 \text{ mm}^2$. This is where $\beta_w = 500$, the so called reference plate girder. From Figure 7-21 and Figure 7-22 it can be seen that the bending moment resistance M_u of this reference girder with a web slenderness $\beta_w = 500$ is much smaller

than the maximum bending moment resistance M_u according to Approach 2 with $\rho=1.0$ and $\beta_w=1450$ for steel grade S235 and with $\beta_w=850$ for steel grade for S460.

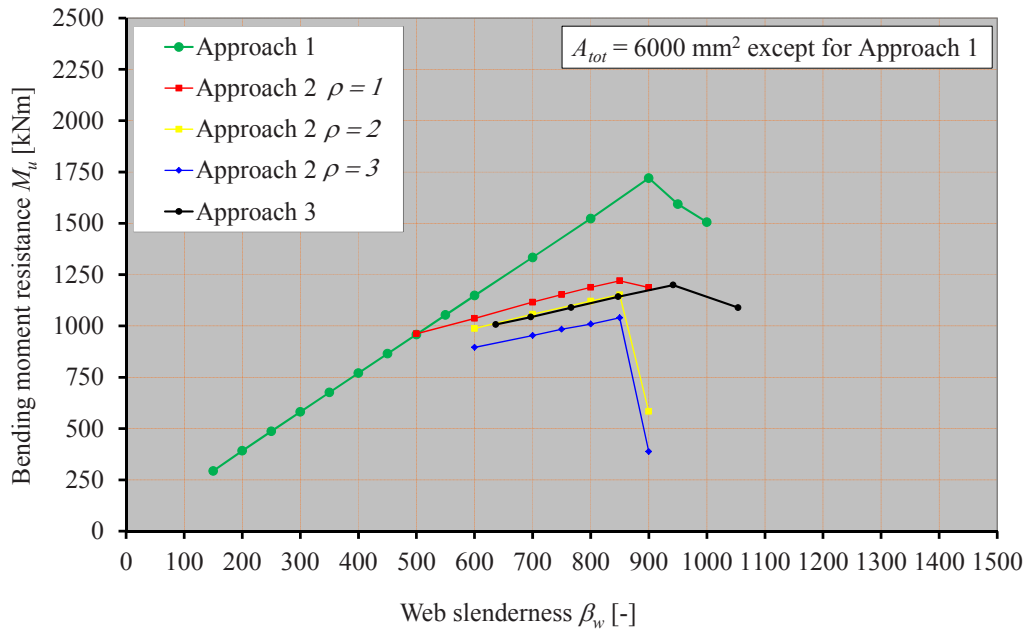


Figure 7-22 Comparison of the bending moment resistances M_u determined by FEM per approach for S460

One of the aims of this research is to find the maximum bending moment resistance M_u for a plate girder with a certain amount of steel. Because the cross-sectional area A_{tot} of the girders using Approach 1 and Approach 2 with $\rho=1.0$ are not the same, except for the girder with $\beta_w=500$, the efficiency value η is introduced. This efficiency value η is defined as the bending moment resistance M_u of a cross-section divided by the weight of that cross-section per unit length, see Eq.(7.17).

$$\eta = \frac{M_u}{\rho_{steel} \cdot A_{tot} \cdot 1} \quad (7.17)$$

where ρ_{steel} is the density of steel. Using Approach 1 for steel grade S235, the maximum bending moment resistance is $M_u=1411.2 \text{ kNm}$ and the cross-sectional area is $A_{tot}=9600 \text{ mm}^2$. The with-

going efficiency value is $\eta = \frac{1411.1}{7850 \cdot 9600 \cdot 10^{-6} \cdot 1} = 18.7 \text{ kNm/kg}$. For this cross-section the ratio of area is $\rho = 2.8$. Using Approach 2 with $\rho = 1.0$ the maximum bending moment resistance is $M_u = 822.4 \text{ kNm}$. In this case the cross-sectional area is $A_{tot} = 6000 \text{ mm}^2$ and so the efficiency value is $\eta = \frac{822.4}{7850 \cdot 6000 \cdot 10^{-6} \cdot 1} = 17.5 \text{ kNm/kg}$. Thus, apart from a larger bending moment resistance M_u , a larger efficiency value η is found when Approach 1 is used.

Using Approach 1 for steel grade S460, the maximum bending moment resistance is $M_u = 1720.0 \text{ kNm}$ and the cross-sectional area is $A_{tot} = 7600 \text{ mm}^2$. The withgoing efficiency value is $\eta = \frac{1720.0}{7850 \cdot 7600 \cdot 10^{-6} \cdot 1} = 28.8 \text{ kNm/kg}$. For this cross-section, the ratio of area is $\rho = 1.8$. Using Approach 2 with $\rho = 1.0$ the maximum bending moment resistance is $M_u = 1220.3 \text{ kNm}$. In this case the cross-sectional area is constant $A_{tot} = 6000 \text{ mm}^2$ and so the efficiency value is $\eta = \frac{1220.3}{7850 \cdot 6000 \cdot 10^{-6} \cdot 1} = 25.9 \text{ kNm/kg}$. Thus, besides a larger bending moment resistance M_u a greater efficiency value η is found when Approach 1 is used. Using Approach 2 with either $\rho = 2$ or $\rho = 3$ leads to lower maximum bending moment resistances M_u and lower efficiency values η compared with using Approach 2 with $\rho = 1$, see Table 7-7 and Table 7-8.

Table 7-7 Bending moment resistances $M_u = M_{FEM}$ for steel grade S235

Approach	M_u	$M_{Abspoel}$	β_w	ρ	η	$h_w \cdot t_w + b \cdot t_f$
	[kNm]	[kNm]	[-]	[-]	[kNm/kg]	[mm x mm + mm x mm]
Approach 1	1411.2	1391.3	1400	2.8	18.7	2800x2+200x10
Approach 2; $\rho = 1$	822.4	819.9	1450	1.00	17.5	1702.9x1.17+200x10
Approach 2; $\rho = 2$	810.1	801.2	1600	2.00	17.2	2190.9x1.37+173.2x8.66
Approach 2; $\rho = 3$	664.3	688.4	1400	3.00	14.1	2.245,0x1.60+154.92x7.75
Approach 3	699.3	694.2	1195	2.08	14.8	1912.6x1.60+171.5x8.57

Table 7-8 Bending moment resistance $M_u = M_{FEM}$ for steel grade S460

Approach	M_u	$M_{Abspoel}$	β_w	ρ	η	$h_w \cdot t_w + b \cdot t_f$
	[kNm]	[kNm]	[-]	[-]	[kNm/kg]	[mm x mm + mm x mm]
Approach 1	1720.0	1728.3	900	1.80	28.8	1800x2+200x10
Approach 2; $\rho = 1$	1220.3	1235.6	850	1.00	25.9	1303.8x1.53+200x10
Approach 2; $\rho = 2$	1151.8	1157.1	850	2.00	24.5	1549.19x1.94+173.21x8.66
Approach 2; $\rho = 3$	1039.9	1034.6	850	3.00	22.1	1749.3x2.06+154.92x7.75
Approach 3	1199.2	1203.7	942	2.07	25.5	1791.66x1.70+171.88x8.59

From the graphs as shown in Figure 7-21 and Figure 7-22 as well as from Table 7-7 and Table 7-8 it can be seen that the maximum bending moment resistance M_u and the largest efficiency value η are found using Approach 1.

It can be questioned whether the maximum bending moment resistances for the maximum web slenderness $\beta_{w,max} = 1400$ for steel grade S235 and $\beta_{w,max} = 900$ for steel grade S460, both determined by using Approach 1, are really the maximum bending moment resistance for the cross-sectional area $A_{tot} = 9600 \text{ mm}^2$ for steel grade S235 and for $A_{tot} = 7600 \text{ mm}^2$ for steel grade S460?

To answer this question for S235, starting with a cross-sectional area $A_{tot} = 9600 \text{ mm}^2$ and for S460, starting with a cross-sectional area $A_{tot} = 7600 \text{ mm}^2$, Approach 2 with $\rho = 1.0$ will be used. Instead of making the calculations to determine the maximum bending moment resistance using FEM-models, it is shown in Chapter 7.3.1 to Chapter 7.3.3 that using the simplified effective width method according to Abspoel determines the maximum bending moment resistances $M_{Abspoel}$ with sufficient accuracy.

The dimensions of the cross-section for steel grade S235 are determined as follows, based on equations as shown Chapter 7.3.2:

$$\text{Eq.(7.8):} \quad A_f = \frac{1}{\rho + 2} \cdot A_{tot} = \frac{1}{1 + 2} \cdot 9600 = 3200 \text{ mm}^2$$

$$\text{Eq.(7.9):} \quad A_w = \frac{\rho}{\rho + 2} \cdot A_{tot} = \frac{1}{1 + 2} \cdot 9600 = 3200 \text{ mm}^2$$

$$\text{Eq.(7.10):} \quad t_w = \sqrt{\frac{\rho}{\rho+2}} \cdot \sqrt{\frac{1}{\beta_w}} \cdot \sqrt{A_{tot}} = \sqrt{\frac{1}{1+2}} \cdot \sqrt{\frac{1}{1400}} \cdot \sqrt{9600} = 1.51 \text{ mm}$$

$$\text{Eq.(7.11):} \quad h_w = \sqrt{\frac{\rho}{\rho+2}} \cdot \sqrt{\beta_w} \cdot \sqrt{A_{tot}} = \sqrt{\frac{1}{1+2}} \cdot \sqrt{1400} \cdot \sqrt{9600} = 2116.6 \text{ mm}$$

$$\text{Eq.(7.12):} \quad t_f = \sqrt{\frac{1}{\rho+2}} \cdot \sqrt{\frac{1}{\beta_f}} \cdot \sqrt{A_{tot}} = \sqrt{\frac{1}{1+2}} \cdot \sqrt{\frac{1}{20}} \cdot \sqrt{9600} = 12.6 \text{ mm}$$

$$\text{Eq.(7.13):} \quad b = \sqrt{\frac{1}{\rho+2}} \cdot \sqrt{\beta_f} \cdot \sqrt{A_{tot}} = \sqrt{\frac{1}{1+2}} \cdot \sqrt{20} \cdot \sqrt{9600} = 253.0 \text{ mm}$$

The effective width b_{eff} of this cross-section under pure bending $\psi = -1.0$ is iteratively determined as shown in Chapter 6.3.2. The effective width is $b_{eff} = 103.8 \text{ mm}$ and so the effective width at the top of the web is $b_{e1} = 0.4 \cdot b_{eff} = 0.4 \cdot 103.8 = 41.5 \text{ mm}$. The bending moment resistance $M_{Abspoel}$ is determined by substituting these dimensions and this effective width in Eq.(7.1):

$$\begin{aligned} M_{Abspoel} &= \left\{ b \cdot t_f \cdot (h_w + t_f) + b_{e1} \cdot t_w \cdot (h_w - b_{e1}) \right\} \cdot f_y = \\ &= \left\{ 253.0 \cdot 12.6 \cdot (2116.6 + 12.6) + 41.5 \cdot 1.51 \cdot (2116.6 - 41.5) \right\} \cdot 235 \cdot 10^{-6} = 1631.8 \text{ kNm} \end{aligned}$$

This bending moment resistance $M_{Abspoel} = 1631.8 \text{ kNm}$ according to Approach 2 with $\rho = 1.0$ is larger than the bending moment resistance $M_u = 1411.2 \text{ kNm}$ determined by FEM according to Approach 1.

The dimensions of the cross-section for steel grade S460 follow from:

$$\text{Eq.(7.8):} \quad A_f = \frac{1}{\rho+2} \cdot A_{tot} = \frac{1}{1+2} \cdot 7600 = 2533 \text{ mm}^2$$

$$\text{Eq.(7.9):} \quad A_w = \frac{\rho}{\rho+2} \cdot A_{tot} = \frac{1}{1+2} \cdot 7600 = 2533 \text{ mm}^2$$

$$\text{Eq.(7.10):} \quad t_w = \sqrt{\frac{\rho}{\rho+2}} \cdot \sqrt{\frac{1}{\beta_w}} \cdot \sqrt{A_{tot}} = \sqrt{\frac{1}{1+2}} \cdot \sqrt{\frac{1}{900}} \cdot \sqrt{7600} = 1.68 \text{ mm}$$

$$\text{Eq.(7.11):} \quad h_w = \sqrt{\frac{\rho}{\rho+2}} \cdot \sqrt{\beta_w} \cdot \sqrt{A_{tot}} = \sqrt{\frac{1}{1+2}} \cdot \sqrt{900} \cdot \sqrt{7600} = 1510.0 \text{ mm}$$

$$\text{Eq.(7.12):} \quad t_f = \sqrt{\frac{1}{\rho+2}} \cdot \sqrt{\frac{1}{\beta_f}} \cdot \sqrt{A_{tot}} = \sqrt{\frac{1}{1+2}} \cdot \sqrt{\frac{1}{20}} \cdot \sqrt{7600} = 11.3 \text{ mm}$$

$$\text{Eq.(7.13):} \quad b = \sqrt{\frac{1}{\rho+2}} \cdot \sqrt{\beta_f} \cdot \sqrt{A_{tot}} = \sqrt{\frac{1}{1+2}} \cdot \sqrt{20} \cdot \sqrt{7600} = 225.1 \text{ mm}$$

The effective width b_{eff} of this cross-section under pure bending $\psi = -1.0$ is iteratively determined as shown in Chapter 6.3.2. The result is $b_{eff} = 82.4 \text{ mm}$ and so $b_{e1} = 0.4 \cdot b_{eff} = 0.4 \cdot 82.4 = 32.9 \text{ mm}$.

The bending moment resistance $M_{Abspoel}$ is determined with Eq.(7.1):

$$\begin{aligned} M_{Abspoel} &= \{b \cdot t_f \cdot (h_w + t_f) + b_{e1} \cdot t_w \cdot (h_w - b_{e1})\} \cdot f_y = \\ &= \{225.1 \cdot 11.3 \cdot (1510.0 + 11.3) + 32.9 \cdot 1.68 \cdot (1510.0 - 32.9)\} \cdot 460 \cdot 10^{-6} = 1810.3 \text{ kNm} \end{aligned}$$

This bending moment resistance $M_{Abspoel} = 1810.3 \text{ kNm}$ according to Approach 2 with $\rho = 1.0$ is larger than the bending moment resistance $M_u = 1720.0 \text{ kNm}$ determined by FEM according to Approach 1. It could be expected that the bending moment resistances according to Approach 2 with $\rho = 1.0$ with similar cross-sectional areas as used in Approach 1, namely $A_{tot} = 9600 \text{ mm}^2$ for S235 and $A_{tot} = 7600 \text{ mm}^2$ for S460, are larger than the bending moment resistances according to Approach 1. It has been proved that a ratio of area $\rho = 1.0$ gives the largest bending moment resistance for a constant cross-sectional area $A_{tot} = 6000 \text{ mm}^2$ for steel grade S235 as well as for S460 for Approach 2, see Chapter 7.3.2. The maximum bending moment resistance $M_{Abspoel}$ according to Approach 1 occurs for a ratio of area $\rho = 2.8$ for steel grade S235, which is close to $\rho = 3.0$ as used in Chapter 7.3.2, and for a ratio of area $\rho = 1.8$ for steel grade S460, which is close to $\rho = 2.0$ as used in Chapter 7.3.2 too.

7.4 PARAMETRIC RESEARCH BASED ON THE SIMPLIFIED EFFECTIVE WIDTH METHOD ACCORDING TO ABSPOEL

7.4.1 THE RATIO OF AREA

The main aim of the parametric research is to determine the maximum bending moment resistance M_u for a certain amount of steel, so for a specific cross-sectional area A_{tot} . This maximum bending moment resistance M_u depends on the maximum web slenderness $\beta_{w,max}$, which is determined by the parametric research using FEM-models and by the optimum ratio of area ρ_{opt} . With a view to Chapter 7.3.4 it can be concluded that Approach 2 gives the maximum bending moment resistance M_u for a ratio of area $\rho = 1.0$, compared with ratios of area $\rho = 2.0$ and $\rho = 3.0$, but it is not clear whether this $\rho = 1.0$ is the optimum itself. In Chapter 7.3.1 to Chapter 7.3.3 it can be seen that the bending moment resistances $M_{Abspoel}$ based on the simplified effective width method according to

Abspoel fit the bending moment resistances M_u based on the FEM-models very well and so it is useful to continue the parametric research by using this simplified effective width method according to Abspoel.

The web thickness t_w , the web height h_w , the flange thickness t_f and the flange width b of the plate girder can be expressed in the cross-sectional area A_{tot} , the ratio of area ρ , the web slenderness β_w and the flange slenderness β_f as given in Eq.(7.10), Eq.(7.11), Eq.(7.12) and Eq.(7.13) respectively.

The bending moment resistance $M_{Abspoel}$ for a specific cross-sectional area A_{tot} and specific web slenderness β_w is maximised by varying the ratio of area ρ , including the iterative calculation to determine the effective width b_{e1} according to EN1993-1-5 [30]. Figure 7-23 presents the optimised ratio of area ρ_{opt} for steel grade S235 and S460 for specific web slenderness's β_w up to the maximum web slenderness $\beta_{w,max}$ as determined with Approach 2 for the corresponding steel grades. From this Figure 7-23, it can be seen that the optimal ratio of area ρ_{opt} is independent on the cross-sectional area A_{tot} , but it is dependent on the web slenderness β_w and the steel grade. Steel grade S235 results in larger optimal ratios of area ρ_{opt} compared with steel grade S460.

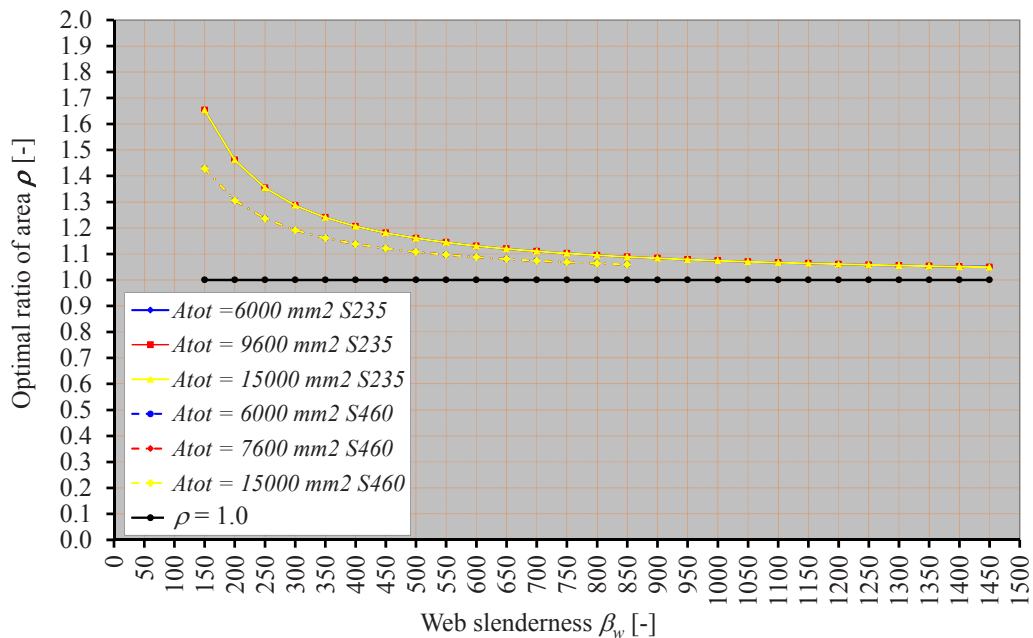


Figure 7-23 Optimal ratio of area ρ versus the web slenderness β_w for S235 and S460

Figure 7-24 and Figure 7-25 show the bending moment resistances based on these optimised ratio of area ρ_{opt} as well as a constant ratio of area $\rho = 1.0$ for steel grades S235 and S460 respectively for cross-sectional areas $A_{tot} = 6000 \text{ mm}^2$ and $A_{tot} = 15000 \text{ mm}^2$. For steel grade S235 also a cross-sectional area $A_{tot} = 9600 \text{ mm}^2$ is used and for steel grade S460 a cross-sectional area $A_{tot} = 7600 \text{ mm}^2$ is used, both corresponding with the cross-sectional areas determined with Approach 1 with the maximum web slenderness's $\beta_{w,max}$ for these steel grades.

From Figure 7-24 and Figure 7-25 it can be seen that the bending moment resistances $M_{Abspoel}$ are hardly influenced by the optimised ratio of area ρ_{opt} . See for bending moment resistances $M_{Abspoel}$ based on the optimised ratio of area ρ_{opt} the dotted lines and for the bending moment resistances $M_{Abspoel}$ based on a constant ratio of area $\rho = 1.0$ the solid lines in Figure 7-24 and Figure 7-25.

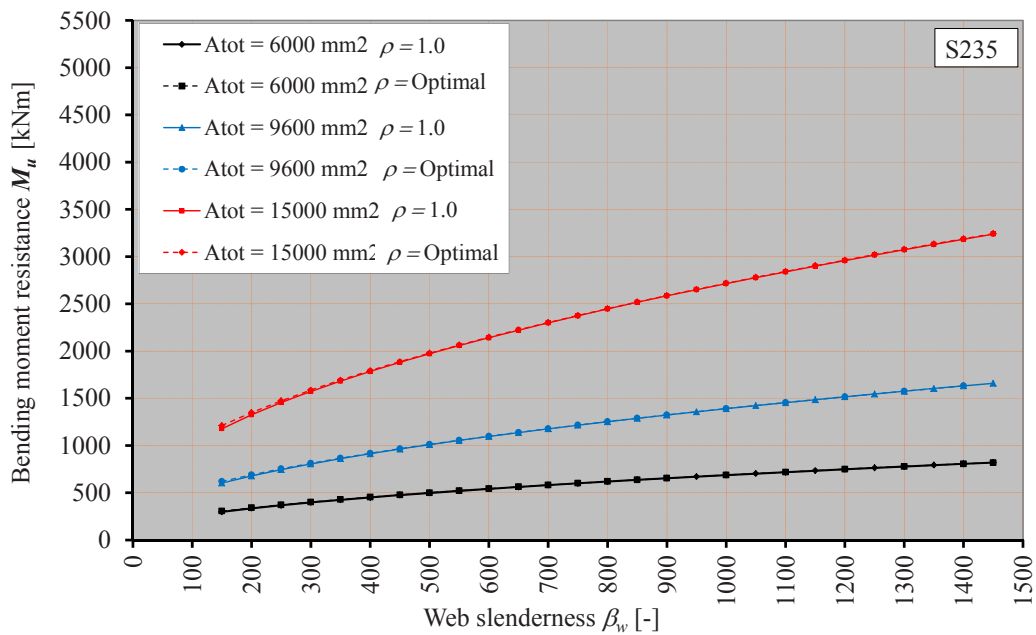


Figure 7-24 Bending moment resistance $M_{Abspoel}$ for $\rho = 1.0$ and an optimal ratio of area, S235

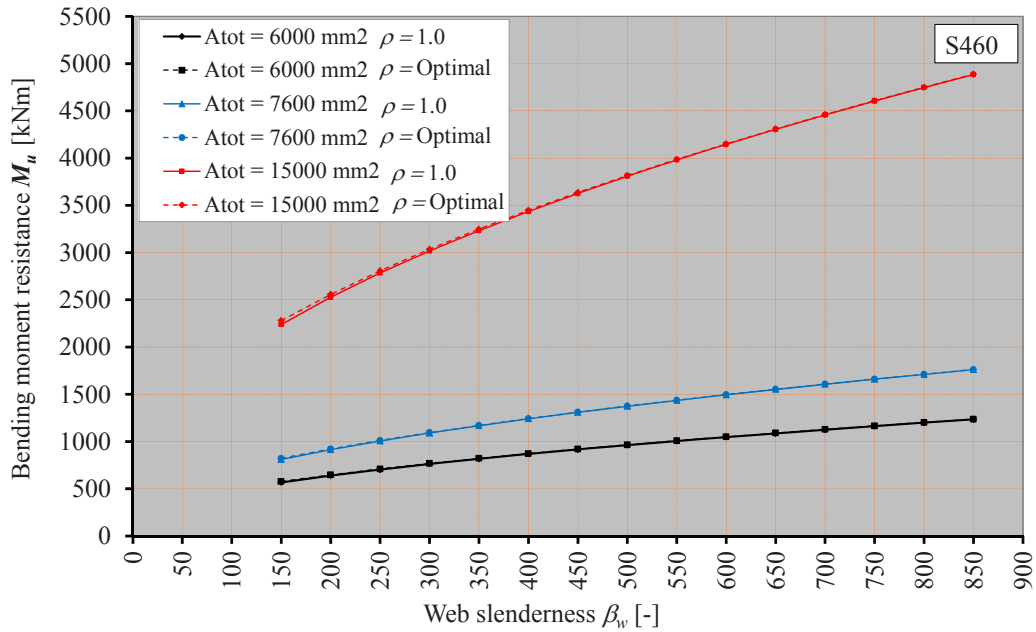


Figure 7-25 Bending moment resistance $M_{Abspoel}$ for $\rho = 1.0$ and an optimal ratio of area, S460

Based on Figure 7-24 and Figure 7-25 it is concluded that the bending moment resistance $M_{Abspoel}$ can be based on the safesided assumption that the ratio of area is constant $\rho = 1.0$ for steel grades S235 and S460.

7.4.2 THE MAXIMUM WEB SLENDERNESS

The maximum web slenderness $\beta_{w,max}$ needs not be based on vertical buckling of the compressive flange into the web as proven by the Delft experiments, see Chapter 6.5. In the parametric research based on FEM-models, see Chapter 7.3, the maximum web slenderness $\beta_{w,max}$ is determined, based on the latest stable result of these FEM-models. Figure 7-21 and Figure 7-22 show this maximum web slenderness, namely $\beta_{w,max} = 1450$ for steel grade S235 and $\beta_{w,max} = 850$ for steel grade S460, both using Approach 2 with $\rho = 1.0$. Nevertheless, the maximum web slenderness will be limited to $\beta_{w,max} = 800$ which is justified by the following arguments:

1. The maximum web slenderness used in the Delft experiments is $\beta_{w,max} = 800$, see Chapter 4;
2. The FEM-results show a maximum web slenderness $\beta_{w,max}$, but it is not clear whether this is due to physical instabilities or to numerical instabilities, see Chapter 7.3;

3. It can be assumed that there are practical limitations on this maximum web slenderness

$\beta_{w,\max}$, especially focused on the fabrication and erection of the plate girder.

The effective width b_{eff} and so the effective part b_{e1} at the top of the web can be iteratively determined according to EN1993-1-5 [30] clause 4.4. In the simplified effective width method according to Abspoel, only the effective width b_{e1} is used, see Eq.(7.1). To avoid the need for an iterative procedure to determine the value of this effective width b_{e1} resulting from b_{eff} , the ratio $\frac{h_w}{b_{e1}}$ between

the web height h_w and this effective width b_{e1} is calculated as a function of the web slenderness β_w . Figure 7-26 shows the ratio $\frac{h_w}{b_{e1}}$ as a result of this iterative procedure as a function of the web slenderness β_w for steel grade S235 and S460. In Figure 7-26, also the mean value regression lines are drawn and the withgoing polynomials of the first degree $c_s(\beta_w, f_y) = \frac{h_w}{b_{e1}}$ are given, see Eq.(7.18)

for steel grade S235 and Eq.(7.19) for steel grade S460.

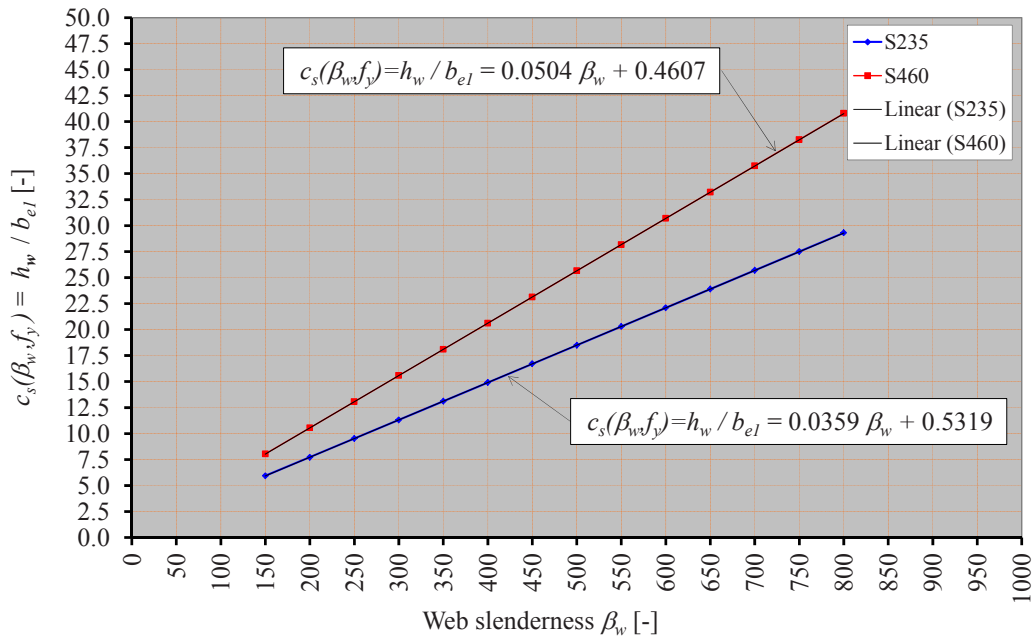


Figure 7-26 The ratio $c_s(\beta_w, f_y) = \frac{h_w}{b_{e1}}$ as a function of the web slenderness β_w for steel grades S235 and S460

$$c_s(\beta_w, f_y) = \frac{h_w}{b_{e1}} = 0.0359 \cdot \beta_w + 0.5319 \text{ for steel grade S235} \quad (7.18)$$

$$c_s(\beta_w, f_y) = \frac{h_w}{b_{e1}} = 0.0504 \cdot \beta_w + 0.4607 \text{ for steel grade S460} \quad (7.19)$$

The ratio $c_s(\beta_w, f_y)$ is independent of the cross-sectional area A_{tot} , which also follows from the effective width method according to EN1993-1-5 [30] as described in Chapter 2.3.

7.4.3 THE MINIMUM FLANGE SLENDERNESS

The flange slenderness, defined as $\beta_f = \frac{b}{t_f}$, will influence the bending moment resistance $M_{Abspoel}$ as well. Up to now, the flange slenderness $\beta_f = 20$ is used for steel grades S235 and S460. This means that for steel grade S235 the flange is a class 2 cross-section or, depending on the web thickness t_w and the type of welds used, even a class 1 cross-section. For steel grade S460 the flange is a class 3 cross-section. The classification of the entire cross-section is always based on the most slender component of the cross-section. In this research, only class 4 webs are considered, combined with flanges of cross-section class 1, 2 or 3. The bending moment resistance $M_{Abspoel}$ deviates less than 2% in case the flange slenderness β_f varies between just being class 2 and just class 3 and the web slenderness β_w is just class 3. This percentage decreases with increasing web slenderness β_w up to a maximum web slenderness $\beta_{w,max} = 800$ to around 0.3% and so the differences in the flange slenderness β_f on the bending moment resistance $M_{Abspoel}$ are negligibly small.

A certain flange width b is necessary when the plate girder is used in a roof structure with trapezoidal roof plates or in a floor structure with a composite floor system to support these plates and so flanges of cross-section class 3 are preferred. Nevertheless, the loads will be introduced into the plate girder rather locally by the webs of these plates and due to this load introduction compact flanges of cross-section class 1 are preferred.

A compact flange is preferred to achieve the maximum bending moment resistance $M_{Abspoel}$, because the lever arm between both flanges will be as large as possible with a large flange thickness t_f . Because of these considerations it is suggested to take the flange slenderness $\beta_f \geq 5$.

7.4.4 THE STEEL GRADE

From Chapter 7.3 it can be observed that the bending moment resistance M_u increases by using higher values for the yield stress f_y , but to what extent? Figure 7-27 assembles the bending mo-

ment resistances M_u from Figure 7-21 and Figure 7-22 according to Approach 2 with the ratio of area $\rho = 1.0$ and a cross-sectional area $A_{tot} = 6000 \text{ mm}^2$ for steel grade S235 and S460, inclusive the related maximum web slenderness's (see the big red dots) $\beta_{w,max}$. Figure 7-27 also shows the bending moment resistances $M_{Abspoel}$ based on the simplified effective width method according to Abspoel for steel grades S355 and S690 for the same cross-sectional area $A_{tot} = 6000 \text{ mm}^2$. In order to find the end of the curves for S355 and S690, which would be determined by instability in FEM-results that can not be detected by the simplified effective width method according to Abspoel, a linear interpolation and an extrapolation (the yellow dots) are used based on the maximum web slenderness's β_w determined using FEM for steel grades S235 and S460 respectively (the red dots).

Table 7-9 shows the maximum bending moment resistance $M_{u(fy)}$, the maximum web slenderness

$\beta_{w,max}$ and the ratios $\frac{M_{u(fy)}}{M_{u(S235)}}$ and $\frac{f_y}{f_{y(S235)}}$.

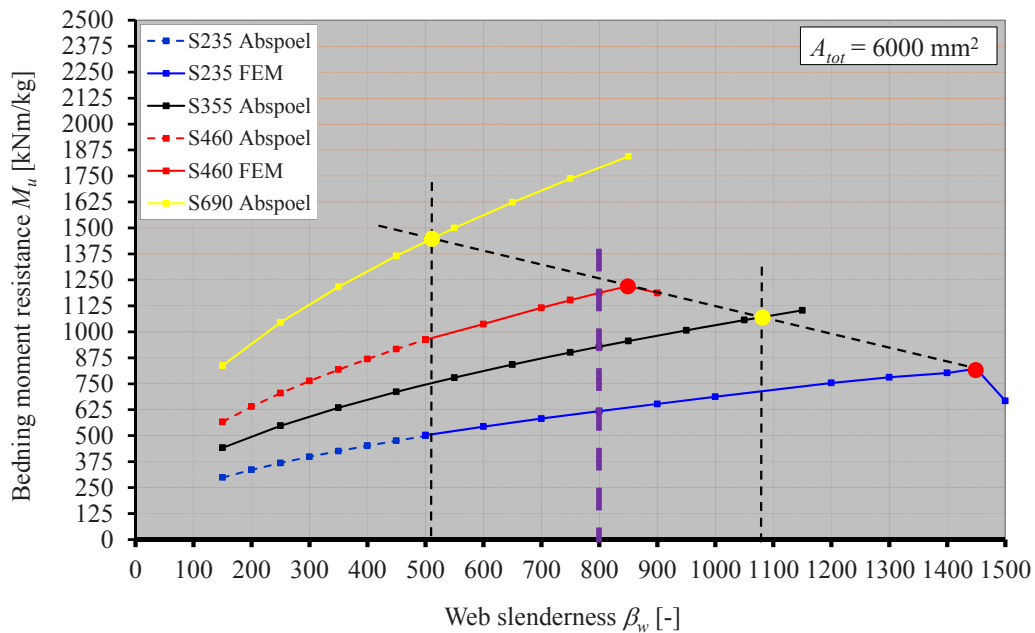


Figure 7-27 Bending moment resistances M_u based on Approach 2 with $\rho = 1$ for several steel grades

Table 7-9 The maximum bending moment resistance $M_{u(f_y)}$, the maximum web slenderness

$$\beta_{w,\max} \text{ and the ratios } \frac{M_{u(f_y)}}{M_{u(S235)}}, \frac{f_y}{f_{y(S235)}} \text{ for several steel grades}$$

	S235	S355	S460	S690
$M_{u(f_y)}$	822.4	1068.5	1220.3	1445.7
$\beta_{w,\max}$	1450	1076	850	509
$\frac{M_{u(f_y)}}{M_{u(S235)}}$	1.00	1.30	1.48	1.76
$\frac{f_y}{f_{y(S235)}}$	1.00	1.51	1.96	2.94

From Table 7-9 it can be seen that the ratio $\frac{M_{u(f_y)}}{M_{u(S235)}}$ increases slower with increasing yield stress

than the ratio $\frac{f_y}{f_{y(S235)}}$ itself. This is mainly due to the fact that the maximum web slenderness $\beta_{w,\max}$

decreases when the yield stress f_y increases and the withgoing web height h_w of the girder also decreases.

In Chapter 7.4.2, motivated considerations are given to limit the maximum web slenderness to $\beta_{w,\max} = 800$. Table 7-10 shows the bending moment resistance $M_{u(f_y)}$ for the web slenderness $\beta_w = 150$ and the cross-sectional areas $A_{tot} = 6000 \text{ mm}^2$, $A_{tot} = 12000 \text{ mm}^2$, $A_{tot} = 15000 \text{ mm}^2$ and $A_{tot} = 18000 \text{ mm}^2$ for the steel grades S235, S355, S460 and S690. Table 7-11 presents the ratios $\frac{M_{u(f_y)}}{M_{u(S235)}}$ based on the bending moment resistance as shown in Table 7-10.

Table 7-12 and Table 7-13 show these results for the web slenderness $\beta_w = 350$, Table 7-14 and Table 7-15 show these results for the web slenderness $\beta_w = 500$ and Table 7-16 and Table 7-17 show the results for the web slenderness $\beta_w = 800$.

Table 7-10 The maximum bending moment resistance $M_{Abspoel(f_y)}$ for a web slenderness $\beta_w = 150$ for several cross-sectional areas A_{tot} and steel grades

Cross-sectional area $A_{tot} [mm^2]$	Steel grade			
	S235	S355	S460	S690
	$M_{Abspoel(f_y)} [kNm]$			
6000	298.2	442.8	568.0	839.5
12000	843.5	1252.5	1606.5	2374.3
15000	1178.9	1750.4	2245.1	3318.2
18000	1549.7	2301.0	2951.3	4361.9

Table 7-11 The ratio $\frac{M_{u(f_y)}}{M_{u(S235)}}$ for a web slenderness $\beta_w = 150$ for several cross-sectional areas A_{tot} and steel grades

Cross-sectional area $A_{tot} [mm^2]$	Steel grade			
	S235	S355	S460]	S690
	$\frac{M_{Abspoel(f_y)}}{M_{Abspoel(S235)}} [-]$			
6000	1.00	1.48	1.90	2.82
12000	1.00	1.48	1.90	2.81
15000	1.00	1.48	1.90	2.81
18000	1.00	1.48	1.90	2.81

Table 7-12 The maximum bending moment resistance $M_{Abspoel(f_y)}$ for a web slenderness $\beta_w = 350$ for several cross-sectional areas A_{tot} and steel grades

	Steel grade			
Cross-sectional area	S235	S355	S460	S690
$A_{tot} [mm^2]$	$M_{Abspoel(f_y)} [kNm]$			
6000	425.7	636.0	819.1	1218.4
12000	1204.0	1798.9	2316.8	3446.2
15000	1682.6	2514.1	3237.9	4816.3
18000	2211.9	3304.9	4256.3	6331.1

Table 7-13 The ratio $\frac{M_{u(f_y)}}{M_{u(S235)}}$ for a web slenderness $\beta_w = 350$ for several cross-sectional areas A_{tot} and steel grades

	Steel grade			
Cross-sectional area	S235	S355	S460]	S690
$A_{tot} [mm^2]$	$\frac{M_{Abspoel(f_y)}}{M_{Abspoel(S235)}} [-]$			
6000	1.00	1.49	1.92	2.86
12000	1.00	1.49	1.92	2.86
15000	1.00	1.49	1.92	2.86
18000	1.00	1.49	1.92	2.86

Table 7-14 The maximum bending moment resistance $M_{Abspoel(f_y)}$ for a web slenderness $\beta_w = 500$ for several cross-sectional areas A_{tot} and steel grades

	Steel grade			
Cross-sectional area	S235	S355	S460	S690
$A_{tot} [mm^2]$	$M_{Abspoel(f_y)} [kNm]$			
6000	498.7	747.1	963.7	1436.5
12000	1410.7	2113.2	2725.7	4063.0
15000	1971.5	2953.3	3809.3	5678.3
18000	2591.6	3882.2	5007.4	7464.3

Table 7-15 The ratio $\frac{M_{u(f_y)}}{M_{u(S235)}}$ for a web slenderness $\beta_w = 500$ for several cross-sectional areas A_{tot} and steel grades

	Steel grade			
Cross-sectional area	S235	S355	S460]	S690
$A_{tot} [mm^2]$	$\frac{M_{Abspoel(f_y)}}{M_{Abspoel(S235)}} [-]$			
6000	1.00	1.50	1.93	2.88
12000	1.00	1.50	1.93	2.88
15000	1.00	1.50	1.93	2.88
18000	1.00	1.50	1.93	2.88

Table 7-16 The maximum bending moment resistance $M_{Abspoel(f_y)}$ for a web slenderness $\beta_w = 800$ for several cross-sectional areas A_{tot} and steel grades

Cross-sectional area $A_{tot} [mm^2]$	Steel grade			
	S235	S355	S460	S690
	$M_{Abspoel(f_y)} [kNm]$			
6000	618.8	929.5	1200.8	-
12000	1750.2	2629.1	3396.2	-
15000	2446.0	3674.2	4746.4	-
18000	3215.4	4829.9	6239.3	-

Table 7-17 The ratio $\frac{M_{u(f_y)}}{M_{u(S235)}}$ for a web slenderness $\beta_w = 800$ for several cross-sectional areas A_{tot} and steel grades

Cross-sectional area $A_{tot} [mm^2]$	Steel grade			
	S235	S355	S460]	S690
	$\frac{M_{Abspoel(f_y)}}{M_{Abspoel(S235)}} [-]$			
6000	1.00	1.50	1.94	-
12000	1.00	1.50	1.94	-
15000	1.00	1.50	1.94	-
18000	1.00	1.50	1.94	-

For girders with an equal web slenderness's β_w , but made from different steel grades and with different cross-sectional areas A_{tot} , the ratios $\frac{M_{u(f_y)}}{M_{u(S235)}}$, see Table 7-11 for $\beta_w = 150$, Table 7-13 for $\beta_w = 350$, Table 7-15 for $\beta_w = 500$ and Table 7-17 for $\beta_w = 800$, are almost equal to the ratios $\frac{f_y}{f_{y(S235)}}$, see Table 7-9, as collected in Table 7-18. These ratios $\frac{M_{u(f_y)}}{M_{u(S235)}}$ and $\frac{f_y}{f_{y(S235)}}$ show that the influence of the yield stress f_y is very large, irrespective the cross-sectional area A_{tot} .

Table 7-18 The ratios $\frac{M_{u(fy)}}{M_{u(S235)}}$ and $\frac{f_y}{f_{y(S235)}}$ for several web slenderness's β_w and steel grades

Web slenderness	S355	S460	S690
	[-]	[-]	[-]
$\frac{M_{u(fy)}}{M_{u(S235)}}$ for $\beta_w = 150$	1.48	1.90	2.82
$\frac{M_{u(fy)}}{M_{u(S235)}}$ for $\beta_w = 350$	1.49	1.92	2.86
$\frac{M_{u(fy)}}{M_{u(S235)}}$ for $\beta_w = 500$	1.50	1.93	2.88
$\frac{M_{u(fy)}}{M_{u(S235)}}$ for $\beta_w = 800$	1.50	1.94	-
$\frac{f_y}{f_{y(S235)}}$	1.51	1.96	2.94

This is valid as long as the maximum web slenderness $\beta_{w,max}$ of girders made of a certain steel grade is larger than the web slenderness β_w under consideration. At a constant value for β_w the dimensions of the cross-section of the girders are the same for different steel grades. It is of interest to look in more detail to the fact that these ratios $\frac{M_{u(fy)}}{M_{u(S235)}}$ are constant for a specific web slenderness β_w and steel grade.

The maximum bending moment resistance $M_{Abspoel}$ based on the simplified effective width method according to Abspoel is determined with Eq.(7.1). The dimensions of the cross-section of a plate girder can be determined by substituting the ratio of area $\rho=1.0$ in Eq.(7.10) to Eq.(7.13):

$$t_w = \sqrt{\frac{1}{3 \cdot \beta_w}} \cdot \sqrt{A_{tot}} \quad (7.20)$$

$$h_w = \sqrt{\frac{\beta_w}{3}} \cdot \sqrt{A_{tot}} \quad (7.21)$$

$$t_f = \sqrt{\frac{1}{3 \cdot \beta_f}} \cdot \sqrt{A_{tot}} \quad (7.22)$$

$$b = \sqrt{\frac{\beta_f}{3}} \cdot \sqrt{A_{tot}} \quad (7.23)$$

The effective width b_{el} is determined with:

$$b_{el} = \frac{h_w}{c_s(\beta_w, f_y)} = \frac{\sqrt{\frac{\beta_w}{3}} \cdot \sqrt{A_{tot}}}{c_s(\beta_w, f_y)} \quad (7.24)$$

The function $c_s(\beta_w, f_y)$ depends on the web slenderness β_w and the steel grade. Substitution of Eq.(7.20) to Eq.(7.23) for the dimensions and equation Eq.(7.24) for the effective width b_{el} into Eq.(7.1) of the bending moment resistance $M_{Abspoel}$ results in:

$$M_{Abspoel} = \left\{ b \cdot t_f \cdot (h_w + t_f) + b_{el} \cdot t_w \cdot (h_w - b_{el}) \right\} \cdot f_y = \left\{ \frac{A_{tot}}{3} \cdot \left(\sqrt{\frac{\beta_w}{3}} \cdot \sqrt{A_{tot}} + \sqrt{\frac{1}{3 \cdot \beta_f}} \cdot \sqrt{A_{tot}} \right) + \right. \\ \left. + \frac{\sqrt{\frac{\beta_w}{3}} \cdot \sqrt{A_{tot}}}{c_s(\beta_w, f_y)} \cdot \sqrt{\frac{1}{3 \cdot \beta_w}} \cdot \sqrt{A_{tot}} \cdot \left(\sqrt{\frac{\beta_w}{3}} \cdot \sqrt{A_{tot}} - \frac{\sqrt{\frac{\beta_w}{3}} \cdot \sqrt{A_{tot}}}{c_s(\beta_w, f_y)} \right) \right\} \cdot f_y$$

which leads to:

$$M_{Abspoel} = A_{tot} \cdot \sqrt{A_{tot}} \cdot \left\{ \left(\sqrt{\frac{\beta_w}{27}} + \sqrt{\frac{1}{27 \cdot \beta_f}} \right) + \frac{1}{c_s(\beta_w, f_y)} \cdot \left(\sqrt{\frac{\beta_w}{27}} - \frac{1}{c_s(\beta_w, f_y)} \cdot \sqrt{\frac{\beta_w}{27}} \right) \right\} \cdot f_y$$

and subsequently to:

$$\frac{M_{Abspoel}}{A_{tot}^{1.5}} = \left\{ \left(\sqrt{\frac{\beta_w}{27}} + \sqrt{\frac{1}{27 \cdot \beta_f}} \right) + \frac{1}{c_s(\beta_w, f_y)} \cdot \left(\sqrt{\frac{\beta_w}{27}} - \frac{1}{c_s(\beta_w, f_y)} \cdot \sqrt{\frac{\beta_w}{27}} \right) \right\} \cdot f_y \quad (7.25)$$

From Eq.(7.25) it can be seen that for a specific steel grade f_y , web slenderness β_w and the flange slenderness β_f , the ratio $\left(\frac{M_{Abspoel}}{A_{tot}^{1.5}} \right)$ is a constant.

The steel grade used in the Delft experiments is S235. Because the actual yield stress $f_{y,act}$ used in the Delft experiments varied between 309 and 350 MPa, which is close to the nominal yield stress f_y of steel grade S355, this steel grade S355 is added. Because of this, Figure 7-26, in which the graphs and equations for $c_s(\beta_w, f_y)$ for steel grade S355 are shown for steel grade S235 and S460, is extended by steel grade S355, see Figure 7-28. The equation for $c_s(\beta_w, f_y)$ steel grade S355 is given in Eq. (7.26).

$$c_s(\beta_w, f_y) = \frac{h_w}{b_{el}} = 0.0443 \cdot \beta_w + 0.4943 \text{ for steel grade S355} \quad (7.26)$$

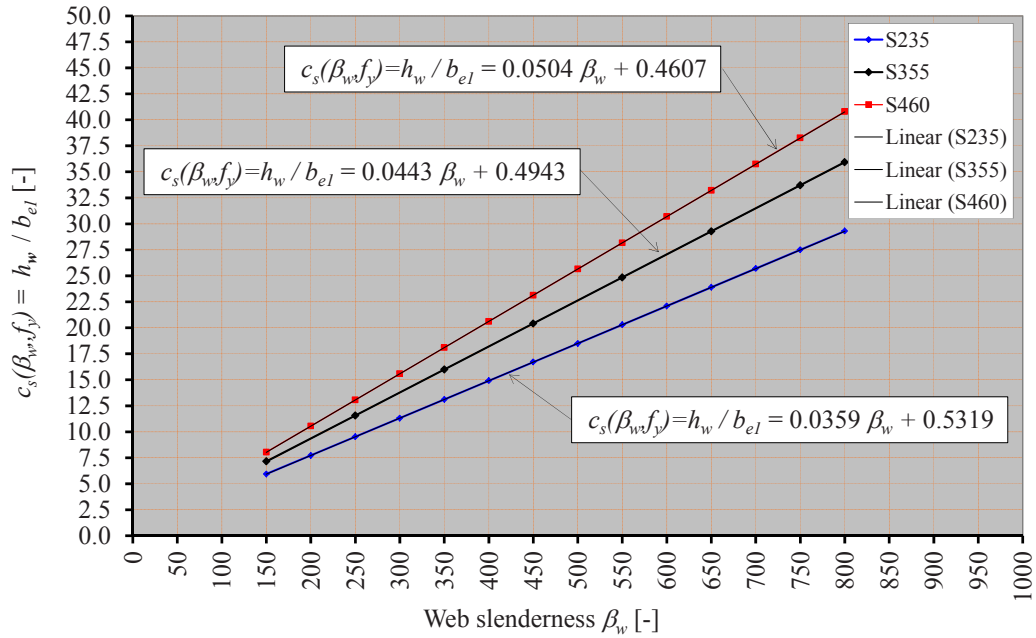


Figure 7-28 The equation $c_s(\beta_w, f_y) = \frac{h_w}{b_{el}}$ as function of the web slenderness β_w for steel grade S235, S355 and S460

7.5 STRATEGY TO DESIGN THE CROSS-SECTION FOR A PLATE GIRDER

The ratio $\left(\frac{M_{Abspoel}}{A_{tot}^{1.5}} \right)$ is a constant for a specific web slenderness β_w , flange slenderness β_f and steel grade f_y , see Eq.(7.25). Please bear in mind that Eq.(7.1) for $M_{Abspoel}$ is in fact the calculation of the bending moment resistance M_u based on the simplified effective width method according to Abspoel. When the bending moment resistance M_u is set equal to the design bending moment M_{Ed} as a result of the factored loading on the structure, the minimum required cross-sectional area $A_{tot.min}$ for the plate girder in the constant moment region can be determined.

In fact, $M_{Abspoel}$ is the characteristic value of the bending moment resistance $M_{Abspoel,Rk}$ and the design value has to be determined with $M_{Abspoel,Rd} = \frac{M_{Abspoel,Rk}}{\gamma_{M0}}$, with γ_{M0} according to the National Annex. In The Netherlands $\gamma_{M0} = 1.0$, but in some other countries $\gamma_{M0} = 1.1$ is used.

$$M_{Abspoel,Rd} = \frac{M_{Abspoel,Rk}}{\gamma_{M0}} = M_{Ed} \quad (7.27)$$

with $M_{Abspoel,Rk} = M_{Abspoel}$

From Eq.(7.25) and Eq.(7.27) the optimal cross-sectional area A_{tot} can be determined:

$$A_{tot} = \frac{(\gamma_{M0} \cdot M_{Ed})^{\frac{2}{3}}}{\left[\left\{ \left(\sqrt{\frac{\beta_w}{27}} + \sqrt{\frac{1}{27 \cdot \beta_f}} \right) + \frac{1}{c_s(\beta_w, f_y)} \cdot \left(\sqrt{\frac{\beta_w}{27}} - \frac{1}{c_s(\beta_w, f_y)} \cdot \sqrt{\frac{\beta_w}{27}} \right) \right\} \cdot f_y \right]^{\frac{2}{3}}} \quad (7.28)$$

The optimal dimensions can be determined with Eq.(7.20) for the web thickness $t_{w,opt}$, Eq.(7.21) for the web height $h_{w,opt}$, Eq.(7.22) for the flange thickness $t_{f,opt}$ and Eq.(7.23) for the flange width b_{opt} . The optimal dimensions are indicated by adding the subscript *opt* to the symbol. The final nominal dimensions are based on the optimal dimensions, but have to be adapted to standardised dimensions. The adapted dimensions are indicated by adding the subscript *ad* to the symbol. These adapted dimensions are subject to additional requirements. First, the contribution of the flanges on the bending moment resistance based on the adapted dimensions should not be smaller than the contribution of the flanges based on the optimal dimensions. Second, the web slenderness $\beta_{w,ad}$ based on the adapted dimensions should not be larger than the web slenderness $\beta_{w,opt}$ related to the optimal dimensions. These additional requirements are expressed in Eq.(7.29) and Eq.(7.30):

$$b_{ad} \cdot t_{f,ad} \cdot (h_{w,ad} + t_{f,ad}) \geq b_{opt} \cdot t_{f,opt} \cdot (h_{w,opt} + t_{f,opt}) \quad (7.29)$$

$$\beta_{w,ad} = \frac{h_{w,ad}}{t_{w,ad}} \leq \beta_{w,opt} = \frac{h_{w,opt}}{t_{w,opt}} \quad (7.30)$$

More attention has to be paid to the last additional requirement, because up to now the maximum web slenderness $\beta_{w,max}$ is based on the parametric study by using FEM for only one cross-sectional area, namely $A_{tot} = 6000 \text{ mm}^2$, see Figure 7-27. It can be questioned what the maximum web slen-

derness $\beta_{w,max}$ will be when other cross-sectional areas A_{tot} are used? To answer this question, additional calculations are made to determine the bending moment resistance $M_u = M_{Abspoel}$ using the simplified effective width method according to Abspoel for another cross-sectional area e.g. $A_{tot} = 12000 \text{ mm}^2$ with steel grades S235, S355, S460 and S690. The maximum web slenderness $\beta_{w,max}$ can't be determined by this method. It is assumed that the maximum web slenderness's $\beta_{w,max}$ for steel grades S235 and S460 for plate girders with the cross-sectional area $A_{tot} = 12000 \text{ mm}^2$ are equal to the maximum web slenderness's $\beta_{w,max}$ for the cross-sectional area $A_{tot} = 6000 \text{ mm}^2$ determined by FEM, see Figure 7-29. The intersection points of these maximum web slenderness's and the curves for S235 and S460 (see the big red dots) are used to interpolate and extrapolate the maximum web slenderness's for steel grade S355 and S690 (see the big yellow dots).

For steel grades S235 and S460, additional FEM-calculations are made for plate girders with a cross-sectional area $A_{tot} = 12000 \text{ mm}^2$ by using Approach 2 with $\rho = 1.0$. The results of these additional FEM-calculations are shown in Figure 7-29 and it can be seen that for both steel grades there are stable points beyond the dotted line through the big red and yellow dots. This means that the maximum web slenderness for plate girders with a cross-sectional area $A_{tot} = 12000 \text{ mm}^2$ is larger than for the ones determined for the cross-sectional area $A_{tot} = 6000 \text{ mm}^2$.

From this, it can be concluded that the maximum web slenderness $\beta_{w,max} = 800$, based on the maximum web slenderness used in the Delft experiments, is safesided and can be used for steel grades S235 and S355 for plate girders with different cross-sectional areas.

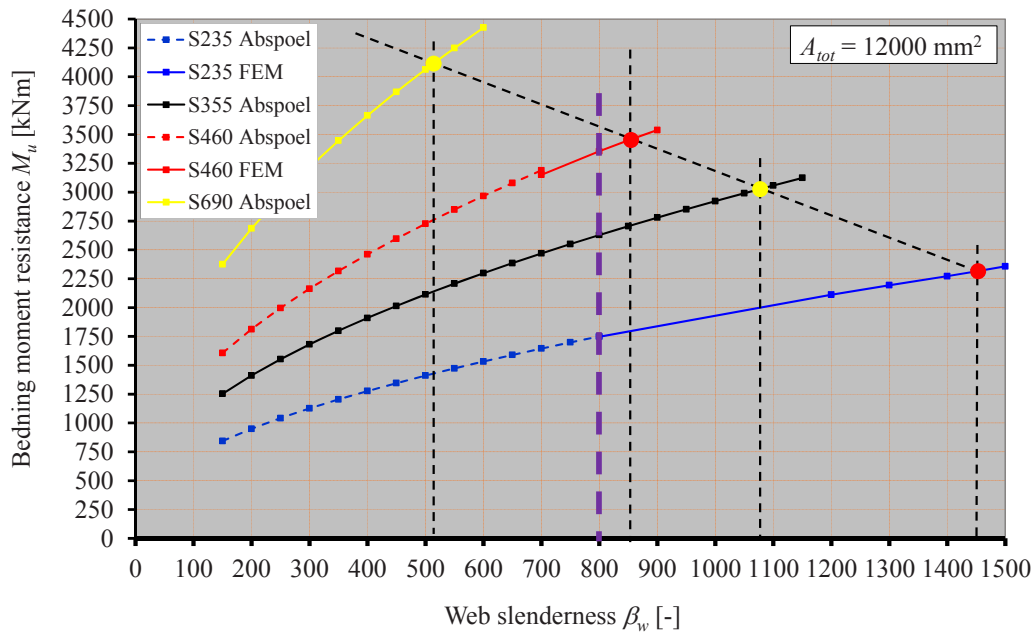


Figure 7-29 Bending moment resistances M_u based on Approach 2 with $\rho = 1$ for several steel grades

7.6 CONCLUSIONS

The following conclusions are drawn:

1. The maximum web slenderness for steel grade S235 achieved with the FEM-model is $\beta_{w,\max} = 1450$ and for steel grade S460 it is $\beta_{w,\max} = 850$. Nevertheless it is suggested to use a maximum web slenderness related to the one used in the Delft experiments $\beta_{w,\max} = 800$;
2. Although higher steel grades are used in the parametric research, it is suggested to use a maximum steel grade S355 related to the maximum actual steel grade used in the Delft experiments. The use of higher web slenderness as well as higher steel grades is not verified with experiments;
3. The optimal ratio of area ρ_{opt} is not a constant for a specific steel grade, but varies depending on the web slenderness β_w and the steel grade used. Nevertheless, the influence of the optimal ratio of area ρ_{opt} on the bending moment resistance M_u is very small compared

with the bending moment resistance M_u based on a fixed ratio of area $\rho = 1.0$, especially for very large web slenderness's β_w ;

4. The bending moment resistance based on the simplified effective width method according to Abspoel fits very well with the bending moment resistances according to the FEM-models. The effective width b_{e1} used in this simplified effective width method is based on a iterative procedure, which could be represented with linear expressions for $c_s(\beta_w, f_y)$ for a specific steel grade;

8 DESIGN PROCEDURE FOR PLATE GIRDERS MADE OF S235 AND S355

8.1 PROCEDURE TO DETERMINE THE MINIMAL CROSS-SECTIONAL AREA

This chapter shows the design procedure to determine the dimensions of a plate girder with a minimal cross-sectional area $A_{tot,min}$ for steel grades S235 and S355, see Chapter 7.4.4, in such a way that the bending moment resistance is equal or larger than the maximum bending moment M_{Ed} as an effect of the factored loading on that plate girder.

The following steps are needed to achieve this aim:

Step 1 Calculate the maximum bending moment M_{Ed} as an effect of the factored loading on the plate girder

Step 2 Take the web slenderness equal to $\beta_{w,max} = 800$

Remark: The web slenderness equal to $\beta_w = \beta_{w,max} = 800$ results into the minimal cross-sectional area $A_{tot,min}$;

Step 3 Take the flange slenderness equal to $\beta_{f,min} = 5$;

Remark: The flange slenderness equal to $\beta_f = \beta_{f,min} = 5$ results into the minimum cross-sectional area $A_{tot,min}$;

Step 4 Choose a steel grade S235 or S355.

Remark: The steel grade with the largest yield stress f_y leads to the minimum cross-sectional area $A_{tot,min}$;

Step 5 Determine the value $c_s(\beta_w, f_y)$ based on the web slenderness $\beta_{w,max} = 800$ (Step 2) and the selected steel grade (Step 4) by using:

$$\text{Eq.(7.18):} \quad c_s(\beta_w, f_y) = \frac{h_w}{b_{e1}} = 0.0359 \cdot \beta_w + 0.5319 \text{ for steel grade S235}$$

$$\text{Eq.(7.26):} \quad c_s(\beta_w, f_y) = \frac{h_w}{b_{e1}} = 0.0443 \cdot \beta_w + 0.4943 \text{ for steel grade S355}$$

Step 6 Determine the minimal cross-sectional area $A_{tot,min}$ required, based on the bending moment M_{Ed} as a result of the factored loading (Step 1), the maximum web slenderness $\beta_{w,max} = 800$ (Step 2), the minimum flange slenderness $\beta_{f,min} = 5$ (Step 3), the selected steel grade (Step 4) and the determined value $c_s(\beta_{w,max}, f_y)$ (Step 5) by using Eq.(7.28):

$$A_{tot,min} = \frac{(\gamma_{M0} \cdot M_{Ed})^{\frac{2}{3}}}{\left[\left(\sqrt{\frac{\beta_{w,max}}{27}} + \sqrt{\frac{1}{27 \cdot \beta_{f,min}}} \right) + \frac{1}{c_s(\beta_{w,max}, f_y)} \cdot \left(\sqrt{\frac{\beta_{w,max}}{27}} - \frac{1}{c_s(\beta_{w,max}, f_y)} \cdot \sqrt{\frac{\beta_{w,max}}{27}} \right) \right]^{\frac{2}{3}} \cdot f_y}$$

Step 7 Determine the optimal dimensions of the cross-section by using the web slenderness $\beta_{w,max} = 800$ (Step 2), the flange slenderness $\beta_{f,min} = 5$ (Step 3) and the determined minimal cross-sectional area $A_{tot,min}$ (Step 6):

$$\text{Eq.(7.20): } t_{w,opt} = \sqrt{\frac{1}{3 \cdot \beta_{w,max}}} \cdot \sqrt{A_{tot,min}}$$

$$\text{Eq.(7.21): } h_{w,opt} = \sqrt{\frac{\beta_{w,max}}{3}} \cdot \sqrt{A_{tot,min}}$$

$$\text{Eq.(7.22): } t_{f,opt} = \sqrt{\frac{1}{3 \cdot \beta_{f,min}}} \cdot \sqrt{A_{tot,min}}$$

$$\text{Eq.(7.23): } b_{opt} = \sqrt{\frac{\beta_{f,min}}{3}} \cdot \sqrt{A_{tot,min}}$$

Step 8 Adapt the determined optimal dimensions of the web and the flanges of the plate girder to standardised dimensions such that:

$$\text{Eq.(7.29): } b_{ad} \cdot t_{f,ad} \cdot (h_{w,ad} + t_{f,ad}) \geq b_{opt} \cdot t_{f,opt} \cdot (h_{w,opt} + t_{f,opt})$$

and:

$$\text{Eq.(7.30): } \beta_{w,ad} = \frac{h_{w,ad}}{t_{w,ad}} \leq \beta_{w,max} = 800$$

Based on these 8 steps, the dimensions of the plate girder are determined. The plate girder has a bending moment resistance $M_{Abspoel,Rd}$ at least equal to the bending moment M_{Ed} as an effect of the factored loading, so $M_{Abspoel,Rd} \geq M_{Ed}$. Herewith, the design procedure is ended.

To complete a structural safety verification procedure the unity check $\frac{M_{Ed}}{M_{Abspoel,Rd}} \leq 1.0$ needs to be shown. M_{Ed} is known from step 1 and $M_{Abspoel,Rd}$ can be calculated based on Eq. (7.1) by using the adapted dimensions and using Eq.(7.18) or Eq.(7.26) to determine the effective width $b_{e1,ad}$ dependent on the selected steel grade S235 or S355.

8.2 EXAMPLES

8.2.1 EXAMPLE 1 PLATE GIRDER WITHOUT ANY LIMITATION OF THE HEIGHT

In this Example 1 the adapted dimensions of the cross-section in step 8 are adapted in such a way that they are all larger than the optimal dimensions.

Step 1 Calculate the maximum bending moment M_{Ed} as an effect of the factored loading on the plate girder. In this example it is assumed that $M_{Ed} = 1250 \text{ kNm}$

Step 2 Take the web slenderness is $\beta_{w,max} = 800$

Step 3 Take the flange slenderness is $\beta_{f,min} = 5$;

Step 4 Choose a steel grade. In this example it is selected S355.

Step 5 Determine the value $c_s(\beta_w, f_y)$:

$$\text{Eq.(7.26): } c_s(\beta_w, f_y) = \frac{h_w}{b_{e1}} = 0.0443 \cdot \beta_w + 0.4943 = 0.0443 \cdot 800 + 0.4943 = 35.93$$

Step 6 Determine the minimal cross-sectional area $A_{tot,min}$, while $\gamma_{M0} = 1.0$ with Eq.(7.28):

$$\begin{aligned} A_{tot,min} &= \frac{(\gamma_{M0} \cdot M_{Ed})^{\frac{2}{3}}}{\left[\left\{ \left(\sqrt{\frac{\beta_{w,max}}{27}} + \sqrt{\frac{1}{27 \cdot \beta_{f,min}}} \right) + \frac{1}{c_s(\beta_{w,max}, f_y)} \cdot \left(\sqrt{\frac{\beta_{w,max}}{27}} - \frac{1}{c_s(\beta_{w,max}, f_y)} \cdot \sqrt{\frac{\beta_{w,max}}{27}} \right) \right\} \cdot f_y \right]^{\frac{2}{3}}} = \\ &= \frac{(1.0 \cdot 1250 \cdot 10^6)^{\frac{2}{3}}}{\left[\left\{ \left(\sqrt{\frac{800}{27}} + \sqrt{\frac{1}{27 \cdot 5}} \right) + \frac{1}{35.93} \cdot \left(\sqrt{\frac{800}{27}} - \frac{1}{35.93} \cdot \sqrt{\frac{800}{27}} \right) \right\} \cdot 355 \right]^{\frac{2}{3}}} = \\ &= \frac{1160397.2}{159.5} = 7272 \text{ mm}^2 \end{aligned}$$

Step 7 Determine the optimal dimensions of the cross-section:

$$\text{Eq.(7.20): } t_{w,opt} = \sqrt{\frac{1}{3 \cdot \beta_{w,max}}} \cdot \sqrt{A_{tot,opt}} = \sqrt{\frac{1}{3 \cdot 800}} \cdot \sqrt{7272} = 1.74 \text{ mm}$$

$$\text{Eq.(7.21): } h_{w,opt} = \sqrt{\frac{\beta_{w,max}}{3}} \cdot \sqrt{A_{tot,opt}} = \sqrt{\frac{800}{3}} \cdot \sqrt{7272} = 1393 \text{ mm}$$

$$\text{Eq.(7.22): } t_{f,opt} = \sqrt{\frac{1}{3 \cdot \beta_{f,min}}} \cdot \sqrt{A_{tot,opt}} = \sqrt{\frac{1}{3 \cdot 5}} \cdot \sqrt{7272} = 22.0 \text{ mm}$$

$$\text{Eq.(7.23): } b_{opt} = \sqrt{\frac{\beta_{f,min}}{3}} \cdot \sqrt{A_{tot,opt}} = \sqrt{\frac{5}{3}} \cdot \sqrt{7272} = 110 \text{ mm}$$

Step 8 Adapt the determined optimal dimensions of the web and the flanges of the plate girder to standardised dimensions:

The web height is taken $h_{w,ad} = 1400 \text{ mm}$ and the web thickness is $t_{w,ad} = 2 \text{ mm}$. The optimal flange width $b_{opt} = 110 \text{ mm}$ is a standardised measure, so $b_{ad} = 110 \text{ mm}$ and the optimal flange thickness $t_{f,opt} = 22.0 \text{ mm}$ is adapted to $t_{f,ad} = 25 \text{ mm}$. The contribution of the flanges to the bending moment resistance is checked:

$$\text{Eq.(7.29): } b_{ad} \cdot t_{f,ad} \cdot (h_{w,ad} + t_{f,ad}) = 110 \cdot 25 \cdot (1400 + 25) = 3918750 \text{ mm}^3 \geq$$

$$b_{opt} \cdot t_{f,opt} \cdot (h_{w,opt} + t_{f,opt}) = 110 \cdot 22.0 \cdot (1393 + 22.0) = 3429113 \text{ mm}^3$$

and:

$$\text{Eq.(7.30): } \beta_{w,ad} = \frac{h_{w,ad}}{t_{w,ad}} = \frac{1400}{2.0} = 700 \leq \beta_{w,max} = 800$$

The bending moment resistance $M_{Abspoel,Rk}$ is determined by using Eq. (7.1) with the adapted dimensions of the plate girder and by using Eq.(7.26) to determine the effective width $b_{e1,ad}$ based on the adapted dimensions:

- Determine $c_{s,ad}(\beta_{w,ad}, f_y)$:

$$\text{Eq.(7.26): } c_{s,ad}(\beta_{w,ad}, f_y) = 0.0443 \cdot \beta_{w,ad} + 0.4943 = 0.0443 \cdot 700 + 0.4943 = 31.50$$

- Determine the effective width $b_{e1,ad}$:

$$b_{e1,ad} = \frac{h_{w,ad}}{c_{s,ad}(\beta_{w,ad}, f_y)} = \frac{1400}{31.50} = 44.4 \text{ mm}$$

- Determine the characteristic bending moment resistance with Eq.(7.1):

$$\begin{aligned} M_{Abspoel,Rk} &= \left(\left\{ b \cdot t_f \cdot (h_w + t_f) + b_{el} \cdot t_w \cdot (h_w - b_{el}) \right\}_{ad} \right) \cdot f_y = \\ &= \{ 110 \cdot 25 \cdot (1400 + 25) + 44.4 \cdot 2.0 \cdot (1400 - 44.4) \} \cdot 355 \cdot 10^{-6} = \\ &= 1391.2 + 42.7 = 1433.9 \text{ kNm} \end{aligned}$$

- Determine the design value of the bending moment resistance with Eq.(7.27):

$$M_{Abspoel,Rd} = \frac{M_{Abspoel,Rk}}{\gamma_{M0}} = \frac{1433.9}{1.0} = 1433.9 \text{ kNm}$$

- The unity check is:

$$\frac{M_{Ed}}{M_{Abspoel,Rd}} = \frac{1250}{1433.9} = 0.87 \leq 1.00$$

- $A_{tot} = 8300 \text{ mm}^2$.

8.2.2 EXAMPLE 2 PLATE GIRDER WITH A WEB HEIGHT BASED ON THE ADAPTED WEB THICKNESS AND MAXIMUM WEB SLENDERNESS

This Example 2 is exactly the same as Example 1, but the dimensions are adapted in such a way that the adapted cross-sectional area is close to the optimal cross-sectional area. The procedure is exactly the same up to Step 8.

Step 8 Adapt the determined optimal dimensions of the web and the flanges of the plate girder to standardised. The adapted web thickness is $t_{w,ad} = 2 \text{ mm}$. The optimal web height $h_{w,opt}$ is adapted in such a way that the adapted web slenderness $\beta_{w,ad}$ is still equal to the maximum web slenderness $\beta_{w,max}$, so:

$$h_{w,ad} = \beta_{w,max} \cdot t_{w,ad} = 800 \cdot 2.0 = 1600 \text{ mm}$$

The flange area can be determined based on the contribution of the flange on the bending moment resistance determined by the optimal dimensions:

$$\begin{aligned} \text{Eq.(7.29): } b_{ad} \cdot t_{f,ad} \cdot (h_{w,ad} + t_{f,ad}) &\geq b_{opt} \cdot t_{f,opt} \cdot (h_{w,opt} + t_{f,opt}) \\ \Rightarrow b_{ad} \cdot t_{f,ad} &= \frac{b_{opt} \cdot t_{f,opt} \cdot (h_{w,opt} + t_{f,opt})}{(h_{w,ad} + t_{f,ad})} \approx \frac{b_{opt} \cdot t_{f,opt} \cdot (h_{w,opt} + t_{f,opt})}{h_{w,ad}} = \frac{3429113}{1600} = 2143 \text{ mm}^2 \end{aligned}$$

The optimal flange width is adapted to $b_{ad} = 140 \text{ mm}$ and the optimal flange thickness is adapted to $t_{f.ad} = 15 \text{ mm}$.

- Determine the characteristic bending moment resistance with Eq.(7.1). $c_{s.ad}(\beta_w, f_y)$ is not changed from previous example:

$$\begin{aligned} M_{Abspoel.Rk} &= \left(\left\{ b \cdot t_f \cdot (h_w + t_f) + b_{e1} \cdot t_w \cdot (h_w - b_{e1}) \right\} \right)_{ad} \cdot f_y = \\ &= \{ 140 \cdot 15 \cdot (1600 + 15) + 35.93 \cdot 2.0 \cdot (1600 - 35.93) \} \cdot 355 \cdot 10^{-6} = \\ &= 1204.0 + 39.9 = 1243.9 \text{ kNm} \end{aligned}$$

- Determine the design value of the bending moment resistance with Eq.(7.27):

$$M_{Abspoel.Rd} = \frac{M_{Abspoel.Rk}}{\gamma_{M0}} = \frac{1243.9}{1.0} = 1243.9 \text{ kNm}$$

- The unity check is:

$$\frac{M_{Ed}}{M_{Abspoel.Rd}} = \frac{1250}{1243.9} = 1.004 > 1.00$$

The plate girder does not fulfil the requirements, the flange area is selected too small and the contribution of the effective parts of the web does not fully compensate.

- The optimal flange width is adapted to $b_{ad} = 110 \text{ mm}$ and the optimal flange thickness is adapted to $t_{f.ad} = 20 \text{ mm}$.

- Determine the characteristic bending moment resistance with Eq.(7.1):

$$\begin{aligned} M_{Abspoel.Rk} &= \left(\left\{ b \cdot t_f \cdot (h_w + t_f) + b_{e1} \cdot t_w \cdot (h_w - b_{e1}) \right\} \right)_{ad} \cdot f_y = \\ &= \{ 110 \cdot 20 \cdot (1600 + 20) + 35.93 \cdot 2.0 \cdot (1600 - 35.93) \} \cdot 355 \cdot 10^{-6} = \\ &= 1265.2 + 39.9 = 1305.1 \text{ kNm} \end{aligned}$$

- Determine the design value of the bending moment resistance with Eq.(7.27):

$$M_{Abspoel.Rd} = \frac{M_{Abspoel.Rk}}{\gamma_{M0}} = \frac{1305.1}{1.0} = 1305.1 \text{ kNm}$$

- The unity check is:

$$\frac{M_{Ed}}{M_{Abspoel.Rd}} = \frac{1250}{1305.1} = 0.96 \leq 1.00$$

- $A_{tot.ad} = 7600 \text{ mm}^2$.

8.2.3 EXAMPLE 3: PLATE GIRDER WITH WEB HEIGHT CLOSE TO THE OPTIMAL WEB HEIGHT

This Example 3 is exactly the same as Example 1, but the dimensions are adapted in such a way that the adapted cross-sectional area is close to the optimal cross-sectional area. The procedure is exactly the same up to Step 8.

Step 8 Adapt the determined optimal dimensions of the web and the flanges of the plate girder to standardised dimensions:

The adapted web thickness is $t_{w.ad} = 2 \text{ mm}$ and adapted web height is $h_{w.ad} = 1375 \text{ mm}$.

The flange area can be determined based on the contribution of the flange determined by the optimal dimensions:

$$\begin{aligned} \text{Eq.(7.29): } b_{ad} \cdot t_{f.ad} \cdot (h_{w.ad} + t_{f.ad}) &\geq b_{opt} \cdot t_{f.opt} \cdot (h_{w.opt} + t_{f.opt}) \\ \Rightarrow b_{ad} \cdot t_{f.ad} &= \frac{b_{opt} \cdot t_{f.opt} \cdot (h_{w.opt} + t_{f.opt})}{(h_{w.ad} + t_{f.ad})} \approx \frac{b_{opt} \cdot t_{f.opt} \cdot (h_{w.opt} + t_{f.opt})}{h_{w.ad}} = \frac{3429113}{1375} = 2494 \text{ mm}^2 \end{aligned}$$

The optimal flange width is adapted to $b_{ad} = 165 \text{ mm}$ and the optimal flange thickness is adapted to $t_{f.ad} = 15 \text{ mm}$.

- Determine the adapted web slenderness:

$$\text{Eq.(7.30): } \beta_{w.ad} = \frac{h_{w.ad}}{t_{w.ad}} = \frac{1375}{2} = 687.5 \leq \beta_{w.max} = 800$$

- Determine $c_{s.ad}(\beta_w, f_y)$:

$$\text{Eq.(7.26): } c_{s.ad}(\beta_{w.ad}, f_y) = 0.0443 \cdot \beta_{w.ad} + 0.4943 = 0.0443 \cdot 687.5 + 0.4943 = 30.95$$

- Determine the effective width $b_{e1.ad}$:

$$b_{e1.ad} = \frac{h_{w.ad}}{c_{s.ad}(\beta_{w.ad}, f_y)} = \frac{1375}{30.95} = 44.4 \text{ mm}$$

- Determine the characteristic bending moment resistance with Eq.(7.1):

$$\begin{aligned} M_{Abspoel.Rk} &= \left(\left\{ b \cdot t_f \cdot (h_w + t_f) + b_{e1} \cdot t_w \cdot (h_w - b_{e1}) \right\}_{ad} \right) \cdot f_y = \\ &= \{ 165 \cdot 15 \cdot (1375 + 15) + 44.40 \cdot 2.0 \cdot (1375 - 44.40) \} \cdot 355 \cdot 10^{-6} = \\ &= 1221.3 + 41.9 = 1263.2 \text{ kNm} \end{aligned}$$

- Determine the design value of the bending moment resistance with Eq.(7.27):

$$M_{Abspoel.Rd} = \frac{M_{Abspoel.Rk}}{\gamma_{M0}} = \frac{1263.2}{1.0} = 1263.2 \text{ kNm}$$

- The unity check is:

$$\frac{M_{Ed}}{M_{Abspoel.Rd}} = \frac{1250}{1263.2} = 0.99 \leq 1.00$$

- $A_{tot.ad} = 7700 \text{ mm}^2$.

8.2.4 EXAMPLE 4: PLATE GIRDER WITH A LIMITED WEB HEIGHT

This Example 3 is exactly the same as Example 1, but the web height is based on a limited height equal to $h = 1000 \text{ mm}$. The procedure is exactly the same up to Step 7.

Step 8 Adapt the determined optimal dimensions of the web and the flanges of the plate girder to

standardised dimensions such that $\beta_{w.ad} = \frac{h_{w.ad}}{t_{w.ad}} \leq 800$ and:

$$(h_{w.ad} + t_{f.ad}) \cdot b_{ad} \cdot t_{f.ad} \geq (h_{w.opt} + t_{f.opt}) \cdot b_{opt} \cdot t_{f.opt}.$$

The web height is taken $h_{w.ad} = 1000 \text{ mm}$ and the web thickness is $t_{w.ad} = 2 \text{ mm}$. The flange area can be determined based on the minimal contribution of the flange and the selected web height $h_{w.ad} = 1000 \text{ mm}$:

$$(A_f)_{ad} \geq \frac{((h_w + t_f) \cdot b \cdot t_f)_{opt}}{(h_w)_{ad}} = \frac{3429113}{1000} = 3429 \text{ mm}^2$$

The optimal flange width is adapted to $b_{ad} = 180 \text{ mm}$ and the optimal flange thickness is adapted to $t_{f.ad} = 20 \text{ mm}$. Finally, the web height is adapted to $h_{w.ad} = 960 \text{ mm}$ and the web thickness is taken $t_{w.ad} = 2 \text{ mm}$.

- Determine the adapted web slenderness $\left(\beta_w = \frac{h_w}{t_w} \right)_{ad} = \frac{960}{2.0} = 480 \leq \beta_{w,max} = 800$;

- Determine $c_{s.ad}(\beta_{w.ad}, f_y)$:

$$\text{Eq.(7.26): } c_{s.ad}(\beta_{w.ad}, f_y) = 0.0443 \cdot \beta_{w.ad} + 0.4943 = 0.0443 \cdot 480 + 0.4943 = 21.76$$

- Determine the effective width $b_{e1.ad}$ based on the adapted dimensions:

$$b_{e1.ad} = \frac{h_{w.ad}}{c_{s.ad}(\beta_{w.ad} \cdot f_y)} = \frac{960}{21.76} = 44.1 \text{ mm}$$

- Determine the characteristic bending moment resistance with Eq.(7.1):

$$\begin{aligned} M_{Abspoel.Rk} &= \left(\left\{ b \cdot t_f \cdot (h_w + t_f) + b_{e1} \cdot t_w \cdot (h_w - b_{e1}) \right\}_{ad} \right) \cdot f_y = \\ &= \{180 \cdot 20 \cdot (960 + 20) + 44.1 \cdot 2 \cdot (960 - 44.1)\} \cdot 355 \cdot 10^{-6} = \\ &= 1252.4 + 28.7 = 1281.1 \text{ kNm} \end{aligned}$$

- Determine the design value of the bending moment resistance with Eq.(7.27):

$$M_{Abspoel.Rd} = \frac{M_{Abspoel.Rk}}{\gamma_{M0}} = \frac{1281.1}{1.0} = 1281.1 \text{ kNm}$$

- The unity check is:

$$\frac{M_{Ed}}{M_{Abspoel.Rd}} = \frac{1250}{1281.1} = 0.98 \leq 1.00$$

- $A_{tot} = 9120 \text{ mm}^2$

8.2.5 COMPARISON WITH A HOT-ROLLED SECTION

It is of interest to compare the resistance of the designed plate girder with the resistance of a comparable hot-rolled section. IPE400 has a cross-sectional area of $A_{tot} = 8446 \text{ mm}^2$, 10% more than the cross-sectional area with standardised dimensions in Example 1.

The bending moment resistance of this IPE400 for steel grade S355, is:

$$M_{pl} = W_{pl} \cdot f_{yd} = 1307 \cdot 10^3 \cdot 355 \cdot 10^{-6} = 464.0 \text{ kNm}$$

This means that, as compared with the hot-rolled section, the plate girder has at least 2.7 times more bending moment resistance.

The second moment of area, or the so called moment of inertia, of the IPE is $I_y = 23128 \cdot 10^4 \text{ mm}^4$.

The second moment of area for the plate girder of Example 1 with the adapted dimensions, based on only the flanges, is $I_y = 239107 \cdot 10^4 \text{ mm}^4$. This means that the second moment of area is at least 10.3 times larger than the second moment of area of the hot-rolled section IPE400. But of course, the height of the plate girder is much higher than the height of the hot-rolled section.

8.3 CONCLUSIONS

The following conclusions are drawn:

1. The developed design procedure is a very easy procedure to determine the minimum cross-sectional area for a double symmetric plate girder under the maximum bending moment as effect of the factored loading acting on this plate girder;
2. The flexural stiffness of an optimised plate girder is very large compared with the flexural stiffness of a hot-rolled section with comparable cross-sectional area and so it is of interest to use steel with a higher steel grade;
3. The minimum cross-sectional area to restrain the maximum bending moment as effect of the factored loading is very small and a reduction of the material use up to 50% is possible.

9 CONCLUSIONS AND RECOMMENDATIONS

9.1 CONCLUSIONS

The following conclusions are drawn:

1. Vertical buckling of the compressive flange into the web does not determine the bending moment resistance of the Delft test specimens, although for 8 of the 10 test specimens the web slenderness is larger than the maximum web slenderness as given in EN1993-1-5 which is based on Basler's theory;
2. The nominal web slenderness's used in the Delft experiments were $\beta_w = 400$, 600 and 800 respectively. The steel grade used in the Delft experiments was S235. However the actual values of the steel material used in the Delft experiments was up to $f_y = 350 \text{ MPa}$ for the flanges, so close to the nominal value for the yield stress of steel grade S355.

Based on this information it can be concluded that the maximum web slenderness related to the steel grade S355 is at least $\beta_{w,\max} = 800$;

3. The maximum web slenderness $\beta_{w,\max}$ is smaller for higher steel grades based on EN1993-1-5 and confirmed by the parametric study in Chapter 7, but based on different criteria. Due to this limitation of $\beta_{w,\max}$ which is dependent on the steel grade, the bending moment resistance of steel plate girders with a web slenderness equal to their steel grade related maximum web slenderness is not linearly dependent on the nominal value of the yield stress of that steel grade;
4. For simplicity a full plastic stress distribution acting on a simplified symmetric effective cross section is used for plate girders to determine the bending moment resistance. The strain distributions found in the Delft experiments confirm the use of this plastic stress distribution and the bending moment resistances determined in the parametric study fit very well with the effective bending moment resistances based on this simplified full plastic distribution;
5. A simple design strategy is presented to determine the dimensions of an optimal plate girder with a web slenderness smaller than or equal to the maximum web slenderness in order to reach a bending moment resistance sufficient to carry the external loading;
6. For cases where the deflection criterion is not governing, it is concluded that possible material savings obtained by using high strength steel grades and by optimising the cross sections of plate girders are possible up to approximately 50% compared to using hot-rolled sections of

mild steel grades with the same bending moment resistance. This is an important finding for reducing the carbon footprint of steel structures.

9.2 RECOMMENDATIONS FOR FUTURE WORK

The following recommendations are made:

1. The maximum web slenderness for plate girders made of steel grade S355 is based on interpolation and for plate girders made of steel grade S690 is based on extrapolation of the results obtained from the parametric study. Additional parametric research using FEM is needed to confirm these interpolated and extrapolated maximum web slenderness's $\beta_{w,max}$;
2. Conduct research into the maximum web slenderness $\beta_{w,max}$ related to practical issues, such as transport and erection on site to prevent damage to plate girders with a very slender web;
3. Additional experiments should be conducted to confirm the maximum web slenderness $\beta_{w,max}$ as determined in the parametric research, but also based on the results of recommendation 2, focusing on the following:
 - a. A constant ratio of area $\rho = \frac{A_w}{A_f} = 1.0$
 - b. Steel grades S460 and S690;
 - c. All test specimens had a nominal web thickness $t_w = 1 \text{ mm}$ to reduce the height and the span of the test specimen to fit in a laboratory situation. It is of interest to conduct additional experiments on plate girders with dimensions and spans which are more realistic with respect to applications in practice;
4. Unprotected steel girders for which the strength is governing instead of the stiffness, like the optimised plate girders or trusses, are very sensitive to fire because the steel heats up quickly.

Although the fire safety requirement for industrial halls in terms of time till failure due to elevated temperatures in The Netherlands is zero minutes, there are two issues of interest to research:

- a. Determine a realistic escape time needed authorised employees to evacuate an industrial hall as function of the area and shape of that industrial hall and the fire load in that hall;
- b. Determine the maximum web slenderness $\beta_{w,max}$ related to fire safety to realise the required escape time based on previous recommendation in cases of unprotected or protected steel plate girders.

10 REFERENCES

- [1] Abspoel, R.: Optimizing plate girder design. Nordic Steel Construction Conference. (2009)
- [2] Abspoel, R.: The maximum web slenderness of plate girders. Eurosteel 2008, proceedings of the 5th European Conference on Steel and Composite Structures. (2008)
- [3] Abspoel, R. and Bijlaard F.S.K.: Optimization of plate girders. Steel Construction, Volume 7 Issue 2. (2014)
- [4] Abspoel, R.: The maximum bending moment resistance of plate girders. Eurosteel 2014, proceedings of the 7th European Conference on Steel and Composite Structures. (2014)
- [5] AISC 360-10 [5]: Specification for structural steel buildings. American National Standard Institute/American Institute of Steel Construction. (2010)
- [6] Basler, K.: Strength of plate girders. PhD dissertation, Lehigh University Bethlehem. (1959)
- [7] Basler, K., Thürlimann, B.: Plate girder research. A.I.S.C. National Engineering Conference, proceedings. (1959)
- [8] Basler, K., Thürlimann, B.: Buckling tests on plate girders. IABSE, conference Stockholm. (1960)
- [9] Basler, K., Yen, B.T., Mueller, J.A., Thürlimann, B.: Web buckling test on welded plate girders. Overall introduction and Part 1: The test girders. Welded plate girders Report, Lehigh University Bethlehem. No. 251-11 (1960)
- [10] Basler, K., Yen, B.T., Mueller, J.A., Thürlimann, B.: Web buckling test on welded plate girders. Part 2: Test on plate girders subjected to bending. Welded plate girders Report, Lehigh University Bethlehem. No. 251-12 (1960)
- [11] Basler, K.: Further test on welded plate girders. National Engineering Conference, Proceedings.. No. 251-16 (1960)
- [12] Basler, K., Thürlimann, B.: Strength of plate girders in bending. Welded plate girders Report, Lehigh University Bethlehem. No. 251-19 (1960)
- [13] Basler, K.: New provisions for plate girder design. AISC 360-10 [5], National Engineering Conference Proceedings. (1961)
- [14] Basler, K., Yen, B.T., Mueller, J.A., Thürlimann, B.: Web buckling tests on welded plate girders. Welding research council. Bulletin No. 64 (1960)
- [15] Basler, K., Thürlimann, B.: Strength of plate girders in bending. Journal Structural Division, ASCE, proceedings. ST 7 (1961)
- [16] Basler, K., Thürlimann, B.: Strength of plate girders in bending. ASCE, proceedings, Journal of the structural division. ST 7 (1961)

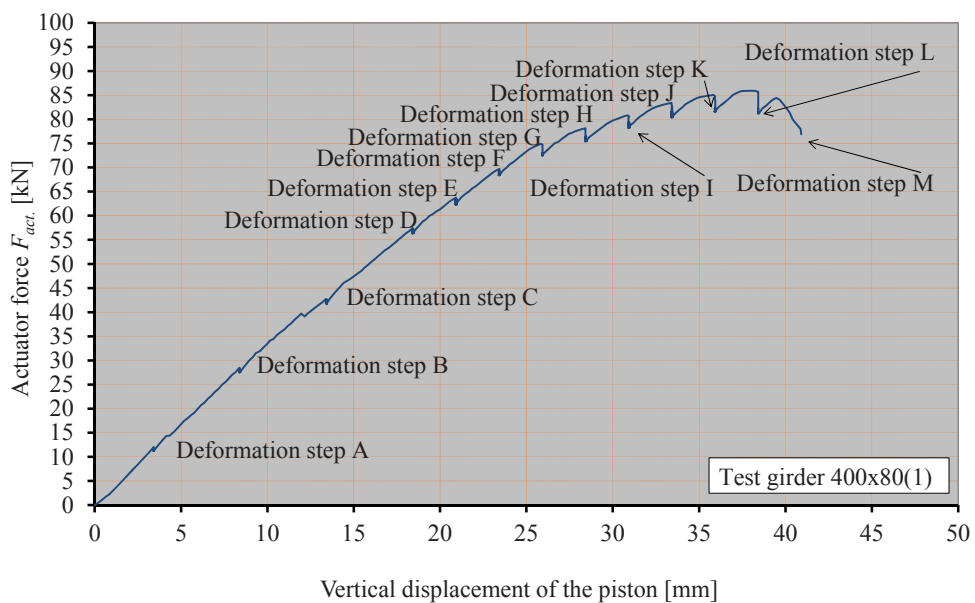
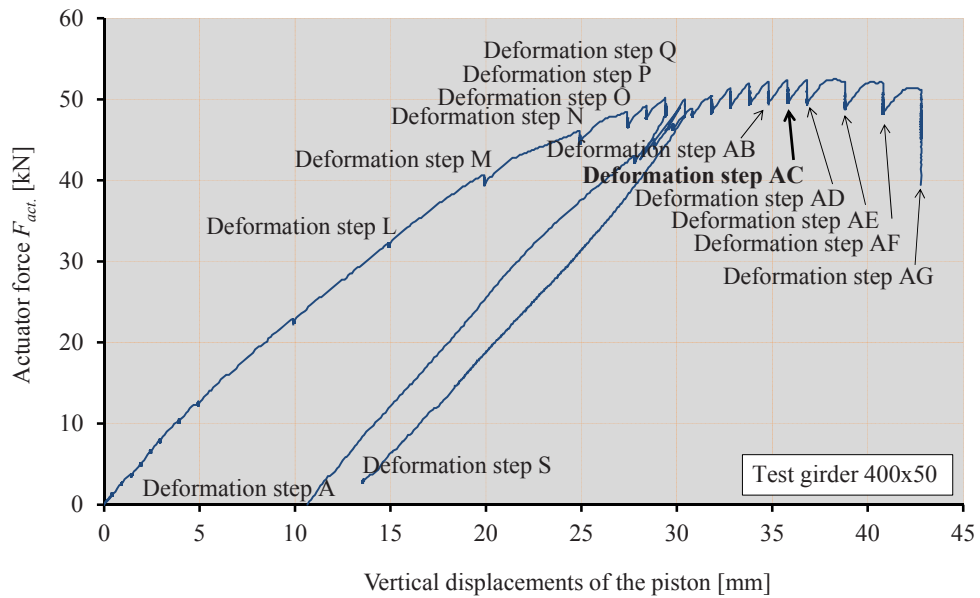
- [17] Bergfelt, A., Hovik, J.: Thin walled deep plate girders under static loads. IABSE, 8th congress, proceedings. (1968)
- [18] Bergfelt, A.: Plate girders with slender web-survey and a modified calculation method. Nordiske forskningsdagar for stålkonstruksjoner. Report No. 11 2.2 (1973)
- [19] Bleich, F.: Die Stabilität dünner Wände gedruckter Stäbe. I.V.B.H., conference Paris. (1932)
- [20] Bleich, F.: Buckling strength of metal structures. McGraw-Hill Company. (1952)
- [21] Bleich, F., Bleich, H.: Bending, torsion and buckling of bars composed of thin walls. IABSE, conference. (1936)
- [22] Borst, R. de, Crisfield, M.A., Remmers, J.J.C., Verhoosel, C.V.: Non-linear finite element analysis of solids and structures. Wiley series in computational mechanics. (2012)
- [23] Bryan, G.H.: On the stability of a plane plate under thrusts in its own plane, with application to the buckling of the sides of a ship. Mathematic Society, conference London. Vol. 22 (1891)
- [24] BSK99: Swedish regulations for steel structures. BSK99. (1999)
- [25] Coan, J.M.: Large deflection theory for plates with small initial curvatures, loaded in edge compression. Journal of the applied mechanics. Vol. 18 No. 2 (1957)
- [26] Cooper, P.B., Lew, H.S., Yen, B.T.: Investigation of web buckling in steel beams. ASCE, proceedings, Journal of the structural division. ST 1 (1964)
- [27] Donnell, L.H., Kármán, T.H., Sechler, E.E.: Strength of thin plates in compression. A.S.M.E., transactions. Vol. 54 (1932)
- [28] Dudley, K.E.: Lateral web deflections of welded test girders. Welded plate girders Report, Lehigh University Bethlehem. No. 303-7 (1965)
- [29] EN 1993-1-1: Eurocode 3: Design of steel structures - Part 1-1: General rules and rules for buildings. EN 1993-1-1. (2006)
- [30] EN 1993-1-5: Eurocode 3: Design of steel structures - Part 1-5: Plated structural elements. EN 1993-1-5. (2006)
- [31] EN10025-1: Hot-rolled products of structural steels - Part 1: General technical delivery conditions. EN 10025-1. (2004)
- [32] EN10025-2: Hot-rolled products of structural steels - Part 2: General technical delivery non-alloy structural steels. EN 10025-2. (2004)
- [33] EN-ISO 6892-1: Metallic materials - Tensile testing - Part 1: Method of test at room temperature (ISO 6892-1:2009, IDT). EN-ISO 6892-1. (2009)
- [34] EUR 8849: Draft Eurocode 3: common unified rules for steel structures. EUR 8849. (1984)

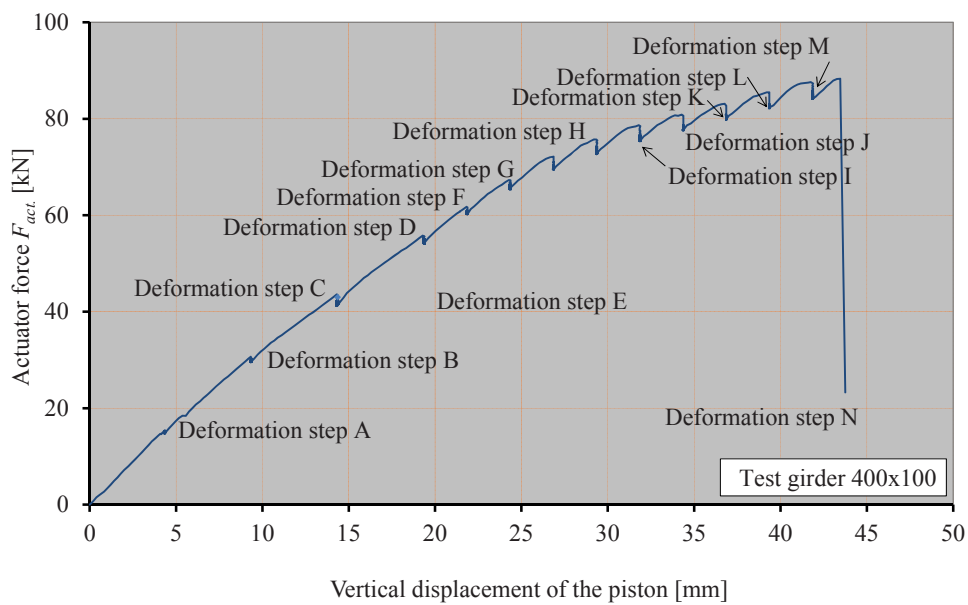
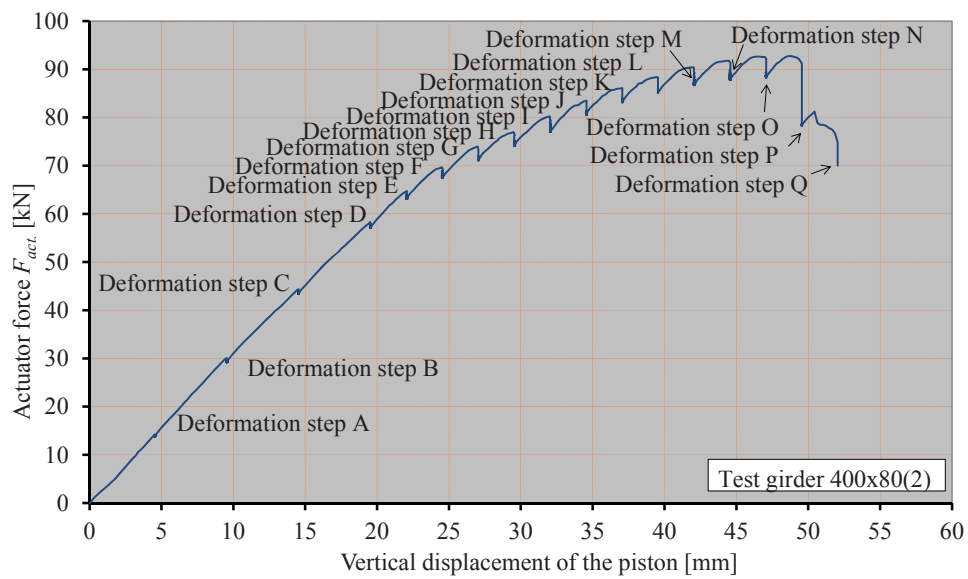
- [35] Fujii, T.: Minimum weight design of structures based on buckling strength and plastic collapse (3rd Report). Journal of the society of naval architects of Japan. Vol. 122 (1967)
- [36] Fujii, T.: On an improved theory for Dr. Basler's theory. IABSE, conference. (1968)
- [37] Fujii, T., Fukumoto, Y., Nishino, F., Okumura, T.: Research works on ultimate strength of plate girders and Japanese provisions on plate girder design. IABSE, conference. (1971)
- [38] Galambos, T.V.: Guide to stability design criteria for metal structures. Book, John Wiley & sons, Inc. (1988)
- [39] Girkmann, K.: Flachentragwerke. Book, Springer Wien. (1956)
- [40] Haaijer, G., Thürlimann, B.: On inelastic buckling in steel. ASCE transactions. Vol. 84 (EM2) (1958)
- [41] Herzog, M.: Die Traglast versteifter, dunwandiger Blechträger. Der Bauingenieur. Heft 9, No. 48 (1973)
- [42] Höglund, T.: Simply supported long thin plate I-girders without web stiffeners subjected to distributed transverse load. IABSE, conference. (1971)
- [43] Hu, P.C., Lundquist, E.E., Batdorf, S.B.: Investigation of web buckling in steel beams. N.A.C.A.. TN 1124 (1946)
- [44] Ivanco (2011), Nonlinear Finite Element Analysis, script of lectures, Technical University of Kosice, Slovakia, (2011)
- [45] Johansson, B., Maquoi, R., Sedlacek, G.: New design rules for plated structures in Eurocode 3. Journal of constructional steel research. 57 (2001)
- [46] Kármán, Th. Von: Encyklopadie der mathematischen Wissenschaften. Book. Vol. 15/4 (1910)
- [47] Kármán, Th. Von, Sechler, E.E., Donnell, L.H.: Strength of thin plates in compression. A.S.M.E., transactions. Vol. 54 (1932)
- [48] Klöppel, K., Scheer, J.: Das praktische Aufstellen von Beul determinanten für Rechteckplatten mit randparallelen Steifen bei Navierschen Randbedingungen. Der Stahlbau. Vol. 25 (1956)
- [49] Kollbrüner, C.F., Meister, M.: Ausbeulen. Book, Springer-Verlag. (1958)
- [50] Lee, G.C.: A survey of literature on the lateral instability of beams. Welding research council. Bulletin No. 63 (1960)
- [51] Levy, S.: Bending of rectangular plates with large deflections. N.A.C.A.. T.N. 846 (1942)
- [52] Levy, S.: Square plate with clamped edges under normal pressure. N.A.C.A.. T.N. 847 (1942)

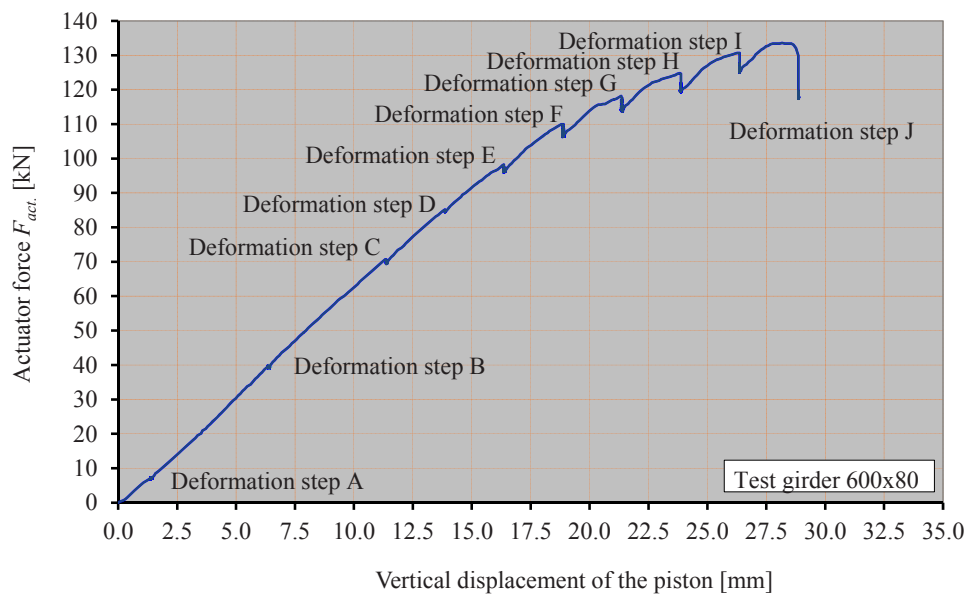
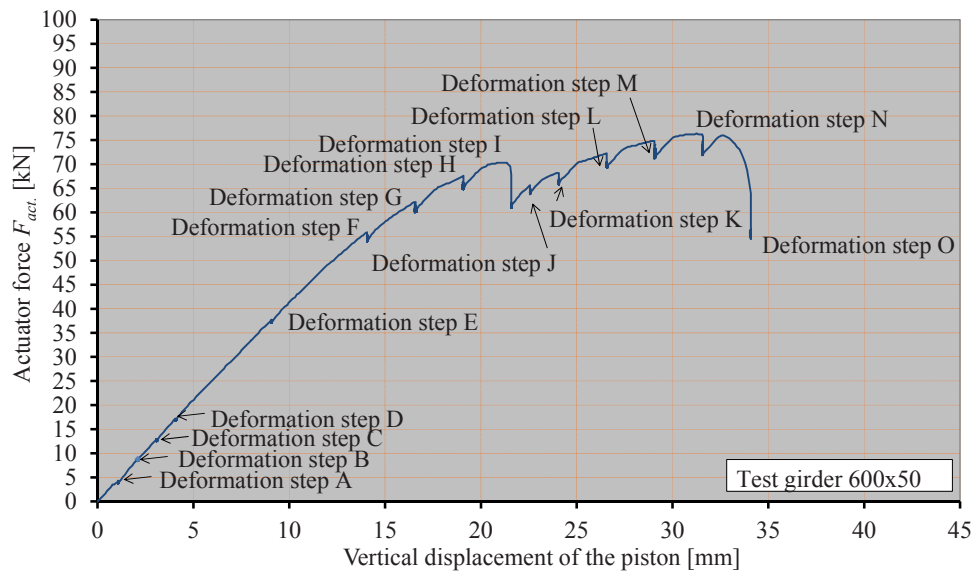
- [53] Lew, H.S., Toprac, A.A.: Research on the static strength of hybrid plate girders. Council Bulletin. No. 64 (1960)
- [54] Longbottom, E., Heyman, J.: Experimental verification of the strengths of plate girders designed in accordance with the revised British Standard 153: Tests on full size and on model plate girders. Institution of Civil Engineers. Paper no. 49 (1956)
- [55] Lündquist, E.E., Stowell, E.Z.: Critical compressive stress for outstanding flanges. N.A.C.A.. T.N. 734 (1942)
- [56] Lyse, I., Godfrey, H.: Investigation of web buckling in steel beams. ASCE, transactions. (1935)
- [57] Marc 2003 and 2012 User guide (2003 and 2012)
- [58] Marquerre, K.: Die mittragende Breite der gedrückten Platte. Luftfahrt Forschung. Vol. 14 (1937)
- [59] Massonnet, Ch.: Stability considerations in the design of steel plate girders. A.S.C.E., proceedings. Vol. 86, No. 2350 (1960)
- [60] Massonnet, Ch.: Thin walled deep plate girders. International Association for Bridge and Structural Engineering, 8th Congress. Theme II C (1968)
- [61] Nadai, A.: Elastischen Platten. Book, Springer Berlin. (1925)
- [62] NEN6771: Technische grondslagen voor bouwconstructies - TGB 1990 - Staalconstructies - Stabiliteit (in Dutch). NEN 6771. (2002)
- [63] Ostapenko, A., Yen, B.T., Lynn, S.: Research on plate girders at Lehigh University. IABSE, conference. (1968)
- [64] Reissner, H.: Über die Knicksicherheit ebener Bleche. Zentralblatt der Bauverwaltung. (1909)
- [65] Ritz, W.: Über eine neue Methode zur Lösung gewisser Variationsproblem der mathematischer Physik. Journal für die reine und angewende Mathematik. Vol. 135 (1909)
- [66] Rocky, K.G., Jenkins, F.: The behaviour of web plates of plate girders subjected to pure bending. Structural Engineer. Vol. 35, No. 5 (1957)
- [67] Rocky, K.G.: Web buckling and plate girder design. Engineering. Vol. 185, No. 4800 (1958)
- [68] Rode, H.H.: Beitrag zur Theorie der Knickscheinungen. Eisenbau. Vol. 7 (1916)
- [69] Sechler, E.E.: Stress distribution of stiffened panels under compression. Journal of the Aeronautic Science (1933)
- [70] Stark, J.W.B.: Berekening van onverstijfde plaatliggers volgens moderne voorschriften. Bouwen met staal, nr. 86 (1988)

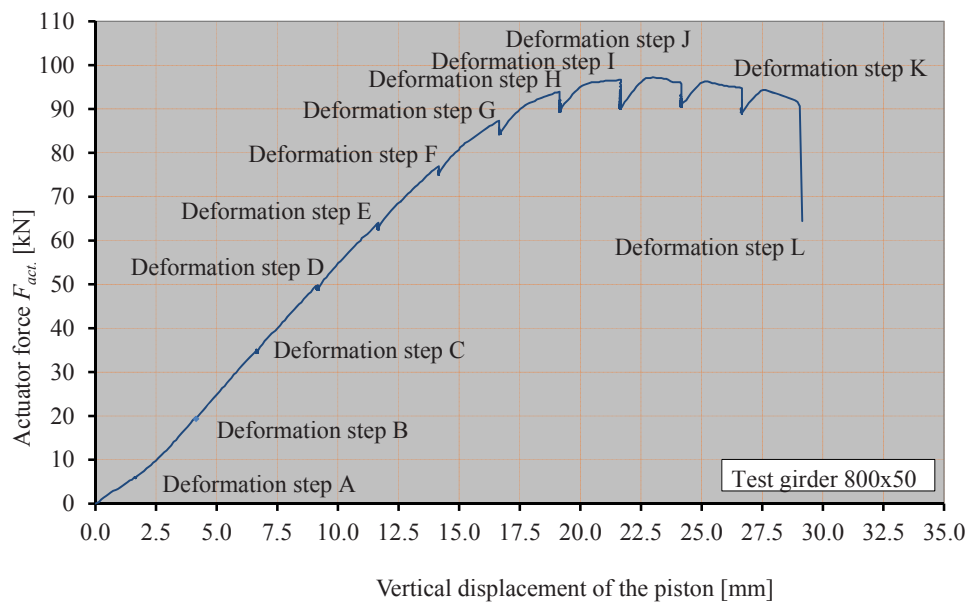
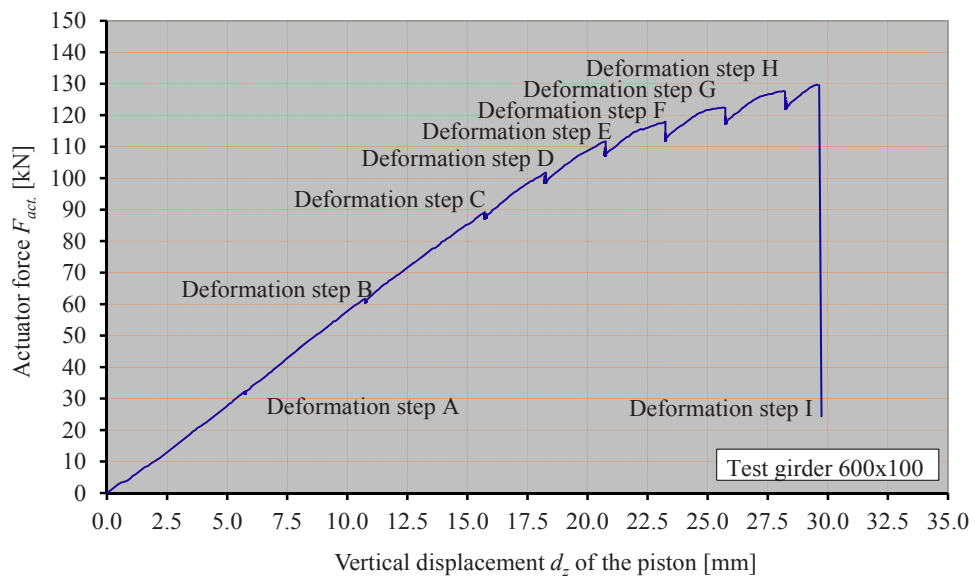
- [71] Timoshenko, S.P., Goodier, J.N.: Theory of elasticity. Book, McGraw-Hill Book Company. (1951)
- [72] Timoshenko, S.P., Gere, J.M.: Theory of elastic stability. Book, McGraw-Hill Book Company. (1961)
- [73] Timoshenko, S.P.: Theory of elastic stability. Book, McGraw-Hill Book Company. (1936)
- [74] Veljkovic, M., Johansson, B.: Design of hybrid steel girders. Journal of construction steel research. (2004)
- [75] Wagner, H.: Ebene Blechwandträger mit sehr dünnen Stegblech. Zeitschrift zur Flügtechnik und Motorluftschiffahrt. 20 (1929)
- [76] Winter, G.: Strength of thin steel compressive flanges. ASCE transactions. Vol. 112 (1947)
- [77] Winter, G.: Post-buckling strength of plates in steel design. IABSE, final report. (1952)
- [78] Yen, B.T., Basler, K.: Results of an investigation of plate girders. Welded plate girders Report, Lehigh University Bethlehem. No. 251-25 (1962)
- [79] Yen, B.T., Beedle, L.S.: A final report on project 251, welded plate girders. Welded plate girders Report, Lehigh University Bethlehem. No. 251-30 (1963)
- [80] Yen, B.T.: Final report on research projects on symmetrical welded plate girders. Welded plate girders Report, Lehigh University Bethlehem. No. 327-10 (1972)

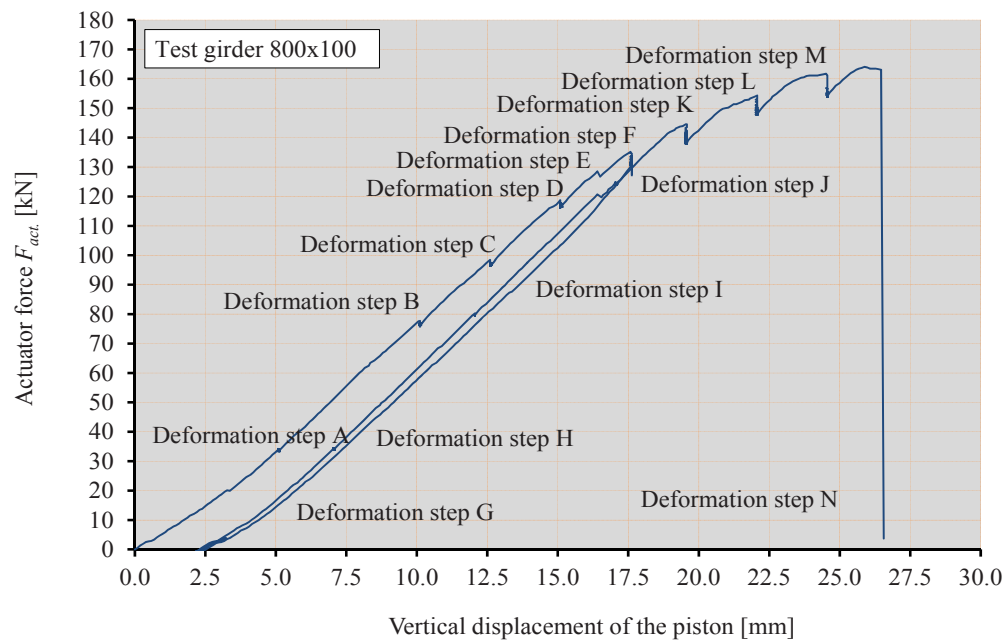
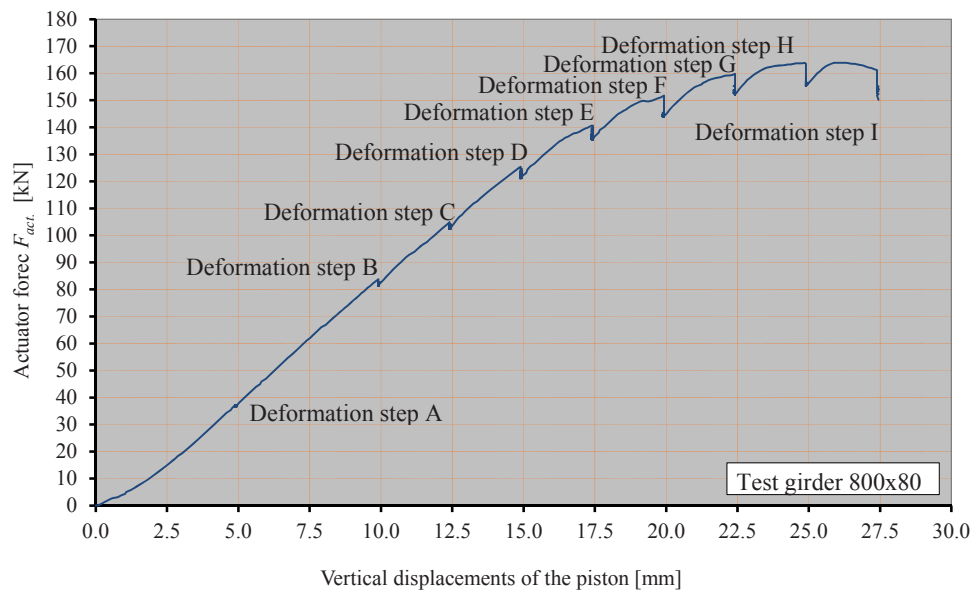
APPENDIX A THE ACTUATOR FORCE VERSUS DISPLACEMENTS OF THE PISTON



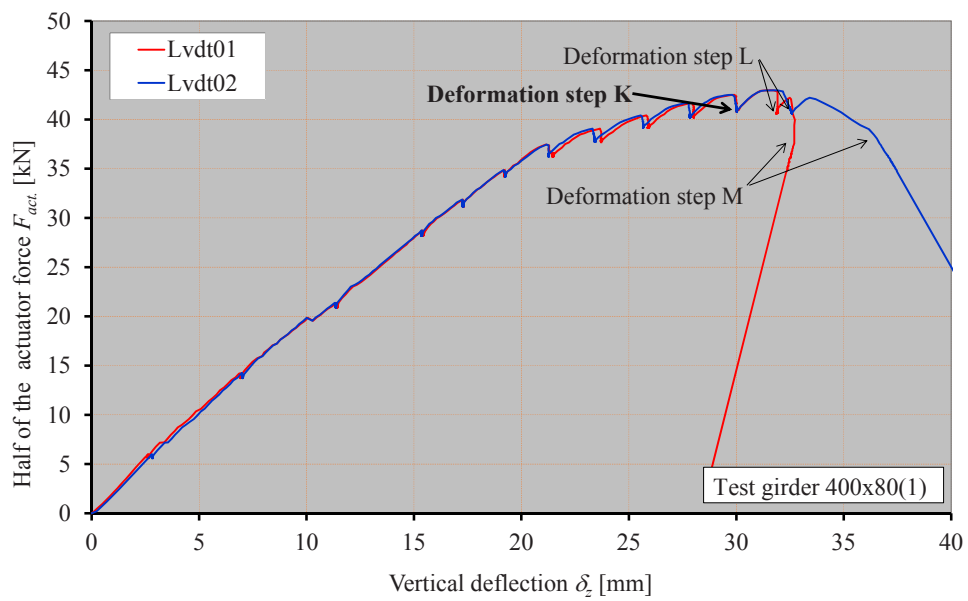
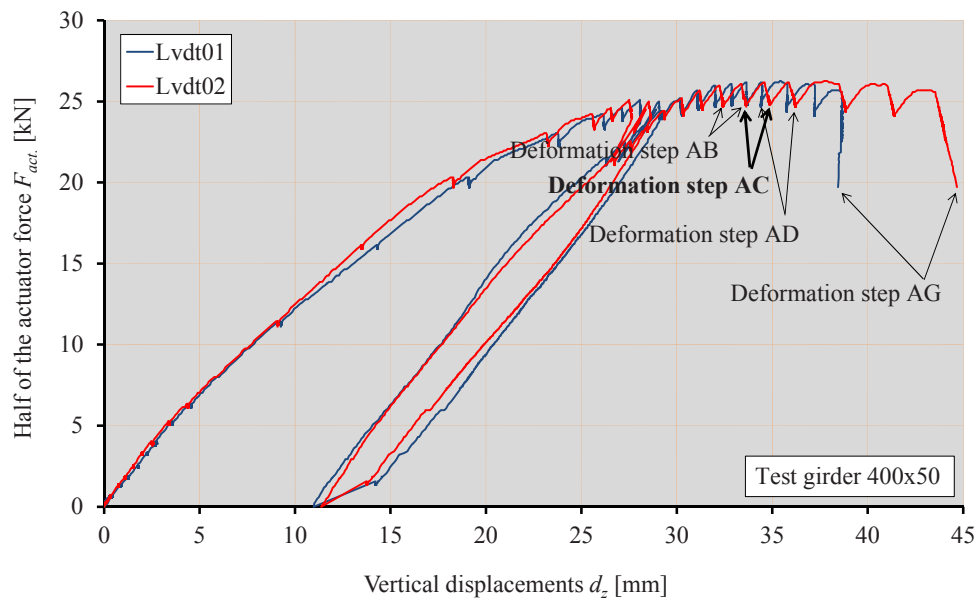


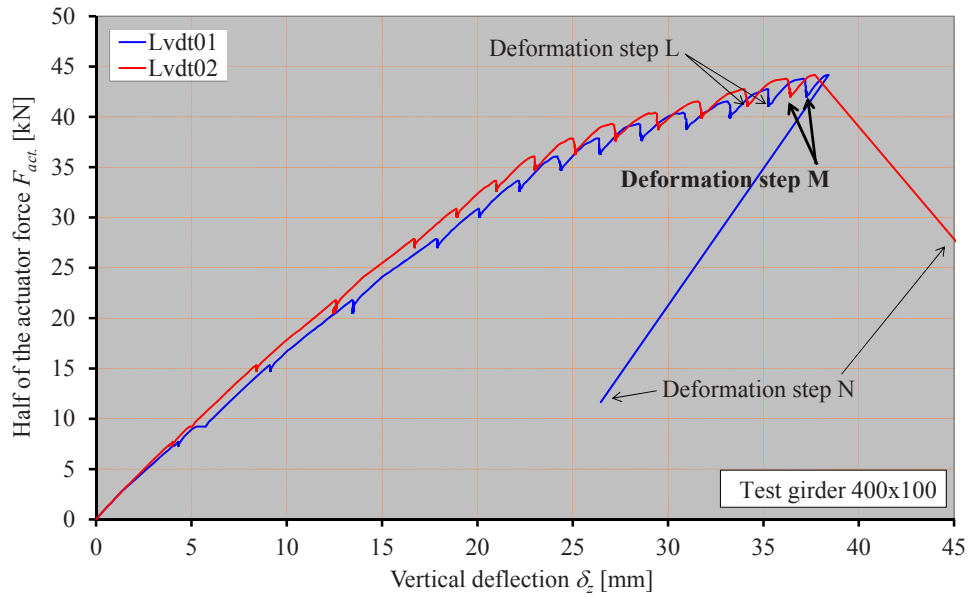
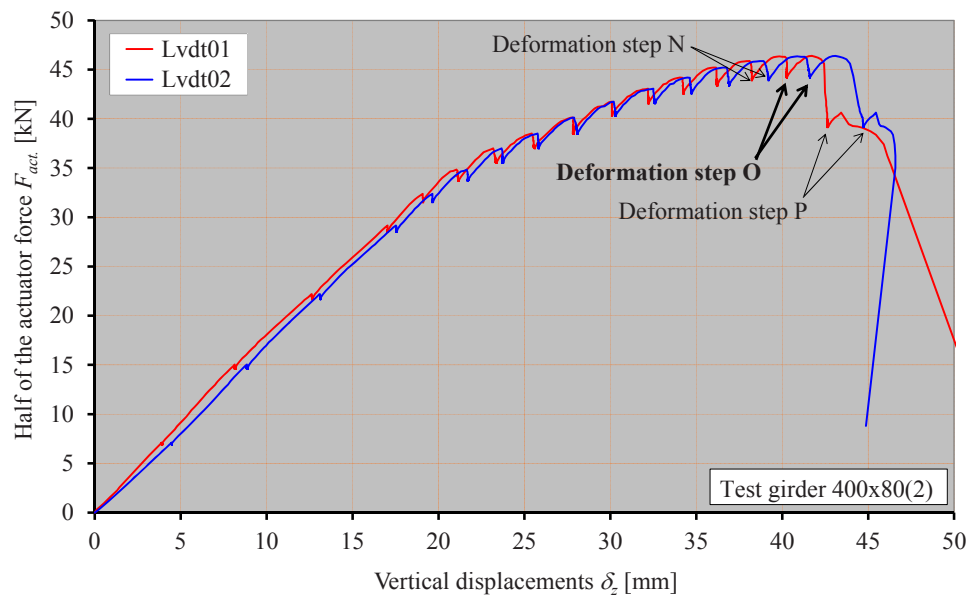


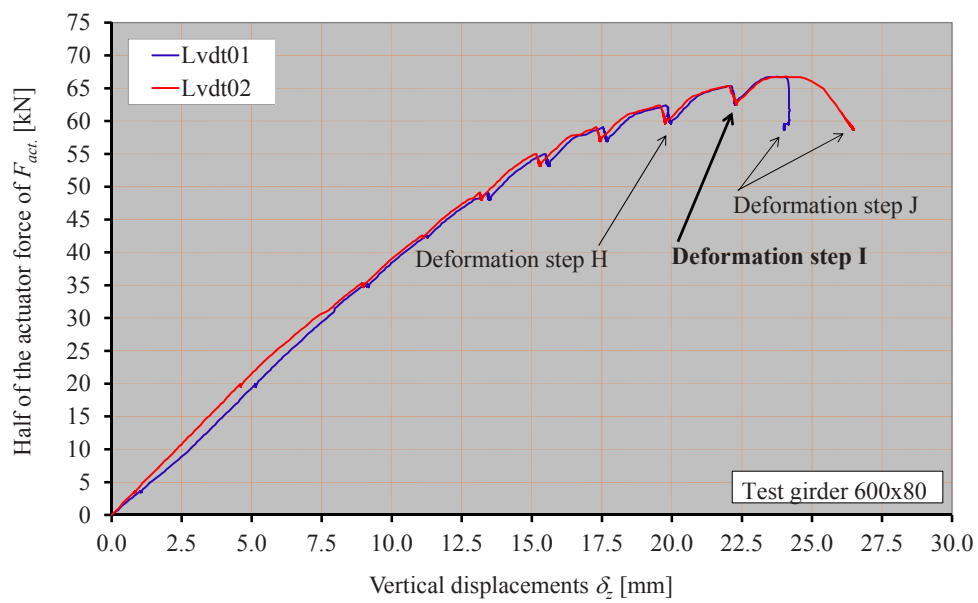
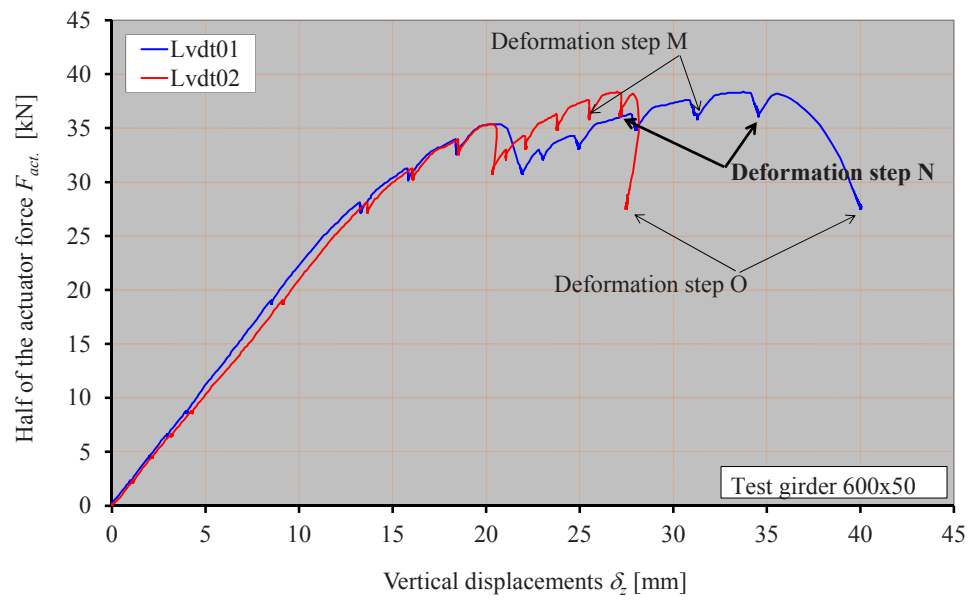


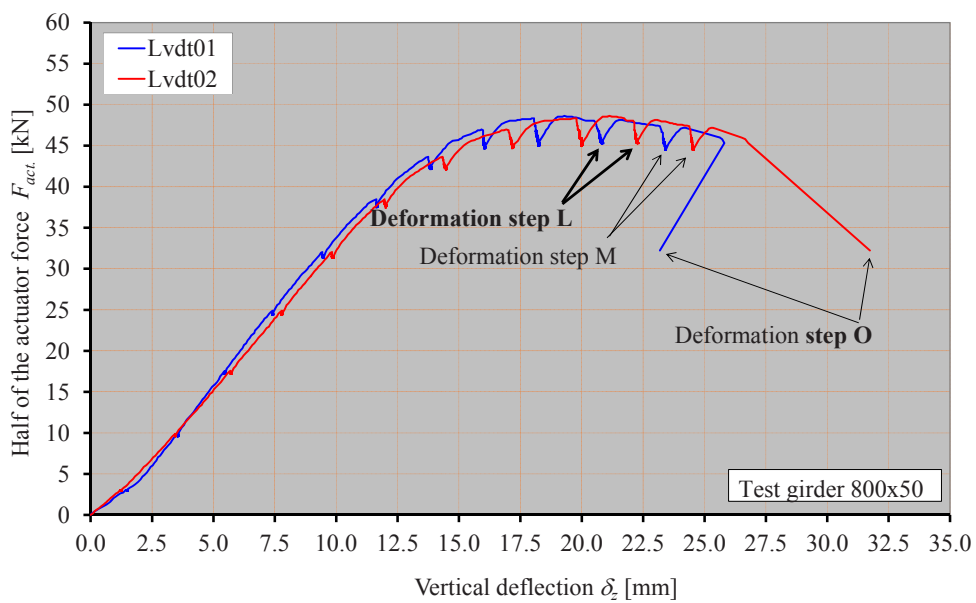
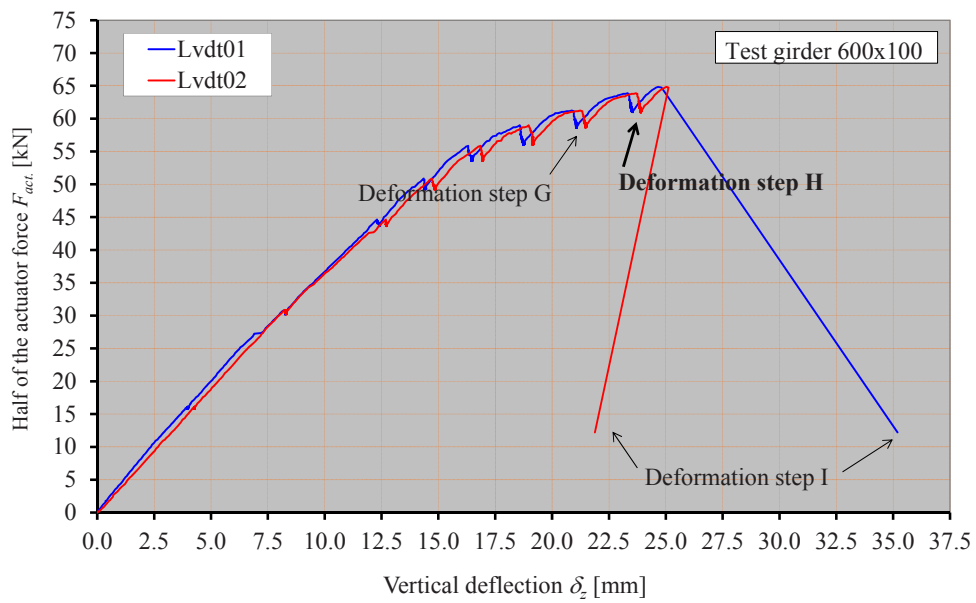


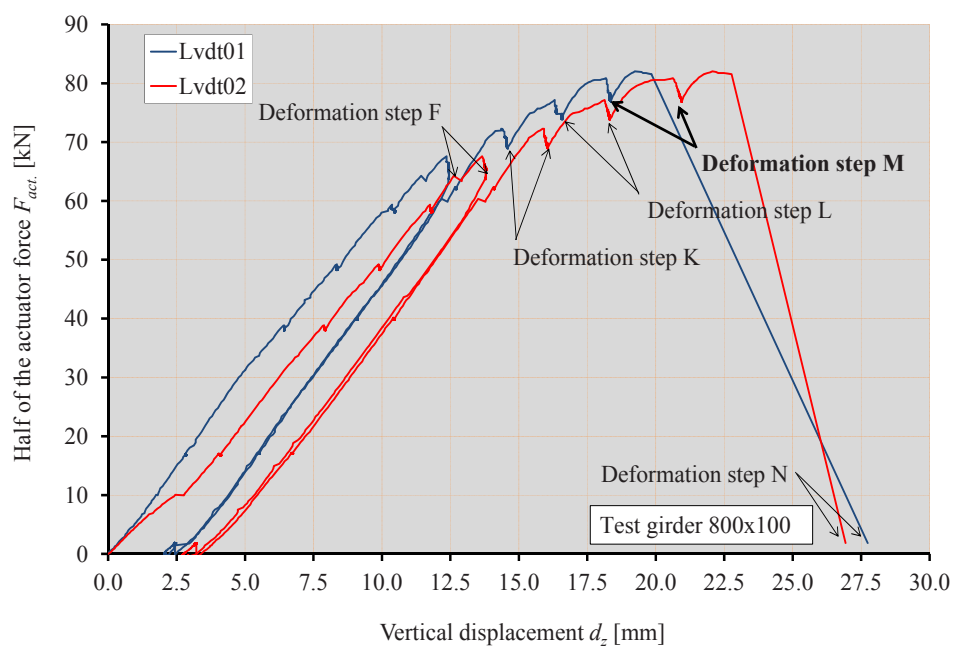
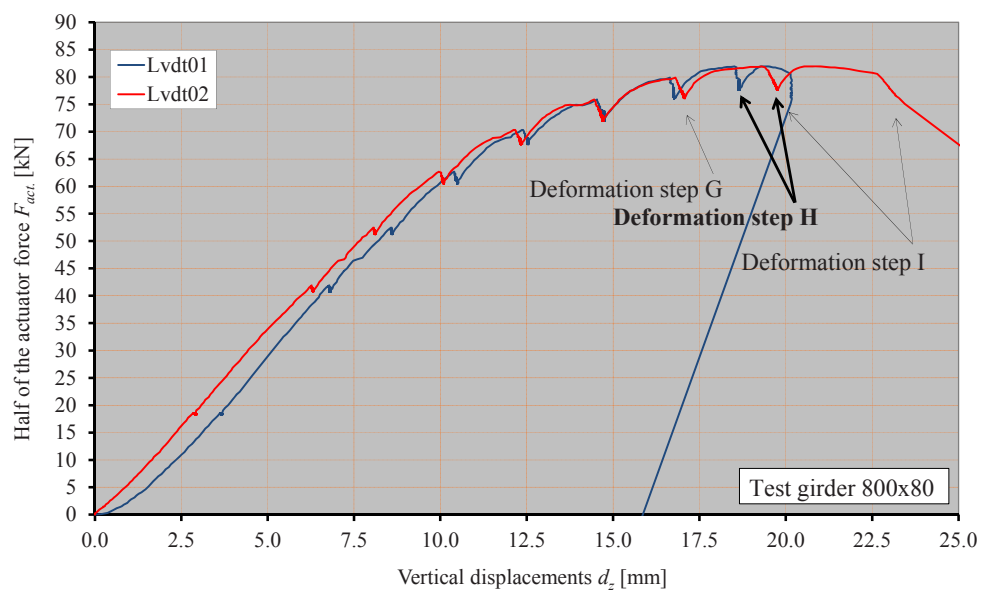
APPENDIX B HALF OF THE ACTUATOR FORCE VERSUS THE VERTICAL DISPLACEMENTS



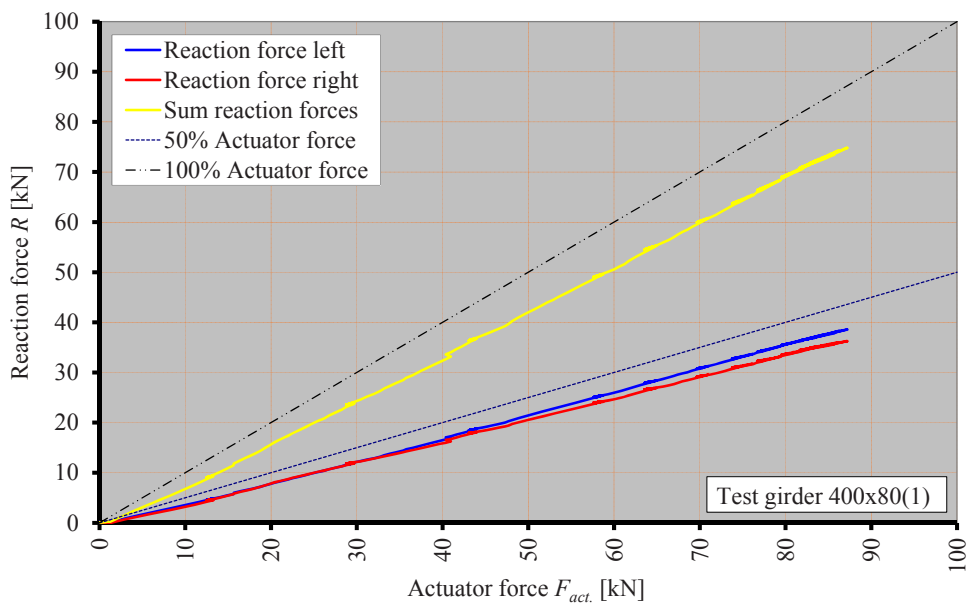
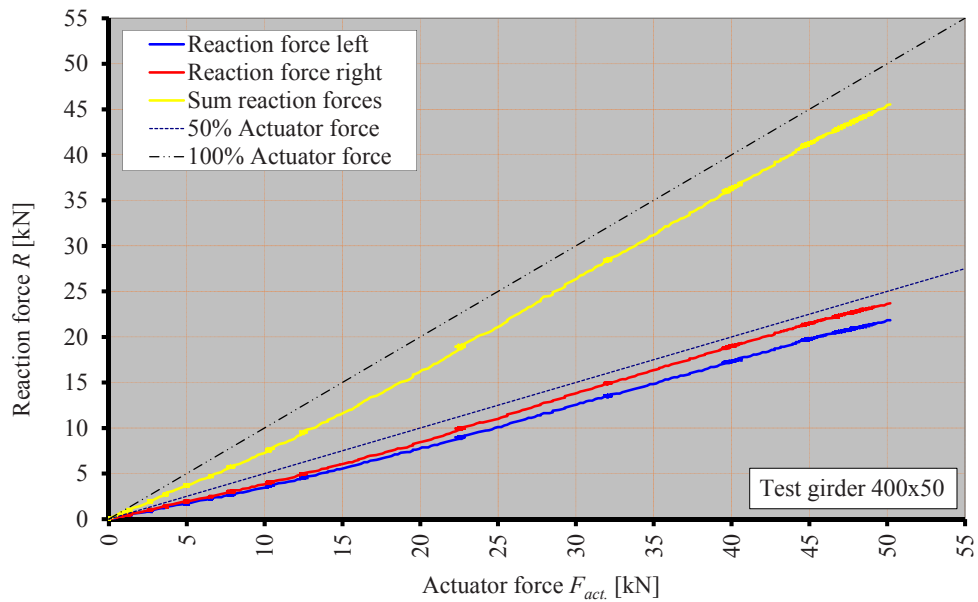


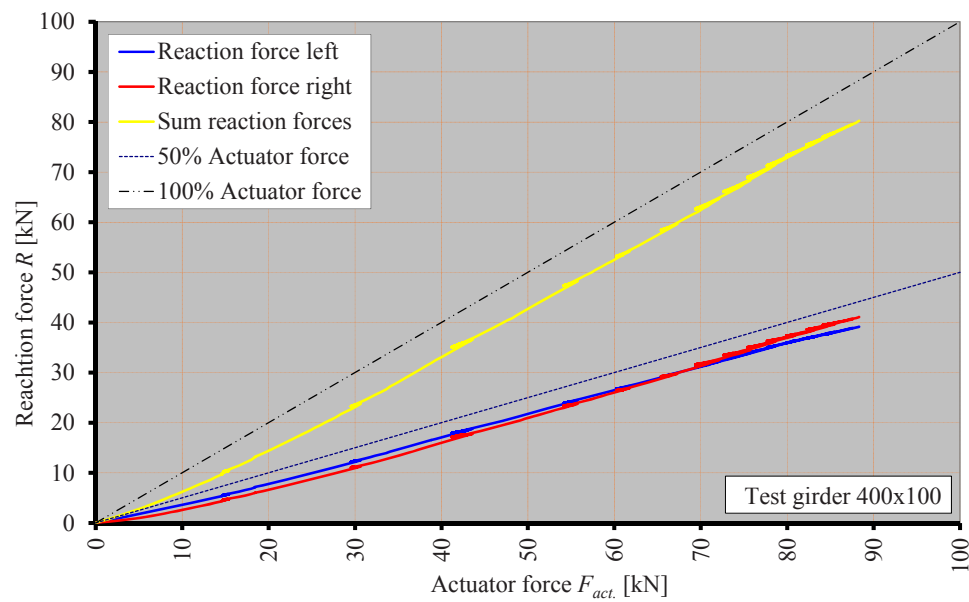
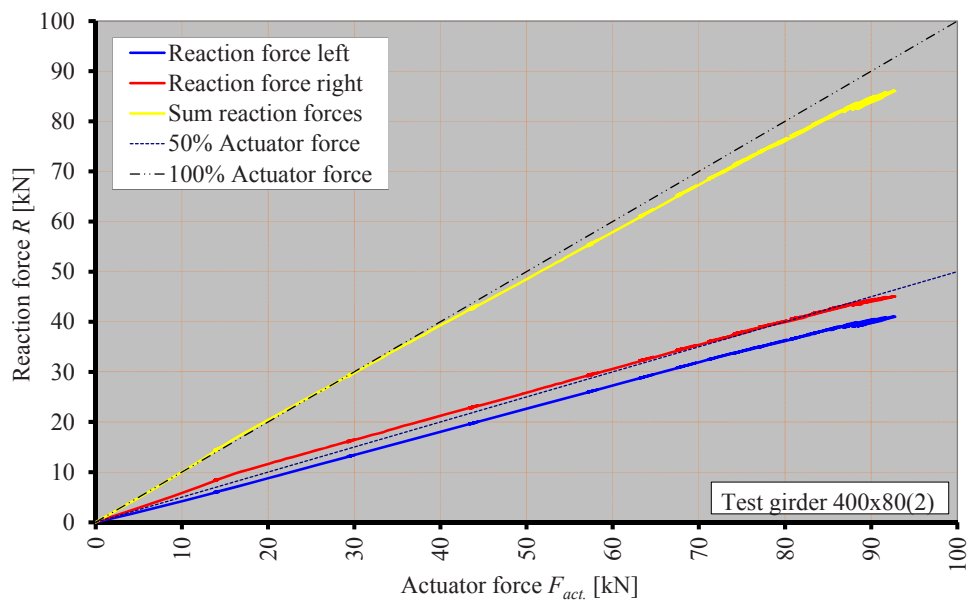


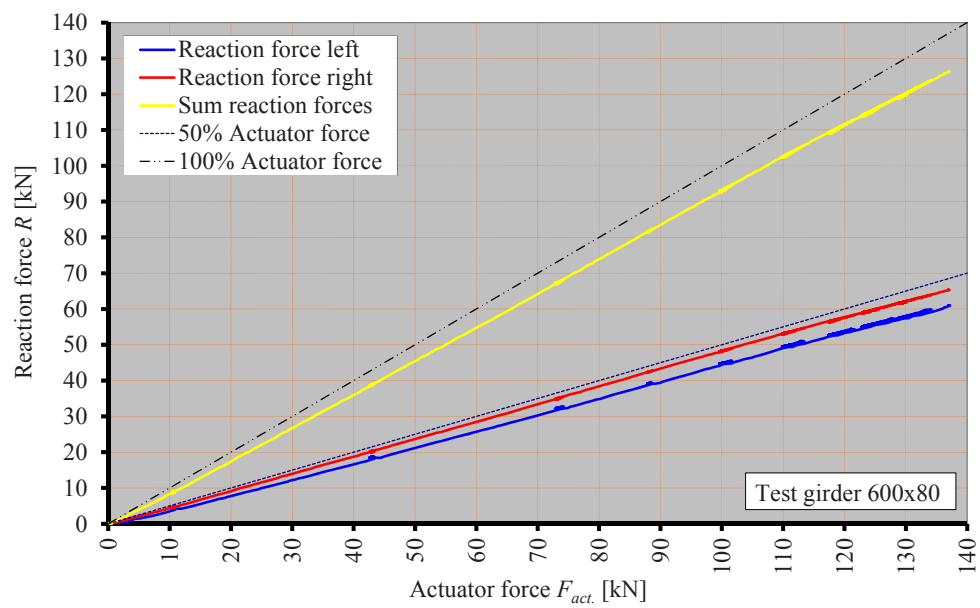
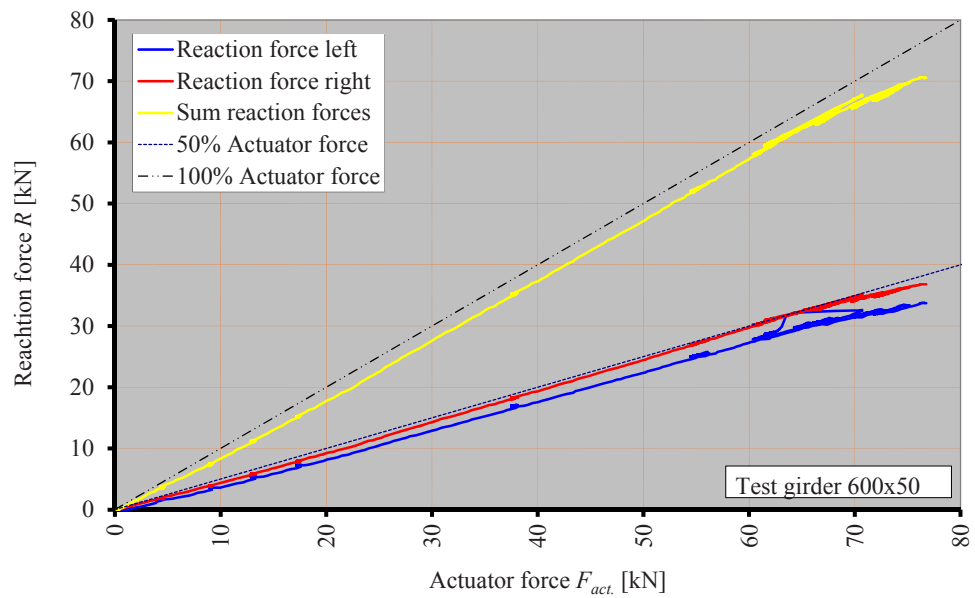


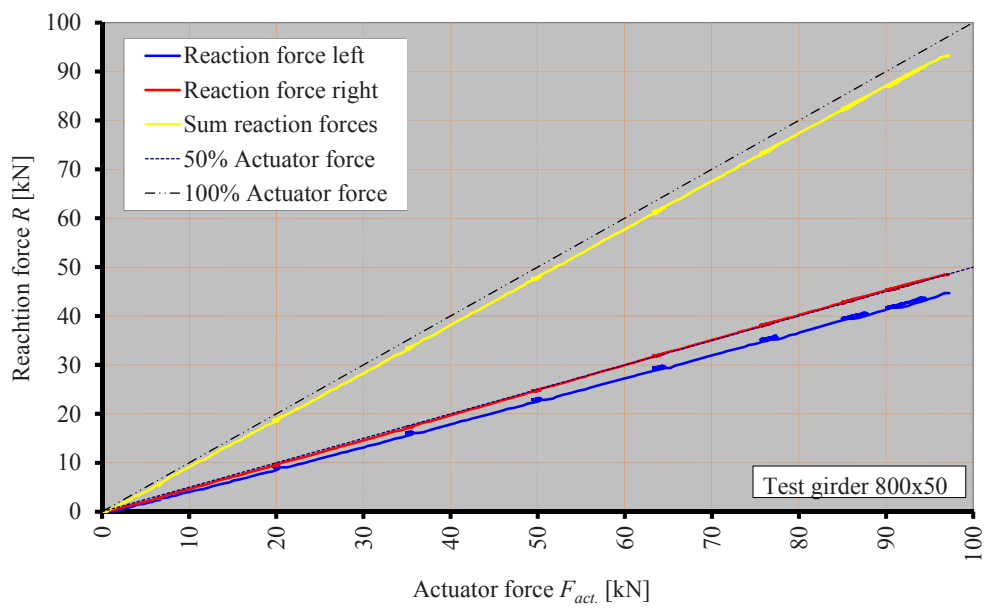
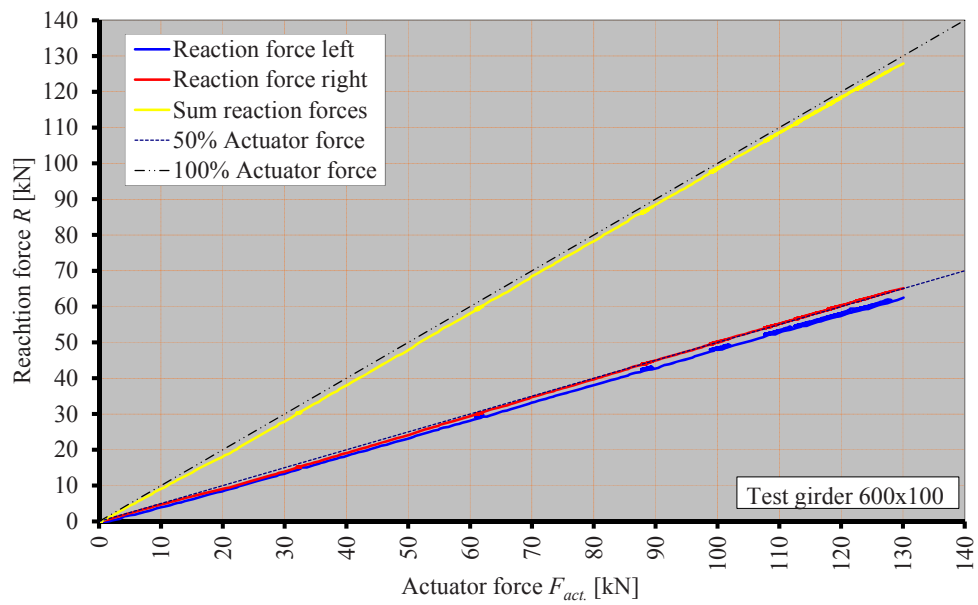


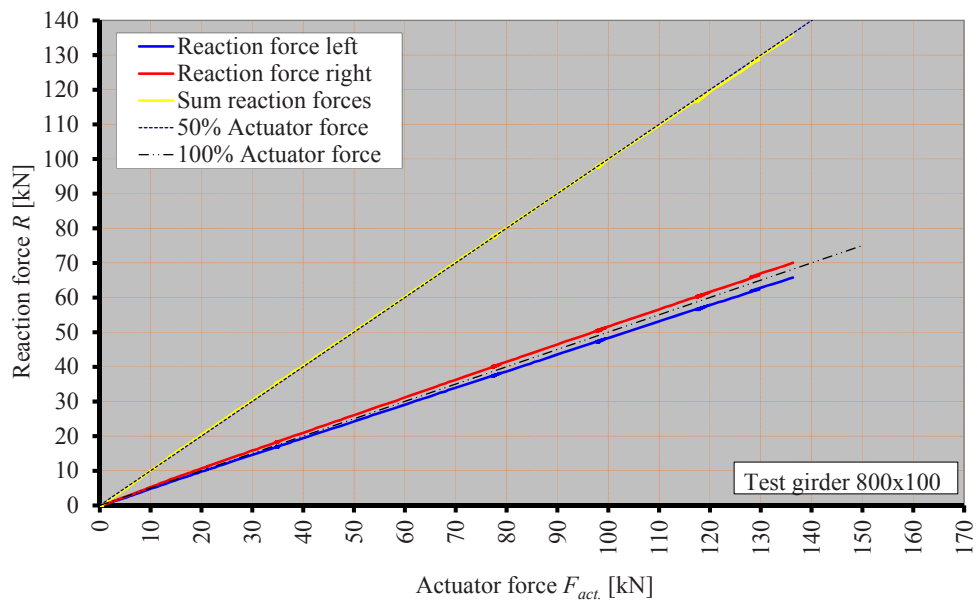
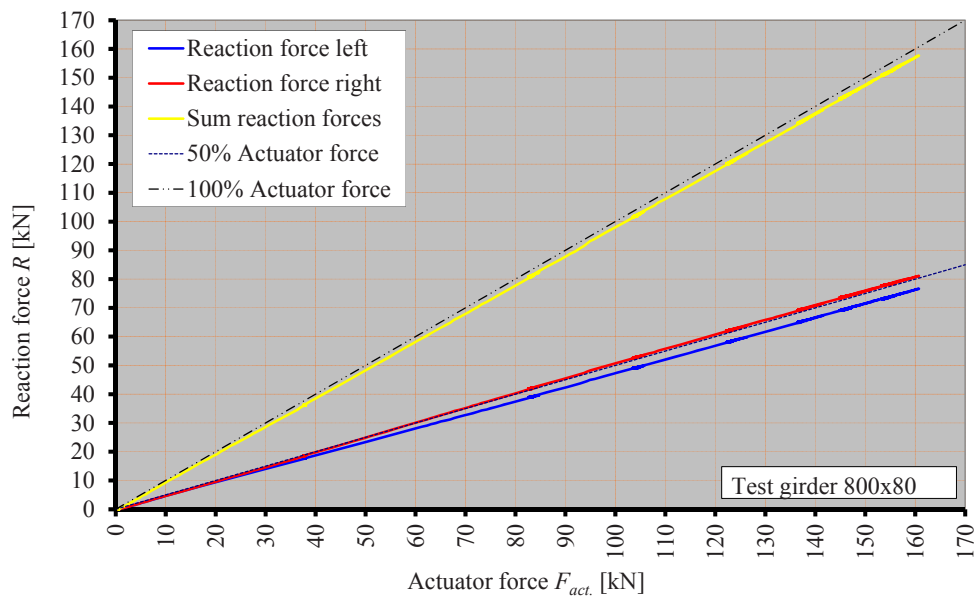
APPENDIX C: GRAPHS OF THE REACTION FORCES VERSUS THE ACTUATOR FORCE



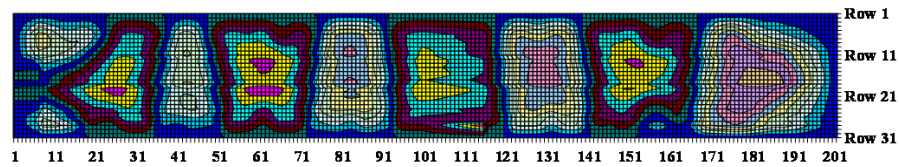




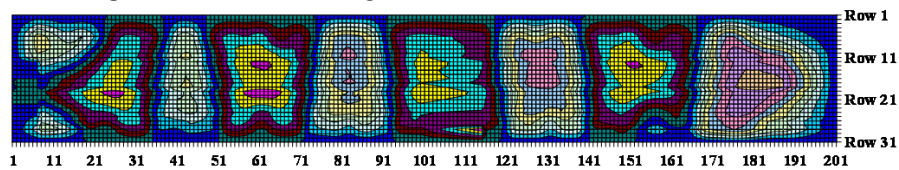




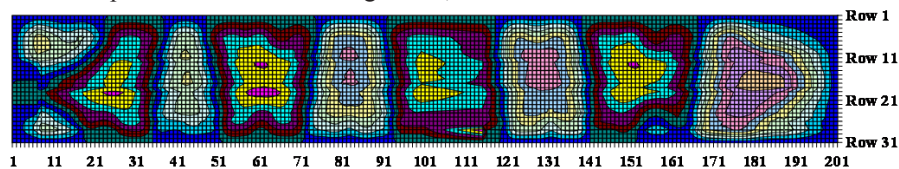
APPENDIX D THE TOTAL OUT-OF-PLANE DEFLECTIONS



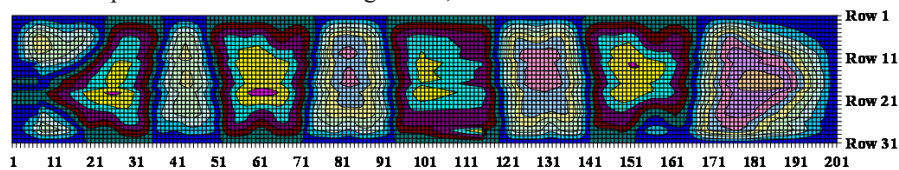
Total out-of-plane deflections of test girder 1, 400x50 DS 0



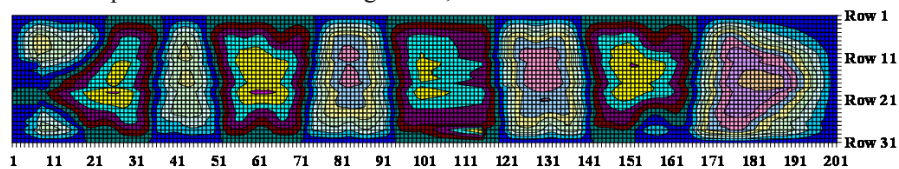
Total out-of-plane deflections of test girder 1, 400x50 DS A



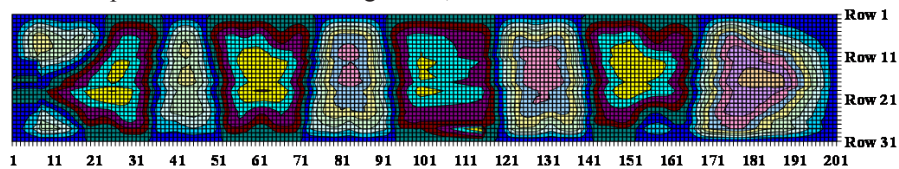
Total out-of-plane deflections of test girder 1, 400x50 DS B



Total out-of-plane deflections of test girder 1, 400x50 DS C

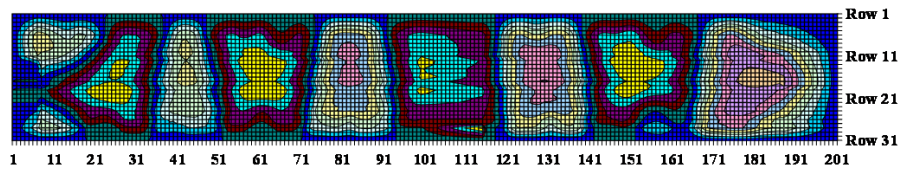


Total out-of-plane deflections of test girder 1, 400x50 DS D

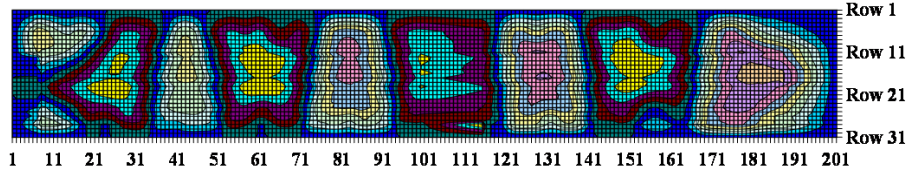


out-of-plane deflections of test girder 1, 400x50 DS E

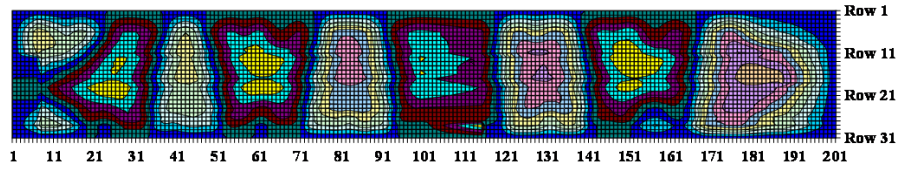
Total



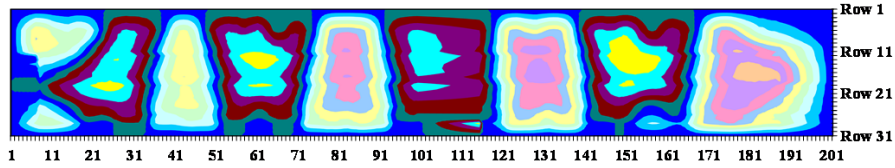
Total out-of-plane deflections of test girder 1, 400x50 DS F



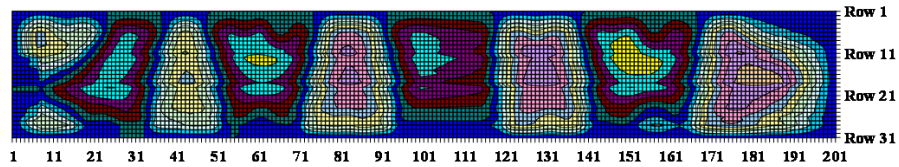
Total out-of-plane deflections of test girder 1, 400x50 DS G



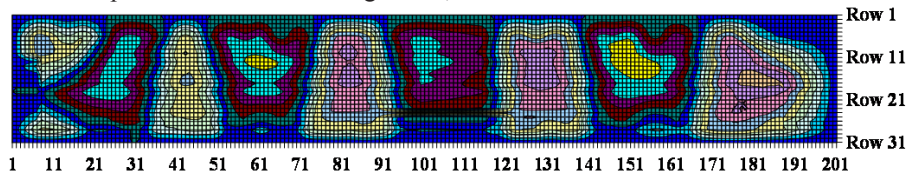
Total out-of-plane deflections of test girder 1, 400x50 DS H



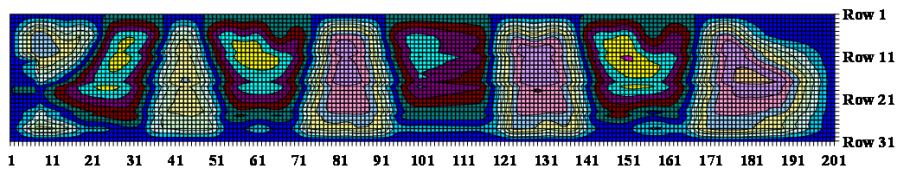
Total out-of-plane deflections of test girder 1, 400x50 DS I



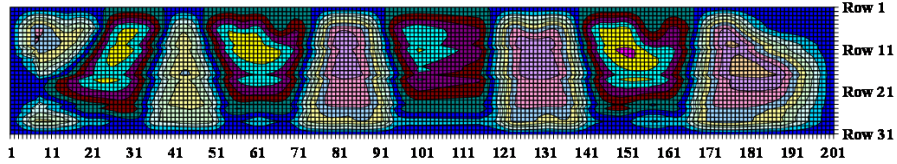
Total out-of-plane deflections of test girder 1, 400x50 DS J



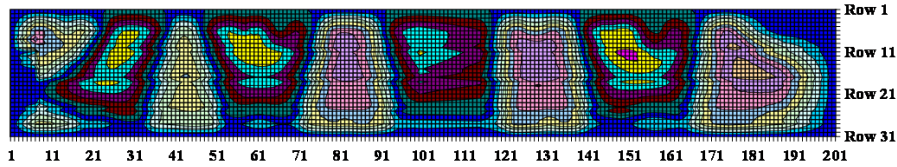
Total out-of-plane deflections of test girder 1, 400x50 DS K



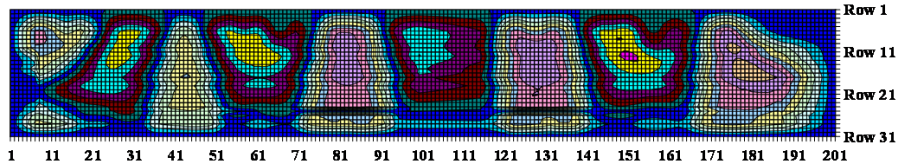
Total out-of-plane deflections of test girder 1, 400x50 DS L



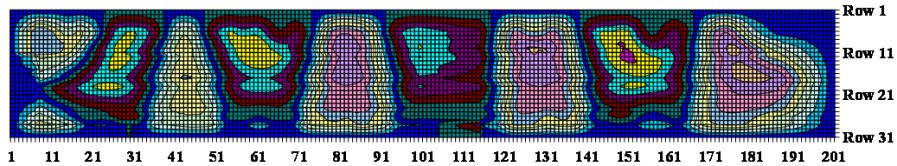
Total out-of-plane deflections of test girder 1, 400x50 DS M



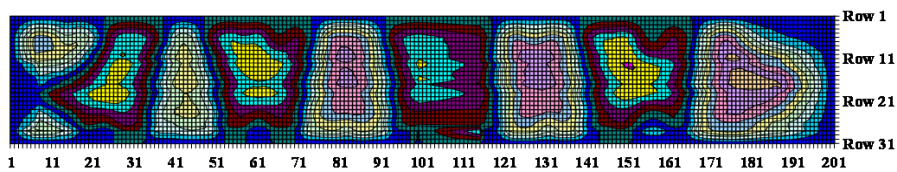
Total out-of-plane deflections of test girder 1, 400x50 DS N



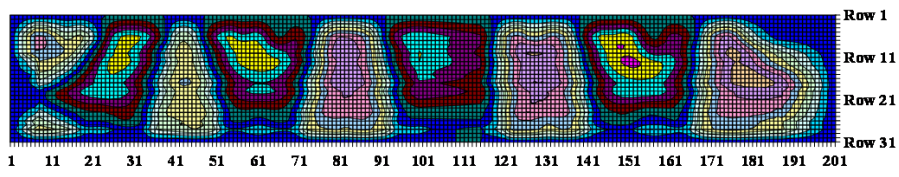
Total out-of-plane deflections of test girder 1, 400x50 DS O



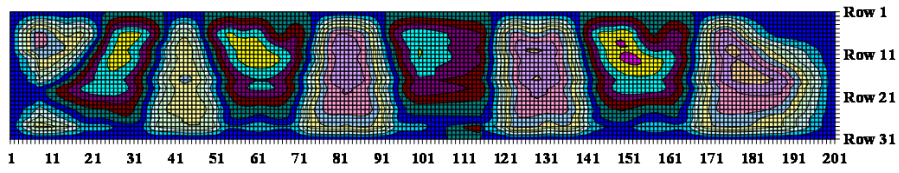
Total out-of-plane deflections of test girder 1, 400x50 DS P



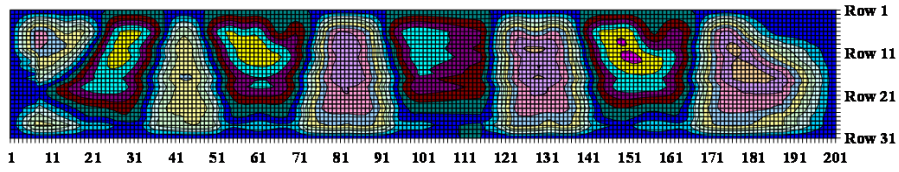
Total out-of-plane deflections of test girder 1, 400x50 DS Q



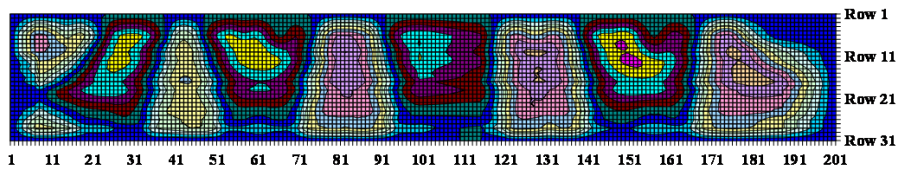
Total out-of-plane deflections of test girder 1, 400x50 DS R



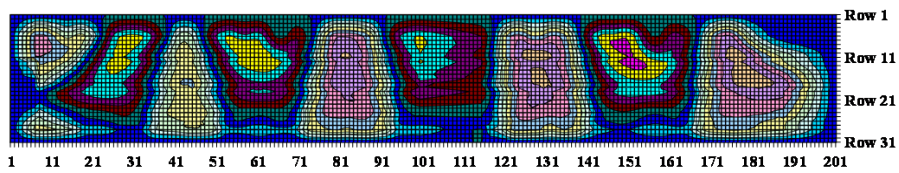
Total out-of-plane deflections of test girder 1, 400x50 DS U



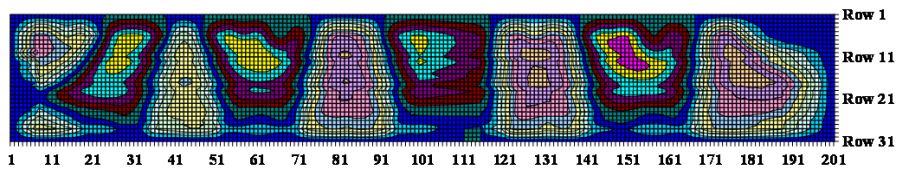
Total out-of-plane deflections of test girder 1, 400x50 DS V



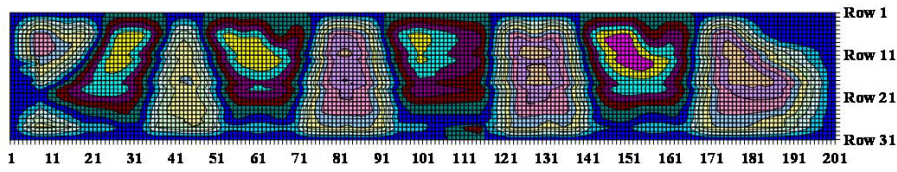
Total out-of-plane deflections of test girder 1, 400x50 DS W



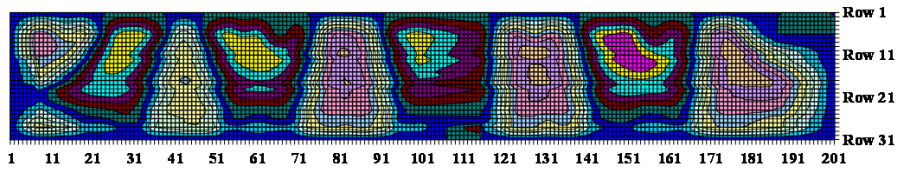
Total out-of-plane deflections of test girder 1, 400x50 DS Y



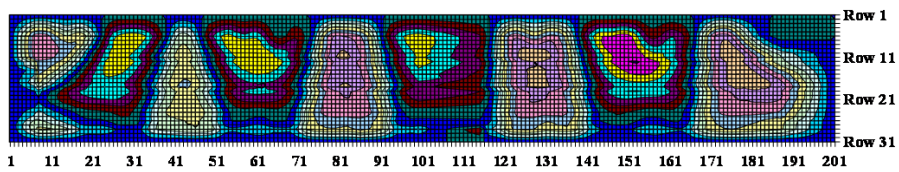
Total out-of-plane deflections of test girder 1, 400x50 DS Z



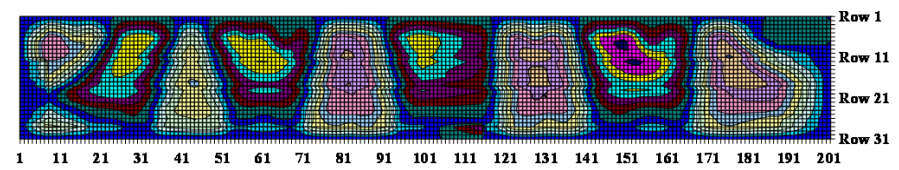
Total out-of-plane deflections of test girder 1, 400x50 DS AA



Total out-of-plane deflections of test girder 1, 400x50 DS AB

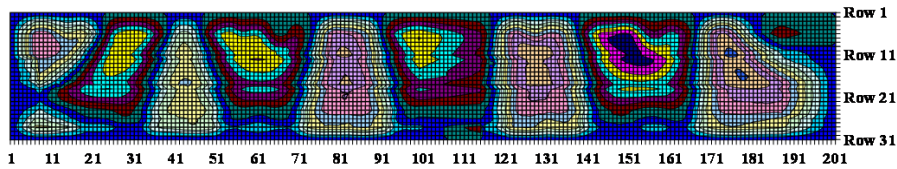


Total out-of-plane deflections of test girder 1, 400x50 DS AC

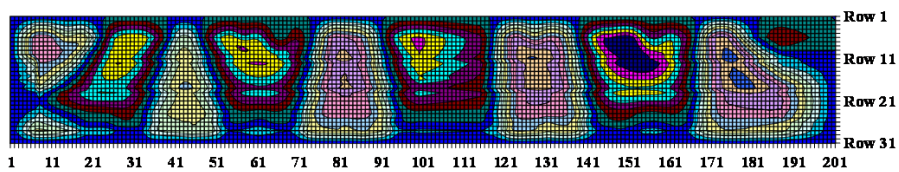


out-of-plane deflections of test girder 1, 400x50 DS AD

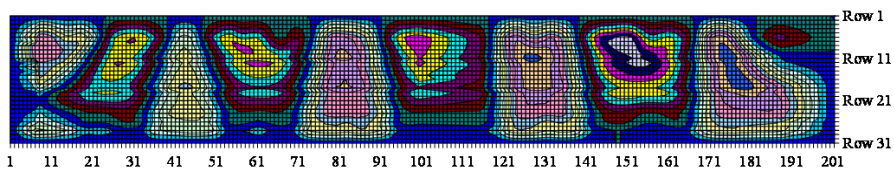
Total



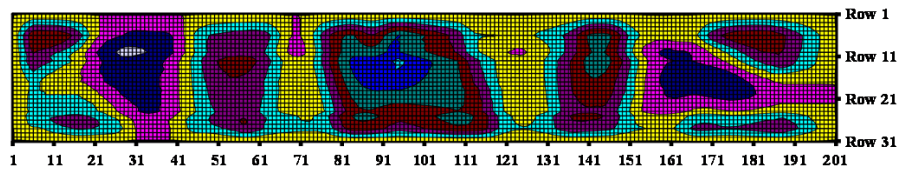
Total out-of-plane deflections of test girder 1, 400x50 DS AE



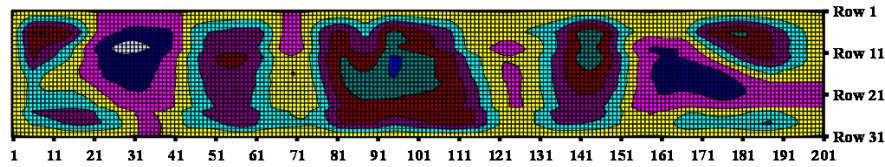
Total out-of-plane deflections of test girder 1, 400x50 DS AF



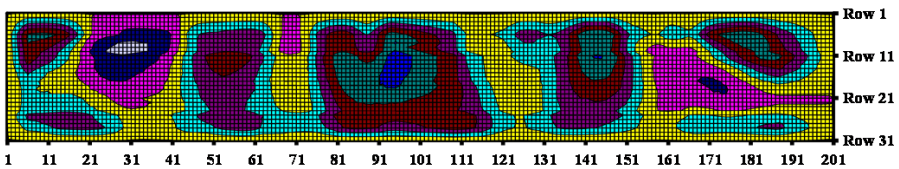
Total out-of-plane deflections of test girder 1, 400x50 DS AG



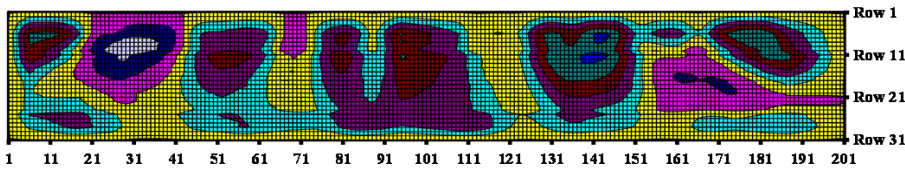
Total out-of-plane deflections of test girder 2, 400x80(1), DS 0



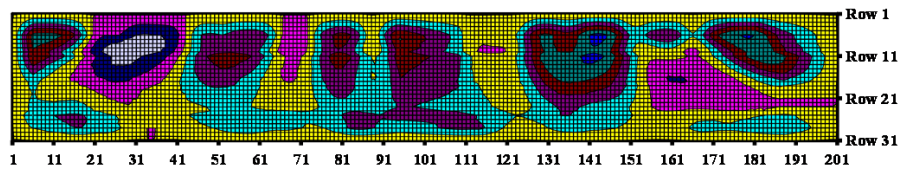
Total out-of-plane deflections of test girder 2, 400x80(1), DS A



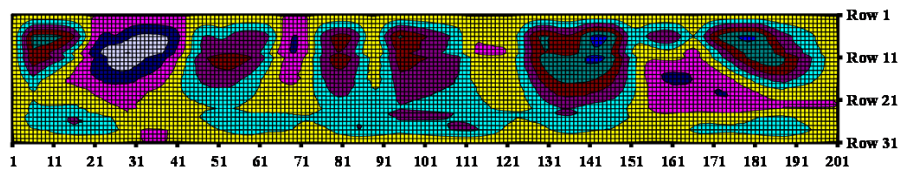
Total out-of-plane deflections of test girder 2, 400x80(1), DS B



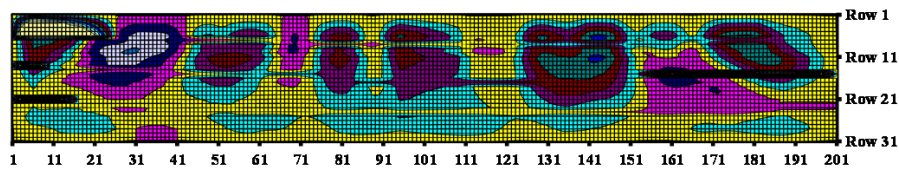
Total out-of-plane deflections of test girder 2, 400x80(1), DS C



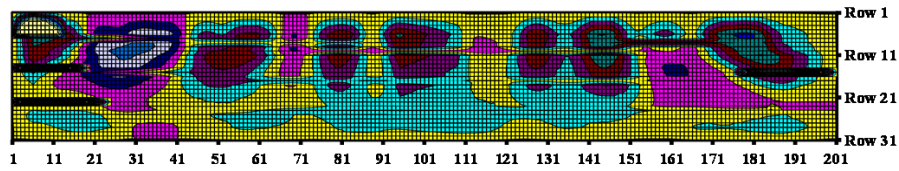
Total out-of-plane deflections of test girder 2, 400x80(1), DS D



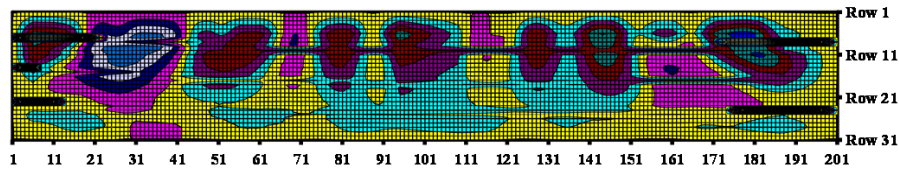
Total out-of-plane deflections of test girder 2, 400x80(1), DS E



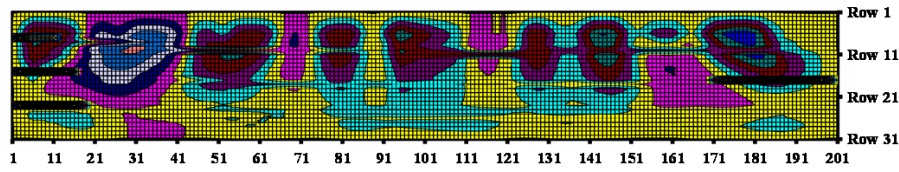
Total out-of-plane deflections of test girder 2, 400x80(1), DS F



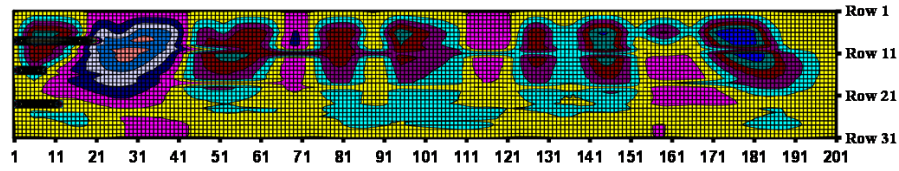
Total out-of-plane deflections of test girder 2, 400x80(1), DS G



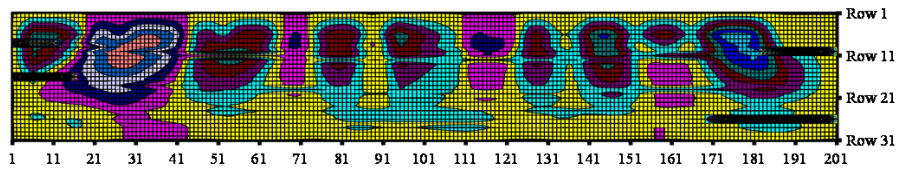
Total out-of-plane deflections of test girder 2, 400x80(1), DS I



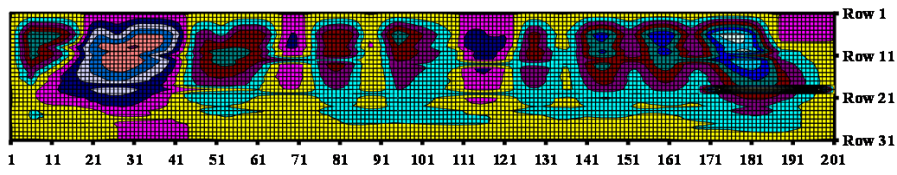
Total out-of-plane deflections of test girder 2, 400x80(1), DS H



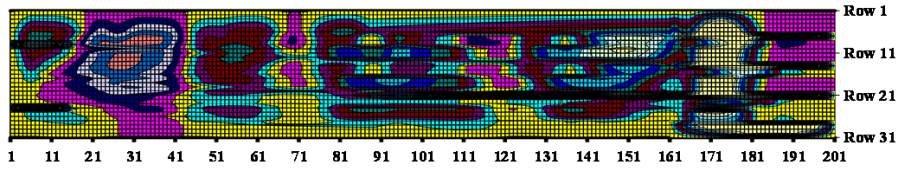
Total out-of-plane deflections of test girder 2, 400x80(1), DS J



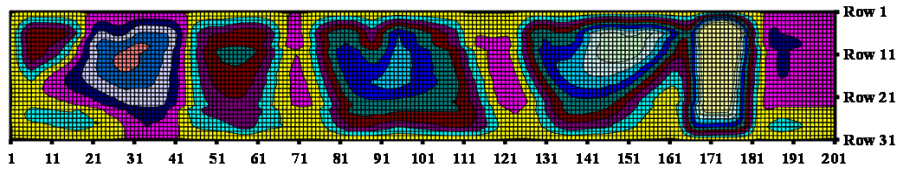
Total out-of-plane deflections of test girder 2, 400x80(1), DS K



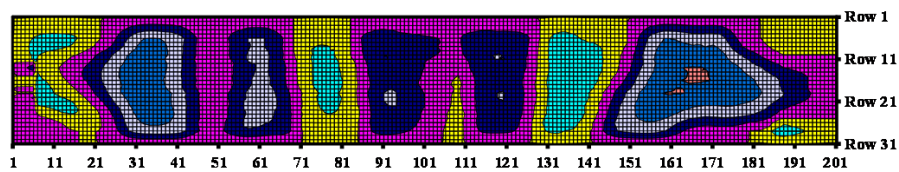
Total out-of-plane deflections of test girder 2, 400x80(1), DS L



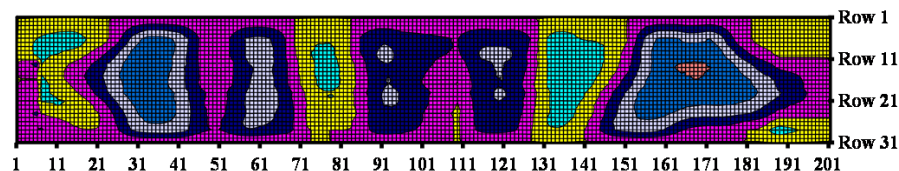
Total out-of-plane deflections of test girder 2, 400x80(1), DS M



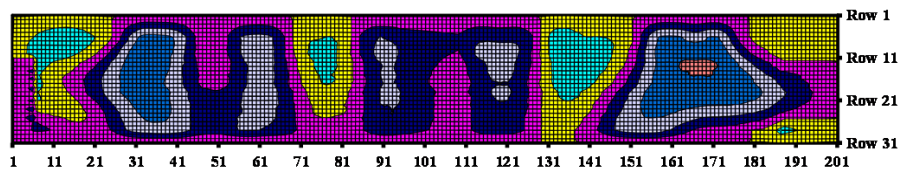
Total out-of-plane deflections of test girder 2, 400x80(1), DS N



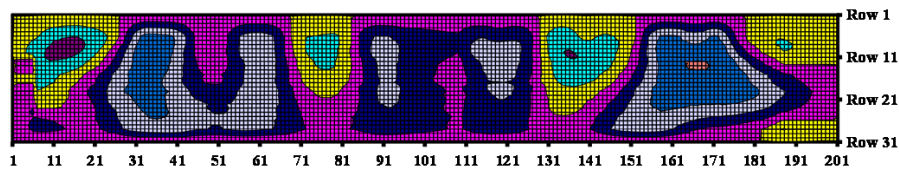
Total out-of-plane deflections of test girder 3, 400x80(2), DS 0



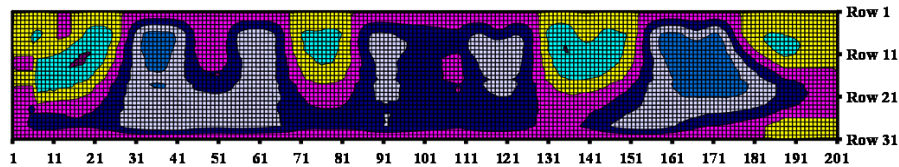
Total out-of-plane deflections of test girder 3, 400x80(2), DS A



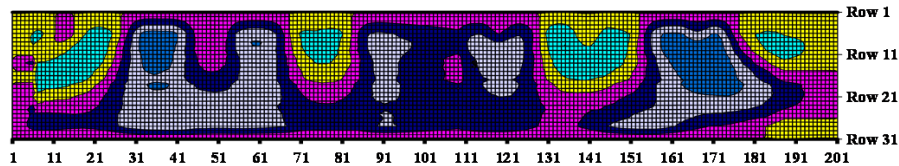
Total out-of-plane deflections of test girder 3, 400x80(2), DS B



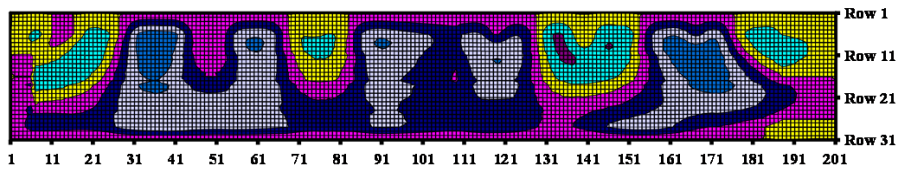
Total out-of-plane deflections of test girder 3, 400x80(2), DS C



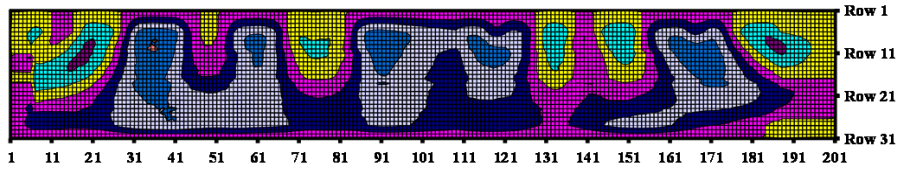
Total out-of-plane deflections of test girder 3, 400x80(2), DS D



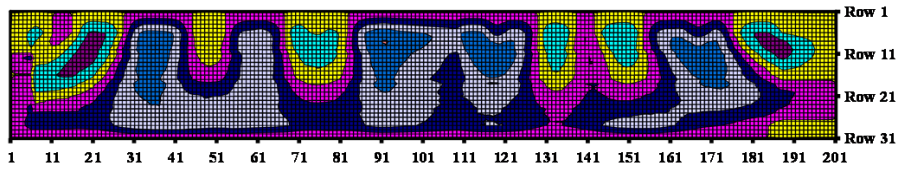
Total out-of-plane deflections of test girder 3, 400x80(2), DS E



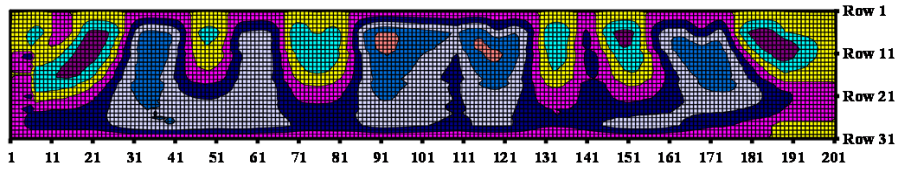
Total out-of-plane deflections of test girder 3, 400x80(2), DS F



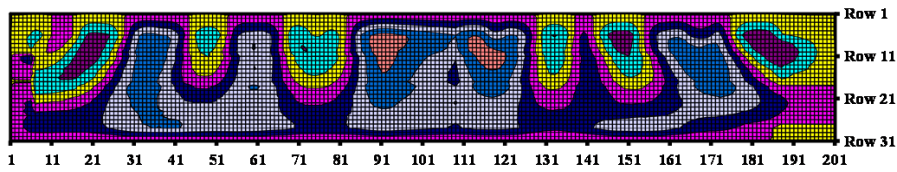
Total out-of-plane deflections of test girder 3, 400x80(2), DS G



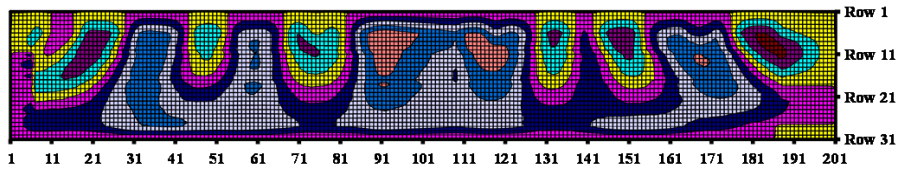
Total out-of-plane deflections of test girder 3, 400x80(2), DS H



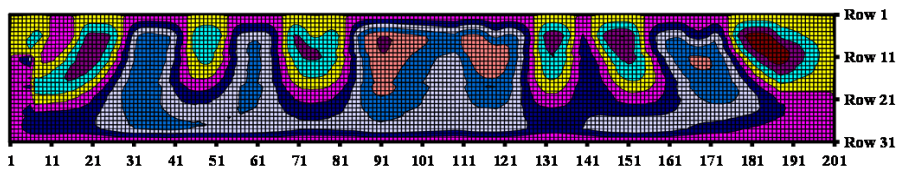
Total out-of-plane deflections of test girder 3, 400x80(2), DS I



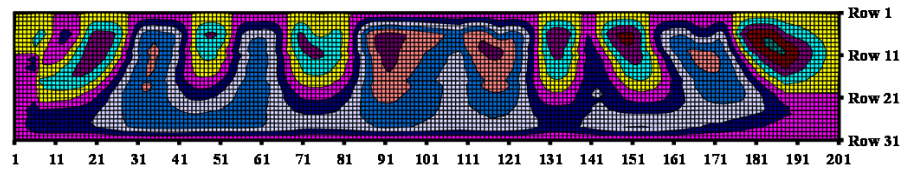
Total out-of-plane deflections of test girder 3, 400x80(2), DS J



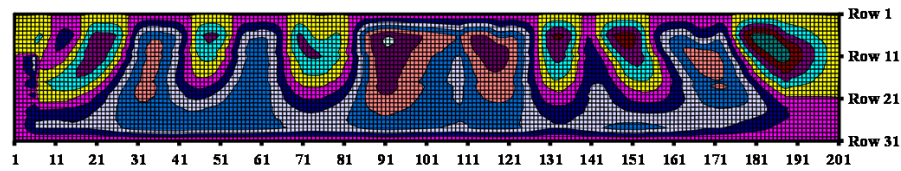
Total out-of-plane deflections of test girder 3, 400x80(2), DS K



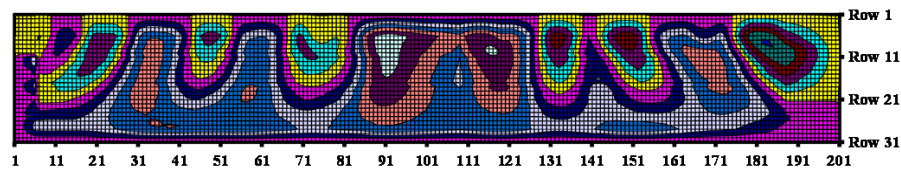
Total out-of-plane deflections of test girder 3, 400x80(2), DS L



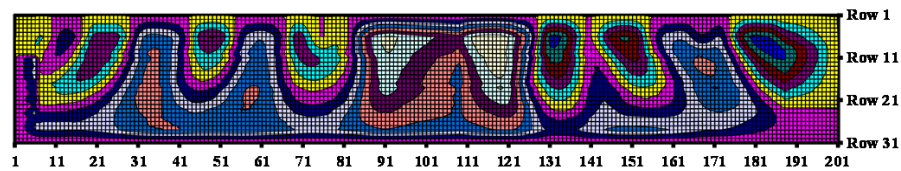
Total out-of-plane deflections of test girder 3, 400x80(2), DS M



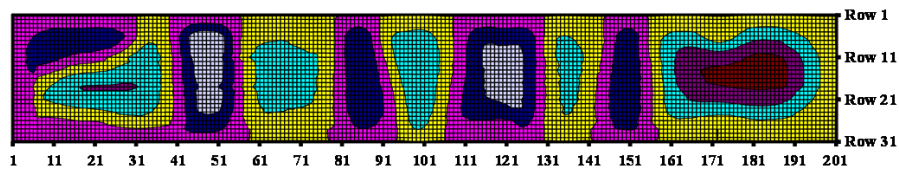
Total out-of-plane deflections of test girder 3, 400x80(2), DS N



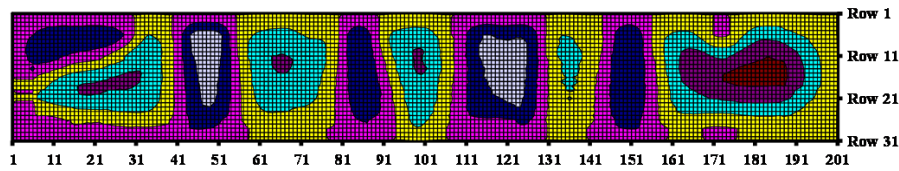
Total out-of-plane deflections of test girder 3, 400x80(2), DS O



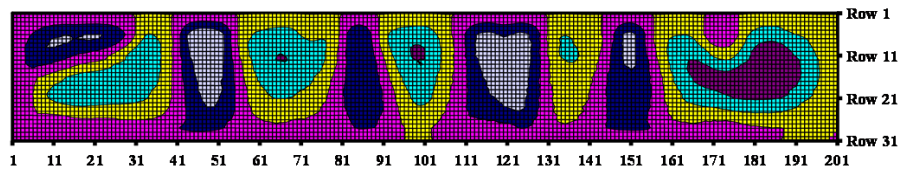
Total out-of-plane deflections of test girder 3, 400x80(2), DS P



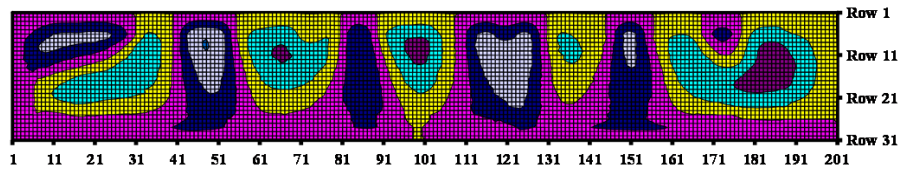
Total out-of-plane deflections of test girder 4, 400x100, DS 0



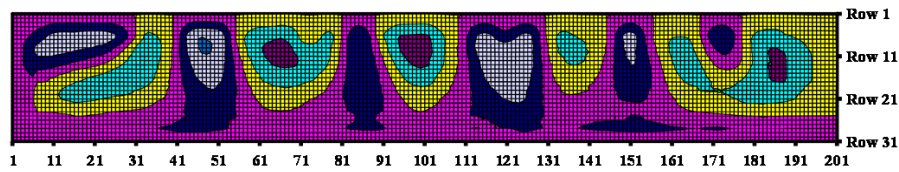
Total out-of-plane deflections of test girder 4, 400x100, DS A



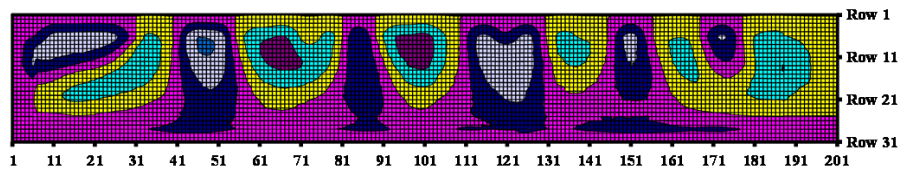
Total out-of-plane deflections of test girder 4, 400x100, DS B



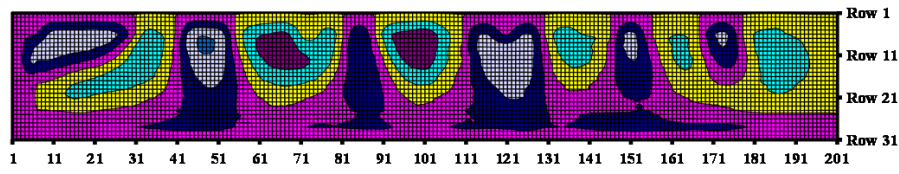
Total out-of-plane deflections of test girder 4, 400x100, DS C



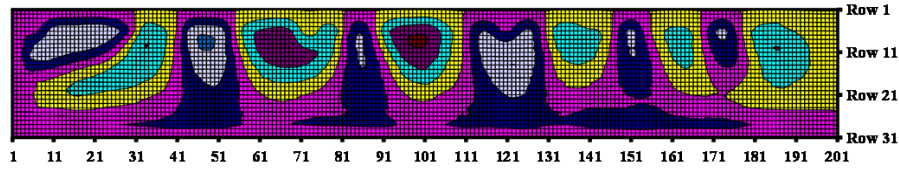
Total out-of-plane deflections of test girder 4, 400x100, DS D



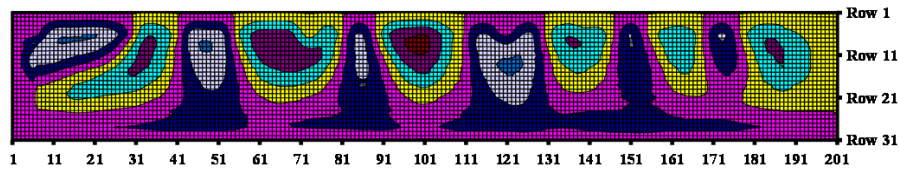
Total out-of-plane deflections of test girder 4, 400x100, DS E



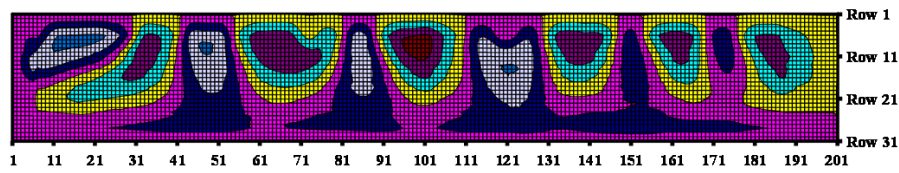
Total out-of-plane deflections of test girder 4, 400x100, DS F



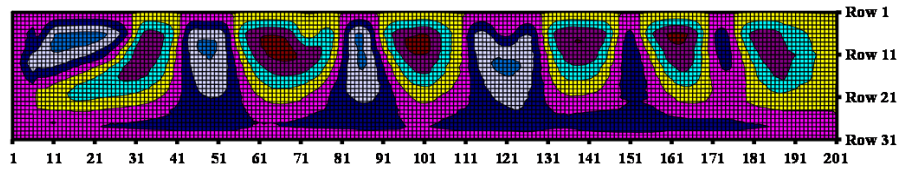
Total out-of-plane deflections of test girder 4, 400x100, DS G



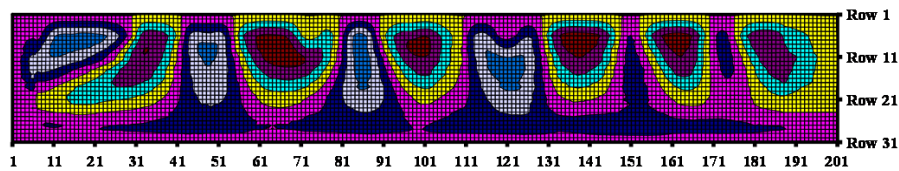
Total out-of-plane deflections of test girder 4, 400x100, DS H



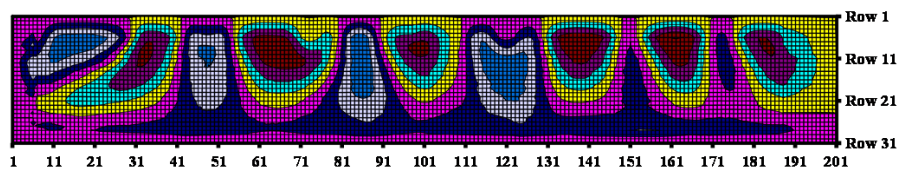
Total out-of-plane deflections of test girder 4, 400x100, DS I



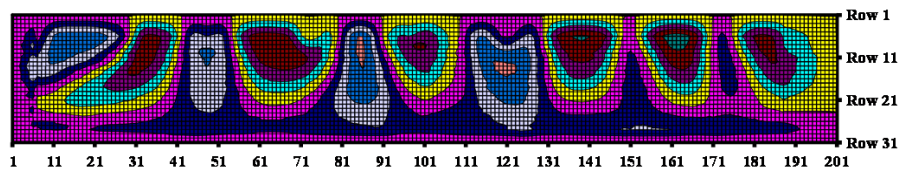
Total out-of-plane deflections of test girder 4, 400x100, DS J



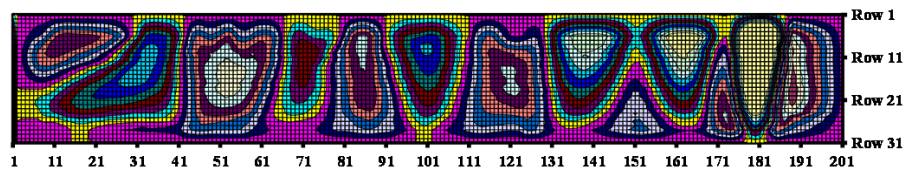
Total out-of-plane deflections of test girder 4, 400x100, DS K



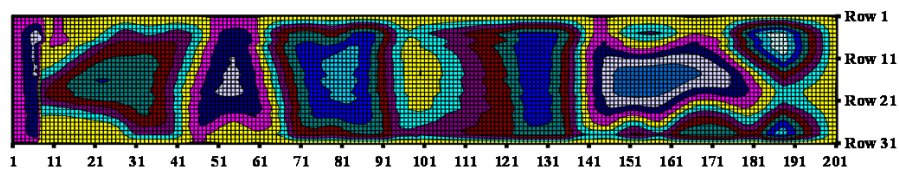
Total out-of-plane deflections of test girder 4, 400x100, DS L



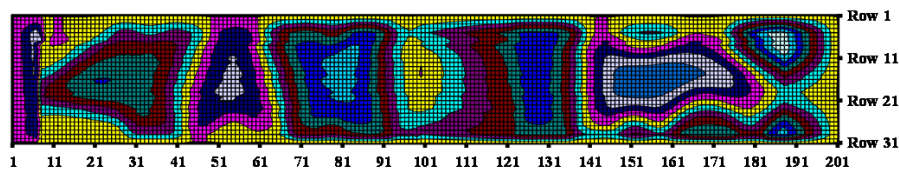
Total out-of-plane deflections of test girder 4, 400x100, DS M



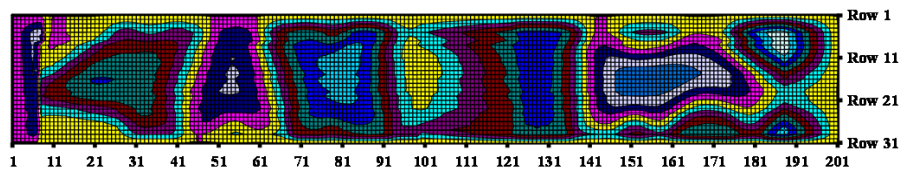
Total out-of-plane deflections of test girder 4, 400x100, DS N



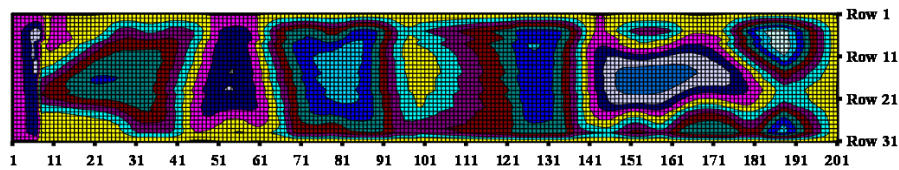
Total out-of-plane deflections of plate girder 5, 600x50, DS 0



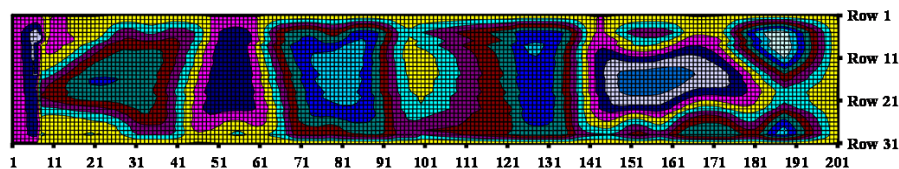
Total out-of-plane deflections of plate girder 5, 600x50, DS A



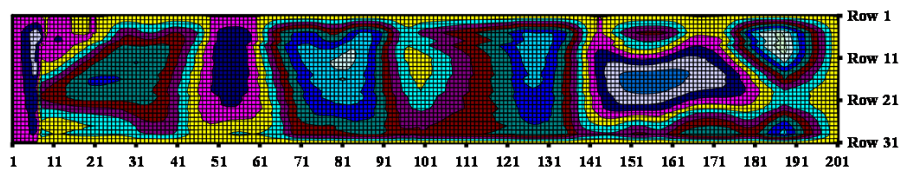
Total out-of-plane deflections of plate girder 5, 600x50, DS B



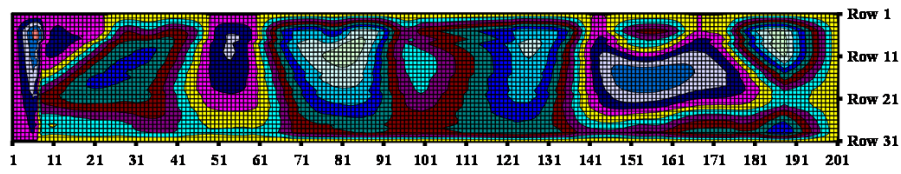
Total out-of-plane deflections of plate girder 5, 600x50, DS C



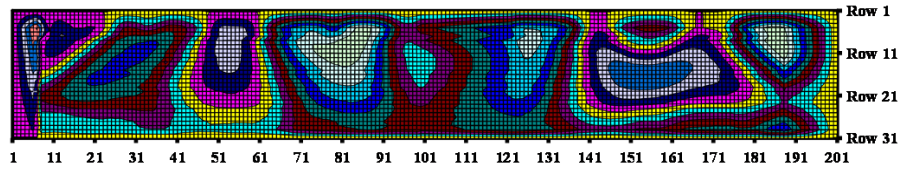
Total out-of-plane deflections of plate girder 5, 600x50, DS D



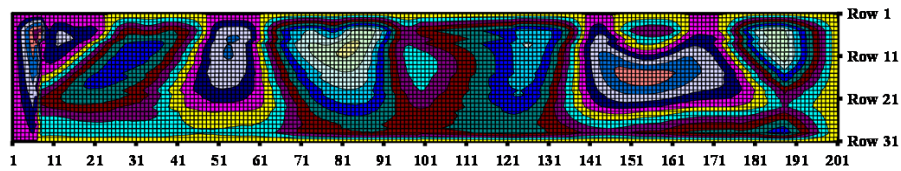
Total out-of-plane deflections of plate girder 5, 600x50, DS E



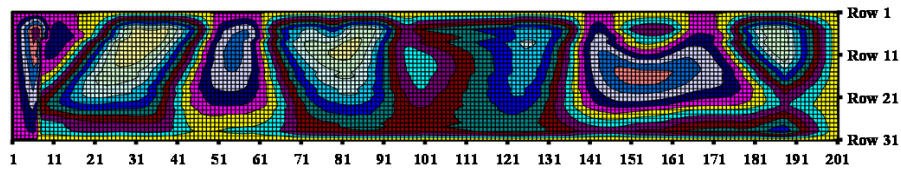
Total out-of-plane deflections of plate girder 5, 600x50, DS F



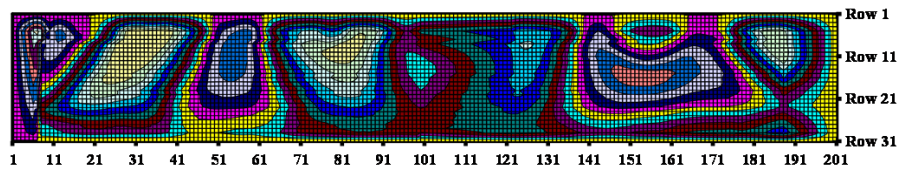
Total out-of-plane deflections of plate girder 5, 600x50, DS G



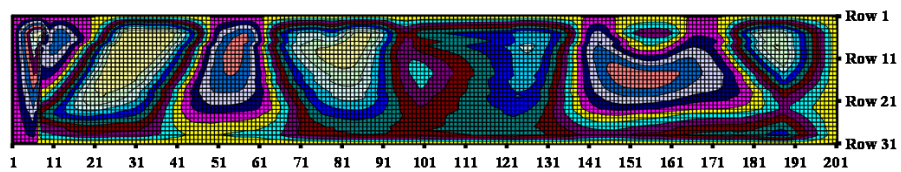
Total out-of-plane deflections of plate girder 5, 600x50, DS H



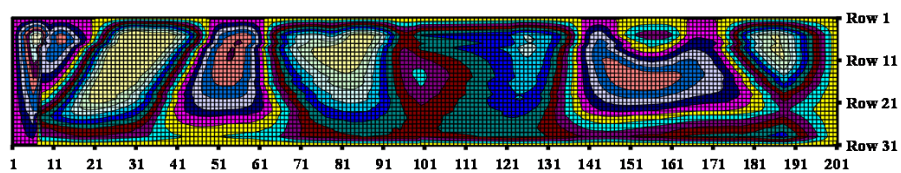
Total out-of-plane deflections of plate girder 5, 600x50, DS I



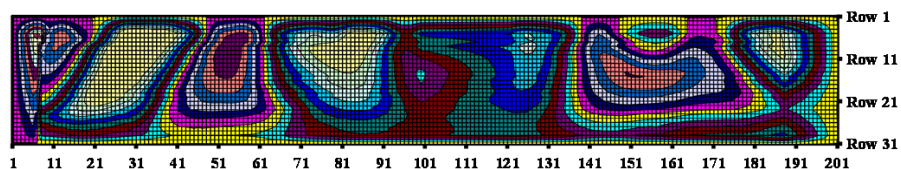
Total out-of-plane deflections of plate girder 5, 600x50, DS J



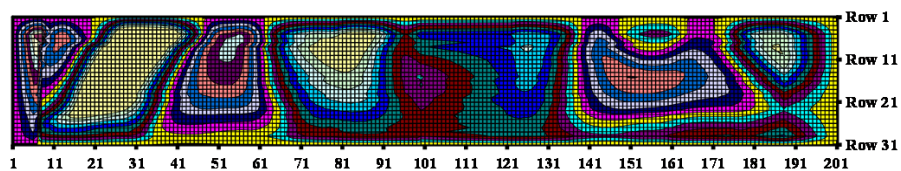
Total out-of-plane deflections of plate girder 5, 600x50, DS K



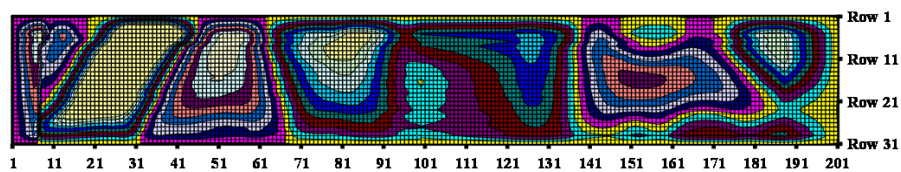
Total out-of-plane deflections of plate girder 5, 600x50, DS L



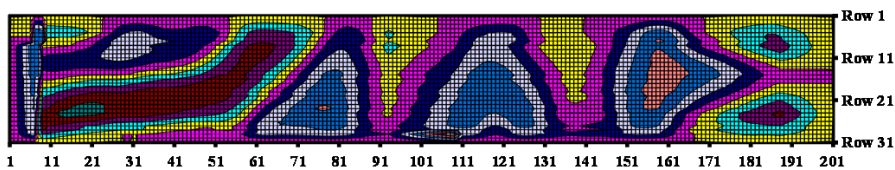
Total out-of-plane deflections of plate girder 5, 600x50, DS M



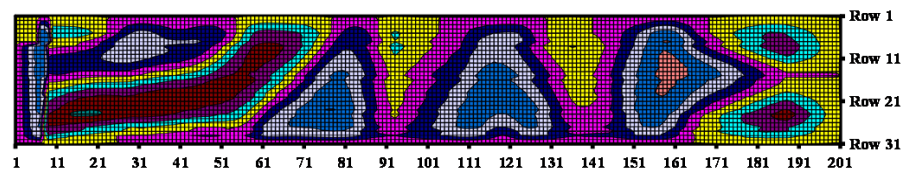
Total out-of-plane deflections of plate girder 5, 600x50, DS N



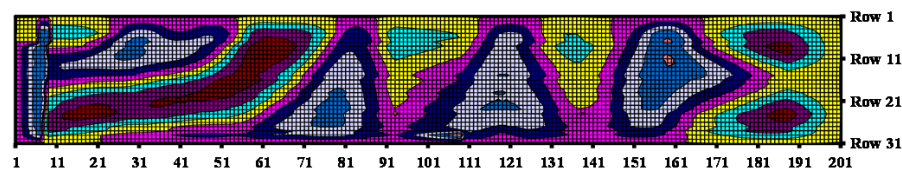
Total out-of-plane deflections of plate girder 5, 600x50, DS O



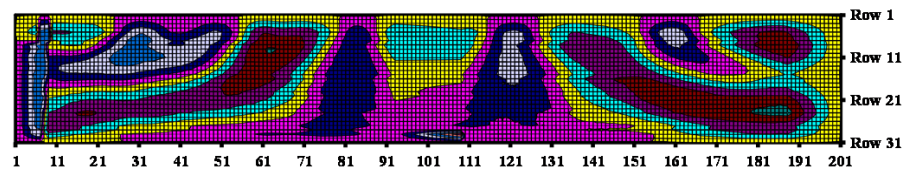
Total out-of-plane deflections of plate girder 6, 600x80, DS 0



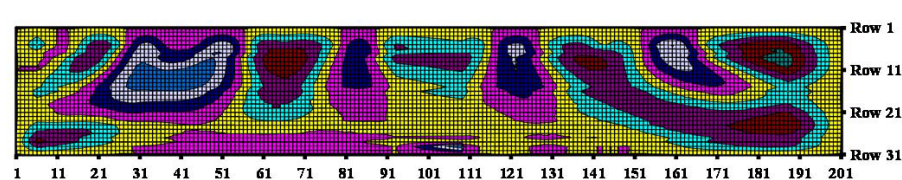
Total out-of-plane deflections of plate girder 6, 600x80, DS A



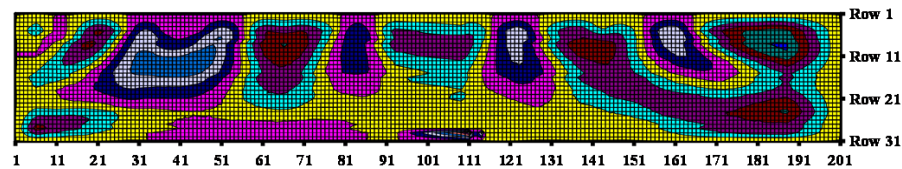
Total out-of-plane deflections of plate girder 6, 600x80, DS B



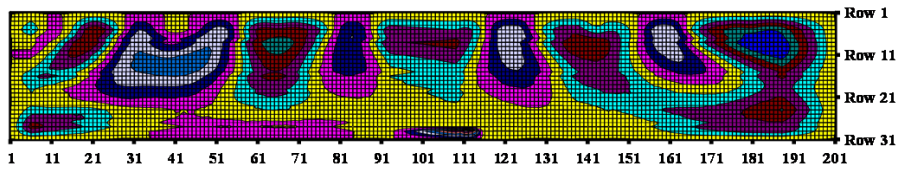
Total out-of-plane deflections of plate girder 6, 600x80, DS C



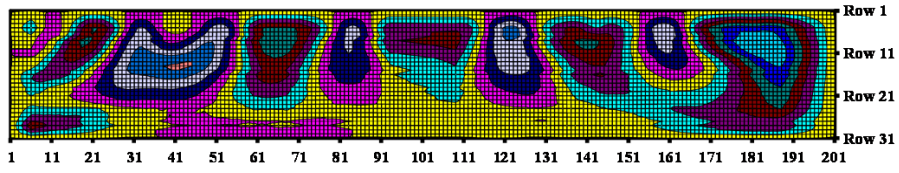
Total out-of-plane deflections of plate girder 6, 600x80, DS D



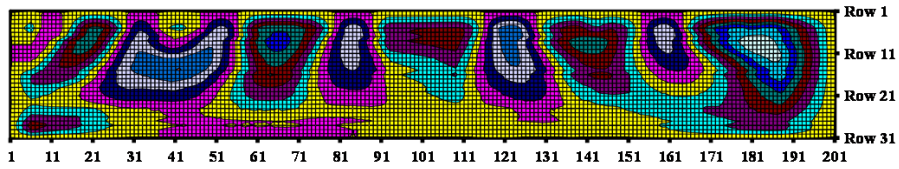
Total out-of-plane deflections of plate girder 6, 600x80, DS E



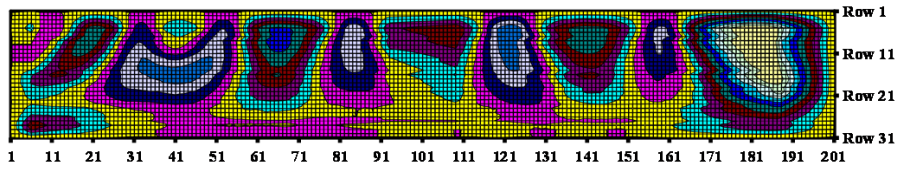
Total out-of-plane deflections of plate girder 6, 600x80, DS F



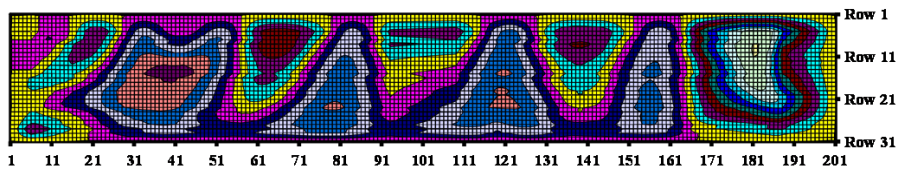
Total out-of-plane deflections of plate girder 6, 600x80, DS G



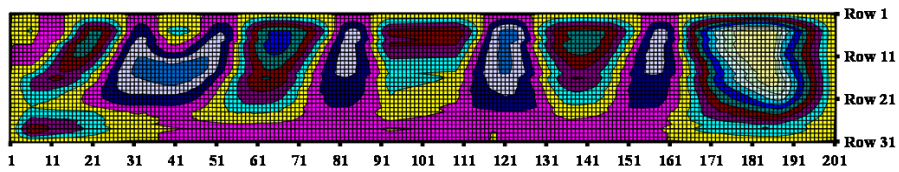
Total out-of-plane deflections of plate girder 6, 600x80, DS H



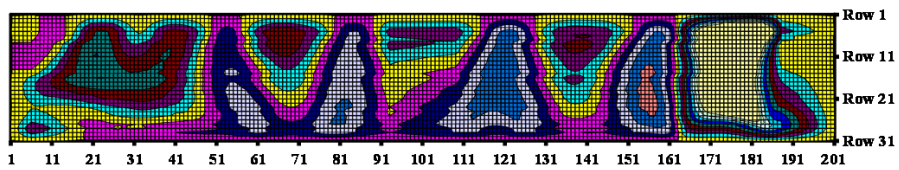
Total out-of-plane deflections of plate girder 6, 600x80, DS I



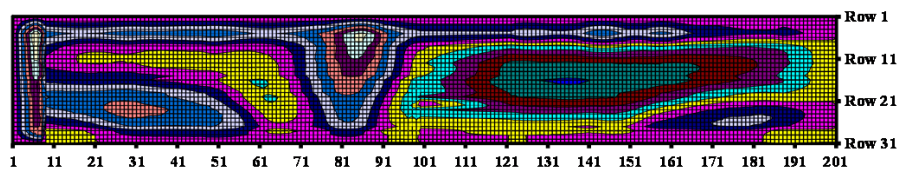
Total out-of-plane deflections of plate girder 6, 600x80, DS J



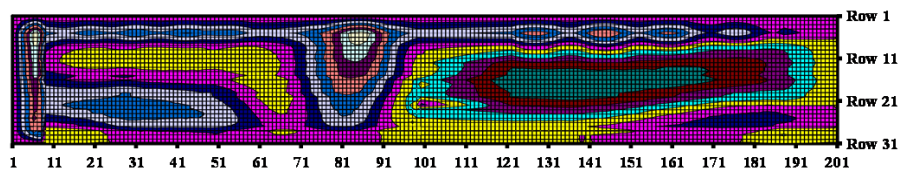
Total out-of-plane deflections of plate girder 6, 600x80, DS K



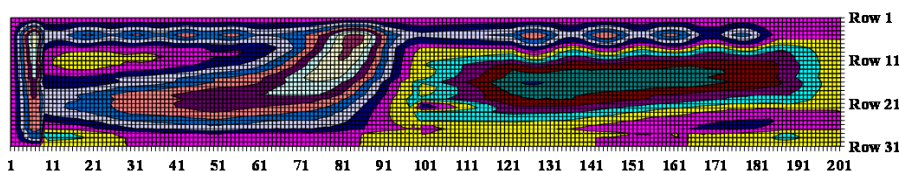
Total out-of-plane deflections of plate girder 6, 600x80, DS L



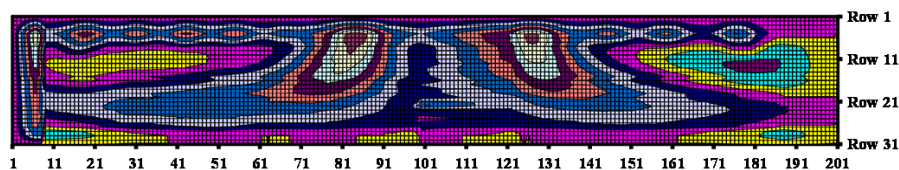
Total out-of-plane deflections of plate girder 7, 600x100, DS 0



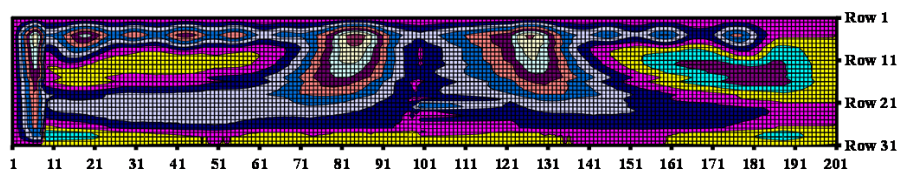
Total out-of-plane deflections of plate girder 7, 600x100, DS A



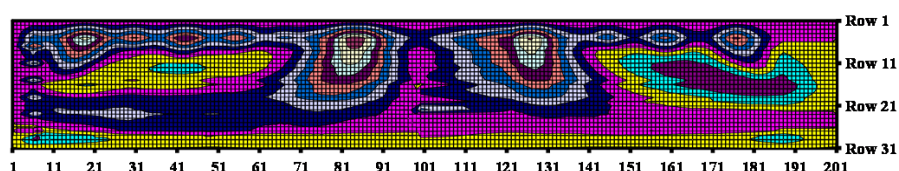
Total out-of-plane deflections of plate girder 7, 600x100, DS B



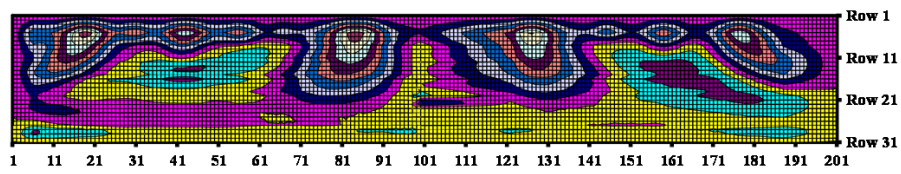
Total out-of-plane deflections of plate girder 7, 600x100, DS C



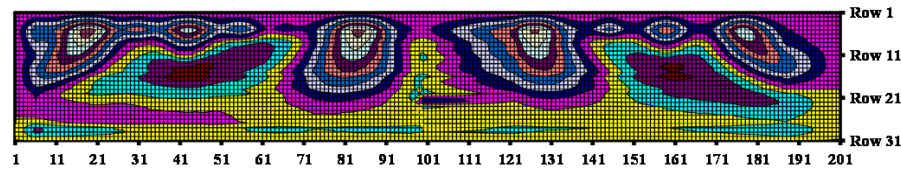
Total out-of-plane deflections of plate girder 7, 600x100, DS D



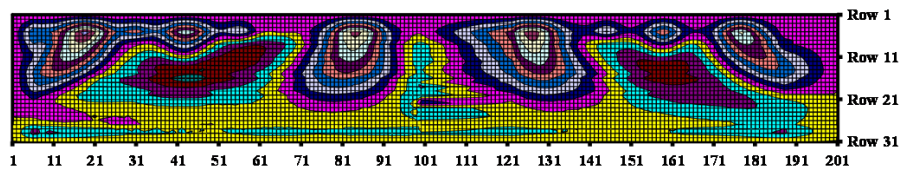
Total out-of-plane deflections of plate girder 7, 600x100, DS E



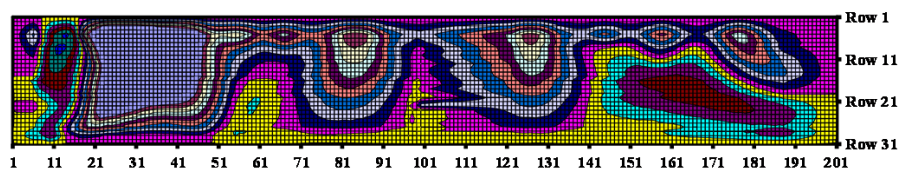
Total out-of-plane deflections of plate girder 7, 600x100, DS F



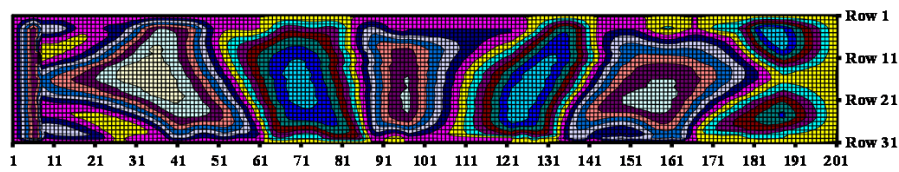
Total out-of-plane deflections of plate girder 7, 600x100, DS G



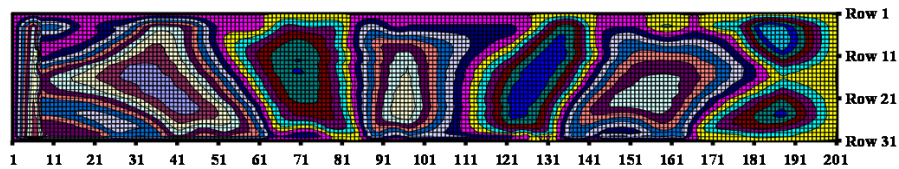
Total out-of-plane deflections of plate girder 7, 600x100, DS H



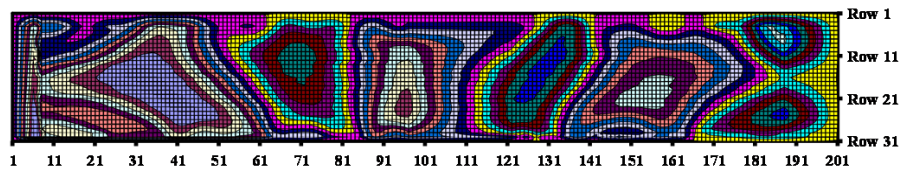
Total out-of-plane deflections of plate girder 7, 600x100, DS I



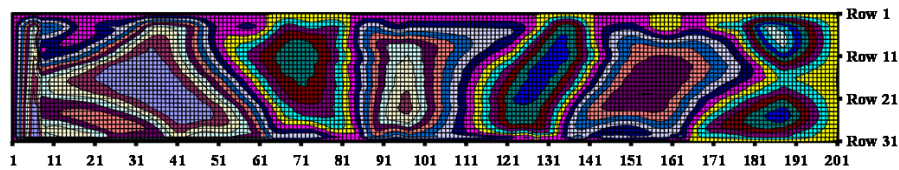
Total out-of-plane deflections of plate girder 8, 800x50, DS 0



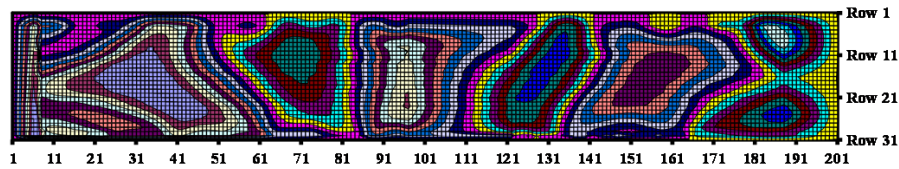
Total out-of-plane deflections of plate girder 8, 800x50, DS A



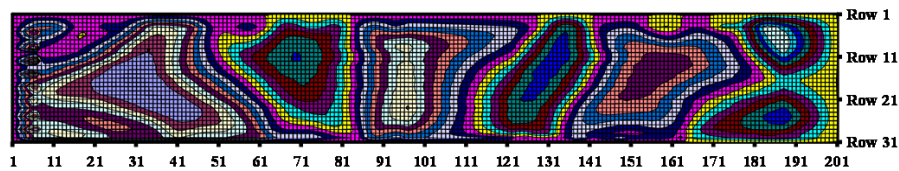
Total out-of-plane deflections of plate girder 8, 800x50, DS B



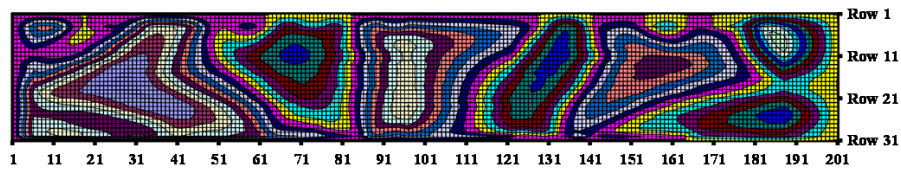
Total out-of-plane deflections of plate girder 8, 800x50, DS C



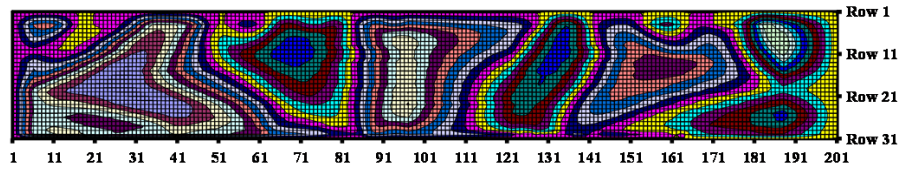
Total out-of-plane deflections of plate girder 8, 800x50, DS D



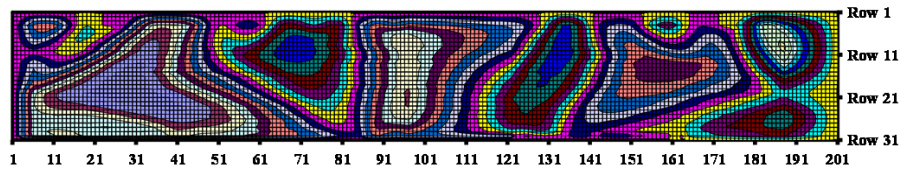
Total out-of-plane deflections of plate girder 8, 800x50, DS E



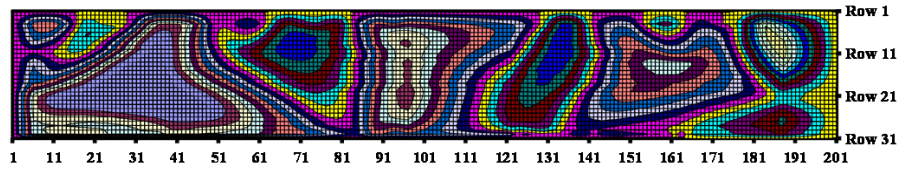
Total out-of-plane deflections of plate girder 8, 800x50, DS F



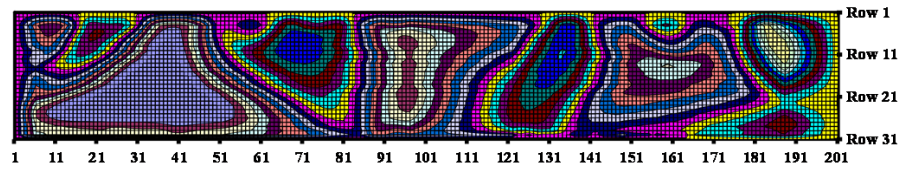
Total out-of-plane deflections of plate girder 8, 800x50, DS G



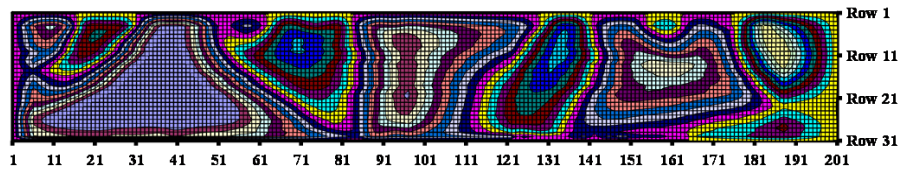
Total out-of-plane deflections of plate girder 8, 800x50, DS H



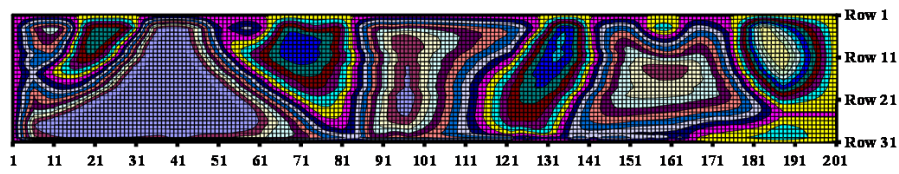
Total out-of-plane deflections of plate girder 8, 800x50, DS I



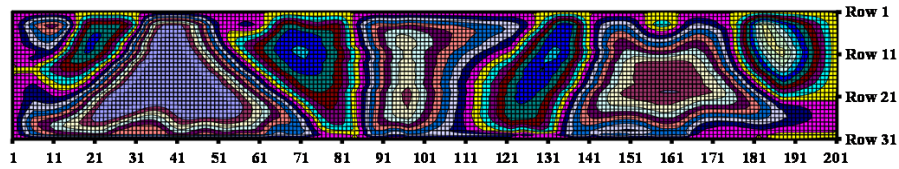
Total out-of-plane deflections of plate girder 8, 800x50, DS J



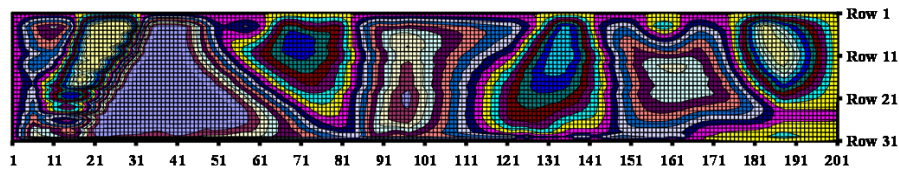
Total out-of-plane deflections of plate girder 8, 800x50, DS K



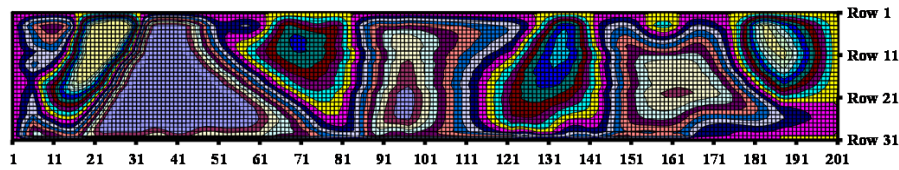
Total out-of-plane deflections of plate girder 8, 800x50, DS L



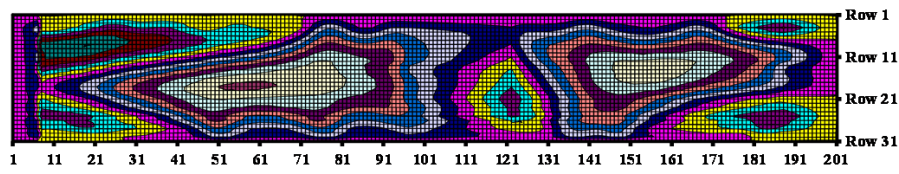
Total out-of-plane deflections of plate girder 8, 800x50, DS M



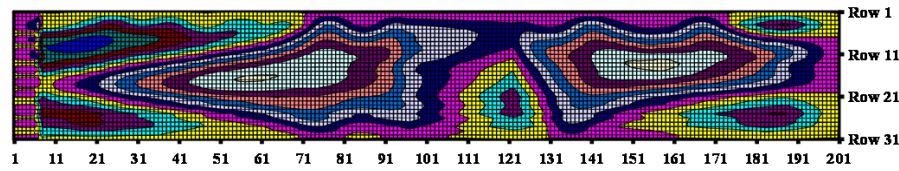
Total out-of-plane deflections of plate girder 8, 800x50, DS O



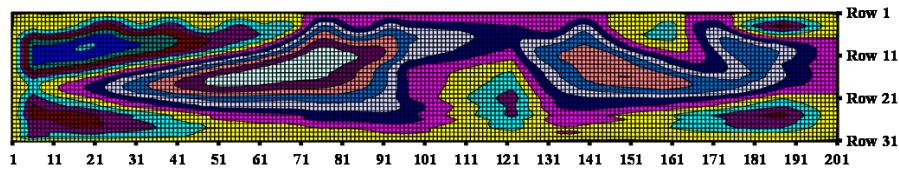
Total out-of-plane deflections of plate girder 8, 800x50, DS P



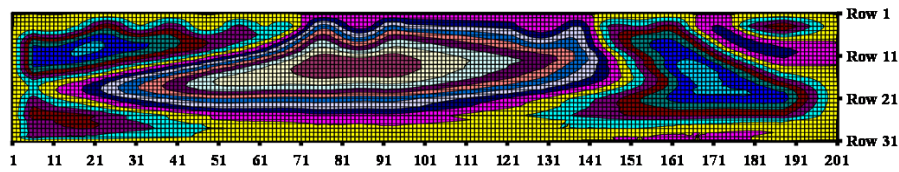
Total out-of-plane deflections of plate girder 9, 800x80, DS 0



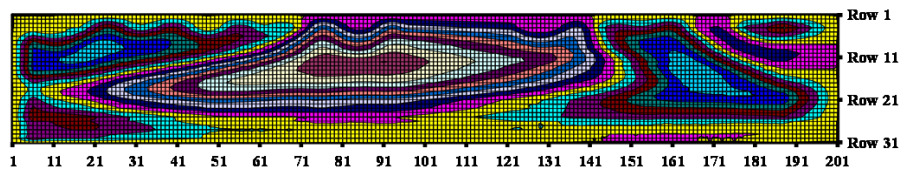
Total out-of-plane deflections of plate girder 9, 800x80, DS A



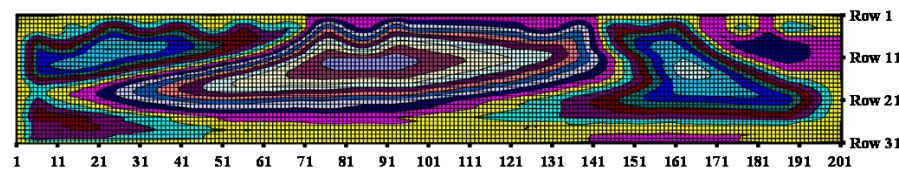
Total out-of-plane deflections of plate girder 9, 800x80, DS B



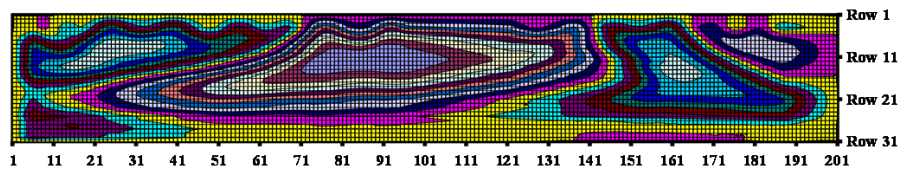
Total out-of-plane deflections of plate girder 9, 800x80, DS C



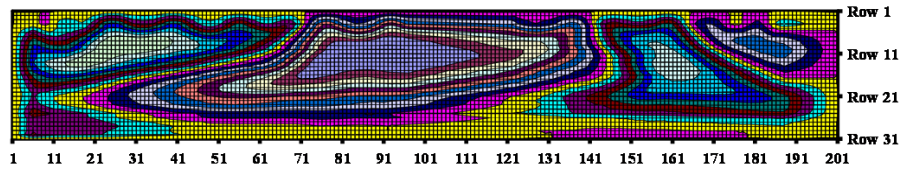
Total out-of-plane deflections of plate girder 9, 800x80, DS D



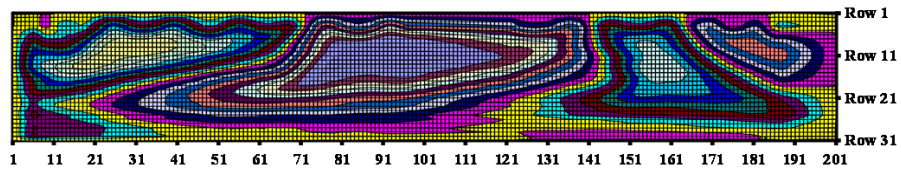
Total out-of-plane deflections of plate girder 9, 800x80, DS E



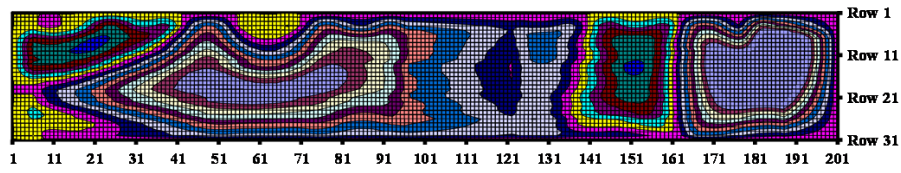
Total out-of-plane deflections of plate girder 9, 800x80, DS F



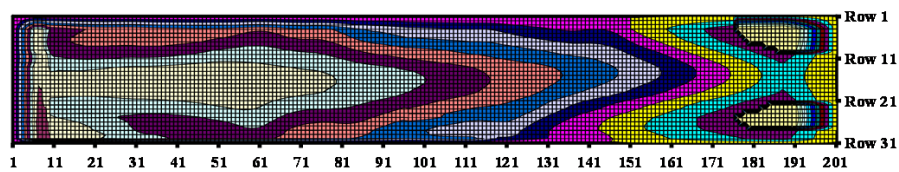
Total out-of-plane deflections of plate girder 9, 800x80, DS G



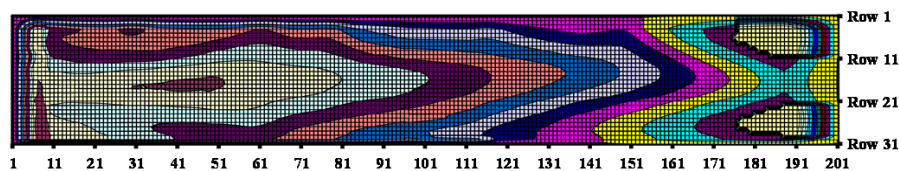
Total out-of-plane deflections of plate girder 9, 800x80, DS H



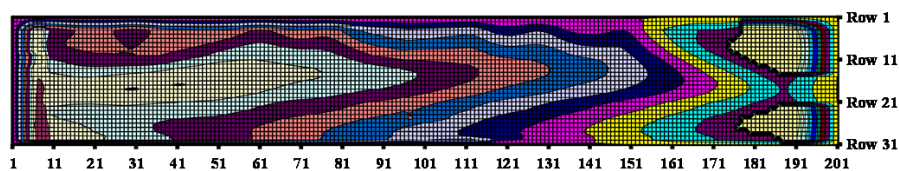
Total out-of-plane deflections of plate girder 9, 800x80, DS I



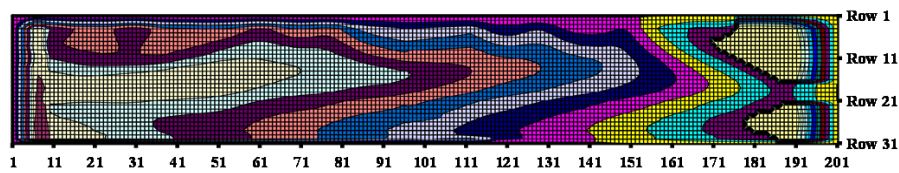
Total out-of-plane deflections of plate girder 10, 800x100, DS 0



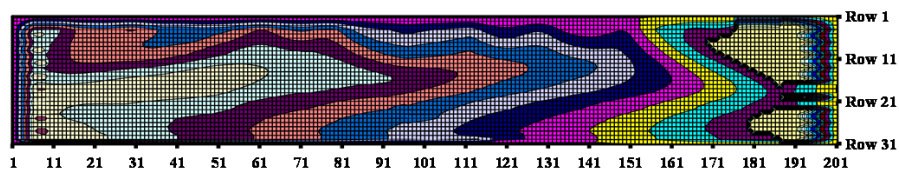
Total out-of-plane deflections of plate girder 10, 800x100, DS A



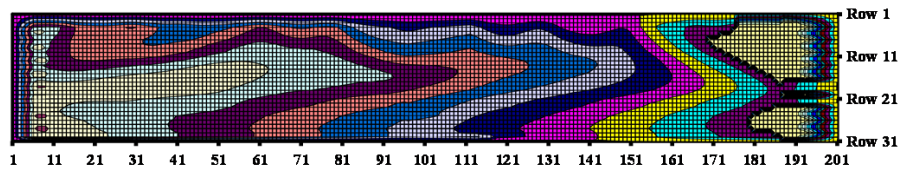
Total out-of-plane deflections of plate girder 10, 800x100, DS B



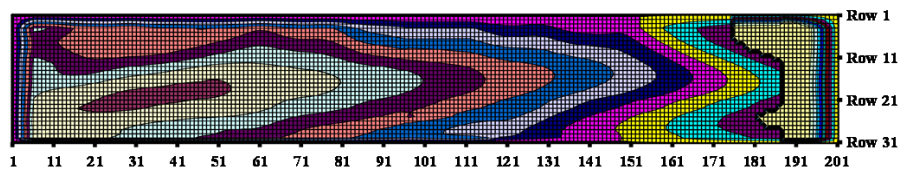
Total out-of-plane deflections of plate girder 10, 800x100, DS C



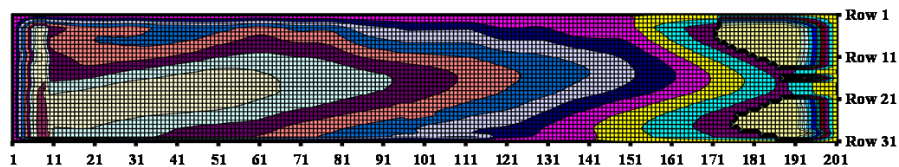
Total out-of-plane deflections of plate girder 10, 800x100, DS D



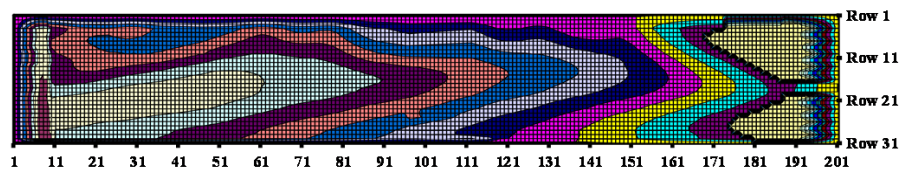
Total out-of-plane deflections of plate girder 10, 800x100, DS E



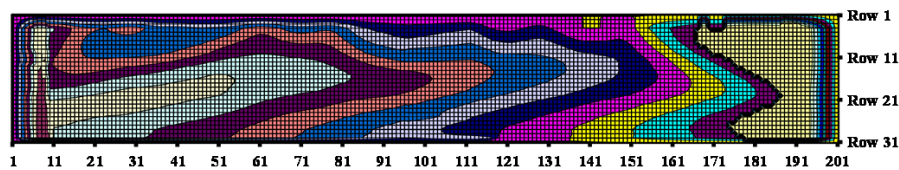
Total out-of-plane deflections of plate girder 10, 800x100, DS F



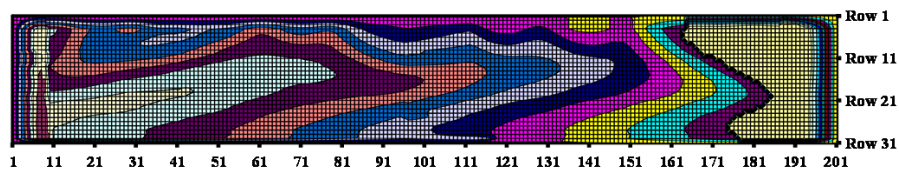
Total out-of-plane deflections of plate girder 10, 800x100, DS G



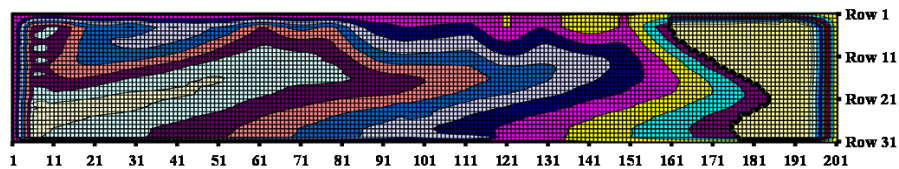
Total out-of-plane deflections of plate girder 10, 800x100, DS H



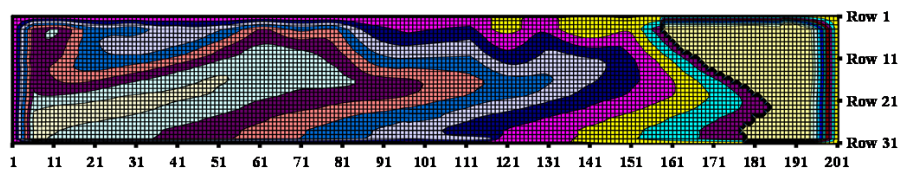
Total out-of-plane deflections of plate girder 10, 800x100, DS I



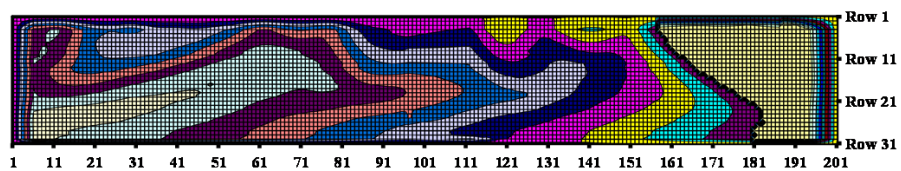
Total out-of-plane deflections of plate girder 10, 800x100, DS J



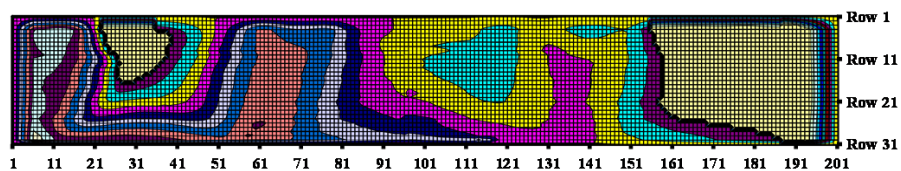
Total out-of-plane deflections of plate girder 10, 800x100, DS K



Total out-of-plane deflections of plate girder 10, 800x100, DS L

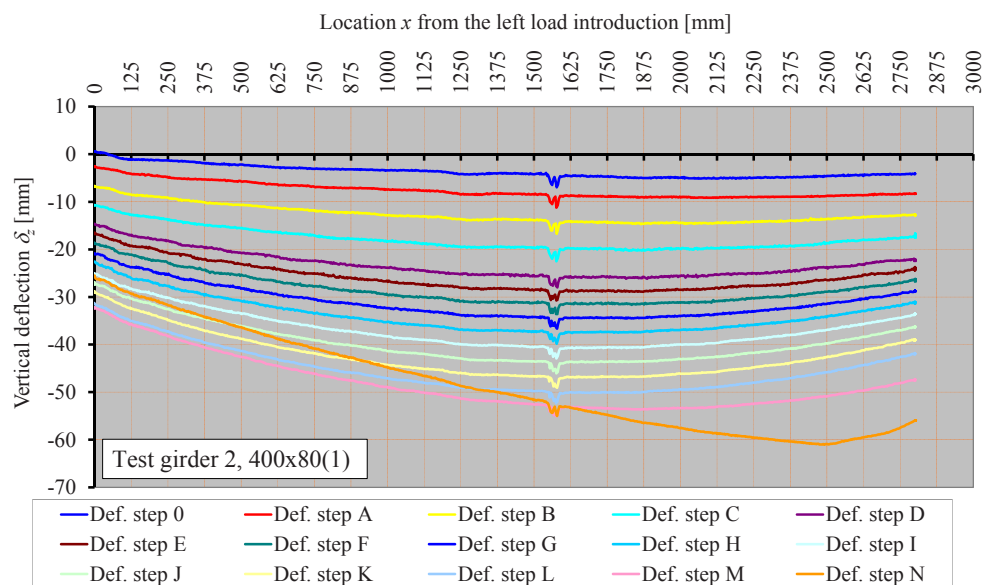
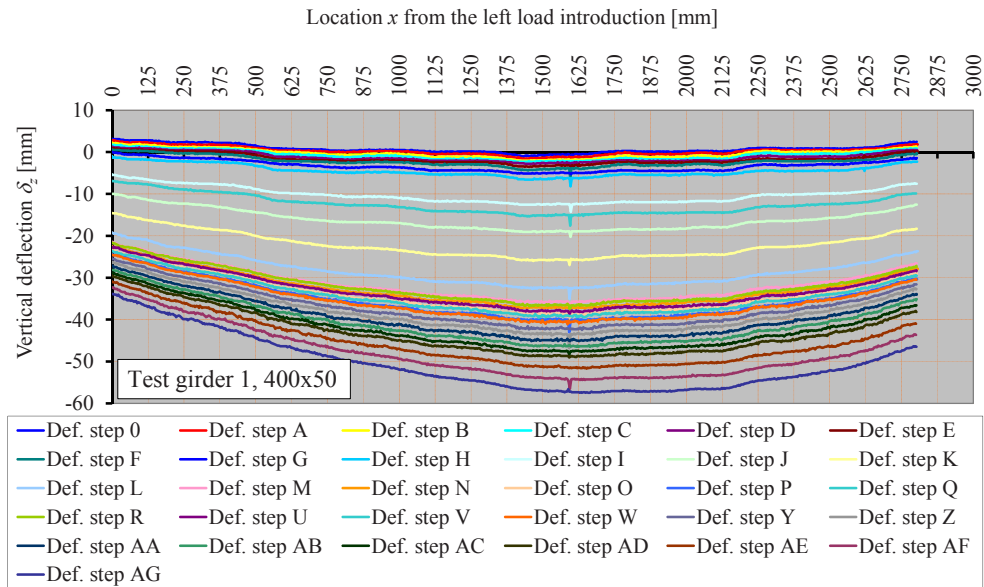


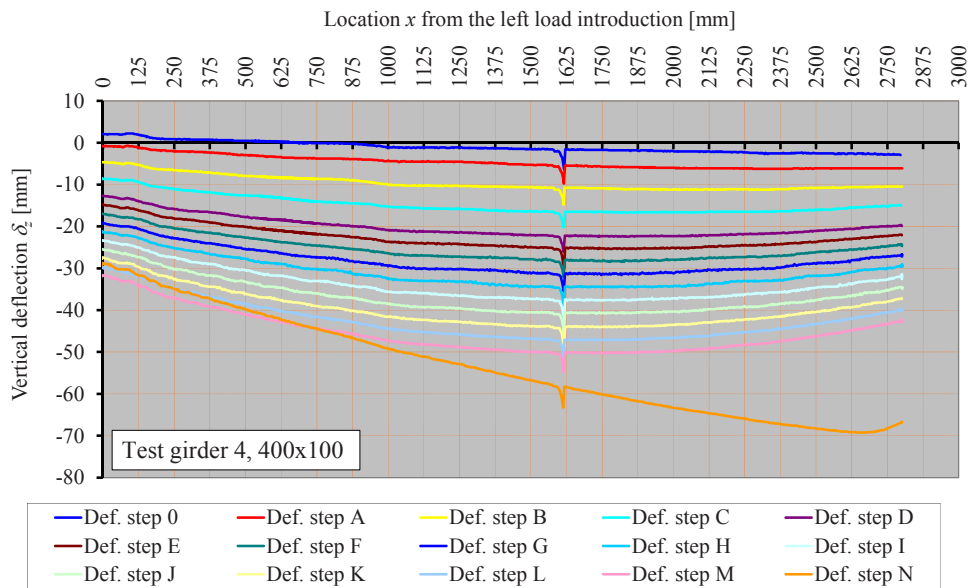
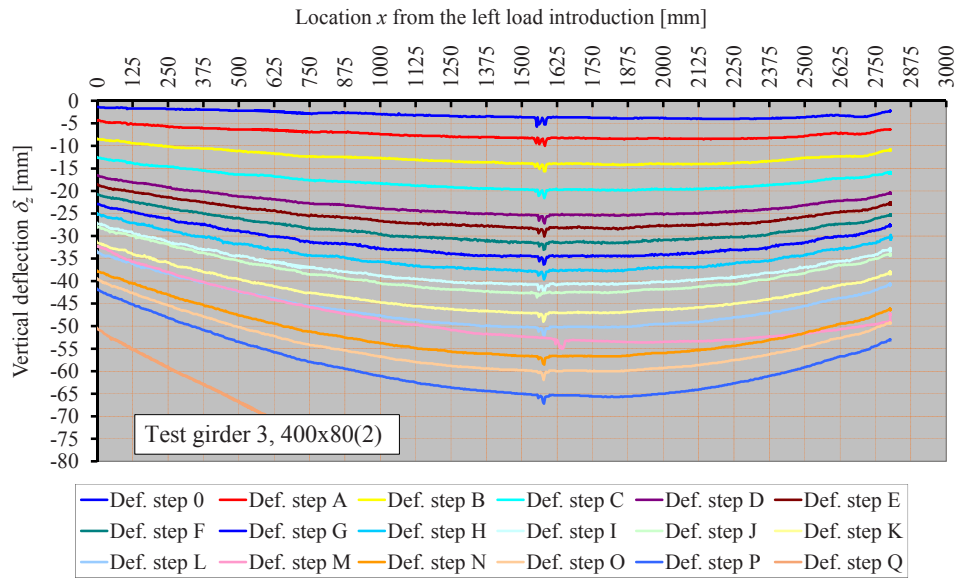
Total out-of-plane deflections of plate girder 10, 800x100, DS M

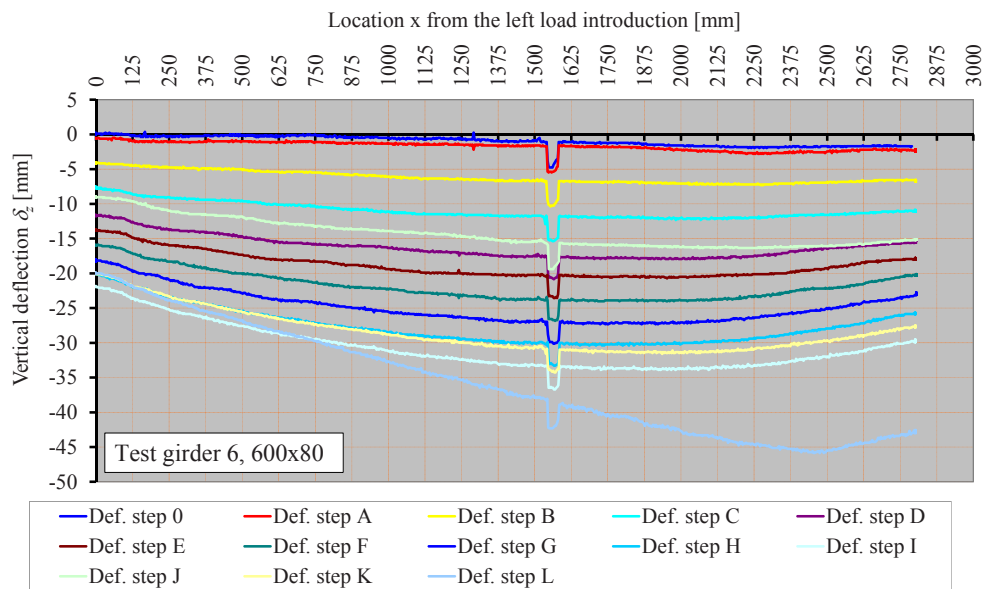
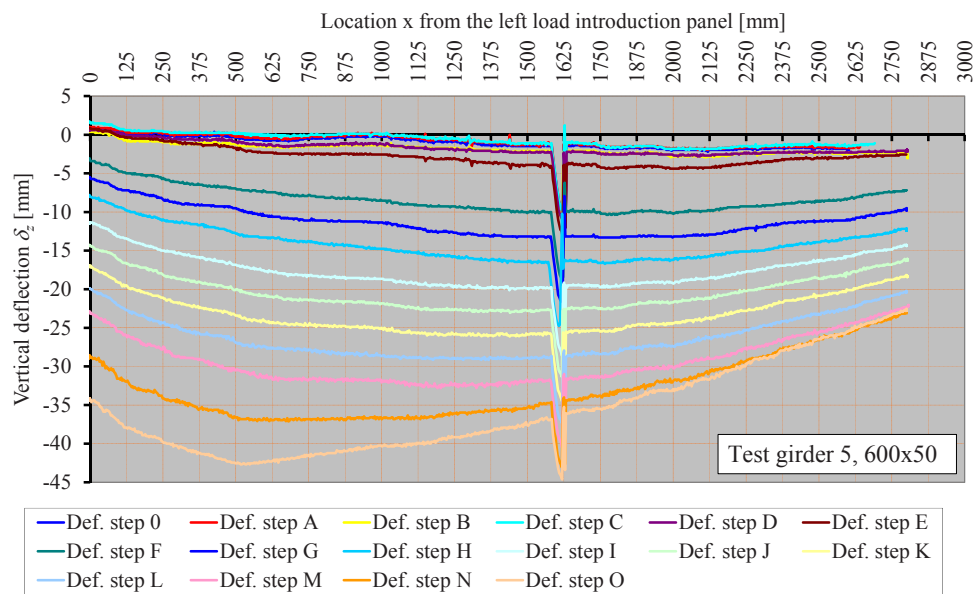


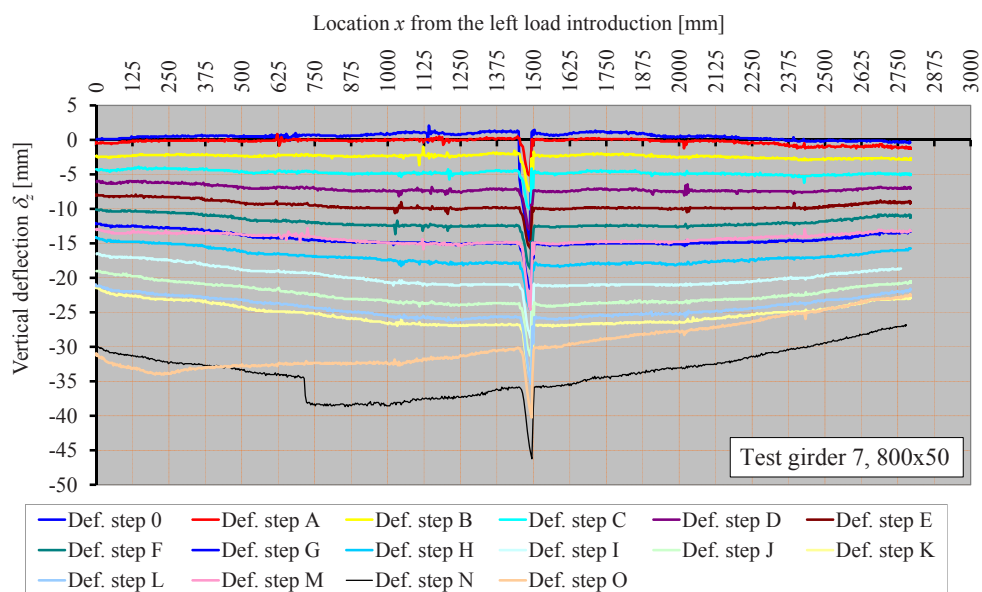
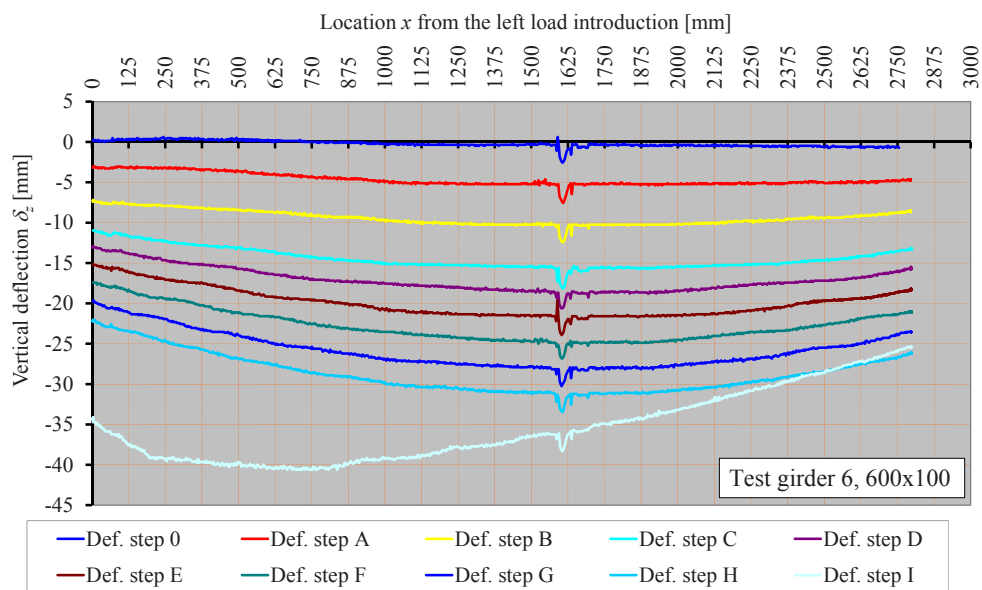
Total out-of-plane deflections of plate girder 10, 800x100, DS N

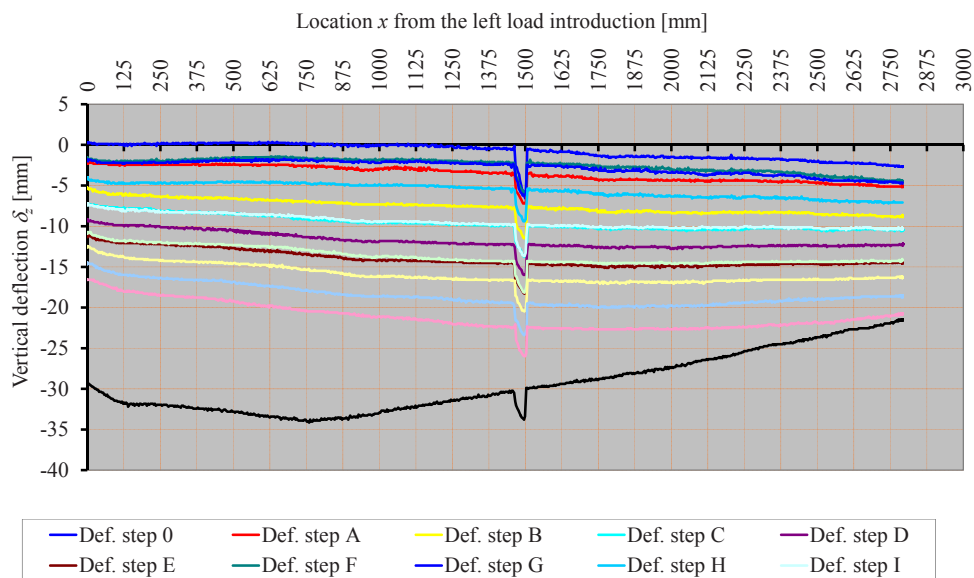
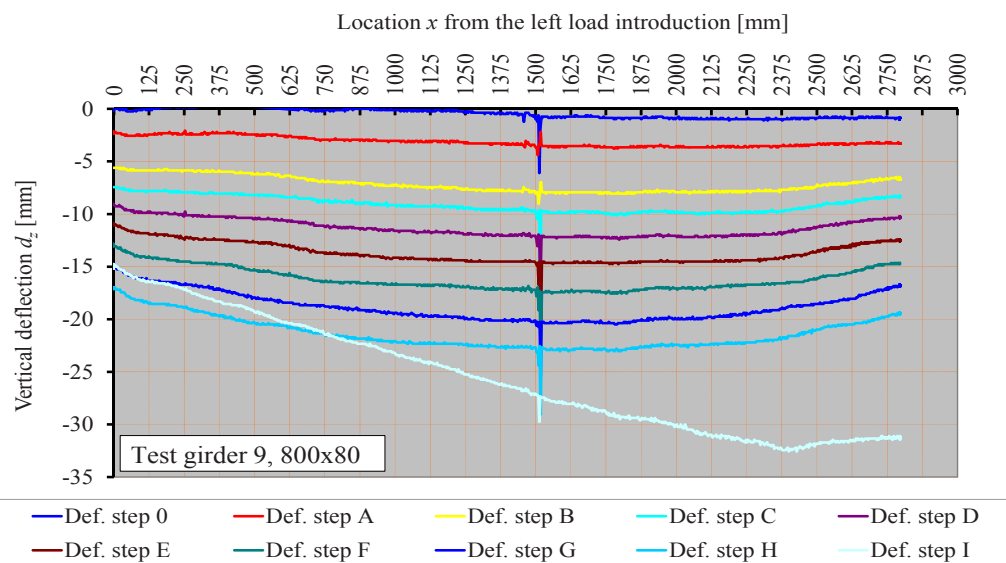
APPENDIX E VERTICAL DEFLECTIONS OF THE BOTTOM FLANGE



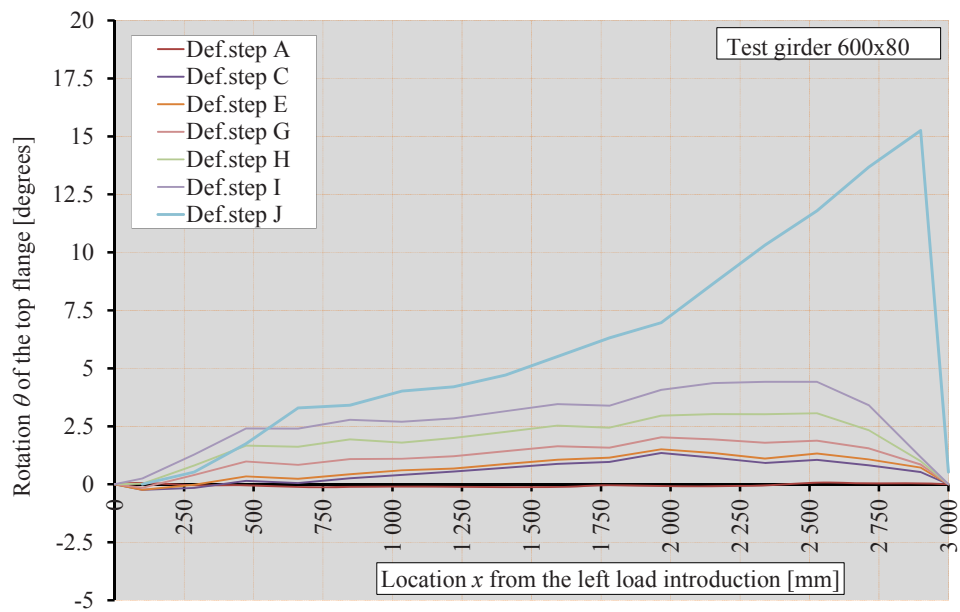
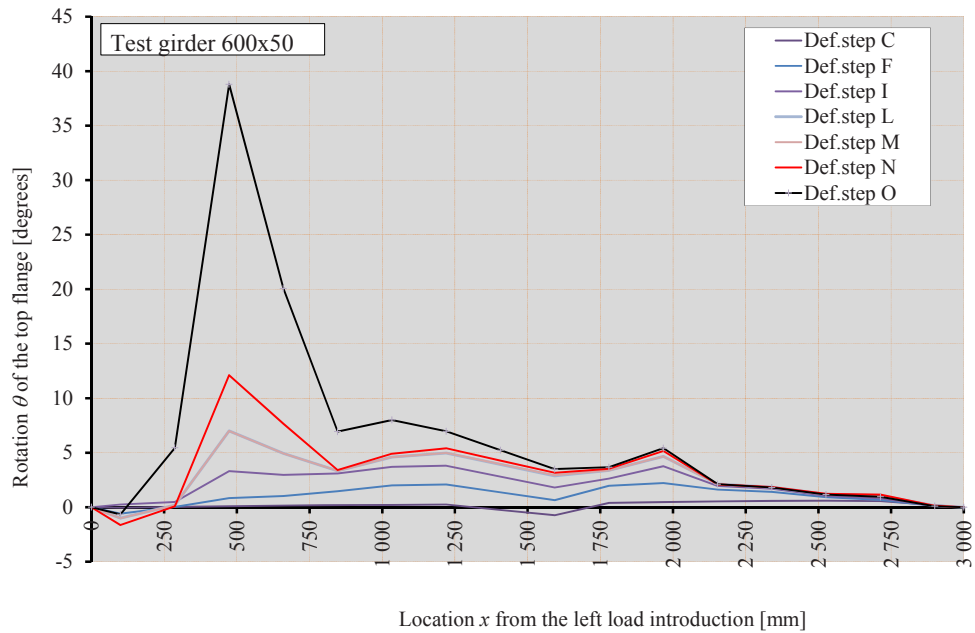


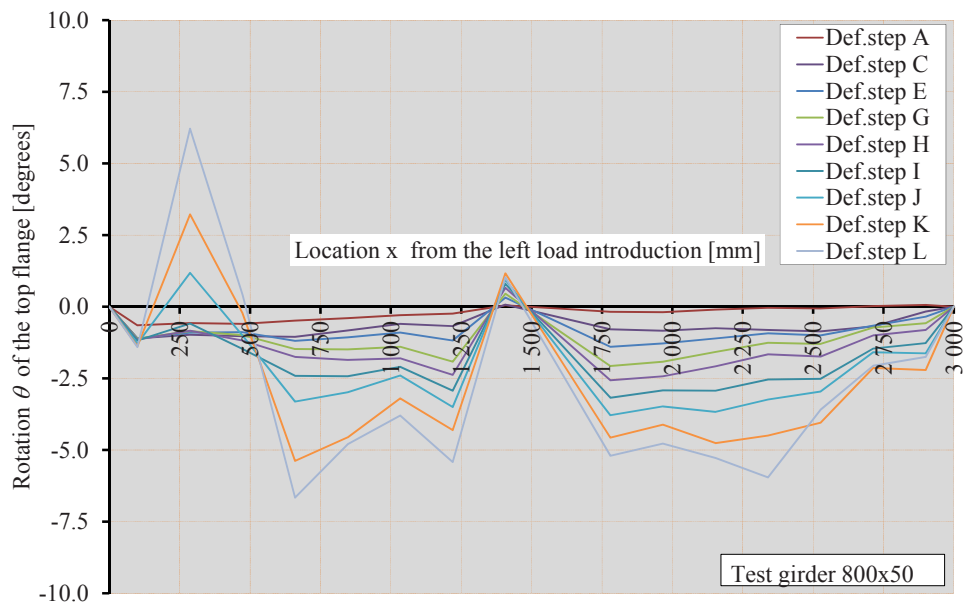
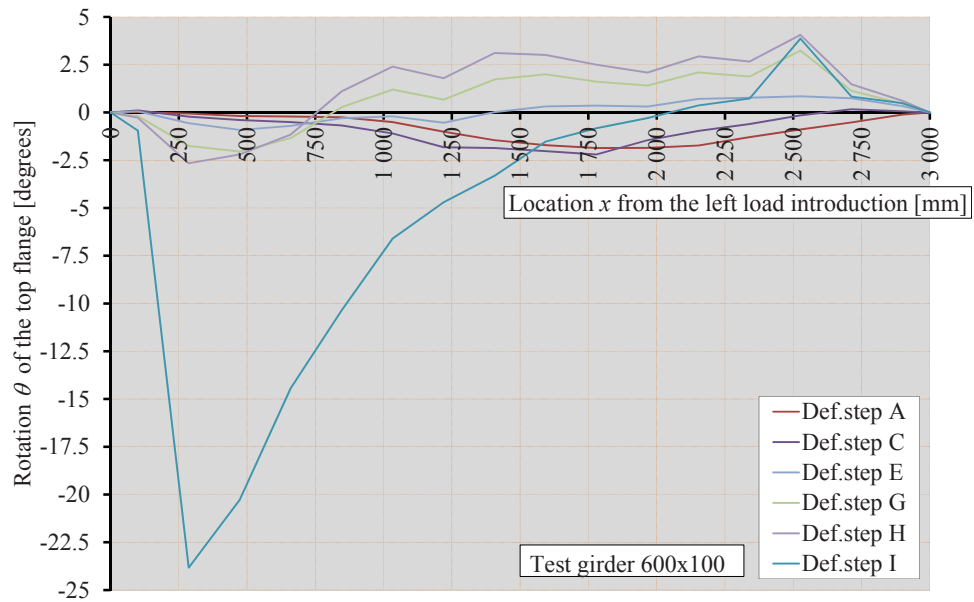


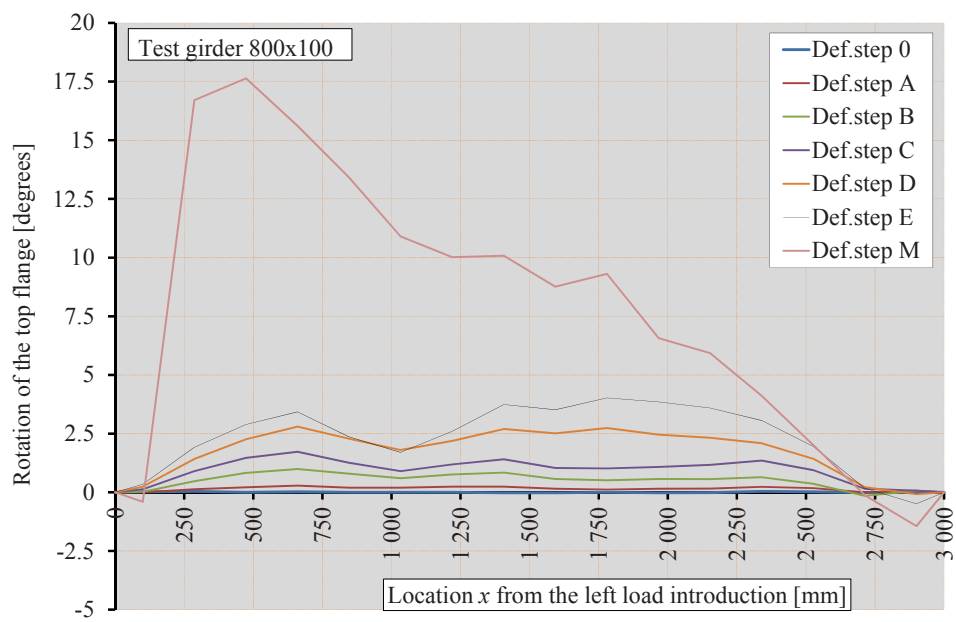
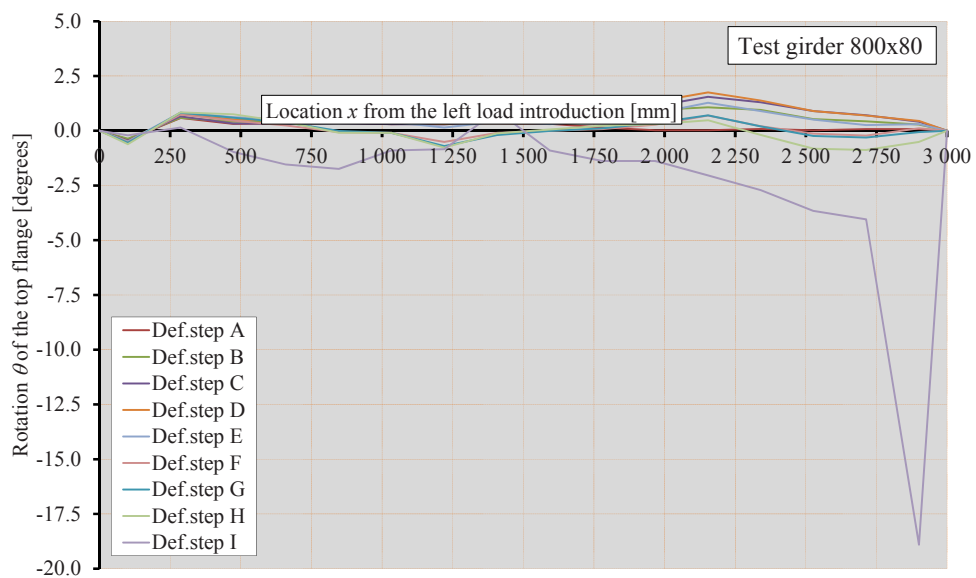




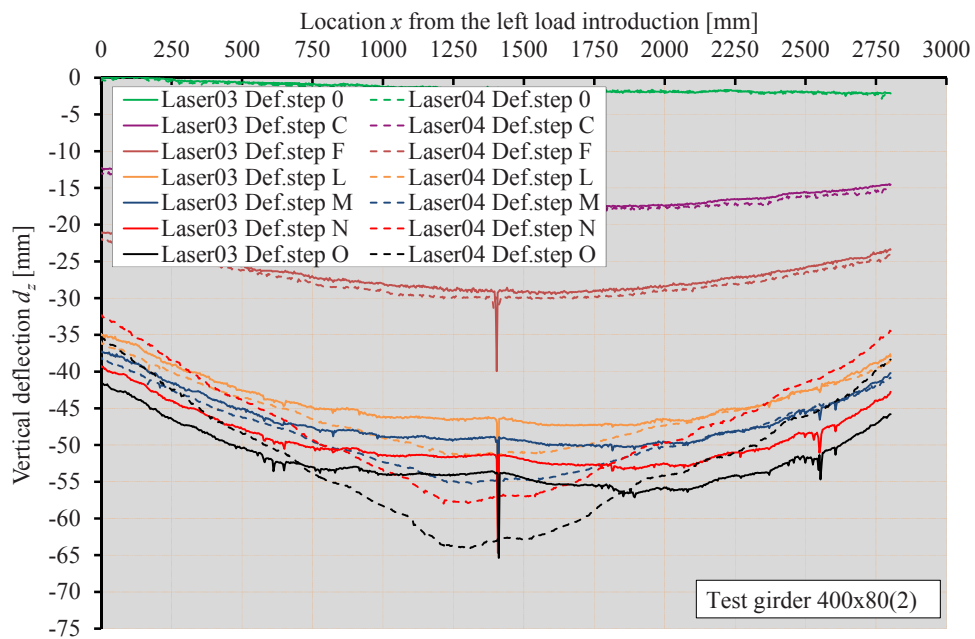
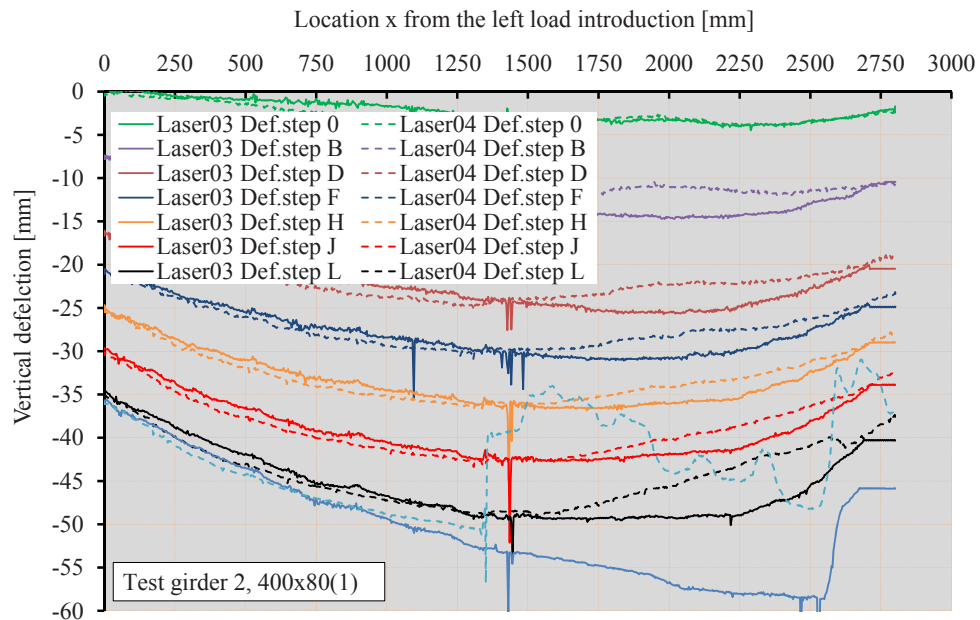
APPENDIX F ROTATION OF THE TOP FLANGE



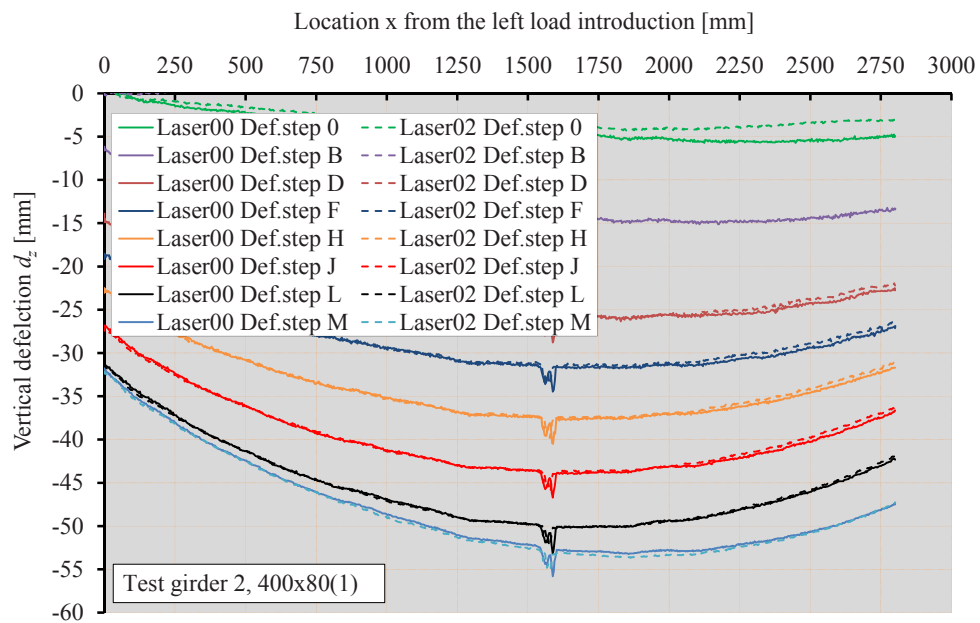
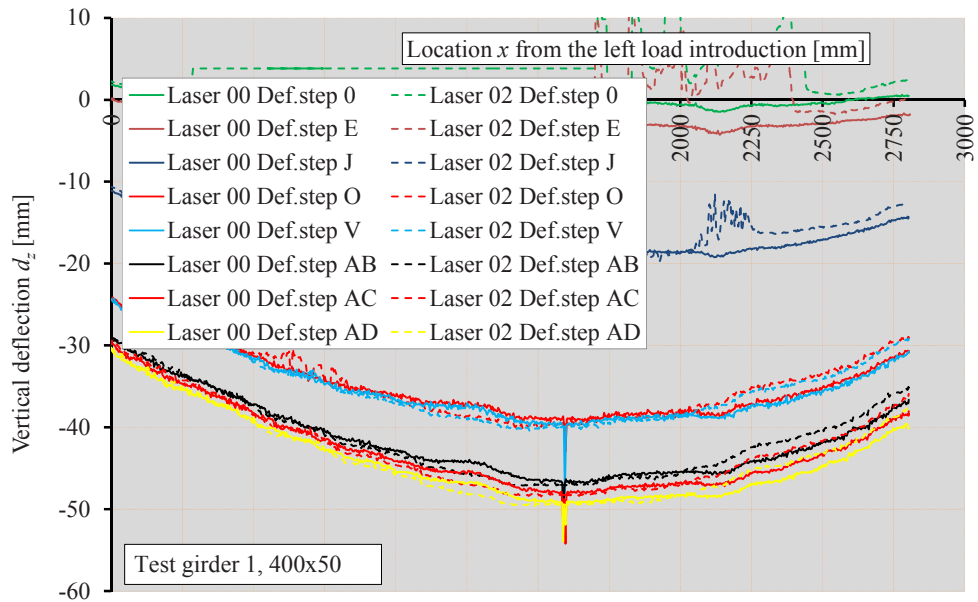


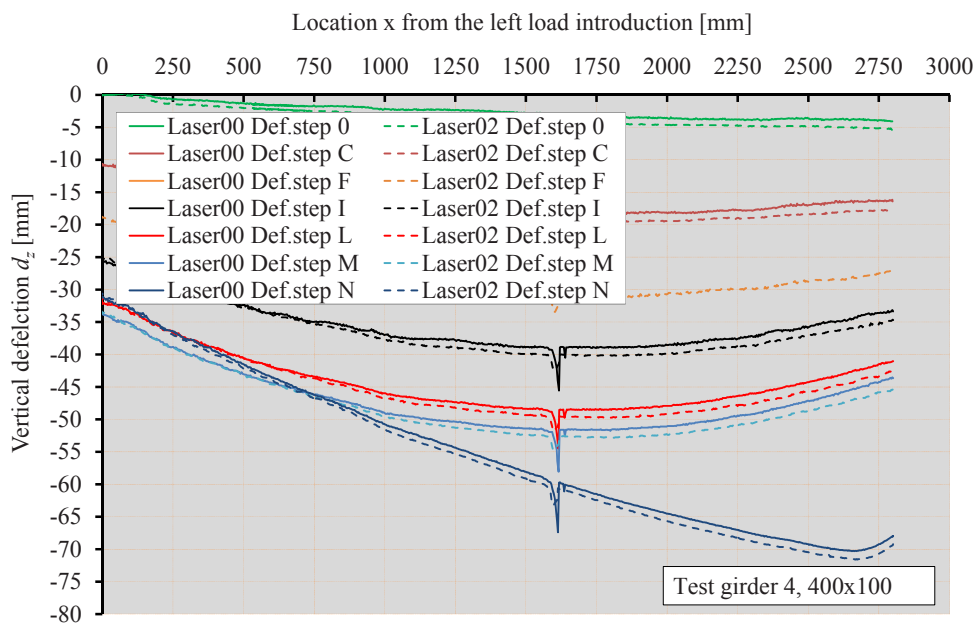
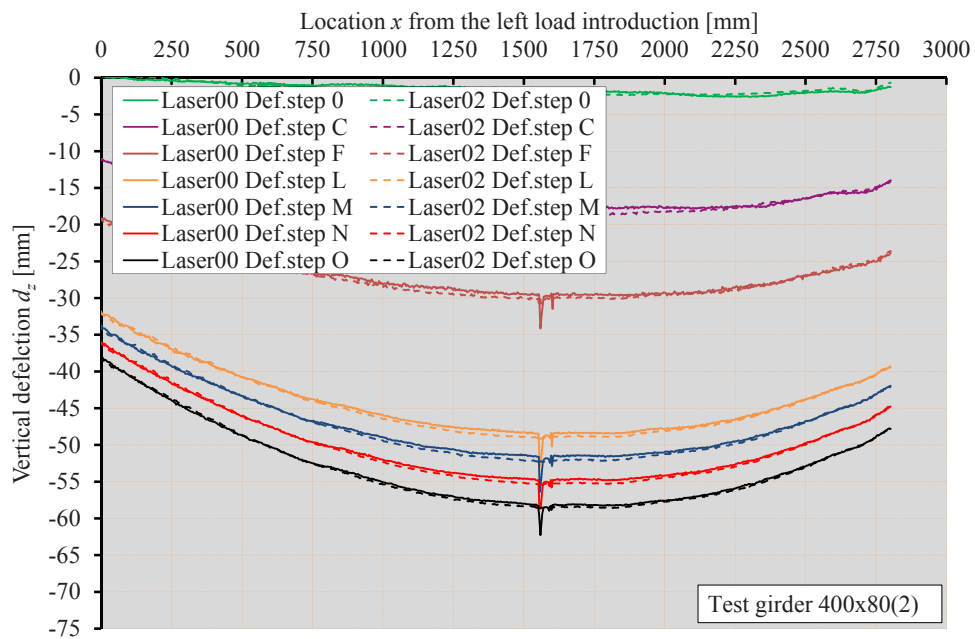


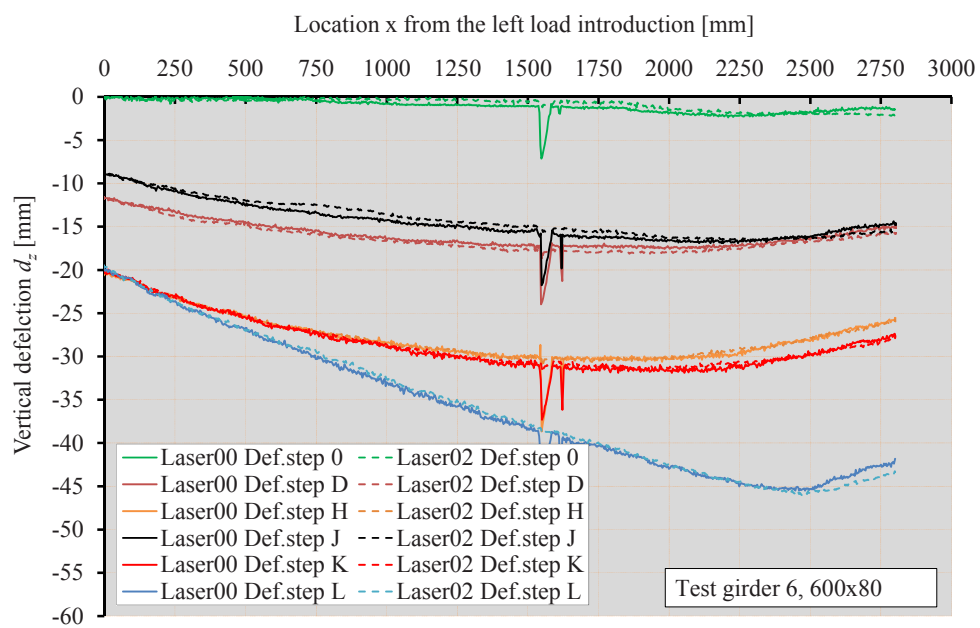
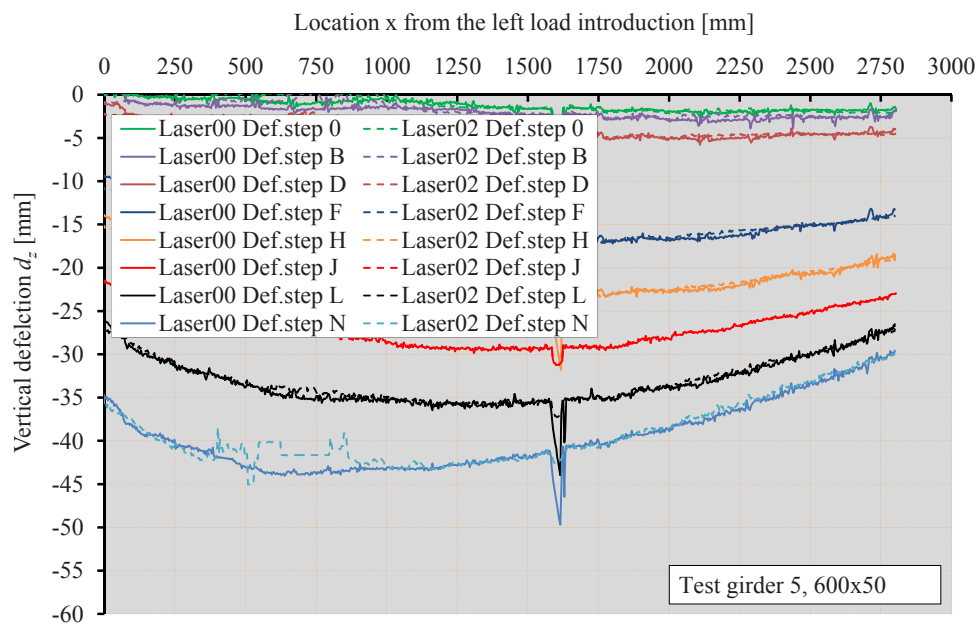
APPENDIX G VERTICAL DEFLECTIONS OF THE TIPS OF THE TOP FLANGE

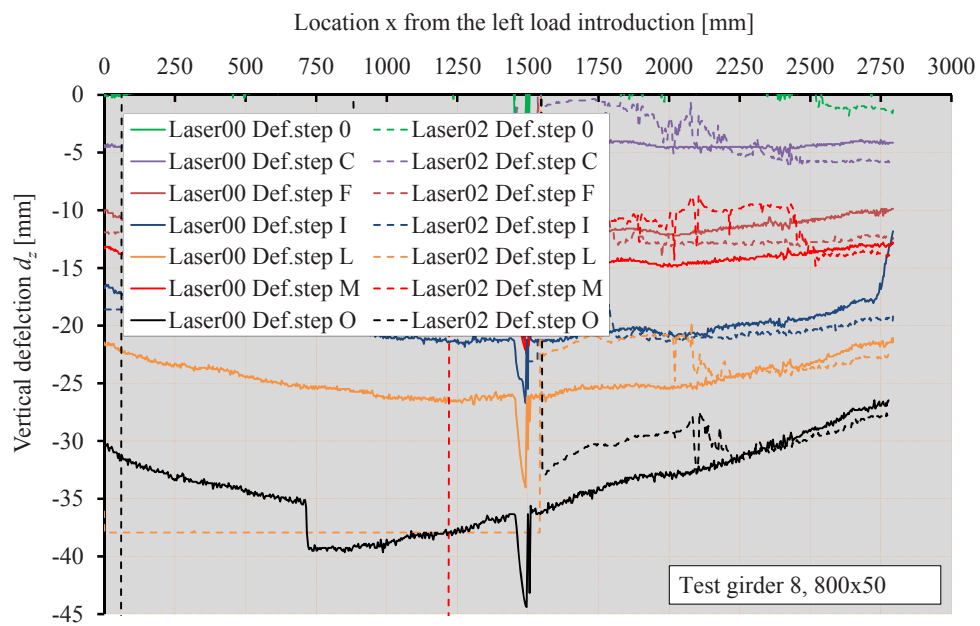
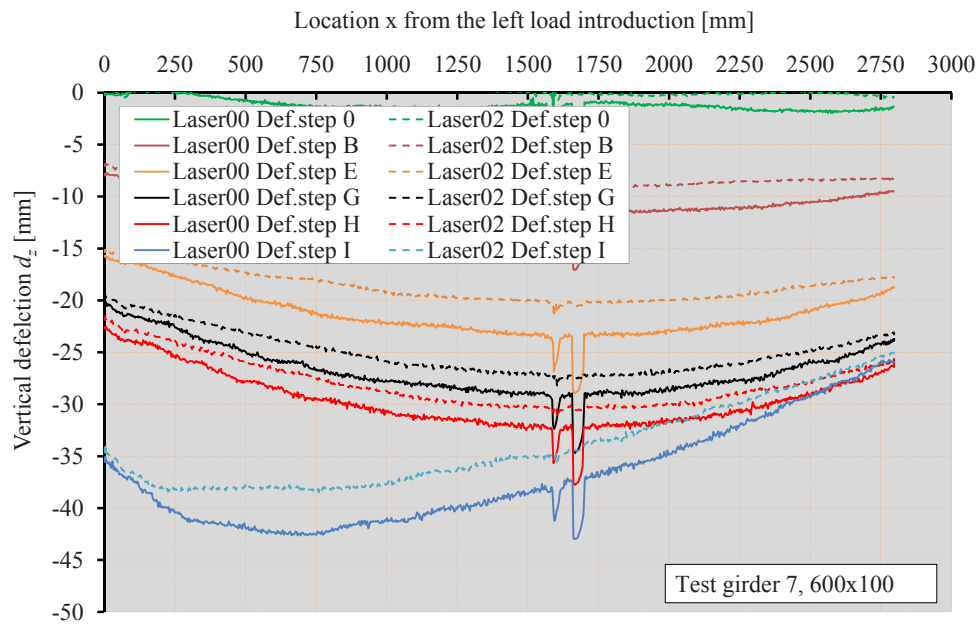


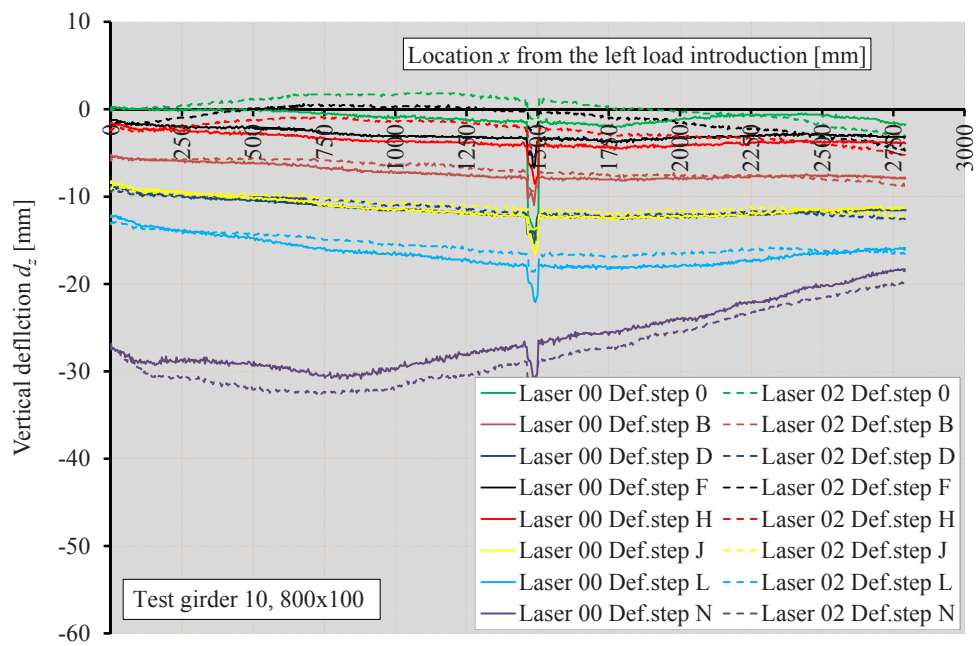
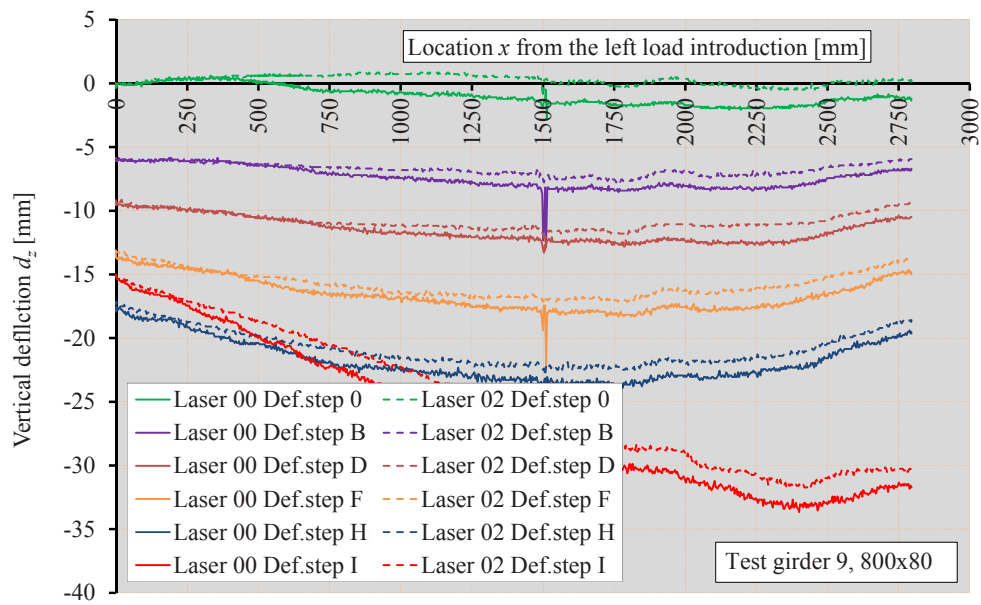
APPENDIX H VERTICAL DEFLECTIONS OF THE TIPS OF THE BOTTOM FLANGE





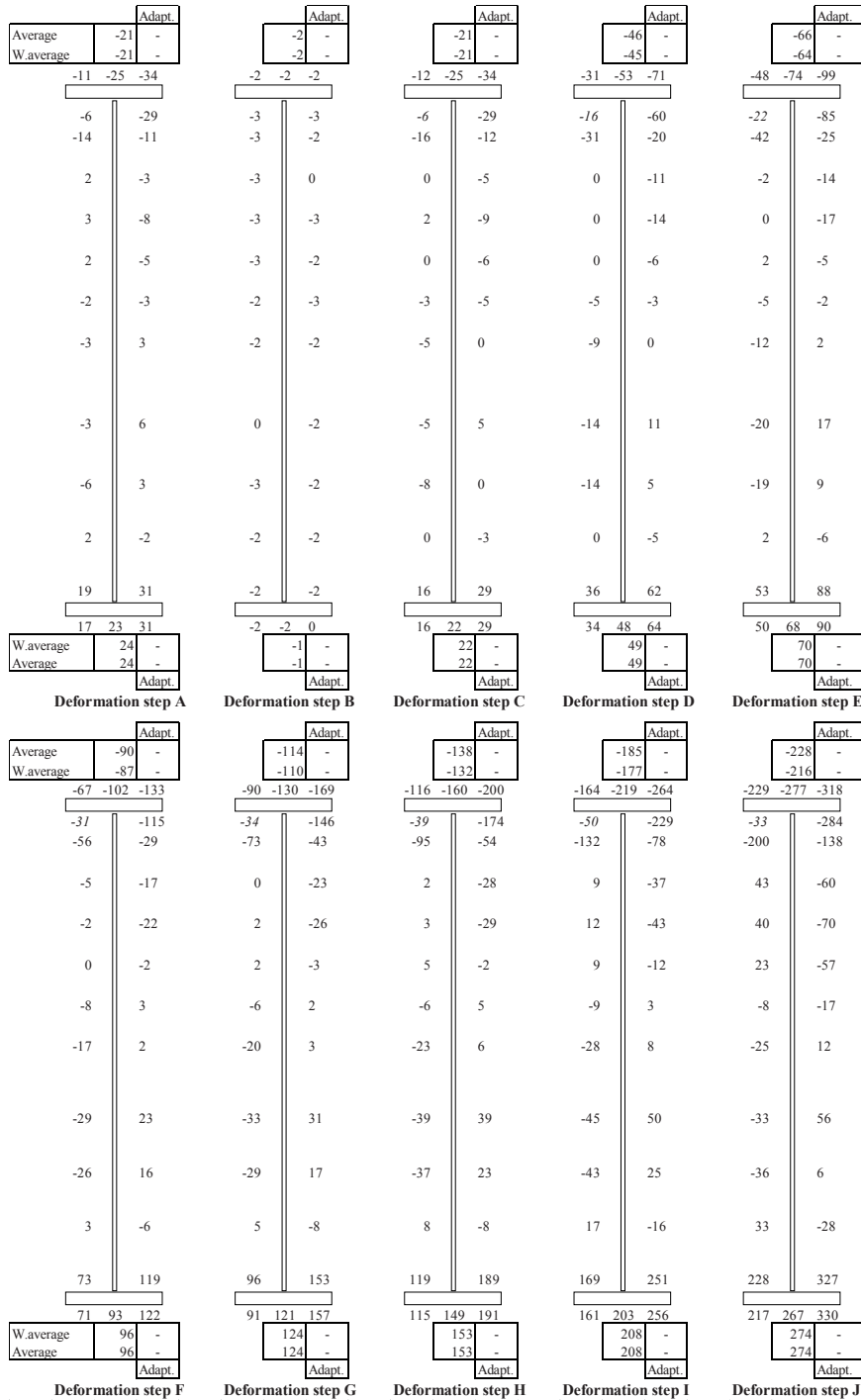






APPENDIX I STRAINS IN THE CROSS-SECTIONS

Test girder 1, 400x50 Deformation steps A - J



Test girder 1, 400x50 Deformation steps K - R

Average		-487	-602	Adapt.
W.average		-458	-599	
-541	-614	-659		
-28	-594			
-510	-312			
140	-140			
109	-150			
62	-149			
-3	-48			
-33	23			
-16	101			
-29	-40			
110	-76			
533	685			
515	586	693		
W.average	604	-		
Average	602	-		
			Adapt.	
Deformation step K				
Average	-662	-1965	Adapt.	
W.average	-336	-1965		
-932	-2187	-2776		
-287	2872			
-747	172			
538	-473			
388	-498			
226	-370			
23	-87			
-90	12			
-2	233			
-43	-90			
374	-81			
1473	1668			
1435	1753	1680		
W.average	1597	-		
Average	1602	-		
			Adapt.	
Deformation step P				
Average	-726	-2067	Adapt.	
W.average	-391	-2067		
-922	-2288	-2992		
-302	2872			
-725	219			
566	-515			
405	-532			
226	-360			
22	-76			
-91	11			
-5	236			
-45	-85			
375	-78			
1491	1666			
1454	1784	1674		
W.average	1608	-		
Average	1614	-		
			Adapt.	
Deformation step Q				
Average	-813	-2214	Adapt.	
W.average	-462	-2214		
-947	-2417	-3277		
-295	2872			
-742	226			
580	-543			
409	-553			
214	-338			
17	-59			
-99	11			
-9	237			
-48	-79			
375	-73			
1507	1671			
1471	1800	1677		
W.average	1619	-		
Average	1625	-		
			Adapt.	
Deformation step R				
Average	-1032	-1264	Adapt.	
W.average	-977	-1276		
-1035	-1271	-1448		
-104	-1301			
-955	-158			
344	-287			
251	-288			
161	-341			
20	-126			
-48	25			
14	188			
-22	-105			
276	-113			
1110	1310			
1082	1175	1332		
W.average	1203	-		
Average	1202	-		
			Adapt.	
Deformation step M				
Average	-1175	-1421	Adapt.	
W.average	-1112	-1415		
-1003	-1693	-1586		
-189	-1403			
-873	-43			
414	-324			
293	-361			
184	-347			
19	-102			
-73	19			
8	215			
-34	-101			
336	-95			
1342	1559			
1279	1166	1561		
W.average	1393	-		
Average	1381	-		
			Adapt.	
Deformation step N				
Average	-610	-1885	Adapt.	
W.average	-291	-1885		
-924	-2097	-2635		
-267	2872			
-752	126			
516	-439			
375	-467			
229	-384			
26	-99			
-85	14			
-2	226			
-43	-93			
361	-81			
1428	1645			
1389	1583	1665		
W.average	1541	-		
Average	1542	-		
			Adapt.	
Deformation step O				

Test girder 1, 400x50 Deformation steps U – Z

Average			-686	-1145	Adapt.
W.average			-356	-1576	
-769	-2201	-3049			
-284	2872				
-569	302				
552	-533				
384	-519				
189	-301				
17	-54				
-87	12				
-5	214				
-42	-84				
326	-90				
1336	1494				
1301	1625	1494			
W.average	1444	-			
Average	1450	-			
Adapt.					
Deformation step U					
Average			-733	-1186	Adapt.
W.average			-395	-1634	
-832	-2279	-3134			
-290	2872				
-631	274				
564	-561				
389	-543				
186	-298				
11	-53				
-96	8				
-9	220				
-45	-87				
343	-87				
1400	1559				
1364	1690	1564			
W.average	1509	-			
Average	1515	-			
Adapt.					
Deformation step V					
Average			-772	-1218	Adapt.
W.average			-428	-1683	
-882	-2347	-3215			
-288	2872				
-680	250				
583	-574				
405	-560				
192	-305				
11	-50				
-99	9				
-9	229				
-48	-82				
363	-78				
1463	1626				
1428	1755	1631			
W.average	1575	-			
Average	1580	-			
Adapt.					
Deformation step W					
Average			-810	-1250	Adapt.
W.average			-460	-1731	
-933	-2426	-3274			
-290	2872				
-729	229				
605	-608				
414	-586				
188	-279				
5	-36				
-109	8				
-12	236				
-50	-76				
378	-68				
1521	1682				
1482	1814	1690			
W.average	1631	-			
Average	1638	-			
Adapt.					
Deformation step X					
Average			-875	-1313	Adapt.
W.average			-516	-1812	
-908	-2882	-3147			
-313	2872				
-688	366				
677	-710				
451	-653				
189	-256				
2	-23				
-118	6				
-20	239				
-54	-68				
380	-62				
1545	1699				
1504	1842	1708			
W.average	1653	-			
Average	1660	-			
Adapt.					
Deformation step Y					
Average			-918	-1352	Adapt.
W.average			-553	-1866	
-902	-3085	-3151			
-326	2872				
-673	412				
702	-761				
456	-685				
177	-214				
-9	-6				
-126	6				
-26	242				
-60	-60				
380	-57				
1545	1711				
1504	1848	1721			
W.average	1660	-			
Average	1666	-			
Adapt.					
Deformation step Z					

Test girder 1, 400x50 Deformation steps AA - AG

Average			Adapt.		
-956			-2436		
W.average			-586		
-888			-3243		
-344			2872		
-639			463		
724			-814		
451			-707		
158			-167		
-19			8		
-132			3		
-25			243		
-60			-59		
378			-57		
1541			1713		
1491			1843		
W.average			1655		
Average			1661		
Adapt.			Adapt.		
Deformation step AA			Deformation step AB		
Average			Adapt.		
-1040			-2566		
W.average			-658		
-877			-3330		
-372			2872		
-685			764		
902			-1198		
330			-668		
40			132		
-71			82		
-171			-11		
-64			242		
-87			-29		
346			-47		
1501			1673		
1448			1797		
W.average			1612		
Average			1618		
Adapt.			Adapt.		
Deformation step AF			Deformation step AG		
Average			Adapt.		
-981			-2481		
W.average			-606		
-884			-3330		
-333			2872		
-632			481		
746			-867		
442			-721		
140			-124		
-28			20		
-138			2		
-28			243		
-62			-57		
375			-57		
1535			1714		
1483			1838		
W.average			1652		
Average			1657		
Adapt.			Adapt.		
Deformation step AC			Deformation step AD		
Average			Adapt.		
-994			-2501		
W.average			-618		
-874			-3330		
-341			2872		
-618			507		
763			-919		
428			-725		
121			-76		
-37			34		
-144			-2		
-33			245		
-65			-53		
372			-56		
1532			1710		
1482			1835		
W.average			1648		
Average			1654		
Adapt.			Adapt.		
Deformation step AE			Deformation step AD		
Average			Adapt.		
-1007			-2521		
W.average			-628		
-843			-3330		
-343			2872		
-615			546		
783			-963		
414			-727		
105			-37		
-45			45		
-149			-3		
-37			245		
-70			-48		
367			-54		
1525			1704		
1473			1826		
W.average			1641		
Average			1647		
Adapt.			Adapt.		
Deformation step AE			Deformation step AE		
Average			Adapt.		
-1026			-2552		
W.average			-644		
-836			-3330		
-344			2872		
-592			637		
834			-1051		
391			-721		
84			28		
-53			60		
-157			-8		
-48			243		
-76			-40		
358			-51		
1514			1691		
1462			1812		
W.average			1629		
Average			1634		
Adapt.			Adapt.		

Test girder 2, 400x80(1) Deformation steps A - J

<table><tr><td>Average</td><td>-137</td><td>-</td></tr><tr><td>Waverage</td><td>-137</td><td>-</td></tr></table>		Average	-137	-	Waverage	-137	-	<table><tr><td>Adapt.</td><td>-</td></tr></table>	Adapt.	-	<table><tr><td>Adapt.</td><td>-</td></tr></table>		Adapt.	-	<table><tr><td>Adapt.</td><td>-</td></tr></table>		Adapt.	-	<table><tr><td>Adapt.</td><td>-</td></tr></table>		Adapt.	-	<table><tr><td>Adapt.</td><td>-</td></tr></table>		Adapt.	-													
Average	-137	-																																					
Waverage	-137	-																																					
Adapt.	-																																						
Adapt.	-																																						
Adapt.	-																																						
Adapt.	-																																						
Adapt.	-																																						
-112 -130 -172		-377 -448 -521		-569 -752 -924		-688 -1042 -1366		-615 -1460 -1417																															
-99 -172		-318 -470		-484 -834		-580 -1245		3184 -1308																															
-110 -53		-171 -135		-268 -228		-415 -329		-547 -357																															
-50 -9		-34 -12		-37 0		-57 0		-60 53																															
-29 19		-26 26		-53 95		-53 136		-53 181																															
-37 22		-48 6		-161 112		-192 153		-212 180																															
-33 3		-51 -17		-231 129		-287 178		-316 202																															
-16 -23		-39 -14		-237 150		-304 212		-332 236																															
6 -47		-19 36		-181 147		-234 236		-253 262																															
12 -19		6 105		-57 174		-34 302		-17 349																															
40 53		116 206		181 315		299 491		361 572																															
167 141		456 409		758 673		1046 927		1175 1045																															
172 164 160		457 445 450		783 756 749		1087 1051 1035		1220 1181 1164																															
<table><tr><td>Waverage</td><td>160</td><td>159</td></tr><tr><td>Average</td><td>161</td><td>153</td></tr></table>		Waverage	160	159	Average	161	153	<table><tr><td>Adapt.</td><td>442</td><td>440</td></tr><tr><td>Adapt.</td><td>443</td><td>430</td></tr></table>		Adapt.	442	440	Adapt.	443	430	<table><tr><td>Adapt.</td><td>739</td><td>740</td></tr><tr><td>Adapt.</td><td>744</td><td>718</td></tr></table>		Adapt.	739	740	Adapt.	744	718	<table><tr><td>Adapt.</td><td>1022</td><td>1025</td></tr><tr><td>Adapt.</td><td>1029</td><td>992</td></tr></table>		Adapt.	1022	1025	Adapt.	1029	992	<table><tr><td>Adapt.</td><td>1149</td><td>1153</td></tr><tr><td>Adapt.</td><td>1157</td><td>1117</td></tr></table>		Adapt.	1149	1153	Adapt.	1157	1117
Waverage	160	159																																					
Average	161	153																																					
Adapt.	442	440																																					
Adapt.	443	430																																					
Adapt.	739	740																																					
Adapt.	744	718																																					
Adapt.	1022	1025																																					
Adapt.	1029	992																																					
Adapt.	1149	1153																																					
Adapt.	1157	1117																																					
Deformation step A		Deformation step B		Deformation step C		Deformation step D		Deformation step E																															
<table><tr><td>Average</td><td>-433</td><td>-1337</td></tr><tr><td>Waverage</td><td>-214</td><td>-1367</td></tr></table>		Average	-433	-1337	Waverage	-214	-1367	<table><tr><td>Adapt.</td><td>-520</td><td>-1445</td></tr><tr><td>Adapt.</td><td>-291</td><td>-1475</td></tr></table>		Adapt.	-520	-1445	Adapt.	-291	-1475	<table><tr><td>Adapt.</td><td>-583</td><td>-1525</td></tr><tr><td>Adapt.</td><td>-355</td><td>-1552</td></tr></table>		Adapt.	-583	-1525	Adapt.	-355	-1552	<table><tr><td>Adapt.</td><td>-634</td><td>-1588</td></tr><tr><td>Adapt.</td><td>-398</td><td>-1601</td></tr></table>		Adapt.	-634	-1588	Adapt.	-398	-1601	<table><tr><td>Adapt.</td><td>-727</td><td>-1704</td></tr><tr><td>Adapt.</td><td>-482</td><td>-1704</td></tr></table>		Adapt.	-727	-1704	Adapt.	-482	-1704
Average	-433	-1337																																					
Waverage	-214	-1367																																					
Adapt.	-520	-1445																																					
Adapt.	-291	-1475																																					
Adapt.	-583	-1525																																					
Adapt.	-355	-1552																																					
Adapt.	-634	-1588																																					
Adapt.	-398	-1601																																					
Adapt.	-727	-1704																																					
Adapt.	-482	-1704																																					
-553 -1815 -1553		-591 -1990 -1668		-574 -2178 -1741		-605 -2364 -1756		-642 -2646 -1828																															
3184 -1426		3184 -1533		3184 -1607		3184 -1628		3184 -1702																															
-642 -394		-716 -419		-814 -462		-894 -474		-964 -474																															
-54 90		-54 112		-45 133		-31 166		-23 202																															
-50 219		-50 245		-48 274		-47 299		-50 327																															
-233 200		-248 219		-270 242		-287 257		-310 274																															
-339 217		-364 236		-392 257		-414 274		-439 295																															
-353 253		-380 271		-406 295		-426 310		-450 332																															
-264 279		-277 295		-308 308		-327 321		-353 333																															
9 391		31 425		12 440		9 456		-6 467																															
428 653		493 727		521 767		558 817		586 857																															
1302 1159		1411 1257		1505 1342		1600 1431		1697 1528																															
1350 1311 1291		1469 1409 1403		1569 1463 1499		1666 1505 1597		1766 1583 1696																															
<table><tr><td>Waverage</td><td>1274</td><td>1278</td></tr><tr><td>Average</td><td>1283</td><td>1239</td></tr></table>		Waverage	1274	1278	Average	1283	1239	<table><tr><td>Adapt.</td><td>1380</td><td>1385</td></tr><tr><td>Adapt.</td><td>1390</td><td>1342</td></tr></table>		Adapt.	1380	1385	Adapt.	1390	1342	<table><tr><td>Adapt.</td><td>1467</td><td>1468</td></tr><tr><td>Adapt.</td><td>1476</td><td>1426</td></tr></table>		Adapt.	1467	1468	Adapt.	1476	1426	<table><tr><td>Adapt.</td><td>1552</td><td>1550</td></tr><tr><td>Adapt.</td><td>1560</td><td>1510</td></tr></table>		Adapt.	1552	1550	Adapt.	1560	1510	<table><tr><td>Adapt.</td><td>1647</td><td>1643</td></tr><tr><td>Adapt.</td><td>1654</td><td>1605</td></tr></table>		Adapt.	1647	1643	Adapt.	1654	1605
Waverage	1274	1278																																					
Average	1283	1239																																					
Adapt.	1380	1385																																					
Adapt.	1390	1342																																					
Adapt.	1467	1468																																					
Adapt.	1476	1426																																					
Adapt.	1552	1550																																					
Adapt.	1560	1510																																					
Adapt.	1647	1643																																					
Adapt.	1654	1605																																					
Deformation step F		Deformation step G		Deformation step H		Deformation step I		Deformation step J																															

Test girder 2, 400x80(1) Deformation steps K – M

Average			Adapt.			Average			Adapt.			Average			Adapt.		
-790			-1783			-815			-1815			235			-932		
W.average			-537			-558			-1784			418			-829		
-671			-2857			-1877			-685			-2989			-1866		
3184			-1728			3184			-1721			3184			-522		
-952			-512			-882			-577			-246			-357		
-17			233			19			265			47			147		
-54			355			-67			378			5			150		
-336			296			-363			315			-68			42		
-470			322			-498			347			-56			-40		
-481			360			-512			388			-25			-67		
-389			352			-420			367			-2			-43		
-45			463			-74			456			8			34		
595			877			594			879			110			174		
1762			1618			1750			1625			355			357		
1837			1595			1733			1837			1586			1811		
W.average			1714			1708			1716			1714			326		
Average			1719			1678			1722			1684			320		
Adapt.			Adapt.			Adapt.			Adapt.			Adapt.			Adapt.		

Deformation step K

Deformation step L

Deformation step M

Test girder 3, 400x80(2) Deformation steps A - J

Average			-220	-	Adapt.
W.average			-219	-	
-242	-228	-194			
-233	-203				
-150	-74				
-113	73				
-87	73				
-56	50				
-29	23				
-9	6				
14	-17				
47	-40				
147	9				
239	222				
214	242	228			
W.average			229	-	
Average			229	-	Adapt.
Deformation step A					
Average			-1060	-	Adapt.
W.average			-1041	-	
-1008	-1559	-842			
-879	-1012				
-456	-538				
-369	256				
-375	285				
-260	181				
-112	48				
19	-60				
195	-178				
490	-37				
1014	414				
1479	1442				
1412	1505	2001			
Average			1550	-	
W.average			1568	-	Adapt.
Deformation step F					
Average			-1133	-	Adapt.
W.average			-1103	-	
-1194	-1744	-820			
-859	-1046				
-440	-632				
-380	291				
-431	339				
-319	233				
-166	93				
-29	-25				
158	-161				
487	-23				
1066	451				
1564	1527				
1497	1592	2032			
Average			1626	-	
W.average			1642	-	Adapt.
Deformation step G					
Average			-1098	-	Adapt.
W.average			-1066	-	
-831	-2077	-772			
-772	-1037				
-353	-729				
-415	344				
-505	412				
-395	298				
-228	149				
-82	22				
112	-136				
457	-19				
1096	473				
1640	1603				
1575	1671	2086			
Average			1699	-	
W.average			1715	-	Adapt.
Deformation step H					
Average			-1136	-	Adapt.
W.average			-1087	-	
-806	-2598	-589			
-825	-862				
-265	-766				
-448	405				
-556	460				
-440	333				
-267	178				
-113	47				
85	-121				
439	-16				
1125	493				
1705	1666				
1637	1735	2159			
Average			1765	-	
W.average			1780	-	Adapt.
Deformation step I					
Average			-1188	-	Adapt.
W.average			-1135	-	
-812	-2779	-618			
-877	-854				
-231	-786				
-463	432				
-580	481				
-460	352				
-282	189				
-126	56				
79	-118				
454	-2				
1180	529				
1781	1744				
1714	1815	2227			
Average			1841	-	
W.average			1856	-	Adapt.
Deformation step J					

Test girder 3, 400x80(2) Deformation steps K - Q

Average			-1278	-	Adapt.
W.average			-1215	-	
-843	-3137	-614			
-986	-811				
-161	-817				
-463	460				
-601	504				
-487	374				
-308	212				
-149	74				
59	-107				
445	5				
1218	555				
1854	1818				
1787	1890	2302			
Average			1915	-	
W.average			1930	-	
					Adapt.

Deformation step K

Average			-1297	-	Adapt.
W.average			-1231	-	
-822	-3179	-673			
-991	-818				
-71	-839				
-476	505				
-629	532				
-515	395				
-333	233				
-172	96				
36	-91				
426	5				
1240	569				
1913	1880				
1849	1964	2347			
Average			1975	-	
W.average			1991	-	
					Adapt.

Deformation step L

Average			-1299	-	Adapt.
W.average			-1236	-	
-792	-3179	-687			
-1012	-826				
-34	-839				
-504	570				
-656	566				
-536	419				
-353	253				
-189	116				
16	-78				
398	3				
1249	575				
1931	1927				
1896	1987	2373			
Average			2007	-	
W.average			2023	-	
					Adapt.

Deformation step M

Average			-24	-822	Adapt.
W.average			-175	-822	
-756	3168	-670			
-1049	-814				
-14	-828				
-544	643				
-682	598				
-550	436				
-360	265				
-194	127				
8	-68				
377	-5				
1251	575				
1928	1961				
1931	1978	2383			
Average			2021	-	
W.average			2036	-	
					Adapt.

Deformation step N

Average			-28	-827	Adapt.
W.average			-189	-827	
-659	3168	-665			
-1163	-823				
-20	-794				
-592	725				
-710	631				
-564	454				
-367	279				
-198	143				
-5	-54				
341	-16				
1237	564				
1921	1976				
1948	1972	2390			
Average			2026	-	
W.average			2041	-	
					Adapt.

Deformation step O

Average			108	-657	Adapt.
W.average			-93	-657	
-42	3168	-395			
-1209	-983				
-186	-448				
-704	910				
-758	713				
-586	527				
-403	363				
-257	239				
-90	51				
152	-54				
1059	448				
1809	1851				
1828	1868	2280			
Average			1911	-	
W.average			1927	-	
					Adapt.

Deformation step P

Average			1109	594	Adapt.
W.average			999	594	
1474	3168	6			
905	-9				
-19	-153				
-687	798				
-699	656				
-574	518				
-485	432				
-420	369				
-321	265				
-157	78				
301	22				
746	853				
880	780	1256			
Average			885	-	
W.average			903	-	
					Adapt.

Deformation step Q

<div><div>Average</div><div>W.average</div></div> <div><div>-200</div><div>-199</div></div> <div><div>Adapt.</div><div>-</div></div>			<div><div>-458</div><div>-456</div></div> <div><div>Adapt.</div><div>-</div></div>			<div><div>-695</div><div>-693</div></div> <div><div>Adapt.</div><div>-</div></div>			<div><div>-748</div><div>-731</div></div> <div><div>Adapt.</div><div>-</div></div>			<div><div>-759</div><div>-730</div></div> <div><div>Adapt.</div><div>-</div></div>		
<div><div>-184</div><div>-198</div><div>-233</div></div>			<div><div>-446</div><div>-460</div><div>-485</div></div>			<div><div>-719</div><div>-701</div><div>-690</div></div>			<div><div>-617</div><div>-1105</div><div>-732</div></div>			<div><div>-505</div><div>-1443</div><div>-680</div></div>		
<div><div>-164</div><div>-135</div></div> <div><div>-220</div><div>-136</div></div>			<div><div>-408</div><div>-274</div></div> <div><div>-490</div><div>-296</div></div>			<div><div>-663</div><div>-380</div></div> <div><div>-702</div><div>-412</div></div>			<div><div>-533</div><div>-553</div></div> <div><div>-753</div><div>-521</div></div>			<div><div>-436</div><div>-674</div></div> <div><div>-730</div><div>-569</div></div>		
<div><div>-68</div><div>-19</div><div>-3</div><div>9</div><div>12</div></div> <div><div>-65</div><div>-8</div><div>5</div><div>-3</div><div>-16</div></div>			<div><div>-113</div><div>-17</div><div>6</div><div>17</div><div>25</div></div> <div><div>-133</div><div>-14</div><div>-9</div><div>-8</div><div>-34</div></div>			<div><div>-135</div><div>6</div><div>34</div><div>40</div><div>54</div></div> <div><div>-177</div><div>-26</div><div>2</div><div>-28</div><div>-67</div></div>			<div><div>-164</div><div>28</div><div>56</div><div>53</div><div>71</div></div> <div><div>-163</div><div>-2</div><div>6</div><div>-45</div><div>-91</div></div>			<div><div>-188</div><div>37</div><div>59</div><div>51</div><div>74</div></div> <div><div>-126</div><div>25</div><div>12</div><div>-51</div><div>-102</div></div>		
<div><div>25</div><div>56</div><div>129</div></div> <div><div>-40</div><div>-43</div><div>98</div></div>			<div><div>62</div><div>129</div><div>293</div></div> <div><div>-82</div><div>-53</div><div>268</div></div>			<div><div>115</div><div>229</div><div>476</div></div> <div><div>-116</div><div>-16</div><div>473</div></div>			<div><div>166</div><div>346</div><div>660</div></div> <div><div>-119</div><div>71</div><div>682</div></div>			<div><div>191</div><div>403</div><div>750</div></div> <div><div>-113</div><div>121</div><div>783</div></div>		
<div><div>211</div><div>214</div><div>214</div><div>330</div></div>			<div><div>510</div><div>527</div><div>400</div><div>660</div></div>			<div><div>815</div><div>854</div><div>994</div><div>925</div></div>			<div><div>1130</div><div>1173</div><div>1921</div><div>1237</div></div>			<div><div>1282</div><div>1328</div><div>2491</div><div>1370</div></div>		
<div><div>W.average</div><div>Average</div></div> <div><div>234</div><div>237</div></div> <div><div>Adapt.</div><div>-</div></div>			<div><div>515</div><div>517</div></div> <div><div>Adapt.</div><div>-</div></div>			<div><div>864</div><div>876</div></div> <div><div>Adapt.</div><div>-</div></div>			<div><div>1280</div><div>1313</div></div> <div><div>Adapt.</div><div>-</div></div>			<div><div>1497</div><div>1543</div></div> <div><div>Adapt.</div><div>-</div></div>		
Deformation step A			Deformation step B			Deformation step C			Deformation step D			Deformation step E		
<div><div>Average</div><div>W.average</div></div> <div><div>-868</div><div>-834</div></div> <div><div>Adapt.</div><div>-</div></div>			<div><div>-1044</div><div>-1031</div></div> <div><div>Adapt.</div><div>-</div></div>			<div><div>-1134</div><div>-1123</div></div> <div><div>Adapt.</div><div>-</div></div>			<div><div>-1217</div><div>-1206</div></div> <div><div>Adapt.</div><div>-</div></div>			<div><div>-1461</div><div>-1495</div></div> <div><div>Adapt.</div><div>-</div></div>		
<div><div>-510</div><div>-1705</div><div>-800</div></div>			<div><div>-546</div><div>-1913</div><div>-826</div></div>			<div><div>-564</div><div>-2164</div><div>-812</div></div>			<div><div>-535</div><div>-2426</div><div>-818</div></div>			<div><div>-521</div><div>-2610</div><div>-839</div></div>		
<div><div>-384</div><div>-778</div></div> <div><div>-942</div><div>-611</div></div>			<div><div>-389</div><div>-848</div></div> <div><div>-1547</div><div>-646</div></div>			<div><div>-363</div><div>-918</div></div> <div><div>-1767</div><div>-657</div></div>			<div><div>-293</div><div>-953</div></div> <div><div>-2010</div><div>-708</div></div>			<div><div>-256</div><div>-983</div></div> <div><div>-3077</div><div>-746</div></div>		
<div><div>-205</div><div>48</div><div>62</div><div>48</div><div>71</div></div> <div><div>-105</div><div>43</div><div>19</div><div>-54</div><div>-107</div></div>			<div><div>-214</div><div>60</div><div>68</div><div>43</div><div>65</div></div> <div><div>-102</div><div>48</div><div>23</div><div>-53</div><div>-109</div></div>			<div><div>-206</div><div>68</div><div>56</div><div>26</div><div>50</div></div> <div><div>-67</div><div>73</div><div>36</div><div>-48</div><div>-107</div></div>			<div><div>-184</div><div>81</div><div>56</div><div>14</div><div>33</div></div> <div><div>-59</div><div>78</div><div>43</div><div>-39</div><div>-102</div></div>			<div><div>-175</div><div>90</div><div>56</div><div>3</div><div>17</div></div> <div><div>-53</div><div>82</div><div>53</div><div>-28</div><div>-93</div></div>		
<div><div>205</div><div>446</div><div>825</div></div> <div><div>-105</div><div>161</div><div>867</div></div>			<div><div>202</div><div>457</div><div>871</div></div> <div><div>-105</div><div>183</div><div>922</div></div>			<div><div>186</div><div>459</div><div>905</div></div> <div><div>-107</div><div>192</div><div>963</div></div>			<div><div>164</div><div>442</div><div>922</div></div> <div><div>-110</div><div>191</div><div>987</div></div>			<div><div>144</div><div>428</div><div>939</div></div> <div><div>-110</div><div>191</div><div>1011</div></div>		
<div><div>1426</div><div>1463</div><div>3142</div><div>1477</div></div>			<div><div>1549</div><div>1572</div><div>3224</div><div>1581</div></div>			<div><div>1656</div><div>1666</div><div>3224</div><div>1621</div></div>			<div><div>1745</div><div>1747</div><div>3224</div><div>1662</div></div>			<div><div>1821</div><div>1815</div><div>3224</div><div>1792</div></div>		
<div><div>W.average</div><div>Average</div></div> <div><div>1713</div><div>1776</div></div> <div><div>Adapt.</div><div>-</div></div>			<div><div>1821</div><div>1882</div></div> <div><div>Adapt.</div><div>-</div></div>			<div><div>1895</div><div>1950</div><div>1631</div><div>1631</div></div> <div><div>Adapt.</div><div>-</div></div>			<div><div>1957</div><div>2008</div><div>1704</div><div>1704</div></div> <div><div>Adapt.</div><div>-</div></div>			<div><div>2025</div><div>2076</div><div>1788</div><div>1788</div></div> <div><div>Adapt.</div><div>-</div></div>		
Deformation step F			Deformation step G			Deformation step H			Deformation step I			Deformation step J		

Test girder 4, 400x100 Deformation steps K - N

		Adapt.				Adapt.				Adapt.				Adapt.																																																																	
Average		-1537	-1101			-1534		-1151			-1570		-1196			-695		-2043																																																													
W.average		-1577	-823			-1556		-856			-1583		-873			-769		-2043																																																													
		-552	-2759	-825			-598	-2920	-820			-589	-3137	-832			718	-2043	130																																																												
		-268		-3283			-265		-3065			-226		-3065			784		-3065																																																												
		-1031		-787			-1070		-836			-1111		-884			-637		-525																																																												
		-169		-37			-163		-14			-167		6			-78		-9																																																												
		91		93			93		104			91		107			-20		101																																																												
		50		60			42		67			39		70			-64		138																																																												
		-8		-20			-20		-14			-28		-9			-65		73																																																												
		3		-87			-9		-79			-17		-76			-33		-65																																																												
		122		-112			110		-112			99		-113			81		-152																																																												
		401		181			392		181			380		177			355		-82																																																												
		942		1020			955		1039			960		1048			349		349																																																												
		1883		1770			1948		1821			1998		1863			882		794																																																												
		1871		3224	1848			1928		3224	1908			1970		3224	1941																																																														
W.average		2071		1843			2119		1902			2155		1943			2011		574																																																												
Average		2119		1843			2166		1902			2199		1943			3141		574																																																												
		Adapt.						Adapt.						Adapt.				Adapt.																																																													
Deformation step K																				Deformation step L																				Deformation step M																				Deformation step N																			

Test girder 5, 600x50 Deformation steps A - J

<table><tr><td>Average</td><td>-75</td><td>Adapt.</td></tr><tr><td>W.average</td><td>-74</td><td>-</td></tr></table>		Average	-75	Adapt.	W.average	-74	-	<table><tr><td>-155</td><td>-</td><td>Adapt.</td></tr><tr><td>-153</td><td>-</td><td>-</td></tr></table>		-155	-	Adapt.	-153	-	-	<table><tr><td>-234</td><td>-</td><td>Adapt.</td></tr><tr><td>-231</td><td>-</td><td>-</td></tr></table>		-234	-	Adapt.	-231	-	-	<table><tr><td>-319</td><td>-</td><td>Adapt.</td></tr><tr><td>-316</td><td>-</td><td>-</td></tr></table>		-319	-	Adapt.	-316	-	-	<table><tr><td>-765</td><td>-</td><td>Adapt.</td></tr><tr><td>-758</td><td>-</td><td>-</td></tr></table>		-765	-	Adapt.	-758	-	-
Average	-75	Adapt.																																					
W.average	-74	-																																					
-155	-	Adapt.																																					
-153	-	-																																					
-234	-	Adapt.																																					
-231	-	-																																					
-319	-	Adapt.																																					
-316	-	-																																					
-765	-	Adapt.																																					
-758	-	-																																					
-79 -79 -78		-164 -164 -158		-248 -246 -239		-339 -336 -324		-823 -800 -763																															
-71 -68		-146 -143		-222 -215		-304 -293		-746 -694																															
-16 -11		-33 -25		-45 -40		-59 -59		-59 -158																															
-9 28		-19 51		-26 73		-34 95		-47 183																															
-17 28		-36 50		-51 73		-67 93		-135 163																															
-22 5		-47 9		-67 14		-91 19		-175 23																															
-2 5		-6 6		-11 8		-16 8		-22 5																															
3 5		5 8		6 9		8 9		17 5																															
8 -2		11 -6		14 -11		12 -16		-9 -50																															
45 -17		88 -34		124 -42		158 -48		220 -59																															
42 -42		82 -87		121 -121		161 -147		380 -104																															
78 85		158 175		239 260		324 350		739 775																															
82 87 60		169 174 119		253 259 177		341 346 236		766 778 518																															
<table><tr><td>W.average</td><td>79</td><td>-</td></tr><tr><td>Average</td><td>78</td><td>-</td></tr></table>		W.average	79	-	Average	78	-	<table><tr><td>160</td><td>-</td><td>Adapt.</td></tr><tr><td>159</td><td>-</td><td>-</td></tr></table>		160	-	Adapt.	159	-	-	<table><tr><td>239</td><td>-</td><td>Adapt.</td></tr><tr><td>237</td><td>-</td><td>-</td></tr></table>		239	-	Adapt.	237	-	-	<table><tr><td>322</td><td>-</td><td>Adapt.</td></tr><tr><td>319</td><td>-</td><td>-</td></tr></table>		322	-	Adapt.	319	-	-	<table><tr><td>722</td><td>-</td><td>Adapt.</td></tr><tr><td>715</td><td>-</td><td>-</td></tr></table>		722	-	Adapt.	715	-	-
W.average	79	-																																					
Average	78	-																																					
160	-	Adapt.																																					
159	-	-																																					
239	-	Adapt.																																					
237	-	-																																					
322	-	Adapt.																																					
319	-	-																																					
722	-	Adapt.																																					
715	-	-																																					
Adapt.		Adapt.		Adapt.		Adapt.		Adapt.																															
Deformation step A		Deformation step B		Deformation step C		Deformation step D		Deformation step E																															
<table><tr><td>Average</td><td>-1116</td><td>Adapt.</td></tr><tr><td>W.average</td><td>-1098</td><td>-</td></tr></table>		Average	-1116	Adapt.	W.average	-1098	-	<table><tr><td>-1239</td><td>-</td><td>Adapt.</td></tr><tr><td>-1213</td><td>-</td><td>-</td></tr></table>		-1239	-	Adapt.	-1213	-	-	<table><tr><td>-1336</td><td>-</td><td>Adapt.</td></tr><tr><td>-1303</td><td>-</td><td>-</td></tr></table>		-1336	-	Adapt.	-1303	-	-	<table><tr><td>-1250</td><td>-</td><td>Adapt.</td></tr><tr><td>-1216</td><td>-</td><td>-</td></tr></table>		-1250	-	Adapt.	-1216	-	-	<table><tr><td>-1288</td><td>-</td><td>Adapt.</td></tr><tr><td>-1251</td><td>-</td><td>-</td></tr></table>		-1288	-	Adapt.	-1251	-	-
Average	-1116	Adapt.																																					
W.average	-1098	-																																					
-1239	-	Adapt.																																					
-1213	-	-																																					
-1336	-	Adapt.																																					
-1303	-	-																																					
-1250	-	Adapt.																																					
-1216	-	-																																					
-1288	-	Adapt.																																					
-1251	-	-																																					
-1339 -1316 -910		-1463 -1631 -933		-1604 -1925 -870		-1635 -1900 -618		-1660 -1993 -651																															
-1217 -798		-1308 -857		-1449 -829		-1497 -597		-1510 -625																															
-8 -163		19 -129		53 -54		78 23		71 25																															
-43 276		-51 329		-71 369		-84 375		-91 384																															
-212 240		-239 268		-260 301		-273 336		-281 352																															
-287 59		-322 60		-366 82		-408 149		-419 171																															
-40 22		-40 17		-71 -3		-157 -14		-184 -26																															
39 6		53 9		65 14		68 34		71 36																															
0 -98		2 -105		0 -109		6 -96		8 -96																															
274 -82		298 -65		319 -42		312 -50		318 -45																															
597 50		701 146		786 231		758 203		781 225																															
1228 1287		1437 1519		1590 1651		1552 1598		1592 1640																															
1223 1443 849		1438 2153 981		1583 2480 1084		1538 2579 1057		1580 2623 1085																															
<table><tr><td>W.average</td><td>1215</td><td>-</td></tr><tr><td>Average</td><td>1206</td><td>-</td></tr></table>		W.average	1215	-	Average	1206	-	<table><tr><td>1501</td><td>-</td><td>Adapt.</td></tr><tr><td>1506</td><td>-</td><td>-</td></tr></table>		1501	-	Adapt.	1506	-	-	<table><tr><td>1668</td><td>-</td><td>Adapt.</td></tr><tr><td>1678</td><td>-</td><td>-</td></tr></table>		1668	-	Adapt.	1678	-	-	<table><tr><td>1650</td><td>-</td><td>Adapt.</td></tr><tr><td>1665</td><td>-</td><td>-</td></tr></table>		1650	-	Adapt.	1665	-	-	<table><tr><td>1689</td><td>-</td><td>Adapt.</td></tr><tr><td>1704</td><td>-</td><td>-</td></tr></table>		1689	-	Adapt.	1704	-	-
W.average	1215	-																																					
Average	1206	-																																					
1501	-	Adapt.																																					
1506	-	-																																					
1668	-	Adapt.																																					
1678	-	-																																					
1650	-	Adapt.																																					
1665	-	-																																					
1689	-	Adapt.																																					
1704	-	-																																					
Adapt.		Adapt.		Adapt.		Adapt.		Adapt.																															
Deformation step F		Deformation step G		Deformation step H		Deformation step I		Deformation step J																															

Test girder 5, 600x50 Deformation steps K - N

Average		-1302	-	Adapt.	Average		-1348	-	Adapt.	Average		-1373	-	Adapt.	Average		-1368	-	Adapt.
W.average		-1264	-		W.average		-1308	-		W.average		-1333	-		W.average		-1328	-	
-1659 -2049 -662					-1651 -2128 -744					-1642 -2167 -797					-1621 -2175 -795				
-1510		-632			-1511		-705			-1508		-753			-1499		-750		
74		40			78		99			82		161			85		202		
-98		394			-110		406			-119		412			-121		408		
-288		367			-291		383			-293		389			-284		380		
-431		212			-425		274			-411		330			-386		329		
-242		-36			-336		-53			-412		-40			-412		-42		
68		42			47		37			-8		16			-33		-6		
12		-90			23		-78			37		-60			43		-56		
321		-39			330		-28			339		-16			341		-17		
797		240			828		271			849		295			853		296		
1618		1666			1673		1718			1711		1738			1721		1738		
1604 2654 1102					1656 2734 1133					1690 2824 1152					1697 2852 1153				
W.average		1715	-		1768		-			1807		-			1815		-		
Average		1729	-		1783		-			1823		-			1832		-		
		Adapt.					Adapt.					Adapt.					Adapt.		
Deformation step K					Deformation step L					Deformation step M					Deformation step N				

Test girder 6, 600x80 Deformation steps A – J

<div>Adapt.</div> <div>Av.strain A-78- Av.strain B-75-</div>			<div>Adapt.</div> <div>-442- -442-</div>			<div>Adapt.</div> <div>-764- -760-</div>			<div>Adapt.</div> <div>-937- -934-</div>			<div>Adapt.</div> <div>-1040- -1031-</div>		
-93-93-93			-451-443-434			-792-781-775			-944-946-955			-916-1192-1125		
-84-29 -5919			-419-465 -132-50			-749-724 -341214			-899-941 -349305			-891-1076 -425411		
-2929			71-37			11-50			-65-56			-96-51		
-1112			-816			937			1457			2354		
-38			-4033			-9150			-10254			-9526		
-33			-3923			-10233			-12122			-91-19		
-83			-342			-81-16			-70-39			87-56		
-140			-19-34			6-57			84-54			211-8		
-6-9			79-45			26240			403116			549226		
7442			380231			738561			913727			1073896		
90115			432498			856952			10621178			12631372		
7887105			406420474			8422764947			107131131198			127131131397		
<div>Av.strain B96- Av.strain A95-</div> <div>Adapt.</div>			<div>449- 446-</div> <div>Adapt.</div>			<div>1211- 1272-</div> <div>Adapt.</div>			<div>1457- 1524-</div> <div>Adapt.</div>			<div>16221326 16831326</div> <div>Adapt.</div>		
Deformation step A			Deformation step B			Deformation step C			Deformation step D			Deformation step E		
<div>Adapt.</div> <div>Av.strain A-209-1117 Av.strain B28-1078</div>			<div>Adapt.</div> <div>-258-1178 -13-1121</div>			<div>Adapt.</div> <div>-487-1464 -269-1572</div>			<div>Adapt.</div> <div>-765-1812 -589-2156</div>			<div>Adapt.</div> <div>-598-1604 -385-1756</div>		
-859-1575-1032			-899-1804-1001			-921-2130-1020			-930-2392-1084			-845-2451-1059		
3424-1001			3424-1008			3424-1787			3424-2844			3424-2060		
-549553			-659617			-749626			-837614			-598206		
-115-28			-47-3			5956			129130			155167		
2364			-382			-5399			-99110			-153110		
-10426			-13647			-17278			-197101			-226130		
-91-20			-130-5			-16419			-18837			-22067		
115-45			84-39			51-34			29-28			-17-20		
26836			25347			22042			19842			1186		
640313			667350			671367			680384			594316		
12001029			12711107			13241164			13751217			12971138		
14371542			15561663			16621762			17721866			17041800		
144231131569			156631131694			167431131800			178131131905			170731131835		
<div>Av.strain B17651497 Av.strain A18201497</div> <div>Adapt.</div>			<div>18671620 19181620</div> <div>Adapt.</div>			<div>19541724 20021724</div> <div>Adapt.</div>			<div>20431831 20871831</div> <div>Adapt.</div>			<div>19851761 20321761</div> <div>Adapt.</div>		
Deformation step F			Deformation step G			Deformation step H			Deformation step I			Deformation step J		

Test girder 7, 600x100 Deformation steps A – I

<table><tr><td>Av.strain A</td><td>-217</td><td>-362</td></tr><tr><td>Av.strain B</td><td>-211</td><td>-363</td></tr></table>		Av.strain A	-217	-362	Av.strain B	-211	-363	Adapt.	<table><tr><td>-430</td><td>-717</td></tr><tr><td>-417</td><td>-714</td></tr></table>		-430	-717	-417	-714	Adapt.	<table><tr><td>-623</td><td>-1038</td></tr><tr><td>-598</td><td>-1016</td></tr></table>		-623	-1038	-598	-1016	Adapt.	<table><tr><td>-672</td><td>-1119</td></tr><tr><td>-626</td><td>-1040</td></tr></table>		-672	-1119	-626	-1040	Adapt.	<table><tr><td>-762</td><td>-1271</td></tr><tr><td>-701</td><td>-1150</td></tr></table>		-762	-1271	-701	-1150	Adapt.
Av.strain A	-217	-362																																		
Av.strain B	-211	-363																																		
-430	-717																																			
-417	-714																																			
-623	-1038																																			
-598	-1016																																			
-672	-1119																																			
-626	-1040																																			
-762	-1271																																			
-701	-1150																																			
0 -366 -353			0 -752 -696			0 -1243 -922			0 -1708 -846			0 -2266 -758																								
-366 0			-704 0			-949 0			-803 0			-787 0																								
-288 -12			-462 -57			-636 8			-566 -96			-555 -11																								
-242 178			-298 226			-395 321			-322 259			-477 419																								
-209 25			-198 25			-155 48			-70 37			-186 74																								
-85 -19			-37 -26			-19 11			-6 25			-19 47																								
-9 2			9 -53			-34 -19			-57 -20			-74 -9																								
-6 -9			2 -93			-23 -42			-42 -43			-65 -42																								
12 -26			82 -76			107 -6			126 16			119 16																								
87 -34			245 26			369 164			450 234			488 268																								
256 79			530 316			809 586			939 708			1026 792																								
358 338			781 721			1203 1102			1389 1266			1536 1401																								
369 372 367			795 729 784			1215 1228 1178			1397 1259 1353			1541 1305 1497																								
<table><tr><td>Av.strain B</td><td>359</td><td>-</td></tr><tr><td>Av.strain A</td><td>361</td><td>-</td></tr></table>		Av.strain B	359	-	Av.strain A	361	-	Adapt.	<table><tr><td>760</td><td>-</td></tr><tr><td>762</td><td>-</td></tr></table>		760	-	762	-	Adapt.	<table><tr><td>1180</td><td>-</td></tr><tr><td>1185</td><td>-</td></tr></table>		1180	-	1185	-	Adapt.	<table><tr><td>1332</td><td>-</td></tr><tr><td>1333</td><td>-</td></tr></table>		1332	-	1333	-	Adapt.	<table><tr><td>1458</td><td>-</td></tr><tr><td>1456</td><td>-</td></tr></table>		1458	-	1456	-	Adapt.
Av.strain B	359	-																																		
Av.strain A	361	-																																		
760	-																																			
762	-																																			
1180	-																																			
1185	-																																			
1332	-																																			
1333	-																																			
1458	-																																			
1456	-																																			
Deformation step A																																				
<table><tr><td>Av.strain A</td><td>-825</td><td>-1375</td></tr><tr><td>Av.strain B</td><td>-745</td><td>-1205</td></tr></table>		Av.strain A	-825	-1375	Av.strain B	-745	-1205	Adapt.	<table><tr><td>-903</td><td>-1505</td></tr><tr><td>-814</td><td>-1312</td></tr></table>		-903	-1505	-814	-1312	Adapt.	<table><tr><td>-950</td><td>-1583</td></tr><tr><td>-852</td><td>-1370</td></tr></table>		-950	-1583	-852	-1370	Adapt.	<table><tr><td>-248</td><td>-413</td></tr><tr><td>-181</td><td>-234</td></tr></table>		-248	-413	-181	-234	Adapt.							
Av.strain A	-825	-1375																																		
Av.strain B	-745	-1205																																		
-903	-1505																																			
-814	-1312																																			
-950	-1583																																			
-852	-1370																																			
-248	-413																																			
-181	-234																																			
0 -2672 -756			0 -2979 -805			0 -3182 -832			0 -2234 691																											
-696 0			-732 0			-733 0			304 0																											
-453 47			-370 113			-285 198			-299 132																											
-645 732			-691 832			-767 882			-521 769																											
-598 287			-758 391			-798 419			-555 341																											
-146 136			-219 192			-175 214			-453 203																											
-102 54			-113 91			-133 96			-171 208																											
-113 -17			-135 -2			-160 0			-149 158																											
91 6			60 -2			37 -11			-121 102																											
508 277			499 277			493 274			5 40																											
1079 840			1121 884			1156 919			313 183																											
1629 1487			1730 1575			1821 1656			702 615																											
1631 1335 1597			1733 1432 1696			1826 1583 1784			694 454 670																											
<table><tr><td>Av.strain B</td><td>1539</td><td>-</td></tr><tr><td>Av.strain A</td><td>1536</td><td>-</td></tr></table>		Av.strain B	1539	-	Av.strain A	1536	-	Adapt.	<table><tr><td>1636</td><td>-</td></tr><tr><td>1633</td><td>-</td></tr></table>		1636	-	1633	-	Adapt.	<table><tr><td>1735</td><td>-</td></tr><tr><td>1734</td><td>-</td></tr></table>		1735	-	1734	-	Adapt.	<table><tr><td>632</td><td>-</td></tr><tr><td>627</td><td>-</td></tr></table>		632	-	627	-	Adapt.							
Av.strain B	1539	-																																		
Av.strain A	1536	-																																		
1636	-																																			
1633	-																																			
1735	-																																			
1734	-																																			
632	-																																			
627	-																																			
Deformation step F																																				
Deformation step G																																				
Deformation step H																																				
Deformation step I																																				

Test girder 8, 800x50 Deformation steps A – J

<table><tr><td>Average</td><td>-76</td><td>Adapt.</td></tr><tr><td>Waverage</td><td>-75</td><td>-</td></tr></table>			Average	-76	Adapt.	Waverage	-75	-	<table><tr><td></td><td>-289</td><td>Adapt.</td></tr><tr><td></td><td>-285</td><td>-</td></tr></table>				-289	Adapt.		-285	-	<table><tr><td></td><td>-543</td><td>Adapt.</td></tr><tr><td></td><td>-535</td><td>-</td></tr></table>				-543	Adapt.		-535	-	<table><tr><td></td><td>-793</td><td>Adapt.</td></tr><tr><td></td><td>-782</td><td>-</td></tr></table>				-793	Adapt.		-782	-	<table><tr><td></td><td>-1033</td><td>Adapt.</td></tr><tr><td></td><td>-1020</td><td>-</td></tr></table>				-1033	Adapt.		-1020	-
Average	-76	Adapt.																																										
Waverage	-75	-																																										
	-289	Adapt.																																										
	-285	-																																										
	-543	Adapt.																																										
	-535	-																																										
	-793	Adapt.																																										
	-782	-																																										
	-1033	Adapt.																																										
	-1020	-																																										
-79 -82 -82	-305 -307 -307	-575 -575 -570	-842 -837 -829	-1084 -1084 -1082																																								
-68 -70	-262 -265	-494 -499	-721 -735	-936 -980																																								
20 -2	0 29	-57 90	-115 157	-144 208																																								
25 -37	43 -102	36 -136	51 -112	107 -37																																								
-8 -20	-54 12	-130 104	-143 99	-43 -53																																								
-20 9	-48 43	-76 82	-85 99	-68 70																																								
-16 29	-42 62	-68 85	-82 107	-82 130																																								
-17 23	-43 59	-67 90	-87 118	-98 141																																								
-8 5	-23 19	-39 34	-60 57	-84 84																																								
-9 3	-25 12	-36 19	-54 29	-76 47																																								
19 5	73 -3	141 -17	260 -48	378 -74																																								
95 73	305 273	543 513	871 871	1211 1228																																								
109 96 82	347 273 304	622 594 569	980 722 929	1345 955 1305																																								
W.average 90 -	299 -	561 -	874 -	1210 -																																								
Average 91 -	300 -	568 -	875 -	1209 -																																								
Adapt.	Adapt.	Adapt.	Adapt.	Adapt.																																								
Deformation step A																																												
<table><tr><td>Average</td><td>-1250</td><td>Adapt.</td></tr><tr><td>Waverage</td><td>-1236</td><td>-</td></tr></table>			Average	-1250	Adapt.	Waverage	-1236	-	<table><tr><td></td><td>-1417</td><td>Adapt.</td></tr><tr><td></td><td>-1396</td><td>-</td></tr></table>				-1417	Adapt.		-1396	-	<table><tr><td></td><td>-1503</td><td>Adapt.</td></tr><tr><td></td><td>-1480</td><td>-</td></tr></table>				-1503	Adapt.		-1480	-	<table><tr><td></td><td>-1554</td><td>Adapt.</td></tr><tr><td></td><td>-1527</td><td>-</td></tr></table>				-1554	Adapt.		-1527	-	<table><tr><td></td><td>-1581</td><td>Adapt.</td></tr><tr><td></td><td>-1555</td><td>-</td></tr></table>				-1581	Adapt.		-1555	-
Average	-1250	Adapt.																																										
Waverage	-1236	-																																										
	-1417	Adapt.																																										
	-1396	-																																										
	-1503	Adapt.																																										
	-1480	-																																										
	-1554	Adapt.																																										
	-1527	-																																										
	-1581	Adapt.																																										
	-1555	-																																										
-1263 -1311 -1350	-1248 -1637 -1620	-1235 -1854 -1693	-1280 -1978 -1719	-1304 -2038 -1724																																								
-1093 -1234	-1108 -1474	-1088 -1643	-1108 -1682	-1136 -1705																																								
-74 189	42 150	174 115	290 101	380 71																																								
177 11	234 33	264 28	284 3	281 -36																																								
81 -205	171 -291	217 -336	245 -380	228 -378																																								
-29 -3	11 -99	40 -136	54 -105	39 -29																																								
-68 147	-50 167	-42 164	-42 155	-56 133																																								
-98 152	-105 167	-105 164	-102 155	-20 143																																								
-99 102	-116 126	-127 132	-121 129	-118 118																																								
-93 60	-112 76	-124 85	-121 81	-116 71																																								
463 -96	530 -110	581 -119	587 -122	587 -126																																								
1522 1556	1758 1789	1907 1933	1944 1969	1938 1961																																								
1677 1397 1660	1939 1800 1939	2091 1966 2108	2119 2003 2141	2111 1993 2134																																								
W.average 1559 -	1833 -	1987 -	2022 -	2014 -																																								
Average 1563 -	1845 -	2001 -	2035 -	2028 -																																								
Adapt.	Adapt.	Adapt.	Adapt.	Adapt.																																								
Deformation step F																																												
<table><tr><td></td><td>-1833</td><td>Adapt.</td></tr><tr><td></td><td>-1845</td><td>-</td></tr></table>				-1833	Adapt.		-1845	-	<table><tr><td></td><td>-1987</td><td>Adapt.</td></tr><tr><td></td><td>-2001</td><td>-</td></tr></table>				-1987	Adapt.		-2001	-	<table><tr><td></td><td>-2022</td><td>Adapt.</td></tr><tr><td></td><td>-2035</td><td>-</td></tr></table>				-2022	Adapt.		-2035	-	<table><tr><td></td><td>-2014</td><td>Adapt.</td></tr><tr><td></td><td>-2028</td><td>-</td></tr></table>				-2014	Adapt.		-2028	-	<table><tr><td></td><td>-2014</td><td>Adapt.</td></tr><tr><td></td><td>-2028</td><td>-</td></tr></table>				-2014	Adapt.		-2028	-
	-1833	Adapt.																																										
	-1845	-																																										
	-1987	Adapt.																																										
	-2001	-																																										
	-2022	Adapt.																																										
	-2035	-																																										
	-2014	Adapt.																																										
	-2028	-																																										
	-2014	Adapt.																																										
	-2028	-																																										
Deformation step G																																												
<table><tr><td></td><td>-1987</td><td>Adapt.</td></tr><tr><td></td><td>-2001</td><td>-</td></tr></table>				-1987	Adapt.		-2001	-	<table><tr><td></td><td>-2022</td><td>Adapt.</td></tr><tr><td></td><td>-2035</td><td>-</td></tr></table>				-2022	Adapt.		-2035	-	<table><tr><td></td><td>-2014</td><td>Adapt.</td></tr><tr><td></td><td>-2028</td><td>-</td></tr></table>				-2014	Adapt.		-2028	-	<table><tr><td></td><td>-2014</td><td>Adapt.</td></tr><tr><td></td><td>-2028</td><td>-</td></tr></table>				-2014	Adapt.		-2028	-	<table><tr><td></td><td>-2014</td><td>Adapt.</td></tr><tr><td></td><td>-2028</td><td>-</td></tr></table>				-2014	Adapt.		-2028	-
	-1987	Adapt.																																										
	-2001	-																																										
	-2022	Adapt.																																										
	-2035	-																																										
	-2014	Adapt.																																										
	-2028	-																																										
	-2014	Adapt.																																										
	-2028	-																																										
	-2014	Adapt.																																										
	-2028	-																																										
Deformation step H																																												
<table><tr><td></td><td>-2022</td><td>Adapt.</td></tr><tr><td></td><td>-2035</td><td>-</td></tr></table>				-2022	Adapt.		-2035	-	<table><tr><td></td><td>-2014</td><td>Adapt.</td></tr><tr><td></td><td>-2028</td><td>-</td></tr></table>				-2014	Adapt.		-2028	-	<table><tr><td></td><td>-2014</td><td>Adapt.</td></tr><tr><td></td><td>-2028</td><td>-</td></tr></table>				-2014	Adapt.		-2028	-	<table><tr><td></td><td>-2014</td><td>Adapt.</td></tr><tr><td></td><td>-2028</td><td>-</td></tr></table>				-2014	Adapt.		-2028	-	<table><tr><td></td><td>-2014</td><td>Adapt.</td></tr><tr><td></td><td>-2028</td><td>-</td></tr></table>				-2014	Adapt.		-2028	-
	-2022	Adapt.																																										
	-2035	-																																										
	-2014	Adapt.																																										
	-2028	-																																										
	-2014	Adapt.																																										
	-2028	-																																										
	-2014	Adapt.																																										
	-2028	-																																										
	-2014	Adapt.																																										
	-2028	-																																										
Deformation step I																																												
<table><tr><td></td><td>-2014</td><td>Adapt.</td></tr><tr><td></td><td>-2028</td><td>-</td></tr></table>				-2014	Adapt.		-2028	-	<table><tr><td></td><td>-2014</td><td>Adapt.</td></tr><tr><td></td><td>-2028</td><td>-</td></tr></table>				-2014	Adapt.		-2028	-	<table><tr><td></td><td>-2014</td><td>Adapt.</td></tr><tr><td></td><td>-2028</td><td>-</td></tr></table>				-2014	Adapt.		-2028	-	<table><tr><td></td><td>-2014</td><td>Adapt.</td></tr><tr><td></td><td>-2028</td><td>-</td></tr></table>				-2014	Adapt.		-2028	-	<table><tr><td></td><td>-2014</td><td>Adapt.</td></tr><tr><td></td><td>-2028</td><td>-</td></tr></table>				-2014	Adapt.		-2028	-
	-2014	Adapt.																																										
	-2028	-																																										
	-2014	Adapt.																																										
	-2028	-																																										
	-2014	Adapt.																																										
	-2028	-																																										
	-2014	Adapt.																																										
	-2028	-																																										
	-2014	Adapt.																																										
	-2028	-																																										
Deformation step J																																												

Test girder 8, 800x50 Deformation steps K – L

		Adapt.			Adapt.
Average	-1589	-	-1226	-	-
W.average	-1561	-	-1201	-	-
-1339 -2060 -1705			-1035 -1680 -1260		
-1159 -1682			-865 -1287		
467 48			414 93		
264 -71			140 -50		
188 -324			37 -53		
20 34			-16 79		
-67 110			-73 70		
-14 133			3158 102		
-110 107			-82 68		
-104 57			-79 29		
578 -129			510 -112		
1900 1921			1584 1581		
2069 1953 2093			1721 1603 1735		
W.average	1974	-	1634	-	-
Average	1987	-	1645	-	-
Adapt.			Adapt.		
Deformation step K			Deformation step L		

Test girder 9, 800x80 Deformation steps A – I

			Adapt.						Adapt.						Adapt.																																																																																																																																																																																																																																																																																																																																																																																																																																																																																																																																																																																																																																																																																																																																																																																																																																																																																																																																																								
Average	-925	-305				-1316	-691				-1490	-866				-1565	-962				-1616	-1035																																																																																																																																																																																																																																																																																																																																																																																																																																																																																																																																																																																																																																																																																																																																																																																																																																																																																																																																																	
W.average	-820	-305				-1206	-691				-1386	-866				-1450	-962				-1486	-1035																																																																																																																																																																																																																																																																																																																																																																																																																																																																																																																																																																																																																																																																																																																																																																																																																																																																																																																																																	
-3406			-312	-329				-3815	-721	-729				-3987	-887	-842				-3978	-1294	-806				-3940	-1714	-746																																																																																																																																																																																																																																																																																																																																																																																																																																																																																																																																																																																																																																																																																																																																																																																																																																																																																																																																											
			-281	-301							-653	-662							-884	-851							-929	-820				-896	-783																																																																																																																																																																																																																																																																																																																																																																																																																																																																																																																																																																																																																																																																																																																																																																																																																																																																																																																																						
			104	-192							358	-386							625	-401							750	-488				775	-470																																																																																																																																																																																																																																																																																																																																																																																																																																																																																																																																																																																																																																																																																																																																																																																																																																																																																																																																						
			64	-62							177	-155							291	-316							386	-417				459	-498																																																																																																																																																																																																																																																																																																																																																																																																																																																																																																																																																																																																																																																																																																																																																																																																																																																																																																																																						
			3	-12							40	0							152	-133							217	-192				277	-270																																																																																																																																																																																																																																																																																																																																																																																																																																																																																																																																																																																																																																																																																																																																																																																																																																																																																																																																						
			-14	8							-20	28							48	-220							105	-321				163	-440																																																																																																																																																																																																																																																																																																																																																																																																																																																																																																																																																																																																																																																																																																																																																																																																																																																																																																																																						
			-16	12							-28	53							37	-138							57	-160				57	-157																																																																																																																																																																																																																																																																																																																																																																																																																																																																																																																																																																																																																																																																																																																																																																																																																																																																																																																																						
			-16	12							-20	73							136	34							149	47				157	54																																																																																																																																																																																																																																																																																																																																																																																																																																																																																																																																																																																																																																																																																																																																																																																																																																																																																																																																						
			-6	-2							-60	43							107	107							129	129				136	132																																																																																																																																																																																																																																																																																																																																																																																																																																																																																																																																																																																																																																																																																																																																																																																																																																																																																																																																						
			-14	-2							-113	116							-25	298							54	381				102	431																																																																																																																																																																																																																																																																																																																																																																																																																																																																																																																																																																																																																																																																																																																																																																																																																																																																																																																																						
			-79	84							-339	553							-239	877							-90	1037				16	1149																																																																																																																																																																																																																																																																																																																																																																																																																																																																																																																																																																																																																																																																																																																																																																																																																																																																																																																																						
			273	339							800	818							995	994							1237	1042				1409	1186																																																																																																																																																																																																																																																																																																																																																																																																																																																																																																																																																																																																																																																																																																																																																																																																																																																																																																																																						
			274	346	394							769	423	944							941	446	1132							1178	440	1361				1347	453	1525																																																																																																																																																																																																																																																																																																																																																																																																																																																																																																																																																																																																																																																																																																																																																																																																																																																																																																																																	
W.average	322	-										761	833							917	1015							1066	1204				1203	1367																																																																																																																																																																																																																																																																																																																																																																																																																																																																																																																																																																																																																																																																																																																																																																																																																																																																																																																																					
Average	325	-										751	833							902	1015							1052	1204				1184	1367																																																																																																																																																																																																																																																																																																																																																																																																																																																																																																																																																																																																																																																																																																																																																																																																																																																																																																																																					
			Adapt.									Adapt.									Adapt.									Adapt.						Adapt.																																																																																																																																																																																																																																																																																																																																																																																																																																																																																																																																																																																																																																																																																																																																																																																																																																																																																																																																			
Deformation step A																								Deformation step B																								Deformation step C																								Deformation step D																								Deformation step E																																																																																																																																																																																																																																																																																																																																																																																																																																																																																																																																																																																																																																																																																																																																																																																																																																																																							
			Adapt.																																																																																																																																																																																																																																																																																																																																																																																																																																																																																																																																																																																																																																																																																																																																																																																																																																																																																																																																																																				

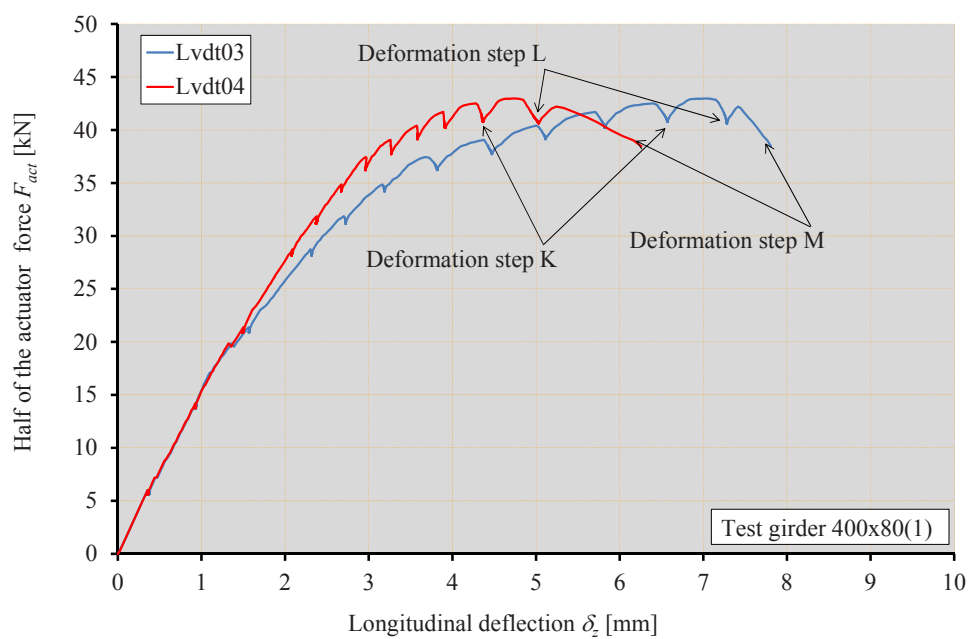
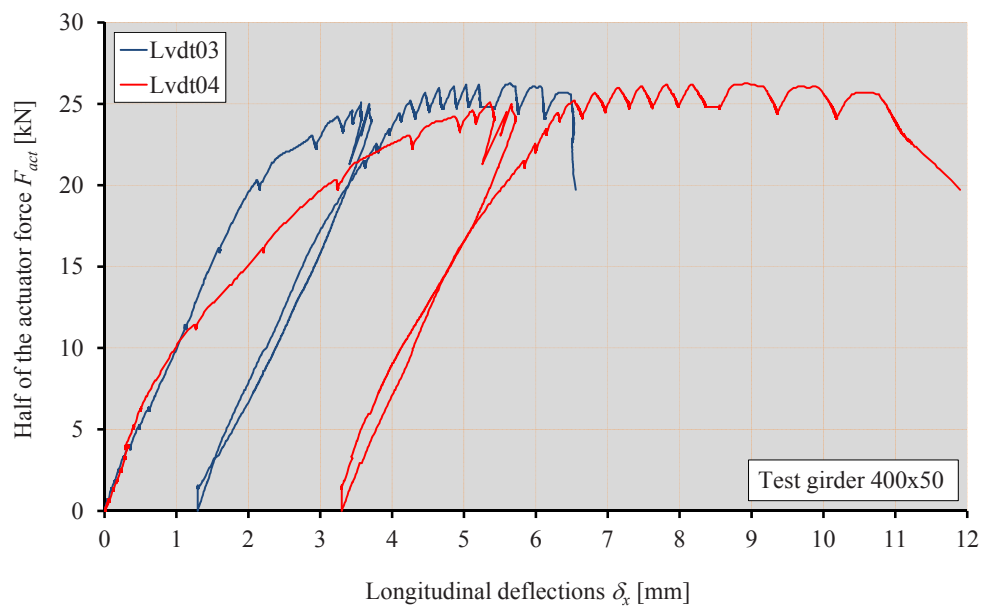
Test girder 10, 800x100 Deformation steps A – E

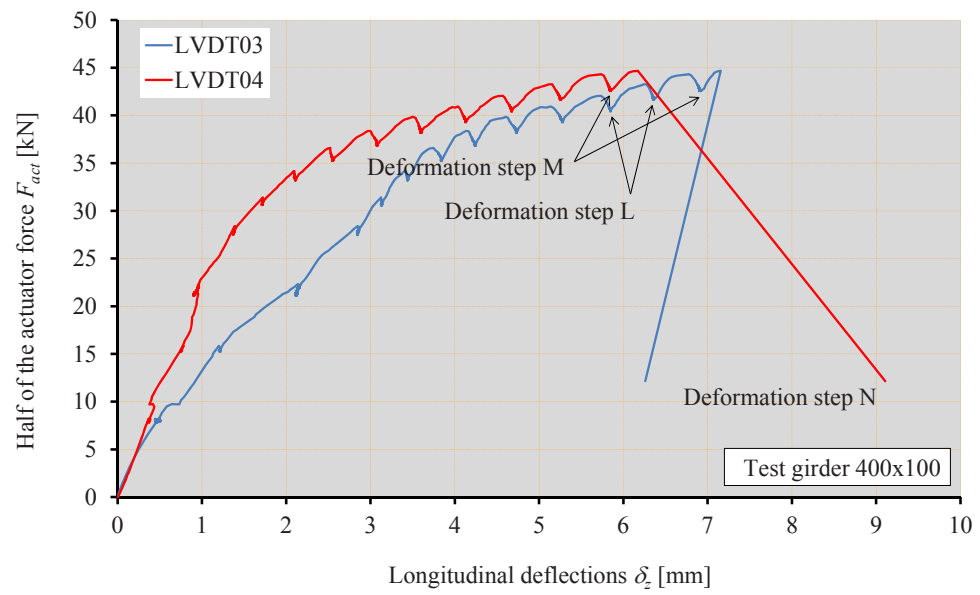
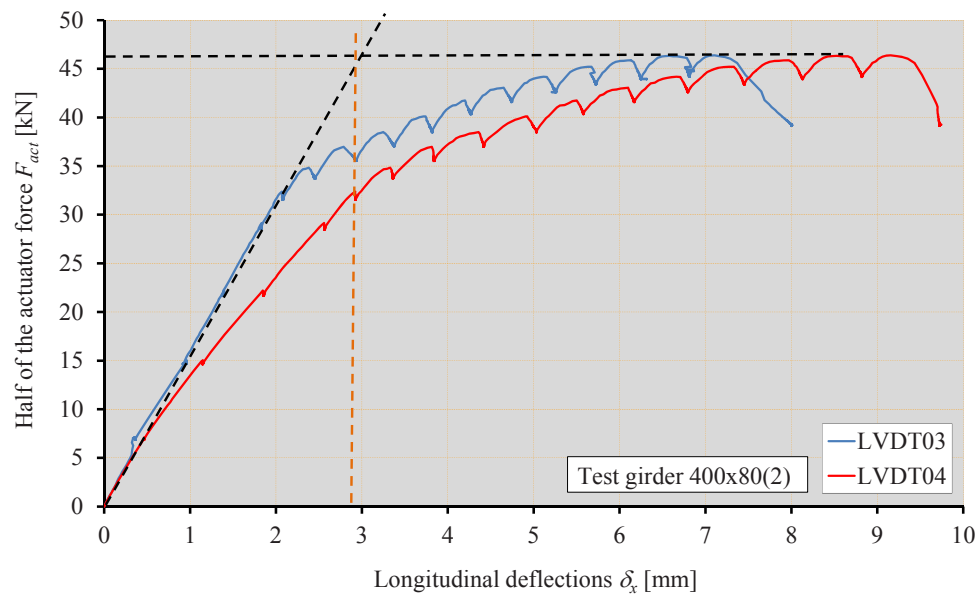
Adapt.			Adapt.			Adapt.			Adapt.			Adapt.		
Av.strain A	-319	-	-700	-	-	-907	-	-	-960	-	-	-1073	-	-
Av.strain B	-317	-	-695	-	-	-900	-	-	-935	-	-	-1042	-	-
-332 -326 -319			-746 -729 -691			-975 -944 -893			-896 -1349 -939			-902 -1685 -995		
-321	-298		-699	-636		-913	-811		-811	-806		-989	-792	
-102	-116		-302	-5		-370	64		-389	133		-374	245	
0	62		-160	270		-191	315		-215	358		-250	394	
-23	42		-121	76		-102	81		-93	101		-102	121	
-79	-37		-95	-138		-51	-178		9	-144		19	-74	
-74	-50		-42	-113		-62	-191		-57	-333		-37	-383	
6	11		20	23		25	26		6	-20		-19	-110	
150	76		200	129		259	181		308	228		346	264	
36	-36		211	71		318	177		420	281		502	369	
-42	39		299	228		463	392		618	546		741	670	
313	324		749	711		972	907		1189	1097		1366	1242	
339 332 344			750 459 781			961 405 994			1164 405 1198			1333 401 1355		
Av.strain B	328	-	697	-		863	-		1033	-		1167	-	
Av.strain A	330	-	690	-		848	-		1011	-		1139	-	
Adapt.			Adapt.			Adapt.			Adapt.			Adapt.		
Deformation step A			Deformation step B			Deformation step C			Deformation step D			Deformation step E		

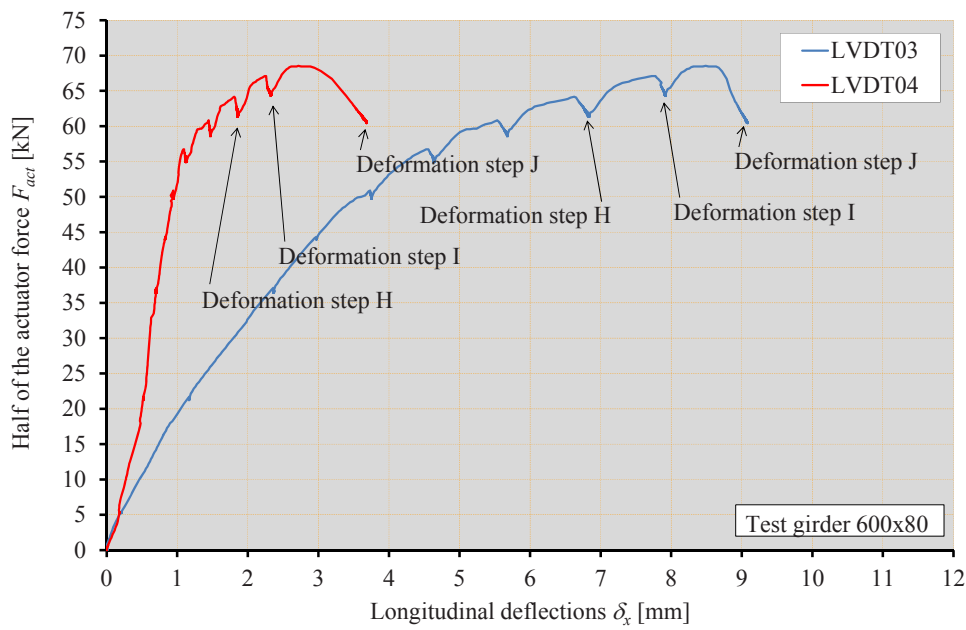
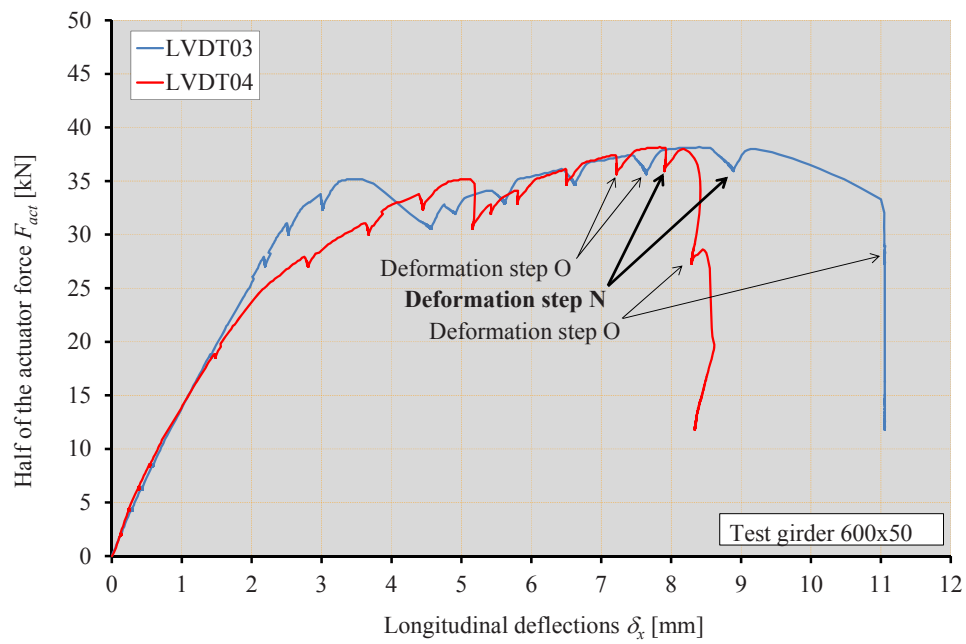
Test girder 10, 800x100 Deformation steps H – N

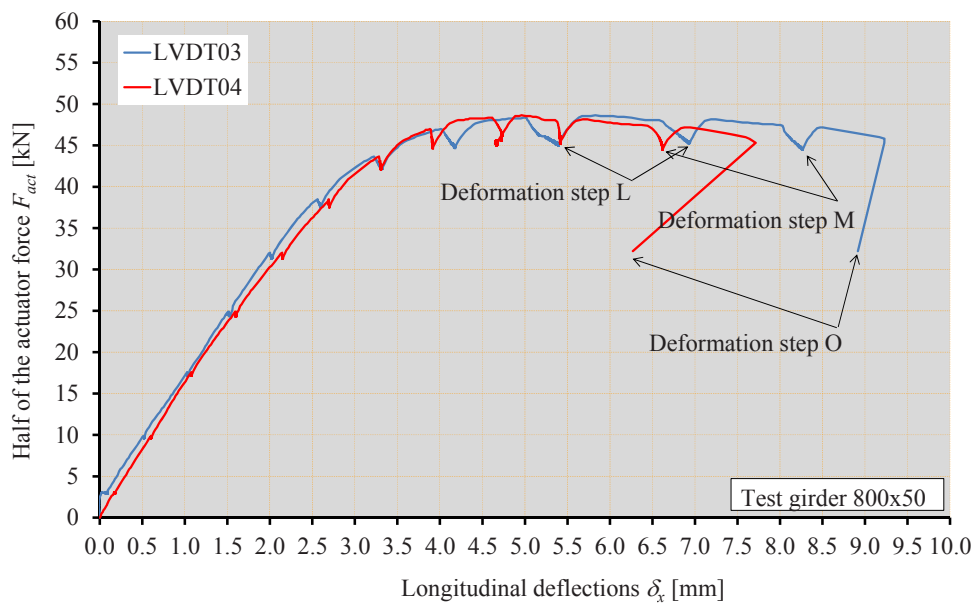
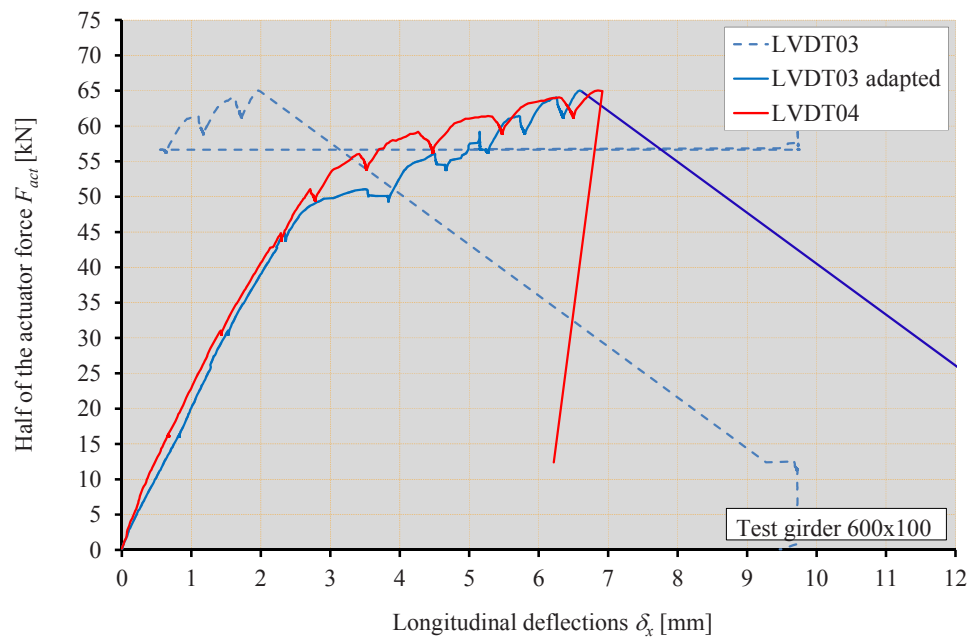
Average			-342	-	Adapt.
W.average			-341	-	
-352	-352	-338			
-366	-304				
-112	-6				
-42	70				
-12	22				
0	-53				
-31	-85				
-19	-19				
74	54				
138	56				
167	110				
287	295				
290	302	322			
W.average			298	-	Adapt.
Average			299	-	
					Adapt.
Deformation step H					
Average			-784	-	Adapt.
W.average			-781	-	
-814	-808	-769			
-845	-687				
-214	-6				
-85	138				
-12	51				
0	-62				
-37	-231				
-34	-71				
157	127				
302	217				
431	369				
649	637				
645	667	702			
W.average			657	-	Adapt.
Average			660	-	
					Adapt.
Deformation step I					
Average			-1234	-	Adapt.
W.average			-1228	-	
-1271	-1271	-1232			
-1308	-1088				
-273	23				
-118	192				
-29	70				
0	-31				
-25	-326				
-29	-132				
237	202				
459	377				
685	623				
1012	967				
1000	1020	1062			
W.average			1008	-	Adapt.
Average			1012	-	
					Adapt.
Deformation step J					
Average			-1537	-	Adapt.
W.average			-1536	-	
-1149	-1793	-1677			
-1510	-1556				
-239	146				
-122	172				
26	-8				
0	-101				
62	-281				
-98	-171				
169	166				
502	419				
784	722				
1175	1108				
1153	1104	1215			
W.average			1150	-	Adapt.
Average			1151	-	
					Adapt.
Deformation step K					
Average			-2001	-	Adapt.
W.average			-1997	-	
-1127	-2100	-2817			
-1547	-2412				
-215	203				
-116	167				
73	-70				
0	-149				
127	-288				
-85	-212				
81	109				
515	429				
856	794				
1313	1228				
1288	1057	1350			
W.average			1251	-	Adapt.
Average			1247	-	
					Adapt.
Deformation step L					
Average			-2429	-	Adapt.
W.average			-2448	-	
-1183	-2455	-3427			
-1615	-3466				
-205	296				
-112	153				
129	-124				
0	-188				
172	-284				
-16	-250				
-40	26				
451	380				
882	815				
1426	1316				
1409	1045	1465			
W.average			1339	-	Adapt.
Average			1332	-	
					Adapt.
Deformation step M					
Average			-1396	-	Adapt.
W.average			-1438	-	
245	-992	-2934			
-96	-3201				
-31	177				
-189	141				
-177	84				
0	181				
-99	161				
-152	57				
-87	50				
22	37				
74	25				
191	184				
163	-208	243			
W.average			127	195	Adapt.
Average			115	195	
					Adapt.
Deformation step N					

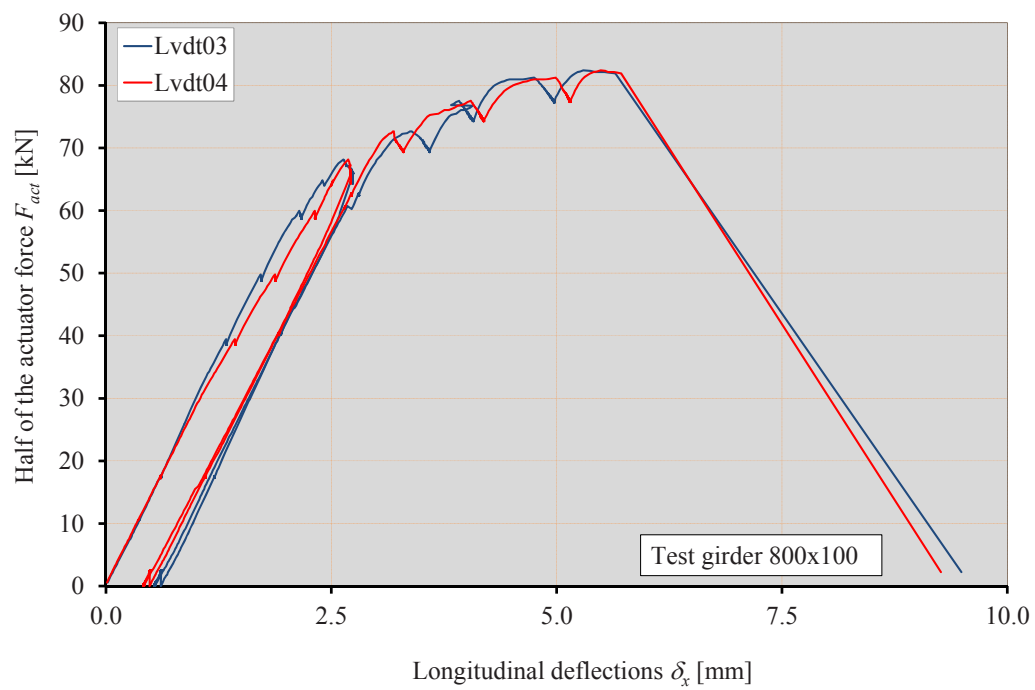
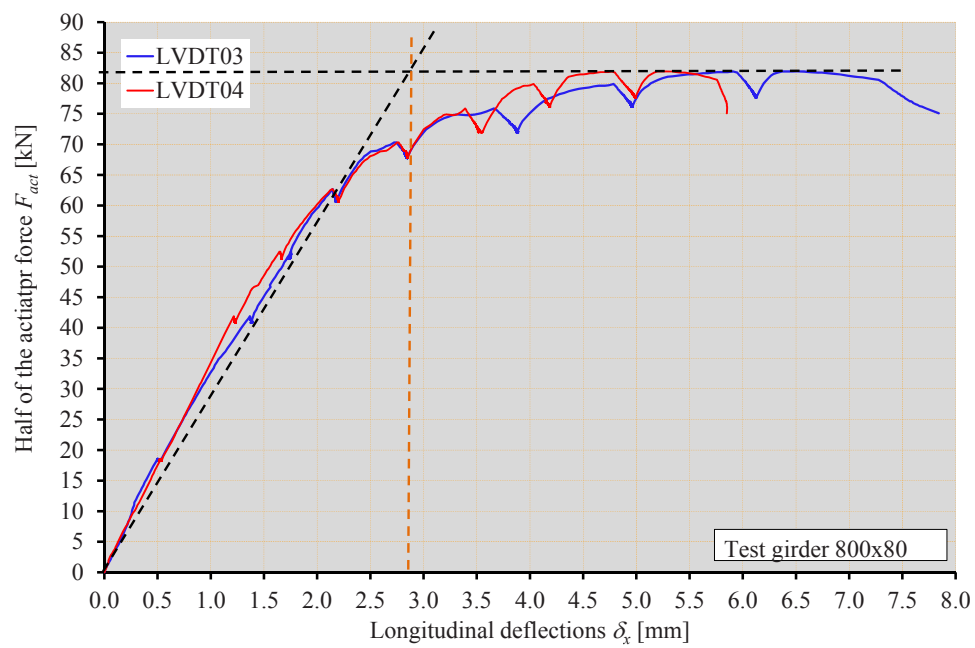
APPENDIX J HALVE OF THE ACTUATOR FORCE VERSUS LONGITUDINAL DEFORMATIONS





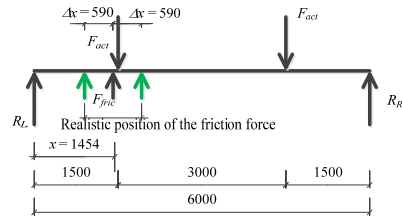




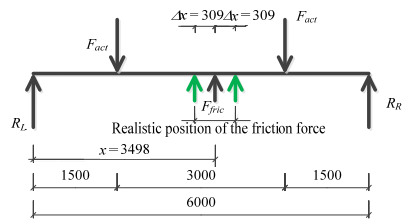


APPENDIX K

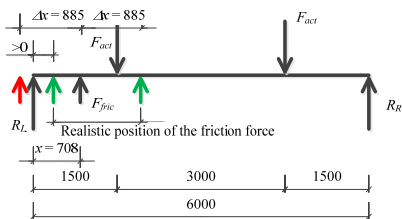
STATIC SCHEMES WITH LOCATIONS OF THE RESULTING FRICTION FORCE RELATED TO THE ERROR PROPAGATION



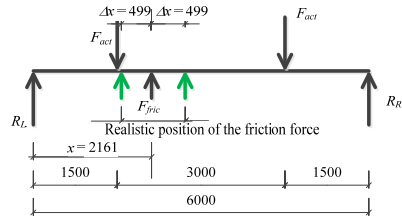
Test girder 1, 400x50



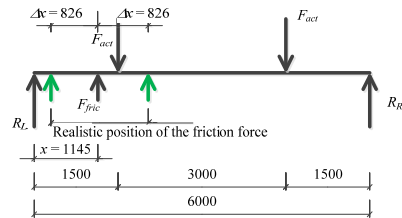
Test girder 2, 400x80(1)



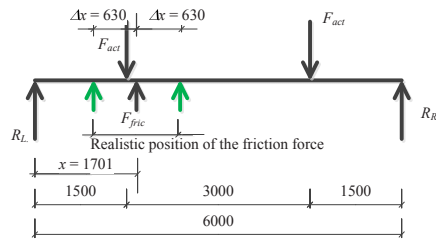
Test girder 3, 400x80(2)



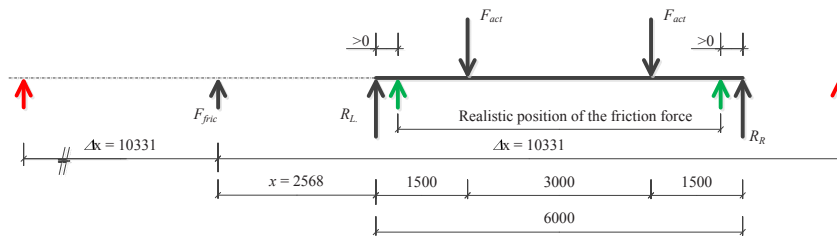
Test girder 4, 400x100



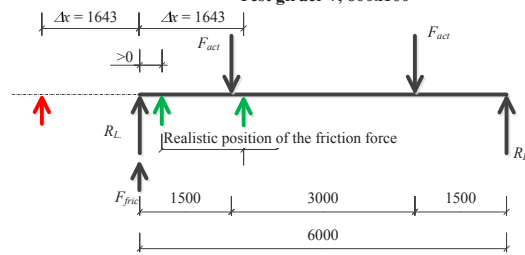
Test girder 5, 600x50



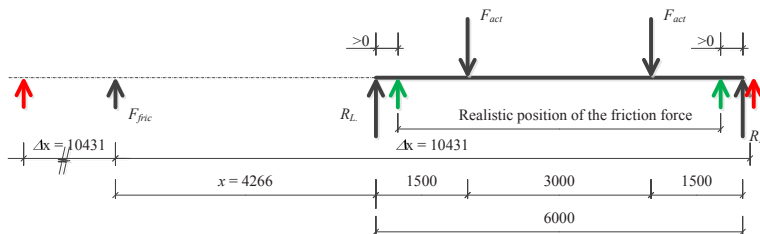
Test girder 6, 600x80



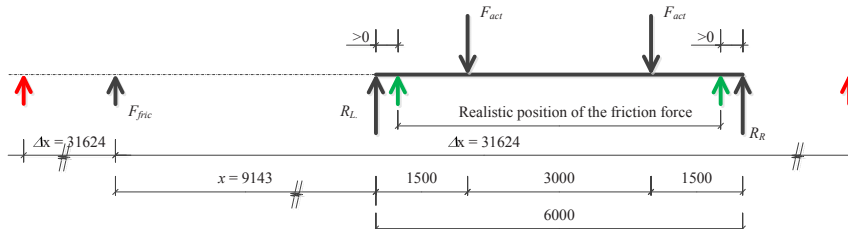
Test girder 7, 600x100



Test girder 8, 800x50

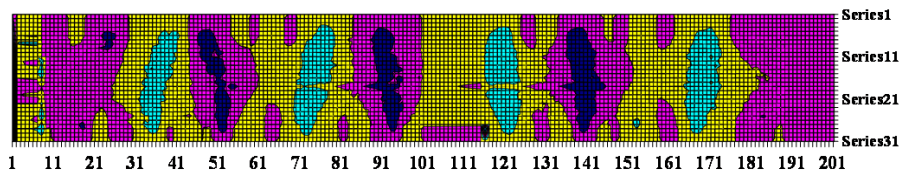


Test girder 9, 800x80

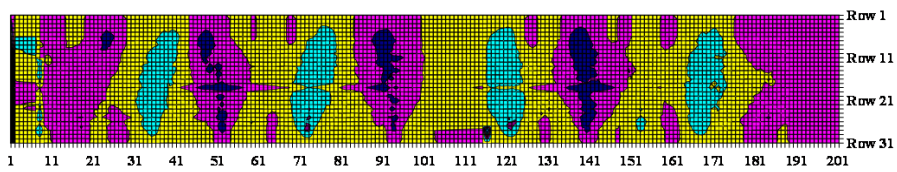


Test girder 10, 800x100

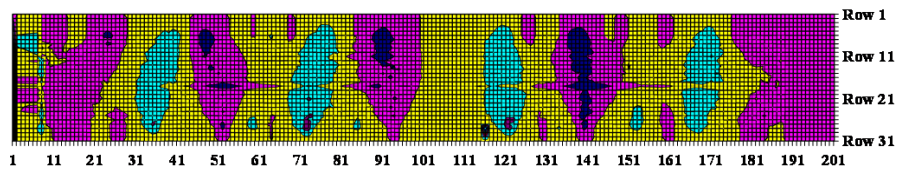
APPENDIX L OUT-OF-PLANE DEFLECTIONS AS FUNCTION OF THE LOAD OF TEST GIRDER 1, 400X50



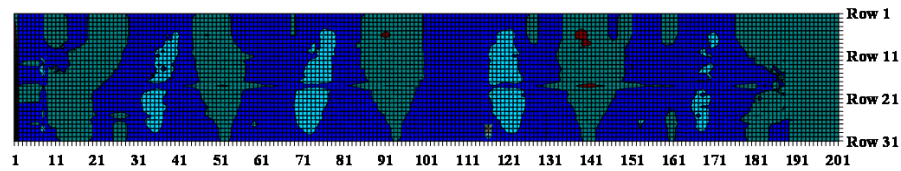
Out-of-plane deflections as function of the load of test girder 1, 400x50, DS A-0



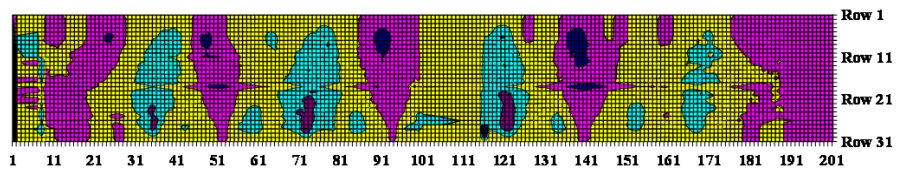
Out-of-plane deflections as function of the load of test girder 1, 400x50, DS B-0



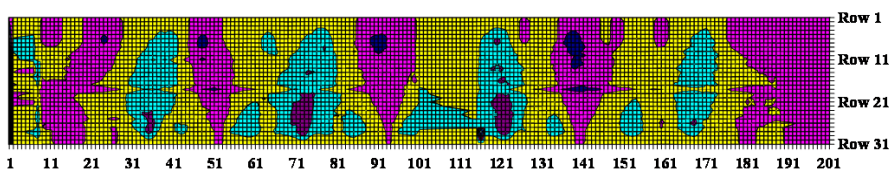
Out-of-plane deflections as function of the load of test girder 1, 400x50, DS C-0



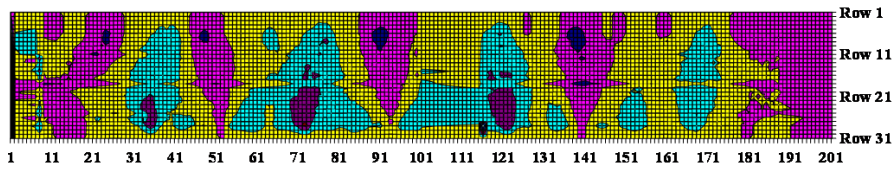
Out-of-plane deflections as function of the load of test girder 1, 400x50, DS D-0



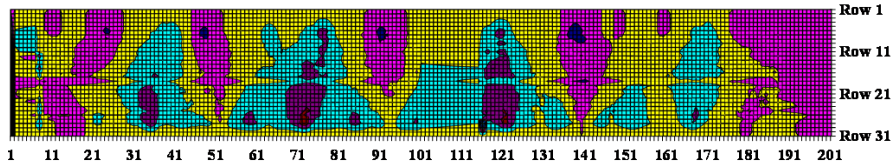
Out-of-plane deflections as function of the load of test girder 1, 400x50, DS E-0



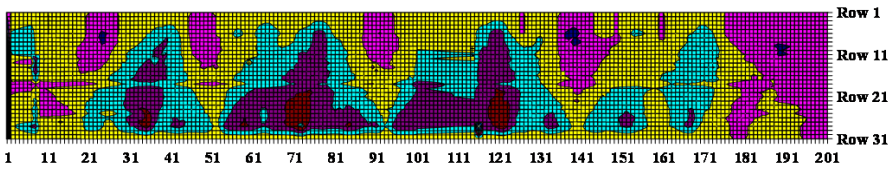
Out-of-plane deflections as function of the load of test girder 1, 400x50, DS F-0



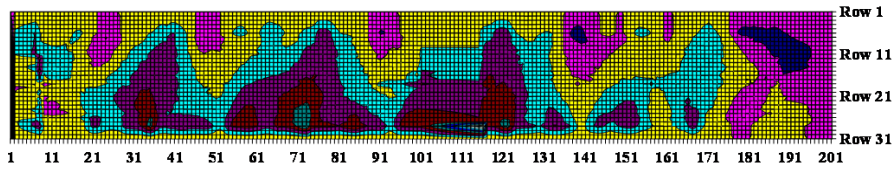
Out-of-plane deflections as function of the load of test girder 1, 400x50, DS G-0



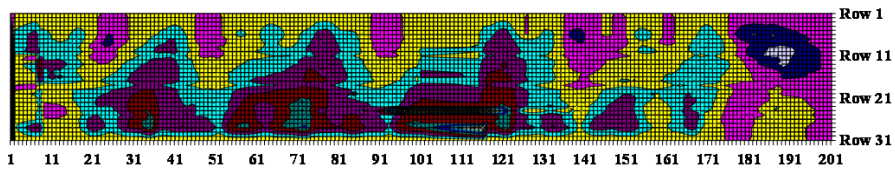
Out-of-plane deflections as function of the load of test girder 1, 400x50, DS H-0



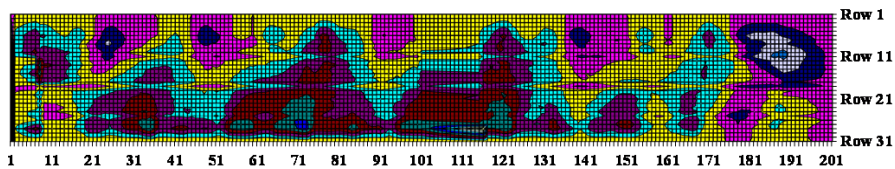
Out-of-plane deflections as function of the load of test girder 1, 400x50, DS I-0



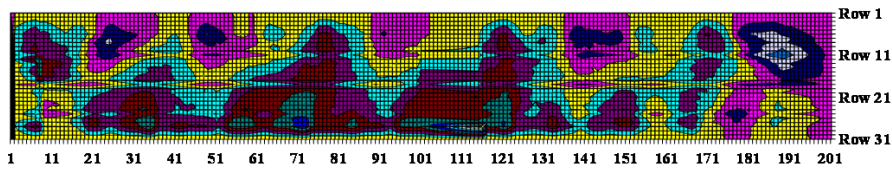
Out-of-plane deflections as function of the load of test girder 1, 400x50, DS J-0



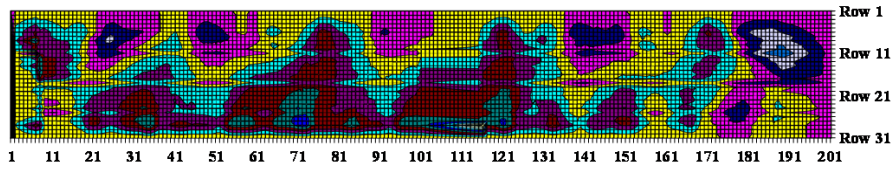
Out-of-plane deflections as function of the load of test girder 1, 400x50, DS K-0



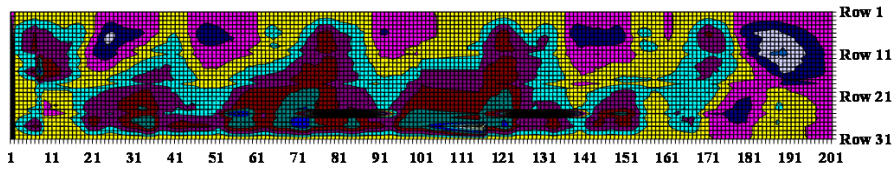
Out-of-plane deflections as function of the load of test girder 1, 400x50, DS L-0



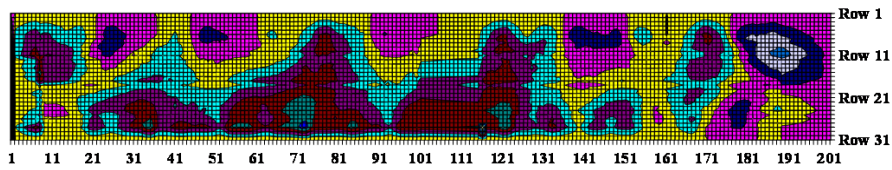
Out-of-plane deflections as function of the load of test girder 1, 400x50, DS M-0



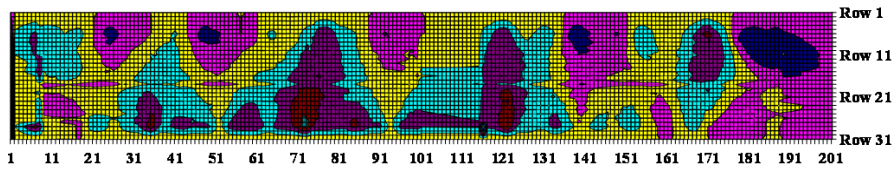
Out-of-plane deflections as function of the load of test girder 1, 400x50, DS N-0



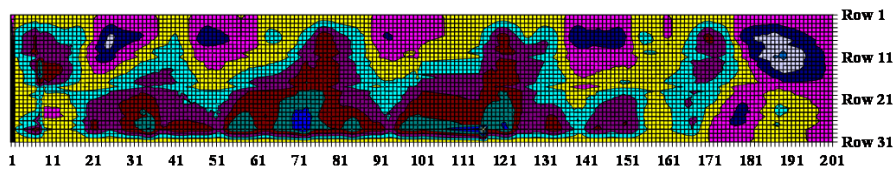
Out-of-plane deflections as function of the load of test girder 1, 400x50, DS O-0



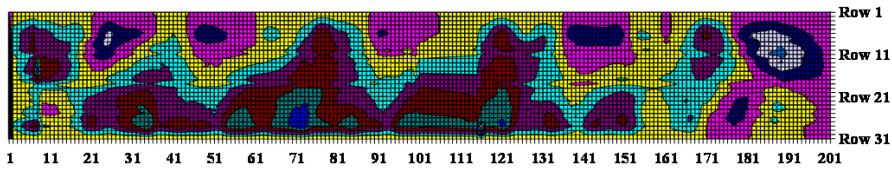
Out-of-plane deflections as function of the load of test girder 1, 400x50, DS P-0



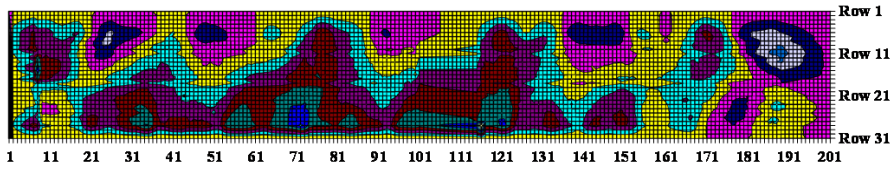
Out-of-plane deflections as function of the load of test girder 1, 400x50, DS Q-0



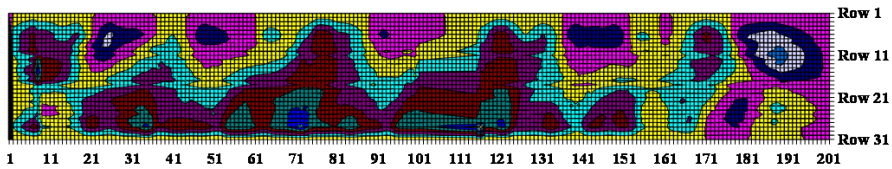
Out-of-plane deflections as function of the load of test girder 1, 400x50, DS R-0



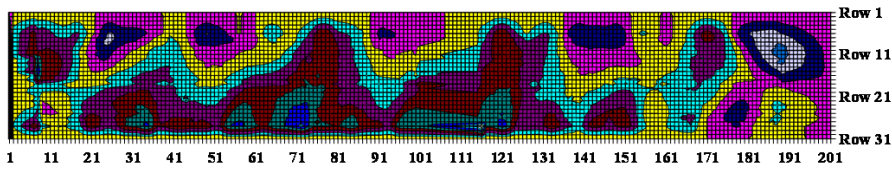
Out-of-plane deflections as function of the load of test girder 1, 400x50, DS U-0



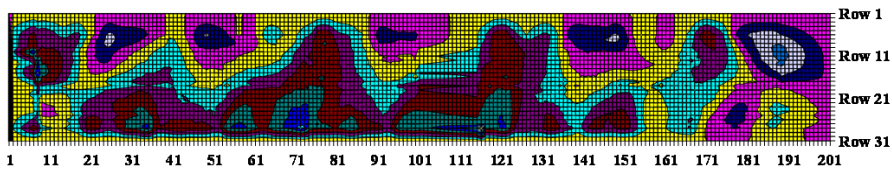
Out-of-plane deflections as function of the load of test girder 1, 400x50, DS V-0



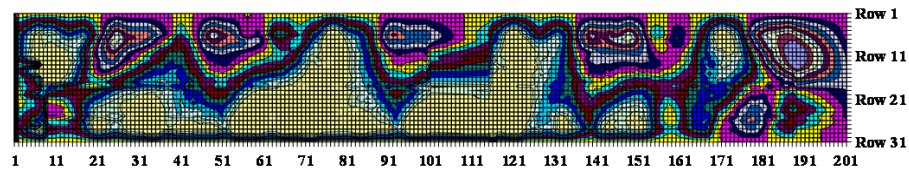
Out-of-plane deflections as function of the load of test girder 1, 400x50, DS W-0



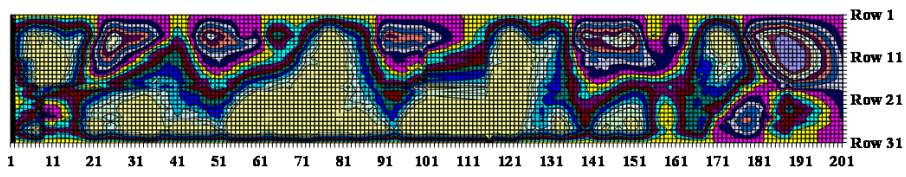
Out-of-plane deflections as function of the load of test girder 1, 400x50, DS Y-0



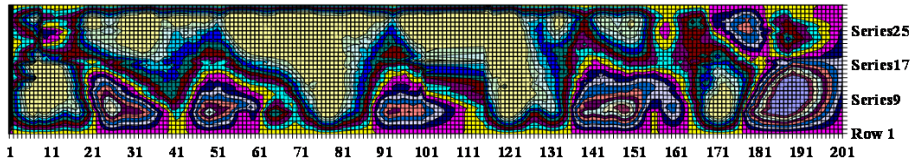
Out-of-plane deflections as function of the load of test girder 1, 400x50, DS Z-0



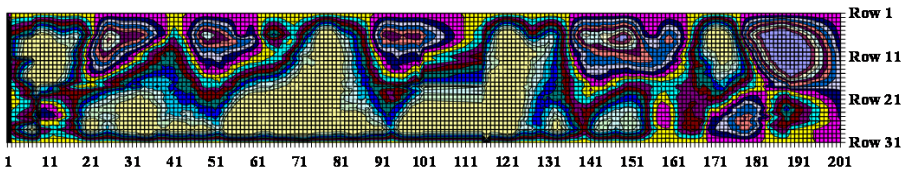
Out-of-plane deflections as function of the load of test girder 1, 400x50, DS AA-0



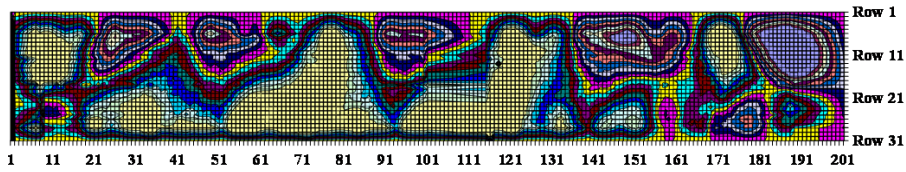
Out-of-plane deflections as function of the load of test girder 1, 400x50, DS AB-0



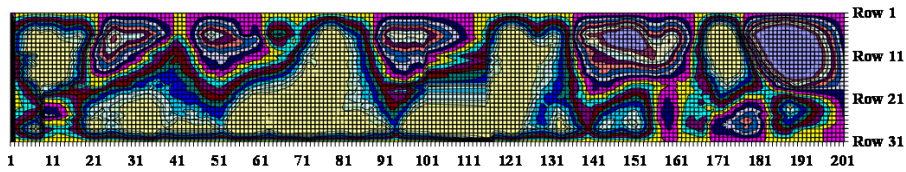
Out-of-plane deflections as function of the load of test girder 1, 400x50, DS AC-0



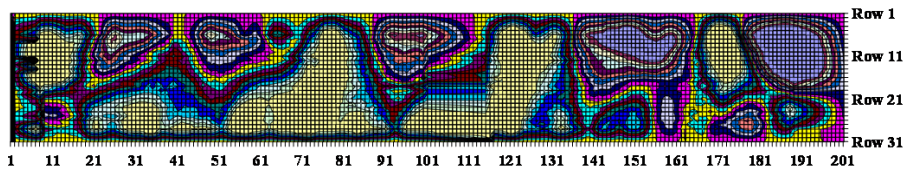
Out-of-plane deflections as function of the load of test girder 1, 400x50, DS AD-0



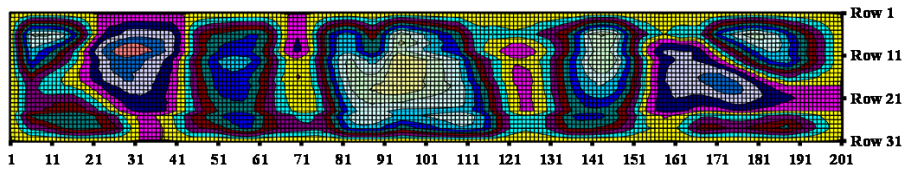
Out-of-plane deflections as function of the load of test girder 1, 400x50, DS AE-0



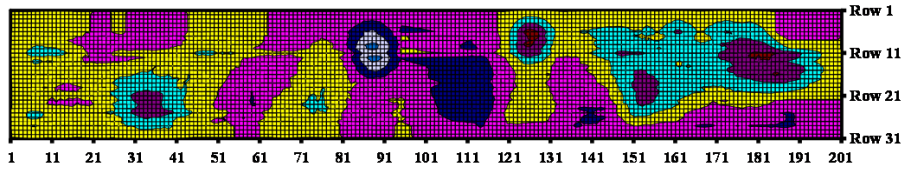
Out-of-plane deflections as function of the load of test girder 1, 400x50, DS AF-0



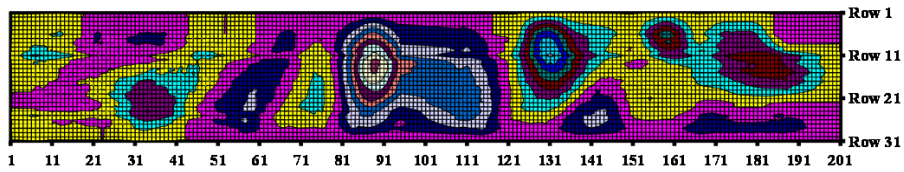
Out-of-plane deflections as function of the load of test girder 1, 400x50, DS AG-0



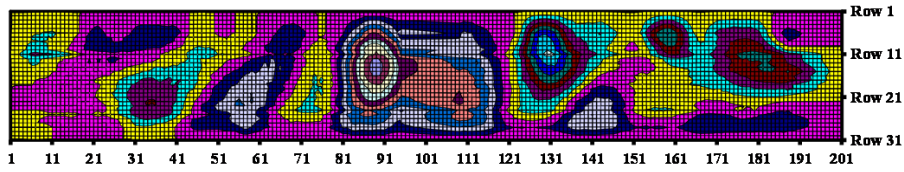
Out-of-plane deflections as function of the load of plate girder 2, 400x80(1), DS A-0



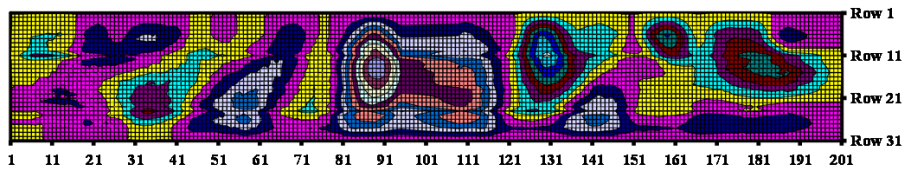
Out-of-plane deflections as function of the load of plate girder 2, 400x80(1), DS B-0



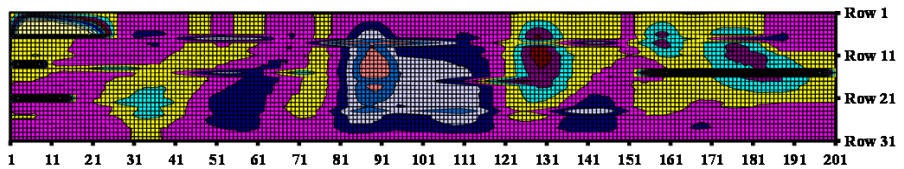
Out-of-plane deflections as function of the load of plate girder 2, 400x80(1), DS C-0



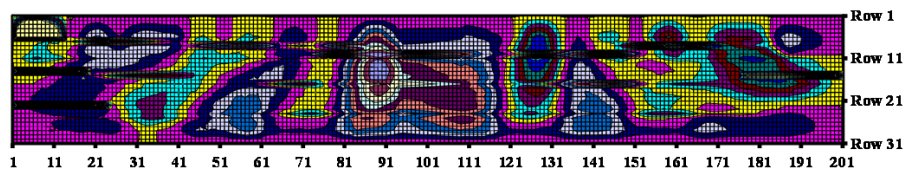
Out-of-plane deflections as function of the load of plate girder 2, 400x80(1), DS D-0



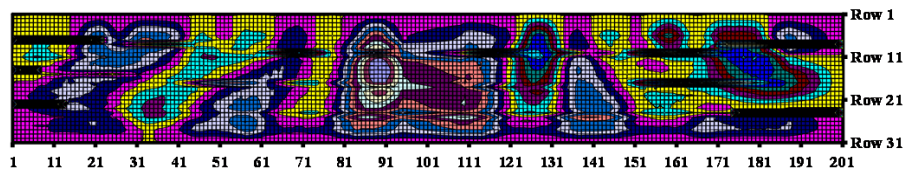
Out-of-plane deflections as function of the load of plate girder 2, 400x80(1), DS E-0



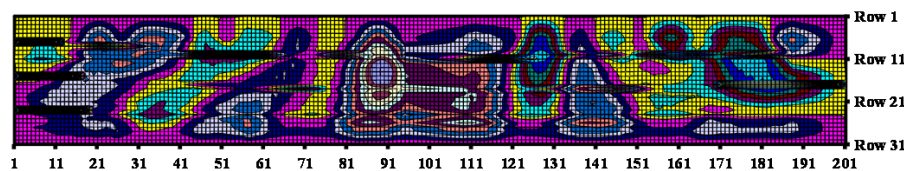
Out-of-plane deflections as function of the load of plate girder 2, 400x80(1), DS F-0



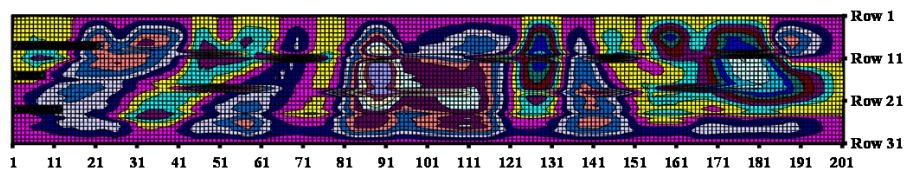
Out-of-plane deflections as function of the load of plate girder 2, 400x80(1), DS G-0



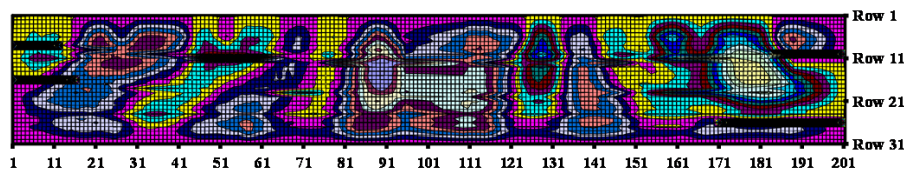
Out-of-plane deflections as function of the load of plate girder 2, 400x80(1), DS H-0



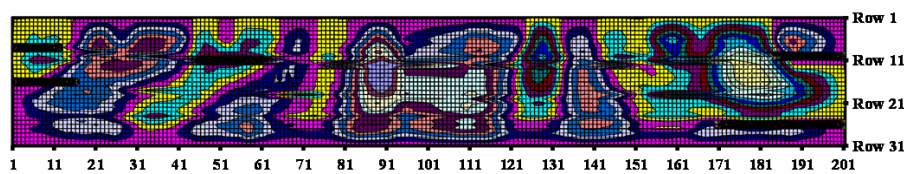
Out-of-plane deflections as function of the load of plate girder 2, 400x80(1), DS I-0



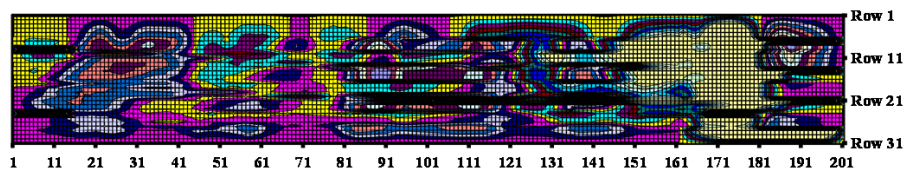
Out-of-plane deflections as function of the load of plate girder 2, 400x80(1), DS J-0



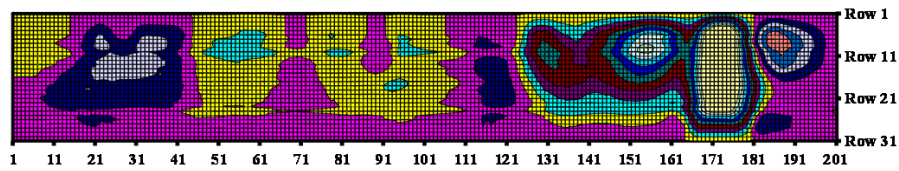
Out-of-plane deflections as function of the load of plate girder 2, 400x80(1), DS K-0



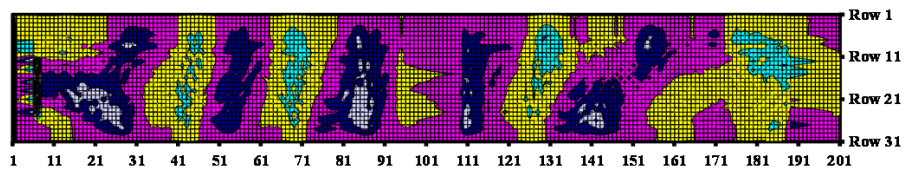
Out-of-plane deflections as function of the load of plate girder 2, 400x80(1), DS L-0



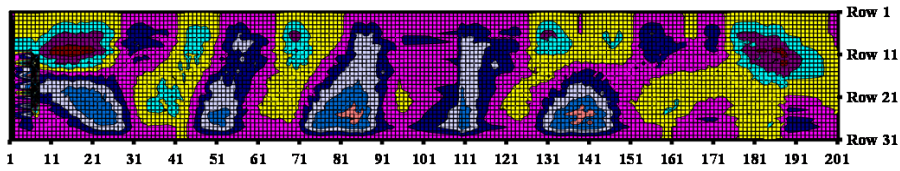
Out-of-plane deflections as function of the load of plate girder 2, 400x80(1), DS M-0



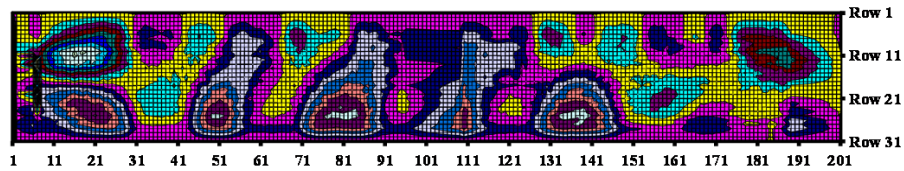
Out-of-plane deflections as function of the load of plate girder 2, 400x80(1), DS N-0



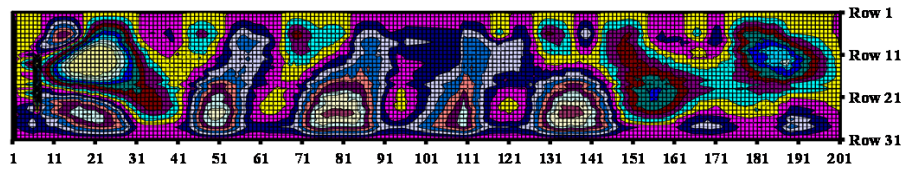
Out-of-plane deflections as function of the load of plate girder 3, 400x80(2), DS A-0



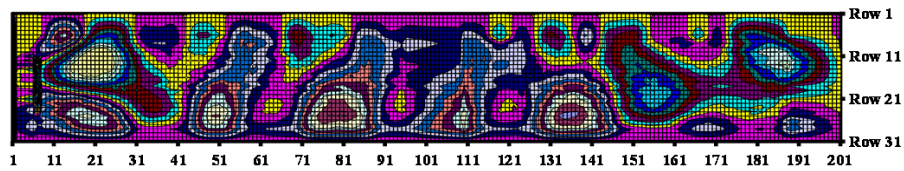
Out-of-plane deflections as function of the load of plate girder 3, 400x80(2), DS B-0



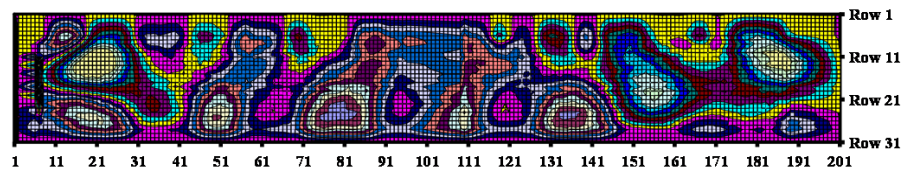
Out-of-plane deflections as function of the load of plate girder 3, 400x80(2), DS C-0



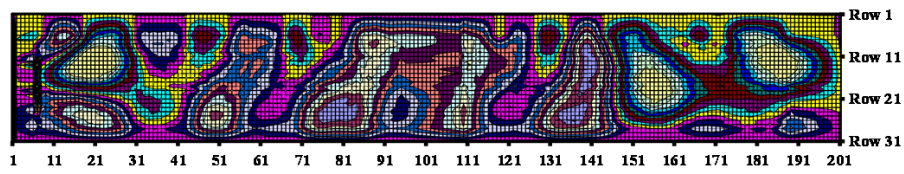
Out-of-plane deflections as function of the load of plate girder 3, 400x80(2), DS D-0



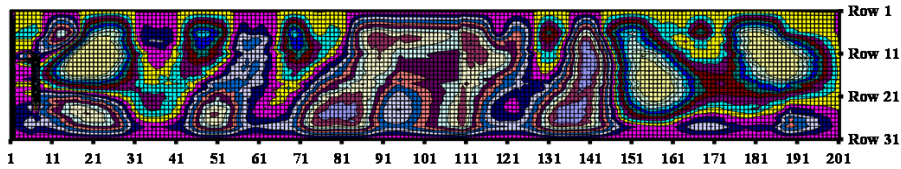
Out-of-plane deflections as function of the load of plate girder 3, 400x80(2), DS E-0



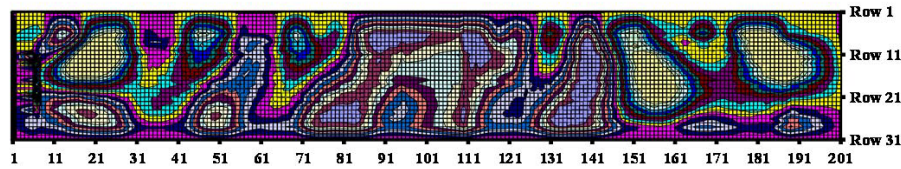
Out-of-plane deflections as function of the load of plate girder 3, 400x80(2), DS F-0



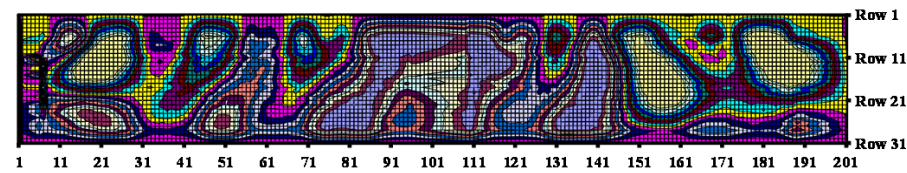
Out-of-plane deflections as function of the load of plate girder 3, 400x80(2), DS G-0



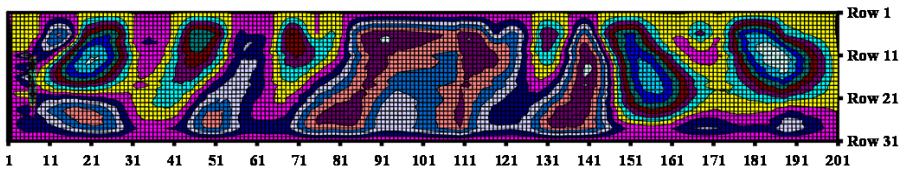
Out-of-plane deflections as function of the load of plate girder 3, 400x80(2), DS H-0



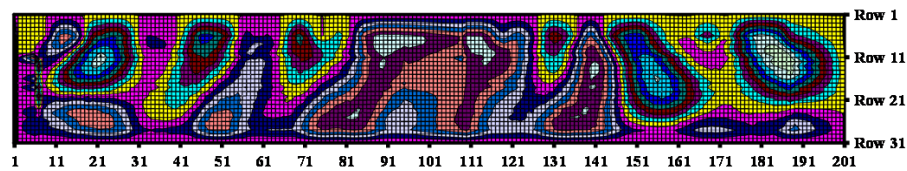
Out-of-plane deflections as function of the load of plate girder 3, 400x80(2), DS I-0



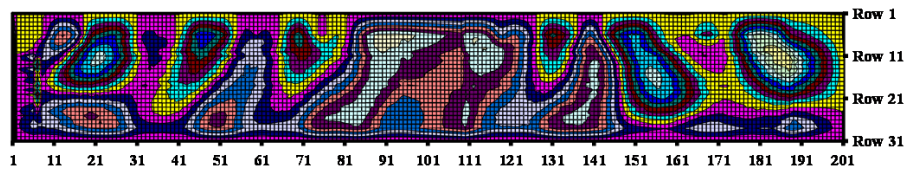
Out-of-plane deflections as function of the load of plate girder 3, 400x80(2), DS J-0



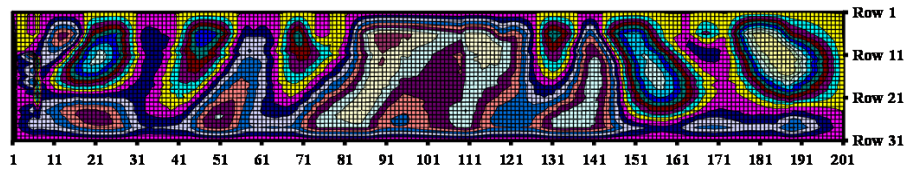
Out-of-plane deflections as function of the load of plate girder 3, 400x80(2), DS K-0



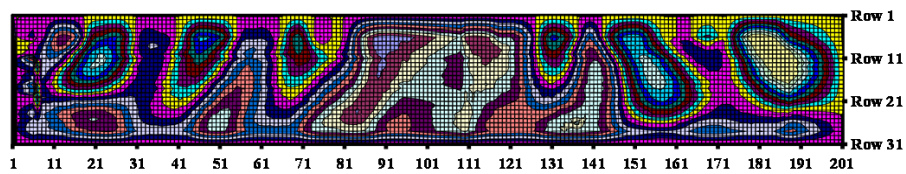
Out-of-plane deflections as function of the load of plate girder 3, 400x80(2), DS L-0



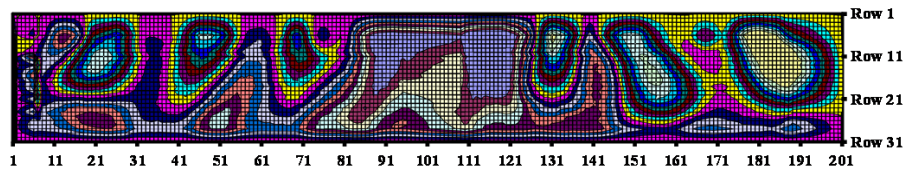
Out-of-plane deflections as function of the load of plate girder 3, 400x80(2), DS M-0



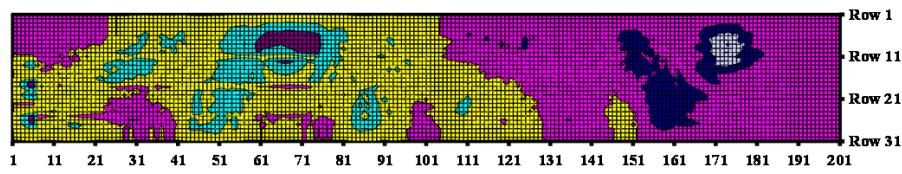
Out-of-plane deflections as function of the load of plate girder 3, 400x80(2), DS N-0



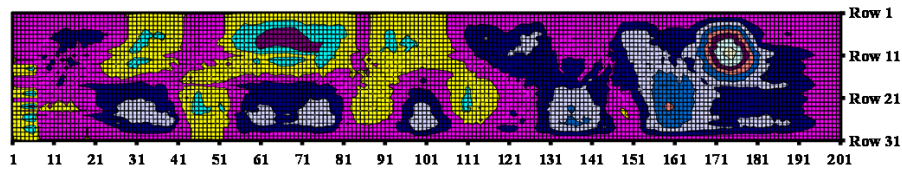
Out-of-plane deflections as function of the load of plate girder 3, 400x80(2), DS O-0



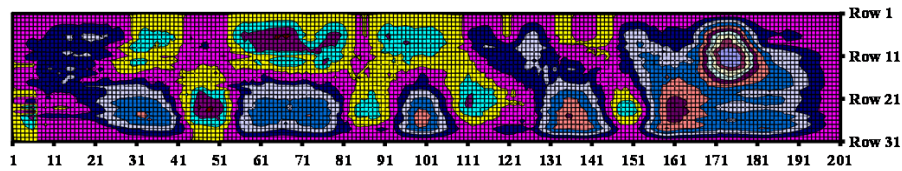
Out-of-plane deflections as function of the load of plate girder 3, 400x80(2), DS P-0



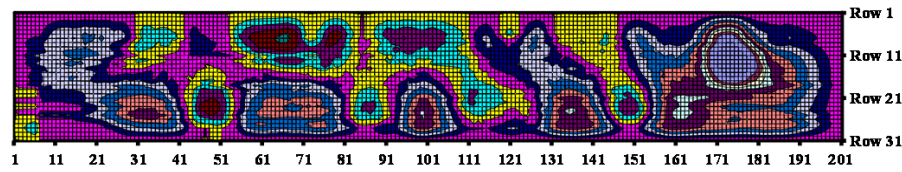
Out-of-plane deflections as function of the load of plate girder 4, 400x100, DS A-0



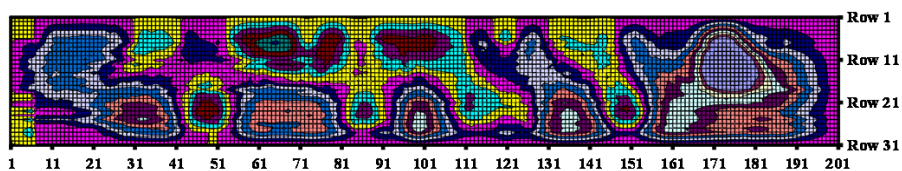
Out-of-plane deflections as function of the load of plate girder 4, 400x100, DS B-0



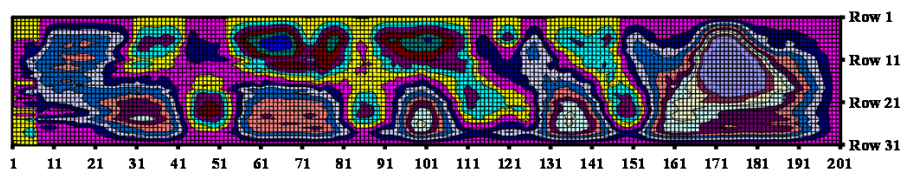
Out-of-plane deflections as function of the load of plate girder 4, 400x100, DS C-0



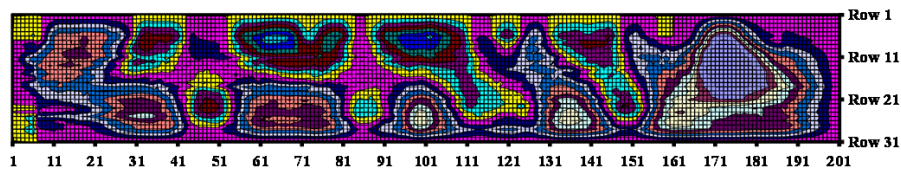
Out-of-plane deflections as function of the load of plate girder 4, 400x100, DS D-0



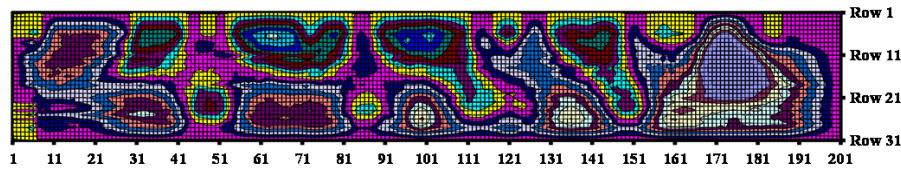
Out-of-plane deflections as function of the load of plate girder 4, 400x100, DS E-0



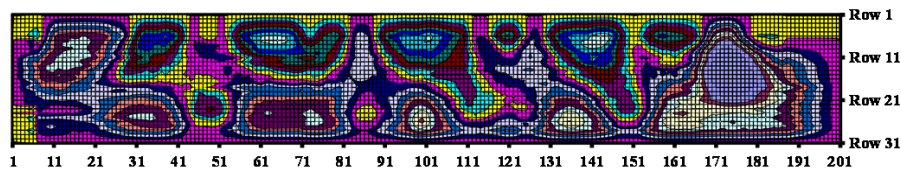
Out-of-plane deflections as function of the load of plate girder 4, 400x100, DS F-0



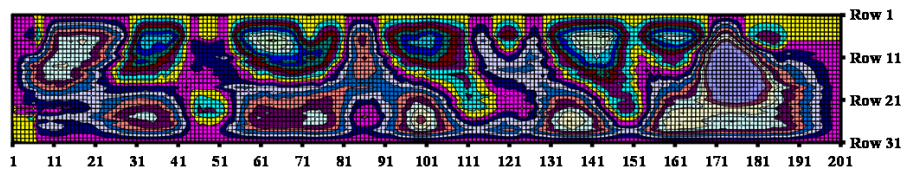
Out-of-plane deflections as function of the load of plate girder 4, 400x100, DS G-0



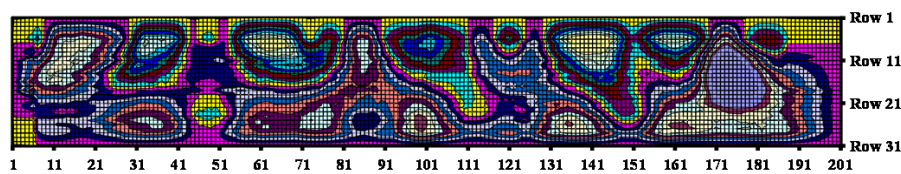
Out-of-plane deflections as function of the load of plate girder 4, 400x100, DS H-0



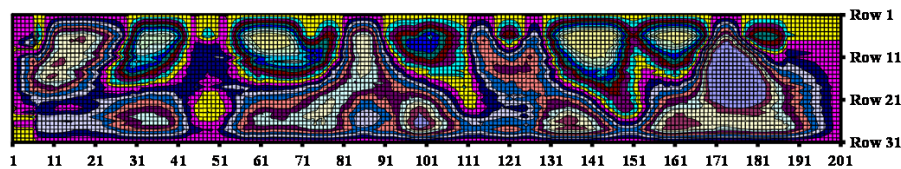
Out-of-plane deflections as function of the load of plate girder 4, 400x100, DS I-0



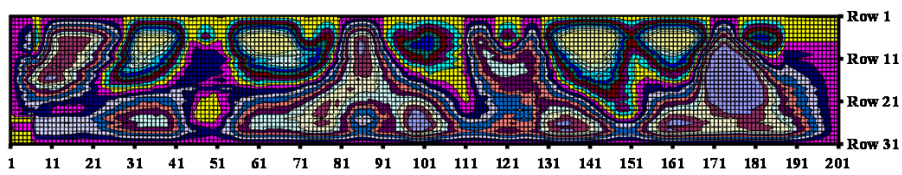
Out-of-plane deflections as function of the load of plate girder 4, 400x100, DS J-0



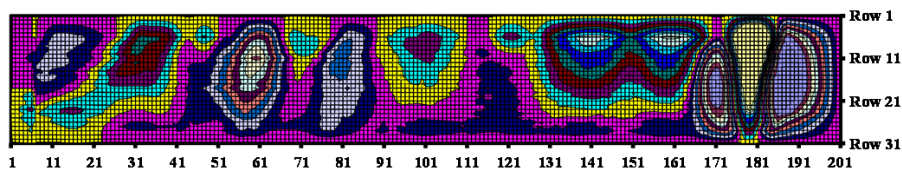
Out-of-plane deflections as function of the load of plate girder 4, 400x100, DS K-0



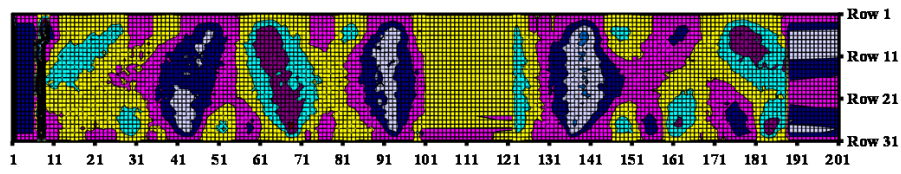
Out-of-plane deflections as function of the load of plate girder 4, 400x100, DS L-0



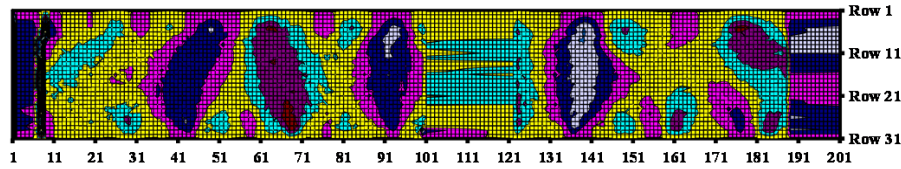
Out-of-plane deflections as function of the load of plate girder 4, 400x100, DS M-0



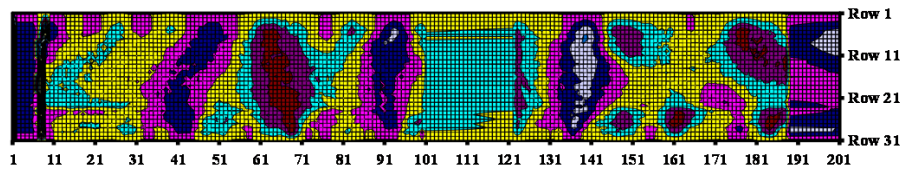
Out-of-plane deflections as function of the load of plate girder 4, 400x100, DS N-0



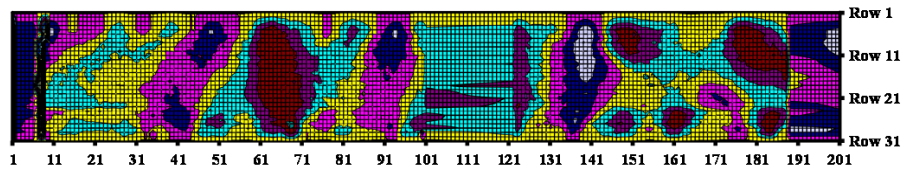
Out-of-plane deflections as function of the load of plate girder 5, 600x50, DS A-0



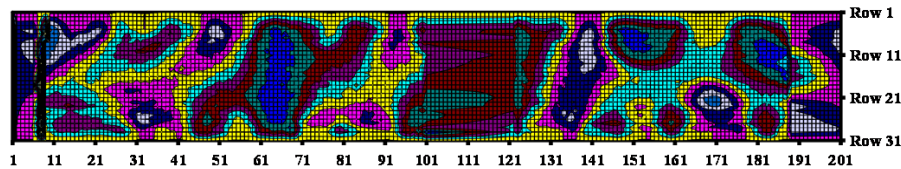
Out-of-plane deflections as function of the load of plate girder 5, 600x50, DS B-0



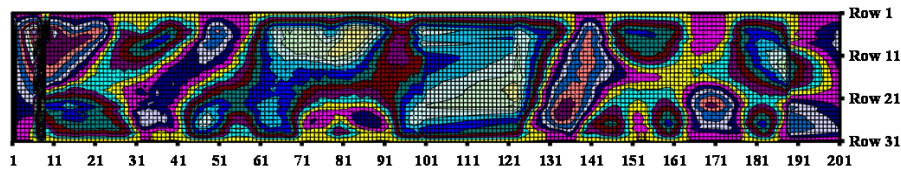
Out-of-plane deflections as function of the load of plate girder 5, 600x50, DS C-0



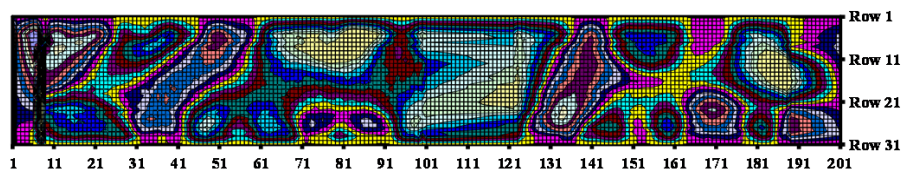
Out-of-plane deflections as function of the load of plate girder 5, 600x50, DS D-0



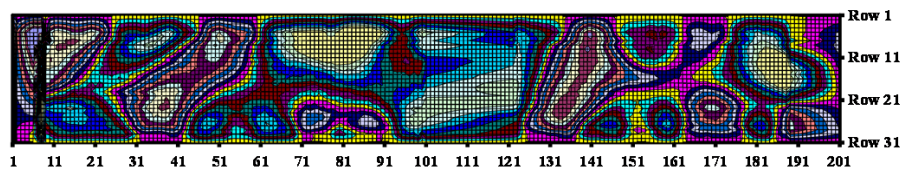
Out-of-plane deflections as function of the load of plate girder 5, 600x50, DS E-0



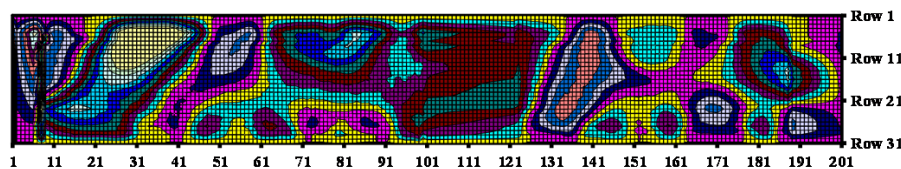
Out-of-plane deflections as function of the load of plate girder 5, 600x50, DS F-0



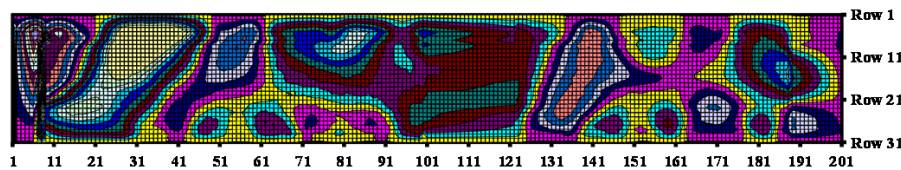
Out-of-plane deflections as function of the load of plate girder 5, 600x50, DS G-0



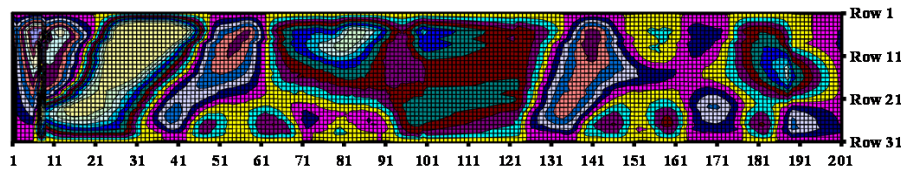
Out-of-plane deflections as function of the load of plate girder 5, 600x50, DS H-0



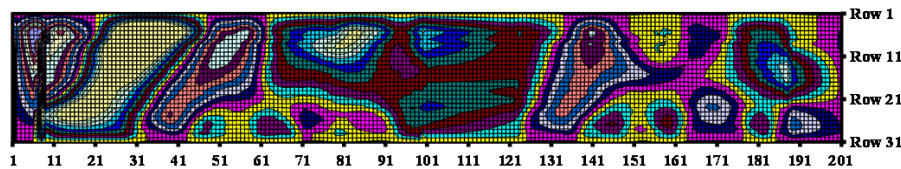
Out-of-plane deflections as function of the load of plate girder 5, 600x50, DS I-0



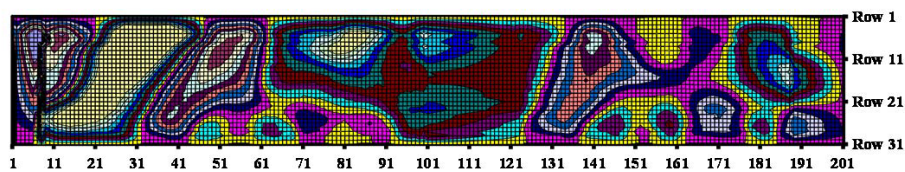
Out-of-plane deflections as function of the load of plate girder 5, 600x50, DS J-0



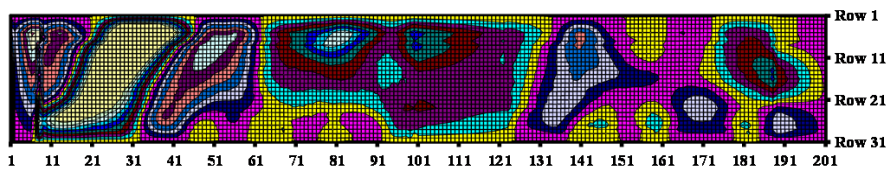
Out-of-plane deflections as function of the load of plate girder 5, 600x50, DS K-0



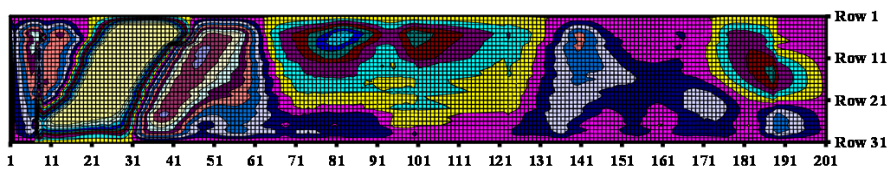
Out-of-plane deflections as function of the load of plate girder 5, 600x50, DS L-0



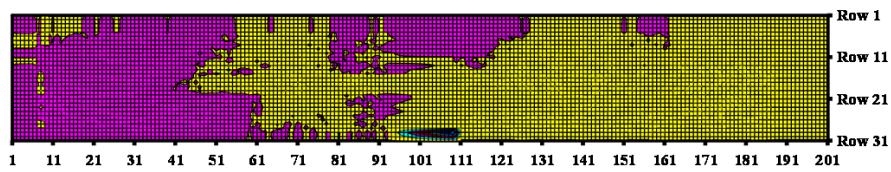
Out-of-plane deflections as function of the load of plate girder 5, 600x50, DS M-0



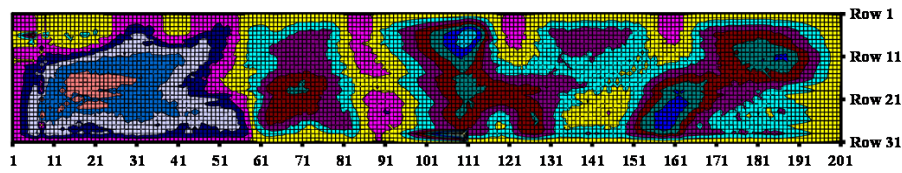
Out-of-plane deflections as function of the load of plate girder 5, 600x50, DS N-0



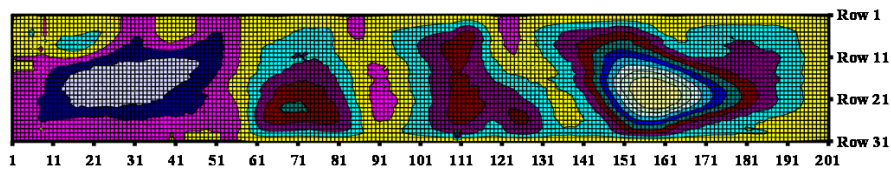
Out-of-plane deflections as function of the load of plate girder 5, 600x50, DS O-0



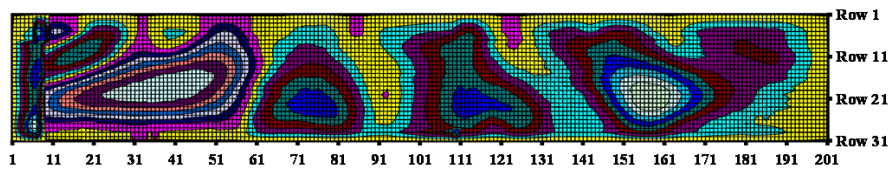
Out-of-plane deflections as function of the load of plate girder 6, 600x80, DS A-0



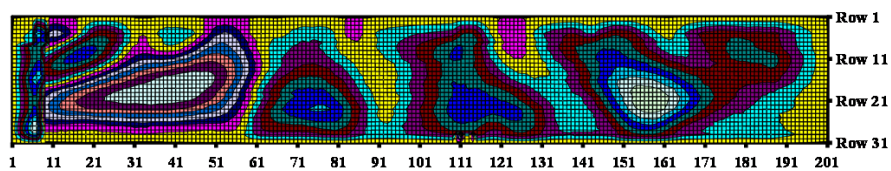
Out-of-plane deflections as function of the load of plate girder 6, 600x80, DS B-0



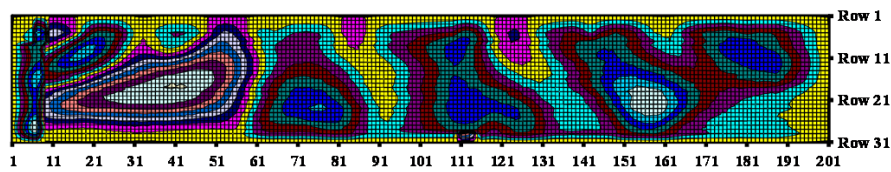
Out-of-plane deflections as function of the load of plate girder 6, 600x80, DS C-0



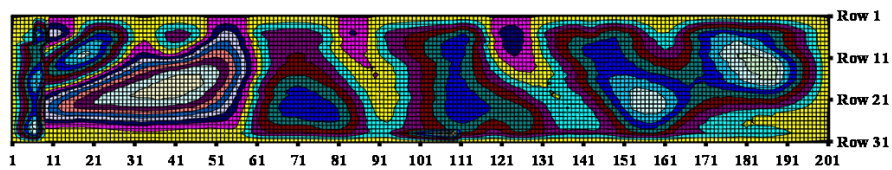
Out-of-plane deflections as function of the load of plate girder 6, 600x80, DS D-0



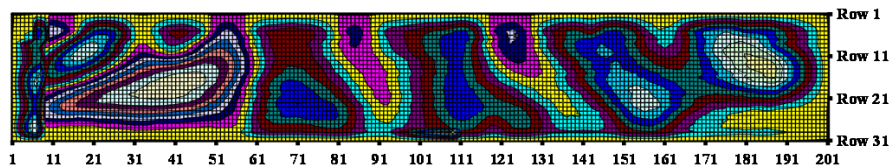
Out-of-plane deflections as function of the load of plate girder 6, 600x80, DS E-0



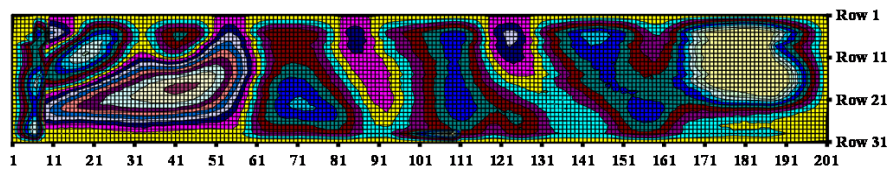
Out-of-plane deflections as function of the load of plate girder 6, 600x80, DS F-0



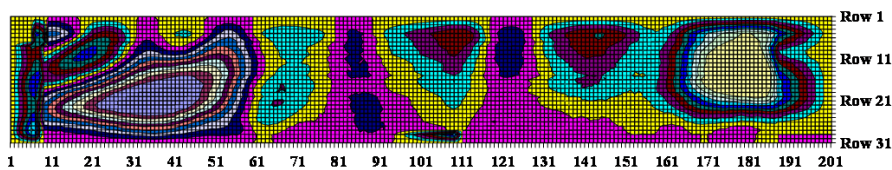
Out-of-plane deflections as function of the load of plate girder 6, 600x80, DS G-0



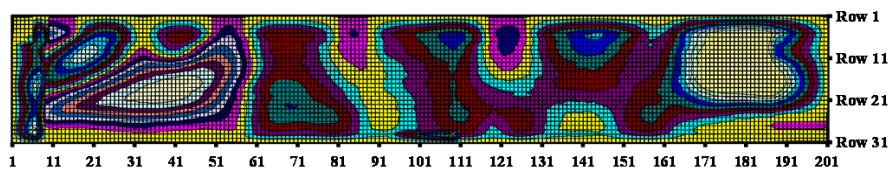
Out-of-plane deflections as function of the load of plate girder 6, 600x80, DS H-0



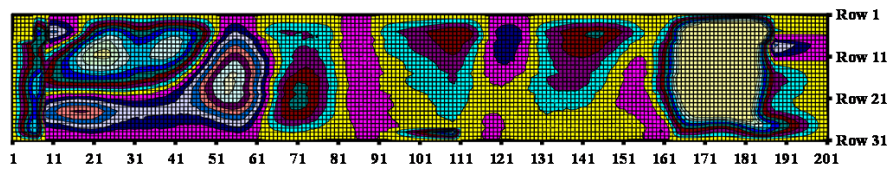
Out-of-plane deflections as function of the load of plate girder 6, 600x80, DS I-0



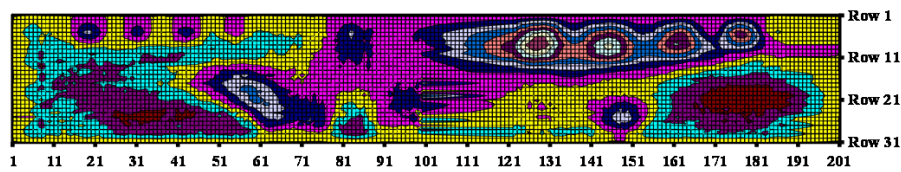
Out-of-plane deflections as function of the load of plate girder 6, 600x80, DS J-0



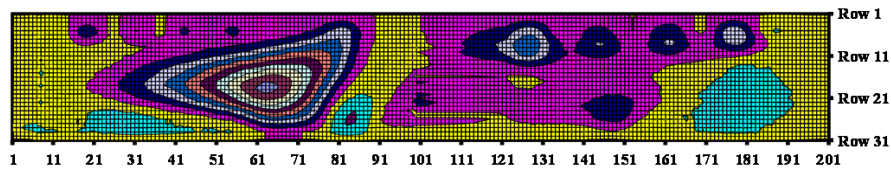
Out-of-plane deflections as function of the load of plate girder 6, 600x80, DS K-0



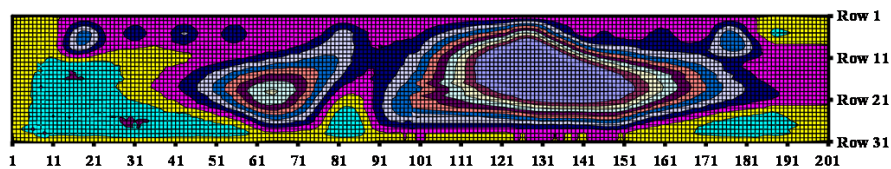
Out-of-plane deflections as function of the load of plate girder 6, 600x80, DS L-0



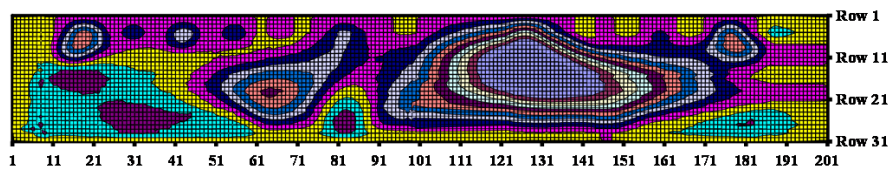
Out-of-plane deflections as function of the load of plate girder 7, 600x100, DS A-0



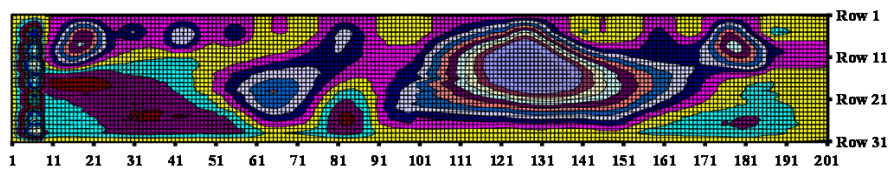
Out-of-plane deflections as function of the load of plate girder 7, 600x100, DS B-0



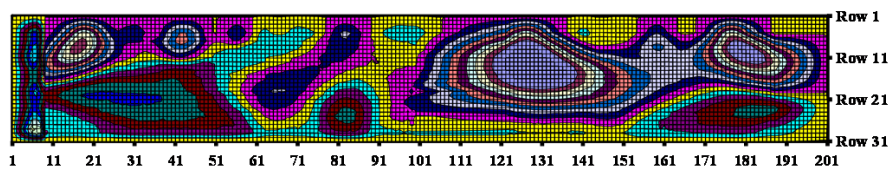
Out-of-plane deflections as function of the load of plate girder 7, 600x100, DS C-0



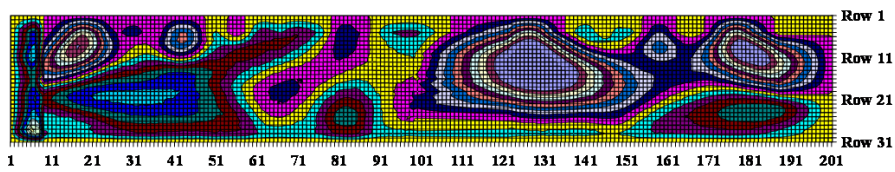
Out-of-plane deflections as function of the load of plate girder 7, 600x100, DS D-0



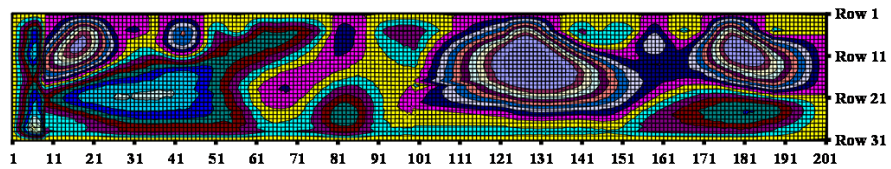
Out-of-plane deflections as function of the load of plate girder 7, 600x100, DS E-0



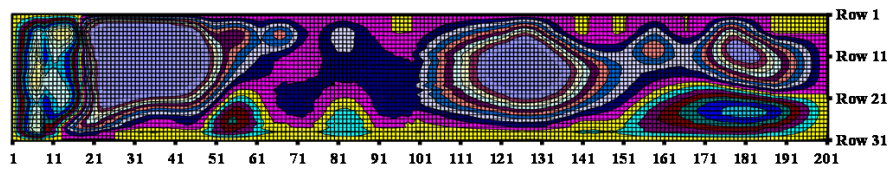
Out-of-plane deflections as function of the load of plate girder 7, 600x100, DS F-0



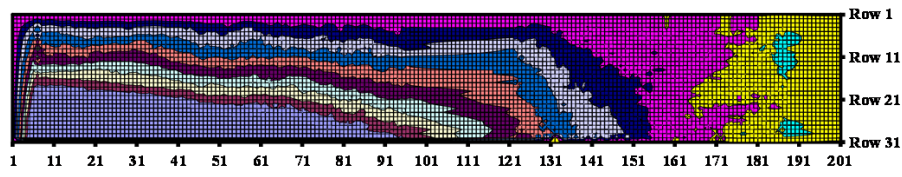
Out-of-plane deflections as function of the load of plate girder 7, 600x100, DS G-0



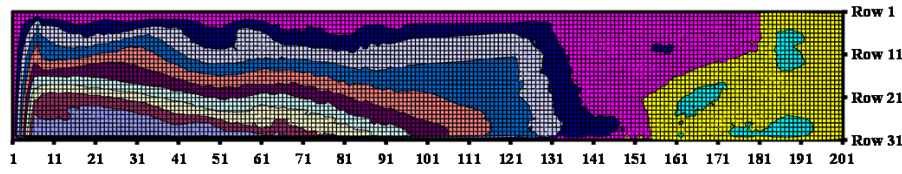
Out-of-plane deflections as function of the load of plate girder 7, 600x100, DS H-0



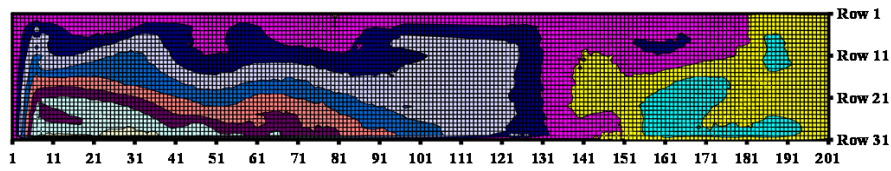
Out-of-plane deflections as function of the load of plate girder 7, 600x100, DS I-0



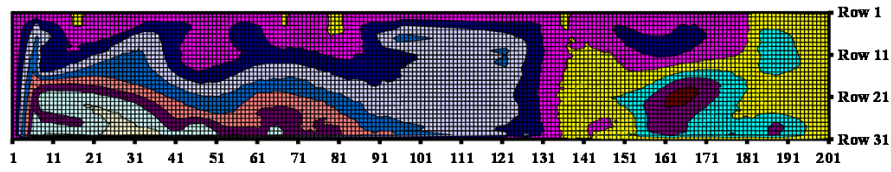
Out-of-plane deflections as functions of the load of plate girder 8, 800x50, DS A-0



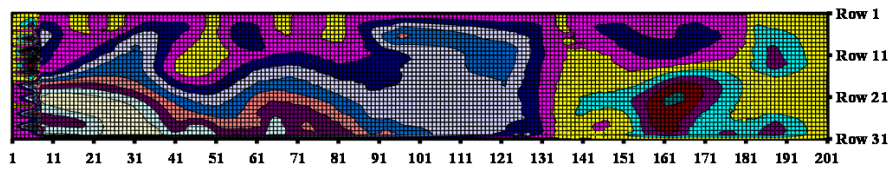
Out-of-plane deflections as functions of the load of plate girder 8, 800x50, DS B-0



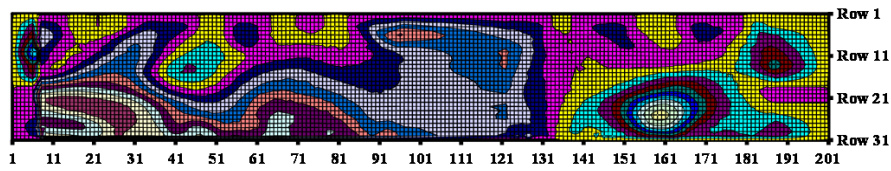
Out-of-plane deflections as functions of the load of plate girder 8, 800x50, DS C-0



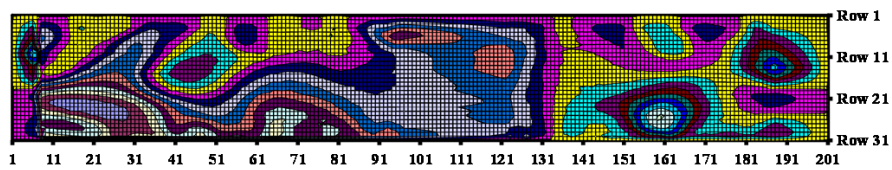
Out-of-plane deflections as functions of the load of plate girder 8, 800x50, DS D-0



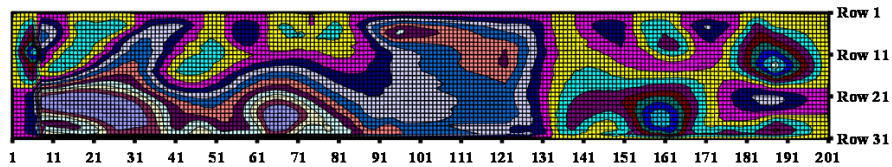
Out-of-plane deflections as functions of the load of plate girder 8, 800x50, DS E-0



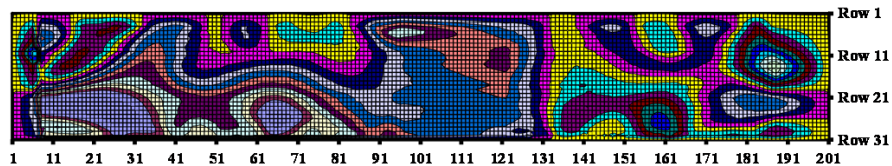
Out-of-plane deflections as functions of the load of plate girder 8, 800x50, DS F-0



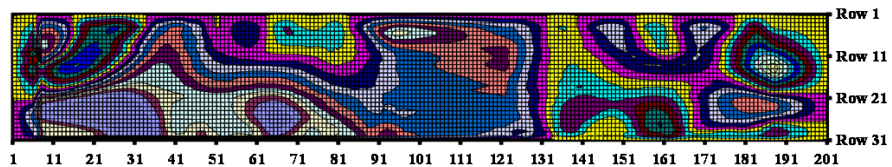
Out-of-plane deflections as functions of the load of plate girder 8, 800x50, DS G-0



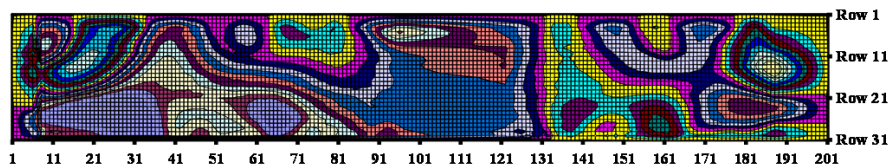
Out-of-plane deflections as functions of the load of plate girder 8, 800x50, DS H-0



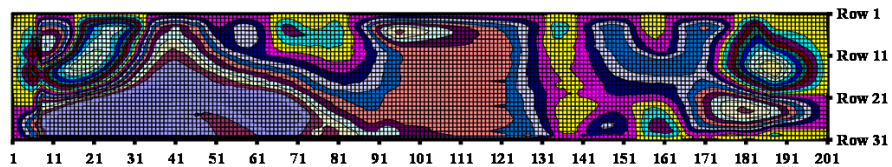
Out-of-plane deflections as functions of the load of plate girder 8, 800x50, DS I-0



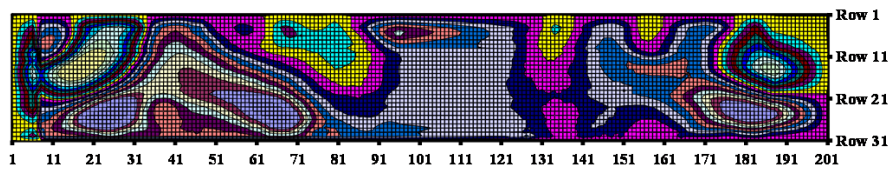
Out-of-plane deflections as functions of the load of plate girder 8, 800x50, DS J-0



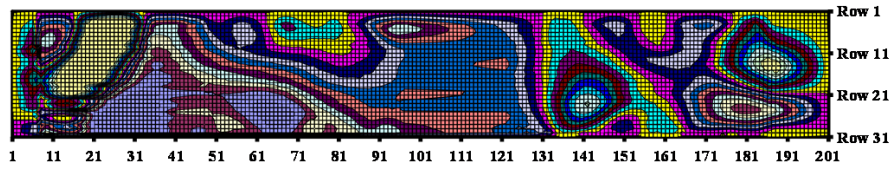
Out-of-plane deflections as functions of the load of plate girder 8, 800x50, DS K-0



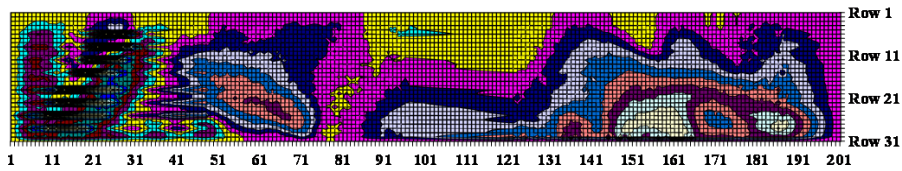
Out-of-plane deflections as functions of the load of plate girder 8, 800x50, DS L-0



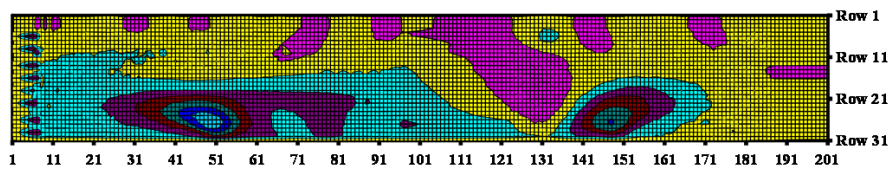
Out-of-plane deflections as functions of the load of plate girder 8, 800x50, DS M-0



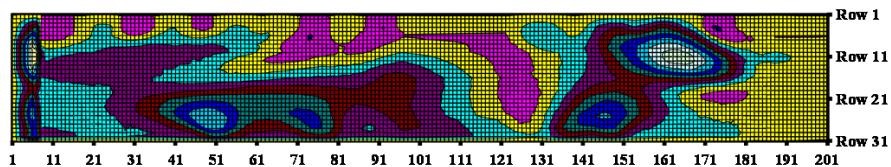
Out-of-plane deflections as functions of the load of plate girder 8, 800x50, DS O-0



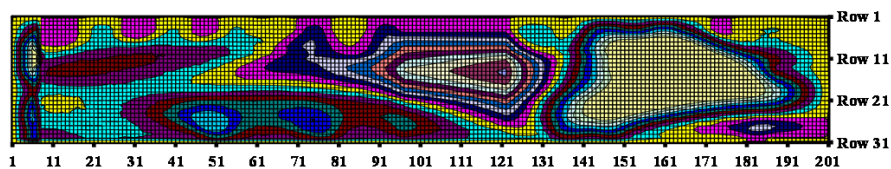
Out-of-plane deflections as functions of the load of plate girder 8, 800x50, DS P-0



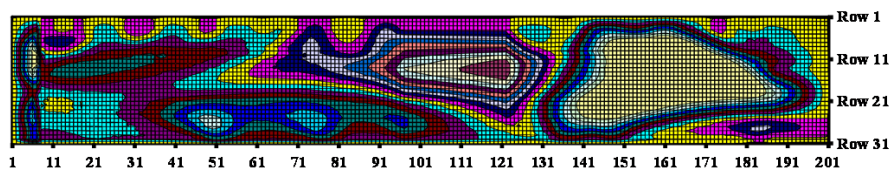
Out-of-plane deflection as function of the load of plate girder 9, 800x80, DS A-0



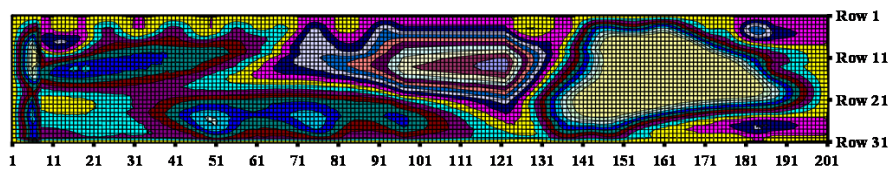
Out-of-plane deflection as function of the load of plate girder 9, 800x80, DS B-0



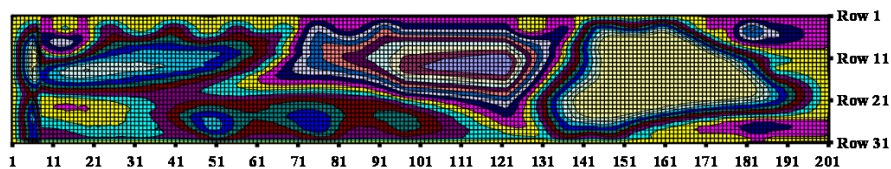
Out-of-plane deflection as function of the load of plate girder 9, 800x80, DS C-0



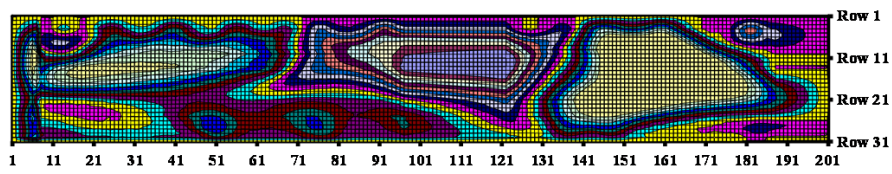
Out-of-plane deflection as function of the load of plate girder 9, 800x80, DS D-0



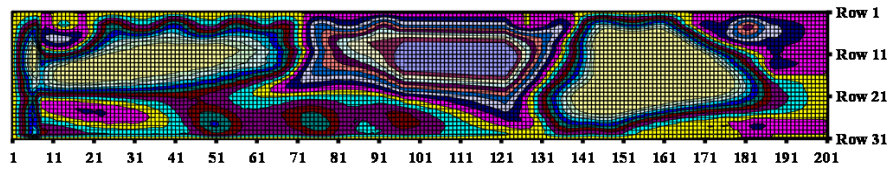
Out-of-plane deflection as function of the load of plate girder 9, 800x80, DS E-0



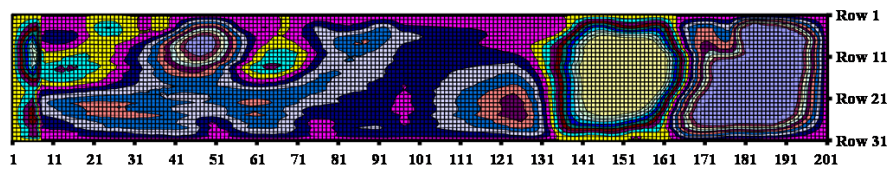
Out-of-plane deflection as function of the load of plate girder 9, 800x80, DS F-0



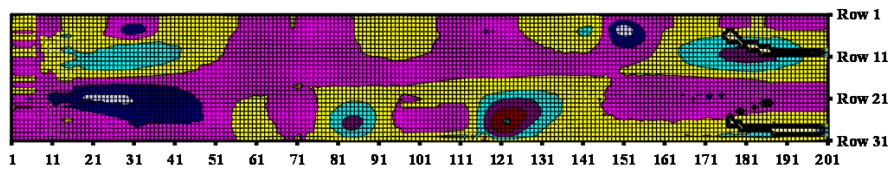
Out-of-plane deflection as function of the load of plate girder 9, 800x80, DS G-0



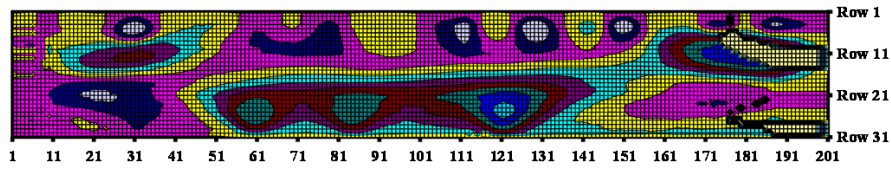
Out-of-plane deflection as function of the load of plate girder 9, 800x80, DS H-0



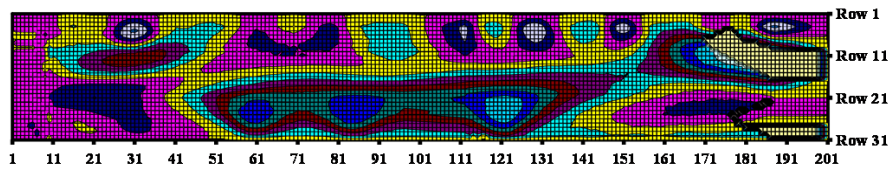
Out-of-plane deflection as function of the load of plate girder 9, 800x80, DS I-0



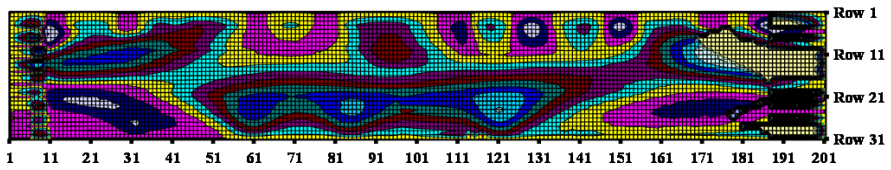
Out-of-plane deflections as function of the load of plate girder 10, 800x100, DS A-0



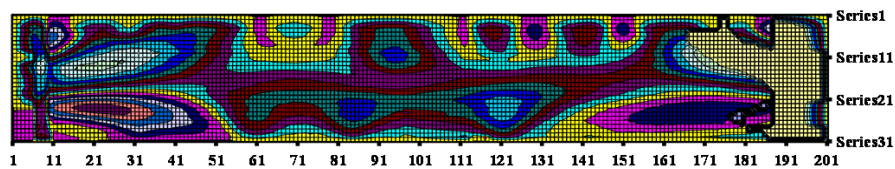
Out-of-plane deflections as function of the load of plate girder 10, 800x100, DS B-0



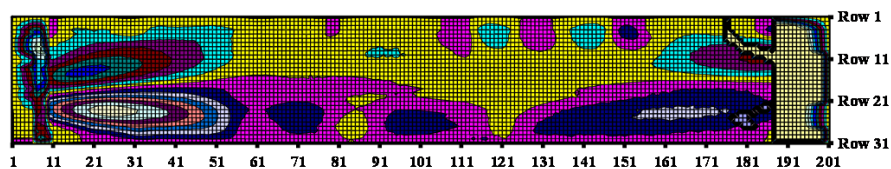
Out-of-plane deflections as function of the load of plate girder 10, 800x100, DS C-0



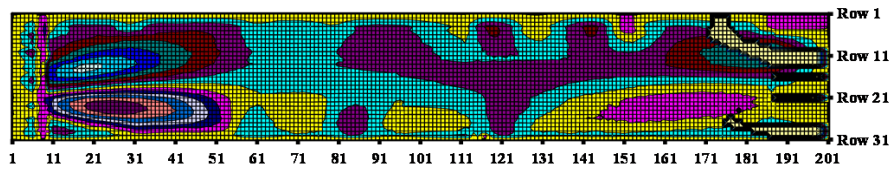
Out-of-plane deflections as function of the load of plate girder 10, 800x100, DS D-0



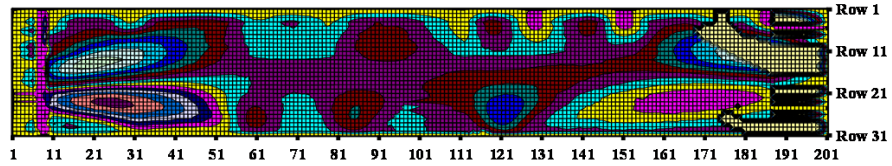
Out-of-plane deflections as function of the load of plate girder 10, 800x100, DS E-0



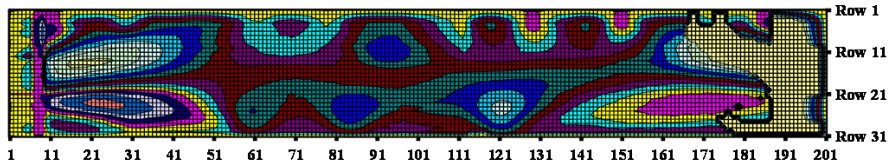
Out-of-plane deflections as function of the load of plate girder 10, 800x100, DS F-0



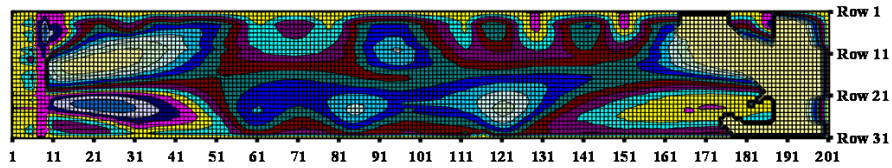
Out-of-plane deflections as function of the load of plate girder 10, 800x100, DS G-0



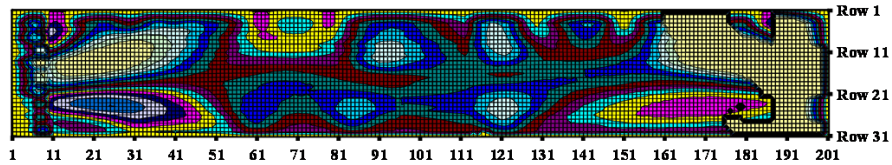
Out-of-plane deflections as function of the load of plate girder 10, 800x100, DS H-0



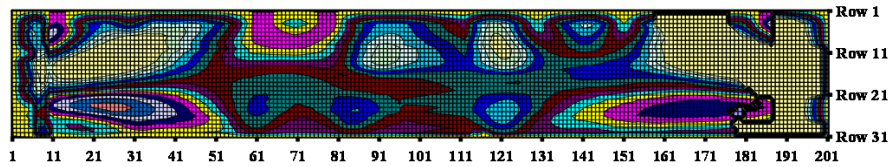
Out-of-plane deflections as function of the load of plate girder 10, 800x100, DS I-0



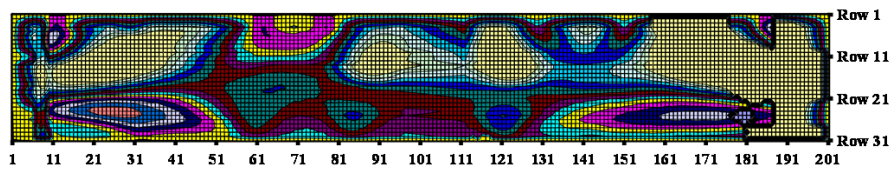
Out-of-plane deflections as function of the load of plate girder 10, 800x100, DS J-0



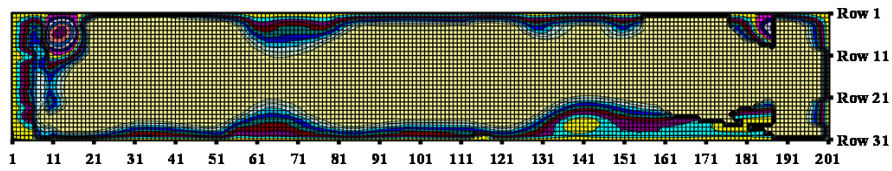
Out-of-plane deflections as function of the load of plate girder 10, 800x100, DS L-0



Out-of-plane deflections as function of the load of plate girder 10, 800x100, DS K-0

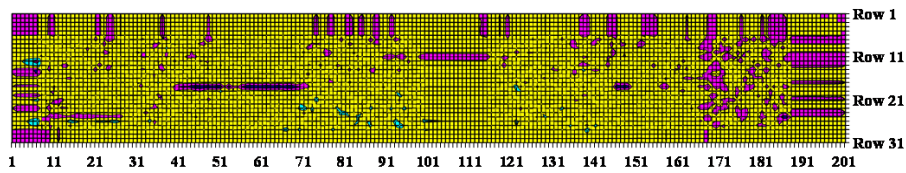


Out-of-plane deflections as function of the load of plate girder 10, 800x100, DS M-0

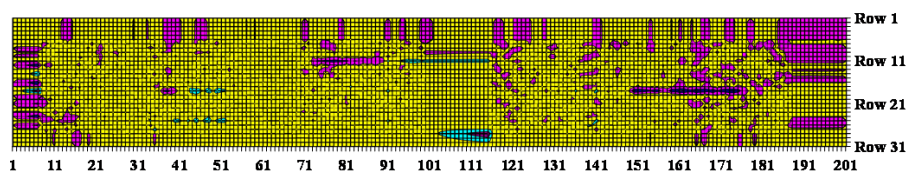


Out-of-plane deflections as function of the load of plate girder 10, 800x100, DS N-0

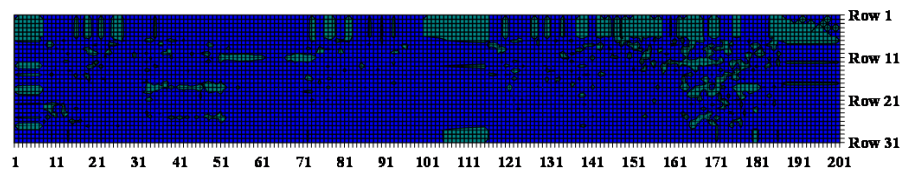
APPENDIX M INCREMENTS IN THE OUT-OF-PLANE DEFLECTIONS AS FUNCTION OF THE LOADING



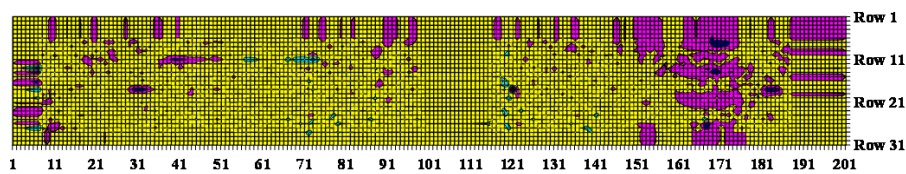
Increments in the out-of-plane deflections as function of the loading of test girder 1, 400x50, DS B-A



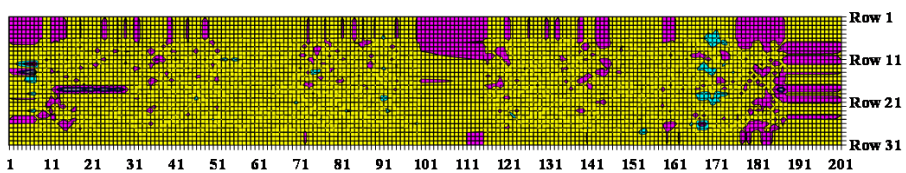
Increments in the out-of-plane deflections as function of the loading of test girder 1, 400x50, DS C-B



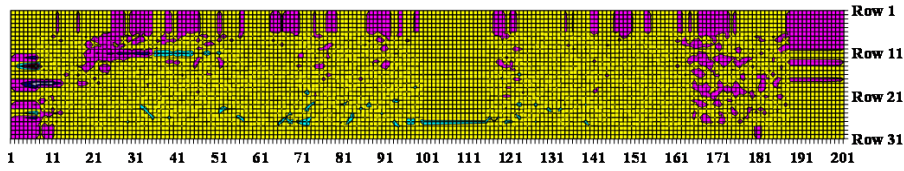
Increments in the out-of-plane deflections as function of the loading of test girder 1, 400x50, DS D-C



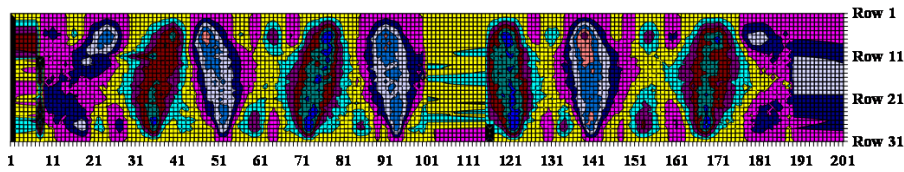
Increments in the out-of-plane deflections as function of the loading of test girder 1, 400x50, DS E-D



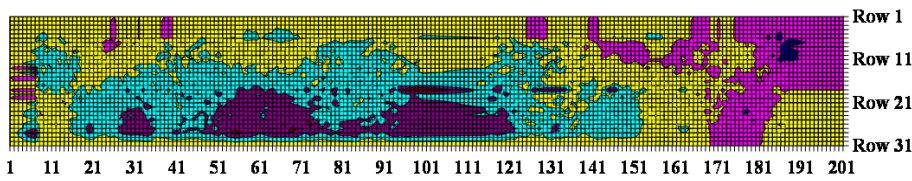
Increments in the out-of-plane deflections as function of the loading of test girder 1, 400x50, DS F-E



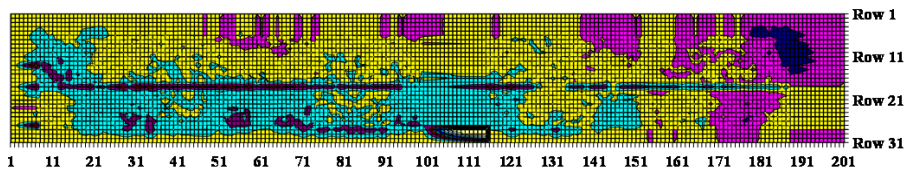
Increments in the out-of-plane deflections as function of the loading of test girder 1, 400x50, DS G-F



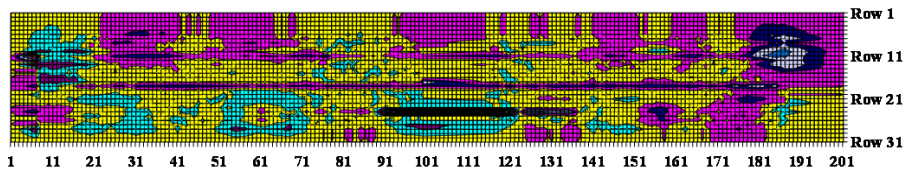
Increments in the out-of-plane deflections as function of the loading of test girder 1, 400x50, DS H-G



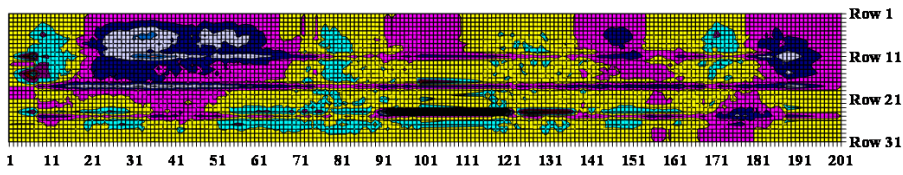
Increments in the out-of-plane deflections as function of the loading of test girder 1, 400x50, DS I-H



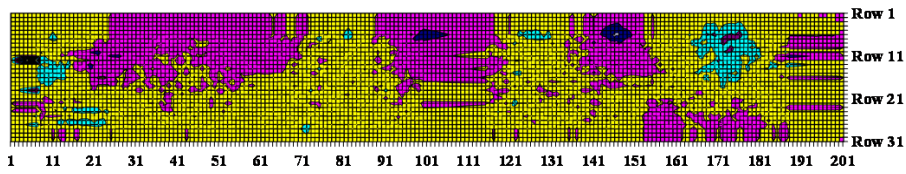
Increments in the out-of-plane deflections as function of the loading of test girder 1, 400x50, DS J-I



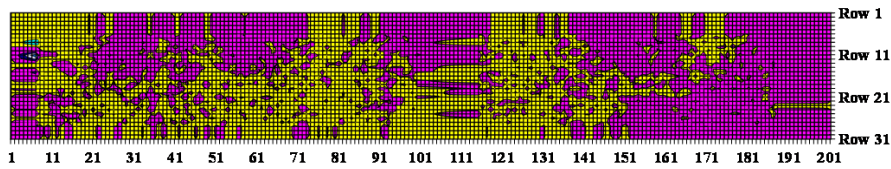
Increments in the out-of-plane deflections as function of the loading of test girder 1, 400x50, DS K-J



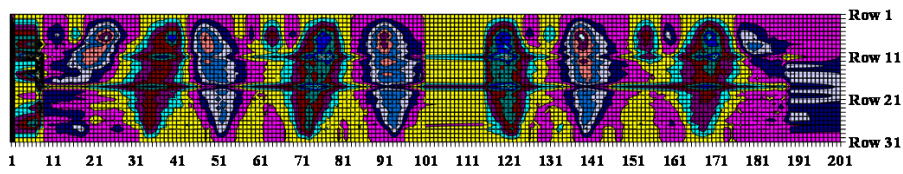
Increments in the out-of-plane deflections as function of the loading of test girder 1, 400x50, DS L-K



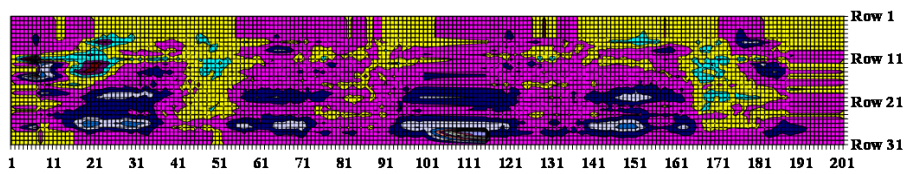
Increments in the out-of-plane deflections as function of the loading of test girder 1, 400x50, DS M-L



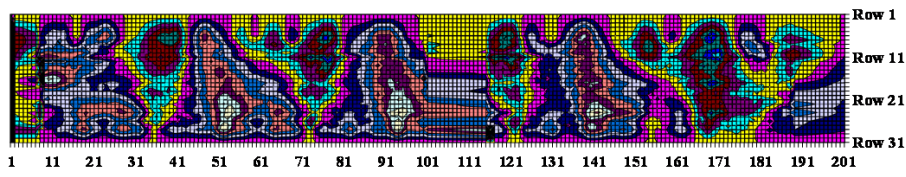
Increments in the out-of-plane deflections as function of the loading of test girder 1, 400x50, DS N-M



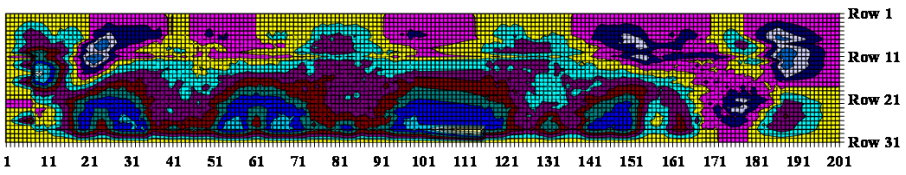
Increments in the out-of-plane deflections as function of the loading of test girder 1, 400x50, DS O-N



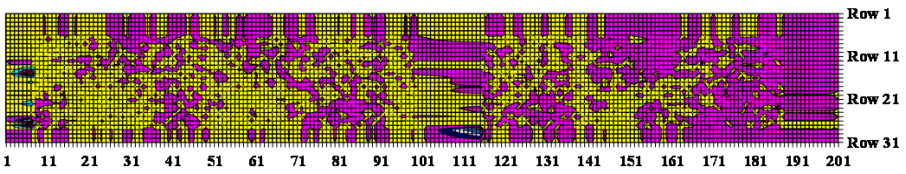
Increments in the out-of-plane deflections as function of the loading of test girder 1, 400x50, DS P-O



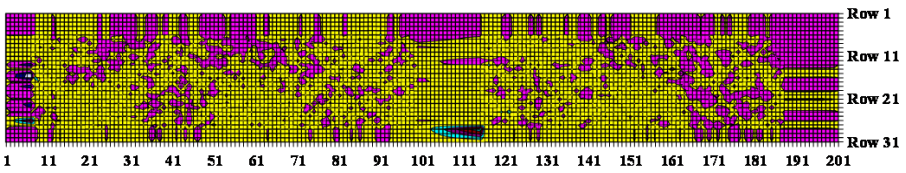
Increments in the out-of-plane deflections as function of the loading of test girder 1, 400x50, DS Q-P



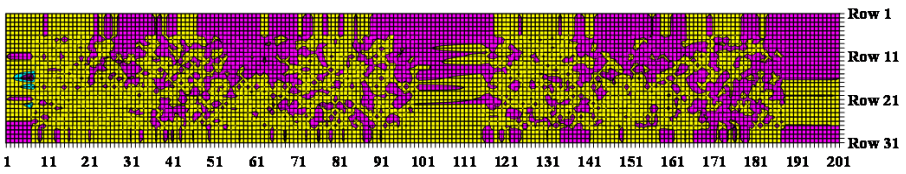
Increments in the out-of-plane deflections as function of the loading of test girder 1, 400x50, DS R-Q



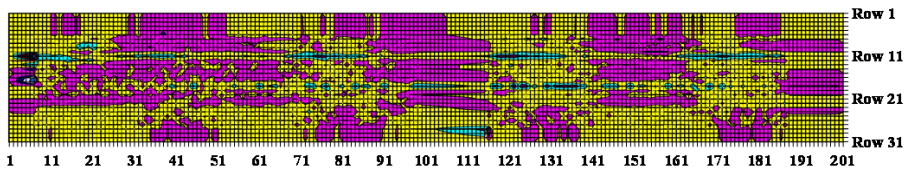
Increments in the out-of-plane deflections as function of the loading of test girder 1, 400x50, DS U-R



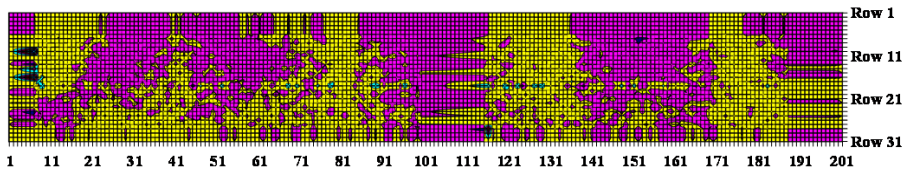
Increments in the out-of-plane deflections as function of the loading of test girder 1, 400x50, DS V-U



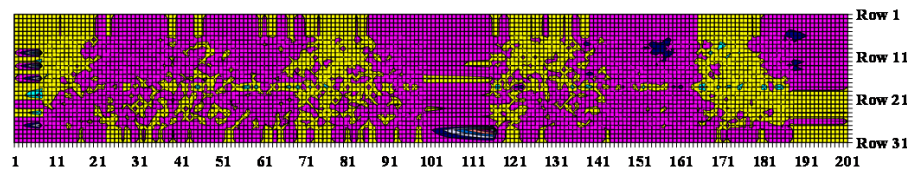
Increments in the out-of-plane deflections as function of the loading of test girder 1, 400x50, DS W-V



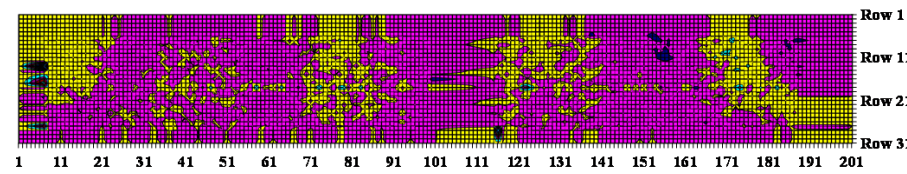
Increments in the out-of-plane deflections as function of the loading of test girder 1, 400x50, DS Y-W



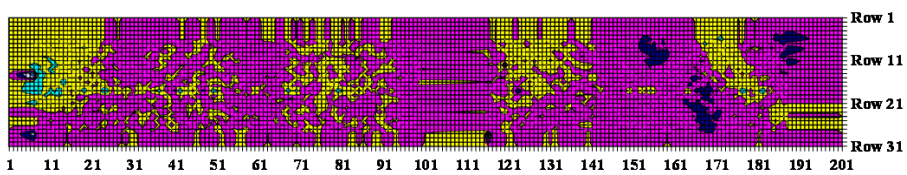
Increments in the out-of-plane deflections as function of the loading of test girder 1, 400x50, DS Z-Y



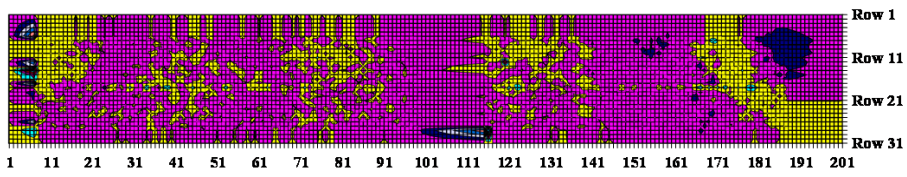
Increments in the out-of-plane deflections as function of the loading of test girder 1, 400x50, DS AA-Z



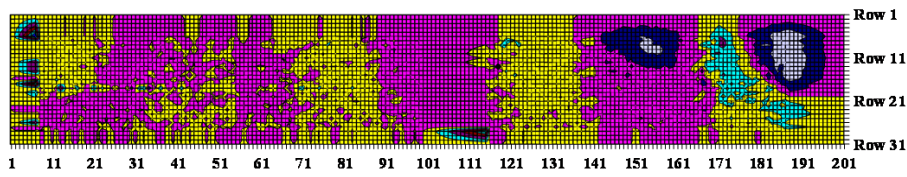
Increments in the out-of-plane deflections as function of the loading of test girder 1, 400x50, DS AB-AA



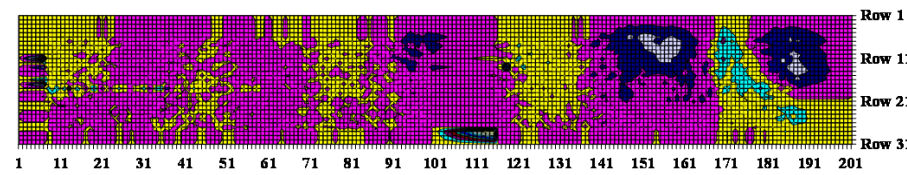
Increments in the out-of-plane deflections as function of the loading of test girder 1, 400x50, DS AC-AB



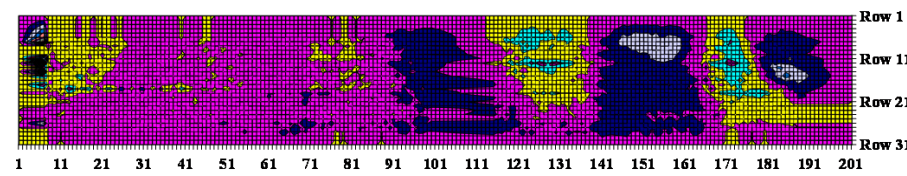
Increments in the out-of-plane deflections as function of the loading of test girder 1, 400x50, DS AD-AC



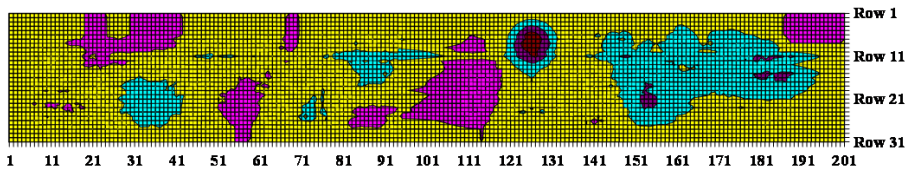
Increments in the out-of-plane deflections as function of the loading of test girder 1, 400x50, AE-AD



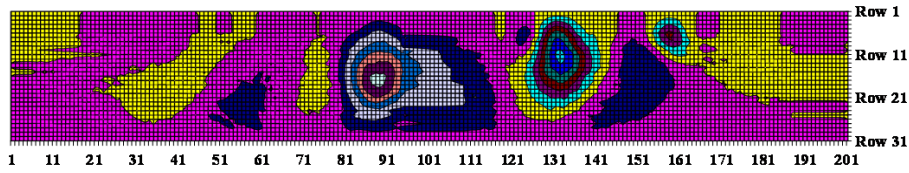
Increments in the out-of-plane deflections as function of the loading of test girder 1, 400x50, DS AF-AE



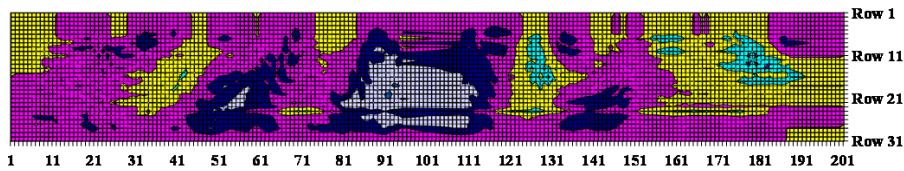
Increments in the out-of-plane deflections as function of the loading of test girder 1, 400x50, AG-AF



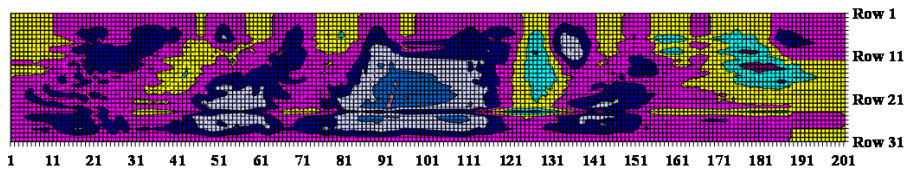
Increments out-of-plane deflections of plate girder 2, 400x80(1), DS B-A



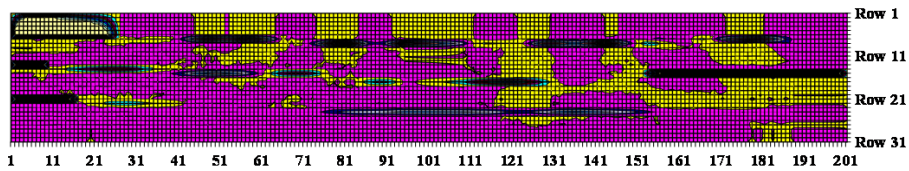
Increments out-of-plane deflections of plate girder 2, 400x80(1), DS C-B



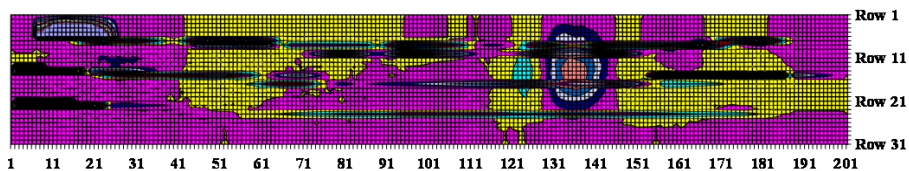
Increments out-of-plane deflections of plate girder 2, 400x80(1), DS D-C



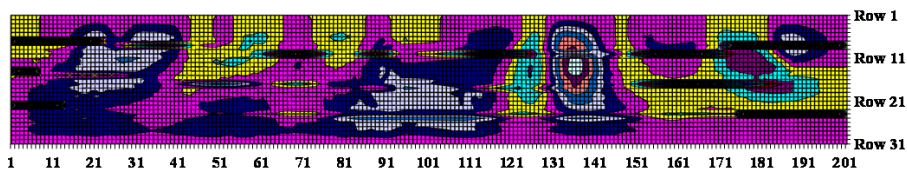
Increments out-of-plane deflections of plate girder 2, 400x80(1), DS E-D



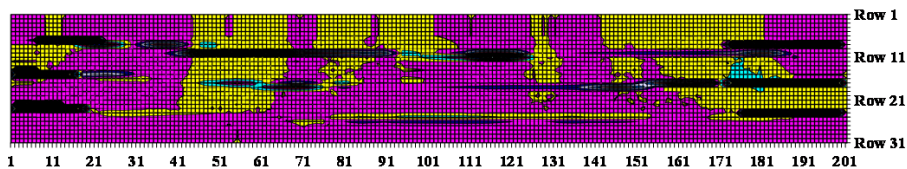
Increments out-of-plane deflections of plate girder 2, 400x80(1), DS F-E



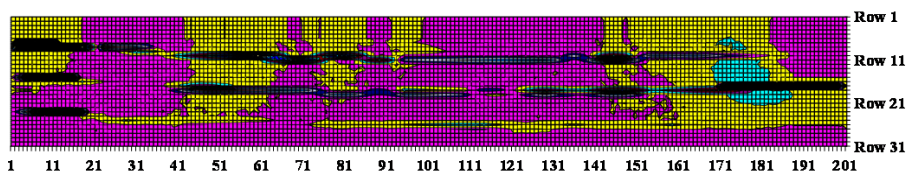
Increments out-of-plane deflections of plate girder 2, 400x80(1), DS G-F



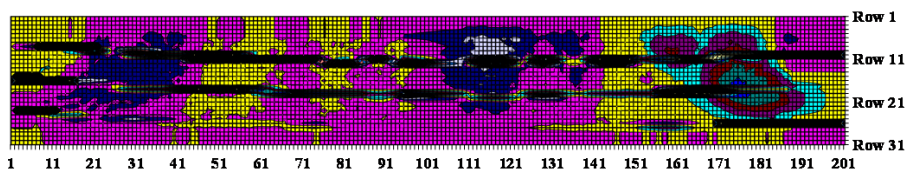
Increments out-of-plane deflections of plate girder 2, 400x80(1), DS H-G



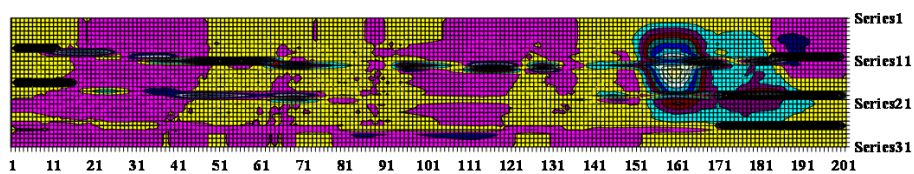
Increments out-of-plane deflections of plate girder 2, 400x80(1), DS I-H



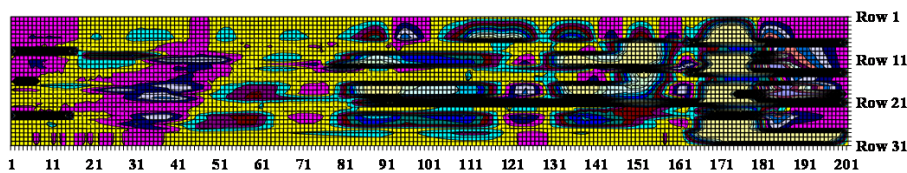
Increments out-of-plane deflections of plate girder 2, 400x80(1), DS J-I



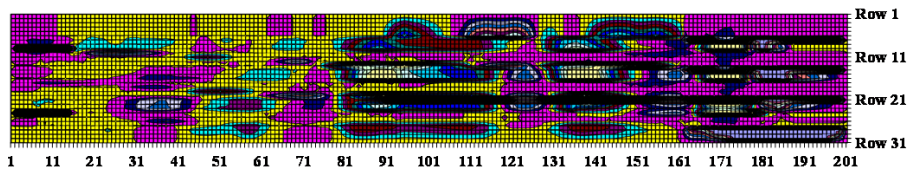
Increments out-of-plane deflections of plate girder 2, 400x80(1), DS K-J



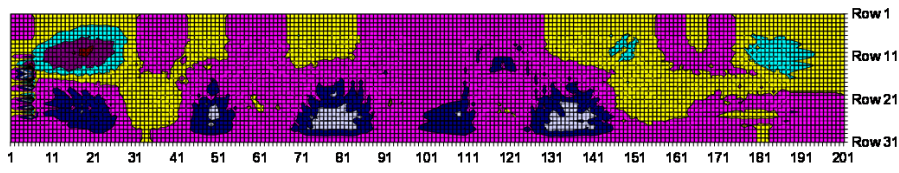
Increments out-of-plane deflections of plate girder 2, 400x80(1), DS L-K



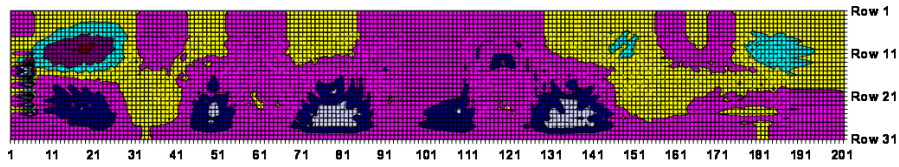
Increments out-of-plane deflections of plate girder 2, 400x80(1), DS M-L



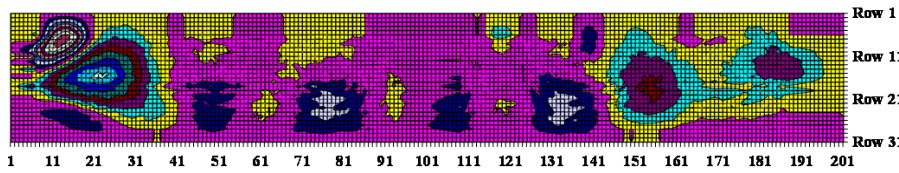
Increments out-of-plane deflections of plate girder 2, 400x80(1), DS N-M



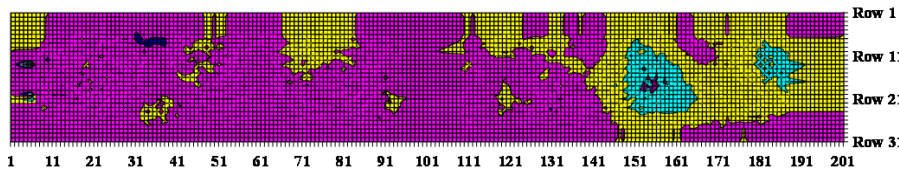
Increment out-of-plane deflections of plate girder 3, 400x80(2), DS B-A



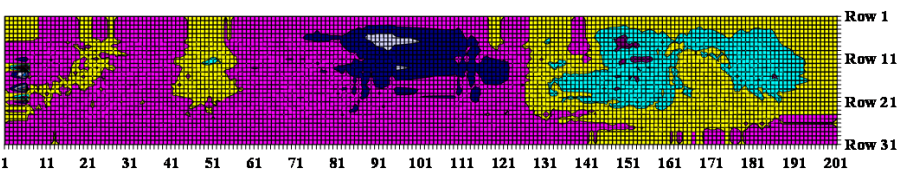
Increment out-of-plane deflections of plate girder 3, 400x80(2), DS C-B



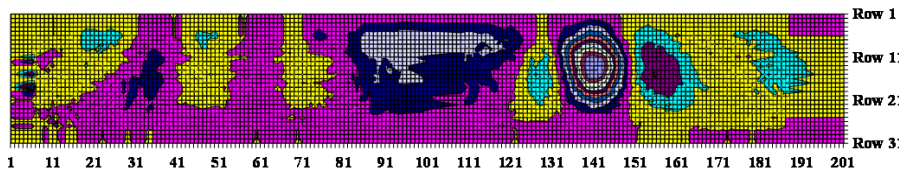
Increment out-of-plane deflections of plate girder 3, 400x80(2), DS D-C



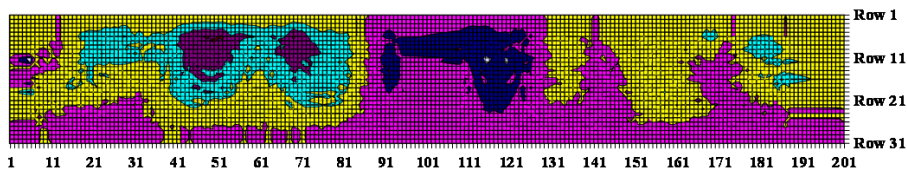
Increment out-of-plane deflections of plate girder 3, 400x80(2), DS E-D



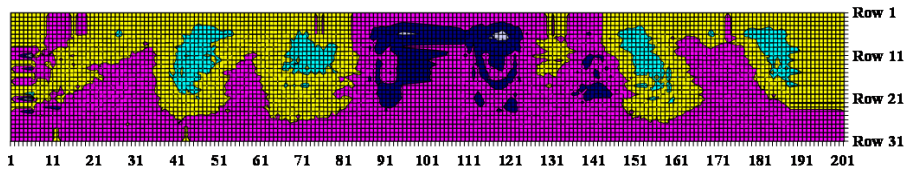
Increment out-of-plane deflections of plate girder 3, 400x80(2), DS F-E



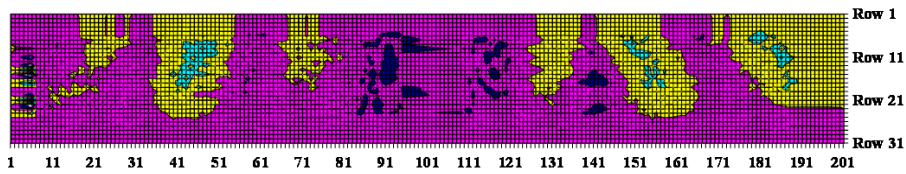
Increment out-of-plane deflections of plate girder 3, 400x80(2), DS G-F



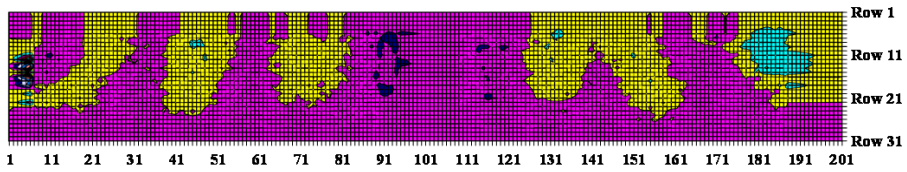
Increment out-of-plane deflections of plate girder 3, 400x80(2), DS H-G



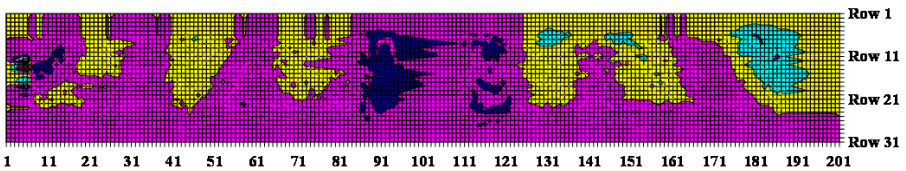
Increment out-of-plane deflections of plate girder 3, 400x80(2), DS I-H



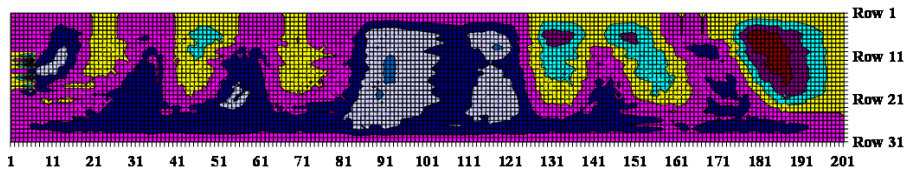
Increment out-of-plane deflections of plate girder 3, 400x80(2), DS J-I



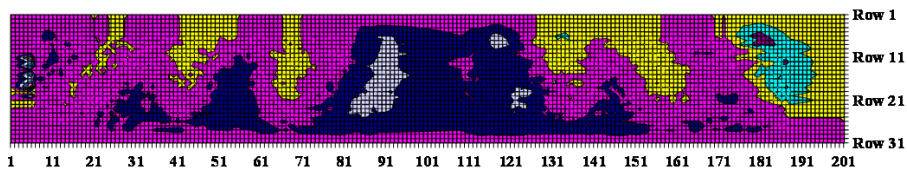
Increment out-of-plane deflections of plate girder 3, 400x80(2), DS K-J



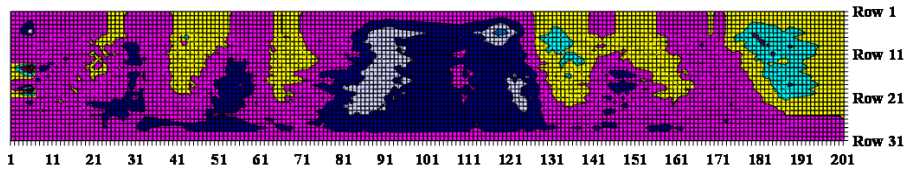
Increment out-of-plane deflections of plate girder 3, 400x80(2), DS M-L



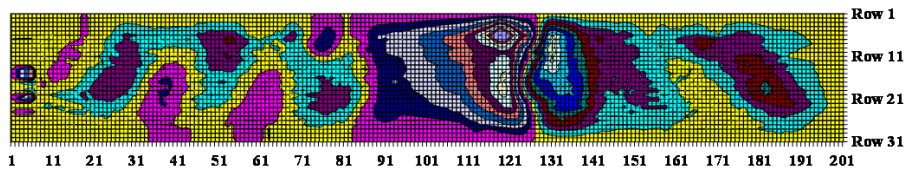
Increment out-of-plane deflections of plate girder 3, 400x80(2), DS L-K



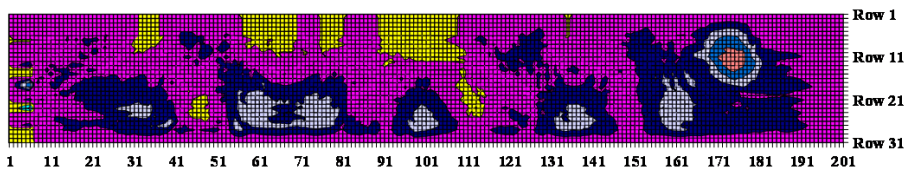
Increment out-of-plane deflections of plate girder 3, 400x80(2), DS N-M



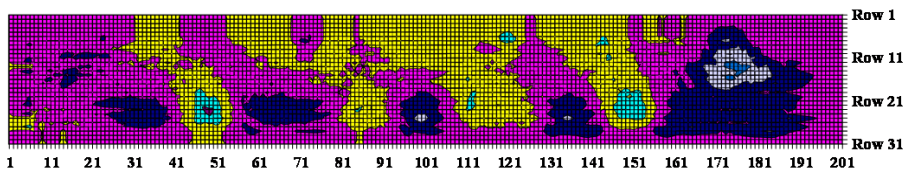
Increment out-of-plane deflections of plate girder 3, 400x80(2), DS O-N



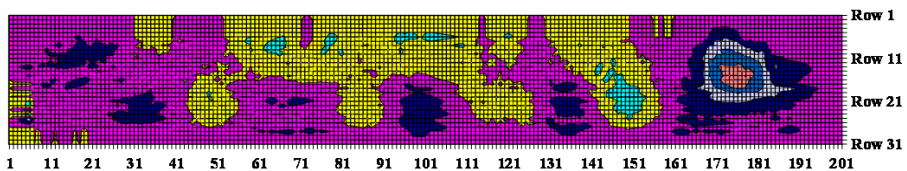
Increment out-of-plane deflections of plate girder 3, 400x80(2), DS P-O



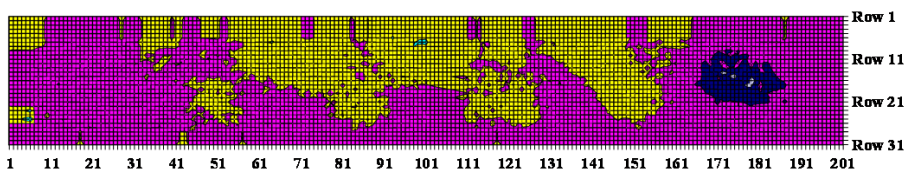
Increment out-of-plane deflections of plate girder 4, 400x100, DS B-A



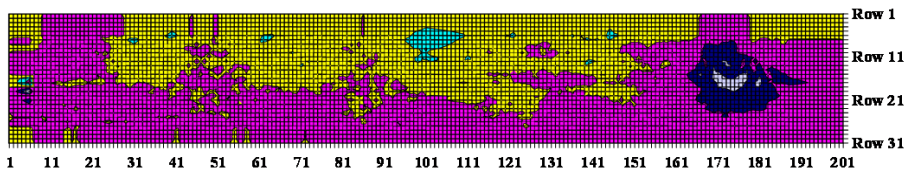
Increment out-of-plane deflections of plate girder 4, 400x100, DS C-B



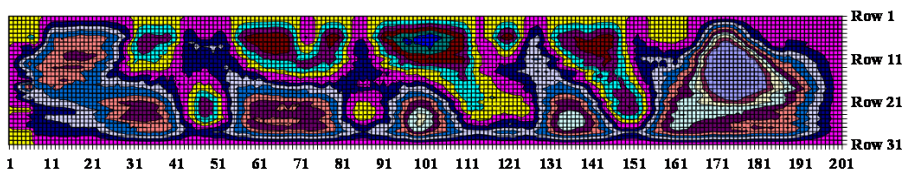
Increment out-of-plane deflections of plate girder 4, 400x100, DS D-C



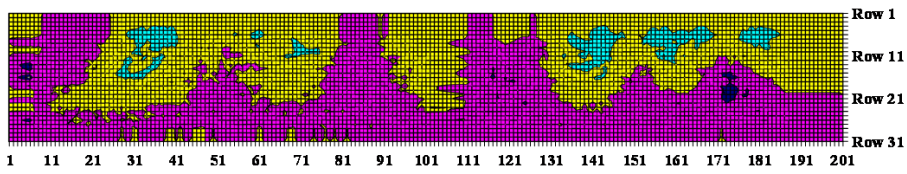
Increment out-of-plane deflections of plate girder 4, 400x100, DS E-D



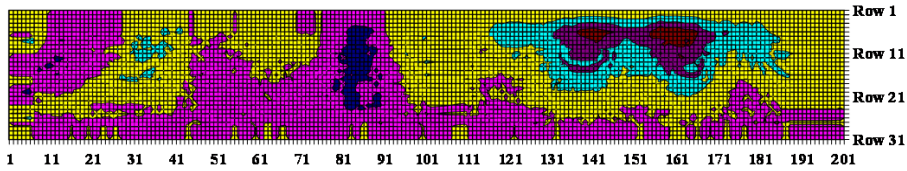
Increment out-of-plane deflections of plate girder 4, 400x100, DS F-E



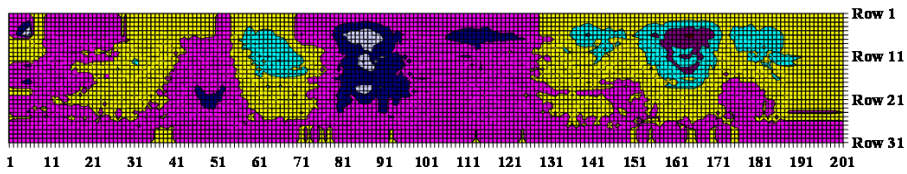
Increment out-of-plane deflections of plate girder 4, 400x100, DS G-F



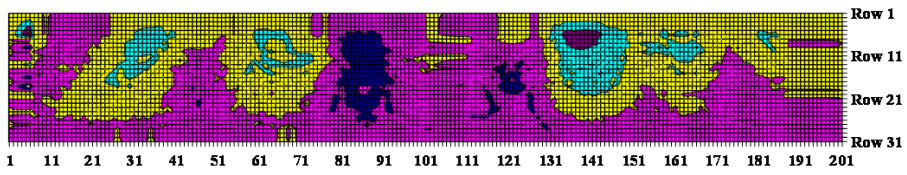
Increment out-of-plane deflections of plate girder 4, 400x100, DS H-G



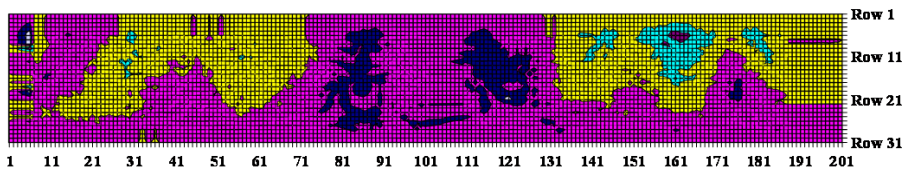
Increment out-of-plane deflections of plate girder 4, 400x100, DS I-H



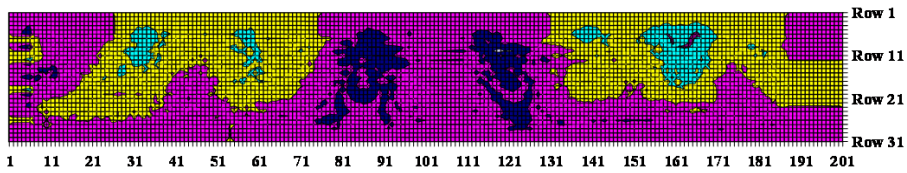
Increment out-of-plane deflections of plate girder 4, 400x100, DS J-I



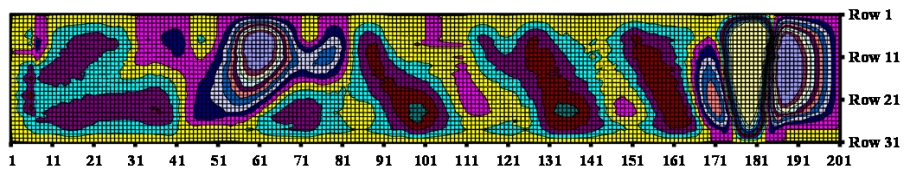
Increment out-of-plane deflections of plate girder 4, 400x100, DS K-J



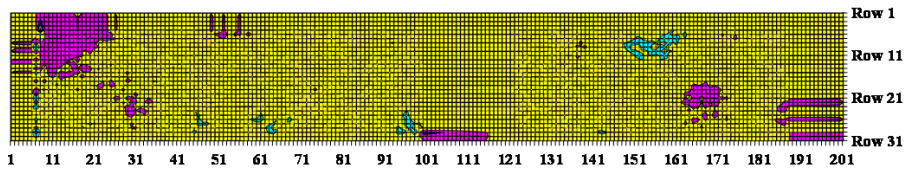
Increment out-of-plane deflections of plate girder 4, 400x100, DS L-K



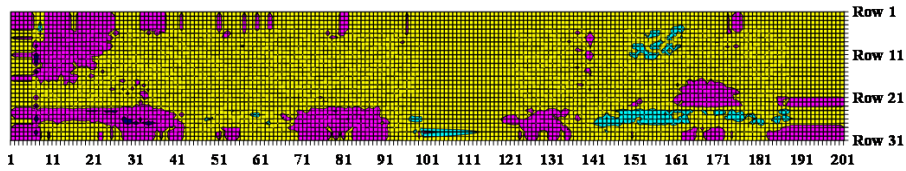
Increment out-of-plane deflections of plate girder 4, 400x100, DS M-L



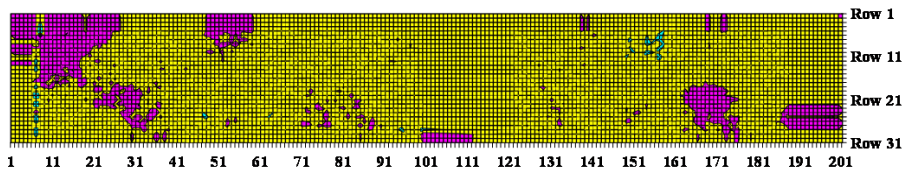
Increment out-of-plane deflections of plate girder 4, 400x100, DS N-M



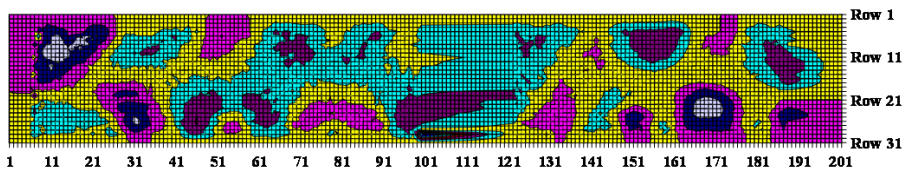
Increment out-of-plane deflections of plate girder 5, 600x50, DS B-A



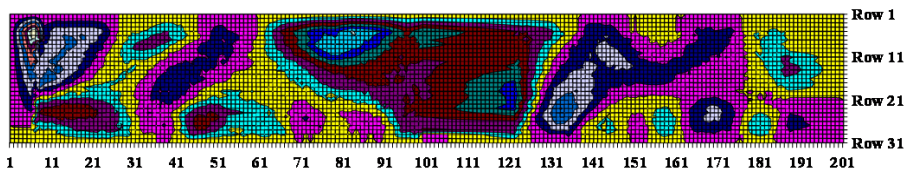
Increment out-of-plane deflections of plate girder 5, 600x50, DS C-B



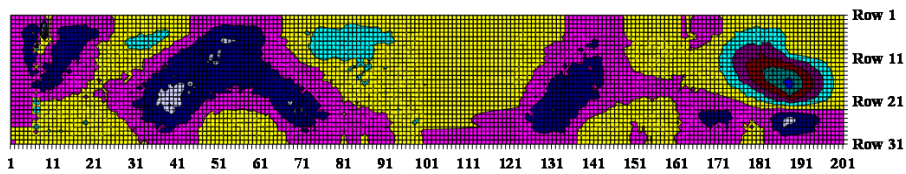
Increment out-of-plane deflections of plate girder 5, 600x50, DS D-C



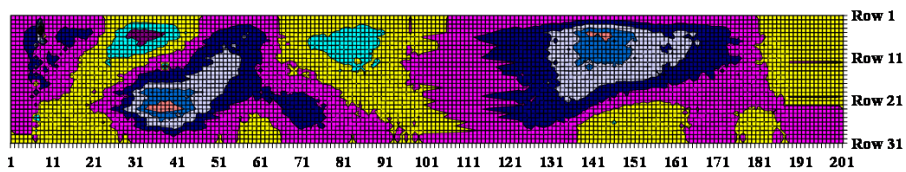
Increment out-of-plane deflections of plate girder 5, 600x50, DS E-D



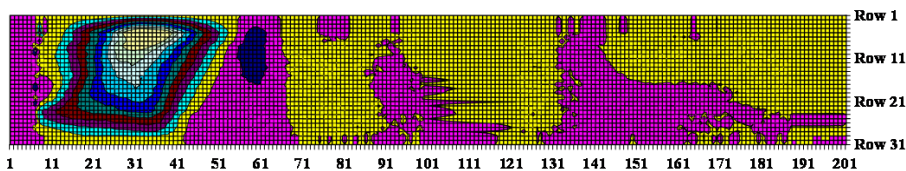
Increment out-of-plane deflections of plate girder 5, 600x50, DS F-E



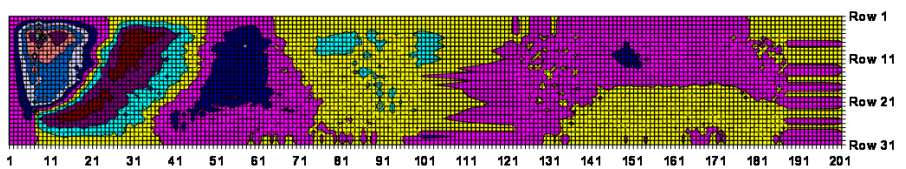
Increment out-of-plane deflections of plate girder 5, 600x50, DS G-F



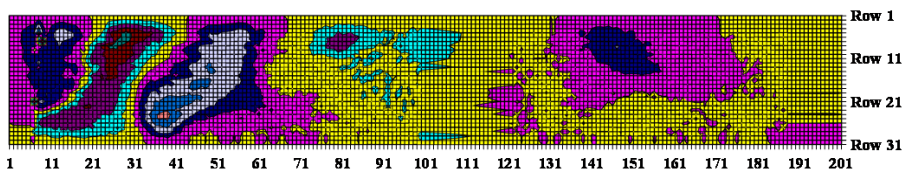
Increment out-of-plane deflections of plate girder 5, 600x50, DS H-G



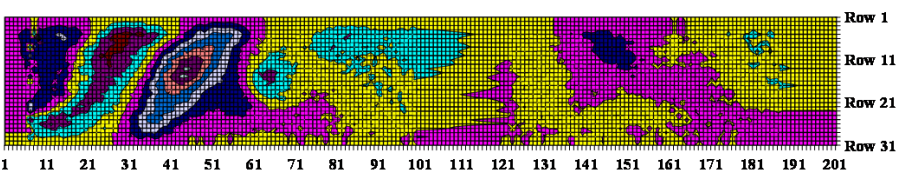
Increment out-of-plane deflections of plate girder 5, 600x50, DS I-H



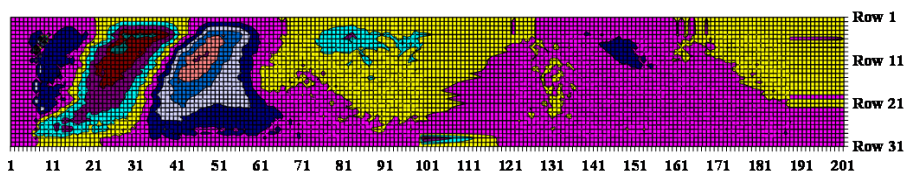
Increment out-of-plane deflections of plate girder 5, 600x50, DS J-I



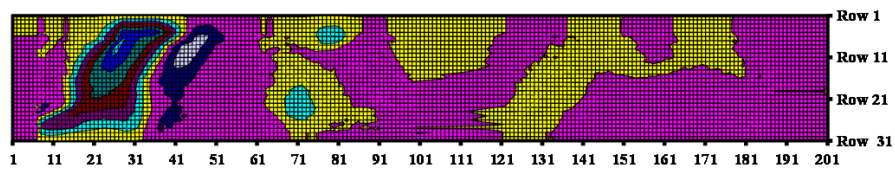
Increment out-of-plane deflections of plate girder 5, 600x50, DS K-J



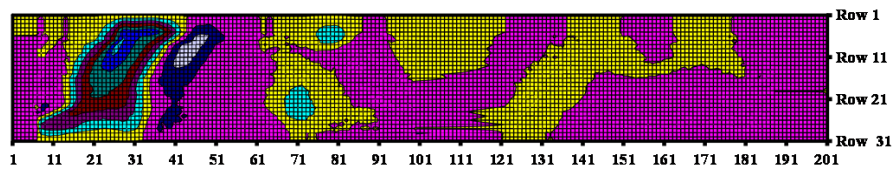
Increment out-of-plane deflections of plate girder 5, 600x50, DS L-K



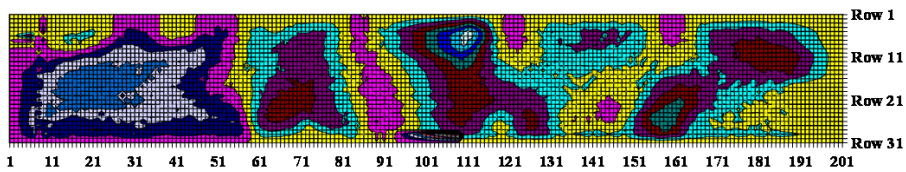
Increment out-of-plane deflections of plate girder 5, 600x50, DS M-L



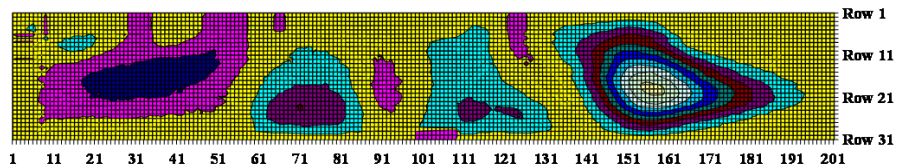
Increment out-of-plane deflections of plate girder 5, 600x50, DS N-M



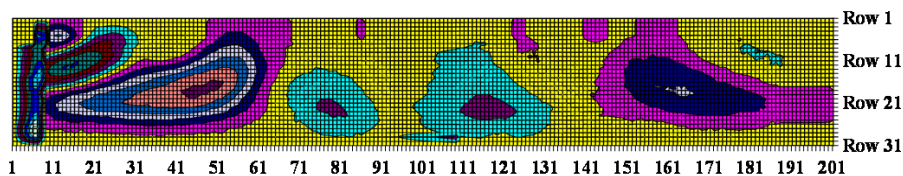
Increment out-of-plane deflections of plate girder 5, 600x50, DS O-N



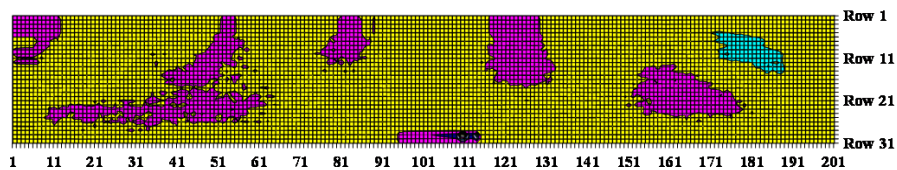
Increment out-of-plane deflections of plate girder 6, 600x80, DS B-A



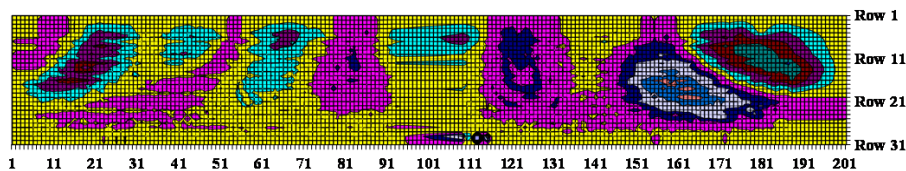
Increment out-of-plane deflections of plate girder 6, 600x80, DS C-B



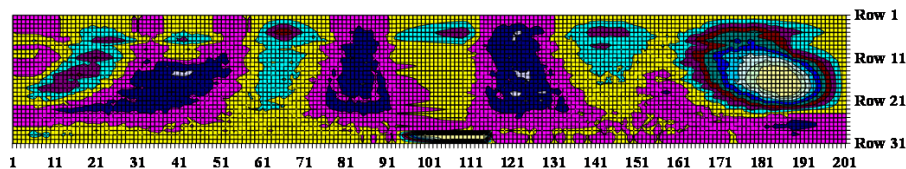
Increment out-of-plane deflections of plate girder 6, 600x80, DS D-C



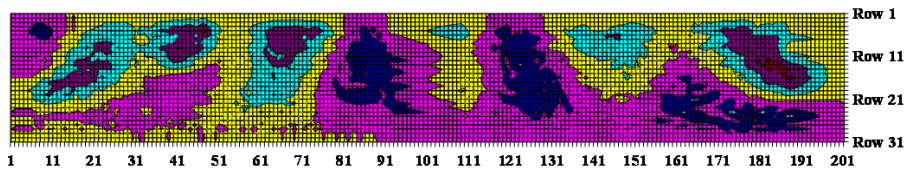
Increment out-of-plane deflections of plate girder 6, 600x80, DS E-D



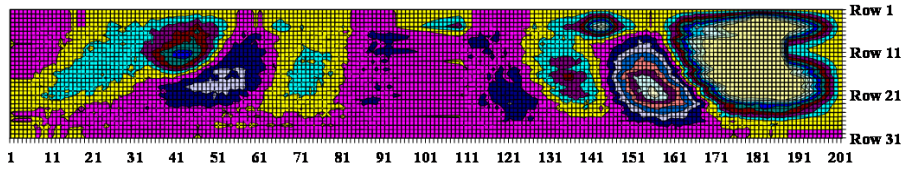
Increment out-of-plane deflections of plate girder 6, 600x80, DS F-E



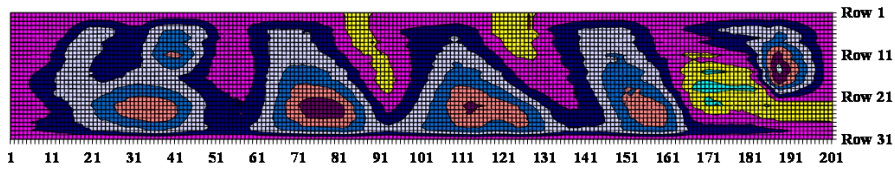
Increment out-of-plane deflections of plate girder 6, 600x80, DS G-F



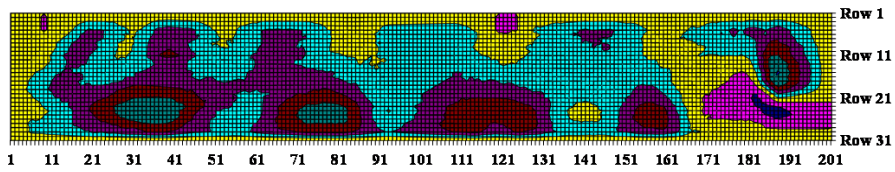
Increment out-of-plane deflections of plate girder 6, 600x80, DS H-G



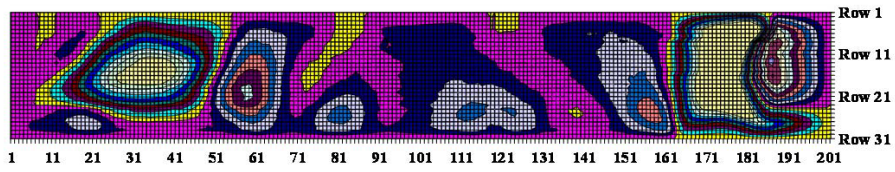
Increment out-of-plane deflections of plate girder 6, 600x80, DS I-H



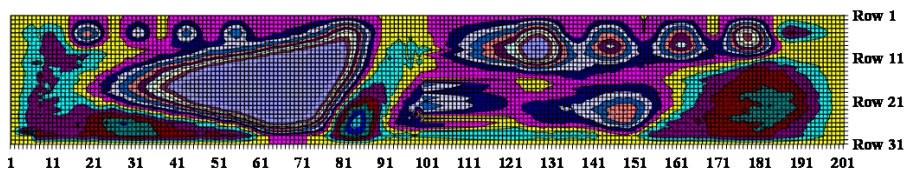
Increment out-of-plane deflections of plate girder 6, 600x80, DS J-I



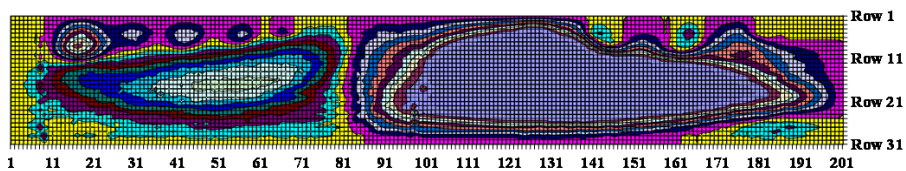
Increment out-of-plane deflections of plate girder 6, 600x80, DS K-J



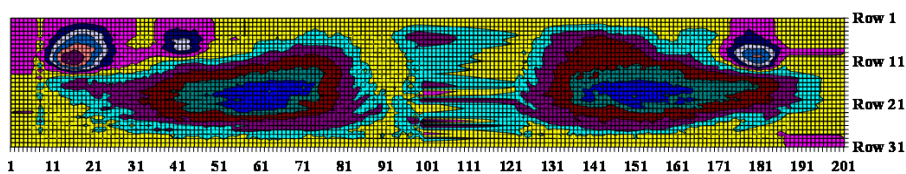
Increment out-of-plane deflections of plate girder 6, 600x80, DS L-K



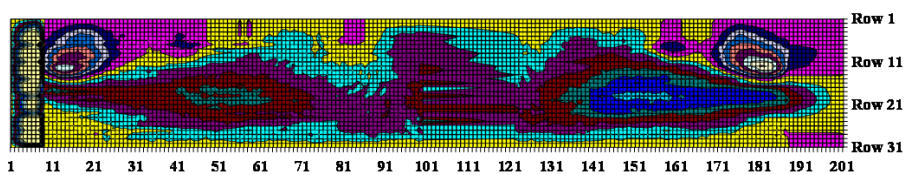
Increment out-of-plane deflections of plate girder 7, 600x100, DS B-A



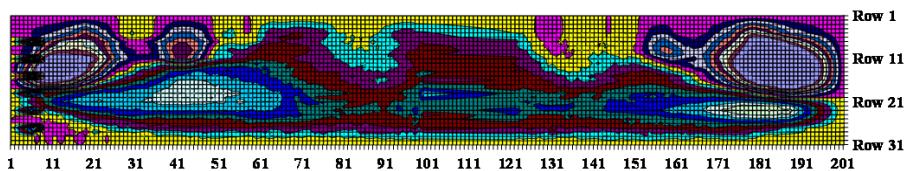
Increment out-of-plane deflections of plate girder 7, 600x100, DS C-B



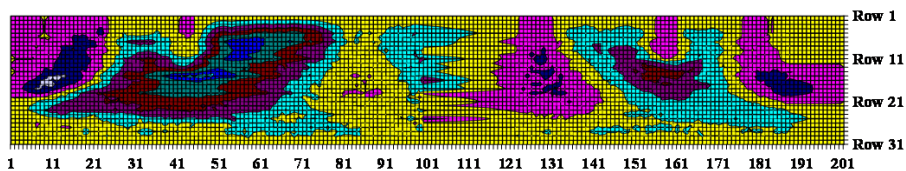
Increment out-of-plane deflections of plate girder 7, 600x100, DS D-C



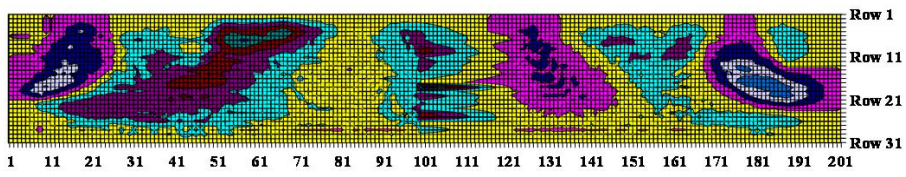
Increment out-of-plane deflections of plate girder 7, 600x100, DS E-D



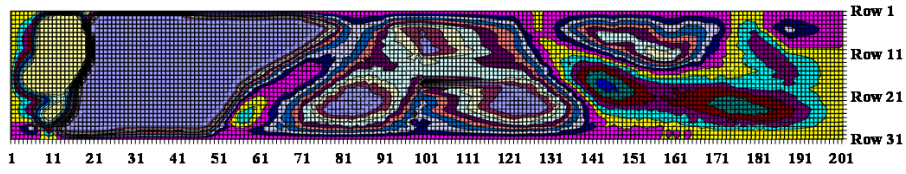
Increment out-of-plane deflections of plate girder 7, 600x100, DS F-E



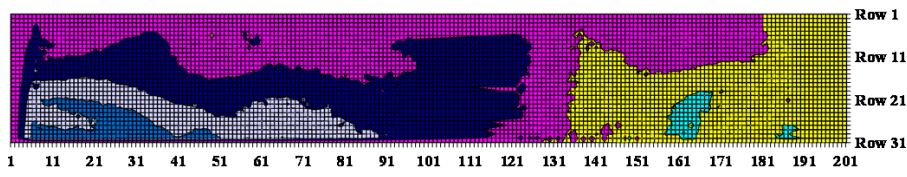
Increment out-of-plane deflections of plate girder 7, 600x100, DS G-F



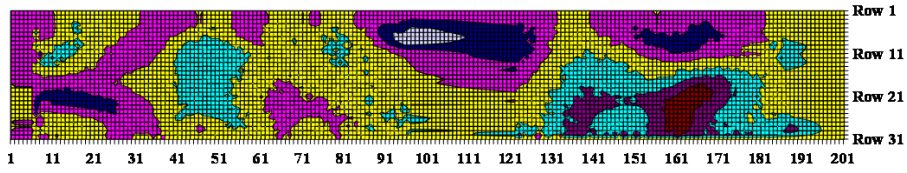
Increment out-of-plane deflections of plate girder 7, 600x100, DS H-G



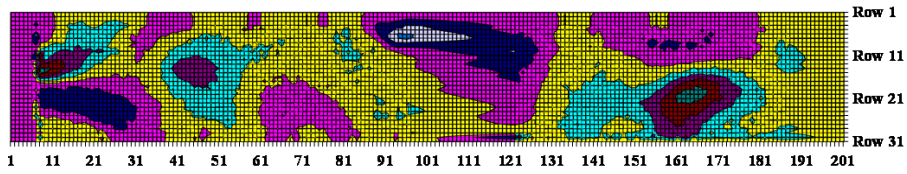
Increment out-of-plane deflections of plate girder 7, 600x100, DS I-H



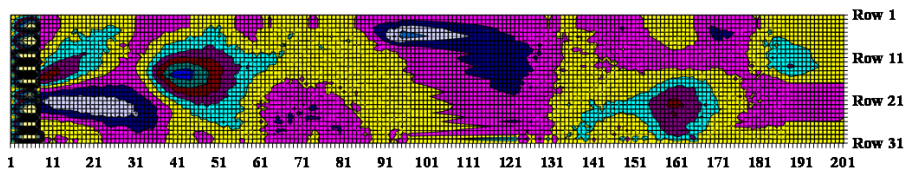
Increment out-of-plane deflections of plate girder 8, 800x50, DS B-A



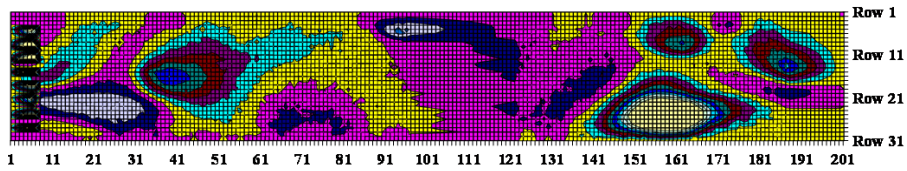
Increment out-of-plane deflections of plate girder 8, 800x50, DS C-B



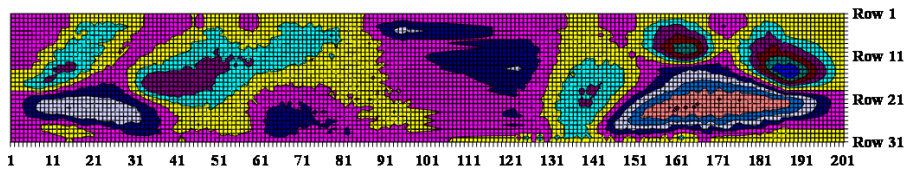
Increment out-of-plane deflections of plate girder 8, 800x50, DS D-C



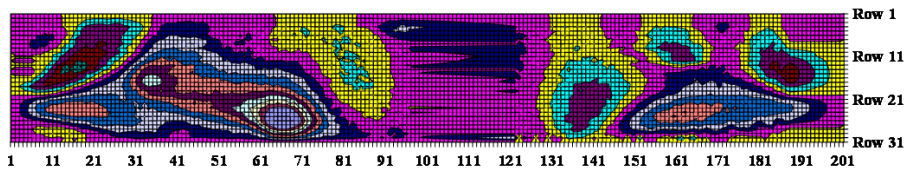
Increment out-of-plane deflections of plate girder 8, 800x50, DS E-D



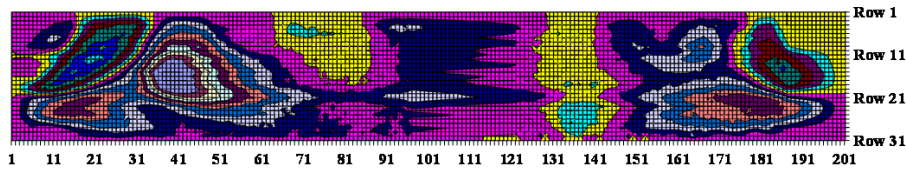
Increment out-of-plane deflections of plate girder 8, 800x50, DS F-E



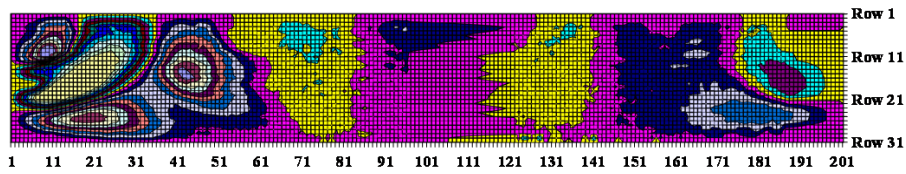
Increment out-of-plane deflections of plate girder 8, 800x50, DS G-F



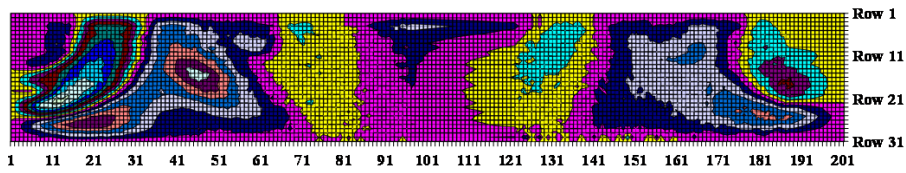
Increment out-of-plane deflections of plate girder 8, 800x50, DS H-G



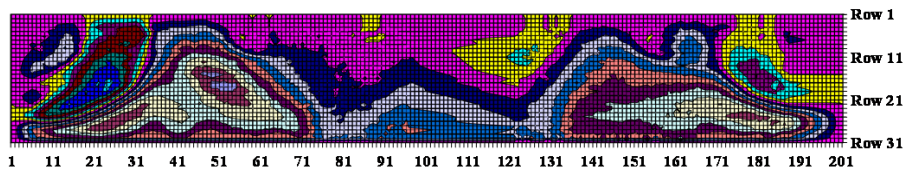
Increment out-of-plane deflections of plate girder 8, 800x50, DS I-H



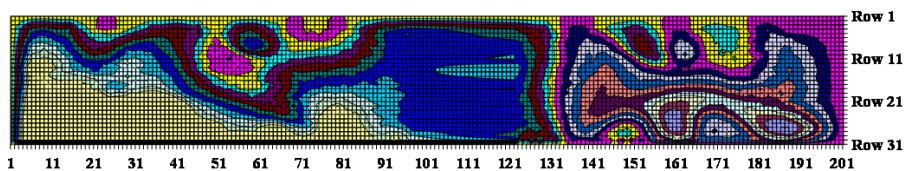
Increment out-of-plane deflections of plate girder 8, 800x50, DS J-I



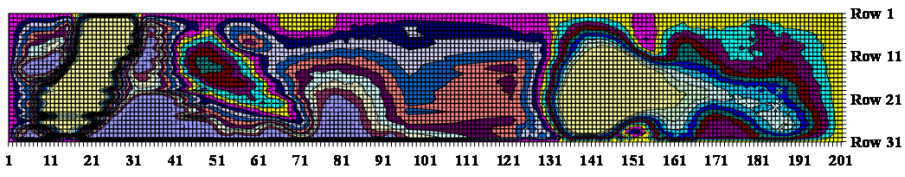
Increment out-of-plane deflections of plate girder 8, 800x50, DS K-J



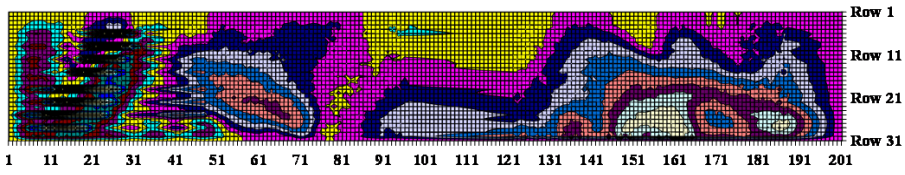
Increment out-of-plane deflections of plate girder 8, 800x50, DS L-K



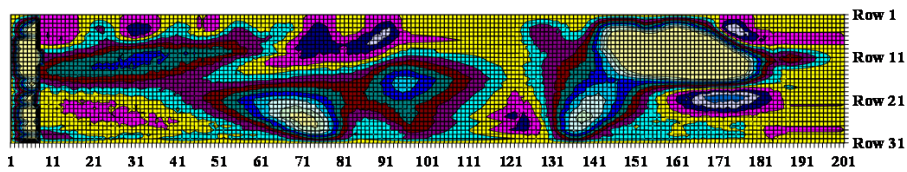
Increment out-of-plane deflections of plate girder 8, 800x50, DS M-L



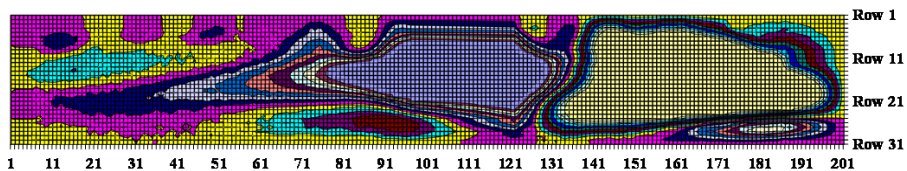
Increment out-of-plane deflections of plate girder 8, 800x50, DS O-N



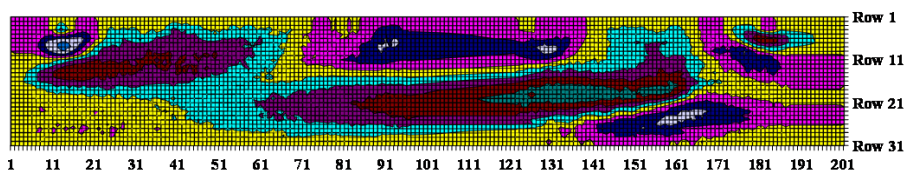
Increment out-of-plane deflections of plate girder 8, 800x50, DS P-O



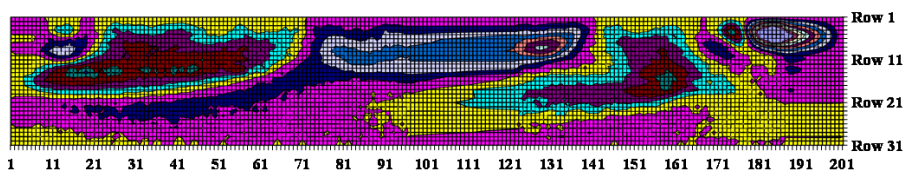
Increment out-of-plane deflections of plate girder 9, 800x80, DS B-A



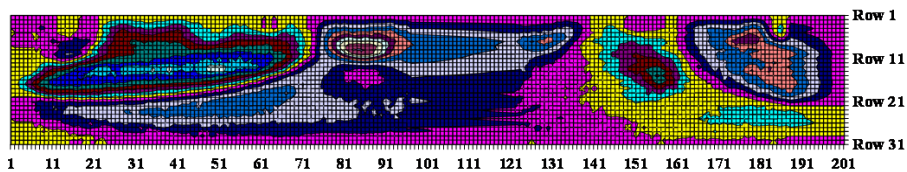
Increment out-of-plane deflections of plate girder 9, 800x80, DS C-B



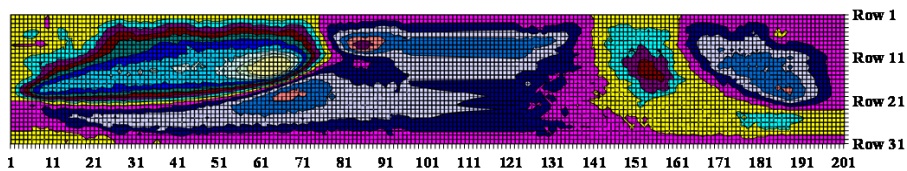
Increment out-of-plane deflections of plate girder 9, 800x80, DS D-C



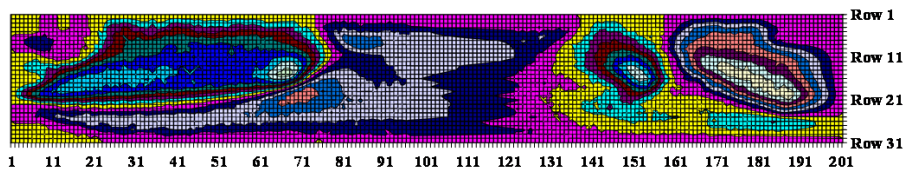
Increment out-of-plane deflections of plate girder 9, 800x80, DS E-D



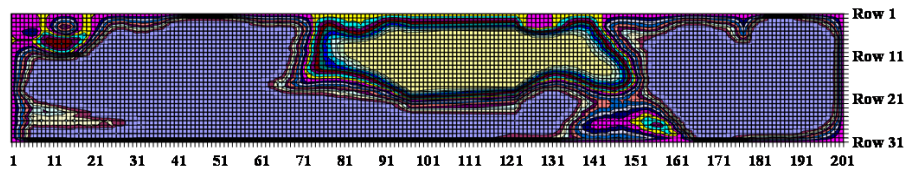
Increment out-of-plane deflections of plate girder 9, 800x80, DS F-E



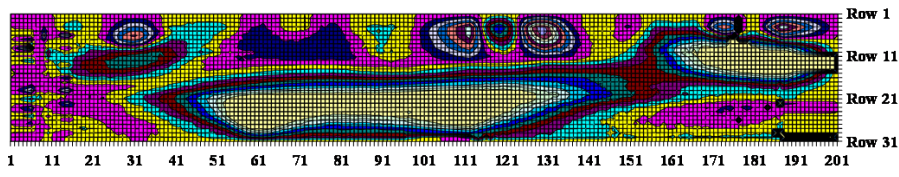
Increment out-of-plane deflections of plate girder 9, 800x80, DS G-F



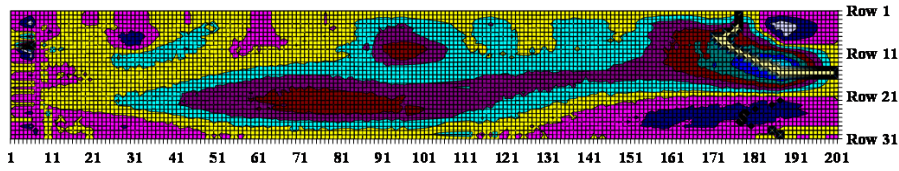
Increment out-of-plane deflections of plate girder 9, 800x80, DS H-G



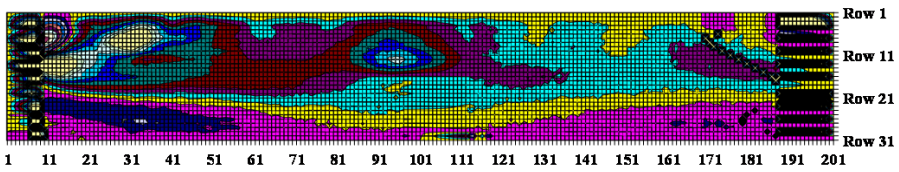
Increment out-of-plane deflections of plate girder 9, 800x80, DS I-H



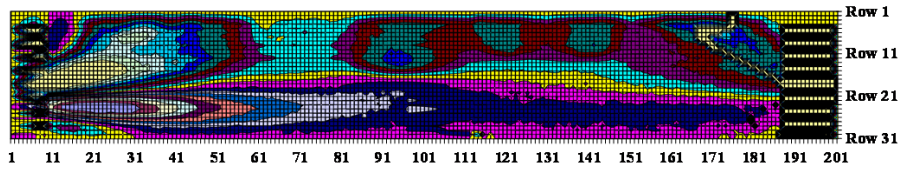
Increment out-of-load deflections of plate girder 10, 800x100, DS B-A



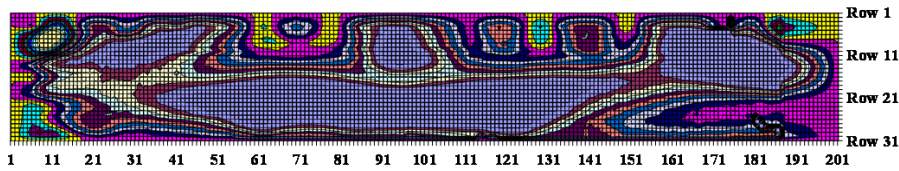
Increment out-of-load deflections of plate girder 10, 800x100, DS C-B



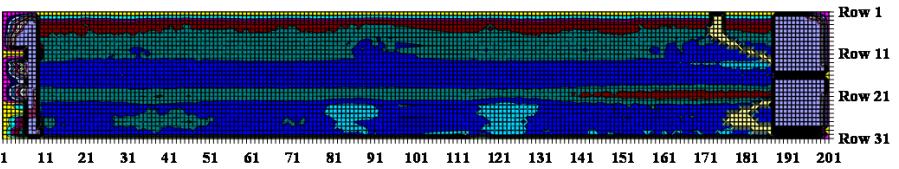
Increment out-of-load deflections of plate girder 10, 800x100, DS D-C



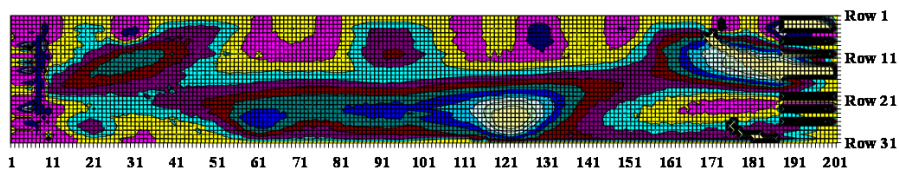
Increment out-of-load deflections of plate girder 10, 800x100, DS E-D



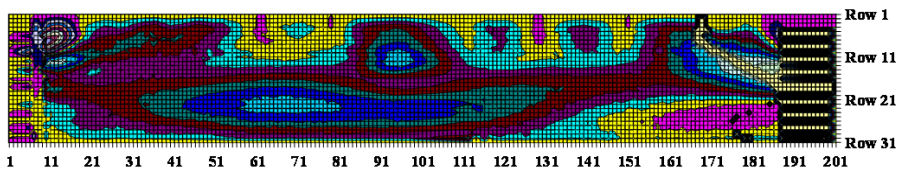
Increment out-of-load deflections of plate girder 10, 800x100, DS F-E



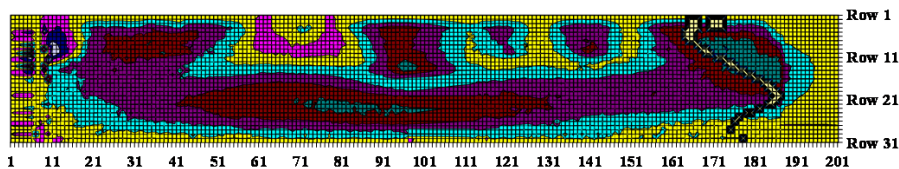
Increment out-of-load deflections of plate girder 10, 800x100, DS G-F



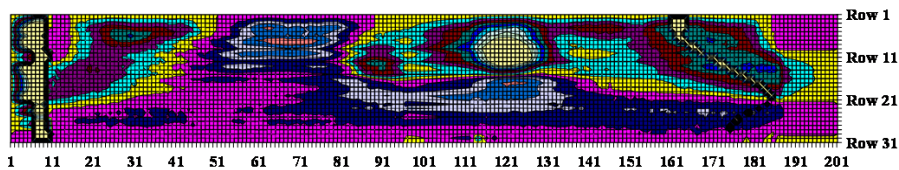
Increment out-of-load deflections of plate girder 10, 800x100, DS H-G



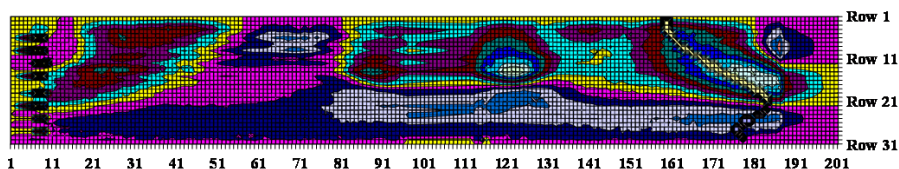
Increment out-of-load deflections of plate girder 10, 800x100, DS I-H



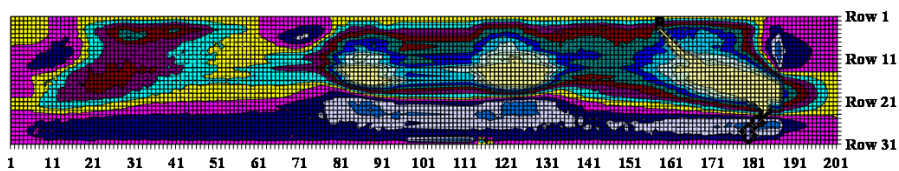
Increment out-of-load deflections of plate girder 10, 800x100, DS J-I



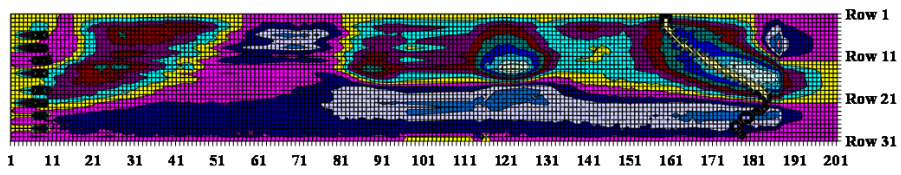
Increment out-of-load deflections of plate girder 10, 800x100, DS K-J



Increment out-of-load deflections of plate girder 10, 800x100, DS L-K

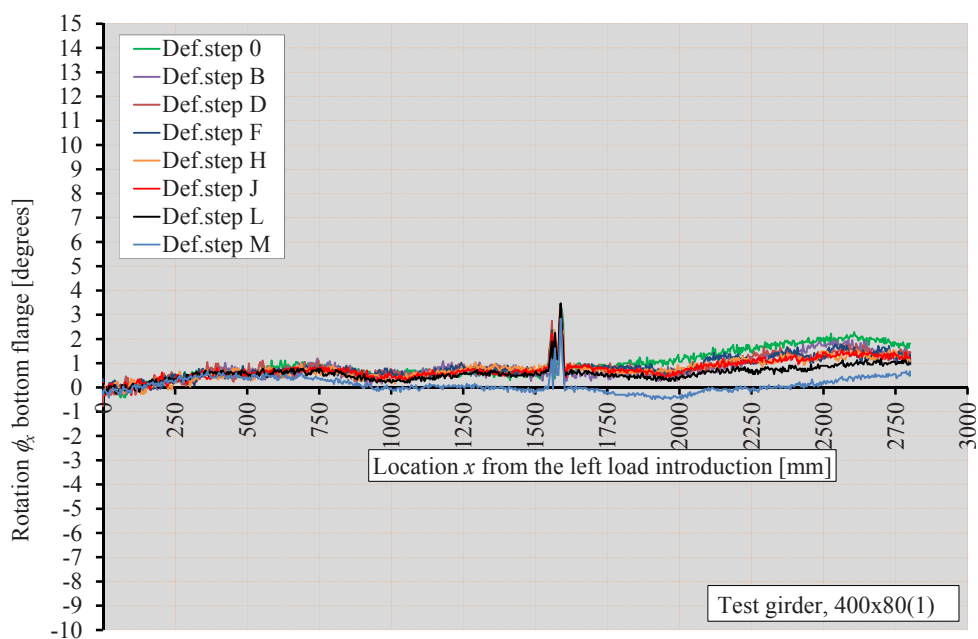
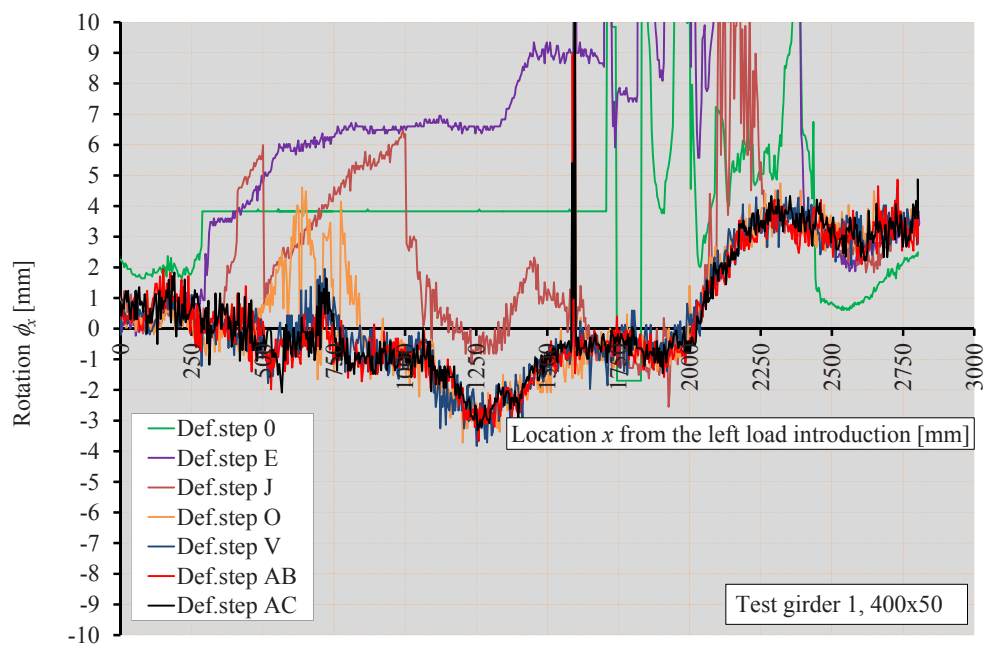


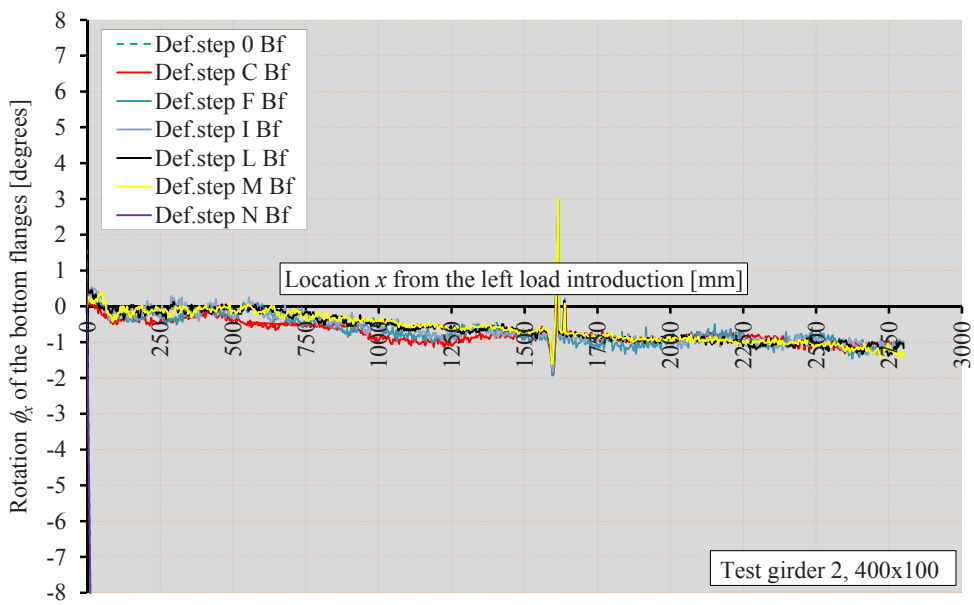
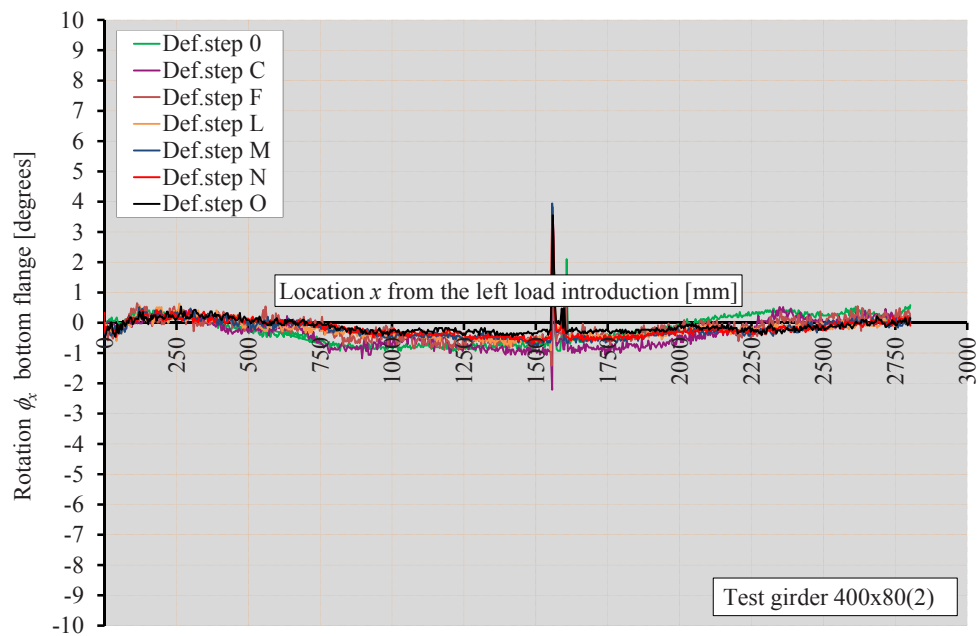
Increment out-of-load deflections of plate girder 10, 800x100, DS M-L

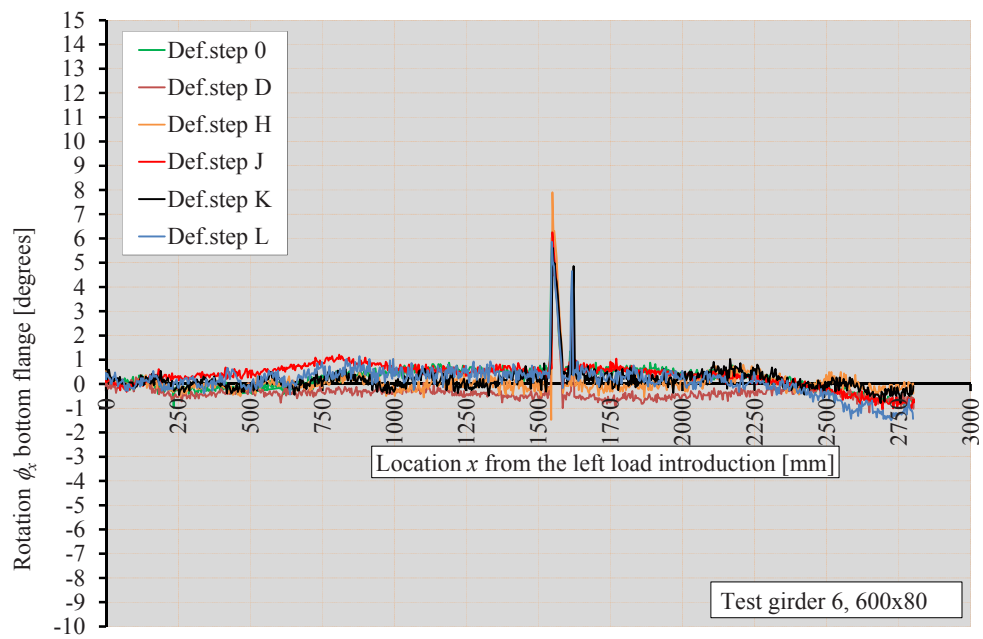
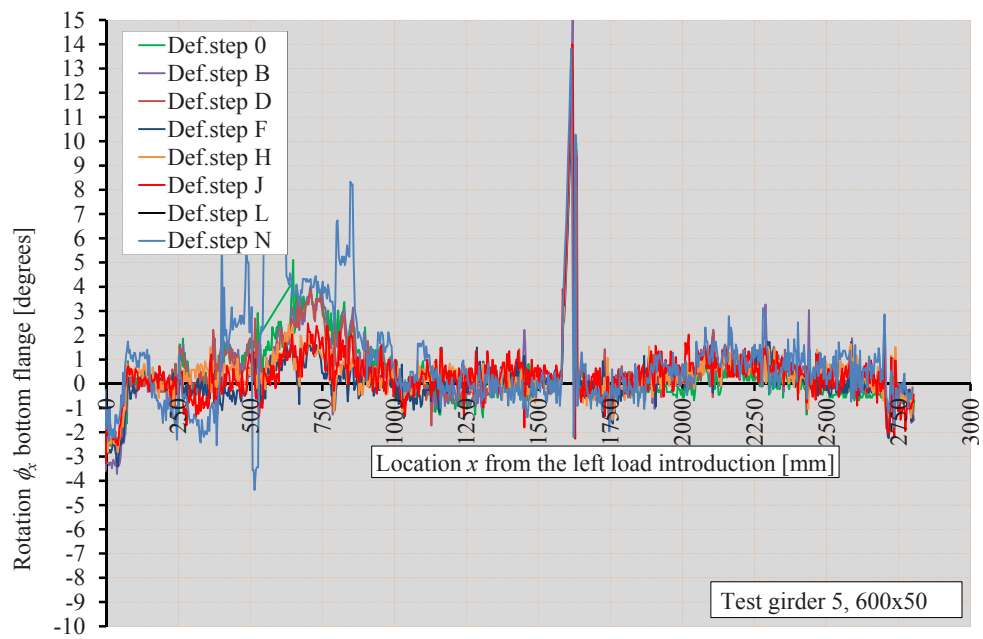


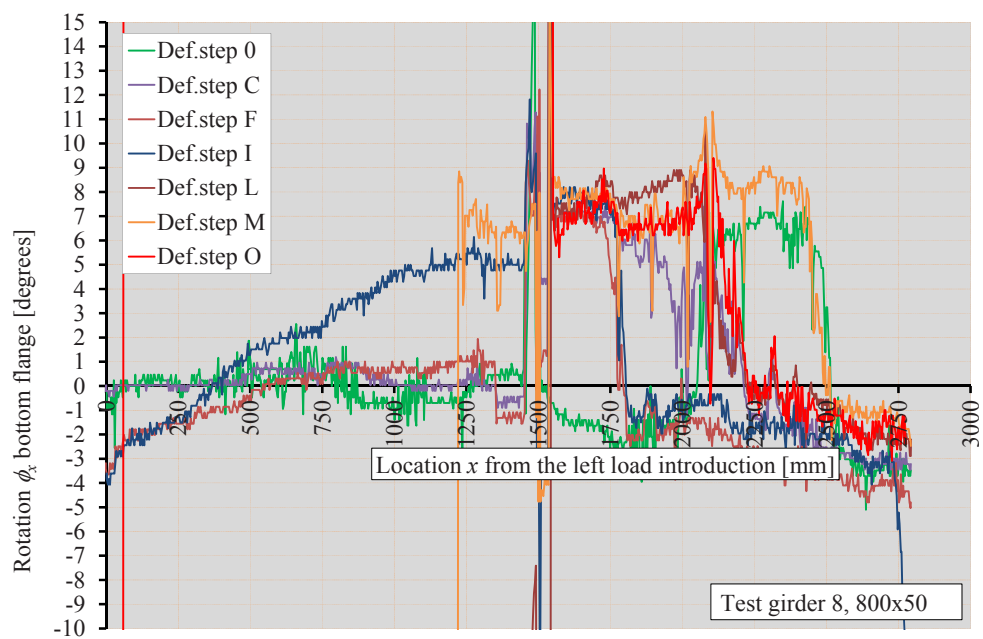
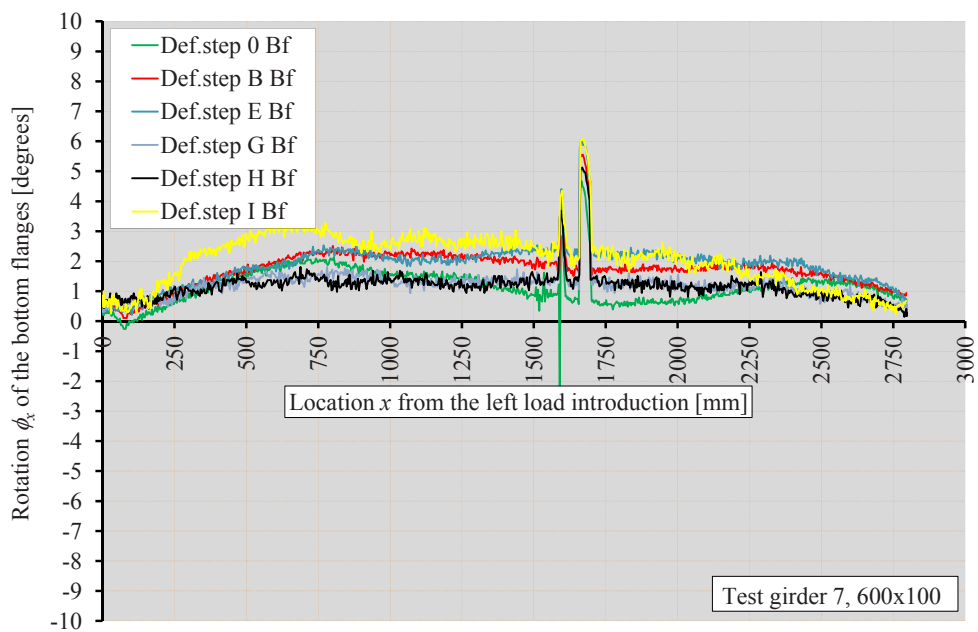
Increment out-of-load deflections of plate girder 10, 800x100, DS N-M

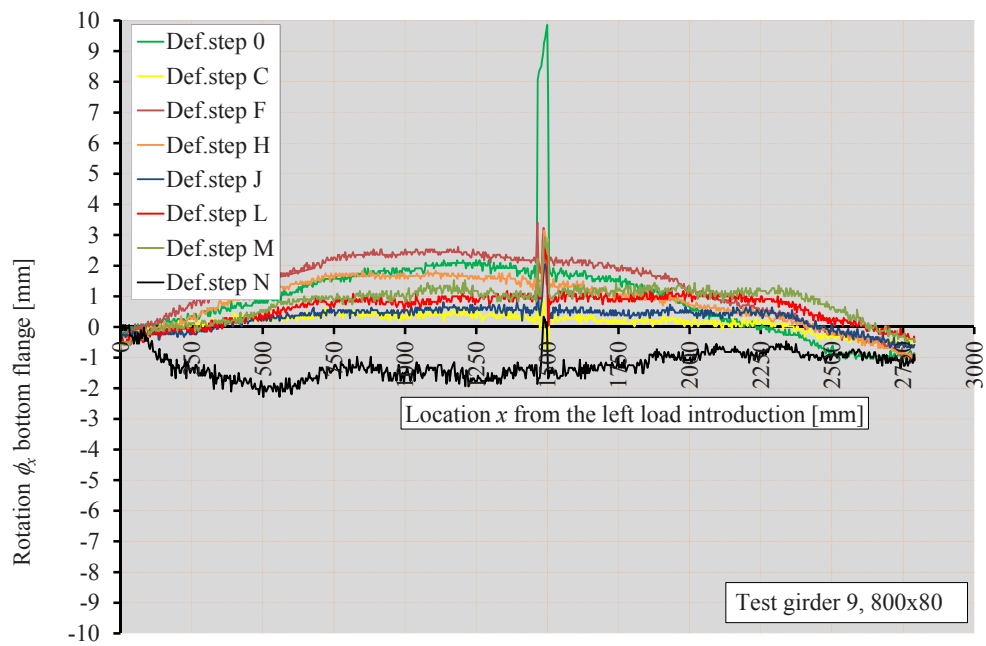
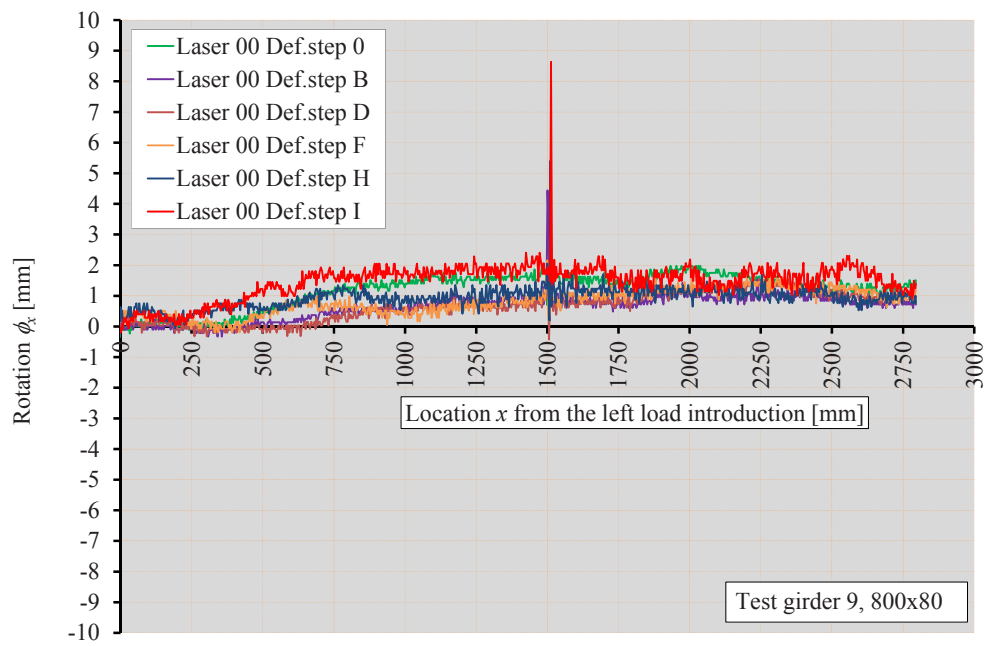
APPENDIX N ROTATIONS BASED ON THE VERTICAL DEFORMATIONS OF THE TIPS OF THE BOTTOM FLANGE



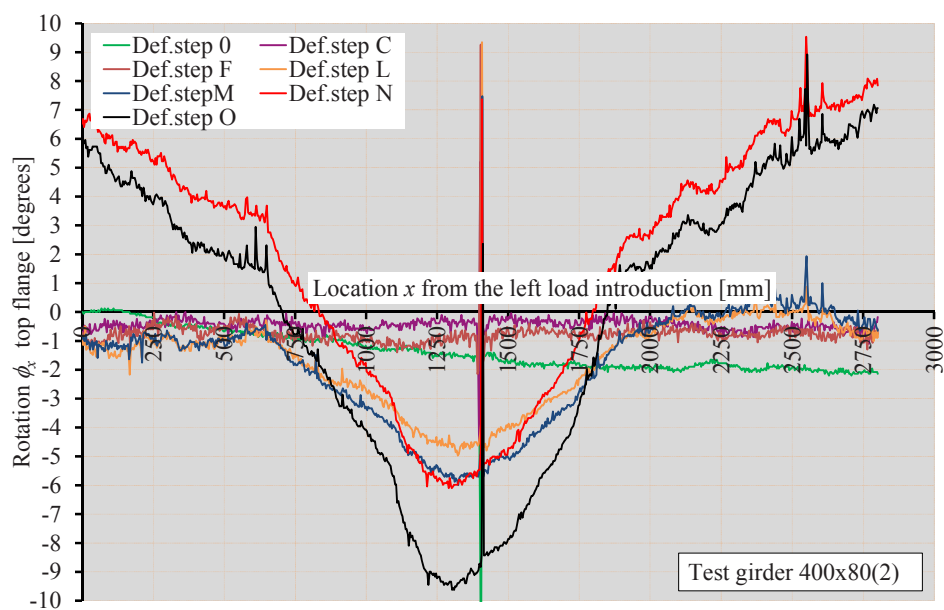
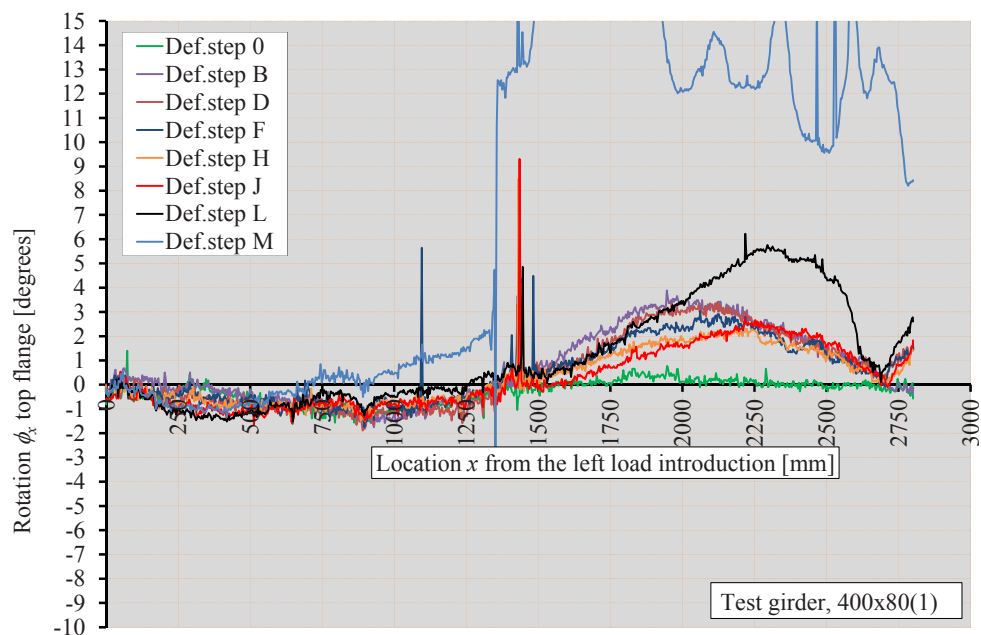


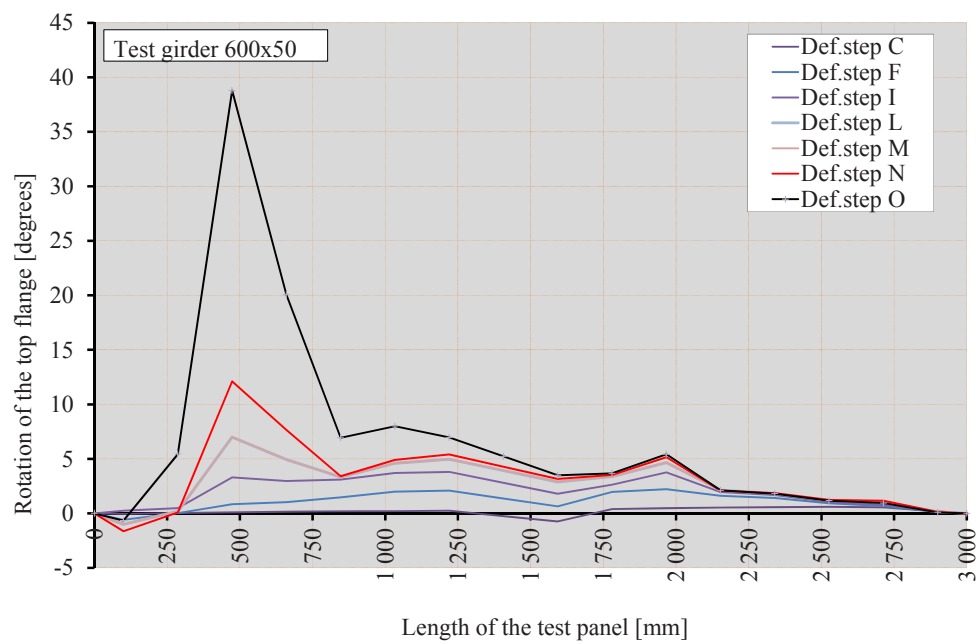
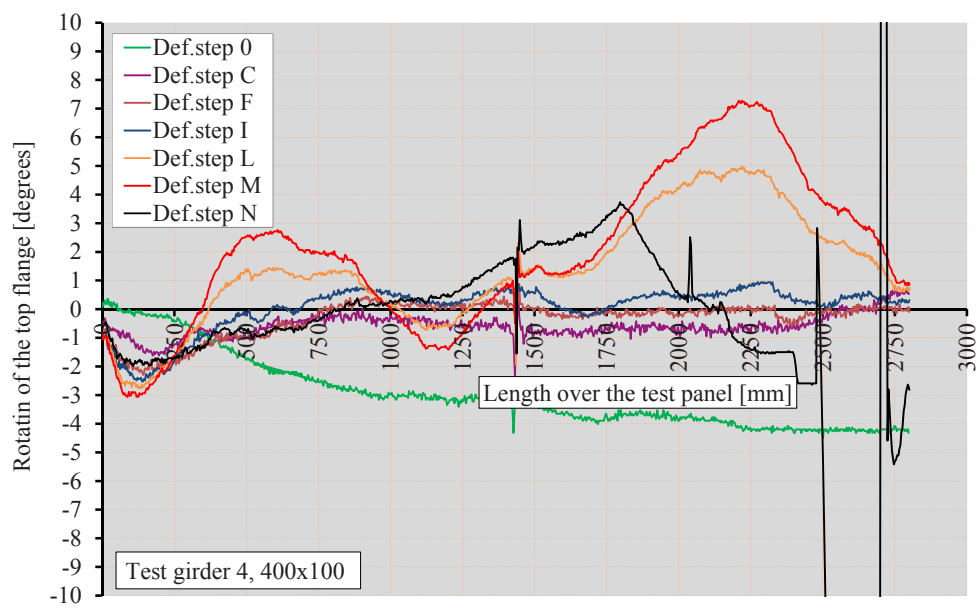


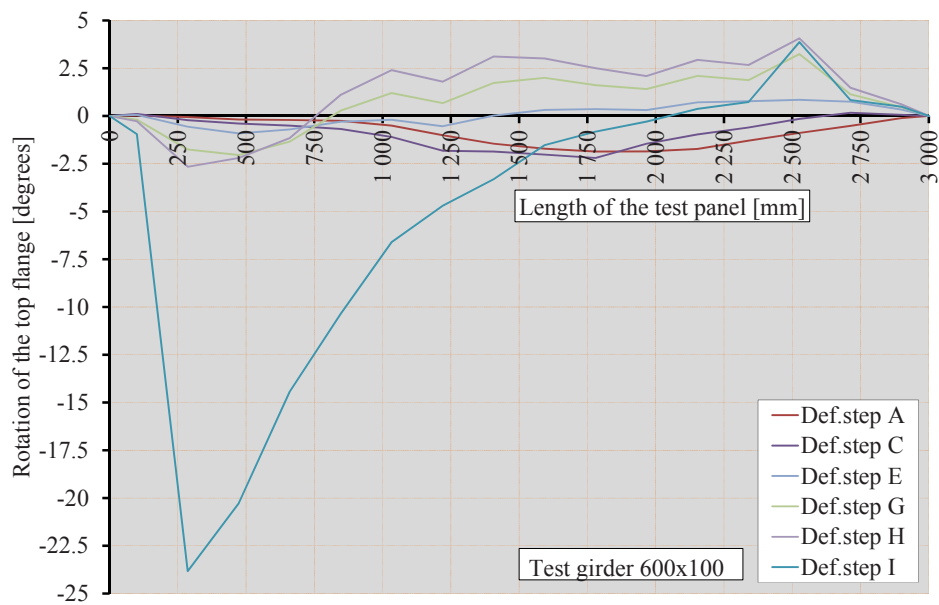
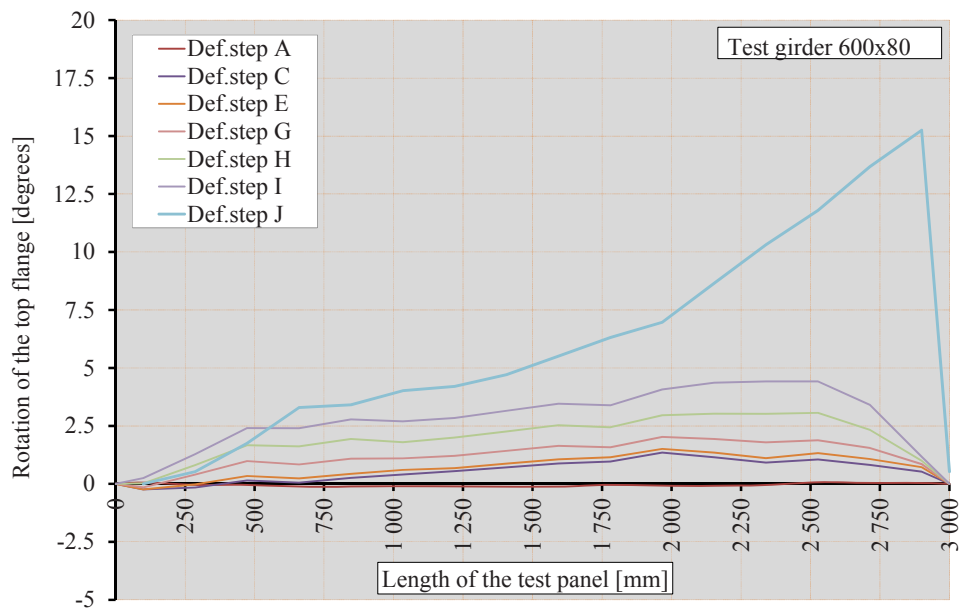


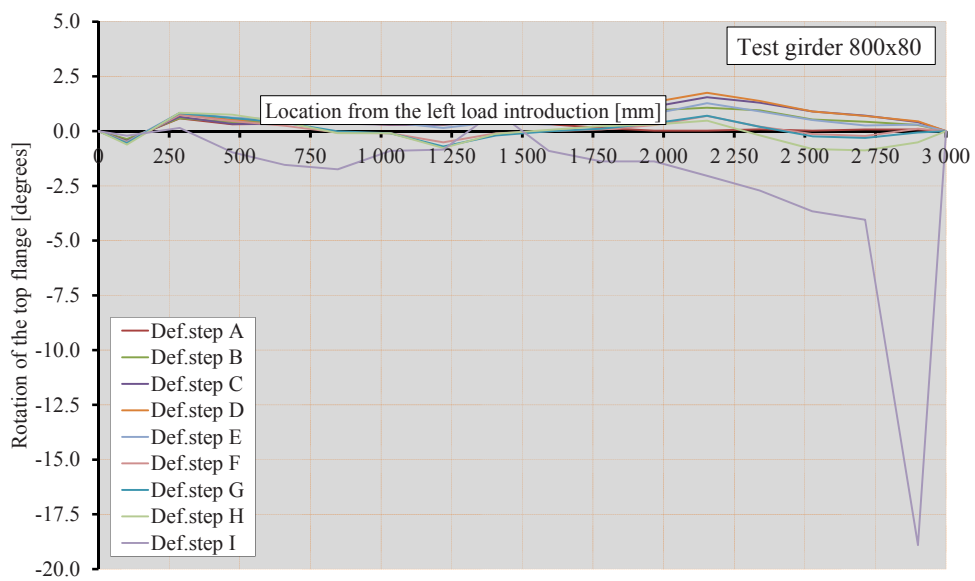
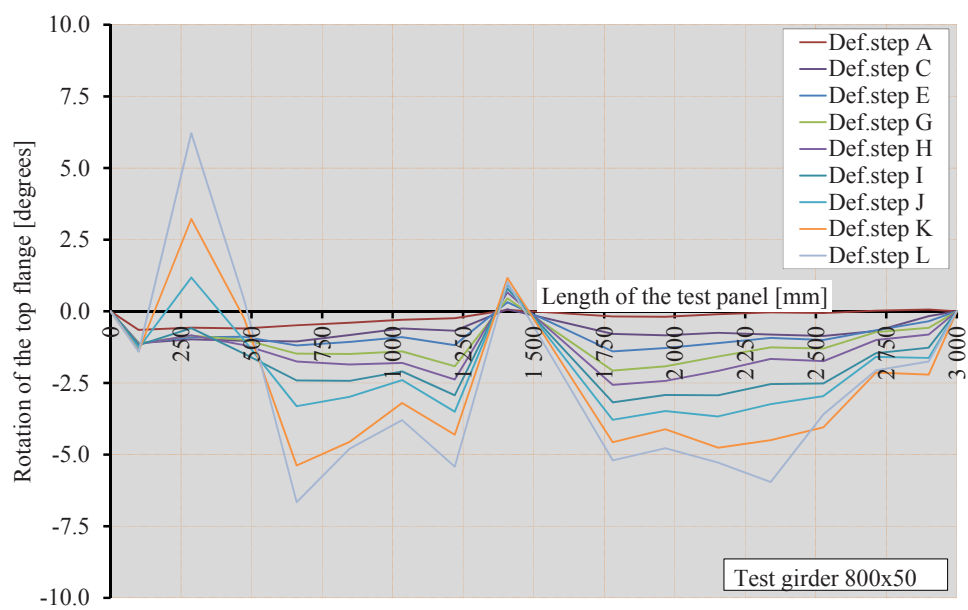


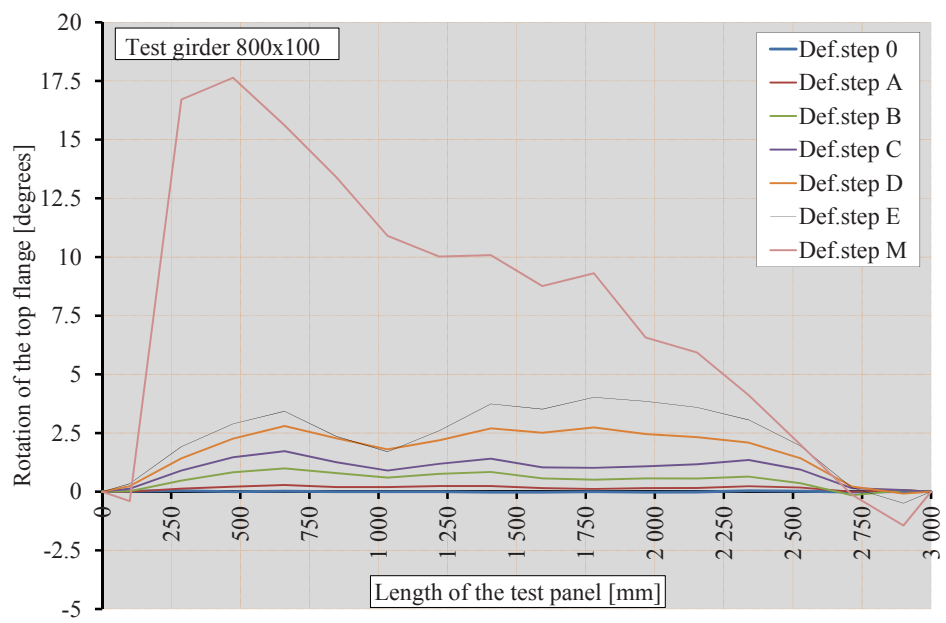
APPENDIX O ROTATIONS OF THE TOP FLANGE





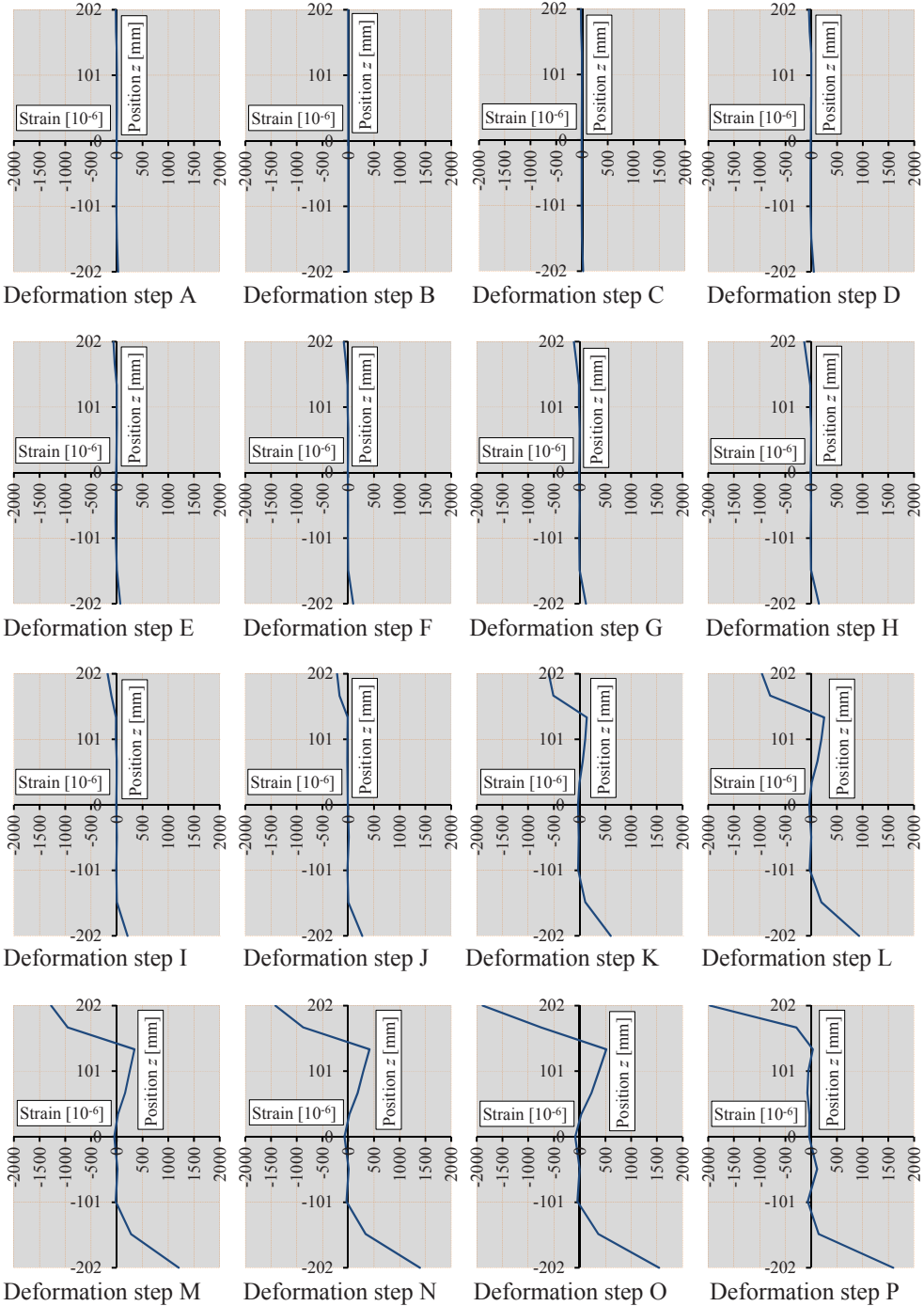


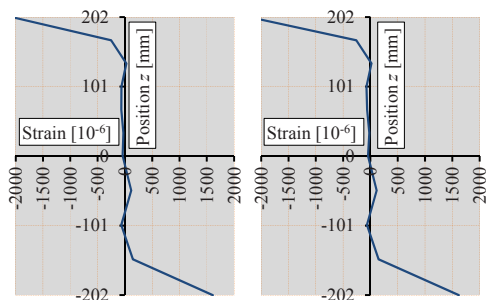




APPENDIX P STRAIN OVER THE HEIGHT OF THE CROSS-SECTION

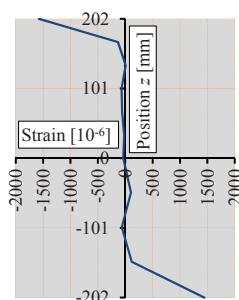
Test girder 1, 400x50 weighed strains: average (average external + average internal)



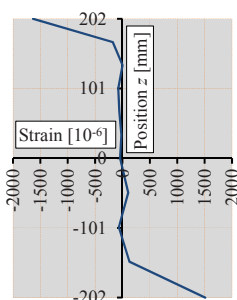


Deformation step Q

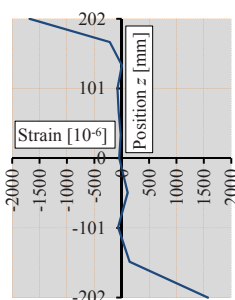
Deformation step R



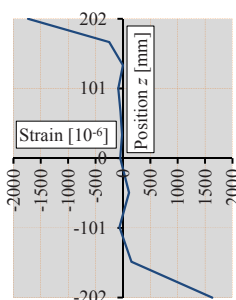
Deformation step U



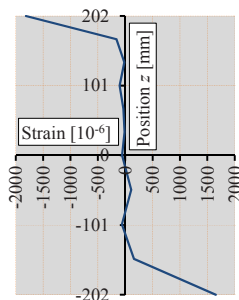
Deformation step V



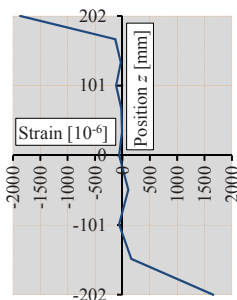
Deformation step W



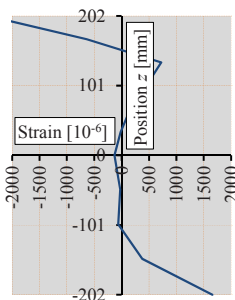
Deformation step X



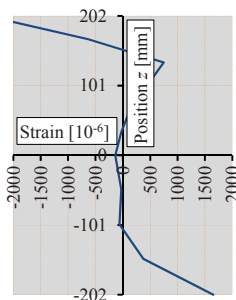
Deformation step Y



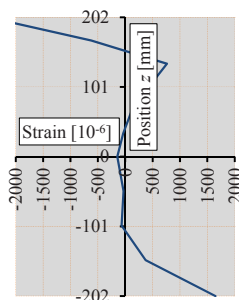
Deformation step Z



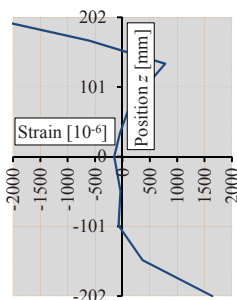
Deformation step AA



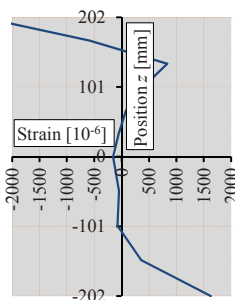
Deformation step AB



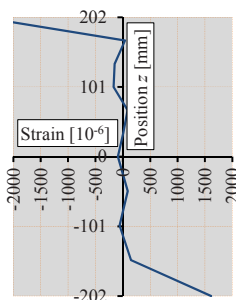
Deformation step AC



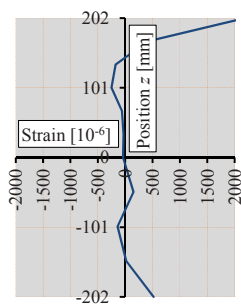
Deformation step AD



Deformation step AE

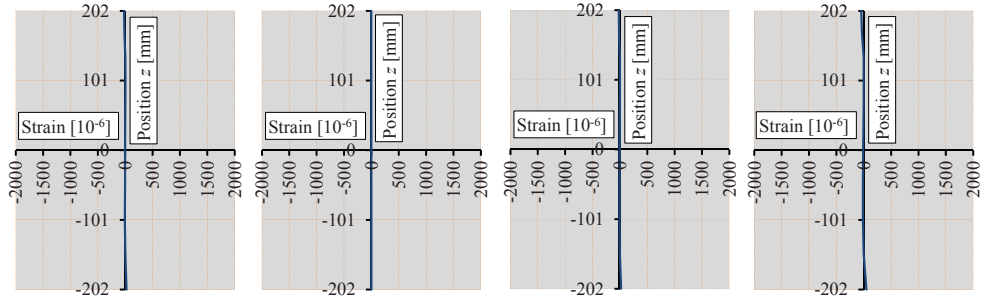


Deformation step AF



Deformation step AG

Test girder 1, 400x50 Average

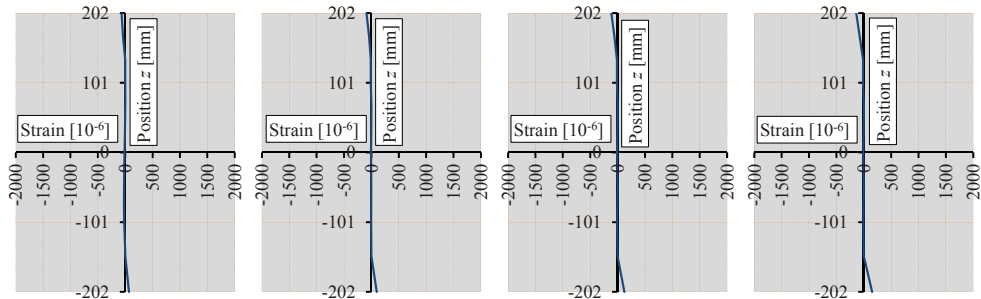


Deformation step A

Deformation step B

Deformation step C

Deformation step D

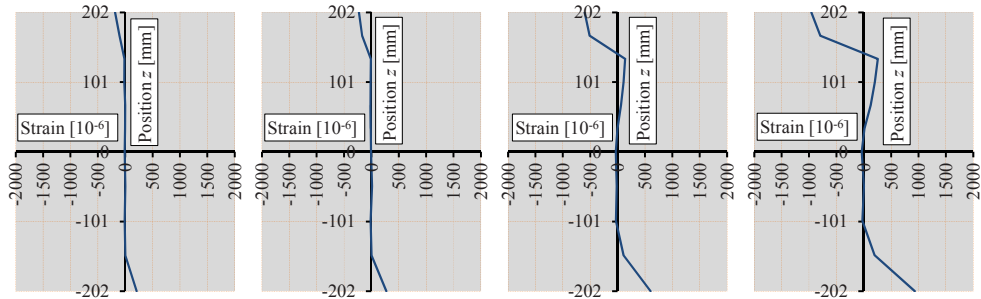


Deformation step E

Deformation step F

Deformation step G

Deformation step H

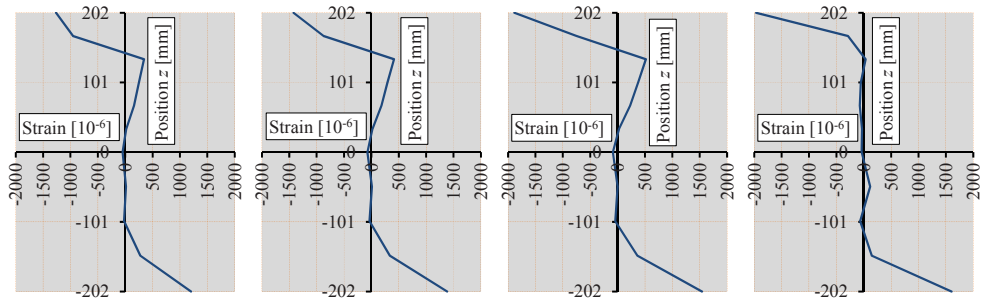


Deformation step I

Deformation step J

Deformation step K

Deformation step L

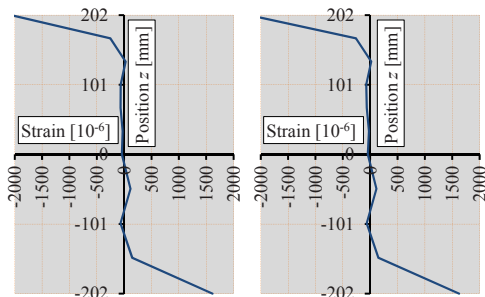


Deformation step M

Deformation step N

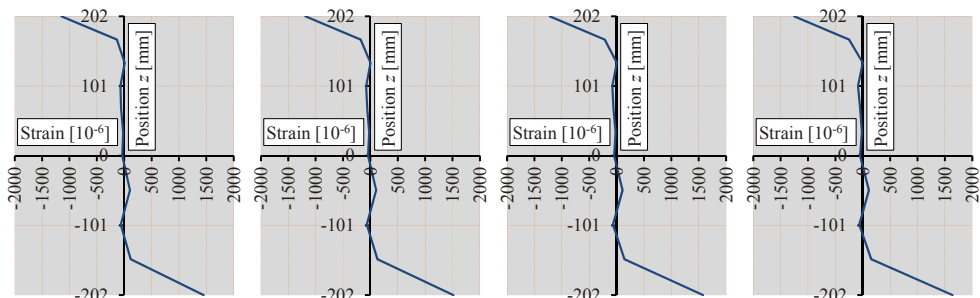
Deformation step O

Deformation step P



Deformation step Q

Deformation step R

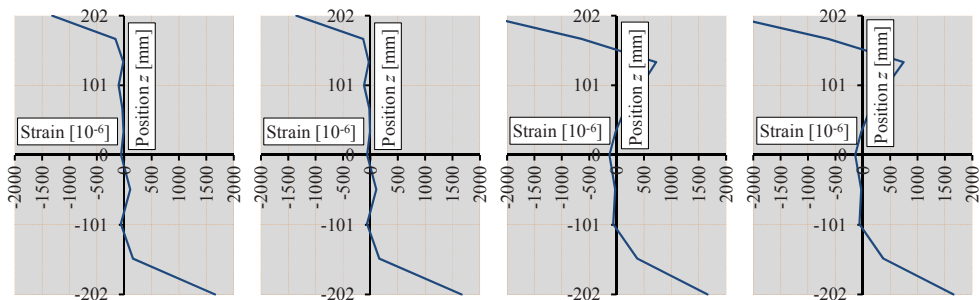


Deformation step U

Deformation step V

Deformation step W

Deformation step X

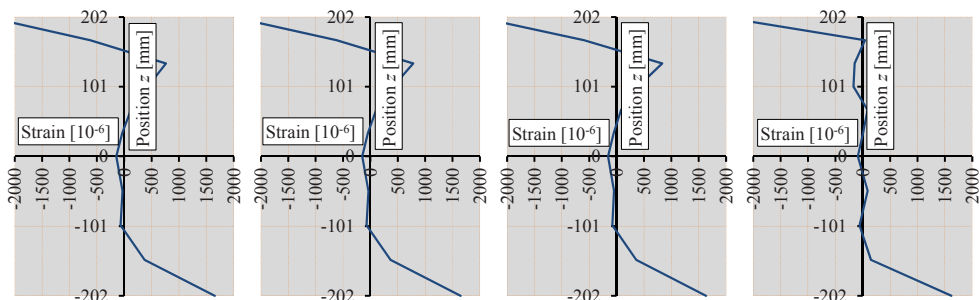


Deformation step Y

Deformation step Z

Deformation step AA

Deformation step AB

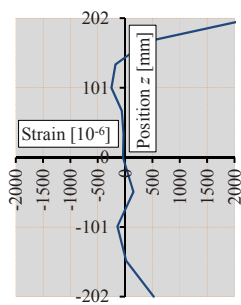


Deformation step AC

Deformation step AD

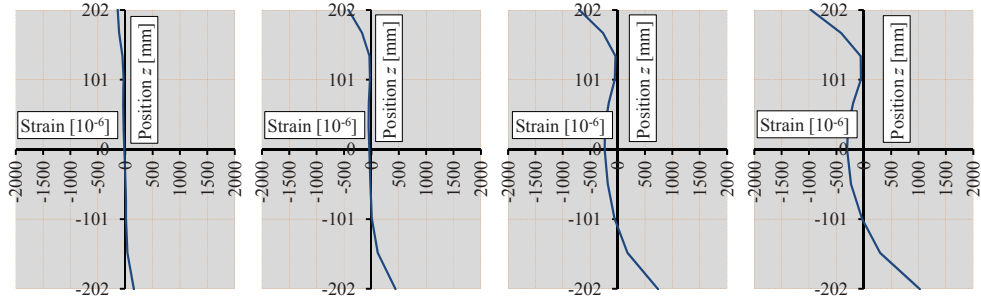
Deformation step AE

Deformation step AF



Deformation step AG

Test girder 2, 400x80(1) weighed strains average (average external + average internal)

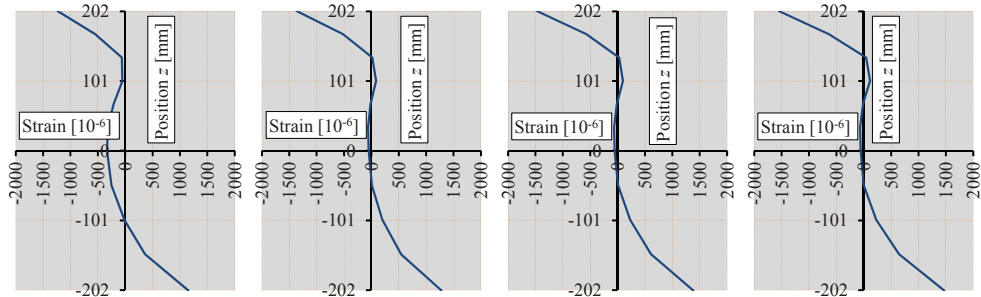


Deformation step A

Deformation step B

Deformation step C

Deformation step D

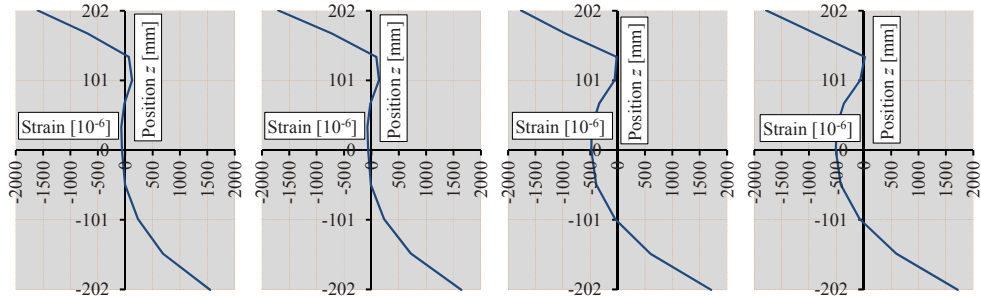


Deformation step E

Deformation step F

Deformation step G

Deformation step H

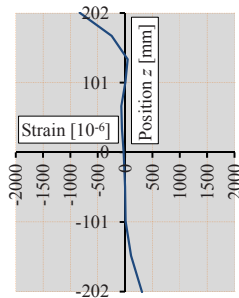


Deformation step I

Deformation step J

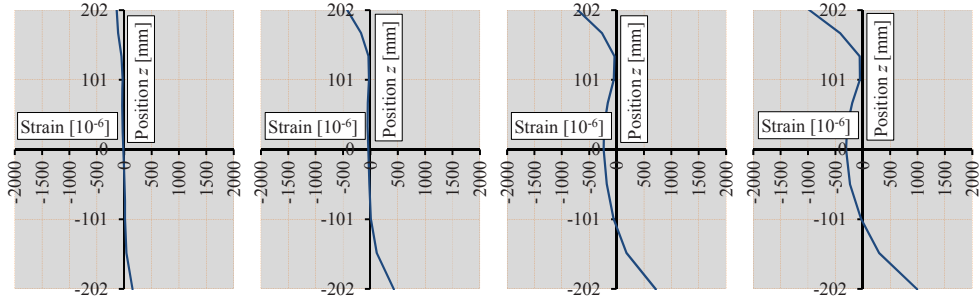
Deformation step K

Deformation step L



Deformation step M

Test girder 2, 400x80(1) Average

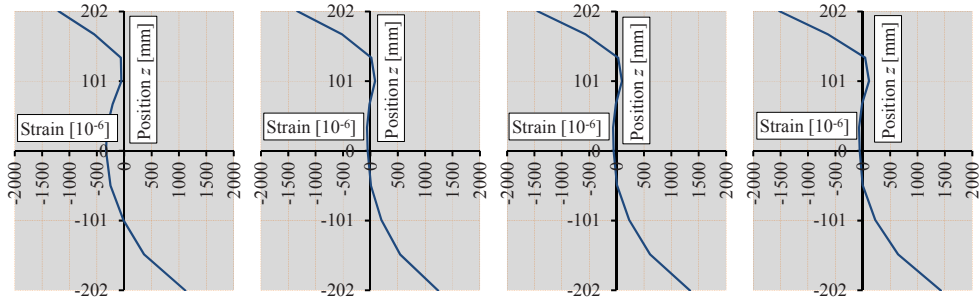


Deformation step A

Deformation step B

Deformation step C

Deformation step D

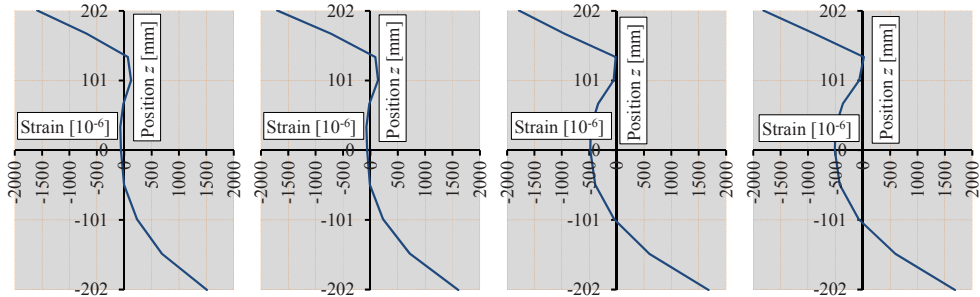


Deformation step E

Deformation step F

Deformation step G

Deformation step H

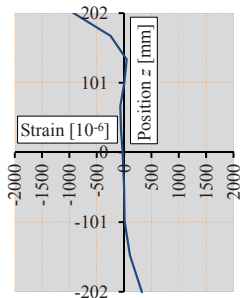


Deformation step I

Deformation step J

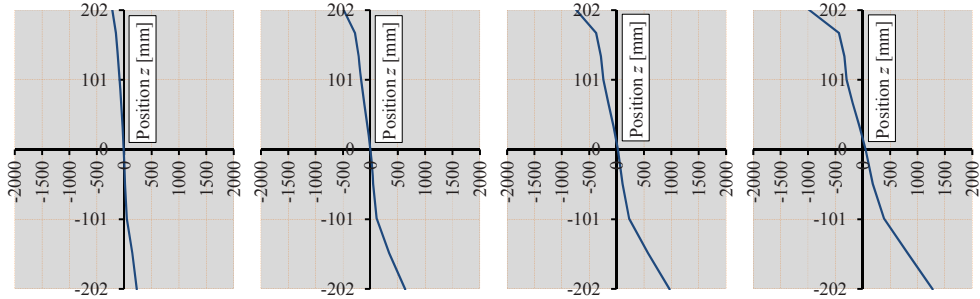
Deformation step K

Deformation step L



Deformation step M

Test girder 3, 400x80(2) weighed strains average (average external + average internal)

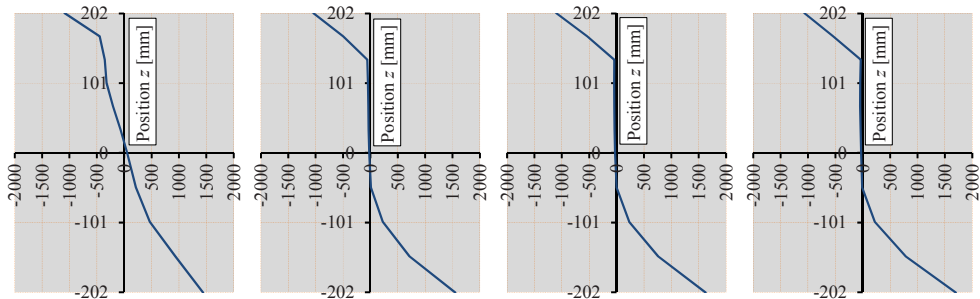


Deformation step A

Deformation step B

Deformation step C

Deformation step D

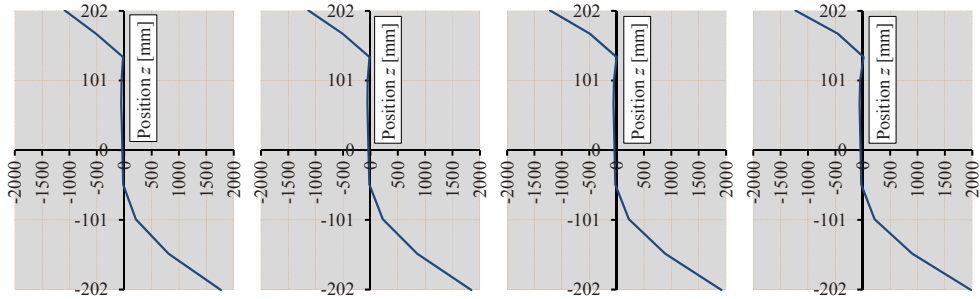


Deformation step E

Deformation step F

Deformation step G

Deformation step H

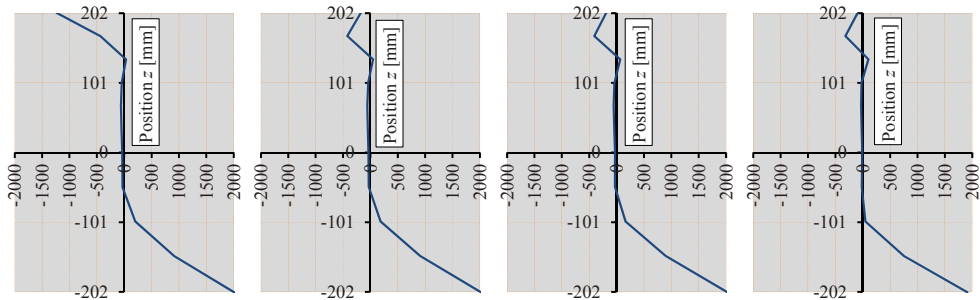


Deformation step I

Deformation step J

Deformation step K

Deformation step L



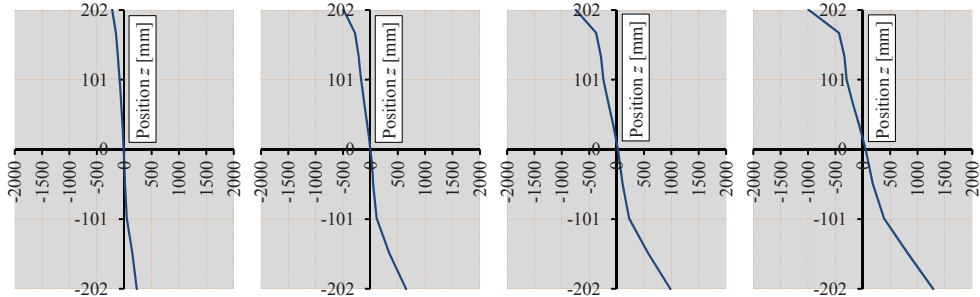
Deformation step M

Deformation step N

Deformation step O

Deformation step P

Test girder 3, 400x80(2) average

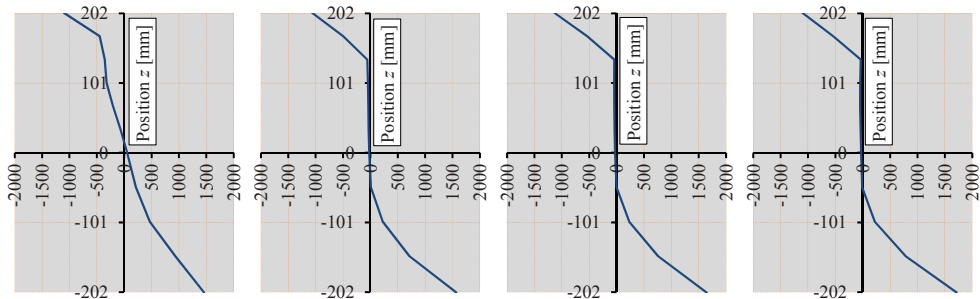


Deformation step A

Deformation step B

Deformation step C

Deformation step D

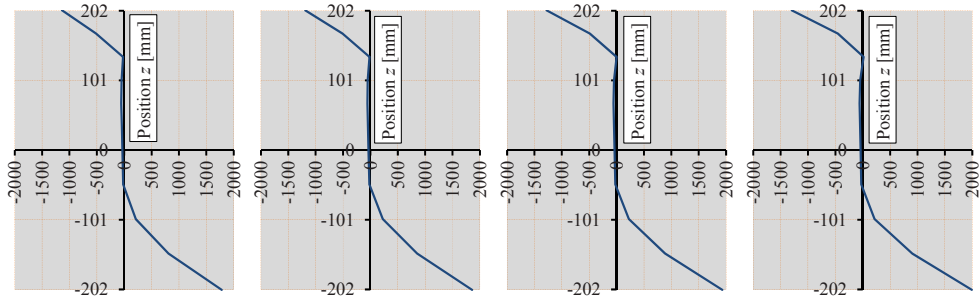


Deformation step E

Deformation step F

Deformation step G

Deformation step H

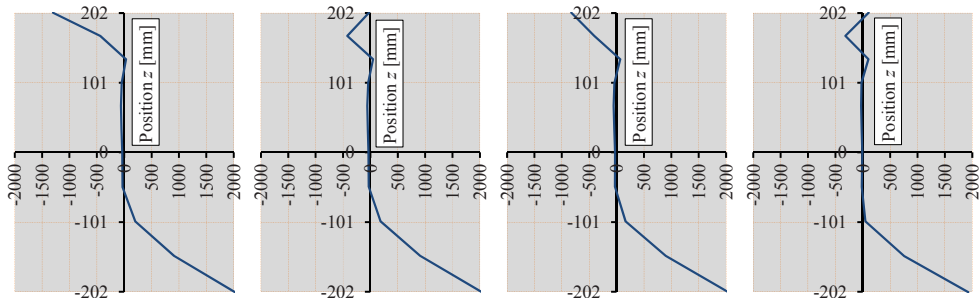


Deformation step I

Deformation step J

Deformation step K

Deformation step L



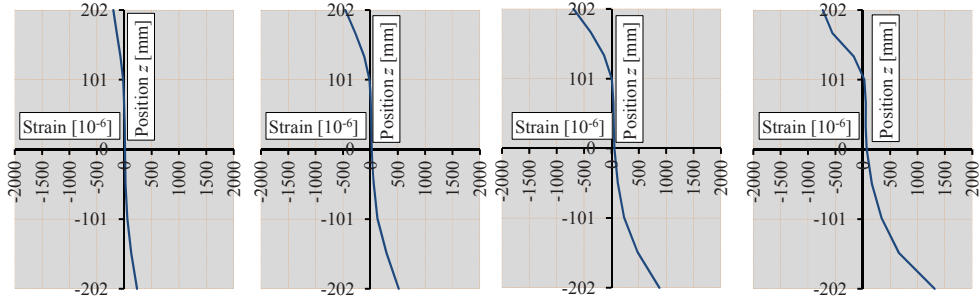
Deformation step M

Deformation step N

Deformation step O

Deformation step P

Test girder 4, 400x100 weighed strains average (average external + average internal)

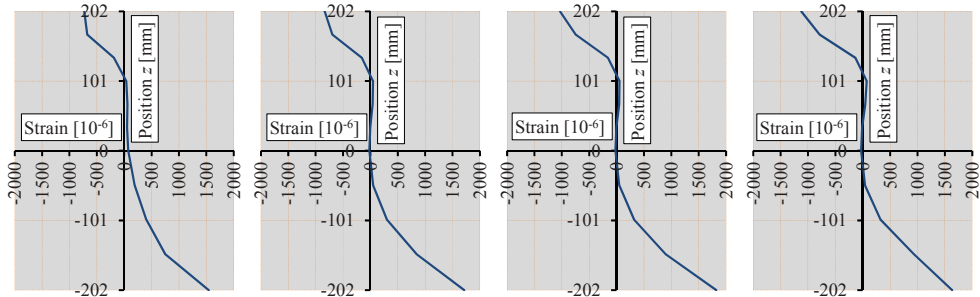


Deformation step A

Deformation step B

Deformation step C

Deformation step D

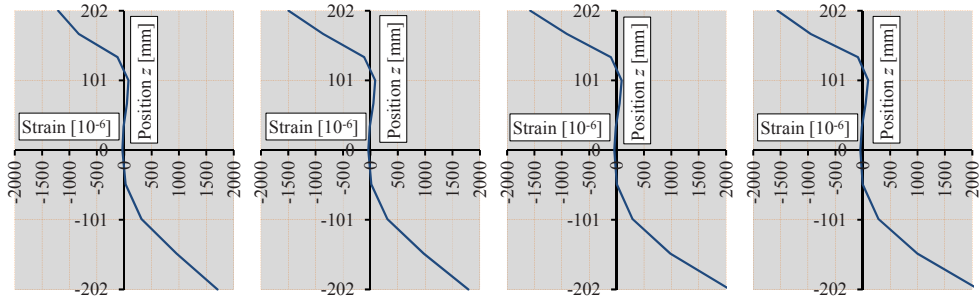


Deformation step E

Deformation step F

Deformation step G

Deformation step H

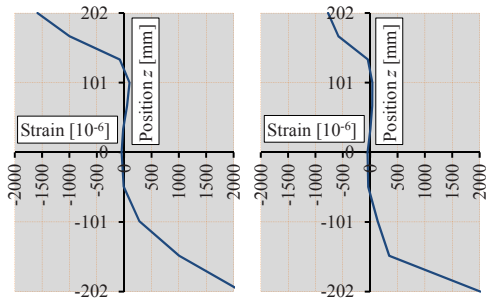


Deformation step I

Deformation step J

Deformation step K

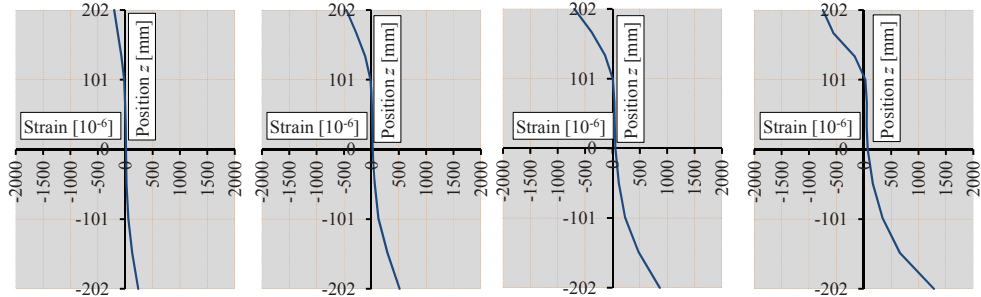
Deformation step L



Deformation step M

Deformation step N

Test girder 4, 400x100 Average strains

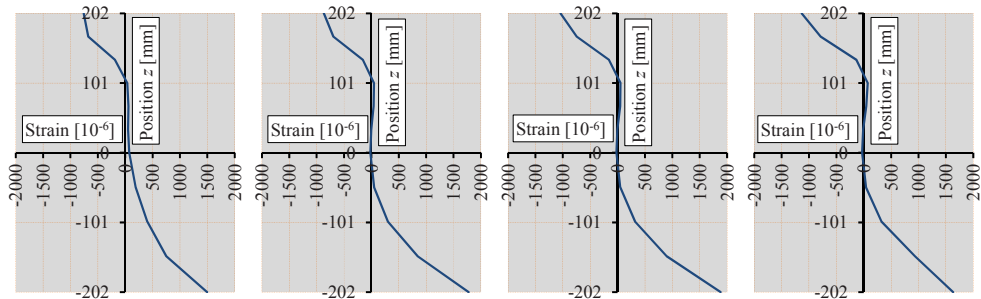


Deformation step A

Deformation step B

Deformation step C

Deformation step D

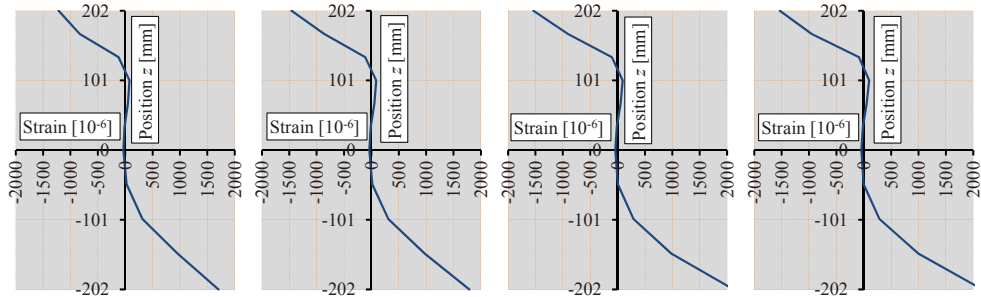


Deformation step E

Deformation step F

Deformation step G

Deformation step H

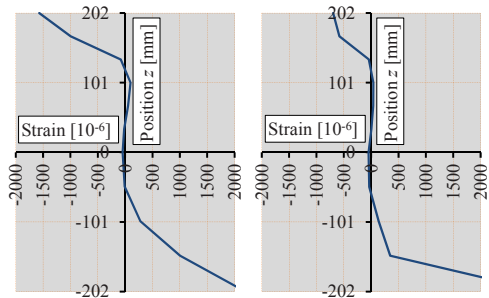


Deformation step I

Deformation step J

Deformation step K

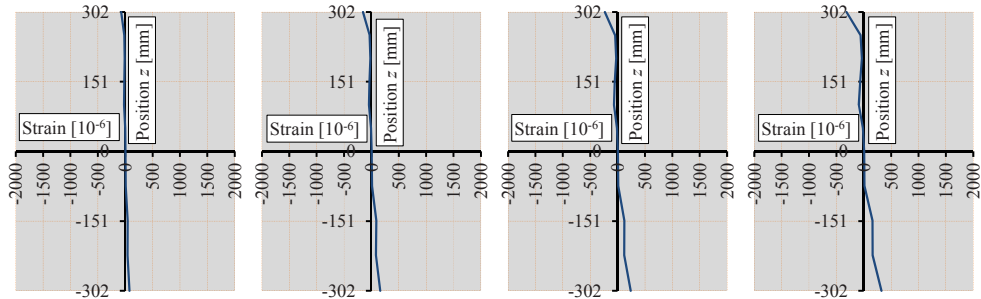
Deformation step L



Deformation step M

Deformation step N

Test girder 5, 600x50 weighed strains average (average external + average internal)

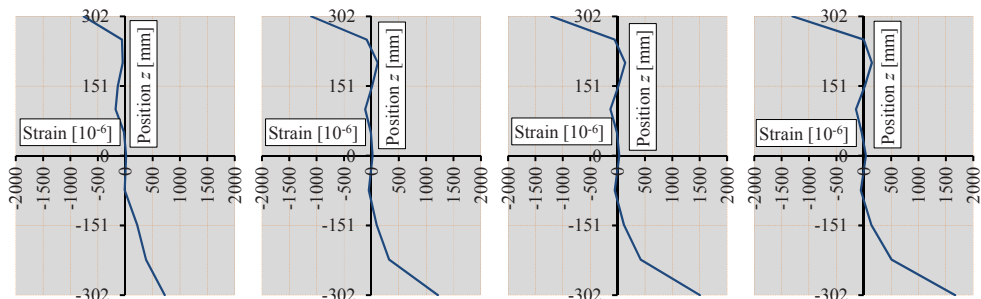


Deformation step A

Deformation step B

Deformation step C

Deformation step D

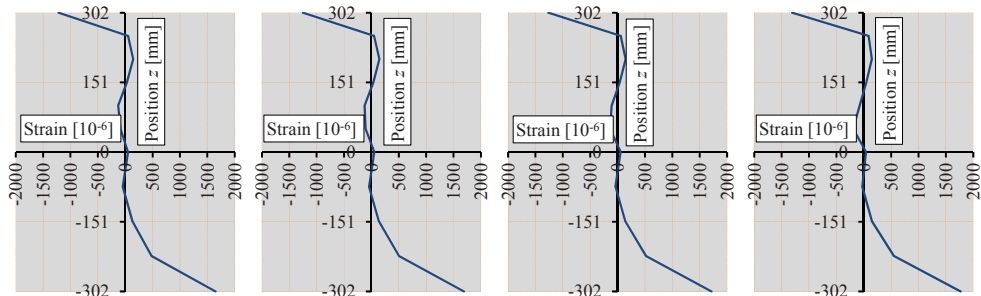


Deformation step E

Deformation step F

Deformation step G

Deformation step H

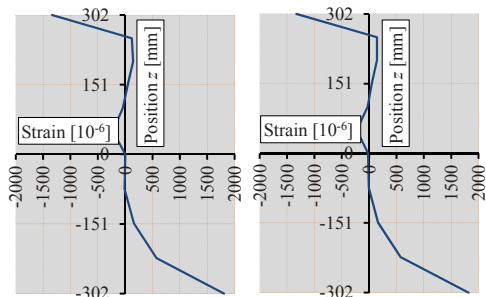


Deformation step I

Deformation step J

Deformation step K

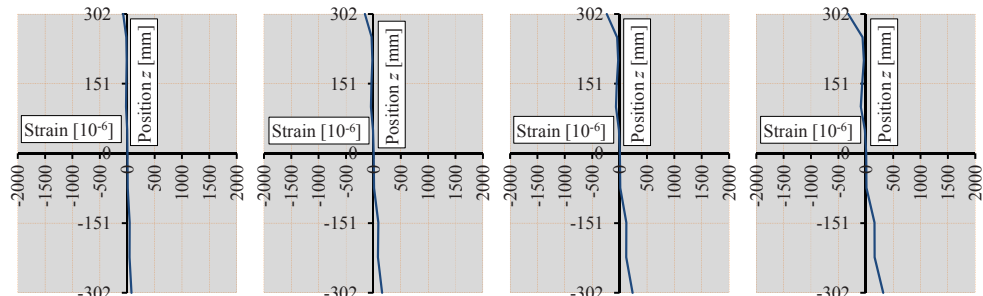
Deformation step L



Deformation step M

Deformation step N

Test girder 5, 600x50 Average strains

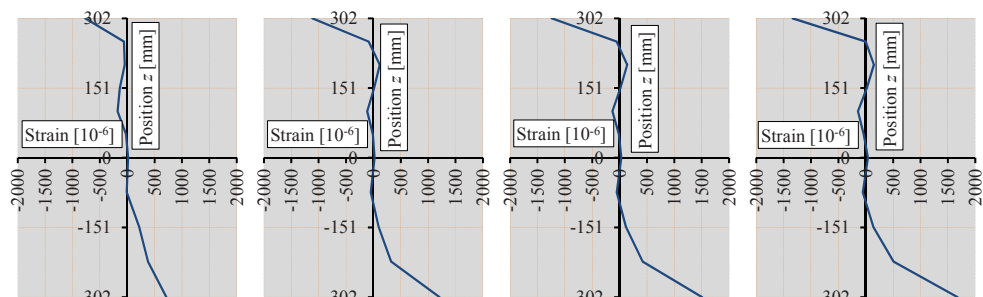


Deformation step A

Deformation step B

Deformation step C

Deformation step D

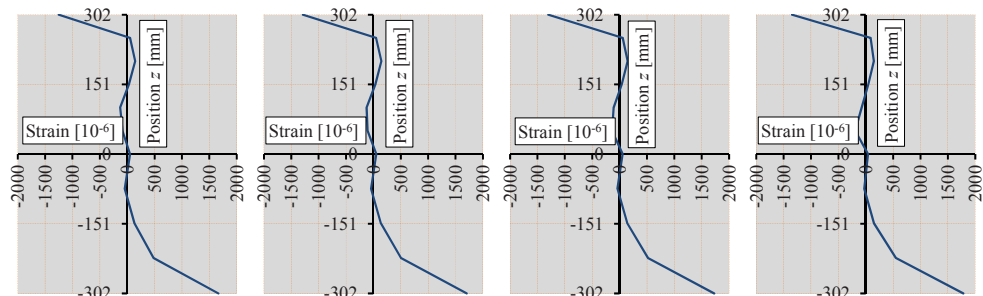


Deformation step E

Deformation step F

Deformation step G

Deformation step H

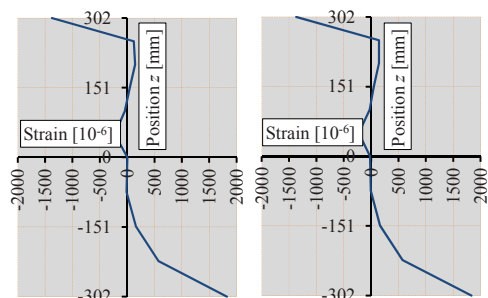


Deformation step I

Deformation step J

Deformation step K

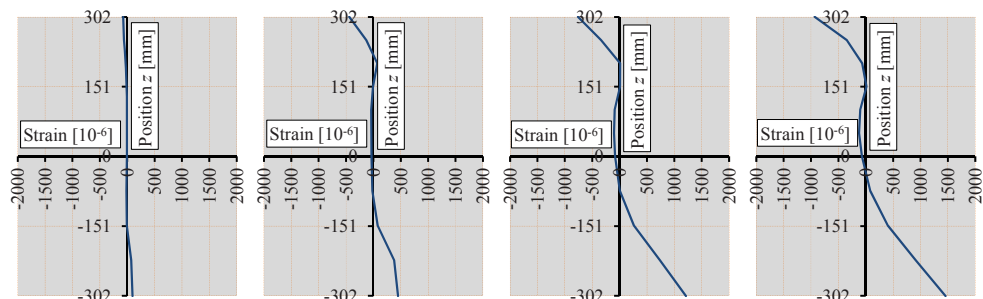
Deformation step L



Deformation step M

Deformation step N

Test girder 6, 600x80 weighed strains average (average external + average internal)

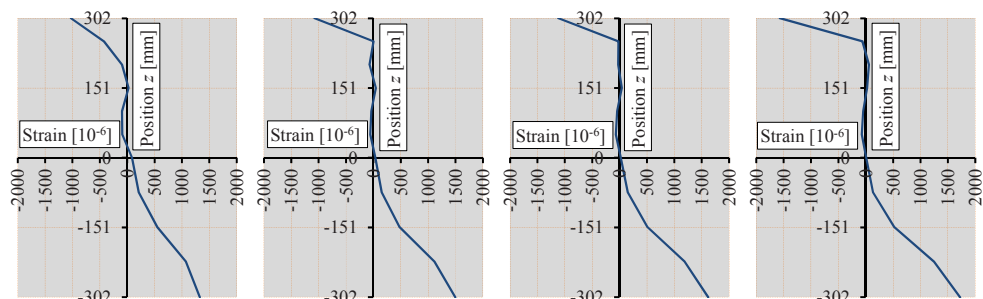


Deformation step A

Deformation step B

Deformation step C

Deformation step D

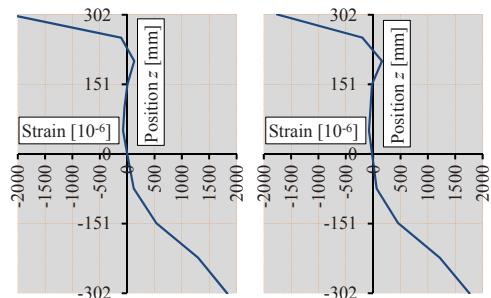


Deformation step E

Deformation step F

Deformation step G

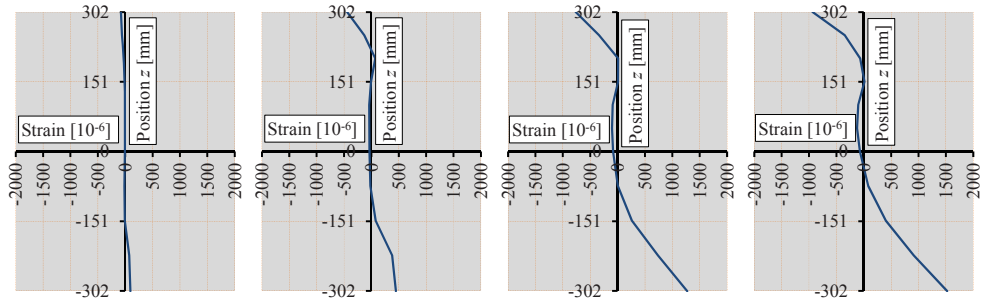
Deformation step H



Deformation step I

Deformation step J

Test girder 6, 600x80 Average

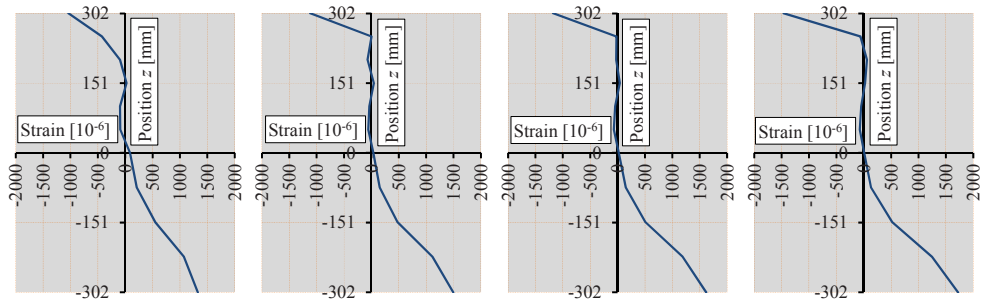


Deformation step A

Deformation step B

Deformation step C

Deformation step D

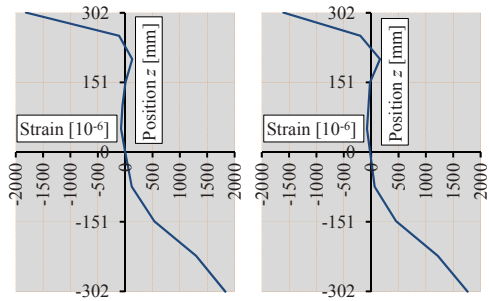


Deformation step E

Deformation step F

Deformation step G

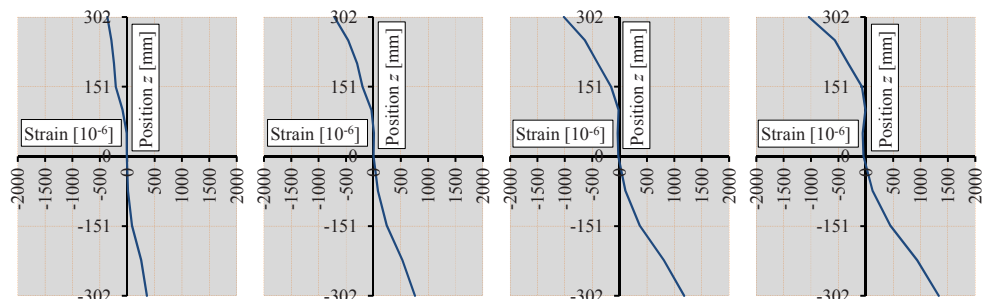
Deformation step H



Deformation step I

Deformation step J

Test girder 7, 600x100 weighed strains average (average external + average internal)

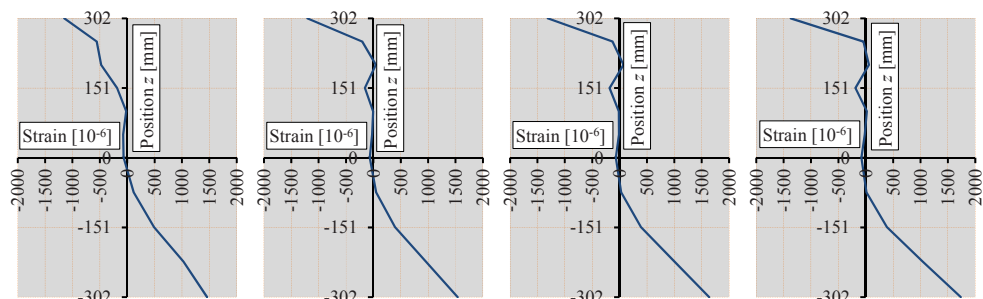


Deformation step A

Deformation step B

Deformation step C

Deformation step D

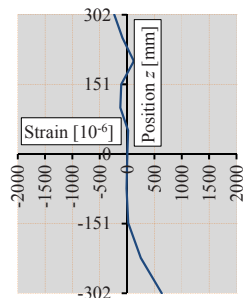


Deformation step E

Deformation step F

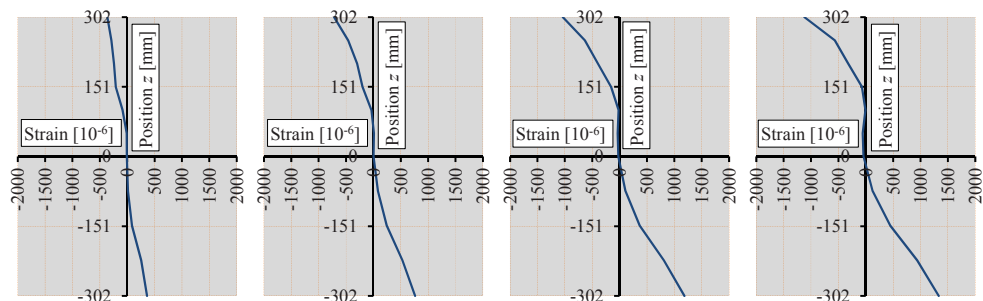
Deformation step G

Deformation step H



Deformation step I

Test girder 7, 600x100 Average

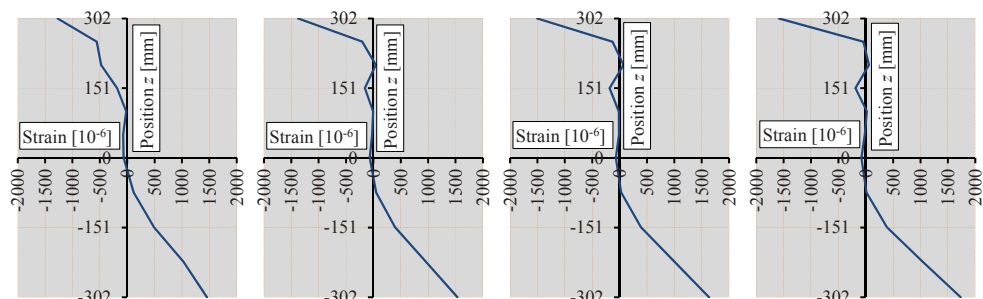


Deformation step A

Deformation step B

Deformation step C

Deformation step D

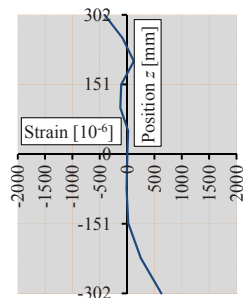


Deformation step E

Deformation step F

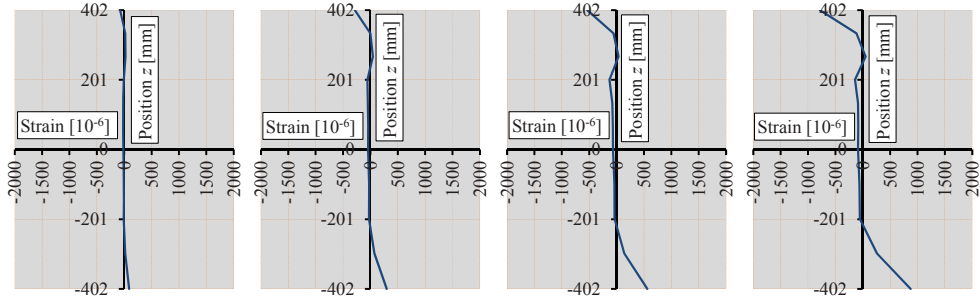
Deformation step G

Deformation step H



Deformation step I

Test girder 8, 800x50 weighed strains average (average external + average internal)

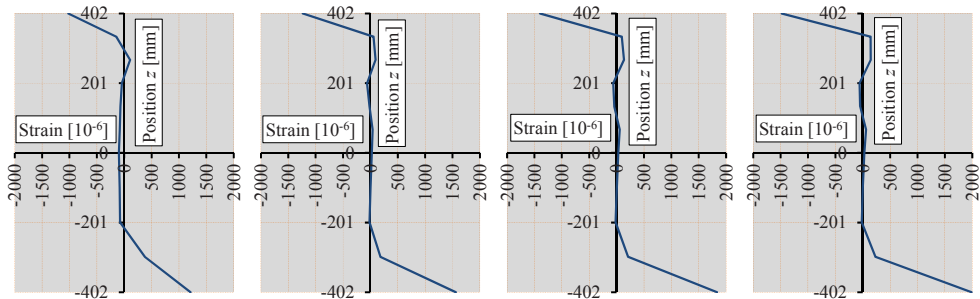


Deformation step A

Deformation step B

Deformation step C

Deformation step D

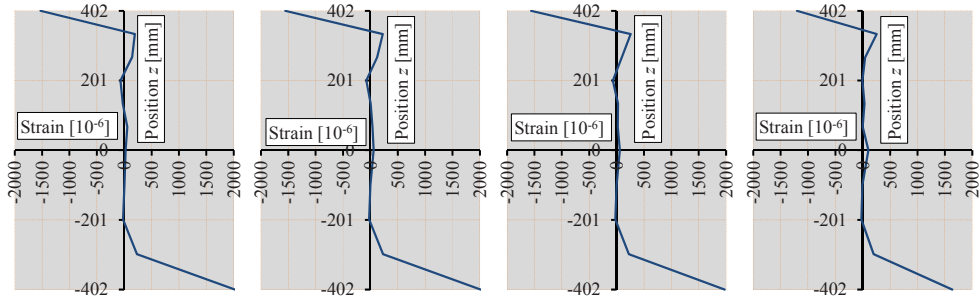


Deformation step E

Deformation step F

Deformation step G

Deformation step H



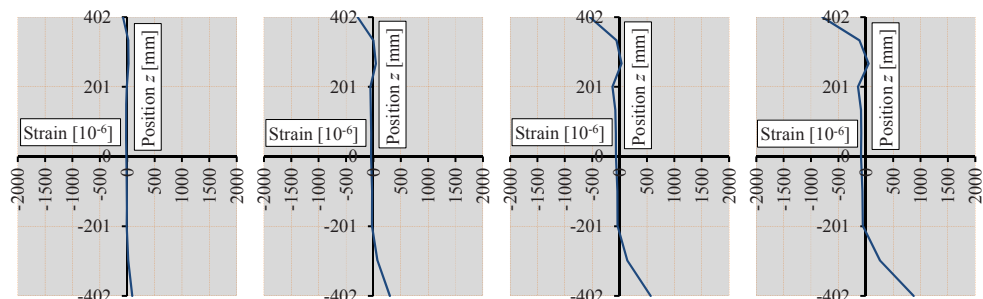
Deformation step I

Deformation step J

Deformation step K

Deformation step L

Test girder 8, 800x50 Average

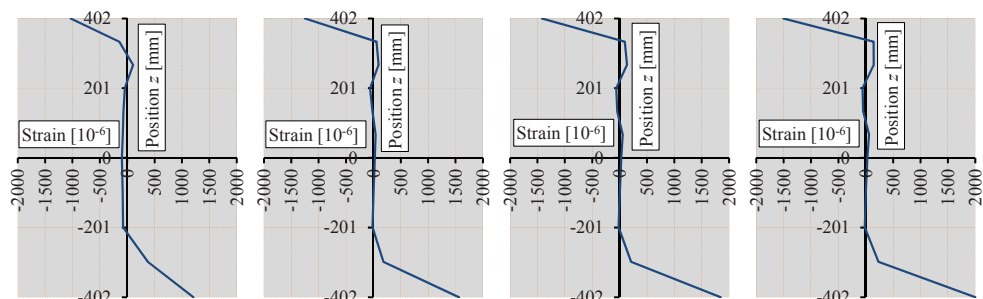


Deformation step A

Deformation step B

Deformation step C

Deformation step D

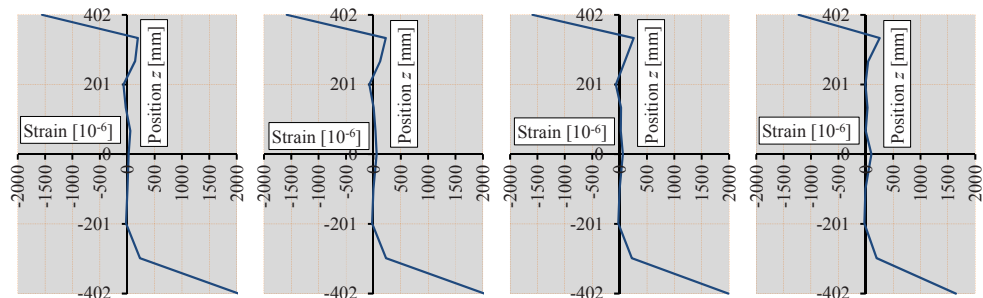


Deformation step E

Deformation step F

Deformation step G

Deformation step H



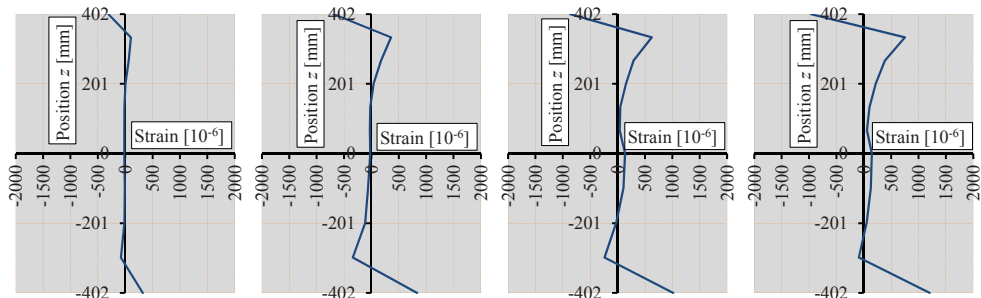
Deformation step I

Deformation step J

Deformation step K

Deformation step L

Test girder 9, 800x80 weighed strains average (average external + average internal)

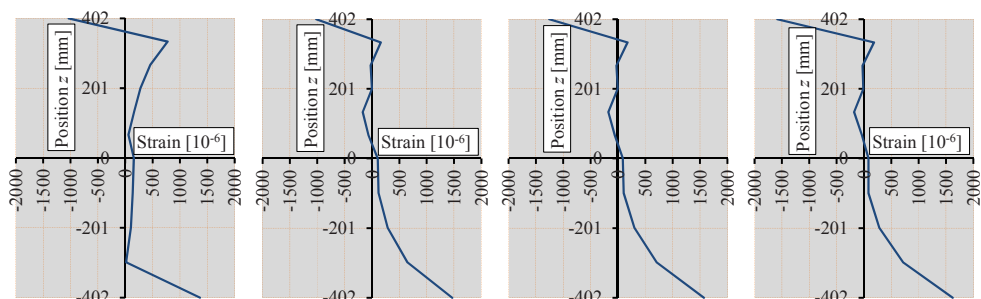


Deformation step A

Deformation step B

Deformation step C

Deformation step D

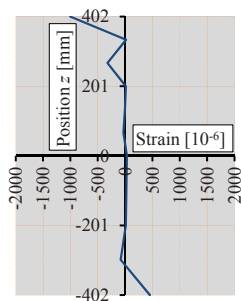


Deformation step E

Deformation step F

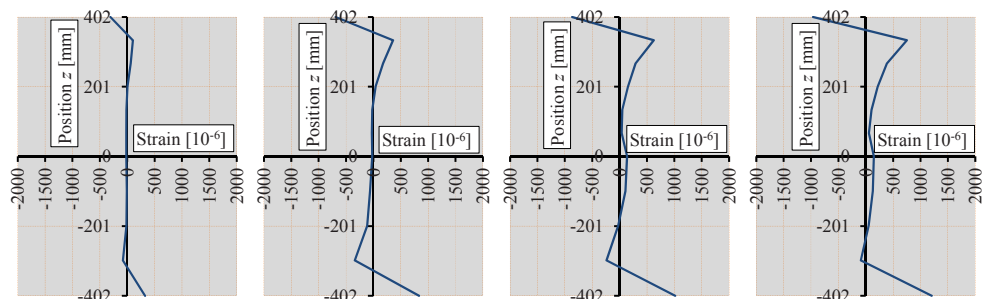
Deformation step G

Deformation step H



Deformation step I

Test girder 9, 800x80 Average

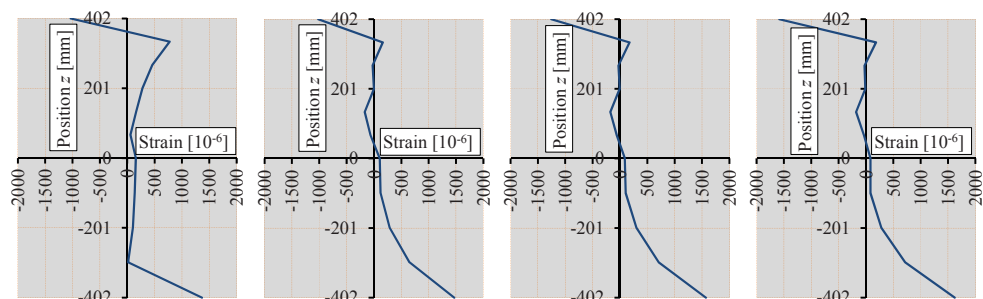


Deformation step A

Deformation step B

Deformation step C

Deformation step D

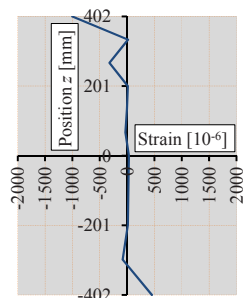


Deformation step E

Deformation step F

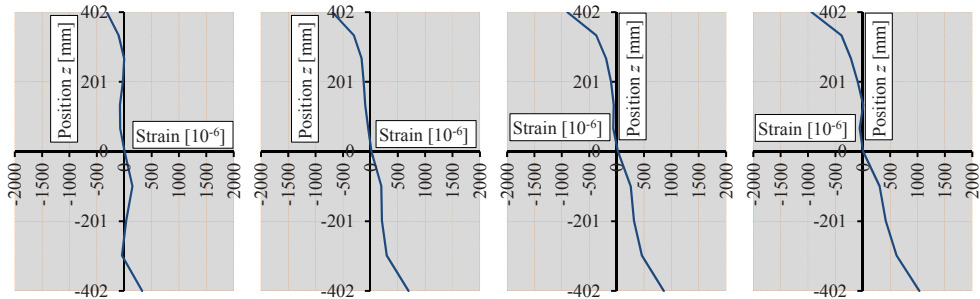
Deformation step G

Deformation step H



Deformation step I

Test girder 10, 800x100 weighed strains average (average external + average internal)

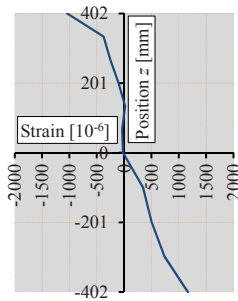


Deformation step A

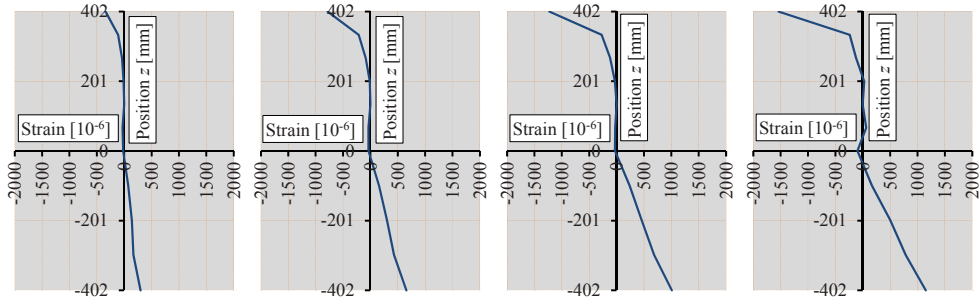
Deformation step B

Deformation step C

Deformation step D



Deformation step E

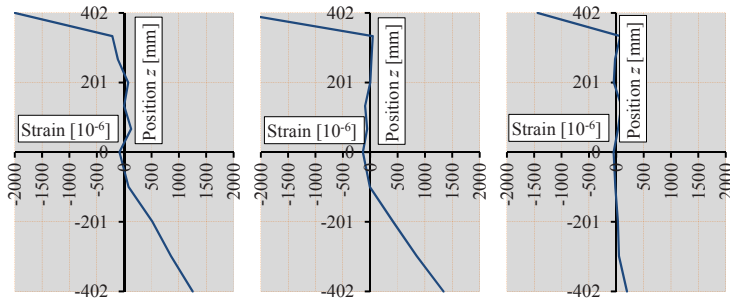


Deformation step H

Deformation step I

Deformation step J

Deformation step K

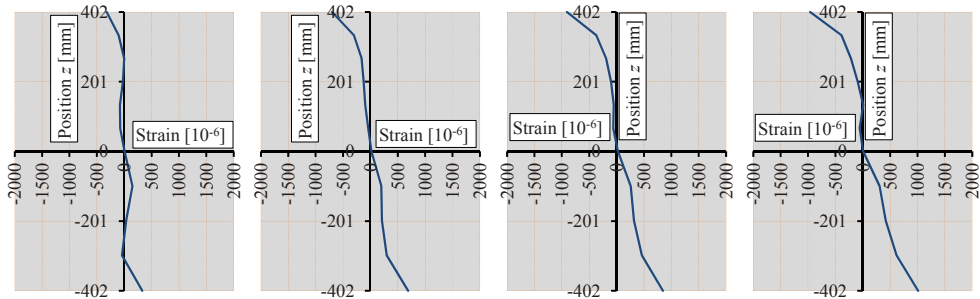


Deformation step L

Deformation step M

Deformation step N

Test girder 10, 800x100 Average

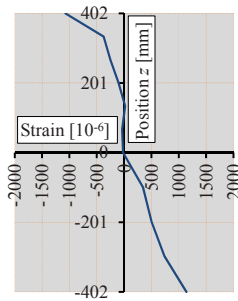


Deformation step A

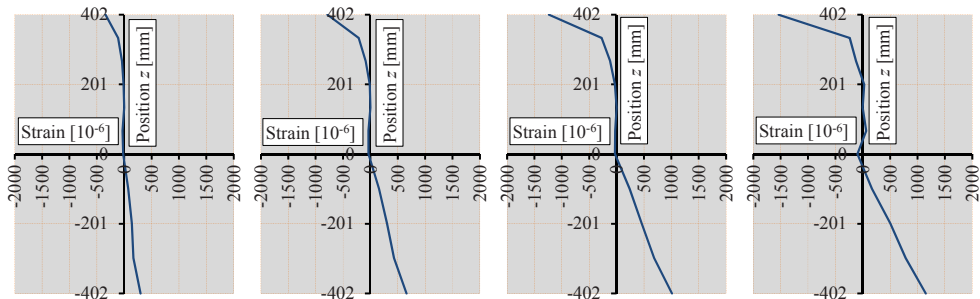
Deformation step B

Deformation step C

Deformation step D



Deformation step E

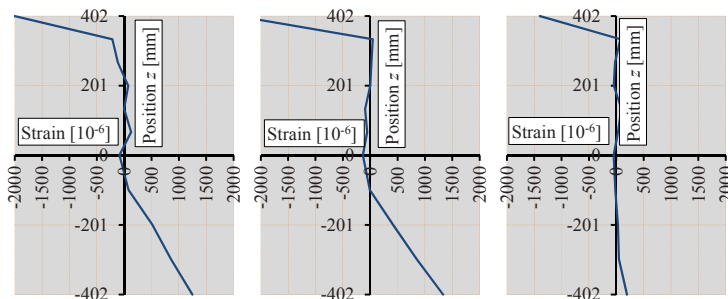


Deformation step H

Deformation step I

Deformation step J

Deformation step K

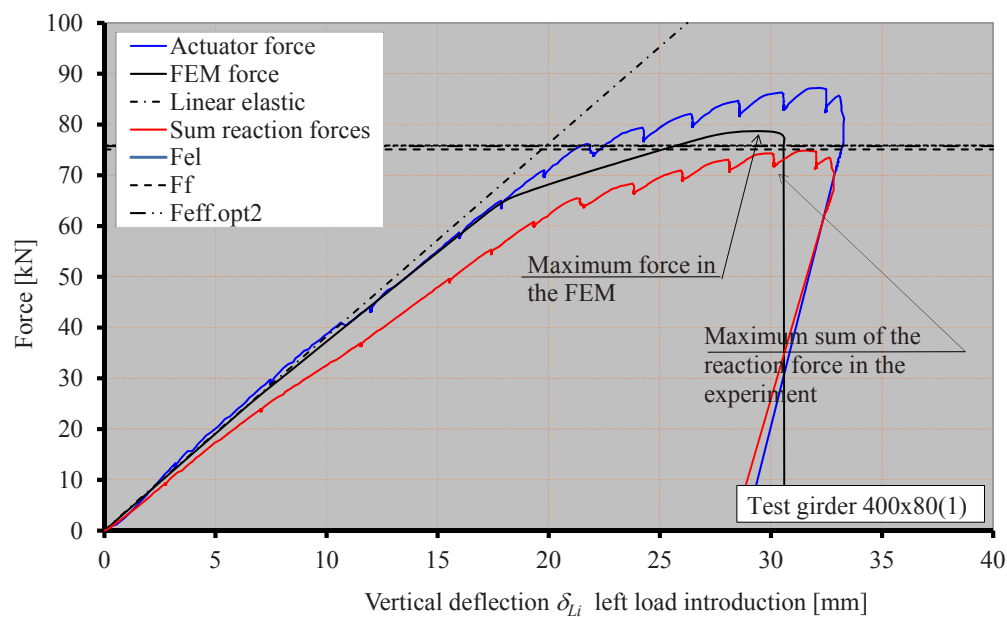
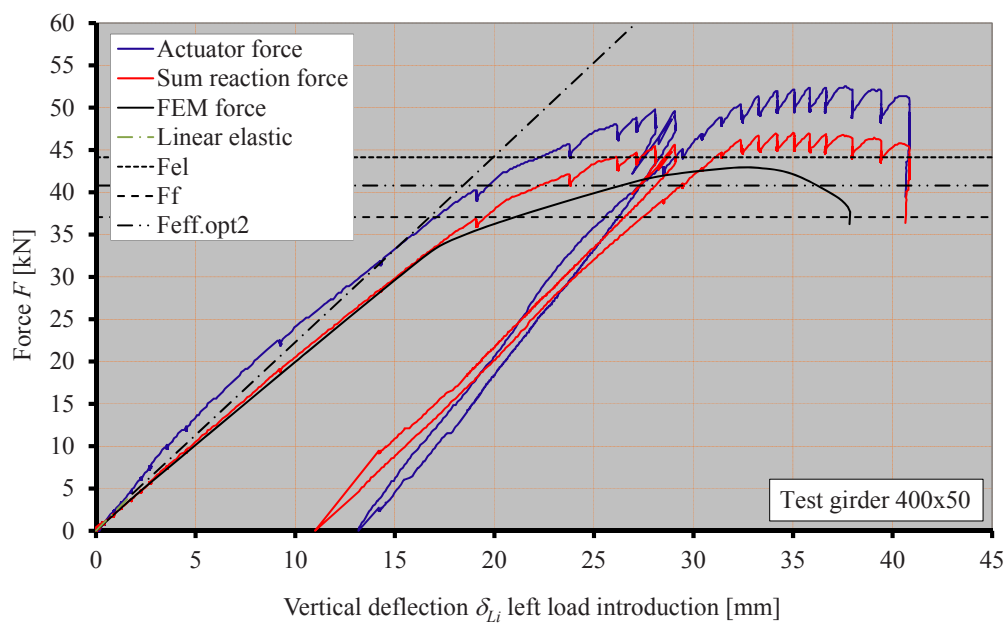


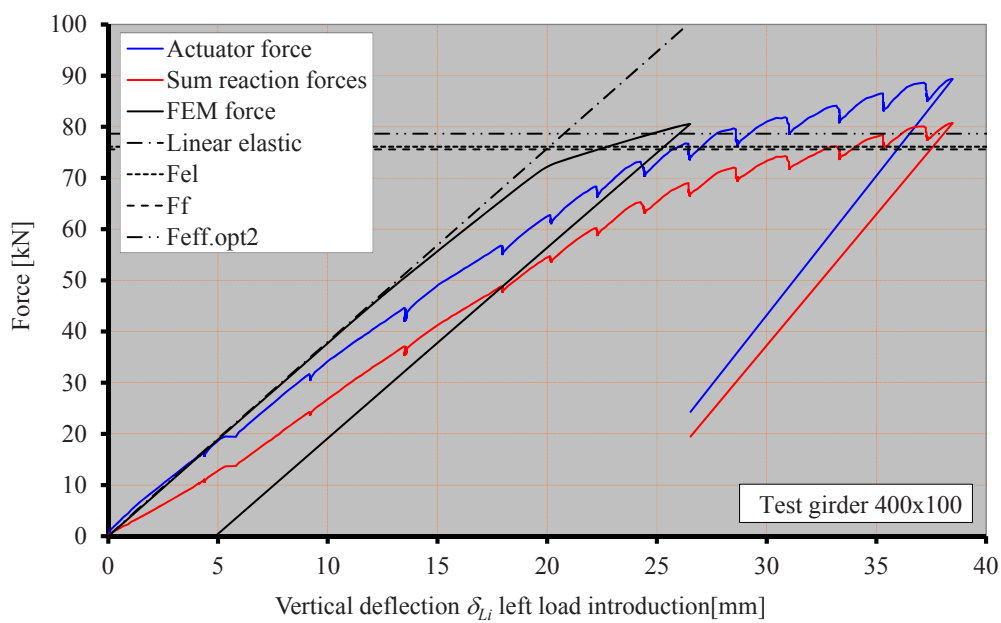
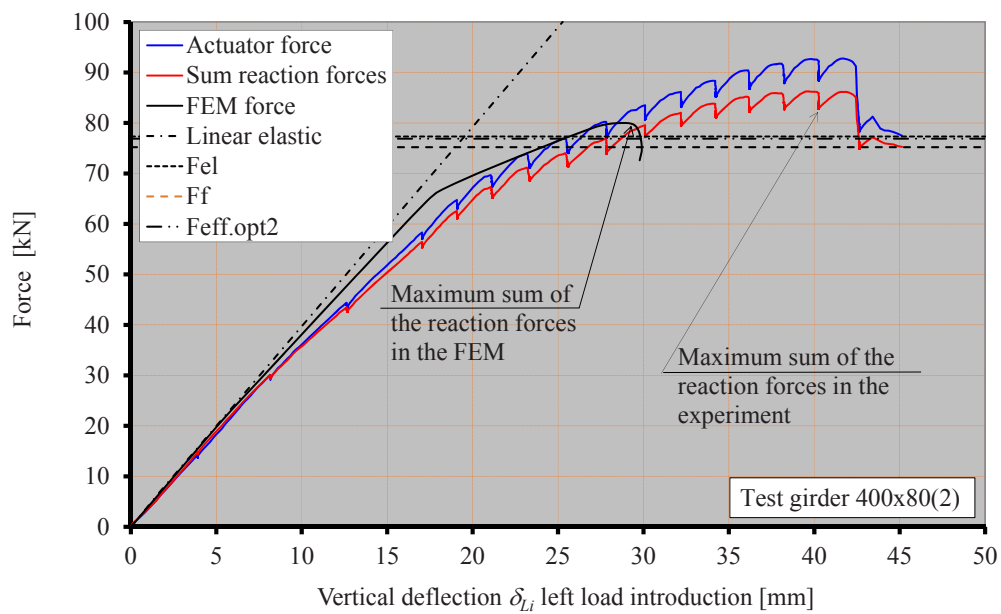
Deformation step L

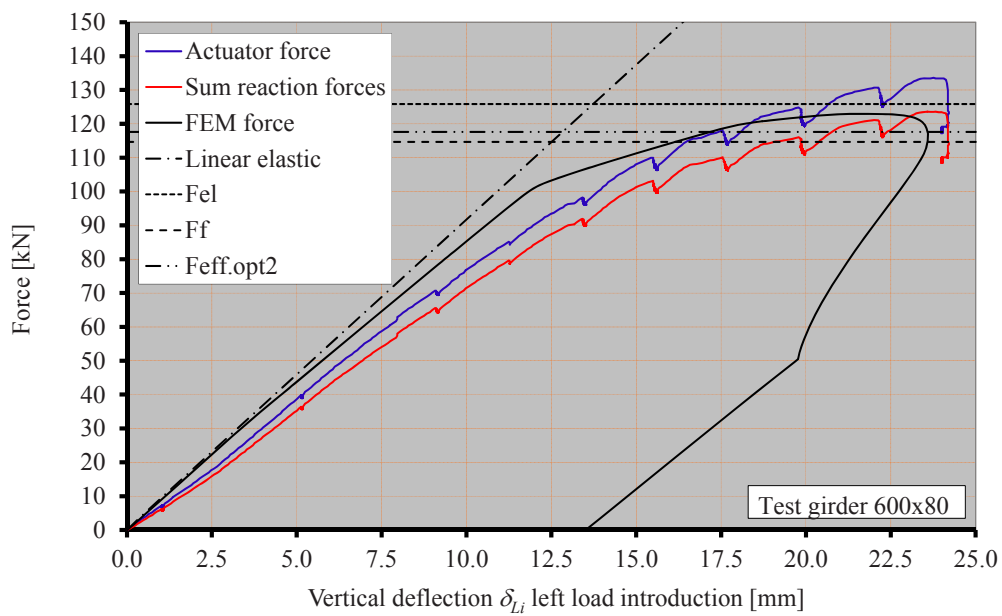
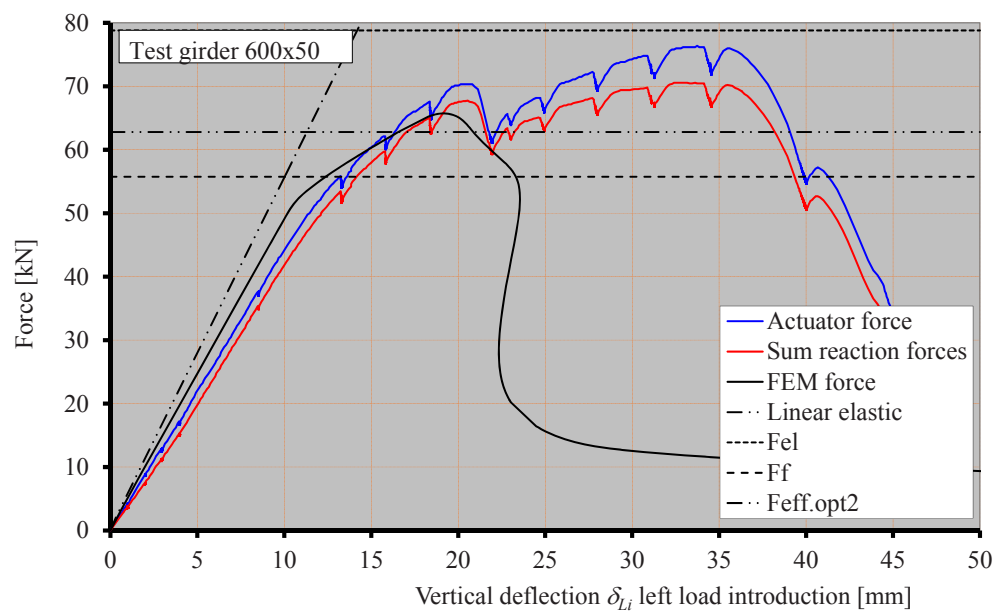
Deformation step M

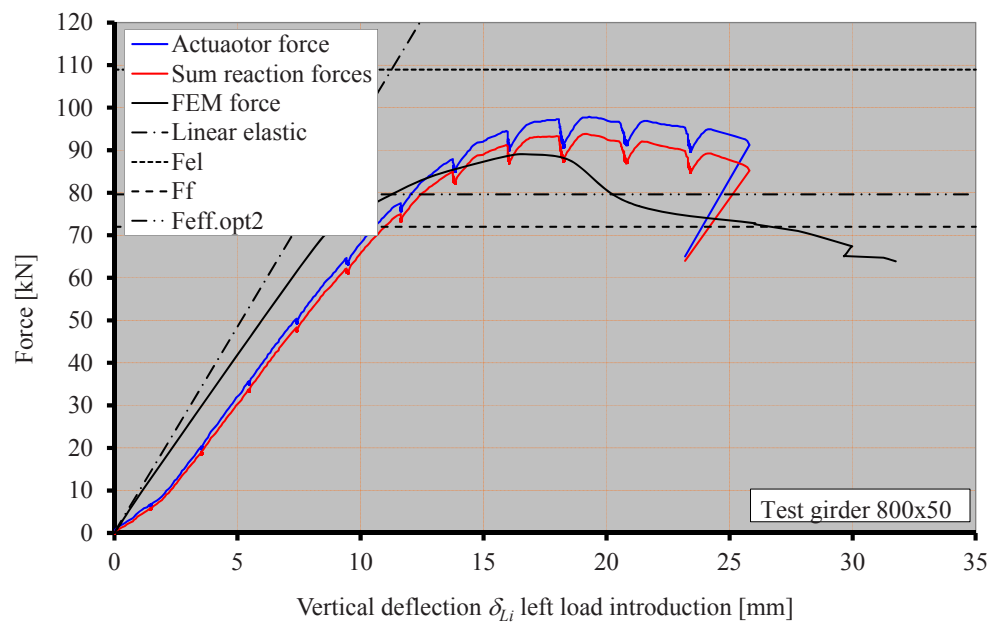
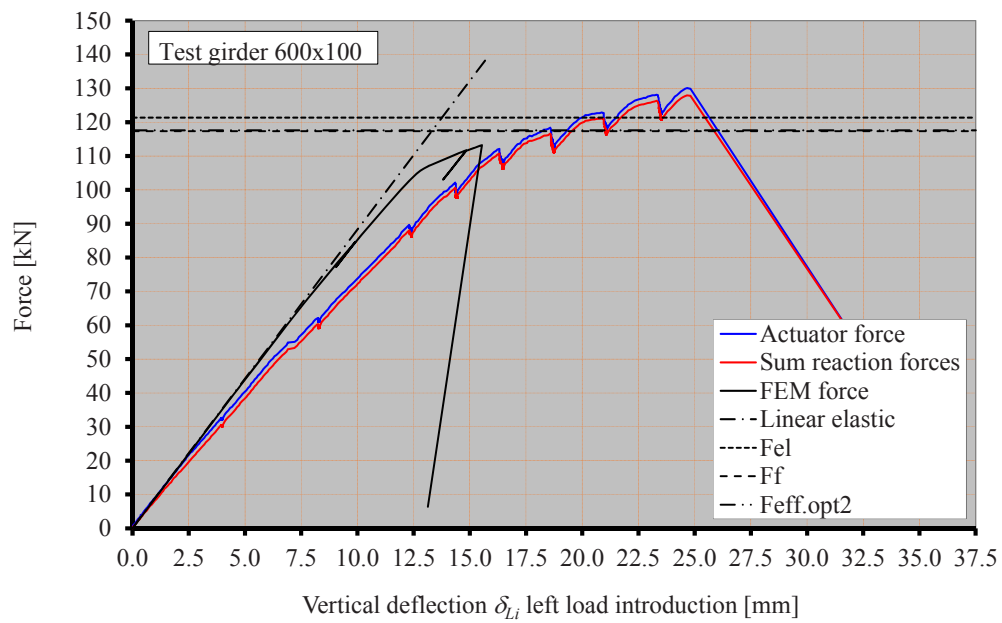
Deformation step N

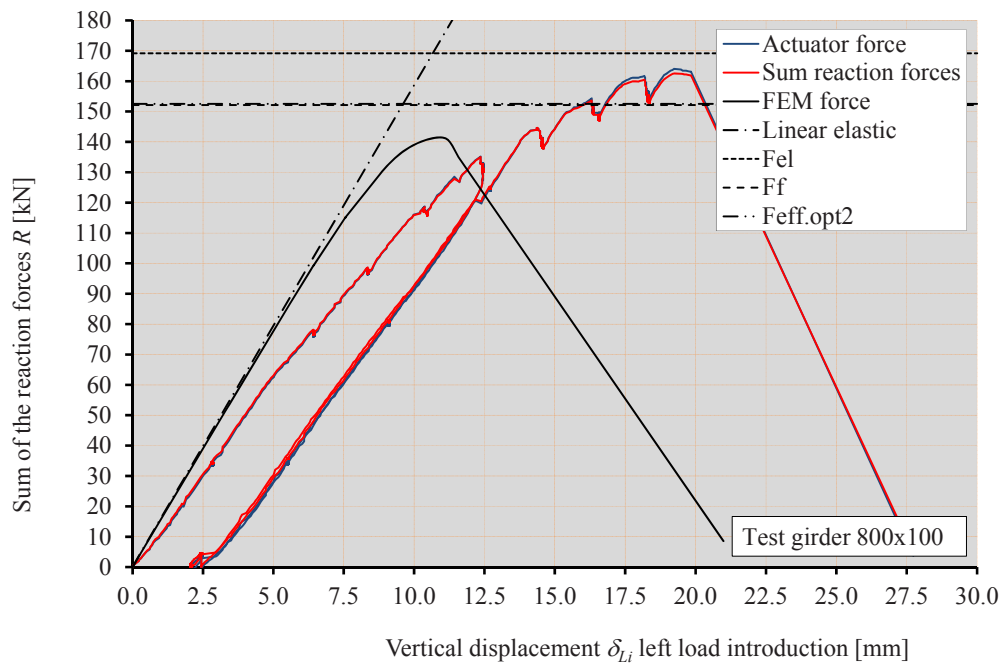
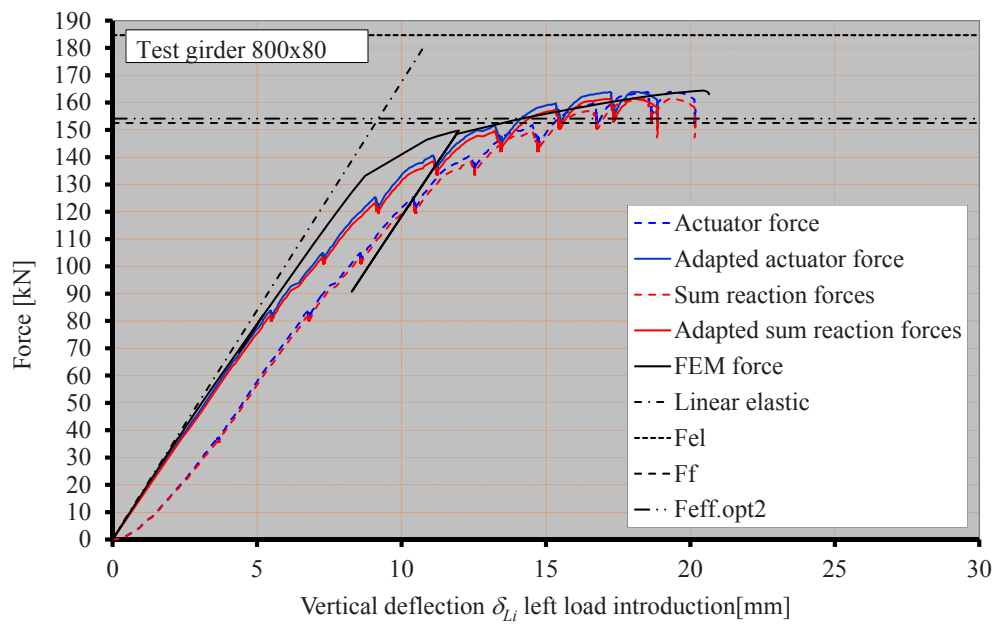
APPENDIX Q COMPARISON OF THE P - δ DIAGRAMS OF THE EXPERIMENTS AND THE FEM-MODELS











Curriculum Vitae

Roland Abspoel was born June 14th 1957 in Leiden, The Netherlands. He attended higher general secondary education at the Agnes Lyceum in Leiden, from which he graduated in 1976. After accomplishing the military services, he attended the Technical College in the Hague, from which he graduated in 1982.

After graduation he took a position as junior structural designer at the international engineering office Tebodin BV in the Hague. He cooperated on many industrial plants for all kind of branches and cooperated on several big hydraulic projects related to the Delta Works send on secondment for the Ministry of Waterways and Public Works and for building consortiums. The most prominent projects were Fuji Photo Tilburg, AVR (processor of residual waste), the extension of the Euromast in Rotterdam, the Eastern Scheldt storm surge barrier, the Maeslant storm surge barrier and the 4th sliding door of the lock in IJmuiden.

Next to his work he began his academic education at the faculty of Civil Engineering and Geosciences at the Delft University of Technology, from which he graduated in 1994. The Masters' thesis also focused on the optimization of plate girders.

From 1994 up to 1997 he worked at the Tebodin BV office in Beverwijk and in 1997 prof.dr.ir. J. Wardenier asked him to join the department of Steel Structures at the Delft University of Technology. One day a week was offered for PhD-research on plate girders, to attractive this position.

He participated in many courses related to steel structures and later on he participated also in two NGO's, one active in the Netherlands and one active in Kenya, both focused on the participation of underprivileged pupils. Especially his contribution on improvements on structures to harvest safe drinking water, strongly related to civil engineering, at 30 primary schools with around 24000 pupils in Kenya, took all his out-of-office time.

From 2012 the focus was on finalizing the PhD-thesis, which was mercilessly interrupted by the illness of his oldest daughter, which was strongly threatened by cancer.

Surname: Abspoel
Birth name: Roland
Address: Beppy Nooijsstraat 31
2331 HT Leiden
The Netherlands
Day of birth: 14-06-1957
E-mail address: r.abspoel@tudelft.nl

PhD-research

1997-2015 Civil Engineering and Geosciences, Delft University of Technology
Subject: 'Optimisation of plate girders'

Scientific publications

Abspoel, R. and Stark, J.W.B. (1999), "Elastic lateral buckling of coped beams" in the proceedings of the international conference on Stability and Ductility of Steel Structures, pages 49-56

Krüse, M., Abspoel, R. (1999), "Roestvast staal in kaart gebracht" in Bouwen met Staal, nr. 150, pages 50-55

Abspoel, R.(2000),

Maljaars, J., Stark, J.W.B., Steenbergen, H.M.G.M. and Abspoel, R. (2005) "Lateral-torsional buckling resistance of coped beams" in the Journal of the Constructional Steel Research, pages 1559-1575

Maljaars, J., Stark, J.W.B., Steenbergen, H.M.G.M. and Abspoel, R. (2005) "Development and validation of a numerical model for buckling of coped beams" in the Journal of the Constructional Steel Research, pages 1576-1593

Abspoel, R. (2008), “The maximum web slenderness of plate girders: State of the art and Laboratory tests” in the proceedings of the 5th European conference on steel and composite structures

Abspoel, R. (2009), “Optimising plate girder design” in the proceedings of the Nordic Steel conference

Abspoel, R. and Bijlaard, F.S.K. (2014) “Optimization of plate girders” in Steel Construction Volume 7, Issue 2, pages 116-125

Abspoel, R. (2014), “The maximum bending moment resistance of plate girders” in the proceedings of the conference Eurosteel 2014

Delgado Ojeda, O., Maljaars, J. and Abspoel, R. (2015) “Fire exposed steel columns with a thermal gradient over the cross-section” in Thin-Walled Structures

